PRE-TRANSMETALATION INTERMEDIATES IN THE SUZUKI-MIYAURA REACTION
REVEALED: THE MISSING LINK

BY

ANDY ALEXANDER THOMAS

DISSERTATION

Submitted in partial fulfillment of the requirements
for the degree of Doctor of Philosophy in Chemistry
in the Graduate College of the
University of Illinois at Urbana-Champaign, 2017

Urbana, Illinois

Doctoral Committee:

    Professor Scott E. Denmark
    Professor Martin D. Burke
    Assistant Professor David Sarlah
    Professor Thomas B. Rauchfuss

ABSTRACT

The Suzuki-Miyaura reaction is currently the most practiced cross-coupling reaction due to its broad applicability, low toxicity of the metal (B), and the wide variety of commercially available boronic acid substrates. Despite the popularity of the Suzuki-Miyaura reaction, the precise manner in which the organic fragment is transferred from boron to palladium has remained elusive for over 30 years. The work described in this dissertation has focused on identifying such species by low temperature rapid injection NMR spectroscopy. For the first time, we were able to detect and characterize the first pre-transmetalation intermediate *"The Missing Link"* in the Suzuki-Miyaura reaction.

The ability to confirm the intermediacy of pre-transmetalation intermediates has provided the opportunity to clarify mechanistic aspects of the transfer of the organic moiety from boron to palladium in the key transmetalation step. Specifically, these studies establish the identity of two different intermediates containing Pd−O−B linkages, a tricoordinate (6-B-3) boronic acid complex and a tetracoordinate (8-B-4) boronate complex, both of which undergo transmetalation leading to the cross-coupling product. Two distinct mechanistic pathways have been elucidated for stoichiometric reactions of these complexes: (1) transmetalation *via* an unactivated 6-B-3 intermediate that dominates in the presence of excess ligand, and (2) transmetalation *via* an activated 8-B-4 intermediate that takes place with a deficiency of ligand.

The successful formation of pre-transmetalation intermediates with arylboronic acids led to the investigation of whether some of the most common arylboronic esters utilized in the Suzuki-Miyaura reaction could also form stable intermediates. Surprisingly, catechol and ethylene glycol arylboronate esters formed Pd-O-B linkages at low temperature and were found to transfer their organic groups directly from boron to palladium with enhanced rates. Specifically, the glycol arylboronate ester was found to transfer its organic group ~25 times faster than the corresponding arylboronic acid analog. These combined results provide the first structure activity relationships on the pre-transmetalation intermediates in the Suzuki-Miyaura reactions which are currently being applied to catalytic reactions.

The work described in the dissertation is dedicated to Professor Dr. Scott E. Denmark whose genius, patience and generous support have made my years in Illinois, chemically and personally, a most enriching and inspiring experience.

ACKNOWLEDGEMENTS

TABLE OF CONTENTS

CHAPTER 1. Introduction

1.1 Palladium Catalyzed Cross-Coupling Reactions

The formation of sp^2-sp^2 carbon-carbon bonds is of profound importance due to the ubiquity of this connection in both synthetic and naturally occurring substances. This fundamental process in organic synthesis is frequently accomplished by the interaction of an organic substrate with a metal catalyst or organometallic reagent. Specifically, palladium has emerged as an excellent metal catalyst for an entire class of reactions known as cross-coupling reactions. Palladium-catalyzed cross-coupling reactions such as the Kumada-Tamao-Corriu[1] (Mg), Suzuki-Miyaura[2] (B), Stille-Migita-Kosugi[3] (Sn), Hiyama-Denmark[4] (Si) and the Negishi[5] (Zn) reactions, have fundamentally changed the practice of organic synthesis in both the academic and industrial settings alike (Figure 1).[6]

M = MgX, BR$_2$, SnR$_3$, ZnX, SiR$_3$
X = Cl, Br, I, OTf, N$_2$+
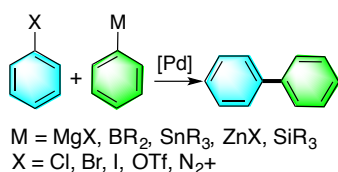
Figure 1. Palladium catalyzed cross-coupling reactions.

Among these reactions, the Nobel Prize sharing Suzuki-Miyaura reaction is the premier cross-coupling process, utilized across all disciplines of chemistry as well as in the industrial synthesis of fine chemicals[7] and pharmaceuticals[8] owing to its demonstrated reliability, broad functional group compatibility, and access to a wide variety of commercially available boron-based reagents. At a fundamental level, all of these reactions share the same basic catalytic cycle comprised of three elementary steps: oxidative addition, transmetalation, and reductive elimination (Figure 2). The oxidative addition and reductive elimination steps are common to all cross-coupling variants; however, because the organic donor is involved only in the transmetalation step, it is this event that preparatively and mechanistically differentiates all of these processes. The desire to understand the relationship between chemical structure and reactivity has led to many mechanistic investigations of these elementary steps. Particularly, the oxidative addition[9] and reductive elimination[10] steps have been extensively studied and those insights are applicable to all of the cross-coupling reactions. However, except for the Stille and more recently the Hiyama-Denmark[11]

couplings, far less is known about the intricate details of the transmetalation step for these cross-coupling reactions.
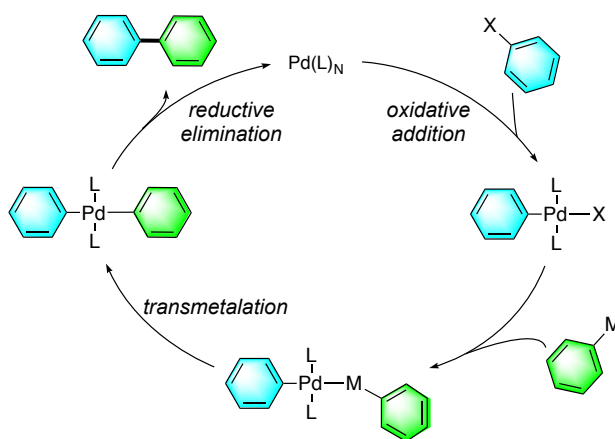
Figure 2. Palladium catalyzed cross-coupling reactions and general mechanism.

1.2 The Mechanism of Cross-Coupling

1.2.1. Oxidative addition step

The oxidative addition of organohalides or triflates is the first step for all palladium catalyzed reactions as well as the Heck process.[12] Many investigations have been conducted on the mechanisms for the oxidative addition step of alkenyl and aryl halides with palladium.[13] The rate of this step has been shown to decrease in the order of PhI > PhBr > PhCl, which is consistent with bond dissociation energies.[14] Specifically, (Ph$_3$P)$_4$Pd has been shown to undergo a prior dissociation event ((Ph$_3$P)$_2$Pd) before oxidative addition with organic halides.[15] After dissociation oxidative addition takes place *via* a three centered transition state to form an initial *cis*-(aryl)PdXL$_2$ **1** complex that undergoes rapid isomerization to the thermodynamic product *trans*-(aryl)PdXL$_2$ **2** because the phosphines exhibit *transphobia* (Figure 3).[16]
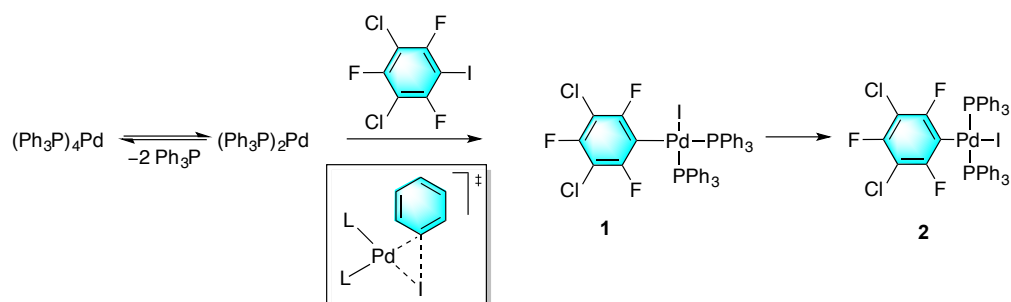
Figure 3. *Cis*- to *trans* isomerization of oxidative addition.

Interestingly, bulky electron rich phosphines have shown increased reactivity towards oxidative addition of aryl chlorides as demonstrated by pioneering work by Fu[17] and Buchwald[18] (Scheme 1).

Scheme 1
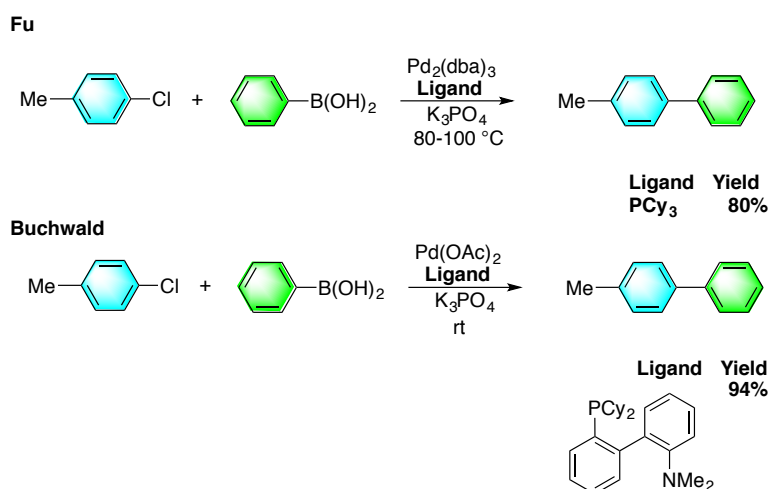
Moreover, the origins of the enhanced rate for bulky phosphines towards oxidative addition has been shown to originate from a prior dissociation event.[2] Hartwig found an inverse dependence for phosphine in the oxidative addition reaction of $[(2\text{-}CH_3C_6H_4)_3P]_2Pd$ with aryl chlorides and bromides demonstrating that a LPd was the active species.[19] Furthermore, palladium halide dimer **3** was isolated. Since then a number of three coordinate T-shaped palladium complexes **4** have been isolated with *t*-Bu$_3$P.[20] Interestingly, these complexes exhibited a empty coordination site *trans* to the aryl substituent most likely due to the larger *trans* influence. Additionally, weak agnostic interactions were observed in the crystal structures of these complexes (Scheme 2).

Scheme 2

L = (o-tol)$_3$P

3

L = t-Bu$_3$P

4
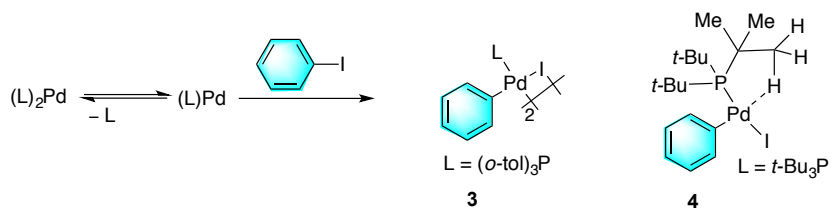
1.2.2. Reductive elimination step

The reductive elimination step is the final step of the catalytic cycle and the bond forming event. Independent kinetic studies by Stille[21] and Yamamoto[22] revealed an inverse order in phosphine for the reductive elimination of isolated L_2PdR_2 complexes. This indicated that an empty coordination site was needed prior to reductive elimination. Moreover, cross-over experiments were executed to determine if an empty coordination site was involved during the reductive elimination step. Interestingly, when *trans*-$(Et_2PPh)_2(CH_3)_2Pd$ **5** and *trans*-$(Et_2PPh)_2(CD_3)_2Pd$ **6** were heated a statistical mixture of CH_3-CH_3, CD_3-CD_3, and CH_3-CD_3 was observed indicating that a bimolecular *trans* to *cis* isomerization was involved. Furthermore, when *cis*-$(Et_2PPh)_2(CH_3)_2Pd$ **7** and *cis*-$(Et_2PPh)_2(CD_3)_2Pd$ **8** were heated only CH_3-CH_3, and CD_3-CD_3 were observed indicating that the reductive elimination from *cis* complexes is unimolecular (Figure 4).
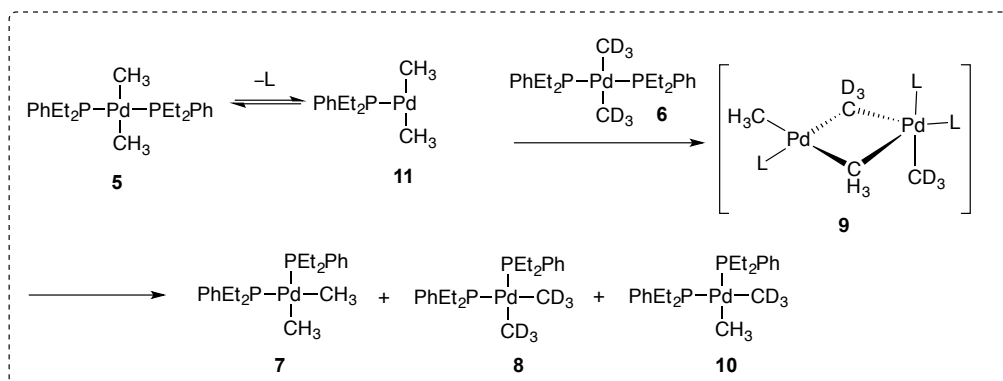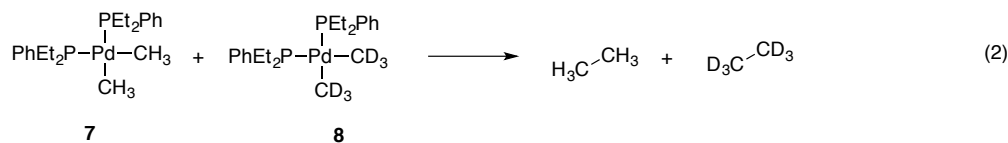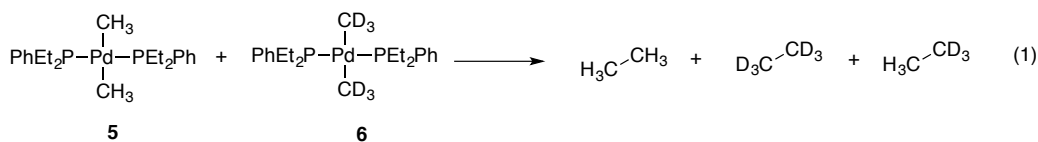
Figure 4. Cross-over experiments during reductive elimination.

To probe the effect of electron rich and poor aryl substituents on the reductive elimination step Hartwig prepared and isolated *bis*-aryl platinum DPPF complexes where interesting rate effects were observed.[23] Upon reductive elimination of symmetrical electron deficient DPPF complex **12** resulted in the slowest rate for reductive elimination. Interestingly, the electron rich DPPF complex **13** was found to only reductive eliminate ~5.35 times faster than the electron deficient analog **12**. Upon, subjecting unsymmetrical complex **14** employing both electron withdrawing and donating groups, a rate enhancement was observed ~17 times faster than complex **12**. This enhancement of rate is manifested from the stabilization of the transition state during the reductive elimination. The accelerating effects of matching electron rich with electron poor substrates is seen in many reactions including the Diels Alder reaction in which optimal reaction conditions involve substrates that can achieve effective LUMO and HOMO mixing (Figure 5).
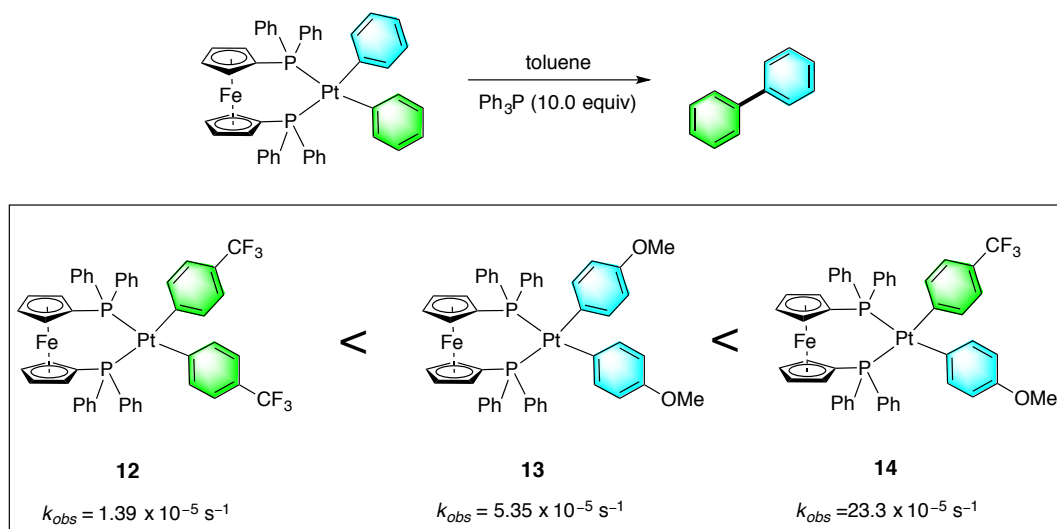
Figure 5. Reductive elimination rates of (DPPF)Pt(Aryl)$_2$ complexes.

1.2.3. Transmetalation step

1.2.3.1. Transmetalation from organotin compounds

In 1977, Migita, Kosugi and Shimizu demonstrated that palladium catalyzed reactions between organo tin compounds were possible.[24] In 1978, Stille's first study appeared on the palladium catalyzed cross-coupling between acid chlorides and organotin compounds to form ketones (Scheme 3).[25] Over the next 10 years Stille performed both extensive mechanistic and synthetic investigations with various electrophiles which is why this reaction bears his name.[26,27]

Scheme 3
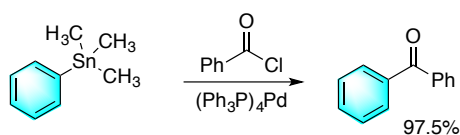
An early investigation on the transfer of the organic group from tin to palladium by Stille and co-workers revealed that electron rich substrates increased the rate.[28] Furthermore, a *p* = + 1.2 value was obtained indicating that a build-up of negative charge was present suggesting that the organic group was transferring to the palladium center in an S$_E$2 fashion or "open transition state." Moreover, the open S$_E$2 mechanism was further supported by the observation that benzylic stereocenters underwent inversion of stereochemistry upon transfer from tin to palladium (Scheme 4).

Scheme 4
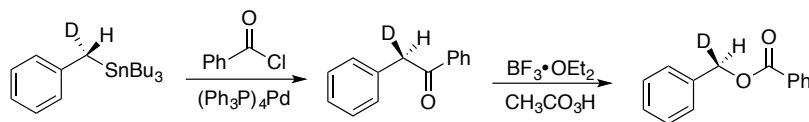
Since then numerous investigations have been undertaken for the transmetalation step in the Stille reaction which have led to two different mechanistic proposals (associative and dissociative) for the transmetalation event (Figure 6). The initial oxidative addition product *cis*-L$_2$PdAryl(X) has been shown kinetically to react directly with the active tin transmetalating agent through an associative pentacoordinate intermediate by Espinet and co-workers.[29] Alternatively, the dissociative process is centered on the proposal that oxidative addition product *trans*-L$_2$PdR(X) is the precursor which needs a prior ligand dissociation (excess ligand slows rate of transmetalation)[30],[31] to open a coordination site on palladium so the active tin transmetalation agent can transfer its organic group.
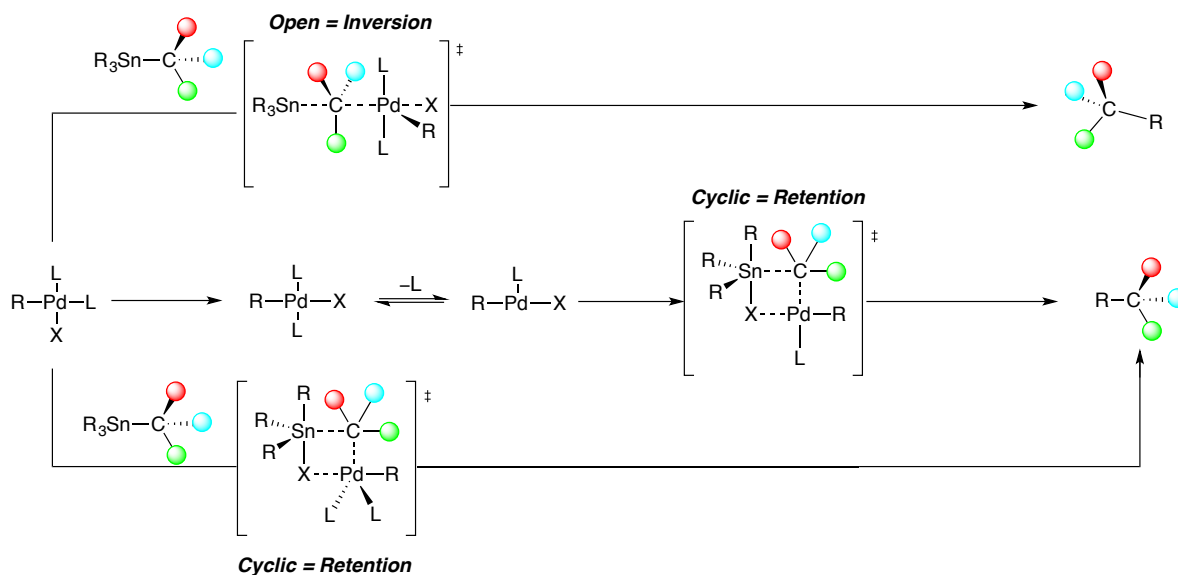
Figure 6. Proposed transition states for transmetalation event with stereochemistry.

These pathways ultimately depend on the reaction conditions; however bulky phosphines are known to form T-shaped organo palladium halides after oxidative addition. [19c] On this note Hartwig and co-workers investigated the transmetalation event between dimeric halide dimer **15** with PhSnMe$_3$ (Figure 7).[32] Interestingly, the reaction was found to exhibit a half order dependence

on the concentration of the dimer **15** indicating that the active species was a T-shaped bromide complex **16** and most likely proceeded through a cyclic S_E2 pathway **17**.[31]

L = (o-tol)$_3$P

15   **16**   **17**

Figure 7. Empty coordination site is needed for the transmetalation event.

1.2.3.2. Transmetalation from organo silicon compounds

In 1982, Kumada and co-workers demonstrated the first silicon mediated cross-coupling between penatafluorosilicates and aryl halides in the presence of a palladium catalyst (Scheme 5, 1).[33] In 1988, Hiyama and co-workers demonstrated that vinyl trimethylsilanes underwent cross-coupling in the presence of a fluoride activator (Scheme 5, 2).[34]

Scheme 5

(51%)   (1)

(89%)   (2)
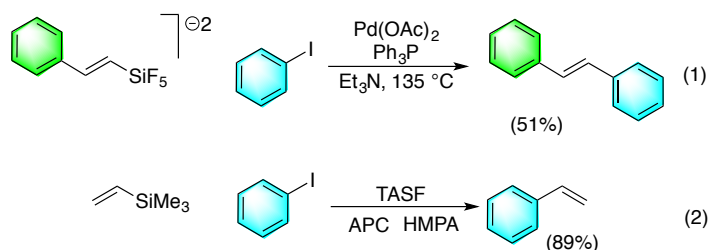
Historically, it was thought that silicon needed an activator to induce transmetalation (ie fluoride activation). However, computational[35] by Hiyama and kinetic studies by Amatore and Jutand[36] have established three roles for fluoride during the transmetalation event. Specifically, the main conclusion was that fluoride does not activate silicon but rather forms a Pd-F intermediate **20** that allows for transmetalation to take place (Figure 8).

18   **19**   **20**   **21**
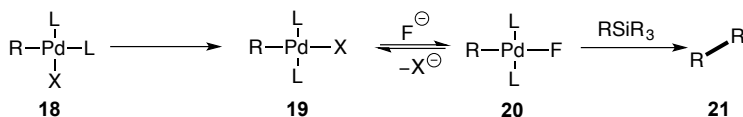
Figure 8. Proposed role of fluoride during transmetalation event.

A related study from Denmark and co-workers on the transmetalation step in the Hiyama-Denmark cross-coupling process described the isolation and single crystal, X-ray diffraction

analysis of several compounds containing Pd-O-Si linkages.[37] These complexes enabled a systematic study on the requirements for the transfer of the organic group from silicon to palladium for both neutral (8-Si-4) and anionic (10-Si-5) pathways.[11b] The N-X-L nomenclature, as introduced by Martin and co-workers designates the bonding about any atom (X) in a resonance structure in terms of the valence shell of electrons (N) formally associated directly with that atom and the number of ligands (L) directly bonded to it.[38] These conclusions contradicted the paradigm that organosilicon compounds *must* be anionically activated to participate in the transmetalation processes. In general, arylsilanolates, require anionic activation and react *via* 10-Si-5 intermediate **22** whereas alkenylsilanolates undergo transmetalation directly from 8-Si-4 intermediate **23** (Figure 9). The ability to perform a similar study with Pd-O-B linkages would be ideal however, the high propensity for transmetalation at room temperature makes their isolation and characterization of them difficult in practice.
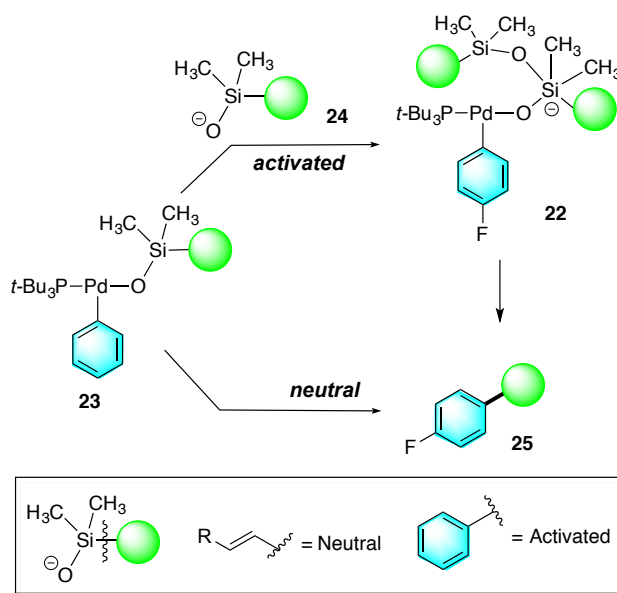
Figure 9. Hiyama-Denmark transmetalation pathways.

1.2.3.3. Transmetalation from organo boron compounds

1.2.3.3.1. Proposed pathways for the organic group transfer from boron to palladium

Currently, two alternative processes (Path A and Path B) have been proposed to initiate the transmetalation event which differ in the precise role of the hydroxide ion which is required for the reaction to proceed.[39] Path A proceeds through saturation of the boron valence in **26** to yield a metal trihydroxyarylboronate salt **27** which then displaces halide from the oxidative addition

product **28** generating species **29** containing the critical Pd-O-B linkage. Path B, proceeds through displacement of halide from the oxidative addition product **28** by hydroxide thus creating a palladium hydroxide complex **30** which then combines with the Lewis acidic arylboronic acid **1** forging the same pre-transmetalation intermediate **29** (Figure 10).
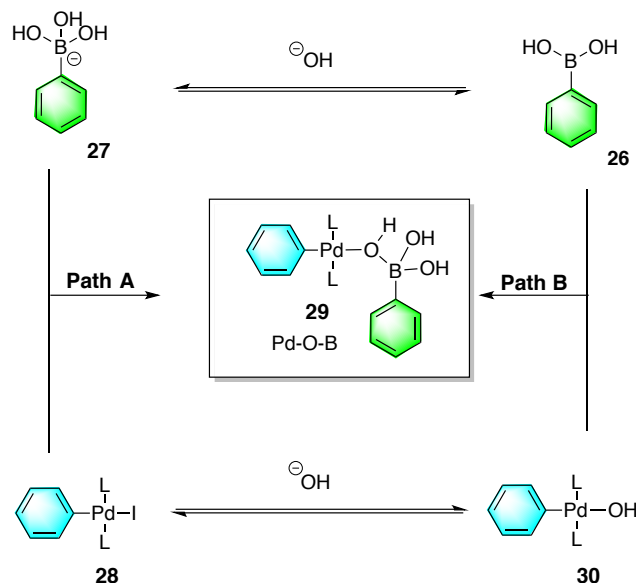
Figure 10. Proposed transmetalation pathways in the Suzuki-Miyaura coupling process.

1.2.3.3.2. Preliminary evidence for a Pd-O-B linkage

Preliminary evidence for the involvement of a Pd-O-B moiety was provided by an early investigation by Soderquist[40] in which the diastereospecificity of the transmetalation step was examined. Subjecting both *syn* (**31**) and *anti* (**32**) deuterium-labeled isomers of *B*-(3,3,-dimethyl-1,2-dideuterio-1-butyl)-9-BBN to standard Suzuki-Miyaura cross-coupling conditions ((THF, NaOH, (Ph$_3$P)$_4$Pd)) leads to complete retention of configuration in the coupling product (Scheme 6). Although no pre-transmetalation intermediate was observed, the retention of configuration indirectly establishes that a Pd-O-B linkage is involved in the transmetalation event.

Scheme 6
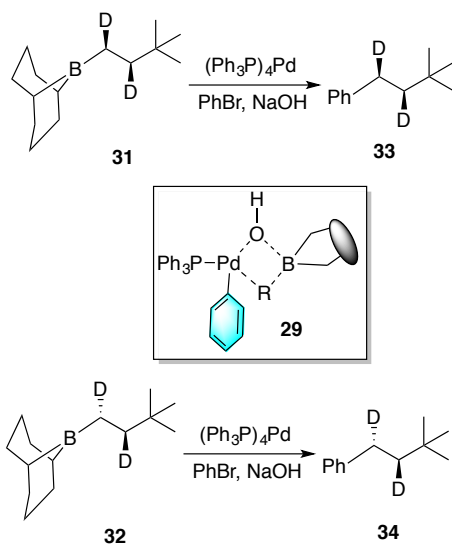
1.2.3.3.3. Computational studies

Distinguishing the way in which Pd-O-B linkages are formed in the Suzuki-Miyaura reaction has proven to be challenging as mechanistic studies are complicated by biphasic reaction conditions (e.g. THF and aqueous base), and by the poor solubility of inorganic bases and metal organoboronate salts in many organic solvents. Consequently, DFT computational studies have provided insights that suggest Path A is responsible for the formation of pre-transmetalation intermediates. Interestingly, in Ph$_3$P-ligated complexes Maseras and Ujaque[41] have calculated that the displacement of bromide from the oxidative addition product **35** with trihydroxyphenylboronate **27** was slightly lower ($\Delta\Delta G^\dagger = 2.6$ kcal/mol) in energy than the reaction of palladium hydroxide complex **36** with **26** suggesting that both paths are capable of forming Pd-O-B linkages. However, the displacement of bromide with hydroxide from complex **35** was found to have a transition state barrier of 18.6 kcal/mol, which suggests that Path A is more favorable than Path B (Figure 11).[42] Moreover, the impact of phosphine ligand on the transmetalation event has been computationally studied in depth by Lloyd-Jones and Harvey using *t*-Bu$_3$P, (CF$_3$)$_3$P, (CH$_3$)$_3$P and Ph$_3$P. In this investigation, the steric parameters were found to be twice as important as the electronic parameters on the transmetalation event.[43]
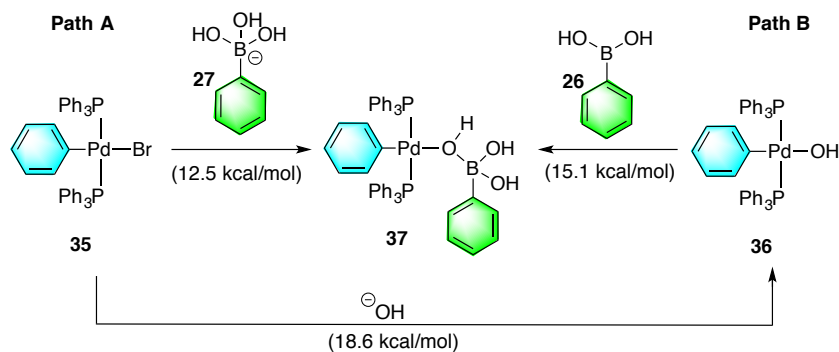
Figure 11. DFT calculated values for transmetalation.

1.2.3.3.4. Experimental studies

Understanding the role of hydroxide in the formation of the "missing link" **29** (i.e. Path A or Path B) has inspired many investigations by Soderquist,[40] Hartwig,[44] Amatore/Jutand[45] and Schmidt.[46] By performing stoichiometric reactions of pre-formed $(Ph_3P)_2PdPhBr$ **35** and $(Ph_3P)_2PdPhOH$[47] **36** with **38** and **39** respectively, Hartwig established that Path B is favored over Path A kinetically by more than 4 orders of magnitude (Scheme 7). Moreover, they established that the equilibrium population of 4-methylphenylboronic acid **39** and potassium 4-methylphenyltrihydroxyboronate **37** in acetone/H_2O in the presence of 2.5 equiv of K_2CO_3 is ca. 1:1. Interestingly, the relative populations of *trans*-$(Cy_3P)_2(C_6H_5)Pd(OH)$ **40** and *trans*-$(Cy_3P)_2(C_6H_5)Pd(I)$ **41** are also approximately equal under simulated catalytic reactions conditions (Scheme 6). This conclusion was reinforced by extensive kinetic studies by Amatore and Jutand who also identified multiple antagonistic roles for hydroxide ion. Although kinetic studies have provided evidence for these pathways, the actual composition and structure of the Pd-O-B containing species has not been determined.

Scheme 7

k = 1.7 x 10^{-7} s^{-1}
estimated rate at –40 °C

k = 2.4 x 10^{-3} s^{-1}
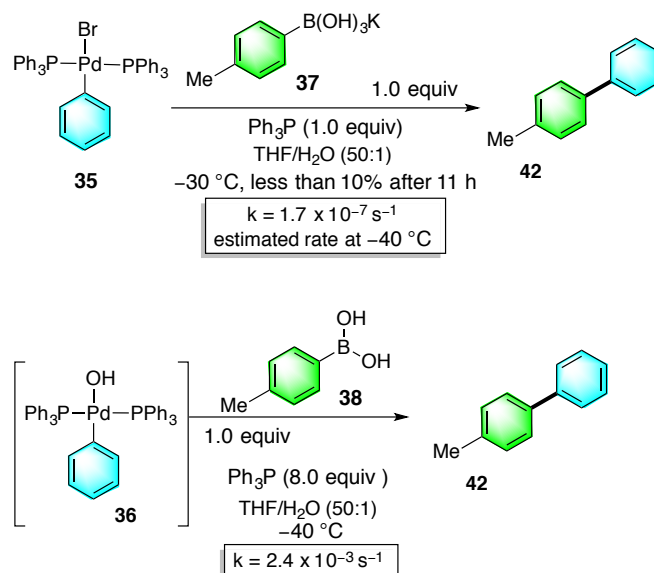
Scheme 8
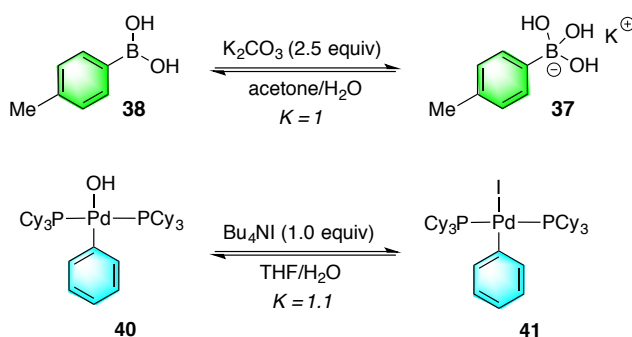
1.2.3.3.5. Attempts to detect reactive intermediates

To observe pre-transmetalation intermediates Canary and co-workers used electrospray mass spectrometry (ESI-MS) to probe the catalytic reaction between phenylboronic acid (**26**) and 3-bromopyridine (**43**) in toluene using (Ph$_3$P)$_4$Pd and sodium carbonate as the base.[48] During the course of these experiments, both [(pyrH)(Br)Pd(Ph$_3$P)$_2$]$^+$ (**44**) and [(pyrH)(Ph)Pd(Ph$_3$P)$_2$]$^+$ (**45**) were detected. The observation of only the oxidative addition intermediate **44** and transmetalation product **45** clearly demonstrates the difficulty in investigating the central transmetalation step of the catalytic process (Scheme 9, top).

Scheme 9

Observed by ESI

44

oxidative addition product

45

transmetalation product
(pre-reductive elimination intermediate)
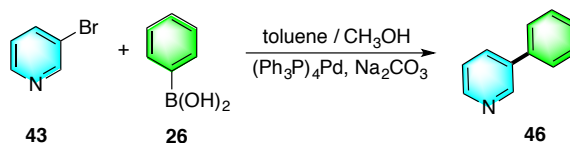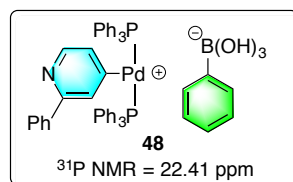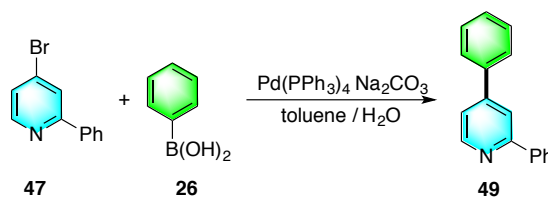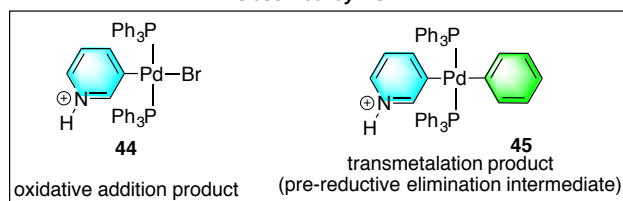
Cid and co-worker's investigation on the transmetalation step of the Suzuki-Miyaura reaction involved the use of ^{31}P NMR spectroscopy and computational methods.[42a] The authors combined 4-bromo-2-phenylpyridine **47** with phenylboronic acid **26** with $(Ph_3P)_4Pd$ and were able to observe a ^{31}P NMR signal at 22.41 ppm, which was assigned to $(Ph_3P)_2PdAr[(HO)_3BAr]$ **48** (Scheme 9, bottom). The predicted structure is based solely on DFT calculations. Although a new peak is observed by ^{31}P NMR spectroscopy no further structure determination was performed thus precluding an assignment.

1.3 Rapid Injection NMR

Because of the apparently transient nature of species containing Pd-O-B linkages, routine methods such as ESI-MS spectrometry and NMR spectroscopy have proven incapable of characterizing these highly reactive intermediates. Clearly, fast and low-temperature techniques

are required to probe the mechanism of this crucial transmetalation step in the Suzuki-Miyaura reaction as low barriers ($\Delta G^{\dagger}$ = 14-22 kcal/mol) to transmetalation have been calculated.[41,42,43] One such technique that has proven invaluable in similar mechanistic studies is Rapid Injection Nuclear Magnetic Resonance spectroscopy (RI-NMR).[49]

RI-NMR is a conceptually simple technique that was developed by McGarrity and co-workers in 1981.[50] His seminal paper entitled *Rapid Injection NMR: a simple technique for the observation of reactive intermediates* appropriately highlights perhaps the most useful feature of RI-NMR, the observation and characterization of reactive intermediates with relatively short half-lives. Furthermore, this investigation led to the first kinetic information for the rate of hydrolysis of the trimethyloxonium tetrafluoroborate (Scheme 10). Since then, various instruments have been developed by Ogle, Reich, and Denmark and used to execute mechanistic investigations.

Scheme 10
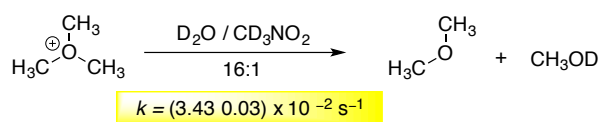
In practical terms, an RI-NMR experiment involves charging a substrate, typically the more sensitive compound, in an NMR tube spinning in the probe of NMR spectrometer. Next, a calibrated syringe assembly is lowered into the magnet, to allow for temperature equilibration, shimming, locking, etc. which is then followed by the injection of another reagent. Acquisition begins simultaneously with injection, which allows for rapid data collection. From the integration of the signals, the quantification of each species in solution can be performed with an internal standard. As a result, detailed quantitative kinetic data can be accessed even for fleeting intermediates.

In the Denmark laboratories, the RI-NMR apparatus in use incorporates a stationary syringe with a movable titanium rod that is filled with a solution of the reagent. The syringe is controlled by a piston coupled to a ceramic pump which is used to dispense the substrate into the tube while providing extremely accurate liquid delivery *via* a ceramic pump. The NMR tube containing the substrate lies inside the magnet, and typically spins at 20 Hz, requiring the liquid to be injected radially for rapid mixing to occur. The injector has a titanium paddle brazed to it, which aids in mixing along with three injection ports 120° apart (Figure 12). If pre-transmetalation intermediates

could be generated and characterized by this method, it would provide the first opportunity to interrogate structure and reactivity relationships of this crucial step.
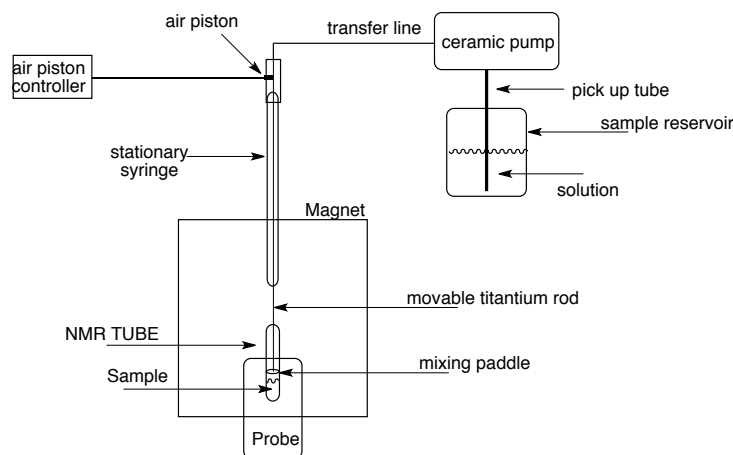
Figure 12. Box diagram of RI-NMR apparatus.

1.4 Project Goals

The aim of this project is to provide a complete understanding for the mechanism of the Suzuki-Miyaura reaction by forming pre-transmetalation intermediates by low temperature and RI-NMR spectroscopy along with computational analysis. Specific goals include: (1) full characterization of reaction intermediates such as the pre-transmetalation species; (2) validation of structure of the proposed intermediates through independent synthesis; (3) demonstration of the kinetic competence of the characterized species containing Pd-O-B linkages to form cross-coupling product, and (4) quantum mechanical simulation of the transmetalation process involving these intermediates by computational modeling.[51] The work described in this dissertation can be best described as follows:

1. The structure elucidation of Pd-O-B linkages from arylboronic acids using various ligands and palladium sources by rapid injection and low temperature NMR spectroscopy (Chapter 2).
2. Kinetic and computational analysis of the identified 6-B-3 and 8-B-4 pre-transmetalation intermediates (Chapter 3).
3. Investigate the effects of aryl boron sources on the structure and reactivity of Pd-O-B linkages structurally, kinetically, and computationally (Chapter 4).

CHAPTER 2: Structure Elucidation and Independent Synthesis of Pd-O-B Linkages in the Suzuki-Miyaura Cross-Coupling Reaction

2.1 Introduction and Background

The transmetalation of arylboronic acids with complexes of late transition metals such as Pd, Rh, and Pt has been postulated in cross-coupling reactions as well as conjugate addition reactions. However, the intermediates involved in the transmetalation steps have rarely been observed for these processes. To date, stable Pt and Rh complexes of arylboronic acids have been characterized by single crystal X-ray diffraction analysis. For example, Osakada[52] prepared Pt-O-B compound **50** by combining $(Me_2PhP)_2Pt(I)Ph$ **51** and 4-methoxyphenylboronic acid **52** with Ag_2O. Complex **50** is stable in THF until base is added, which induces transmetalation to the diarylpalladium intermediate **53** (Scheme 11).

Scheme 11
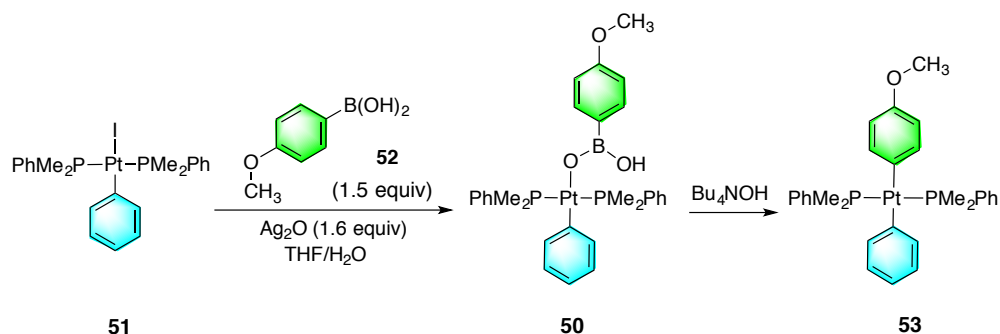
A similar Rh-O-B complex **54** prepared by Hartwig, undergoes transmetalation to form $(Et_3P)_2Rh(Ph)(C_6H_4-OMe)$ **55** when heated to 70 °C (eq 4).[53] Interestingly, both of these M-O-B complexes contain trigonal boron centers in which the Rh-O-B complex is proposed to undergo transmetalation without prior activation of the boron center (Scheme 12).

Scheme 12
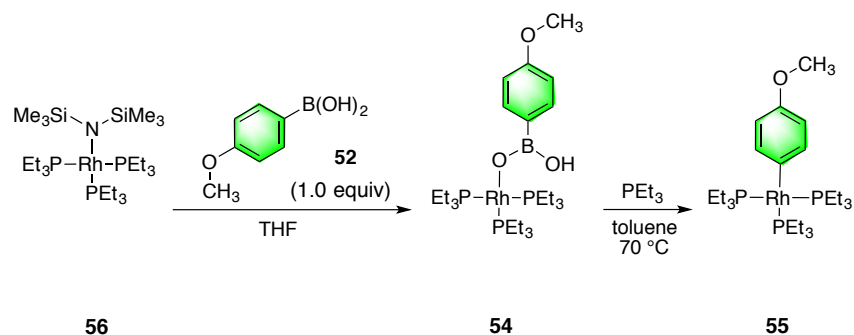
2.2. Objectives

As the transmetalation pathway in the Suzuki-Miyaura is the often the cross-coupling method of choice in both the academic and industrial settings it is crucial to know the structures of the active transmetalating agent. Moreover, the ability to identify such a complex would allow for reaction conditions to be optimized to ensure adequate formation of such intermediate complexes. Although the intermediacy of a species containing a Pd−O−B linkage has been proposed, its observation and characterization have eluded chemists for over 30 years. Indeed, a recent review by Lennox and Lloyd-Jones states that,[39]

"The barrier of this process was predicted computationally to be low (14–22 kcal mol⁻¹), suggesting specialist techniques will need to be applied to detect and confirm the identity of [37] experimentally."

The primary objective of this chapter is to identify and fully characterize pre-transmetalation intermediates in the Suzuki-Miyaura cross-coupling reaction by rapid injection and low temperature NMR spectroscopy. Various 2D NMR techniques were employed for structure determination and the validity of these structures were confirmed *via* independent synthesis.

2.3. Results and Discussion

2.3.1. Investigations of trans-(Ph₃P)₂(Aryl)Pd(OH) with Arylboronic Acids

2.3.1. Investigations of trans-(Ph$_3$P)$_2$(Aryl)Pd(OH) with Arylboronic Acids

Previous investigations that employed palladium complex $[(Ph_3P)(C_6H_5)Pd(OH)]_2$ as described above directed our studies to the use of fluorine labeled derivatives $[(Ph_3P)(4-FC_6H_4)Pd(OH)]_2$ (**57**) and 4-fluorophenylboronic acid (**58**) using ^{19}F and ^{31}P NMR spectroscopy.[54] To be a viable route, a convenient and reproducible preparation of **57** was needed therefore two different reaction sequences were explored. Following literature precedent oxidative addition product *trans*-(Ph$_3$P)$_2$(4-FC$_6$H$_4$)Pd(I) (**59**) (from (Ph$_3$P)$_4$Pd^0 and 4-fluoroiodobenzene **60**)[55] was reacted with 10.0 equiv of CsOH•H$_2$O in THF at room temperature for 12 h yielding 87 mg (30%).[56] However, the reproducibly of this reaction was found to be highly stir rate dependent which led to minimal success upon scale up due to incomplete conversions and side reactions. Additionally, the hydration state of CsOH•H$_2$O was found to be batch dependent which led to drastic changes in yield further complicating the reaction system. An alternative approach for the synthesis of **57** involved the combination of (Ph$_3$P)$_2$PdCl$_2$ (**61**) 4-fluoroiodobenzene, and KOH in an aqueous benzene mixture employing a catalytic amount of phase transfer catalyst 18-crown-6 at 80 °C for 3 h yielding 192 mg 42% (Scheme 13, 2).[57] This reaction was found to be successful up to a 1.0 g scale allowing for bulk quantitates of **57** to be prepared.

Scheme 13
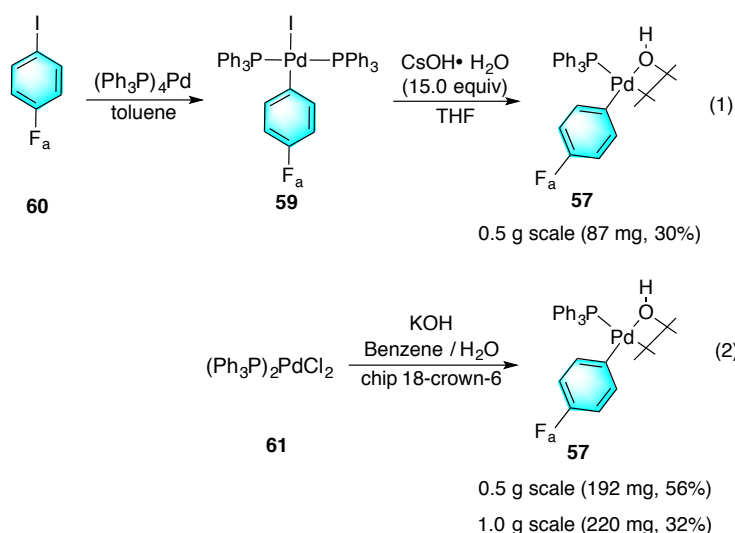
The addition of 4.0 equiv of Ph₃P to a THF solution of dinuclear complex **57** resulted in

only trace conversion to *trans*-(Ph$_3$P)$_2$(4-FC$_6$H$_4$)Pd(OH) **62** indicating a thermodynamic preference for the Pd-(μ-OH)-Pd moiety (Scheme 14, 1).[58] However, the addition of 4-fluorophenylboronic acid (**58**) (1.0 equiv/Pd in) to this solution at −50 °C followed by warming to −50 °C resulted in the observation of a new complex (**63**) by ^{31}P and ^{19}F NMR spectroscopy. Interestingly, the ^{31}P NMR spectrum displayed two singlets at −6.5 ppm (free Ph$_3$P) and 20.60 ppm in a ratio of 1:1, implying that the complex contained two molecules of Ph$_3$P based on the initial stoichiometry of starting materials (Figure 13). The ^{19}F NMR spectrum displayed a new set of signals at −116.74 and −125.40 ppm in a 1:1 ratio (Figure 14). The observation of two ^{19}F NMR resonances excluded the assignment of the new species as the product of transmetalation, *trans*-(Ph$_3$P)$_2$(4-FC$_6$H$_4$)$_2$Pd, (should appear as a single resonance) and was consistent with the assignment of an unsymmetrical species containing a Pd-O-B linkage such as **63**.

Scheme 14
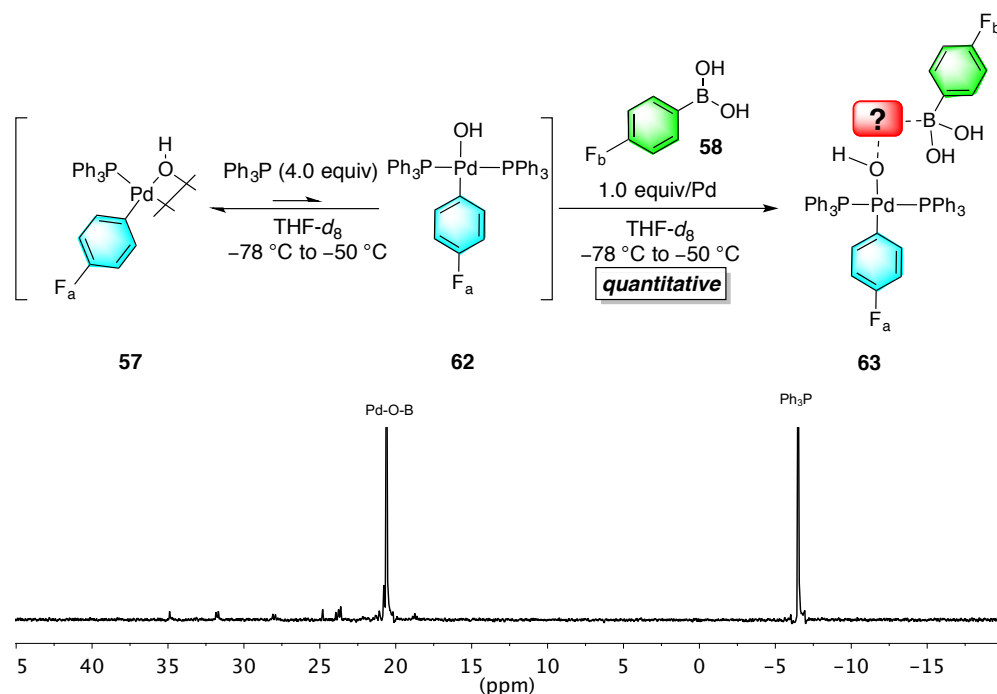
Figure 13. ^{31}P NMR spectrum of complex **63**.
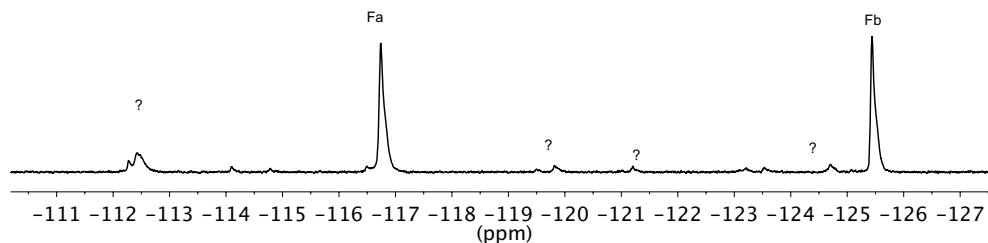
Figure 14. ^{19}F NMR spectrum of complex **63**.

The ability to observe an intermediate prior to transmetalation led us to investigate other palladium sources [(Ph$_3$P)(Y-C$_6$H$_4$)Pd(OH)]$_2$ (Y = F, **57**; CF$_3$ **64**) with excess Ph$_3$P and boronic acids such as 4-fluorophenylboronic acid **58**, 4-trifluoromethylboronic acid **65** or 3-fluoro-4methyoxyphenylboronic acid **66** (Table 1).

To probe the effects of electron poor and rich boronic acids, **65** and **66** were both separately reacted with a THF solution containing **57** and Ph$_3$P (1.5 equiv/Pd) in an NMR tube at −50 °C (Table 1). In both cases the starting materials reacted slowly at −50 °C, therefore the solutions were annealed at −40 °C over ~30 min, resulting in near quantitative conversions to both **67** an **68** by ^{31}P and ^{19}F NMR spectroscopy. Additionally, electron deficient palladium complex **64** also reacted with boronic acid **58** upon annealing at −40 °C by ^{31}P and ^{19}F NMR spectroscopy.

Table 1: ^{19}F, and ^{31}P NMR chemical shifts (ppm) for starting materials, products and complexes using Ph$_3$P as ligand.
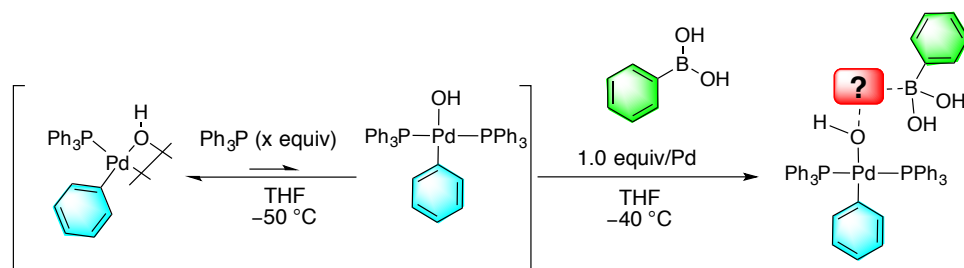
Entry	Pd-Aryl/sm	B-Aryl/sm	Complex
1[a]	**57**	**58**	**63**
2	**57**	**65**	**67**
3	**57**	**66**	**68**
4	**64**	**58**	**69**

Experiments were conducted by cooling in dewar to −78 °C and placing in the NMR spectrometer pre-cooled to −50 °C.

Unfortunately, the ^{31}P and ^{19}F NMR chemical shifts are not sufficient to unambiguously assign complexes **63**, **67, 68** and **69** as Pd-O-B linkages, thus complex **63** was selected to investigate the remaining structure information such as ^1H, ^{13}C, and ^{11}B NMR chemical shifts. However, the ^{11}B NMR spectrum was non-conclusive due to significant broadening and borosilicate glass in the NMR probe. Furthermore, the complexity of the aromatic region in the ^1H and ^{13}C NMR spectra prohibited assignments thus making it impossible to unambiguously identify the structures of these new species. Therefore, to clear the aromatic region of interfering signals the Ph$_3$P ligand was replaced with a trialkylphosphine, i-Pr$_3$P, which readily forms stable mononuclear bis-phosphine palladium hydroxide complexes such as $trans$-(i-Pr$_3$P)$_2$(4-FC$_6$H$_4$)Pd(OH) (**70**).[57] Thus, our efforts switched to the study of mononuclear bis phosphine palladium complexes to identify the key intermediate.

Table 2: ^{19}F, and ^{31}P NMR chemical shifts (ppm) for starting materials, products and complexes using Ph$_3$P as ligand.

Entry	complex	^{31}P	^{19}F$_a$	^{19}F$_b$
1	**58**	–	–	−111.21
2	**57**	34.83	−123.79	–
3	**63**	20.60	−125.40	−116.74
4	**65**	–	–	−61.84
5	**57**	34.83	−123.79	–
6	**67**	21.30	−125.48	−62.18
7	**58**	–	–	−111.21
8	**64**	34.64	−62.18	–
9	**69**	21.11	−61.10	−118.50
10	**66**	–	–	−139.39
11	**57**	34.83	−123.79	–
12	**68**	19.95	−126.47	−141.31

2.3.2. Investigations of trans-(i-Pr$_3$P)$_2$(4-FC$_6$H$_4$)Pd(OH) with 4-Fluorophenylboronic Acid and 4-Fluorophenylboroxine

Combination of *trans*-(*i*-Pr$_3$P)$_2$(4-FC$_6$H$_4$)Pd(OH) (**70**) and arylboronic acid **58** with 2.0 equiv of *i*-Pr$_3$P[59] in THF-*d$_8$* at −78 °C followed by warming to −60 °C did not result in the formation of a new intermediate. Upon annealing the solution at −30 °C for 3 h, quantitative conversion to a new discrete species was observed (Scheme 15, left). The use of extensive 1D and 2D NMR techniques at −30 °C lead to the structure elucidation of the newly formed species as complex **71** containing a Pd−O−B linkage. The bonding connectivity of the new species was established by the observation of strong, through-space interactions between aryl protons H$_b$ and H$_d$ with the methyl hydrogens on the *i*-Pr$_3$P group in the NOESY spectrum (Figure 15). This interaction reveals that both aryl residues were proximal to the phosphines and thus established the presence of a Pd-O-B linkage.

Scheme 15
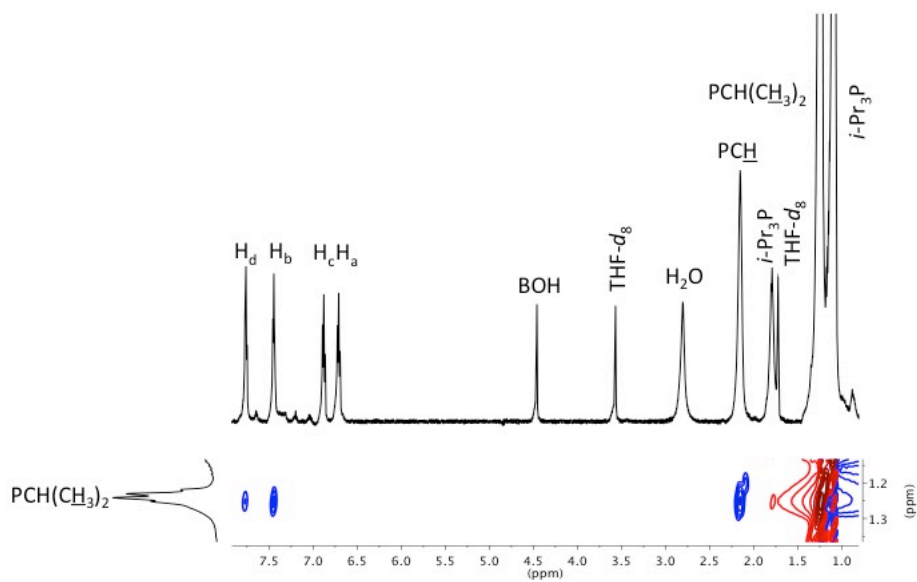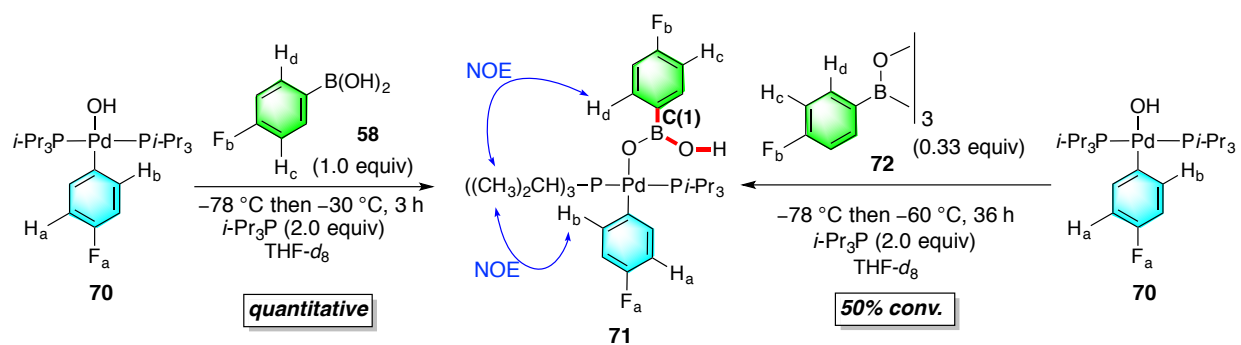
Figure 15. NOESY spectrum of complex **71**.

Table 3 ^{1}H, ^{19}F, ^{11}B and ^{31}P NMR chemical shifts (ppm) for starting materials, products and complexe

Entry	complex	^{11}B	^{31}P	^{19}F$_a$	^{19}F$_b$	^{1}H$_a$	^{1}H$_b$	^{1}H$_c$	^{1}H$_d$	^{1}HO
1	**70**	–	33.00	−124.68	–	6.64	7.35	–	–	3.60
2	**58**	29	–	–	−111.21	–	–	7.04	7.86	7.06
3[a]	**71**	29	29.98	−123.77	−115.75	6.71	7.45	6.88	7.76	4.47
4	**76**	–	30.36	−122.52	–	6.73	7.28	–	–	–
5	**79**	4	–	–	−118.41	–	–	6.79	7.43	3.74
6[b]	**71**	N.D.	29.02	−123.72	−115.73	N.D	N.D	N.D	N.D	N.D.
7[c]	**71**	28	29.98	−123.76	−115.74	6.72	7.46	6.88	7.78	4.48
8	**80**	–	45.55	−122.61	–	6.67	7.36	–	–	−1.74
9[d]	**88**	Broad	45.62	−123.67	−113.40	6.74	7.41	7.04	7.86	10.22
10	**90**	–	43.99	−123.25	–	6.66	7.35	–	–	–
11[e]	**88**	N.D.	46.12	−123.59	−113.36	6.72	7.39	7.06	7.87	10.21
12	**103**	–	75.68	−125.18	–	6.58	7.30	–	–	−2.23
13	**104**	N.D.	N.D.	N.D.	N.D.	6.76	7.46, 7.28	6.76	7.13	9.51
14	**106**	28	–		−111.38			7.08	7.67	–
15	**107**	9	51.00	−121.01	−118.33	6.85	7.45	6.95	7.68	4.02
16[g]	**107**	–	–	–	–	6.84	7.46	6.92	7.70	4.01
17	**58**	–	34.83	−123.79	–	6.33	6.92	–	–	−1.78
18	**106**	10	34.86	−121.09	−118.16	6.60	7.05	6.99	7.76	4.14
19	**109**	–	28.42(P1) 8.96(P2)	−123.63	–	6.93	6.34	–	–	0.45
20	**111**	N.D.	33.06(P1) 11.47(P2)	−122.35	−116.47	7.08	6.97	6.45	6.97	N.D.
21	**73**	–		−116.45	–	7.65	7.21	–	–	–

[a] 6-B-3 complex **71** was prepared from **70** and **58**. [b] 6-B-3 complex **71** was prepared from **76** and **71**. [c] 6-B-3 complex **71** was prepared from **70** and **76**. [d] Complex **88** was prepared from **80** and **90**. [e] Complex **88** was prepared from **90** and **79**. [f] Complex **107** was prepared from **80** and **58** in THF/CH$_3$OH. [g] Complex **107** was prepared from **80** and **106** in THF/CH$_3$OH.

The identity of the carbon bound to the boron atom C(1) was revealed in the HMBC (^{1}H-^{13}C) spectrum by the observation of cross peaks between the BOH hydrogen with a single ^{13}C signal at 138.68 ppm (red bonds) (Figure 16).
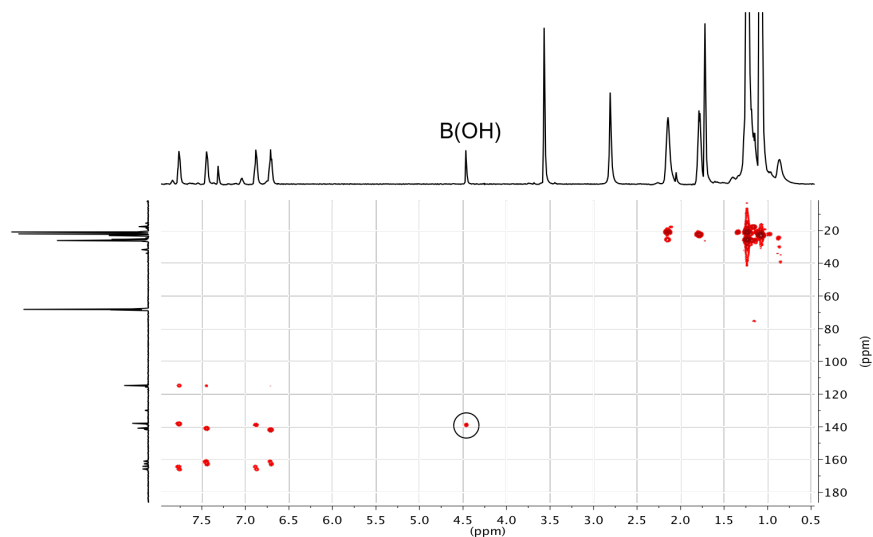
Figure 16. gHMBC spectrum of **71** at −30 °C, referenced to THF-d_8 (1.72 and 68.21 ppm).

The coordination geometry at the palladium atom was established by the appearance of the ^{13}C NMR signal of the isopropyl methine carbon (PCH) at 25.38 ppm as an apparent triplet (J_{P-C} = 10 Hz) owing to virtual coupling[60] along with a solitary ^{31}P NMR signal at 29.98 ppm. These data indicate a *trans* arrangement of phosphine ligands bound to palladium (Figure 17).
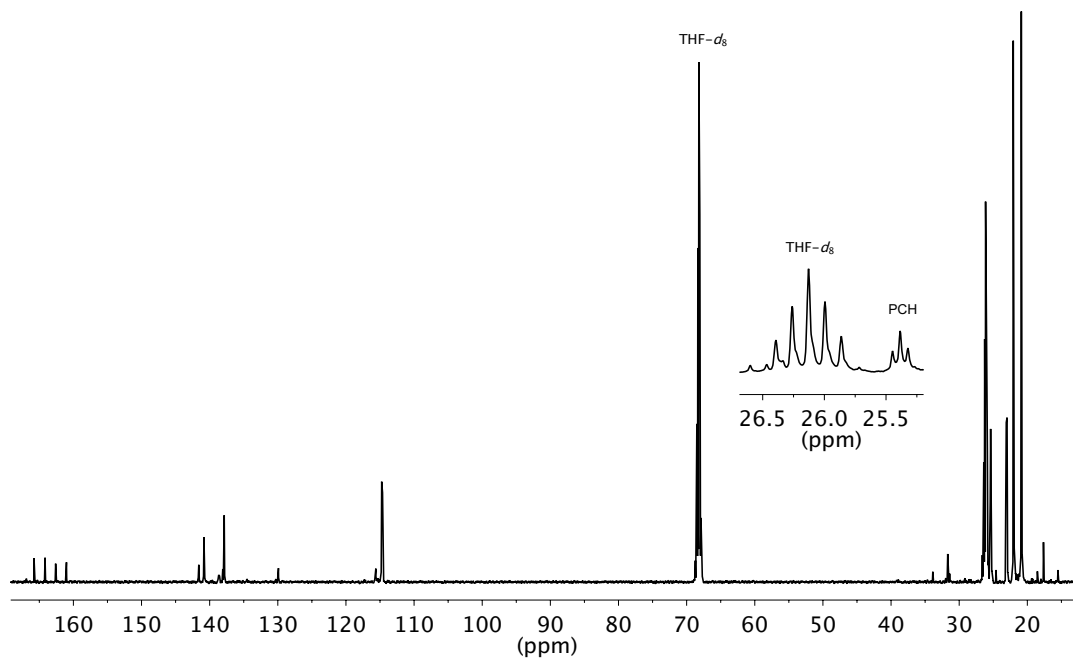
Figure 17. Left is ^{13}C NMR spectrum for complex **71** displaying signal at 25.38 ppm.

The coordination geometry at boron was established by the observation of a ^{11}B NMR signal at 29 ppm indicating a tricoordinate geometry (6-B-3)' that was also seen in the Pt **50** and Rh **54** complexes mentioned above (Scheme 11) [Ph$_4$BNa was used as a reference standard at −6.15 ppm]. The surprising observation that species **71** contained a trigonal boron atom required that the complexation resulted in the loss of a molecule of water from the kinetically generated 8-B-4 complex that was expected (see Figure 10).
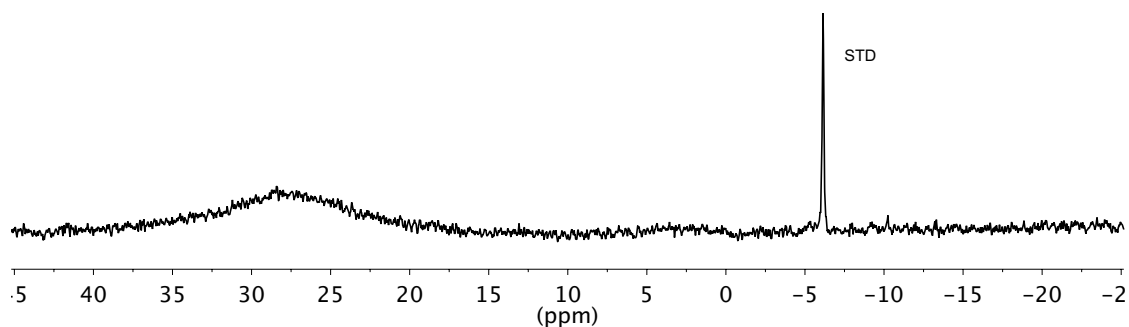
Figure 18. ^{11}B NMR spectrum for complex **71**.

Support for the structural assignment of complex **71** was provided by an independent preparation from 4-fluorophenylboroxine (**72**) (0.33 equiv) and complex **70** with 2.0 equiv of *i*-Pr$_3$P in THF-*d$_8$* at −78 °C followed by warming to −60 °C. Under these conditions, a ca. 50% conversion to complex **71** was observed with the remainder forming 4,4'-difluorobiphenyl cross-coupling product **73** (Scheme 15, right). The similarity of the spectroscopic data from these two independent syntheses, including the NOE cross peaks and ^{11}B NMR chemical shifts, provides compelling support for the structural assignment of **71** as a 6-B-3 palladium(II) complex containing a Pd–O–B linkage.

2.3.3. Investigations of trans-(i-Pr$_3$P)$_2$(2-napth)Pd(OH) with 4-Fluorophenylboronic Acid

The ability to prepare 6-B-3 complex **71** with a 4-fluorophenyl ligand bound to the palladium atom led us to explore the generality of this approach by preparing 2-nathylpalladiumhydroxide dimer **74** followed by reacting it with 4-fluorophenylboronic acid **58** in the presence of 0.5 equiv of *i*-Pr$_3$P in THF-*d$_8$* at −30 °C where a quantitative formation to 6-B-3 complex **75** was observed by ^{31}P and ^{1}H NMR spectroscopy The ^{31}P NMR chemical shift at 28.51

ppm is in good agreement with 6-B-3 complex **74**. The ^{1}H NMR chemical shifts were assigned with the aid of ^{1}H-^{1}H COSY experiment (Figure 19). This complex was ultimately prepared to create a larger π-surface that could aid in crystallization experiments. However, all attempts at crystallizing this 6-B-3 complex failed.

Scheme 16
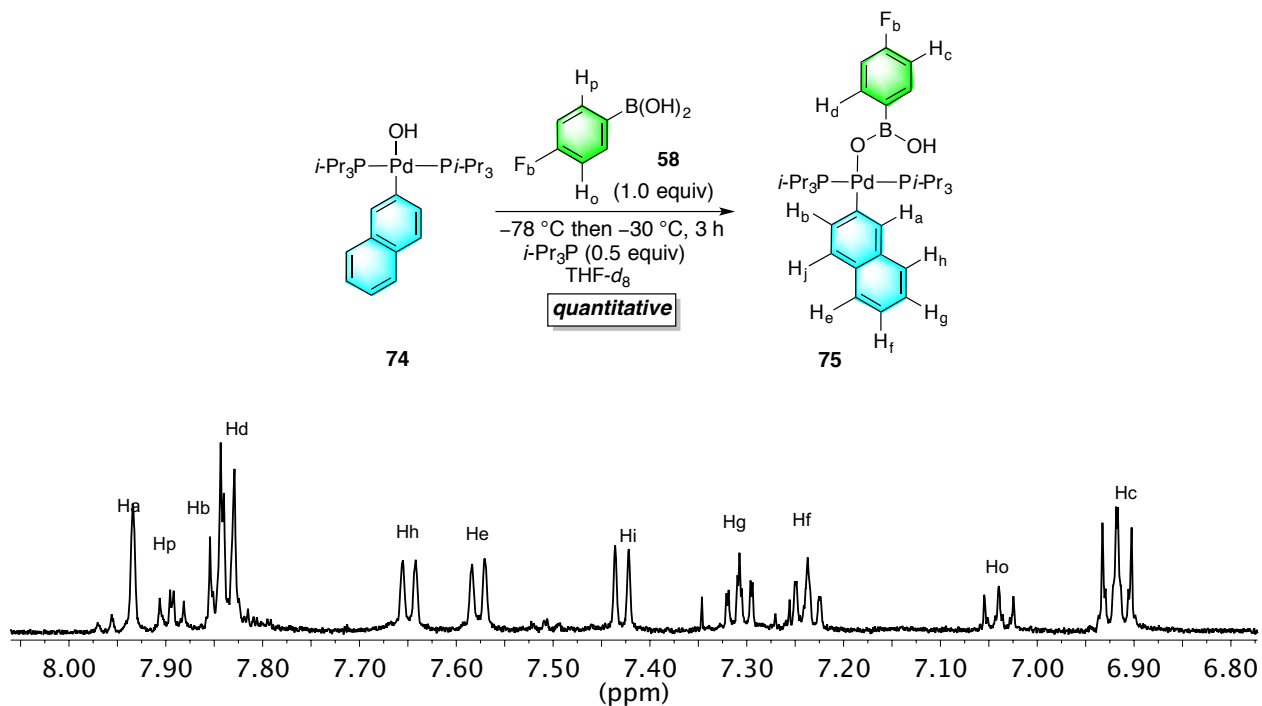
Figure 19. ^{1}H NMR spectrum for 6-B-3 complex **75**.

2.3.4. Investigations of trans-(i-Pr$_3$P)$_2$(4-FC$_6$H$_4$)Pd(X) with 4-Fluorophenylboronate Salts

An alternative preparation of the intermediate involves the direct displacement of halide from the bis-phosphine ligated oxidative addition product, *trans*-(i-Pr$_3$P)$_2$(4-FC$_6$H$_4$)Pd(I) (**76**). To be a viable route, a convenient and reproducible preparation of **76** was needed. Therefore, complex **76** was prepared by the combination of CpPdallyl **77** with 4-fluoroiodobenzene which formed complex **76** in a 78% yield. (Scheme 17). Complex **76** has remained shelf stable (freezer) for over 2 years outside the glovebox.

Scheme 17

(0.1 mmol scale, 51 mg, 78%)
(1.0 mmol scale, 416 mg, 64%)

Treatment of a THF solution of complex **76** with 3.0 equiv of potassium 4-fluorophenylboronate **78** at −30 °C in THF with 2.0 equiv of i-Pr$_3$P resulted in no reaction (Scheme 18, left). Even upon warming to 30 °C, no cross-coupling product **73** was observed. The lack of reaction is most likely due to the steric hindrance at the palladium center provided by the bulky phosphine ligands, as well as the low solubility of **78** in THF.

To activate the palladium center toward nucleophilic attack, complex **76** was combined with 3.0 equiv of thallium 4-fluorphenylboronate (**79**) containing 1.0 equiv of i-Pr$_3$P and dibenzo-22-crown-6[61] to facilitate halide abstraction (Scheme 18, right). Although only a 10% conversion to **71** was observed by ^{19}F and ^{31}P NMR spectroscopy, the experiment demonstrated that intermediate **71** could be formed directly from complex **76**.

Scheme 18

Based on the 10% conversion to 6-B-3 complex **71** using thallium boronate **79,** we envisioned generating a cationic palladium complex from **80**. Tri-isopropylphosphonium tetrafluoroborate was prepared and reacted with [(i-Pr$_3$P)(4-FC$_6$H$_4$)Pd(OH)]$_2$ (**80**) at room temperature where a quantitative conversion to a single cationic *trans*-(i-Pr$_3$P)$_2$Pd(4-FC$_6$H$_4$)(OH$_2$)$^+$BF$_4$$^-$ (**81**) complex was observed which was characterized by NMR spectroscopy (Scheme 19). The cationic complex **81** was identified as *trans* because a single ^{31}P NMR signal was observed. In addition to the aryl group and two i-Pr$_3$P ligands, a molecule of H$_2$O was

coordinated to the complex as observed by ^{1}H NMR spectroscopy. Attempts to isolate this complex resulted in decomposition.[62]

Scheme 19

80   81
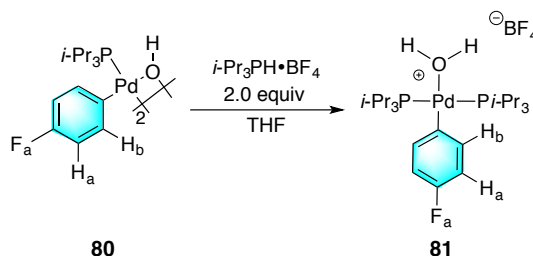
This attempt at the synthesis of the 6-B-3 intermediate **71** involved combining cationic aqua complex *trans*-(*i*-Pr$_3$P)$_2$Pd(4-FC$_6$H$_4$)(OH$_2$)$^+$BF$_4^-$ (**81**) with sodium 4-fluorophenylboronate **82** (Scheme 20). In this experiment, complex **81** and 1.0 equiv of *i*-Pr$_3$P were added to a suspension of sodium 4-fluorophenylboronate **82** in THF-d_8 at −78 °C in a dry ice acetone bath followed by placement into the NMR spectrometer set to −30 °C. A ~50% conversion to 6-B-3 complex **71** was observed at −30 °C (Scheme 20). In an attempt to observe chemical exchange between **74** and unbound 4-flurophenylboronic acid **58**, a 2D-EXSY experiment was performed. Although no exchange was detected between **74** and **58**, exchange *was* observed between free arylboronic acid **58** and sodium boronate **82** on the NMR time scale. However, for this route to be considered an independent synthesis of 6-B-3 complex **74** the possibility of **82** deprotonating complex **81** needed to be unambiguously ruled out.

Scheme 20

81   71
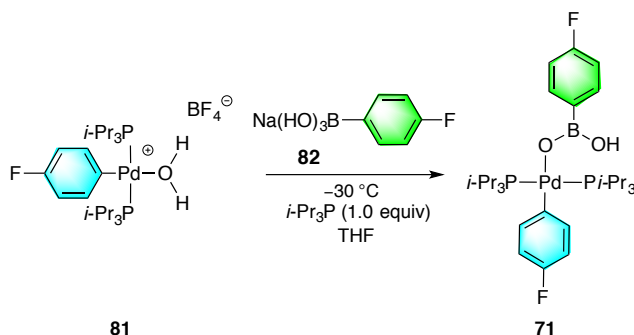
To probe this hypothesis, an experiment was designed to react the aqua complex **81** with sodium 4-fluorophenylboronate **82** at a temperature in which the palladium hydroxide **70** and arylboronic acid **58** did not react to form the 6-B-3 complex **71.** It is conceivable that if palladium

hydroxide complex **70** and arylboronic acid **58** was being formed during the experiment they would be detected at low temperature by ^{19}F NMR spectroscopy. Upon the combination of a THF solution of the aqua complex **81** and sodium 4-fluorophenylboronate **82** (3.0 equiv/Pd) at −55 °C the palladium hydroxide **70** and arylboronic acid **58** were observed by ^{19}F NMR spectroscopy indicating that this reaction is proceeding through a deprotonation event and not through a direct displacement of water with the sodium arylboronate **82** (Scheme 21).

Scheme 21
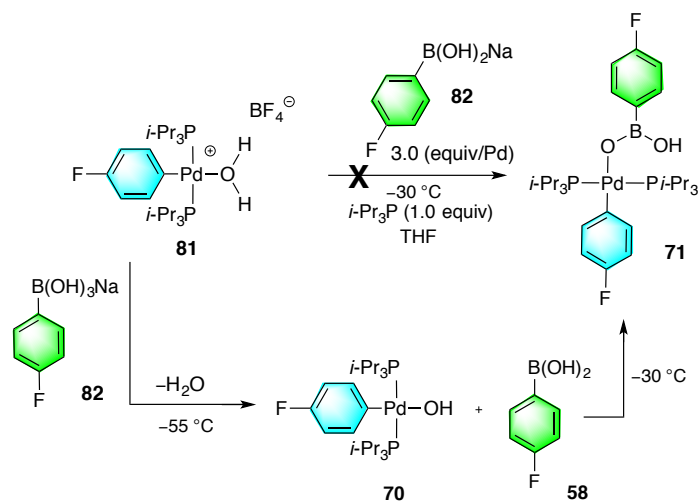
*2.3.5. Attempts to generate an 8-B-4 Complex from **71***

The formation of 6-B-3 complex **71** must arise from a kinetically generated 8-B-4 complex **83** followed by rapid elimination of a single molecule of water. Because these experiments were performed in anhydrous THF, it is conceivable that the 8-B-4 complex **83** is thermodynamically unstable. Thus, a number of attempts to add water back were undertaken, beginning with generating **71** in THF/H$_2$O (99:1) mixtures. However, no change in the ^{31}P, ^{19}F or ^{11}B NMR spectra were observed at −30 °C (Scheme 22).

Scheme 22
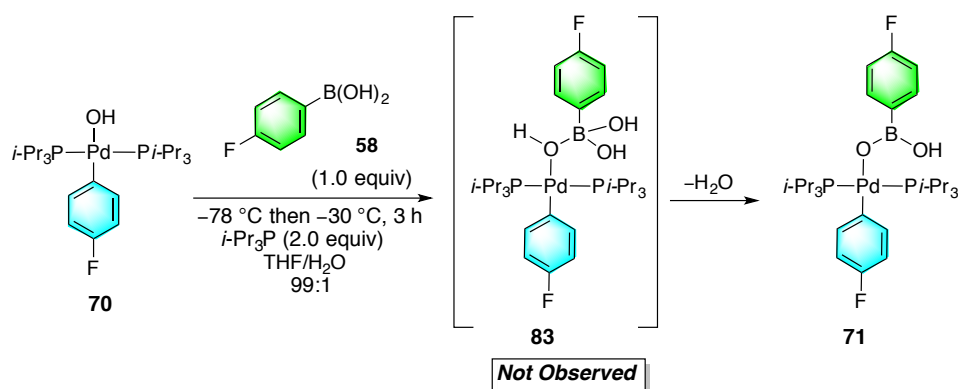
Secondly, the use of inorganic hydroxide bases were explored by combining 6-B-3 complex **71** in THF at with a solution of CsOH•H_2O in THF/CH_3OH (10:1) in attempts to saturate the boron valences. [Attempts to solubilize MOH bases in aqueous THF mixtures resulted in insoluble hydroxides or bi-phasic mixtures.]

Complex **71** (from **70** and **58,** *vide supra*) in THF at −78 °C was combined with a solution of CsOH•H_2O (5.0 equiv) in methanol. The sample was monitored at −30 °C, but no changes in the ^{19}F, ^{31}P or ^{11}B NMR spectra were observed. However, after warming the sample in 10 °C intervals up to 20 °C, cesium 4-fluorophenylboronate **84** and complex **70** were observed by ^{19}F and ^{31}P NMR spectroscopy indicting that the arylboronic acid had been displaced from the palladium center (Scheme 23, Figure 20). The identity of the cesium 4-fluorophenylboronate **59** was confirmed by mixing an isolated sample in THF/CH_3OH where an identical ^{19}F NMR signal was observed. This experiment supported the notion that arylboronate complexes such as **83** are indeed unstable. The reason for their instability was revealed by thermochemical calculations as detailed below.

Scheme 23
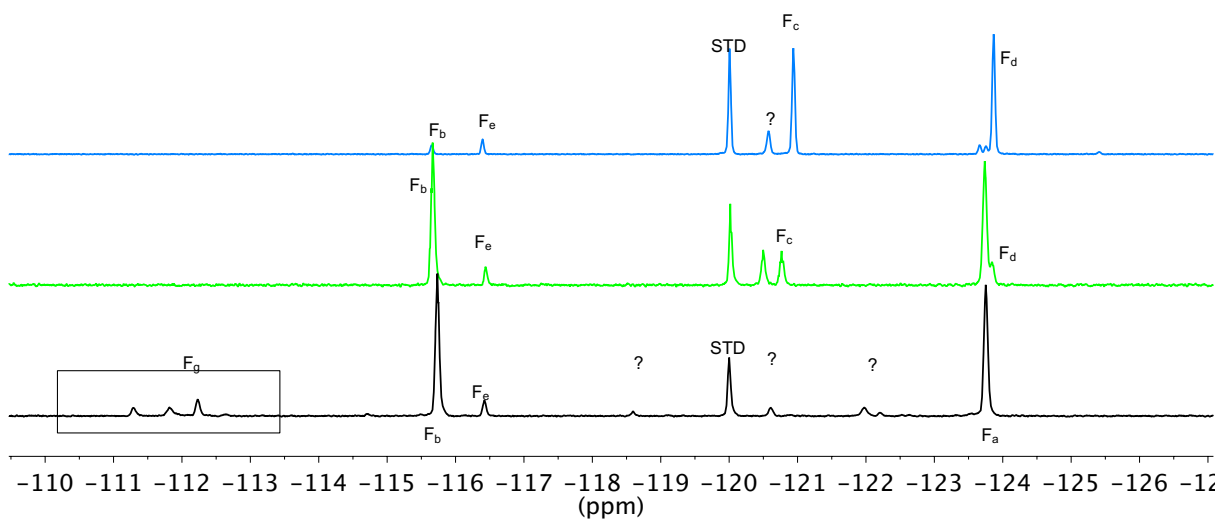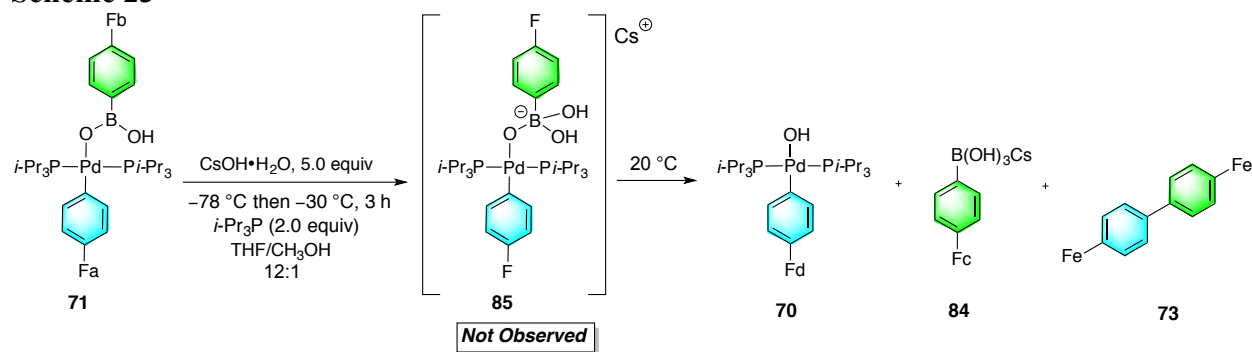
Figure 20. Black ^{1}H NMR spectrum for 6-B-3 complex **71** in THF at −30 °C. Green ^{1}H NMR spectrum for 6-B-3 complex **71** in THF/CH$_3$OH at −30 °C. Blue ^{1}H NMR spectrum for 6-B-3 complex **71** in THF/CH$_3$OH at 20 °C.

2.3.6. Thermochemical calculations on 6-B-3 and 8-B-4 Complexes[*]

To gain further insight into the lack of stability of 8-B-4 complex **83**, ground state equilibrium energies were calculated using M06-2X /6-31G(d) on B3LYP/6-31(d) optimized structures with a THF continuum solvent field. The loss of water from an initially formed 8-B-4 complex **83** yielding 6-B-3 complex **74** was found to be highly exergonic ($\Delta G^{\circ} = -10.8$ kcal/mol). Surprisingly, the entropic advantage ($\Delta S^{\circ} = 0.048$ kcal/mol K) is not offset by the expected enthalpic disadvantage of creating a coordinatively unsaturated boron ($\Delta H^{\circ} = 1.0$ kcal/mol) (Figure

21).

Inspection of space filling models of **83** reveals that the OH groups on boron penetrate the van der Waals radii of the isopropyl methyl groups on phosphorus thus destabilizing the four-coordinate geometry. Therefore, the instability of **83** is not related to the medium, but rather to the bulk of the two i-Pr$_3$P groups attached to palladium (F- and B-strain).[63] The solution to this problem then became obvious; remove a phosphine ligand from the complex. Indeed, calculation of the ground state energies for monoligated T-shaped complexes **86** and **87** reversed the equilibrium position now substantially favoring the 8-B-4 complex ($\Delta G^{\circ} = -6.9$ kcal/mol) despite an unfavorable entropy ($\Delta S^{\circ} = -0.045$ kcal/mol K). This preference is driven by the overwhelming enthalpic benefit of saturating the valences on boron ($\Delta H^{\circ} = -17.9$ kcal/mol). Accordingly, the focus of the investigation switched to the study of monoligated arylpalladium(II) complexes to enable the generation of the long-sought, 8-B-4 activated adduct.
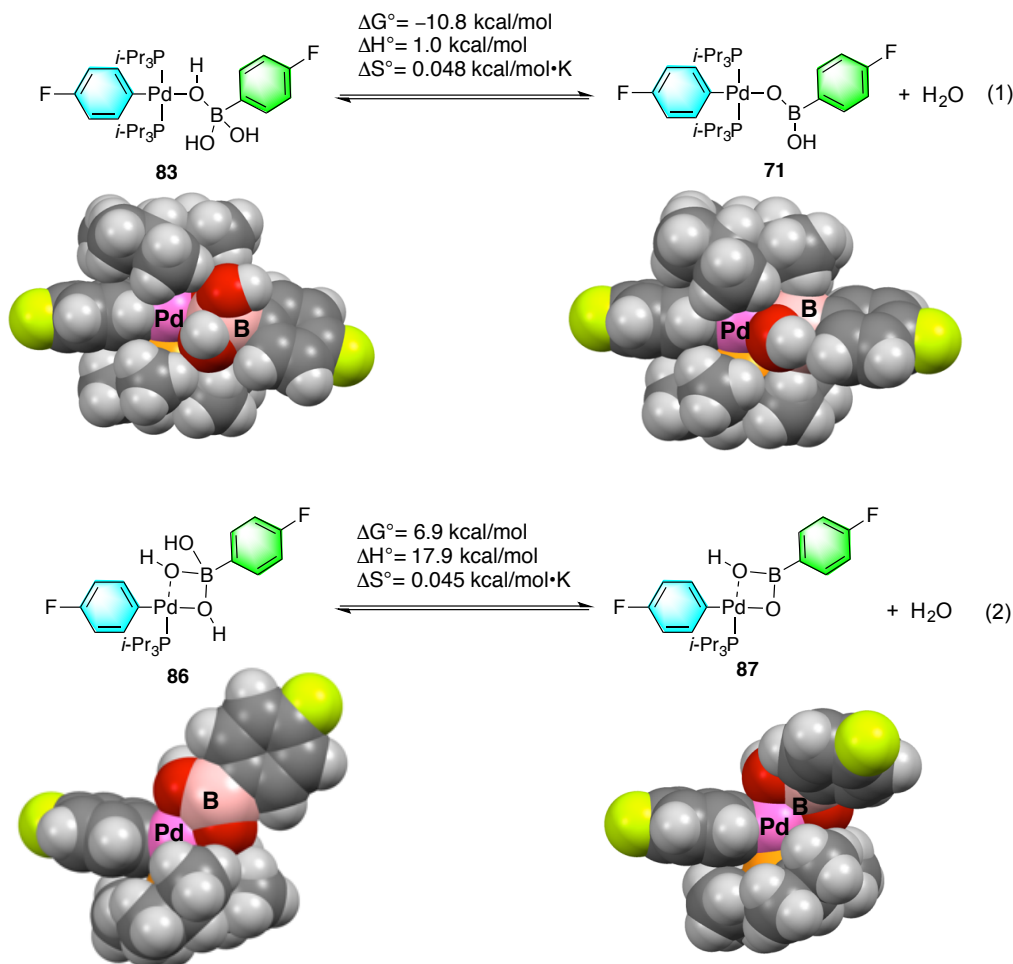
Figure 21. Calculated equilibria for loss of water from 8-B-4 species **83** and **86**.

34

2.3.7. Reaction of [(i-Pr₃P)(4-FC₆H₄)Pd(OH)]₂ with 4-Fluorophenylboronic Acid

Addition of a THF solution of **58** (1.0 equiv/Pd) to dimeric complex [(*i*-Pr₃P)(4-FC₆H₄)Pd(OH)]₂ (**80**) in THF-d_8 at −78 °C followed by warming to −50 °C resulted in no change in the ¹H NMR spectrum (Scheme 34). However, the ¹⁹F NMR spectrum displayed a sharp signal for F_a at −123.35 ppm but an extremely broadened signal for F_b at approximately −111.98 ppm signifying a dynamic process. Moreover, the staring dimeric complex **80** exists as a *cis-trans* mixture that upon the addition of the boronic acid **58** had converted to a single isomer further signifying a dynamic process. Upon cooling this solution to −100 °C new signals appeared in the aromatic region of the ¹H NMR spectrum along with complete loss of the signals of **80** but surprisingly 50% of **58** remained (Scheme 24).

Scheme 24
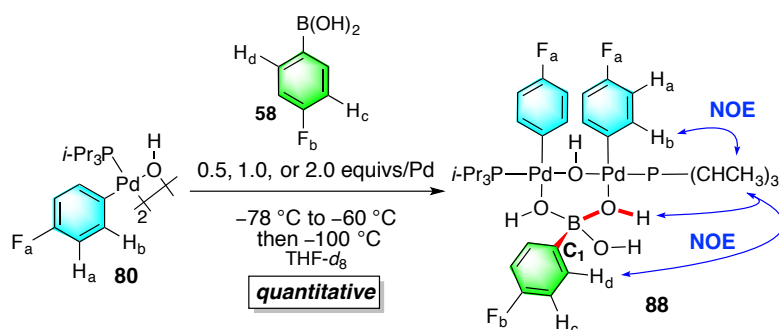
The incomplete consumption of the boronic acid could be interpreted as an unfavorable equilibrium or a different stoichiometry of complexation. The former interpretation was eliminated by the addition of 2.0 equiv/Pd of **58** to complex **80** whereupon no further incorporation of the arylboronic acid was observed (Scheme 25, Figure 22).

Scheme 25
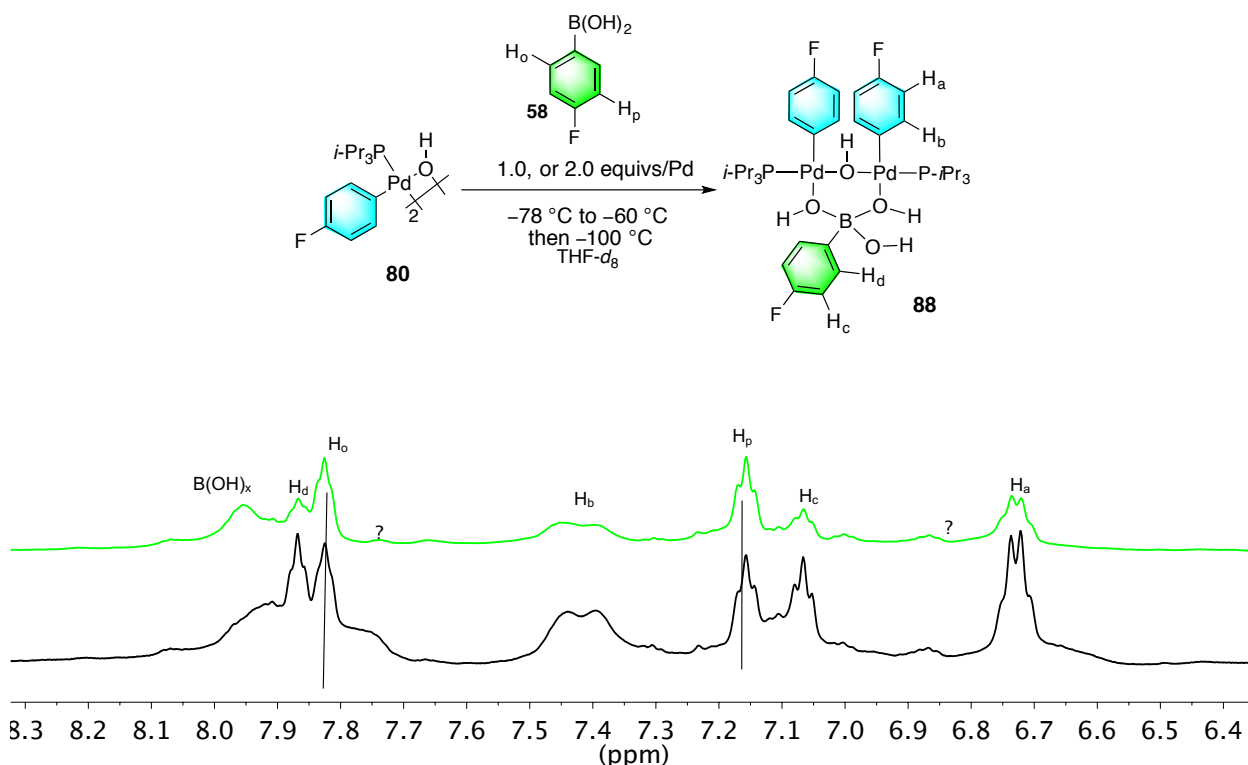
Figure 22. Black ^{1}H NMR spectrum is 1.0 equiv/Pd of **58** to complex **80** at −100 °C. Green ^{1}H NMR spectrum is 2.0 equiv/Pd of **58** to complex **80** at −100 °C.

The connectivity in complex **88** was established by the observation of 1D-NOE, positive cross peaks between H_b, H_d and the bridging OH group with the methyl hydrogens on the i-Pr$_3$P group. The observation of *positive* NOE cross peaks indicates slow molecular movements (tumbling) consistent with the larger molecular size of the 2:1 complex. Interestingly, the resonances for H_b and for the methyl hydrogens on the i-Pr$_3$P group were exceptionally broadened at −100 °C indicating an observable barrier to rotation about both the P-Pd and aryl-Pd bonds. On the basis of the available data, the structure of this complex was assigned as the bridged *bis*-arylpalladium arylboronate complex **88**, which represents direct insertion of **58** into the dimeric complex **80** without further dissociation.[64]

The unexpected 2:1 stoichiometry of complex **88** was confirmed by combining a THF-d_8 solution of **58** (0.5 equiv/Pd) with a THF-d_8 solution of **80** at −60 °C, followed by cooling to −100 °C whereupon a quantitative conversion to **88** was observed (Figure 23).

36
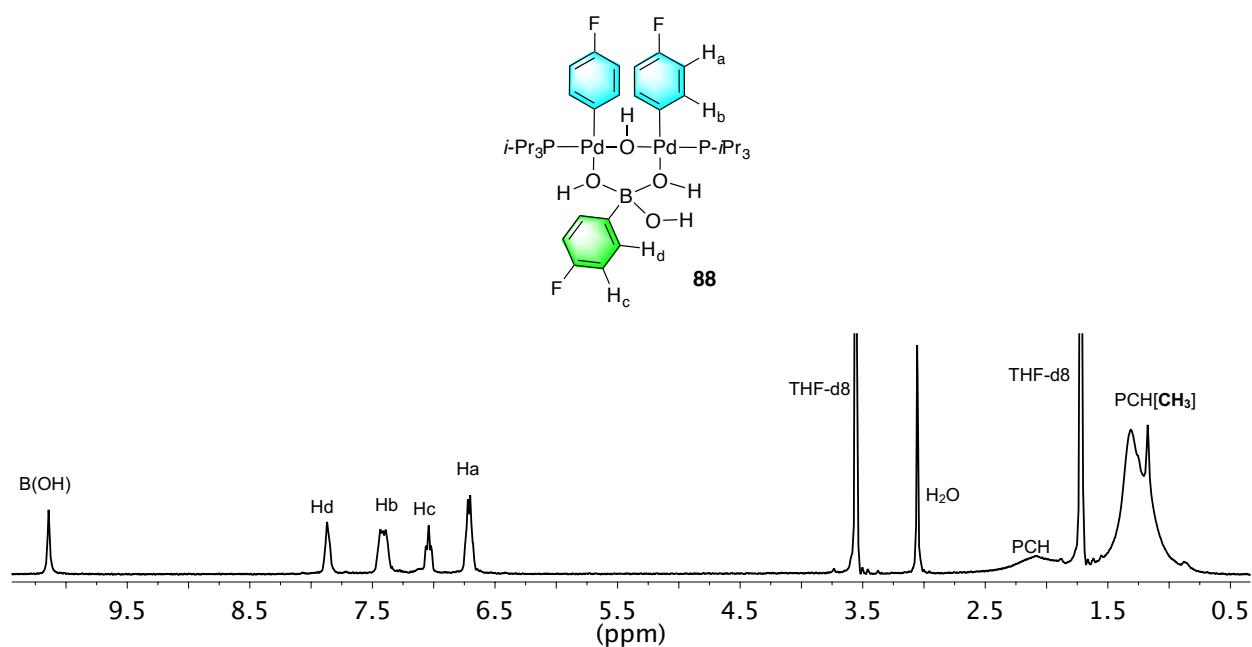
Figure 23. ^{1}H NMR spectrum of 0.5 equiv/Pd of complex **88** at −100 °C.

The ^{11}B NMR spectrum of complex **88** did not reveal a discrete signal, owing to the rapid exchange between the arylboronic acid **58** with the palladium hydroxide complex **80** as confirmed by EXSY experiments.

2.3.8. Reaction of [(i-Pr$_3$P)(4-FC$_6$H$_4$)Pd(I)]$_2$ with Thallium 4-Fluorophenylboronate

To support our structural assignment an independent synthesis of complex **88** was desired. The success with the previous thallium boronate reaction led our next set of investigations to react [(*i*-Pr$_3$P)(4-FC$_6$H$_4$)Pd(I)]$_2$ (**90**) with thallium boronate **79**. In order to probe this process an efficient synthesis of [(*i*-Pr$_3$P)(4-FC$_6$H$_4$)Pd(I)]$_2$ **90** was needed. An initial route to this complex involved the combination of Pd(dba)$_2$ to 25.0 equiv of 4-fluoroiodobenzene in THF with 1.1 equiv of *i*-Pr$_3$P. Unfortunately, palladium black was observed which is most likely the result of disproportionation of subvalent LPd^0 complexes.[65] An alternative synthesis involved performing a stoichiometric cross-coupling reaction between [(*i*-Pr$_3$P)(4-FC$_6$H$_4$)Pd(OH)]$_2$ **80** and 4-fluorophenylboronic acid **58** in the presence of 4-fluoroiodobenzene in aqueous benzene. Additionally, 10.0 equiv of NaI was added to the reaction mixture to both stabilize (disproportionation) and enhance the reactivity of *i*-Pr$_3$P-Pd^0 by forming anionic [*i*-Pr$_3$P-Pd^0-I]Na which should rapidly undergo oxidative

addition to the aryl halide.[66] Interestingly, this method resulted in a 45 % yield of complex **90** after crystallization (Scheme 26).

Scheme 26

(1)

(2)
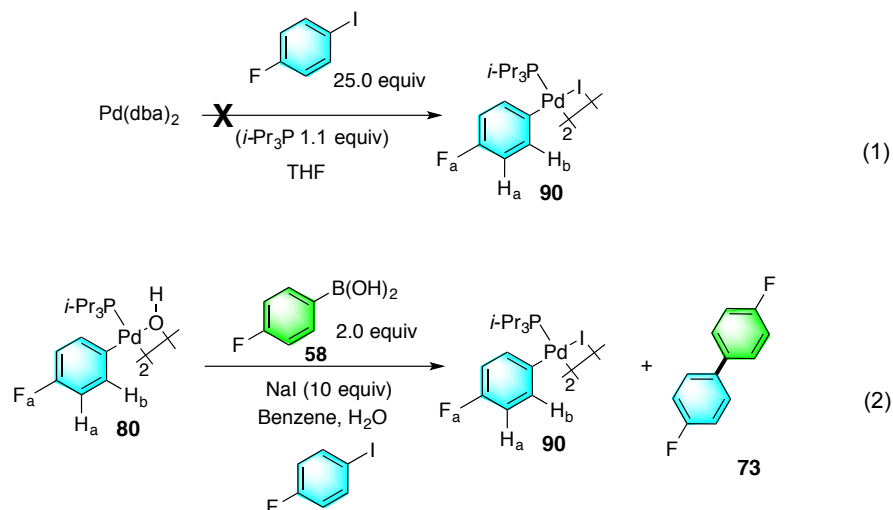
With complex **90** in hand an independent synthesis was performed by combining 1.5 equiv/Pd of thallium arylboronate **79** with $[(i\text{-Pr}_3\text{P})(4\text{-FC}_6\text{H}_4)\text{Pd(I)}]_2$ (**90**) in THF-d_8 at −78 °C followed by warming to −50 °C. By cooling the mixture to −100 °C the identity of complex **88** was confirmed in a 1:1 ratio with cross-coupling product **73** by ^{1}H, ^{19}F and ^{31}P NMR spectroscopy, indicating the ability to form the Pd-O-B linkage in **79** with complex **90** directly (Scheme 27).

Scheme 27
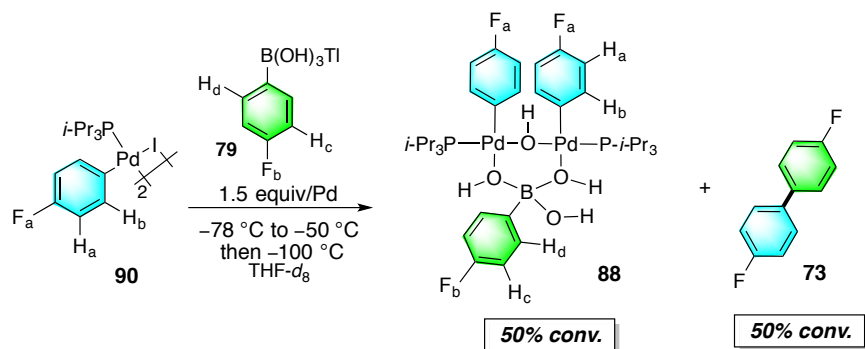
2.3.9. Variable temperature NMR analysis of complex 88

The activation energy of exchange between complex **88** and arylboronic acid **58** was measured by variable temperature NMR spectroscopy. The ^{19}F NMR spectra of a 1:1 ratio of complex **88** and unbound **58** were recorded at temperatures ranging from −100 °C to −10 °C in THF (Figure 24). The rapid exchange of **88** and unbound **58** is evidenced by the overlapping and broadening of their ^{19}F NMR signals at higher temperatures (> −50 °C) and the slow exchange is evidenced at lower temperatures by the decoalescence of the ^{19}F signals into well resolved peaks. An approximate coalescence temperature (T_c) was measured at –40 °C by the signals merging with the baseline. The rate constant k_c at coalescence was measured using $k_c = \pi \Delta v / \sqrt{2}$, where Δv is the maximum chemical shift difference (1068 Hz) between **88** and **58** at −100 °C. Using the Eyring equation $\Delta G_e^{\neq} = -RT_c \ln(k_c \hbar / k_B T_c)$, the activation of exchange was measured to be approximately $\Delta G_e^{\neq} = 11$ kcal/mol. This low barrier of exchange between **88** and **58** suggests that the broad ^{11}B NMR signal is caused by rapid changes in the coordination state of boron.
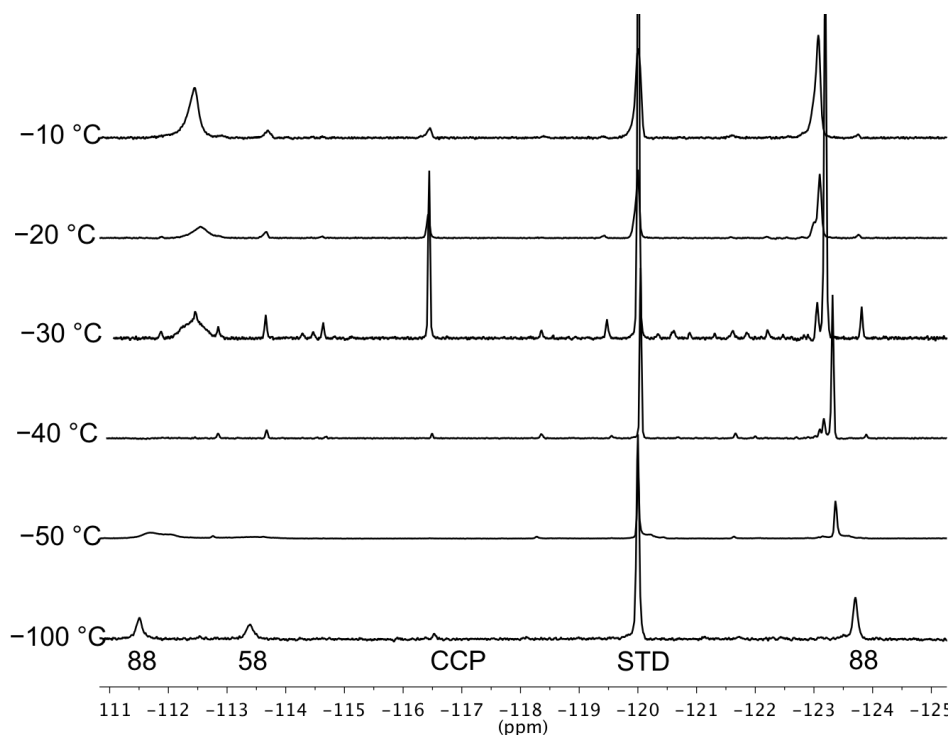
Figure 24. Stacked plot of ^{19}F NMR spectra recorded for a THF solution of 1.0 equiv of **88** and 1.0 equiv of **58** over a range of temperatures (−100 °C to −10 °C).

39

2.3.10. Reaction of [(i-Pr₃P)(Aryl)Pd(OH)]₂ with arylboronic acids

The inability to incorporate two boronic acids into the dimeric complex **80** is conceivably due to the strength of the Pd-(μ-OH)-Pd moiety as observed by Grushin.[57] In attempts to favor a 1:1 Pd/B stoichiometry additions of various [(*i*-Pr₃P)(Y-C₆H₄)Pd(OH)]₂ (Y = F, **80**; CF₃, **64**; Me, **93**) with either 4-fluorophenylboronic acid **58**, 4-trifluoromethylboronic acid **65** or 3-fluoro-4methyoxyphenylboronic acid **66** were performed. Addition of boronic acid **58** to electron deficient complex **64** at −78°C followed by placement into the NMR set to −60°C resulted in a complex aromatic region in the ^{1}H NMR spectrum. Upon cooling to −100 °C the ^{1}H NMR spectra were indiscernible to interpret due to signal overlapping. However, the ^{19}F NMR spectrum revealed two signals at −61.69 ppm and −113.18 ppm in a ratio of 6:1 indicating that the pseudodimer **94** was observed as in complex **88** (Table 4, entry 2)**.** Furthermore complex **93** was unable to form 1:1 Pd/boron stoichiometries, however it did form a 2:1 (Pd/B) as observed by diagnostic signals in the ^{1}H NMR spectrum (entry 3). Similarly, electron deficient complex **64** was also incapable of forming a 1:1 adduct even when electron deficient boronic acid **65** was employed (Table 4, entry 4). Ultimately, it also formed a 2:1 complex as in **88**. It was conceivable that an electron rich boronic acid **66** was needed to form a 1:1 Pd/B adduct however it formed a 2:1 complex as in complex **88** when subjected to the standard reaction conditions (entry 5).

Table 4: Screen of substrates in attempts to form 1:1 Pd/B complexes
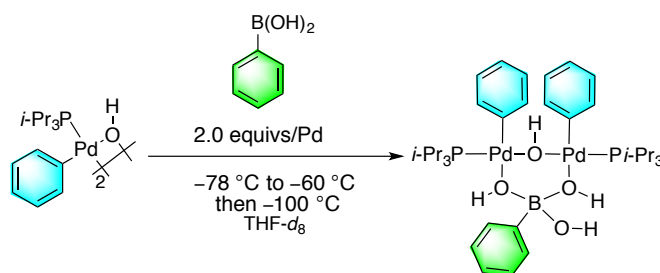
Entry	Pd-Aryl/sm	B-Aryl/sm	1,2-Complex
1	**80**	**58**	88
2	**64**	**58**	94
3	**93**	**58**	96
4	**64**	**65**	97
5	**80**	**66**	98
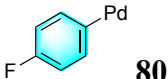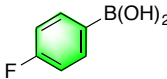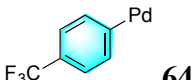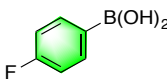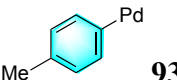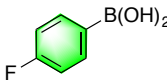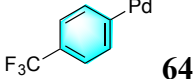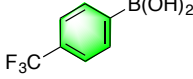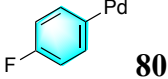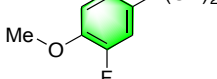
Experiments were conducted by cooling in dewar to −78 °C and placing in the NMR spectrometer pre-cooled to −60 °C followed by cooling to −100 °C.

2.3.11. Reaction of [(t-Bu₃P)(4-FC₆H₄)Pd(OH)]₂ with 4-Fluorophenylboronic Acid

The inability to form a 1:1 Pd/B stoichiometry, was hypothesized to be caused by the *i*-Pr₃P ligand not being large enough to break the Pd-(μ-OH)-Pd dimer bond. Interestingly, upon comparison of mono-ligated phosphine halide complexes containing ligands such as *i*-Pr₃P and *t*-Bu₃P the *i*-Pr₃P ligand forms dimeric complexes (i.e. **90**) where *t*-Bu₃P is known to form T-shaped palladium halide complexes (i.e. **99**) (Figure 25).[20] Therefore, we were interested in preparing T-shaped phosphine arylpalladium hydroxide complexes in monomeric form.
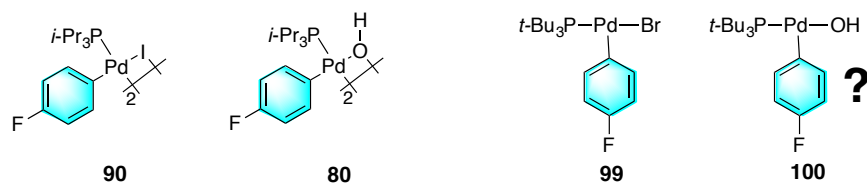
Figure 25. Dimeric and T-shaped phosphine complexes.

The first attempt at synthesizing (Path 1) T-Shaped t-Bu$_3$P complex **100** was attempted by combining (t-Bu$_3$P)$_2$PdCl$_2$ (**101**) with KOH, benzene, and 4-fluorochlorobenzene at reflux; however, palladium black was observed. Path 2 involved reacting T-shaped t-Bu$_3$P complex **101** with 10.0 equiv of CsOH•H$_2$O in THF were palladium black was also observed. A third synthetic route was envisioned by first attempting to prepare TMEDAPd(Aryl)OH[67] **102** which then upon protonation and removal of TMEDA with t-Bu$_3$PH•BF$_4$ lead to complex **100** (Path 3). However, screening the three sets of reaction conditions all led to palladium black indicating that the hydroxide complex **102** was unstable. The final synthesis involved the addition of thallium hydroxide to complex **101** where a white solid was obtained in 17% yield (Scheme 28). We then investigated if the newly formed complex was a T-shaped or dimeric complex in solution.

Scheme 28
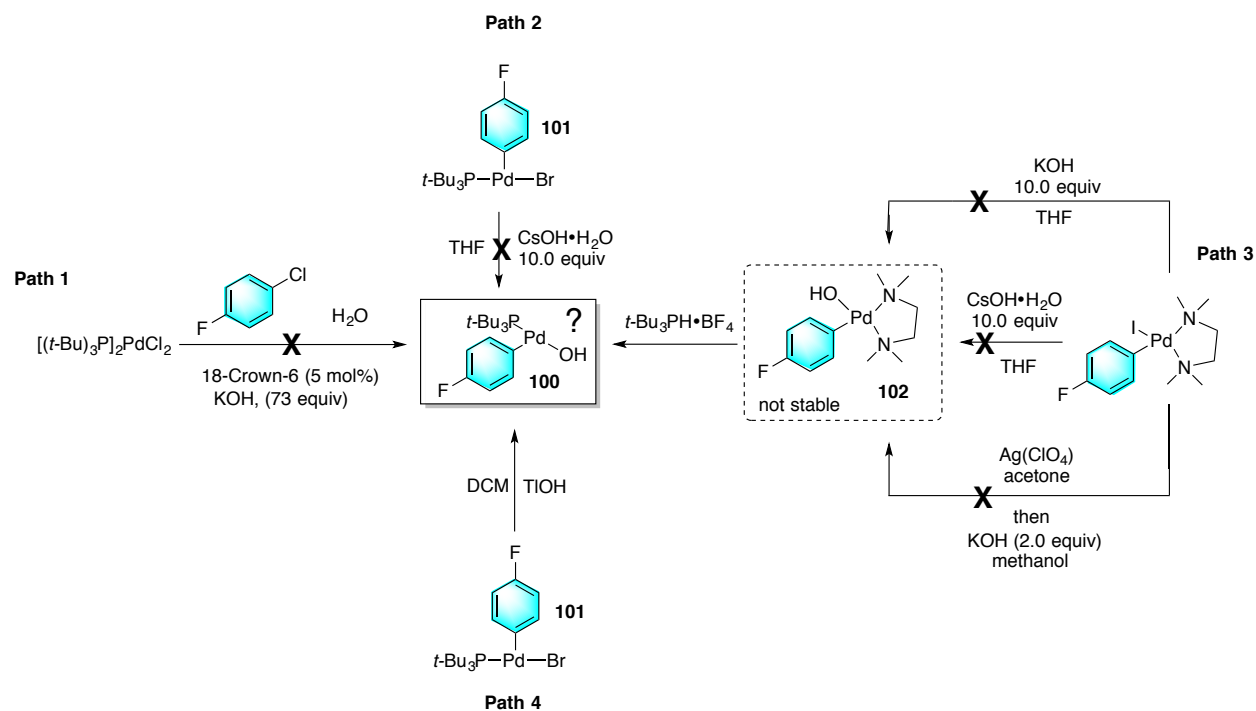
Upon dissolving the powder in THF a dimeric structure was observed in a *trans*:*cis* ratio of 1:1 indicating that the *t*-Bu₃P ligand was not bulky enough to form a monomeric palladium hydroxide dimer (Figure 26). Nevertheless, complex **103** was reacted with boronic acid **58.**
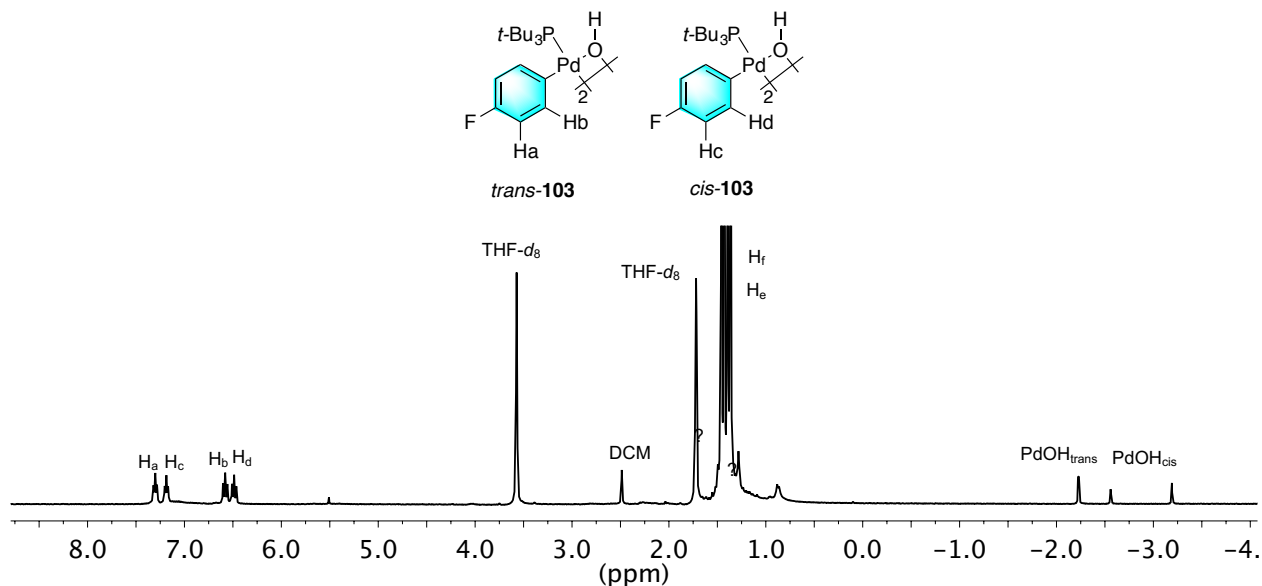
Figure 26. ^{1}H NMR spectrum of complex **103**.

In an attempt to form a complex with 1:1 Pd/B stoichiometry, the larger *t*-Bu₃P ligand was employed to weaken the Pd-(μ-OH)-Pd bonds and form a T-shaped palladium hydroxide complex. Thus, addition of a THF-*d₈* solution of complex **103** to a THF-*d₈* solution of **38** (1.0 equiv/Pd) at −78 °C followed by warming to −60 °C produced no new complexes. However, upon cooling the solution to −100 °C a new complex emerged with complete consumption of **103** with 1.0 equiv of **58** remaining (Scheme 29). The structure of this complex was assigned as the bridged *bis*-arylpalladium arylboronate complex, **104**, by analogy to complex **88.** Two discrete Hᵦ signals were observed at −100 °C wherein the barrier to rotation about the palladium aryl bond was found to be 10 kcal/mol (Figure 27).

Scheme 29
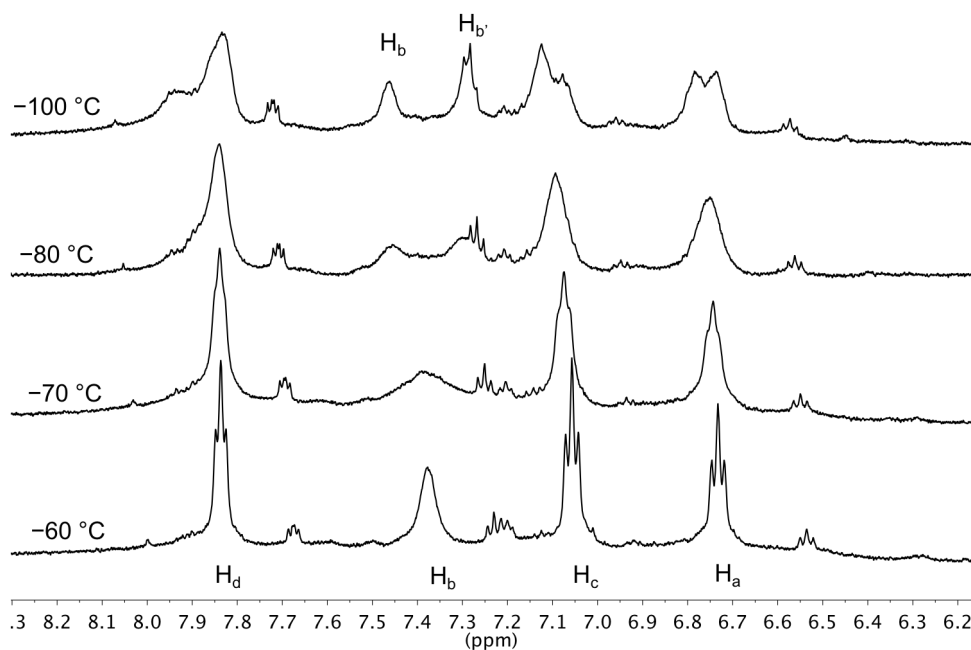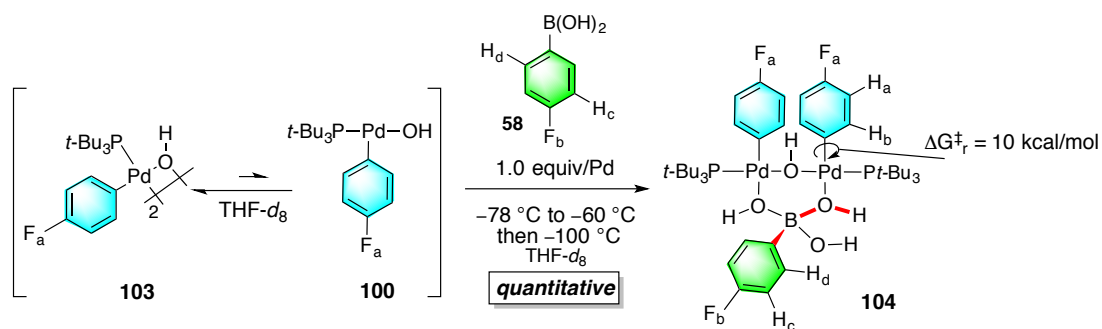
Figure 27. VT-NMR spectra of complex **104**.

2.3.12. Reaction of [(i-Pr₃P)(4-FC₆H₄)Pd(OH)]₂ with 4-Fluorophenylboronic acid in THF/CH₃OH

The surprising formation of 2:1 complex **88** raised a number of questions regarding the origin of its stability. Because this structure is heavily dependent upon the bridging capability of various oxygen atoms, it seemed logical to examine the effect of other donors, such as water, on the stability of this complex. Due to the low temperatures needed for intermediate formation methanol was chosen over water. In order to add methanol, the rapid injection NMR apparatus was used to performed the addition so we could monitor the sample accurately at low temperature.

Rapid injection of CH$_3$OH (60 μL) into a THF-d_8 solution of **88** with 1.0 equiv of **58** (from **80** and **58**, *vide supra*) at −55 °C resulted in the quantitative formation of a new species **86** by ^{1}H NMR spectroscopy (Figure 28).

Figure 28. ^{1}RI-NMR spectra (^{1}H NMR) of methanol injection into complex **88**.

Immediately, this experiment was repeated in CD$_3$OD to characterize the newly formed complex by NMR spectroscopy (Figure 29). The presence of a Pd-O-B linkage in **105** was established by the observation of NOE cross peaks between the methyl hydrogens on the *i*-Pr$_3$P group with both H$_b$ and H$_d$. Interestingly, complex **105** was found to form cross coupling product

73 over ~3-4 h at −55 °C indicating the complex was prone for transmetalation compared to complex **88**.

Scheme 30
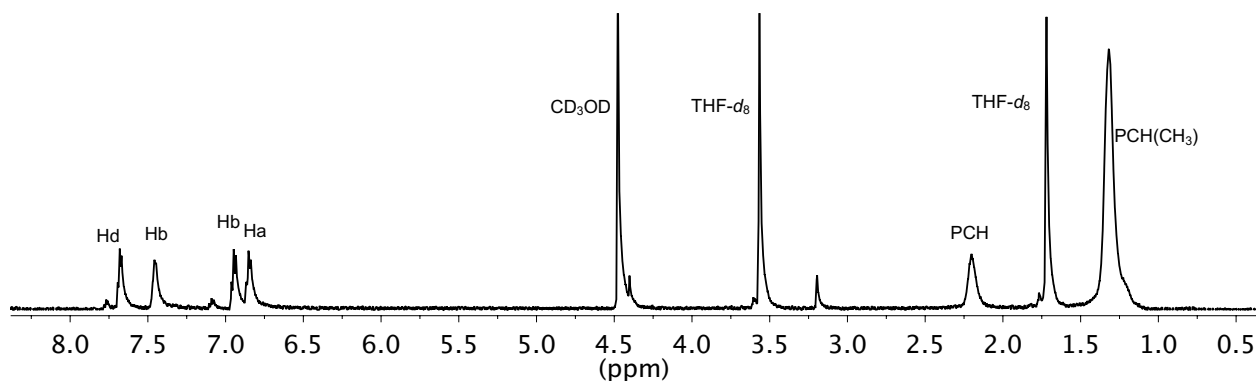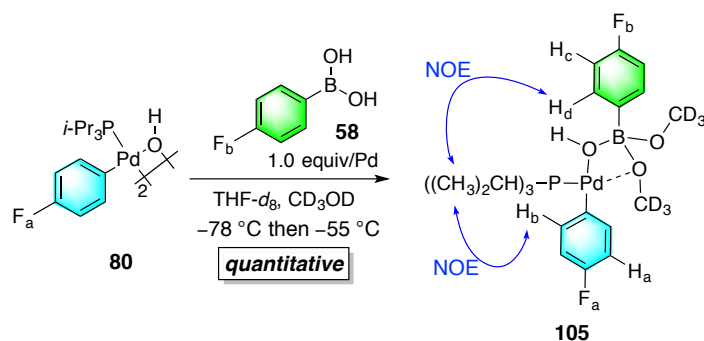
Figure 29. ^{1}H NMR spectrum of complex **105**.

The ^{11}B NMR signal at 9 ppm was well within the chemical shift regime for tetracoordinate boron (8-B-4) complexes (Figure 30). However, the ^{11}B NMR chemical shift of arylboronic acid **58** was needed in THF/CH$_3$OH (10:1) to confirm that methanol had not simply coordinated the boron atom. Addition of arylboronic acid **58** to a THF/CH$_3$OH solution resulted in a broad signal at 30 ppm in the ^{11}B NMR indicating that methanol is not sufficiently Lewis basic to coordinate to the boron atom whereas a Pd-OH is.
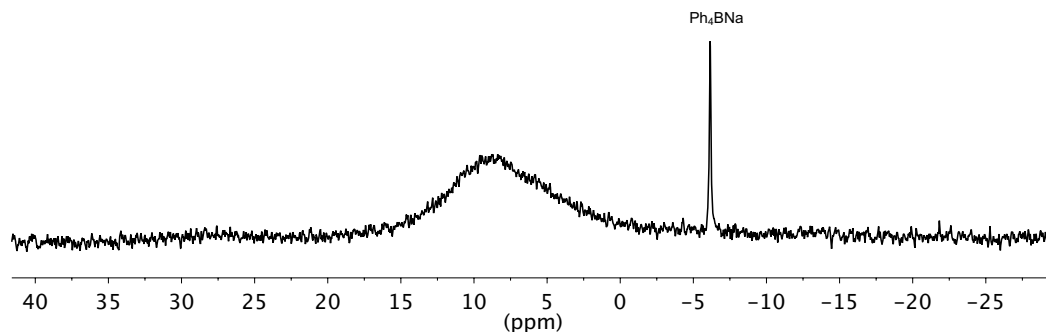
Figure 30. ^{11}B NMR spectrum of 8-B-4 complex **105**.

Attempts to confirm the incorporation of methanol into complex **105** by NMR spectroscopy were unsuccessful most likely because of rapid exchange with free methanol in solution. Attempting to prepare complex **105** with lower THF/CH$_3$OH ratios resulted in cross coupling product even at low temperature (−55 °C) indicating that methanol may be incorporated into the structure and excess methanol in solution may stabilize the complex. To determine if methanol was incorporated into the structure an independent synthesis was investigated between 4-fluorophenyldimethoxyboronate **106** and complex **80**.

The identity of complex **105** was verified by the reaction of 1.0 equiv/Pd of 4-fluorophenyldimethoxyboronate **106** with palladium dimer **80** at −78 °C in THF-d_8/CD$_3$OD followed by warming to −55 °C whereupon a quantitative formation to complex **105** was observed by ^{1}H and ^{13}C NMR spectroscopy (Scheme 31, right). This experiment clearly demonstrates that the hydroxyl groups had been replaced by methanol; however, this result did not provide any information on if the starting binuclear arylpalladium hydroxide complex had converted to a T-shaped complex.

Scheme 31
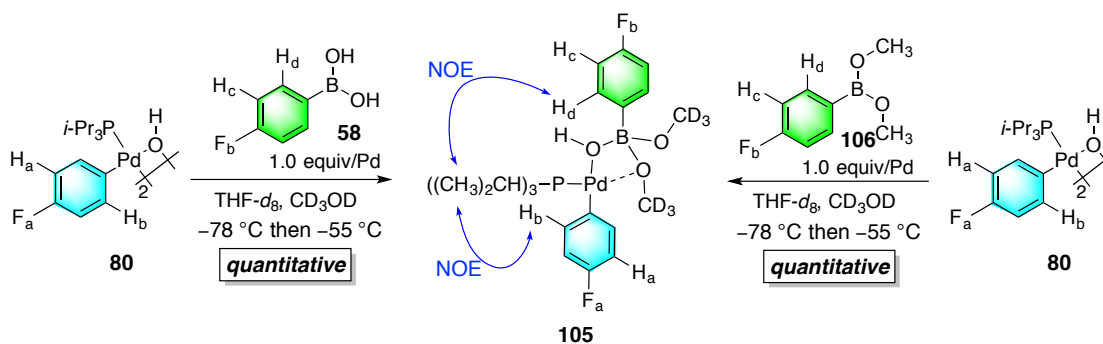
The hypothesis that methanol was not breaking the Pd-(μ-OH)-Pd moiety was confirmed by mixing complex **80** in THF/CH$_3$OH where upon **80** was still observed by ^{1}H NMR

spectroscopy. Moreover, the addition of methanol (60 µL) to a THF solution of complex **88** at −78 °C followed by warming to −60 °C resulted in a quantitative conversion to both **105** and **80** in a ratio of 1 : 0.5, indicating that the Pd-(µ-OH)-Pd is not broken by methanol (Figure 31).
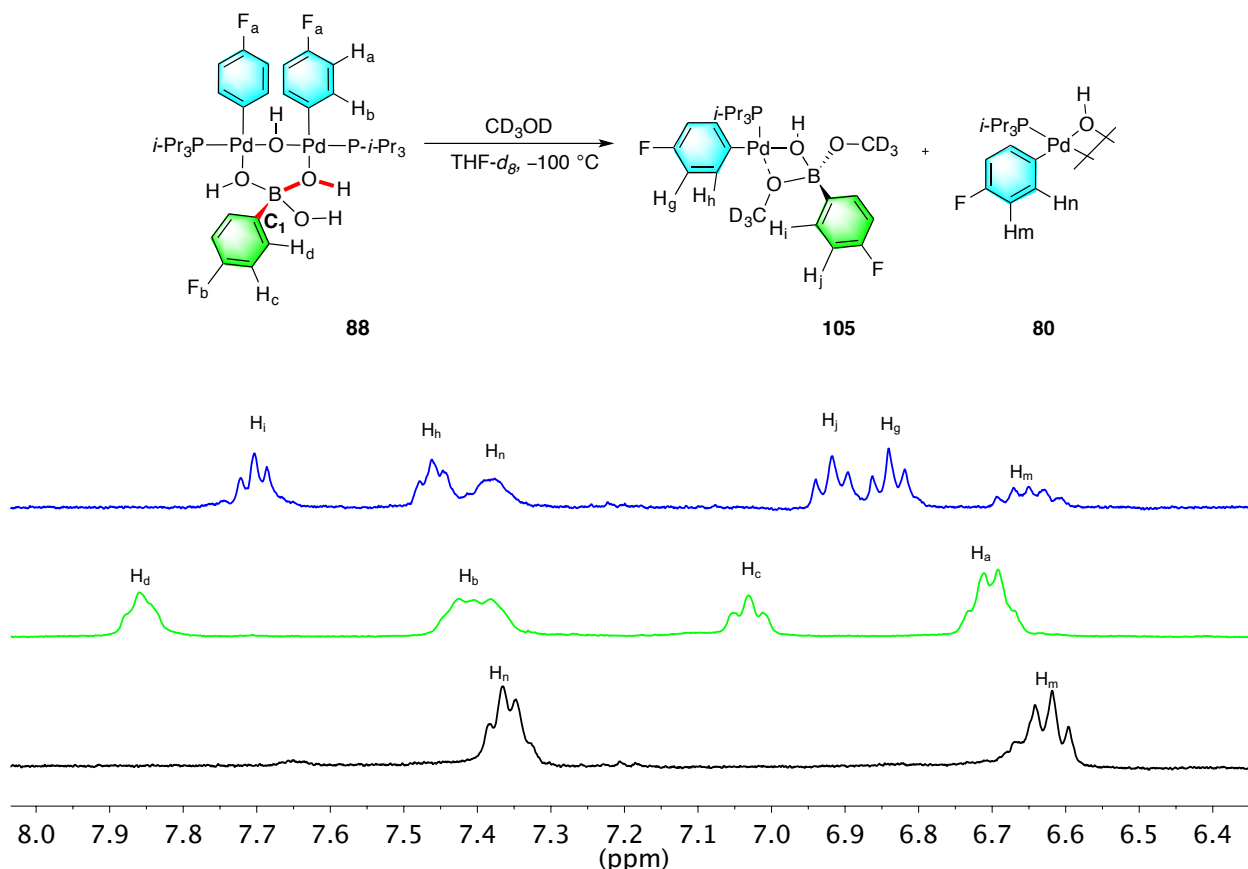
Figure 31. Black ^{1}H NMR spectrum is complex **80** at −100 °C in THF/CH$_3$OH. Green ^{1}H NMR spectrum is complex **88** in THF. Blue ^{1}H NMR spectrum is methanol addition to complex **88**.

2.3.13. Reaction of [(Ph$_3$P)(4-FC$_6$H$_4$)Pd(OH)]$_2$ with 4-Fluorophenylboronic acid in THF/CH$_3$OH

To establish if similar 1:1 complexes can be formed with other ligands, [(Ph$_3$P)(4-FC$_6$H$_4$)Pd(OH)]$_2$ (**57**) was combined with 1.0 equiv/Pd of **58** at −78 °C in THF-*d$_8$*/CD$_3$OD followed by warming to −55 °C. A new complex **107** was formed quantitatively, which displays spectroscopic characteristics similar to the other complexes (^{1}H, ^{13}C, ^{19}F, ^{31}P and ^{11}B NMR) along with HMBC and HSQC experiments to establish connectivity (Scheme 32).

Scheme 32

2.3.14. Reaction of [cis-(L₂)(4-FC₆H₄)Pd(OH)] with 4-Fluorophenylboronic acid in THF

The preference for a tricoordinate boron atom in 6-B-3 complex **74** arose from the presence of two, bulky *i*-Pr₃P ligands arranged in a *trans* configuration about the palladium (F− and B−strain).[68] It was of interest to investigate whether arranging the ligands in a *cis* coordination geometry would allow the boron atom to adopt a tetracoordinate state. Therefore, following literature precedent,[69] (D^{t}BPP)(4-FC₆H₄)Pd(OH) **108** and (DPPF)(4-FC₆H₄)Pd(OH) **109** were prepared by combining complex **57** with 2.0 equiv of either D^{t}BPP or DPPF in THF to form complexes **108** and **109** (Scheme 33). These complexes were characterized by NMR spectroscopy. The isolated arylpalladium hydroxide complexes showed two ^{31}P signals accompanied by $^2J_{PP}$ *cis* coupling, indicating an unsymmetrically coordinating bis-phosphine ligand was present.

Scheme 33

Next, D^{t}BPP complex **108** was combined with arylboronic acid **58** at −78 °C followed by warming to −55 °C which resulted in no reaction even upon warming to −30 °C, most likely due to the bulk of the chelate ligand (Scheme 34).

Scheme 34
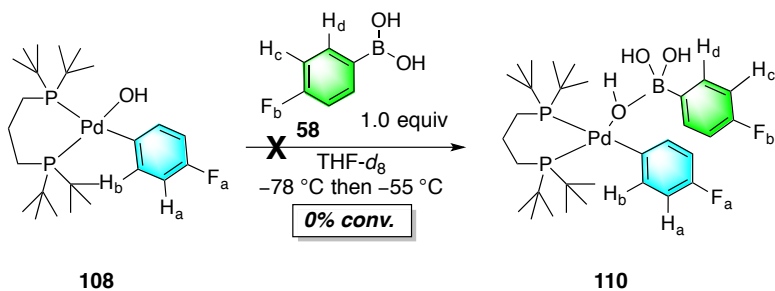
Secondly, complex **109** was combined with arylboronic acid **58** at −55 °C which resulted in the quantitative conversion to a new species, **111** (Scheme 35). Complex **111** was characterized by ^{1}H, ^{31}C, ^{19}F, ^{11}B and ^{31}P NMR spectroscopy with the HMBC (^{1}H−^{13}C and ^{1}H−^{31}P) and HSQC (^{1}H−^{31}C) experiments establishing the connectivity. At −55 °C, the assignment of the P(1)-atom (11.47 ppm) in **111** was enabled by the observation of *trans* couplings across the Pd center to H$_b$ (${}^4J_{P-H}$) and to H$_a$ (${}^5J_{P-H}$), establishing a *trans* relationship between P(1) and the aryl group bound to palladium (Figure 32).[70] The ^{11}B NMR chemical shift was merged with the baseline, suggesting a rapid equilibrium between **111** and starting materials.

Scheme 35
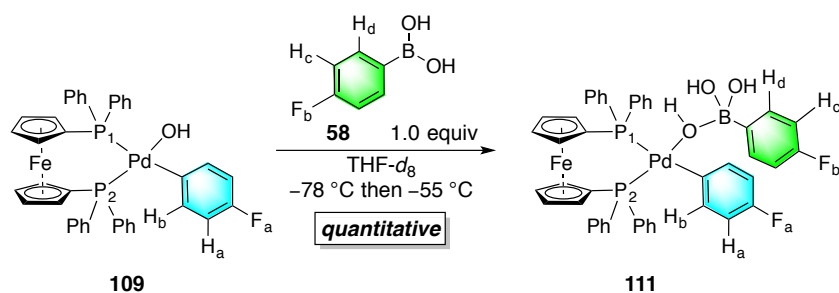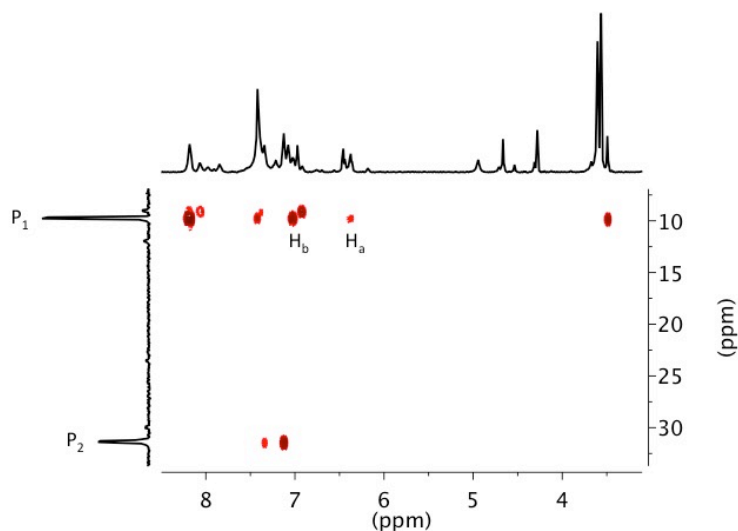
Figure 32. HMBC (^{1}H-^{31}P) spectrum of complex **111**.

2.4 Conclusions

For the first time Pd-O-B linkages *"the missing links"* in the Suzuki-Miyaura have been observed and fully characterized by NMR spectroscopy. The characterization of these complexes was made possible by low temperature and rapid injection NMR spectroscopy. During this study, four types of Pd-O-B linkages were formed and found to display different coordination environments about both the boron and palladium atoms. The structures are shown in general terms in Figure 33.
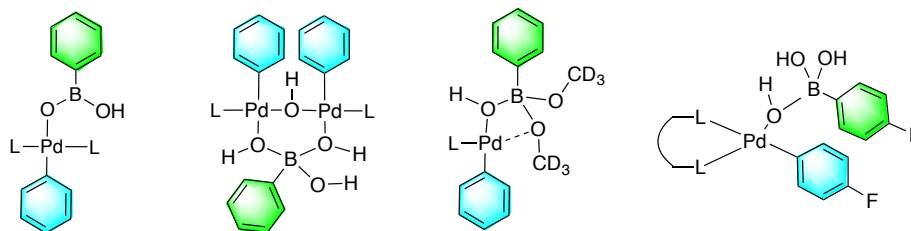
Figure 33. Types of Pd-O-B linkages characterized with arylboronic acids.

The structures of these intermediates were assigned based on 1D and 2D NMR spectroscopy with the NOE and HMBC experiments being crucial in solving the structures.

Moreover, multiple independent synthesis validated our structure determinations. Additionally, these syntheses allowed for the coordination environments about boron to be confirmed. Interestingly, various phosphine ligands such as Ph_3P, i-Pr_3P and DPPF were found to form Pd-O-B linkages that could be characterized by NMR spectroscopy. Furthermore, solvent was found to dramatically affect the structures of these complexes (ie 1:1 Pd/B ratio). The first goal of this project was completed upon the elucidation of these putative intermediates. The next chapter is centered on characterizing these species both kinetically and computationally allowing for the first structure reactivity relationships to be determined for pre-transmetalation intermediates in the Suzuki-Miyaura reaction.

CHAPTER 3: Kinetic and Computational Characterization of Pre-transmetalation Intermediates in the Suzuki-Miyaura Reaction with Aryl Boronic Acids

3.1 Introduction and Background

The past 30 years has seen tremendous advancement in the realm of cross-coupling reactions. Specifically, the advent of electron rich and sterically hindered ligands has allowed for reaction conditions to be tuned in a manner that allows for the oxidative additions of aryl chlorides. Furthermore, the rate of reductive elimination has also been shown to be enhanced by the employment of large phosphine ligands (Scheme 36).[71] The key to this technology is the ability of the ligand to control the coordination number of the palladium atom. Specifically, the Buchwald ligands and *t*-Bu$_3$P work by both stabilizing and keeping an empty coordination site free on the metal center.

Scheme 36
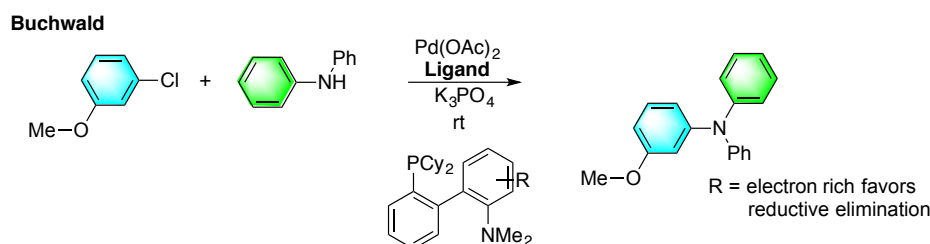
Interestingly, while the oxidative addition and reductive elimination steps have seen many investigations on the impact of ligand, solvent and various other reactions conditions these effects are virtually unknown for the transmetalation step in cross-coupling reactions except for the Stille and Hiyama-Denmark reactions. Echavarren and co-workers[72,73] were able to investigate the intramolecular transmetalation event by forming pre-reductive elimination intermediates (Figure 34). Oxidative addition of aryl iodide **112** with (Ph$_3$P)$_4$Pd in toluene at 40 ºC resulted in the formation of palladacycle **113**. Interestingly, upon changing the ligand to DPPF oxidative addition product **114** was isolated. Evidently, the transmetalation to form palladacycle **114** is inhibited by the lack of an activated palladium center. However, the transmetalation was induced to form palladacycle **115** by the addition of Ag$_2$CO$_3$. These studies reveal the importance of choice of reaction conditions as well as the ligands employed.
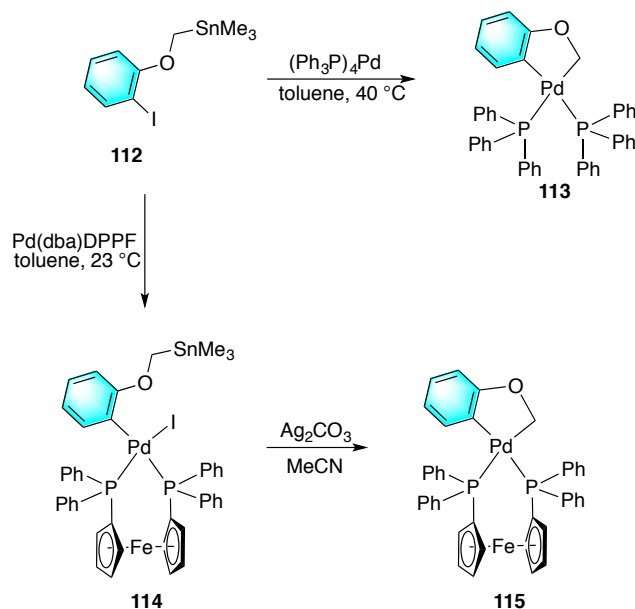
Figure 34. Isolated pre-reductive elimination palladacycles in the Stille reaction.

3.2 Objectives

The ability to generate pre-transmetalation intermediates with different coordination environments around both the boron and palladium atoms provided the opportunity to interrogate kinetic aspects of the transmetalation event. The primary objective is to explore the effect of ligand, solvent and organoboron sources on the transfer of the organic group from boron to palladium. These studies were performed by kinetically monitoring the decay of Pd-O-B linkages under different reaction conditions by ^{19}F NMR spectroscopy as well as monitoring the rates of cross-coupling products to determine the rate determining step. Additionally, Dr. Hao Wang and Andrew Zhart performed DFT calculations to validate my measured results.

3.3 Results and Discussion

3.3.1. Kinetic analysis of Complex 88 from [(i-Pr₃P)(4-FC₆H₄)Pd(OH)]₂ and 4-Fluorophenylboronic acid

*3.3.1. Kinetic analysis of Complex **88** from [(i-Pr$_3$P)(4-FC$_6$H$_4$)Pd(OH)]$_2$ and 4-Fluorophenylboronic acid*

Complex **88** was prepared as described in Section 2.3.8. by the addition of a THF solution of **58** (1.0 equiv/Pd) to a THF solution of **80** at −78 °C. To establish the kinetic behavior, the sample was warmed to −30 °C and the ^{19}F NMR signals for both **86** and **73** were monitored. First order plots of [**86**] and [**73**] *versus* time were fitted using functions [A]=[A]$_0$e^{-kt} and [P]=[A]$_0$(1−e^{-kt}), respectively, where [A] is the concentration of **86**, [A]$_0$ is the initial concentration of **86**, [P] is the concentration of **73**, k is the rate constant, and t is time. These functions provided accurate values for k (the observed kinetic constant) for the decay of **86** (5.78 ± 0.13 x 10^{-4} s^{-1}) and the formation of **73** (7.59 ± 0.58 x 10^{-4} s^{-1}) (Figure 35). The similarity of rates for appearance of **73** and consumption of **86** suggests that transmetalation is the rate-determining step for this process. Moreover, the first order behavior confirms that the transmetalation is in an intramolecular process proceeding through either **86** or **73**. As described in chapter 2 it is not possible to confirm which complex is actually present at –30 ºC because of the rapid exchange among **88**, **58**, and **86** and the resulting coincidence of their NMR signals. The proposal that arylboronate complex **88** converts to **86** prior to transmetalation is supported by an Arrhenius analysis and computational investigation as described below.
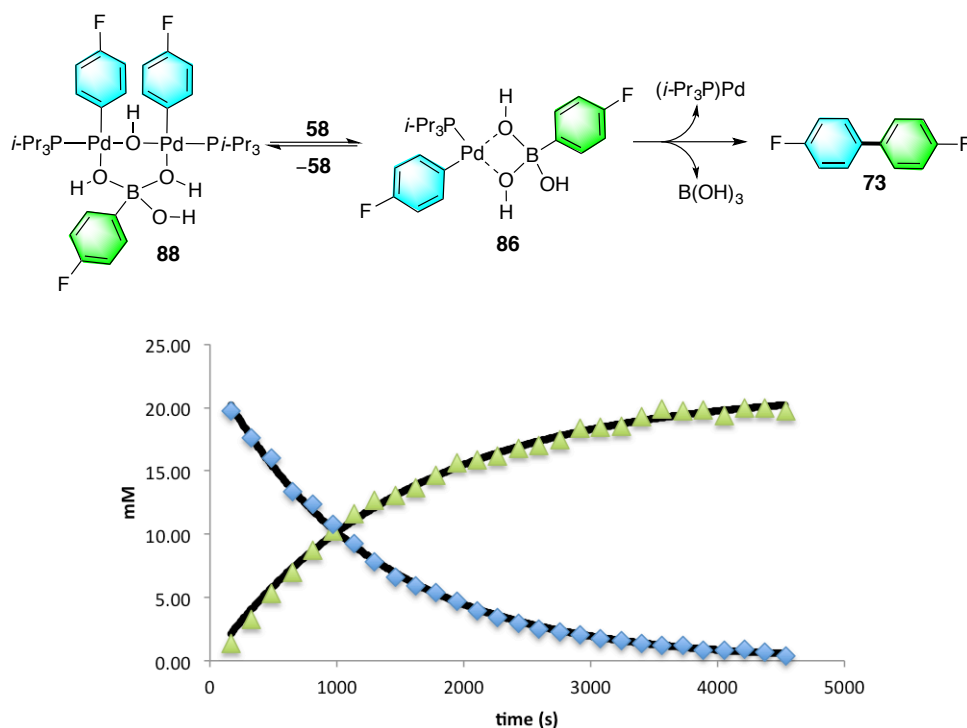
Figure 35. Decay of complex **86** and formation of **73** at −30 °C.

To obtain the activation parameters, the rates of formation of **73** were measured by ^{19}F NMR spectroscopy at four different temperatures ranging from −40 °C to −10 °C in THF. First order plots of [**86**] and [**73**] *versus* time were obtained for all measurements and fitted as described above. Upon plotting ln(k/T) *vs.* T^{-1} a linear slope was obtained which allowed for the activation parameters to be extracted from the data using the Eyring equation **1** (Figure 36).

Equation 1.

$$ln\frac{k}{T} = \frac{-\Delta H^{\ddagger}}{R}\frac{1}{T} + ln\frac{k_B}{h} + \frac{\Delta S^{\ddagger}}{R}$$

The enthalpic ($\Delta H^{\neq}_{243.15}$ = 15.98 ± 0.79 kcal/mol) and entropic ($\Delta S^{\neq}_{243.15}$ = −0.0069 ± 0.0032 kcal/mol) values obtained were strikingly similar to computationally derived parameters strongly suggest that complex **88** has rearranged to **86** prior to transmetalation (Table 5).

56

Table 5: Activation Parameters for the Transmetalation Step.
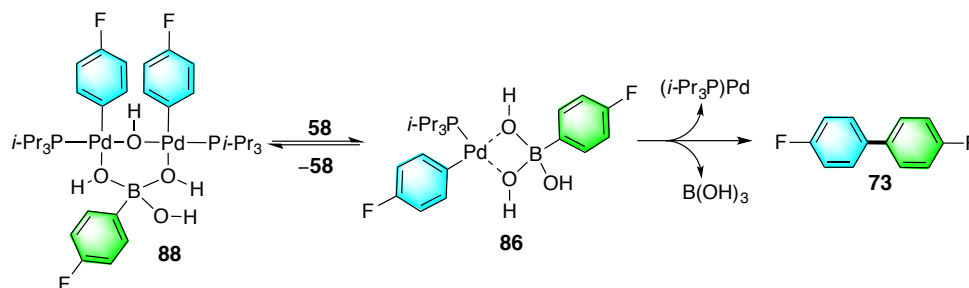
entry	$\Delta G^{\ddagger}_{243.15}$ kcal/mol	$\Delta H^{\ddagger}_{243.15}$ kcal/mol	$\Delta S^{\ddagger}$ kcal/mol•K
measured[a]	17.7 ± 1.1	15.98 ± 0.79	-0.0069 ± 0.0032
calculated	15.38	14.57	-0.003

[a] Average of triplicate runs.

$$y = -(8065 \pm 398)x + (20.3 \pm 1.6)$$
$$R^2 = 0.995 \pm 0.145$$
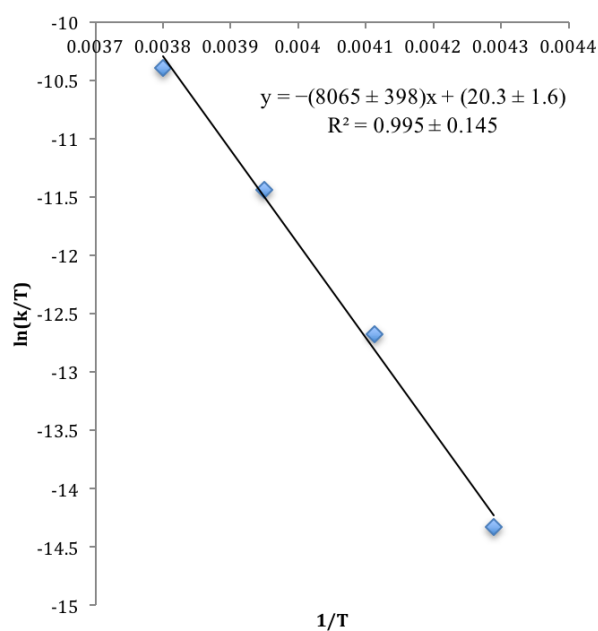
Figure 36. Eyring plot for the decay of complex **86** over a range of temperatures.

3.3.2. Effect of Phosphine ligand on the rate of the transmetalation step

To establish the effect of phosphine ligand (Ph₃P, *i*-Pr₃P, DPPF) on the rate of transmetalation, complexes **86, 116,** and **111** were freshly generated at −78 ºC followed by warming to −10 ºC in THF such that their ^{19}F NMR signals could be monitored. Each complex demonstrated first order behavior providing accurate values for *k* (Table 6, Figure 6). However, an accurate rate value for the formation of cross-coupling product **75** could not be obtained for DPPF complex **11** because its ^{19}F NMR signal (−116.47 ppm) overlapped with the product **73** (−116.45). Furthermore, the matching of the decay and formation of products from Ph₃P complex **116** demonstrated that the transmetalation step is rate determining for this complex as well. The slower reaction rate from using the DPPF ligand compared to Ph₃P and *i*-Pr₃P ligated complexes **116** and **86** respectively suggests that a ligand dissociation event must take place prior to the transmetalation event in complex **111**. The rate of transmetalation from the Ph₃P complex **116** was slightly faster than the *i*-Pr₃P complex **86** indicating the increased rate is not related to the size of the ligand, but rather to the electrophilicity of the palladium center. This conclusion is supported by the observation of a positive rho value for a Hammett study on the transmetalation step in the related cross coupling of arylsilanolates.[74] From these data the rate of the transmetalation process follows the trend Ph₃P > *i*-Pr₃P > DPPF, highlighting the need for generating a coordinatively unsaturated and electrophilic palladium atom during the transmetalation process.

Table 6: Effect of Phosphine Ligand on Rate.[a]
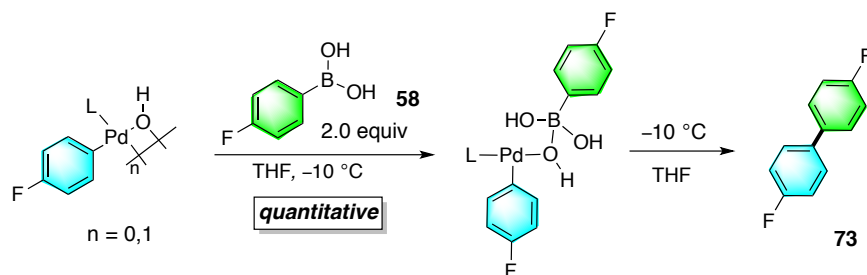
entry	complex	ligand	k,[a] 10^{-3} s^{-1} (decay)	k,[a] 10^{-3} s^{-1} (form)	k_{rel}
1	**111**	DPPF	2.75 ± 0.05	–	1.00
2	**86**	*i*-Pr₃P	8.09 ± 0.86	4.65 ± 0.36	2.94
3	**116**	Ph₃P	9.95 ± 0.71	10.6 ± 0.2	3.61

[a] Average of triplicate runs.

3.3.3. Effect of solvent on transmetalation event

The observation of complex **105** in THF/CH$_3$OH (10:1) raised a concern that the excess methanol in solution may impact the formation of cross-coupling product. This trepidation about the role of methanol sparked a series of kinetic experiments to probe the effect of solvent on the rate of transfer for the organic fragment from boron to palladium. First, the kinetic behavior of arylpalladium complex **105** in THF/CH$_3$OH (a fully characterized 1:1 complex) revealed a clean, first-order decay of **105** and formation of **73** with *k* values of 1.55 ± 0.09 x 10^{-3} s^{-1} and 1.41 ± 0.02 x 10^{-3} s^{-1} respectively, (Scheme 37, 1). These values are very similar (k$_{rel}$ = 2.68) to the rates observed with complex **86** in pure THF (Scheme 37, 2).

Scheme 37
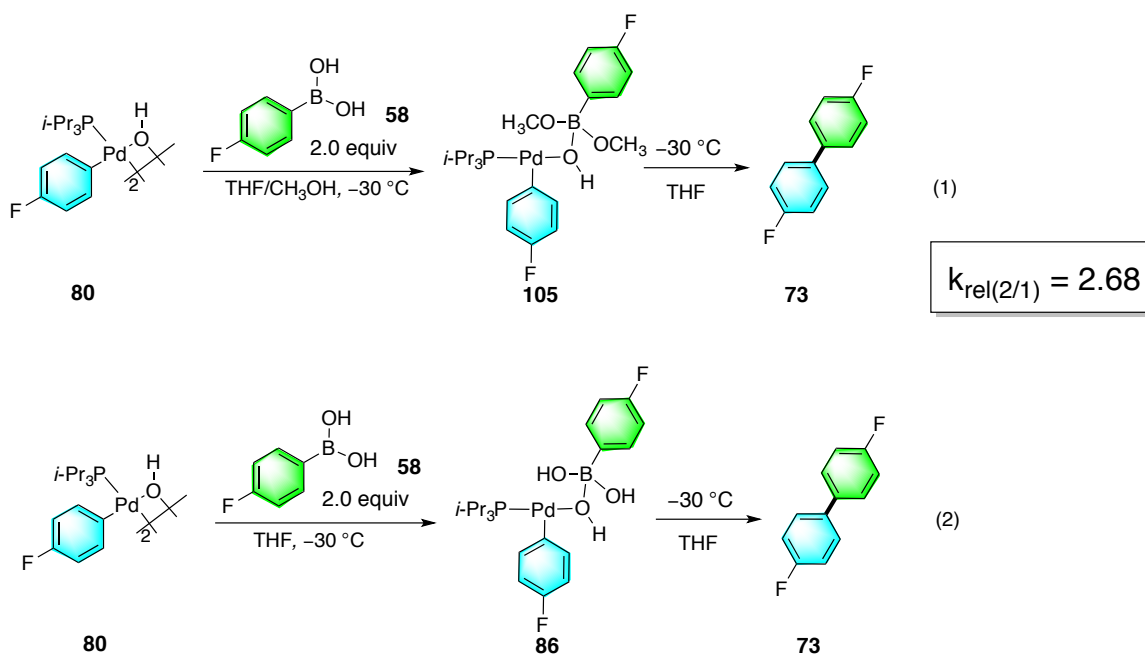
Secondly, the kinetic behavior of Ph$_3$P complex **107** in (10:1) THF/CH$_3$OH revealed a clean, first-order decay of **107** and formation of **73** with *k* values of 6.63 ± 0.32 x 10^{-3} s^{-1} and 7.45 ± 0.36 x 10^{-3} s^{-1} respectively (Table 7, entry 2). Comparing the rates of the *i*-Pr$_3$P complex **105** in (10:1) THF/CH$_3$OH revealed that the Ph$_3$P complex was 4.8 times faster, which is a very similar magnitude increase in rate (k$_{rel}$ was 2.27) for the reactions in pure THF (i.e. no methanol) as described above at -10 °C indicating that methanol does not have much of an impact on the rate between these two ligands (Table 7, entries 3 and 4).

Table 7: Effect of solvent and ligand on rate[a]
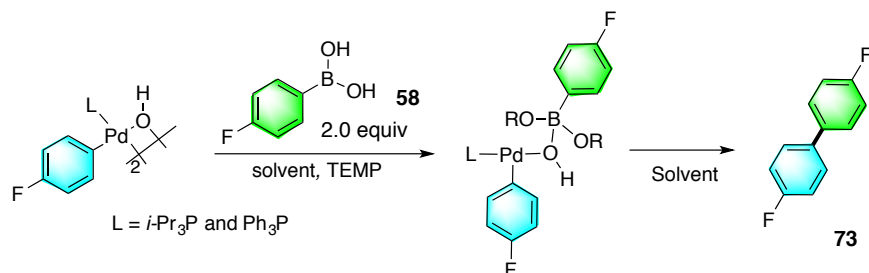
entry	complex	Temp	solvent	ligand	$k,^a\ 10^{-3}\ s^{-1}$ (decay)	$k,^a\ 10^{-3}\ s^{-1}$ (form)	k_{rel}
1	**105**	−30 °C	THF/CH$_3$OH	i-Pr$_3$P	1.41 ± 0.02	1.55 ± 0.09	4.8
2	**107**	−30 °C	THF/CH$_3$OH	Ph$_3$P	6.63 ± 0.32	7.45 ± 0.36	
3	**86**	−10 °C	THF	i-Pr$_3$P	8.09 ± 0.86	4.65 ± 0.36	2.27
4	**116**	−10 °C	THF	Ph$_3$P	9.95 ± 0.71	10.6 ± 0.2	

[a] Average of triplicate runs.

The formation of i-Pr$_3$P complex **105** in pure THF (from dimethyl ester **106** and **80**) at −78 °C followed by warming to −30 °C resulted in the first order formation of cross-coupling product **73** with a remarkable rate increase at $12.4 \pm 0.02 \times 10^{-3}\ s^{-1}$ (Table 8). The decay of complex **105** could not be monitored in this case because the ^{19}F NMR signal was too broad to accurately integrate. The enhanced rate (21.45 times faster) for the appearance of **73** relative to the arylboronic acid complex **86** suggests two things: 1) there is a solvent effect and 2) the methyoxy groups in pure THF are increasing the rate for transmetalation. A full discussion for the origins of this effect is in chapter 4**.** Moreover, these observations led us to investigate the effects of the ligand bound to boron (i.e. arylboronate esters) on the rate for transmetalation.

Table 8: Effect of solvent on rate.[a]
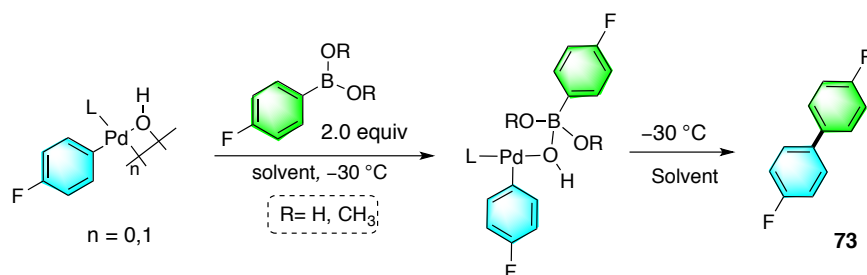
entry	complex	solvent	ligand	k,[a] 10^{-3} s^{-1} (decay)	k,[a] 10^{-3} s^{-1} (form)	k_{rel}
1	**86**	THF	i-Pr$_3$P	0.759 ± 0.058	0.578 ± 0.013	1.00
2	**105**	THF/CH$_3$OH	i-Pr$_3$P	1.41 ± 0.02	1.55 ± 0.09	2.68
3	**105**	THF	i-Pr$_3$P	–	12.4 ± 0.2	21.45

[a] Average of triplicate runs.

3.3.4. Kinetic analysis of 6-B-3 Complex 71

Complex **71** was thermally stable at −30 °C for more than 24 h in the presence of i-Pr$_3$P indicating that a higher temperature would be needed to form cross-coupling product **73**. In fact, warming a THF solution of **71** to 20 °C resulted in the formation of **73** however, not with the first-order behavior observed for the previous complexes, but rather exhibiting *S*-shaped concentration *vs*. time curves. The kinetic order in phosphine was determined by monitoring the rate of formation of **73** in THF solutions containing increasing amounts of i-Pr$_3$P ranging from 97 to 294 mM at 20 °C (Table 9). The *S*-shaped kinetic profiles were fitted using rate equation **2** to solve for kc (rate for catalyzed pathway) and q (a constant) (Figure 37). [75]

Equation 2.

$$[A] = ([A]_0 + q)\frac{[A]_0}{[A]_0 + q \cdot exp[k_c([A]_0 + q)t]}$$

Equation 3.

$$v = k_c\left\{\left(\frac{[A]_0 + q}{2}\right)^2 - \left([A] - \frac{[A]_0 + q}{2}\right)^2\right\}$$

Using equation **3** these values were used to generate a concentration [A] *vs* rate [*v*] plot

which allowed for a maximum rate v_{max} to be was extracted from the data (Figure 38).[75] Plotting log[v_{max}] *versus* log[i-Pr$_3$P] provided a straight line with a slope of -1.05 ± 0.05, consistent with an inverse dependence on phosphine (Scheme 38, Figure 39). This dependence indicates that a phosphine ligand must dissociate in a pre-equilibrium process that leads to putative 14-electron palladium complex **87** (Scheme 38). The requirement for this dissociation event is supported by computational studies that reveal high barriers for direct transmetalation from intermediates such as **87**.

Scheme 38
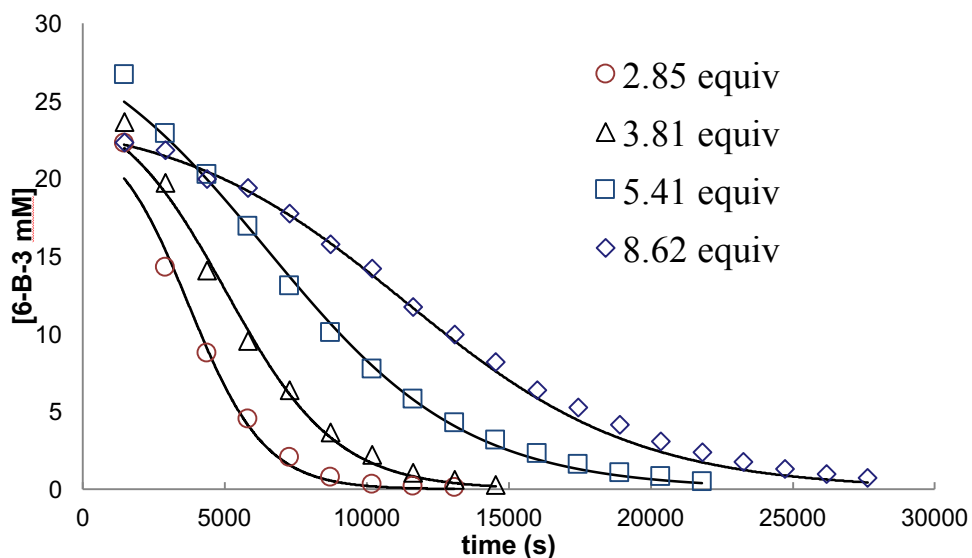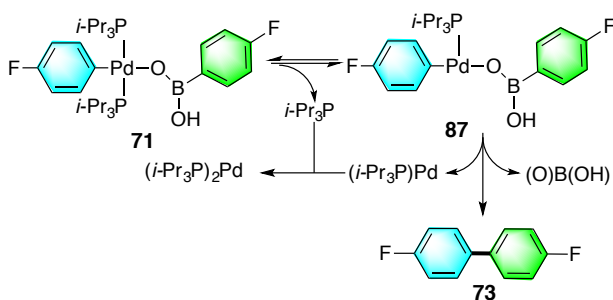
Figure 37. Decay of complex **71** in the presence of varying amounts of i-Pr$_3$P.
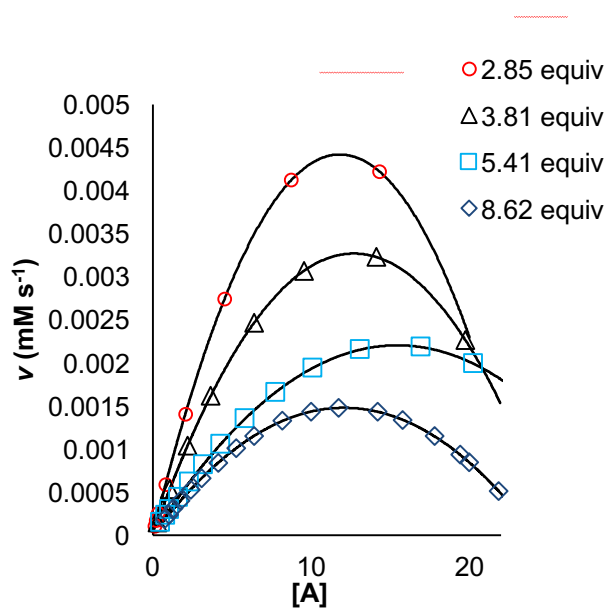
Figure 38. Rate *vs*. concentration curve for varying amounts of *i*-Pr₃P.

$$y = -(1.05 \pm 0.05)x - (0.25 \pm 0.12)$$
$$R^2 = 0.995 \pm 0.019$$
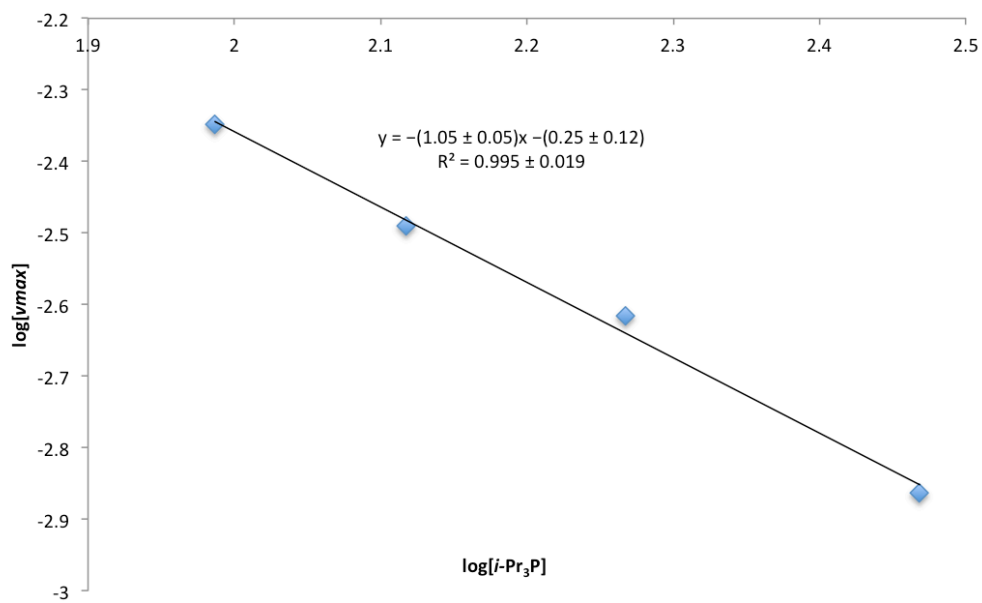
Figure 39. Order determination of *i*-Pr₃P for complex **71**

Table 9. Rates of cross-coupling product formation from **71**.
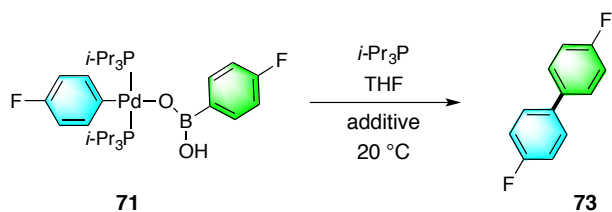
entry	equiv i-Pr$_3$P	additive	rate[a] 10^{-3} mM s^{-1}
1	2.85	–	4.48 ± 0.65
2	3.81	–	3.24 ± 0.12
3	5.41	–	2.42 ± 0.48
4	8.62	–	1.37 ± 0.96
5	3.81	–	3.24 ± 0.12
6[b]	3.81	(i-Pr$_3$P)$_2$Pd	2.99 ± 0.36
7[b]	3.81	(i-Pr$_3$P)$_3$Pd	2.19 ± 0.11
8	5.41	–	2.42 ± 0.48
9[c]	5.41	H$_2$O	1.11 ± 0.04
10	3.81	–	3.24 ± 0.12
11[d]	3.81	–	3.26 ± 0.17

[a] Average of triplicate runs. [b] 0.25 equiv of L$_x$Pd was added. [c] 10 equiv of water was added. [d] From **72** and **70**.

3.3.4.1. Effect of (i-Pr$_3$P)$_x$Pd on the Rate of the Transmetalation from 6-B-3 Complex 71

The *S*-shaped kinetic profiles observed during the reactions outlined above are indicative of autocatalytic behavior which conceivably could be caused by the Pd(0) initial byproduct (*i*-Pr$_3$P)Pd or (*i*-Pr$_3$P)$_2$Pd scavenging *i*-Pr$_3$P. However, this should not be the case as there is an excess of *i*-Pr$_3$P is in solution in a range from 2.85 to 8.62 equiv, which means the Pd(0) species should be saturated. To probe if this was the case ideally one would want to add mono-ligated complex (*i*-Pr$_3$P)Pd to the system, however, zero valent mono-ligated palladium complexes are known to dispropionate and from palladium black.[76] However, both (*i*-Pr$_3$P)$_2$Pd and (*i*-Pr$_3$P)$_3$Pd are known compounds which were prepared by performing a ligand exchange with TMEDAPdMe$_2$[77] followed by rapid reductive elimination to yield (*i*-Pr$_3$P)$_2$Pd and (*i*-Pr$_3$P)$_3$Pd depending on the

amount of $i\text{-Pr}_3\text{P}$ added (Scheme 39).[78]

Scheme 39
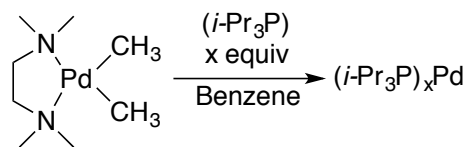
Interestingly, upon dissolving $(i\text{-Pr}_3\text{P})_3\text{Pd}$ in THF both $(i\text{-Pr}_3\text{P})_2\text{Pd}$ and $i\text{-Pr}_3\text{P}$ are observed which means the palladium center cannot accept a third ligand in solution. Nevertheless, upon the addition of 0.25 equiv of $(i\text{-Pr}_3\text{P})_3\text{Pd}$ to a solution of **71** with 3.81 equiv of $i\text{-Pr}_3\text{P}$ the v_{max} was found to be $(2.19 \pm 0.11) \times 10^{-3}$ mM s^{-1} which was slower than in the absence of the additive $(3.24 \pm 0.12) \times 10^{-3}$ mM s^{-1} indicating that the $(i\text{-Pr}_3\text{P})_3\text{Pd}$ had released free $i\text{-Pr}_3\text{P}$ to the system (Table 9). Additionally, 0.25 equiv of $(i\text{-Pr}_3\text{P})_2\text{Pd}$ was added to a freshly generated THF solution of 6-B-3 complex **71** (from **58** and **70)** with 3.81 equiv of $i\text{-Pr}_3\text{P}$. The observed v_{max} was found to be slightly slower than without the additive (Table 9). The lack of rate increase further supports the notion that $(i\text{-Pr}_3\text{P})_2\text{Pd}$ does not have a strong affinity for $i\text{-Pr}_3\text{P}$. These experiments clearly indicate that no order dependence is observed for the Pd(0) byproducts during the reaction, leaving only the boron by-products or water as the next most likely culprit for the *S*-shaped profiles.

*3.3.5. Probing the Transmetalation from 6-B-3 Complex **71** after Phosphine Dissociation: Autocatalysis Explained*

Because **87** is formed in such a low equilibrium concentration, it is not possible to determine if transmetalation occurs directly from the 6-B-3 complex **87** or if coordination of another group on boron (to form an 8-B-4 species) is necessary. Two pathways (Path C and Path D) that differ in the coordination state of boron can be formulated for this process (Figure 40). In Path C the B-aryl group transfers directly to palladium from **87** whereas in Path D water (present in stoichiometric amounts, c.f. Chapter 2, Figure 21) combines with **87** to form **86** prior to the aryl migration. Accordingly, the next stage of this study focused on the role of water during the transmetalation event.

The reaction of 6-B-3 complex **71** (freshly generated in THF from **70** and **58)** containing 5.41 equiv of $i\text{-Pr}_3\text{P}$ and an additional 10.0 equiv of water was monitored by ^{19}F NMR spectroscopy. The v_{max} was unexpectedly found to be slower than with no additional water present

(Table 9, entry 9). This observation suggests that if complex **86** were being formed (from **87** and water) that it reverts to **71** by recombination with i-Pr$_3$P faster than it undergoes transmetalation at 20 °C.

To test the validity of this hypothesis it was necessary to demonstrate the ability to independently convert **86** to **71** in the presence of i-Pr$_3$P. Thus, a solution of complex **86** was prepared from **58** (1.0 equiv/Pd) and **80** in THF at −78 °C followed by warming to −55 °C. As previously described, a mixture of **88** (which is in equilibrium with **86**) and 1.0 equiv of **58** was observed by ^{31}P and ^{19}F NMR analysis (Scheme 40). Upon addition of 60 µL of a 1.6 M THF solution of i-Pr$_3$P at −78 °C to this solution followed by warming to 20 °C, 6-B-3 complex **71** was observed along with minor amounts of cross-coupling product **73**. The formation of complex **71** from this method was verified kinetically by monitoring the formation of cross-coupling product **73** by ^{19}F NMR which was found to have a v_{max} matching the formation of **71** from **70** and **58** (Table 9, entries 2 and 11) further indicating that **71** was indeed formed. Thus, it appears that water is in fact inhibiting the cross coupling by shunting **87** to 8-B-4 intermediate **86** which is captured by the excess phosphine to arrive at the resting state **74**. As a final proof of this scenario, complex **71** would need to be prepared under *anhydrous* conditions thus forcing the reaction through Path C.

Scheme 40
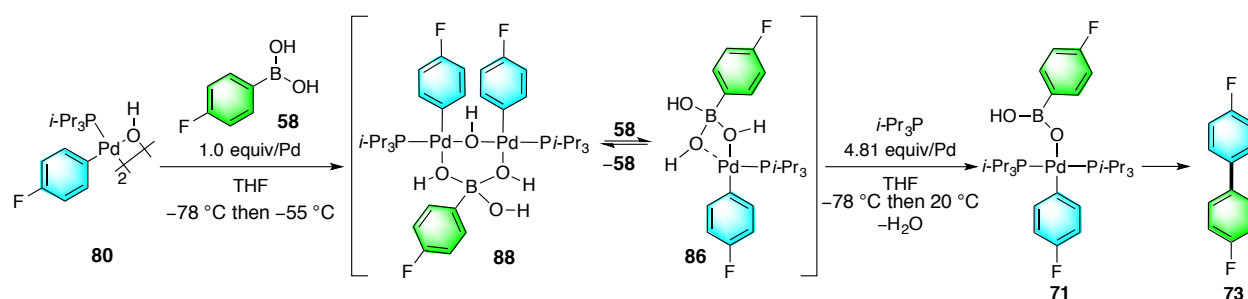
The water-free preparation of **74** has already been accomplished as part of the structural proof by combination of complex **70** and arylboroxine **72** (0.33 equiv) in THF. Repeating this procedure at −78 °C in the presence of 5.41 equiv of i-Pr$_3$P resulted in substantial amounts of cross-coupling product **73**. Therefore, complex **71** (from **40** and **72**) was generated with 15.03 equiv of i-Pr$_3$P which allowed for its kinetic competence to be studied (Scheme 41). *Clean first order kinetic behavior was observed for decay of **71** (1.25 ± 0.60 x 10^{-4} s^{-1}) and formation of **73** (7.14 ± 0.43 x 10^{-5} s^{-1}).* The absence of *S*-shaped kinetic profiles strongly suggests that water is somehow

involved in the rate increase during the reaction of **71** formed from **58** and **70**. The equivalent of water generated from the combination of **58** and **70** (Figure 40) inhibits the transmetalation via **87** by redirecting this intermediate to 8-B-4 complex **86** which is kinetically incompetent in the presence of excess *i*-Pr$_3$P. However, as the reaction proceeds, the metaboric acid byproduct (BO(OH)) scavenges the water to form boric acid and consumes the inhibitor (water) thus accounting for the observed auto-catalytic behavior; *ipso facto,* path C, via a 6-B-3 species, is operative (Figure 40).

Scheme 41
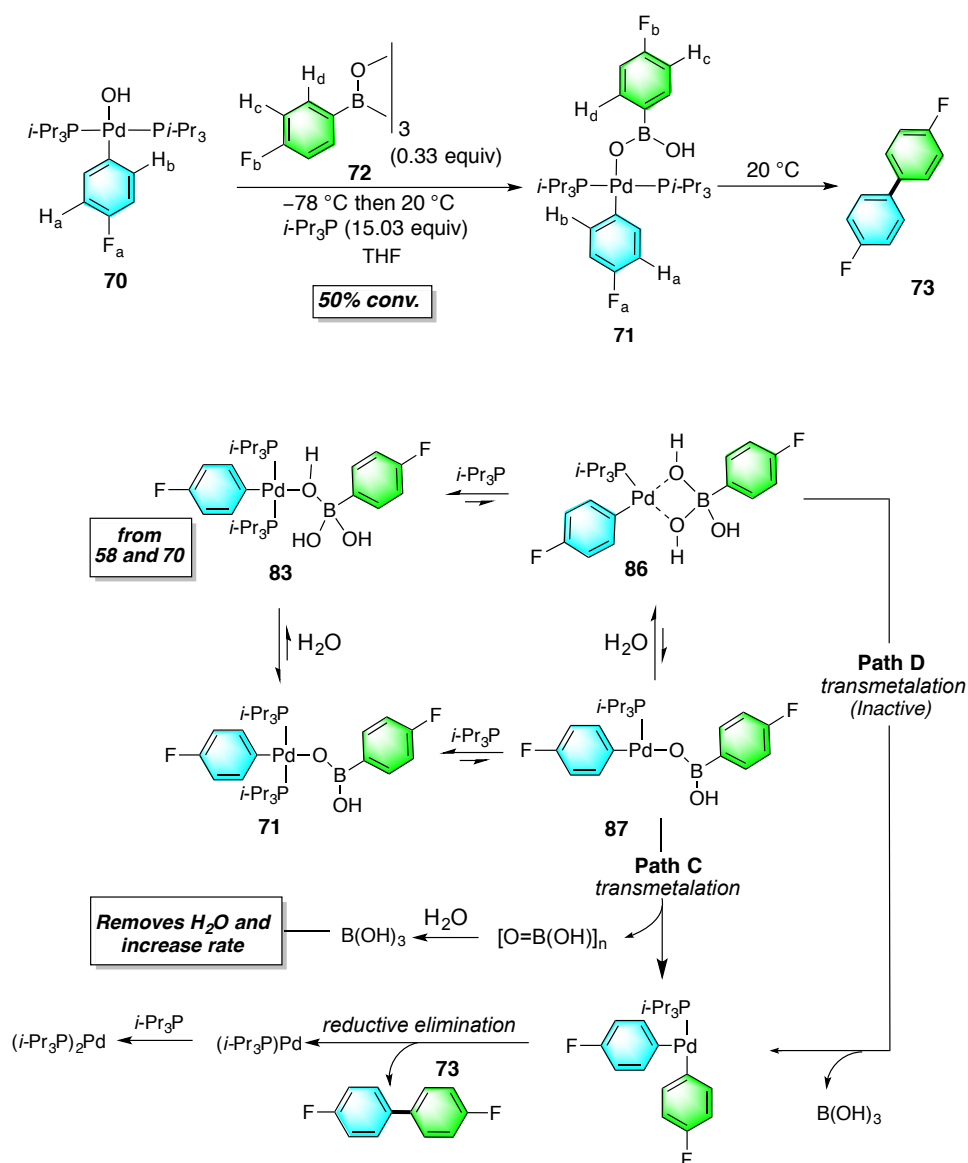
Figure 40. Proposed mechanism for cross-coupling formation from 6-B-3 complex **71.**

3.4. Computational Analysis of the Reaction Profile for Complexes Containing Pd-O-B Linkages

To gain further insight into the transmetalation step, transition state structures were calculated at the M06-2X/6-31G(d) on B3LYP/6-31(d) optimized structures with a THF continuum solvent field for the activated 8-B-4 complex **86** along with unactivated 6-B-3 complex **87**. Our previous computational investigation of arylpalladium arylsilanolate complexes revealed a significant difference in the energy profiles of isomeric, T-shaped arylpalladium complexes.[79] These three-coordinate species can exist in two configurations about palladium in which an empty site is either *trans* to the aryl group *(TA)* or to *trans* to the phosphine *(TP)*. For completeness both isomers were calculated for all the ground states, intermediates, transition states and products.

3.4.1. Computational analysis of Complex 86

The energy profile for the transmetalation event from 8-B-4 complex **86** is summarized in Figure 41. The experimentally observed ground state structure **86**-*GS* has two bridging hydroxyl groups bound to the palladium atom; however, for the transmetalation event to take place, an empty coordination site is needed. The two bridging hydroxyl groups are nonequivalent, one is trans to the aryl group (red) and the other is trans to the phosphine (black). Cleavage of either of these groups will lead to their respective coordinatively unsaturated complexes described above which are "*TA*" (red) or the *i*-Pr$_3$P group "*TP*" (black). The activation barriers for the formation for the two different T-shaped complexes **86**-*Inter-TA* and **86**-*Inter-TP* are 9.37 and 8.44 kcal/mol respectively. The electronic and steric parameters (aryl group and phosphine) lead to the observed differences in energies. Clearly, the steric parameter is the dominating factor because the arylgroup has a stronger kinetic *trans* effect[80] when compared to the *i*-Pr$_3$P ligand (leading to **86**-*InterTS-TP*). Moreover, in all succeeding steps on energy profile, the steric parameter is observed in the in the *TA* family as they are significantly higher energy than those in the *TP* family. The activation energies for the B-aryl transfer for **86**-*TS-TA* and **86**-*TS-TP* are 25.06 and 15.38 kcal/mol, respectively, reflecting a remarkable activation energy difference of 9.7 kcal mol^{-1}. The greater activation barrier to B-aryl migration for **86**-*TS-TA* can be attributed to the significant steric congestion around the palladium atom caused by the presence of the bulky *i*-Pr$_3$P group, whereas

migration of the B-aryl group to the empty coordination site in **86-TS-TP** is free of such repulsions and thus is energetically more favorable (Figure 42). An additional electronic contribution comes from migration of the B-aryl group to the site opposite to the substituent with the stronger *trans* effect in **86-TS-TA** thus constituting a kinetic deterrent. The activation barrier for the **86-TS-TP** (15.38 kcal/mol) transition state was found to be consistent with the experimentally measured value of 17.7 ± 1 kcal/mol (Table 5).

After the transmetalation event, the immediate product is either **86-Prod-Trans** or **86-Prod-Cis** diarylpalladium complex with the coordinated B(OH)$_3$ *trans* to *i*-Pr$_3$P or the 4-fluorophenyl group. The reductive elimination is presumably initiated by the dissociation of boric acid, thus generating the active tricoordinate diarylpalladium complexes *Pd-Prod-Trans* or *Pd-Prod-Cis*, which are poised to form cross-coupling products.
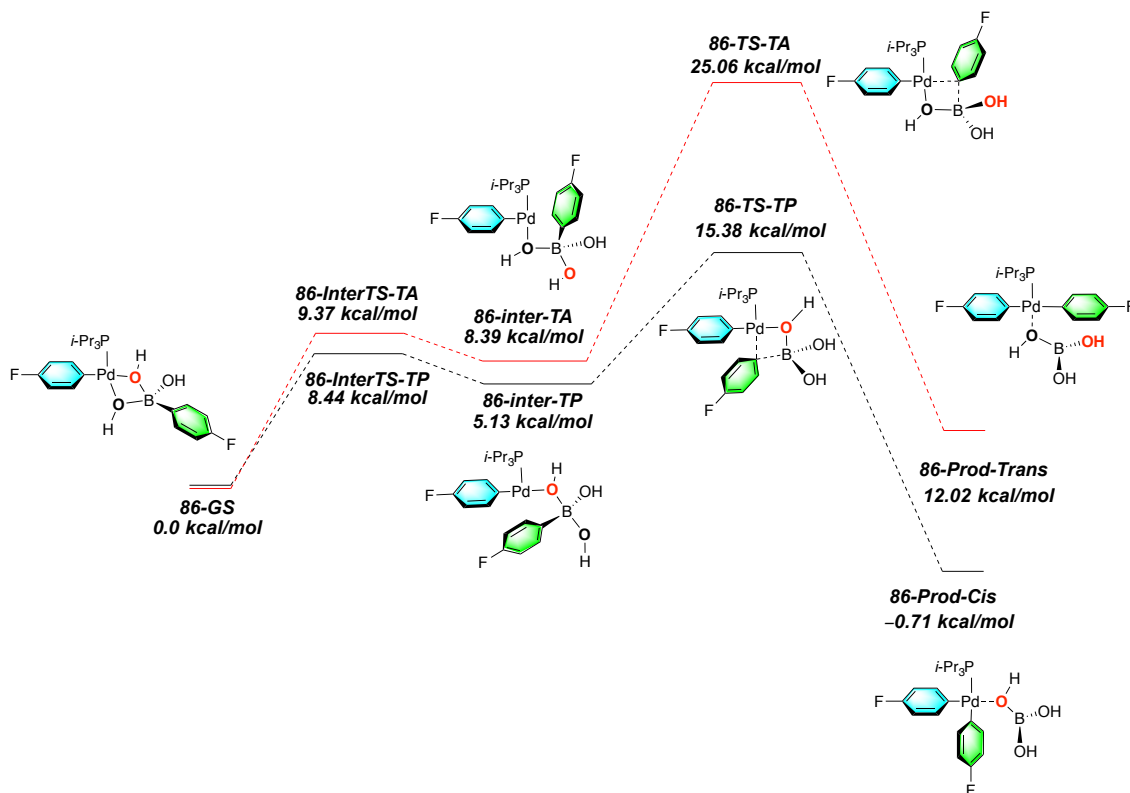
Figure 41. Energy profile for the transmetalation of **86**. Free energies are calculated using M062X/LANL2DZ – 6-31G(d) with CPCM solvation modeling (solvent = THF) for single point energies with thermal corrections from B3LYP/LANL2DZ – 6-31G(d) at 243.15 K.

86-TS-TA

86-Prod-Trans

86-TS-TP

86-Prod-Cis
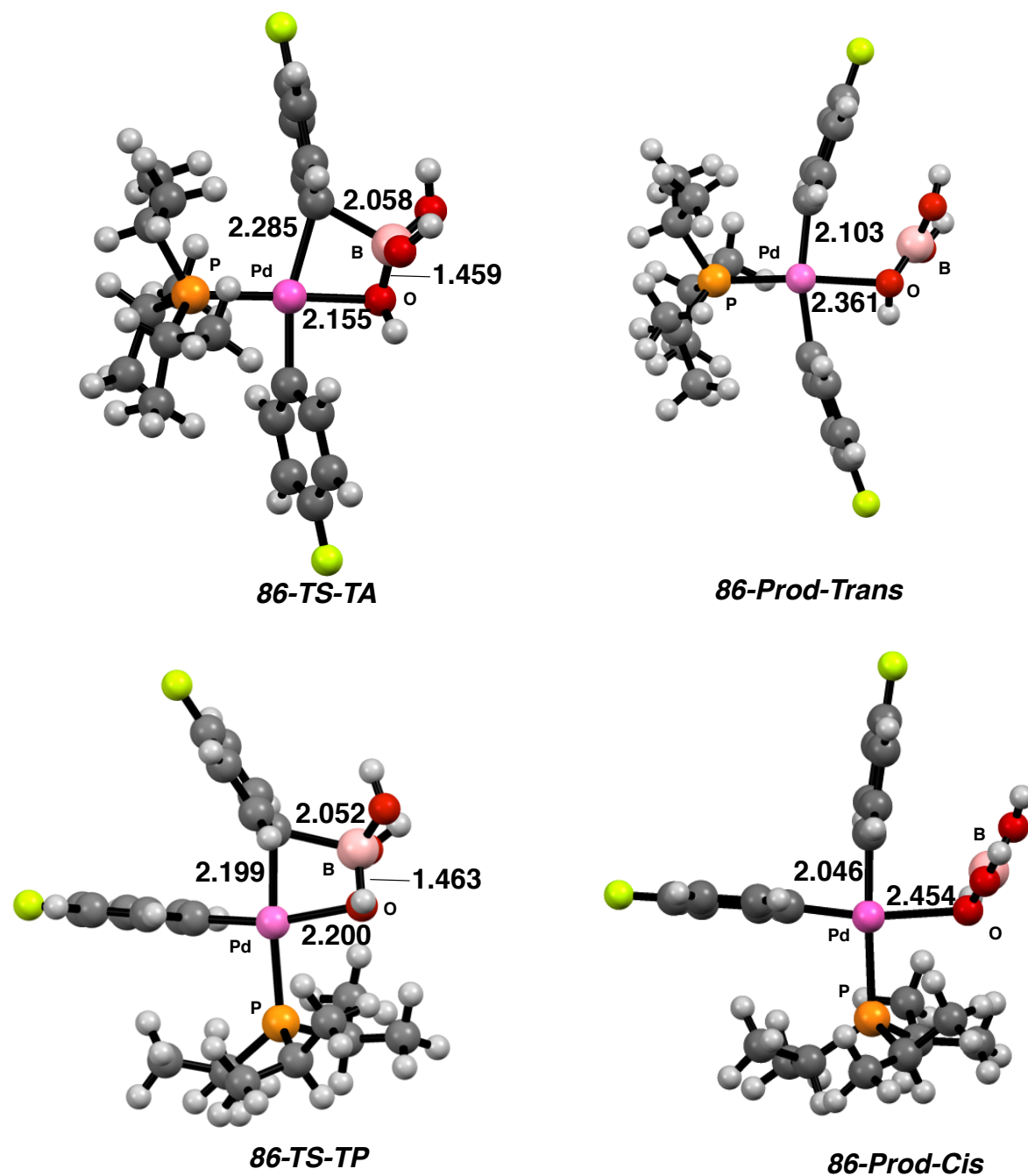
Figure 42. Energy profile for the transmetalation of **86**. Energies are single point solvation energies (THF) using M062X/6-31G(d) on the B3LYP/6-31G(d) optimized structures.

3.4.2. Computational analysis of Complex 87

The energy surface calculated for the 6-B-3 complex **87** is shown in Figure 11. Inspection of the energy profile reveals that the *TA* transition state and structures further along the energy profile are significantly higher in energy (~13 kcal mol^{-1}) compared to the *TP* series. This behavior can be understood in terms of the same steric and electronic influences as was seen in the 8-B-4 transition state structures (Figure 43). After the transmetalation event, the diarylpalladium complexes (**87-Prod-Cis, 87-Prod-Trans**) are only 0.78 – 1.13 kcal/mol downhill thus indicating very late transition states. The existence of late transition states is clearly signaled by the small difference in lengths of the forming bonds between the *ipso* carbon on the migrating group and the palladium atom for both **87-TS-TP** (2.085 Å) and **87-TS-TA** (2.171 Å) compared to **87-Prod-Cis** (2.069 Å) and **87-Prod- Trans** (2.154 Å), respectively. In this series the bonds are shortened by only 0.016 – 0.017 Å, whereas in the 8-B-4 series the corresponding changes for **87-TS-TP** (2.199 Å) and **87-TS-TA** (2.285 Å) compared to **87-Prod-Cis** (2.046 Å) and **87-Prod-Trans** (2.103 Å), are much larger (0.153 – 0.182 Å, Figure 44).
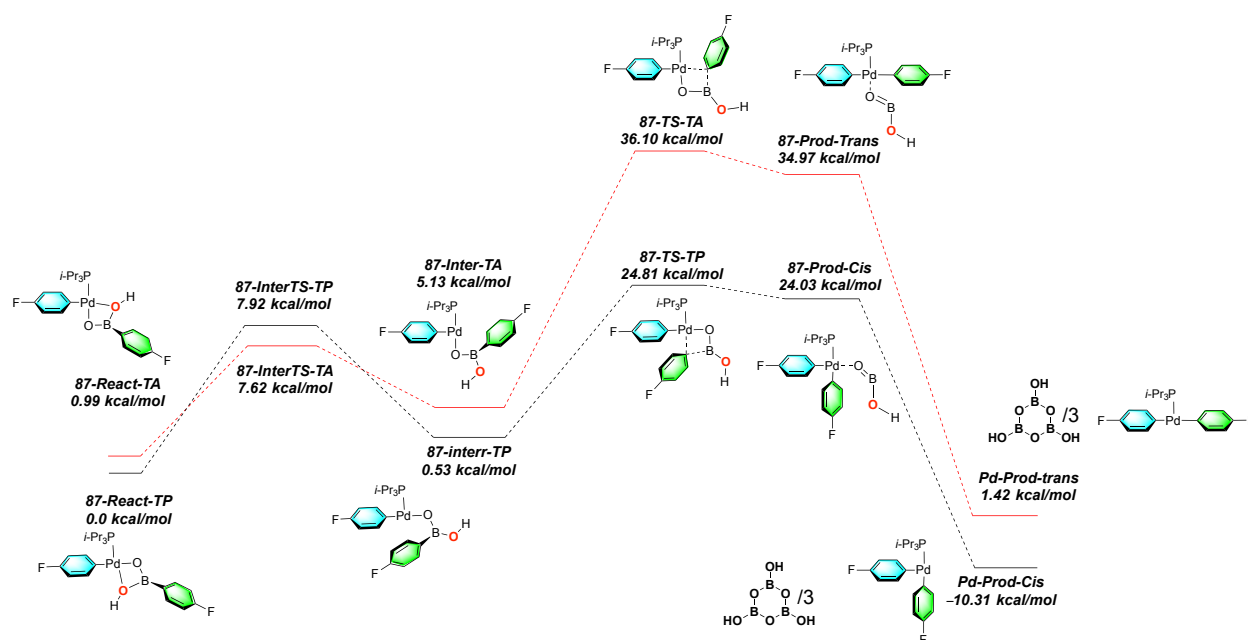
Figure 43. Energy profile for the transmetalation of 6-B-3 species **87**. Free energies are calculated using M062X/LANL2DZ – 6-31G(d) with CPCM solvation modeling (solvent = THF) for single point energies with thermal corrections from B3LYP/LANL2DZ – 6-31G(d) at 243.15 K.

The subsequent reductive elimination is presumably initiated by the dissociation of the

boron species to form free diarylpalladium complexes (*Pd-Prod-Cis, Pd-Prod-Trans*). However, the computational modeling of this event leads to a prohibitively endergonic process, which is most likely ascribable to the high energy of the O=B(OH) moiety. Solvation corrections lower the energies of the two products (32.7 kcal/mol and 19.1 kcal/mol for *Pd-Prod-Trans* and *Pd-Prod-Cis*), but they are still higher than those in the 8-B-4 processes. To solve this problem, we assume that some kind of bimolecular oligomerization takes place to remove O=B(OH) as a byproduct. Thus, to calculate the energies of the final reductive elimination products, instead of directly using the energy of O=B(OH), one-third energy of the O=B(OH) trimer, metaboric acid, was computed and added to the tricoordinate diarylpalladium complexes, which in turn gives more reasonable energies to both *Pd-Prod-Trans* (−2.8 kcal/mol) and *Pd-Prod-Cis* (−16.5 kcal/mol).[81]

87-TS-TA

87-Prod-Trans

87-TS-TP

87-Prod-Cis
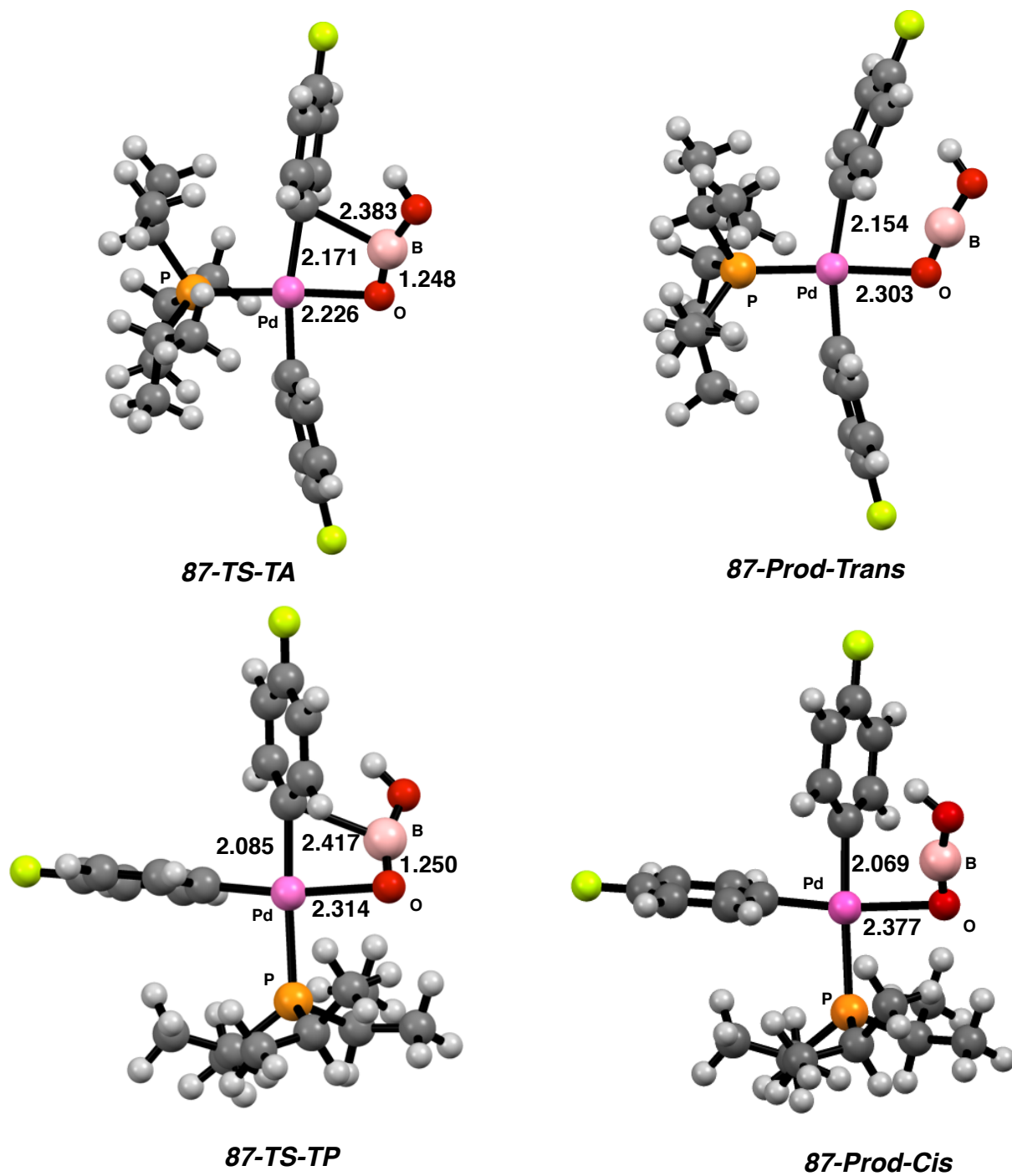
Figure 44. Transition-state and complexed product structures for transmetalation of **87.**

3.5 Conclusions

The combination of low temperature and rapid injection NMR spectroscopic analysis has allowed the unambiguous demonstration that Pd-O-B linkages form prior to the transmetalation event in the Suzuki-Miyaura cross-coupling reaction. Structures of the intermediates identified were assigned by NMR spectroscopy with the NOE and HMBC experiments being crucial in determining the bonding connectivity (Chapter 2). These structural assignments were supported by independent synthesis, which clearly demonstrated that under certain reaction conditions both path A and B can lead to pre-transmetalation intermediates. The ability to form Pd-O-B linkages provided the unprecedented opportunity to probe the effect of the phosphine ligand on both structure and reactivity. Furthermore a series of structural, kinetic and computational investigations revealed two mechanistically distinct pathways: (1) transmetalation *via* a 6-B-3 intermediate that dominates in the presence of excess phosphine, and (2) transmetalation *via* an anionic 8-B-4 intermediate that dominates in mono-ligated or *cis*-chelated systems. The demonstration of a direct transmetalation event from a tri-coordinate boron center (complex **86**) challenges the current dogma that boron must have base activation prior to transmetalation. Overall, the critical feature that enables the transfer of the organic fragment from boron to palladium is the availability of an empty coordination site on the palladium atom. The importance of a coordinatively unsaturated palladium atom was revealed by both the inverse first order dependence on *i*-Pr$_3$P and inhibitory effects of water for the formation of cross-coupling product from the 6-B-3 intermediate **71**. The importance of a subligated palladium atom was further demonstrated by the DFT calculations and rapid transmetalation observed in 8-B-4 complex **105** that contained a single *i*-Pr$_3$P ligand bound to palladium. Further effects of solvent, boron sources and additives on the transmetalation event are discussed in Chapter 4.

CHAPTER 4: Kinetic and Computational Characterization of Pre-transmetalation Intermediates in the Suzuki-Miyaura Reaction with Aryl Boronic Acids

4.1 Introduction

Currently, the Suzuki-Miyaura reaction is arguably the most practiced carbon-carbon forming reaction practiced in both academics and industrial settings as recognized by its share in the 2010 Nobel prize.[6a] The success of this coupling technology originates in its organo boron donor reagents innate ability to undergo rapid transmetalation with transition metals such as palladium and rhodium as well as the coinage metals in the presence of base.[82] Moreover, these reagents are straightforward to prepare, exceptionally stable, and environmentally benign.[83] From a historical perspective (1979) the first coupling reported was between catechol alkenylboranes and bromoalkenes (Scheme 42, 1). In 1981, Suzuki and Miyaura demonstrated that organoboronic acids could lead to favorable cross coupling reactions with organohalides (Scheme 42, 2).[84]

Scheme 42
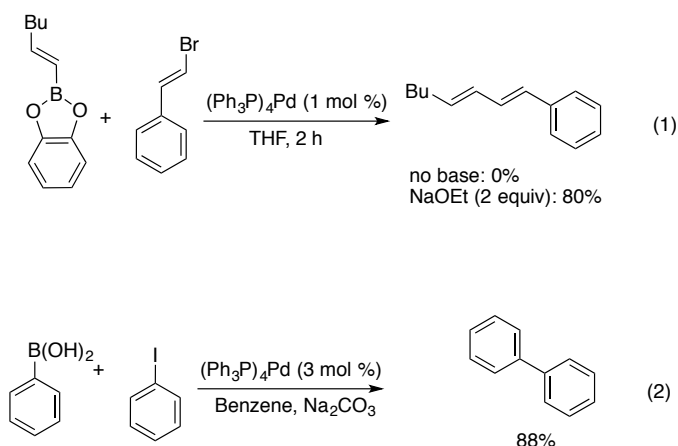
Currently, boronic acids are the most employed coupling reagent in both the academic and industrial settings because of their ease of preparation and high atom economy. The primary method of preparing boronic acids is the trapping of organo lithium or magnesium reagents with boric esters such as $B(O\text{-}i\text{-}Pr)_3$ and $B(OMe)_3$ followed by an acidic workup (Scheme 43, 1).[85] However, this method suffers from low functional group compatibility because of the employment of the lithium or magnesium based reagents and furthermore these reagents also can effectively serve as cross-coupling partners (Kumada). To circumvent this problem many mild methods of generating boronic acids have been developed which include boronic ester hydrolysis and palladium catalysis (Scheme 43, 2 and 3).[86]

Scheme 43
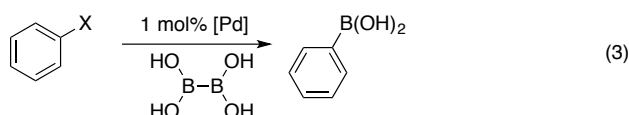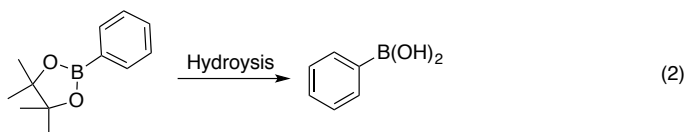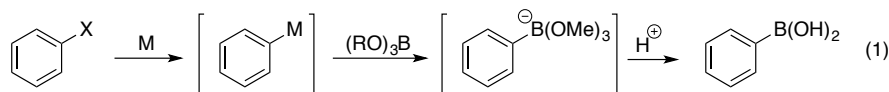
Boronic acids have been employed in the commercial synthesis of BASFs fungicide Boscalide[87] on more than a 1000 tonnes annually with a Suzuki-Miyaura cross coupling of an arylboronic acid being a key step.[88] Additionally, Merck's and Abbott laboratories have made extensive use of arylboronic acids in the synthesis of Losartan[89] and ANT-963[90] respectively on multikilogram scale (Figure 45). Additionally, countless examples of using these reagents have been employed in total synthesis of natural products.[91]

Boscalid   **Losartan**   **ABT-963**
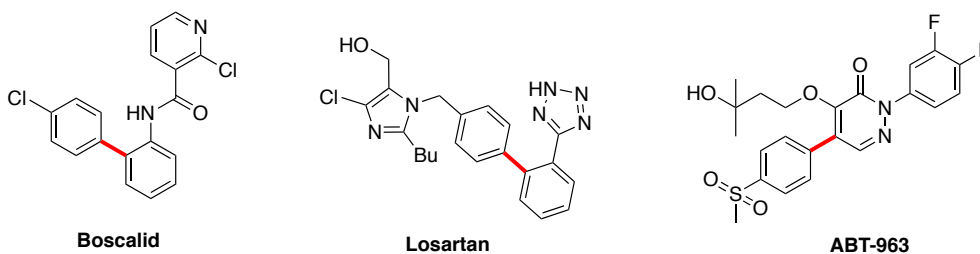
Figure 45. Industrial examples of late stage coupling with boronic acids.

However, these reagents are not without limitations as coupling partners such as vinyl, cyclopropyl, and electron rich heterocyclic derivatives are prone to undergo protodeboronation and oxidation. As these functional groups are ubiquitous in active pharmaceutical agents, especially heterocycles, intense effort over the past 30 years has gone into the development of a variety of masked reagents which include boronic esters, trifluoroborates and MIDA boronates to increase the stability of these coupling partners (Figure 46). [The masking term was defined by Lloyd Jones and co-workers: masking is distinct from "protection" because protection requires that a deprotection step take place prior to use.[88]]
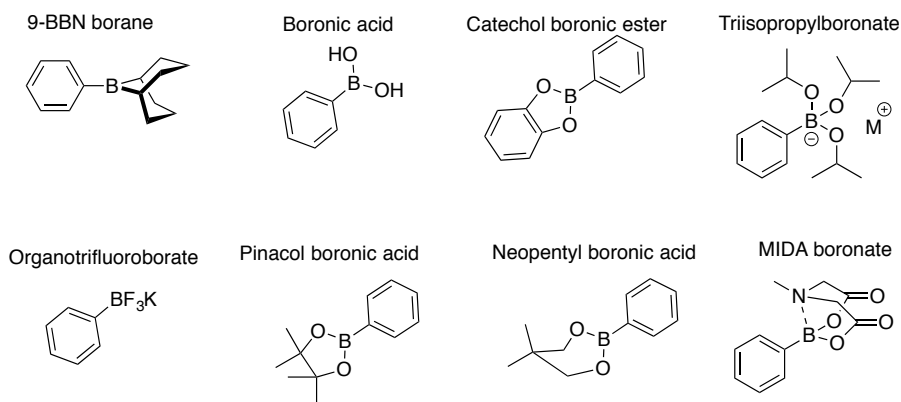
Figure 46. Examples of some of the most popular boron coupling partners.

4.2 Background

4.2.1. Boronic esters

Boronic esters exhibit greater chemical stability than their corresponding boronic acids for a number of reasons.[92] The primary reason is that the Lewis acidity of the boron atom is lower due to the increased overlap of the oxygen lone pairs into boron's empty p orbital. Furthermore, these reagents are often liquids or free flowing powders which makes for the ease of isolation during synthesis. Two of the most common methods of accessing boronic esters is the hydroboration[93] of alkenes or alkynes and the Miyaura borylation[94] protocol. The Miyaura borylation protocol is a palladium catalyzed cross coupling reaction between an aryl or alkenyl halide with *bis*-pinacol borane as the typical borane source. Additionally, CH activation[95] protocols have also been developed that have found widespread use. Moreover, boronic acids readily condense with alcohols or diols under dehydrating conditions such as a Dean Stark apparatus making them easily accessible (Scheme 44).

Scheme 44

Hydroboration

(1)

Miyaura borylation

(2)

C-H activation

(3)

Condensation

(4)
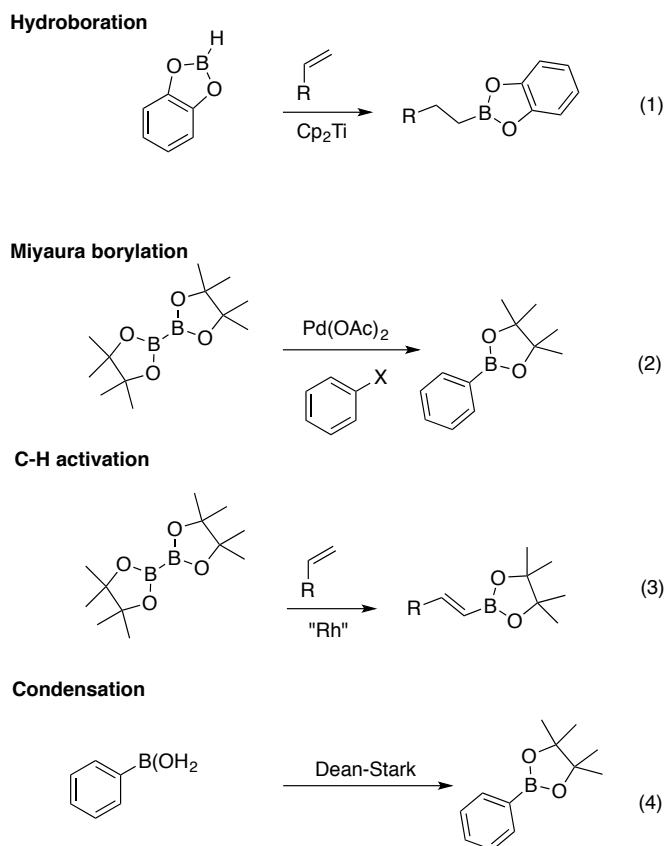
Boronic esters, especially pinacol boronates, have been employed as late stage coupling partners in many convergent syntheses of active pharmaceuticals agents. Two illustrative examples from Abbott Laboratories include the synthesis of kinase inhibitor ABT-869 which is under development for a possible cancer treatment and diacyl glycerolacyltransderase inhibitor DGAT-1.[96,97] Additionally, a potent and selective mesenchymal epithelial transition factor/anaplastic lymphoma kinase inhibitor Crizotinib has been synthesized *via* a late stage Suzuki-Miyaura coupling (Figure 47).[98]
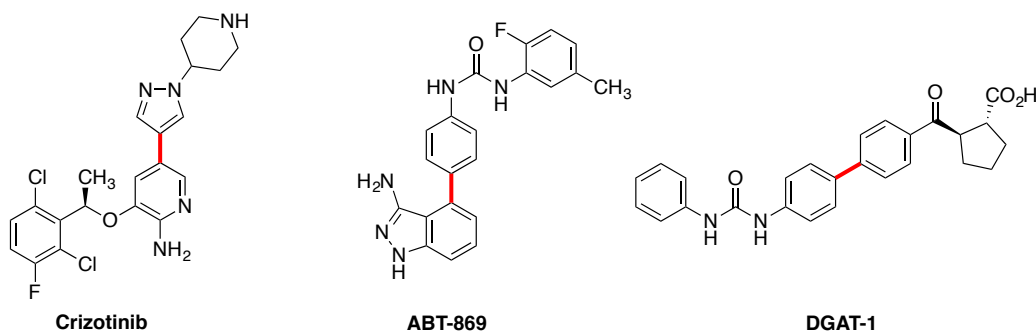
Figure 47. Industrial examples of late stage coupling with boronic esters.

While, boronic esters enjoy increased stability on the bench they are prone to hydrolysis. As almost half of the reported Suzuki-Miyaura cross coupling reactions reported from 1981 to 2011 are performed under basic biphasic systems it is suspected that the boronic esters are typically unmasked under the reaction conditions.[39] Therefore, it is difficult to control the release of the valuable organic coupling partner which can be problematic and lead to decomposition as described above. Therefore, intense effort has gone into the development of masking agents that allow for slow or controlled release under the reaction conditions. Two of the most developed systems are N-methylimidodiacetic acid esters "MIDA boronates" by Burke and co-workers[99] and potassium trifluoroborates by Molander and co-workers.[100]

4.2.2. MIDA boronates

The N-methylimidodiacetic acid esters "MIDA boronates" have substantial chemical stability over boronic acids and esters because the boron atoms valences are saturated. The quaternisation of the boron atom makes these compounds free flowing powders that are stable to column chromatography and other standard purification techniques. The most common method of preparing these compounds is to condense boronic acids with methylimidodiacetic acid using a Dean Stark apparatus (Scheme 45).

Scheme 45
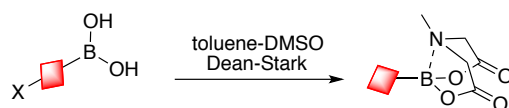
MIDA boronates have found great utility as iterative cross-coupling partners in the synthesis of natural products by the development of halo-MIDA building blocks which has been applied to the synthesis of antifungal heptaene amphotericin B.[101] The key to this coupling technology is the ability to control when the active coupling partner (boronic acid) is released. Specifically, MIDA boronates can be unmasked (hydrolysis) within minutes with aqueous NaOH at room temperature or remain relatively untouched by K_3PO_4.[102,103] This allows for high chemoselectivity when multiple boron centers are present (Figure 48). Recently, Burke, Lloyd Jones, Cheong, and Houk identified two general mechanisms for the hydrolysis of MIDA boronates that differed in ester *vs* B-N cleavage.[104] First, under the KOH conditions, the fast

release, was found to predominantly undergo rapid ester cleavage. Secondly, under K_3PO_4 conditions the reagents were unmasked slowly by a B-N cleavage event.
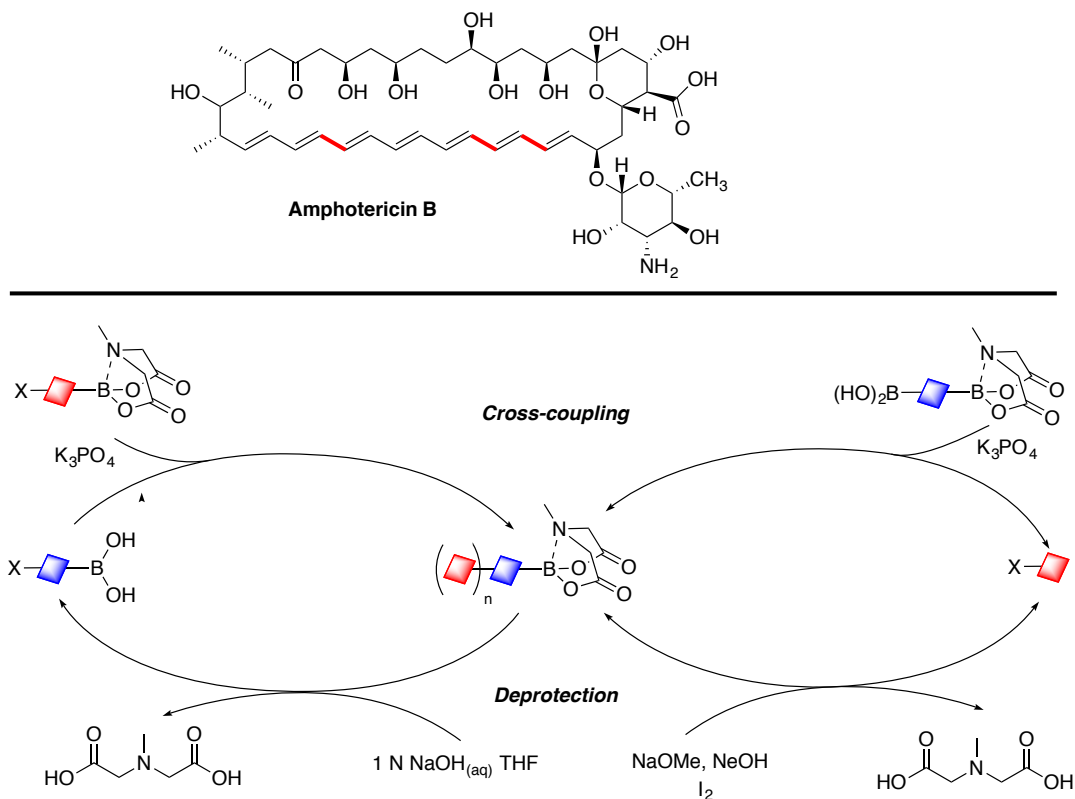
Figure 48. Iterative cross-coupling method with MIDA boronates.

4.2.3. Potassium Trifluoroborates

In 1960, potassium trifluoroborate salts were characterized by Chambers; however, the utility of these reagents remained overlooked for almost 30 years.[105] While Genet[106] demonstrated the first cross-coupling with potassium trifluoroborate salts it was Molander[107] who ultimately developed these reagents.[108] These reagents exhibit similar stabilities to MIDA boronates described above because the boron atom is also quaternized. These reagents are predominantly free flowing powders that are typically prepared from the combination of HKF_2 to the boronic acid of choice. Due to the corrosive nature of HKF_2 milder methods have also been developed for the installation of fluoride by KF/tartaric acid (Scheme 46).[109,110]

Scheme 46
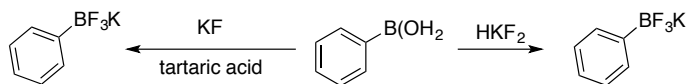
Potassium trifluoroborates, have been employed as late stage coupling partners in many convergent syntheses in both synthetic and natural products as well as active pharmaceuticals agents.[111] An illustrative example is the late stage installation of a vinyl group in the large scale synthesis of 4-hydoxyethylsulfonylstyrene.[112] Additionally, a key carbon-carbon forming event in the synthesis of oximidine II was found to be effective by Molander and co-workers (Figure 49).[113]
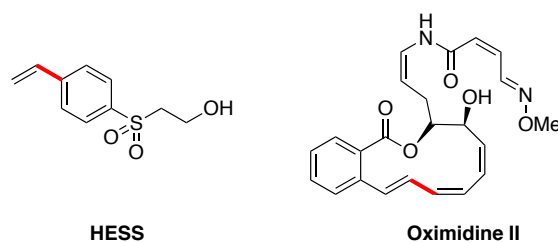
Figure 49. Examples of some of the most popular boron coupling partners

While, potassium trifluoroborates enjoy increased stability on the bench they must be hydrolyzed under the reaction conditions for the coupling reaction to take place. Indeed, an investigation by Lloyd Jones and co-workers demonstrated that a prior hydrolysis step precedes the cross-coupling event.[114] Moreover, the unmasking event was found to be greatly affected by the pH of the solution, vessel and substrate indicating the reason why these reactions are often hard to control.

4.3 Objectives

While the reagents mentioned above have all been well documented to work under Suzuki-Miyaura reaction conditions the precise manner in which the reagents undergo the crucial transmetalation event is lacking. A recent review by Lennox and Lloyd-Jones states that:

"Evidently boronic esters exhibit greater stability than their corresponding boronic acids, but it is not clear what the active transmetalating species is during their Suzuki-Miyaura coupling."[116]

The aim of the research presented in this chapter is to determine if pre-transmetalation

intermediates can be formed from boronic esters by low temperature NMR spectroscopy. Specific goals include: (1) full characterization of reaction intermediates such as the pre-transmetalation species; (2) demonstration of the kinetic competence of the characterized species containing Pd-O-B linkages to form cross-coupling product, and (3) quantum mechanical simulation of the transmetalation process involving these intermediates.[115]

4.4 Results and Discussion

4.4.1. Reactions of L₂PdOH with arylboronate esters

The results presented in this section involve reactions between *trans*-(i-Pr₃P)₂(4-FC₆H₄)Pd(OH) (**70**) and various arylboronate esters at low temperature (neopentyl, pinacol and catechol). It should be noted that this line of investigation presented below was performed prior to the synthesis of 1:1 B/Pd Pd-O-B linkages as described above. However, these results disserve some comment.

Addition of a THF solution of neopentyl ester **117** (1.0 equiv/Pd) to *trans*-(i-Pr₃P)₂(4-FC₆H₄)Pd(OH) (**70**) in THF with 4.0 equiv of i-Pr₃P at −78 °C followed by warming to −60 °C resulted in the observation of some cross coupling product **75** (<5%) by ^{19}F NMR spectroscopy (Scheme 47, Figure 50). Interestingly, while the palladium complex **70** remained unchanged the ^{19}F NMR signal corresponding to ester **112** was extremely broadened. A possible explanation of the observed broadening is a rapid equilibrium between the starting materials.

Scheme 47
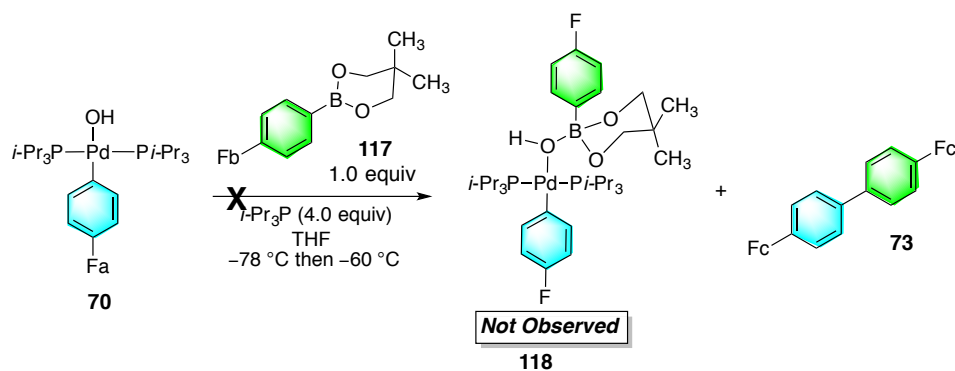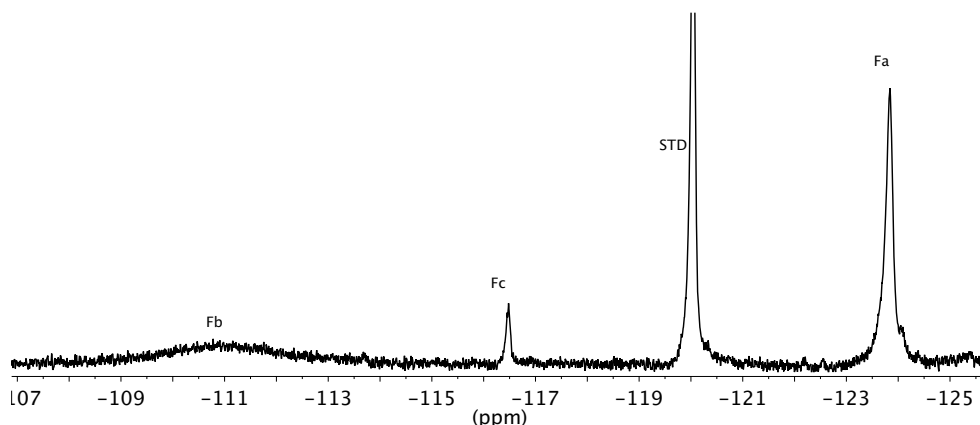
Figure 50. ^{19}F NMR spectrum of reaction mixture of **70** and **117.**

Similarly the addition of a THF solution of pinacol ester **119** (1.0 equiv/Pd) to *trans*-(*i*-Pr$_3$P)$_2$(4-FC$_6$H$_4$)Pd(OH) (**70**) in THF with 3.0 equiv of *i*-Pr$_3$P at −78 °C followed by warming to −60 °C resulted in no detected intermediate. This suggests that the boron atoms in esters **119** and **117** are not sterically accessible or Lewis acidic enough to coordinate with **70**.

Scheme 48
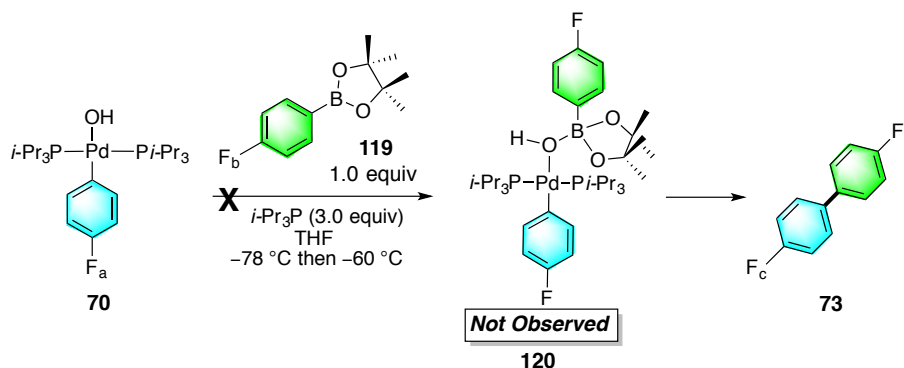
The last ester investigated with *trans*-(*i*-Pr$_3$P)$_2$(4-FC$_6$H$_4$)Pd(OH) (**70**) was the catechol ester **121**. Interestingly, upon the addition of a THF solution of catechol ester complex **121** (1.0 equiv/Pd) to *trans*-(*i*-Pr$_3$P)$_2$(4-FC$_6$H$_4$)Pd(OH) (**70**) with 3.0 equiv of *i*-Pr$_3$P in THF at −78 °C followed by warming to −60 °C resulted in new signals by ^{19}F NMR spectroscopy (Scheme 49, Figure 51). At least one new species was being formed under these reaction conditions however the spectrum was difficult to interpret because of multiple fluorine signals were present. Therefore, our rapid injection apparatus was called into action.

Scheme 49
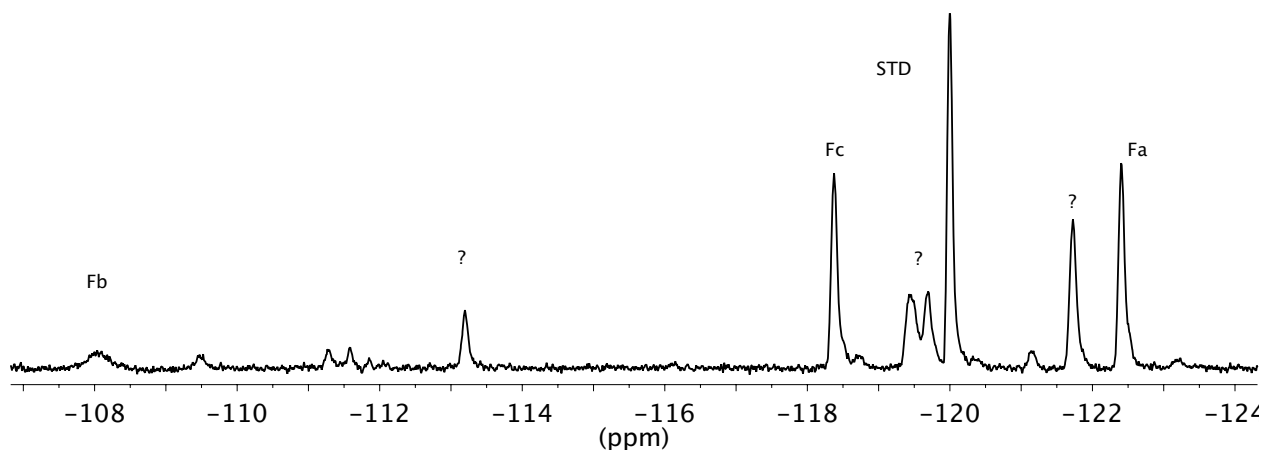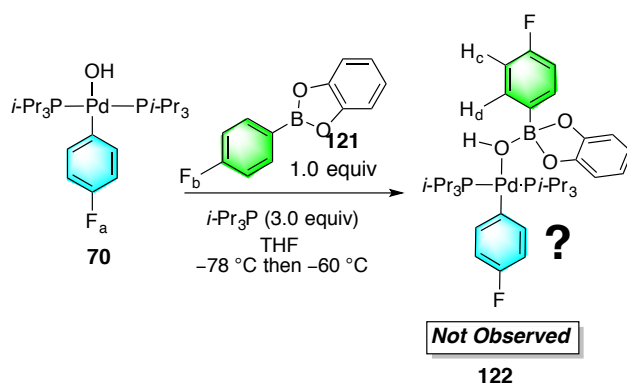
Figure 51. ^{19}F NMR spectrum of reaction of **70** and **121.**

Injection of catechol ester 1.0 equiv/Pd into a THF solution of complex **70** at −60 °C resulted in the instantaneous formation of a clean ^{19}F NMR spectrum containing two new signals at −121.98 ppm (F$_a$) and −119.58 ppm (F$_b$) (Figure 52). Interestingly, over a matter of minutes two broad peaks began to grow into the ^{19}F NMR spectrum at −120.77 ppm and −117.43 ppm (Figure 53). Upon collecting a ^{31}P NMR spectrum (after ~10 min) the mixture two signals were observed at 29.90 ppm (P$_1$) and 33.72 (P$_2$) along with unbound i-Pr$_3$P (Figure 54). The range of the ^{31}P NMR chemical shifts suggests that two i-Pr$_3$P ligands are bound to both complexes. Based on the similarity of both the ^{31}P and ^{19}F NMR chemical shifts between aqua cationic palladium complex **81** (^{31}P NMR at 33.02 ppm; ^{19}F NMR at −122.49 ppm) suggests that the catechol boronate displaced hydroxide from palladium complex **70** and formed a cationic palladium species **123**. Moreover, the ^{19}F NMR chemical shift at −119.58 ppm is in the diagnostic region for

tetracoordinate boron complexes such as cesium trihydroxyboronate **84** (−120.81 ppm) as described in Chapter 2. This result suggests that boron in catechol ester **121** is more Lewis acidic than the palladium atom in complex **70**.

Scheme 50
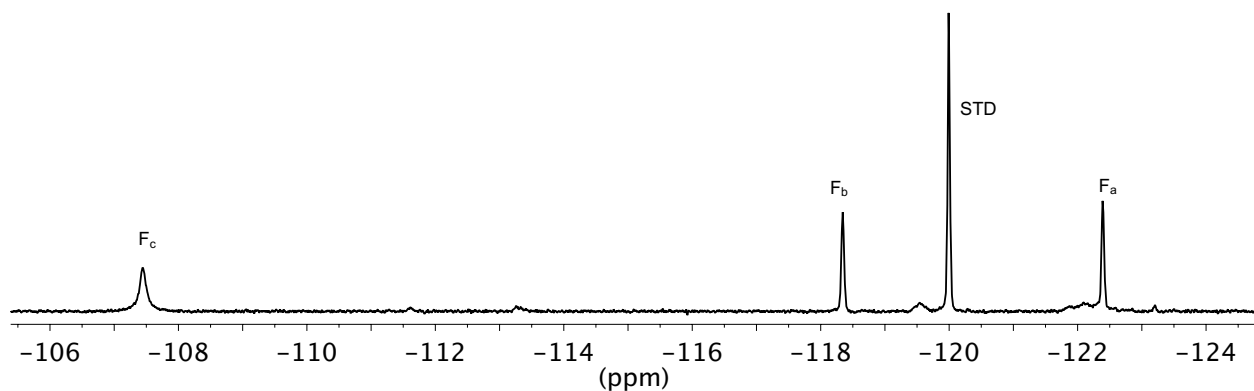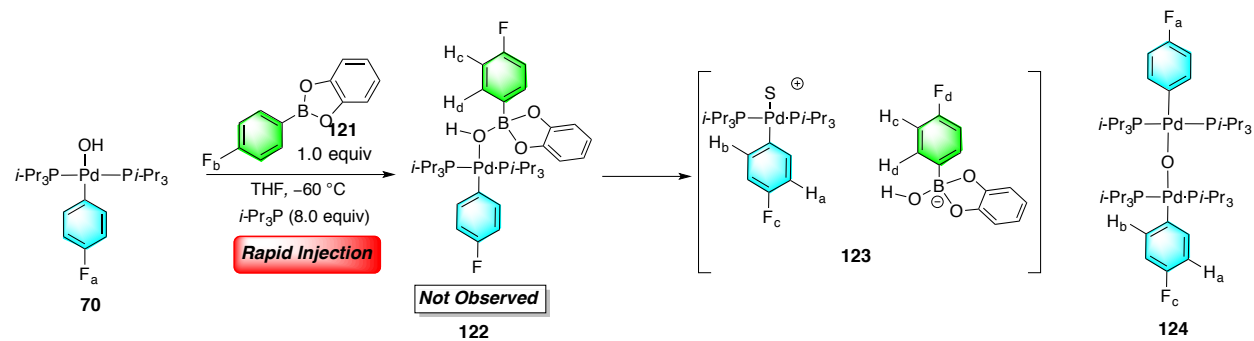
Figure 52. Initial ^{19}F NMR spectrum of reaction mixture of complex **70** and **121.**
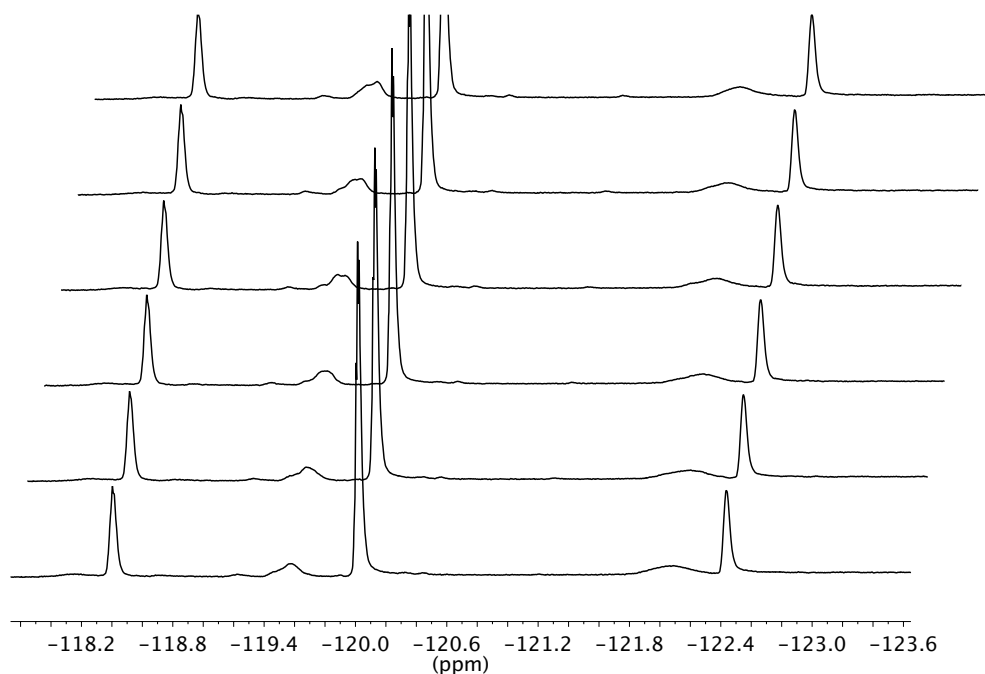
Figure 53. ^{19}F NMR spectra of reaction mixture of complex **70** and **121.**
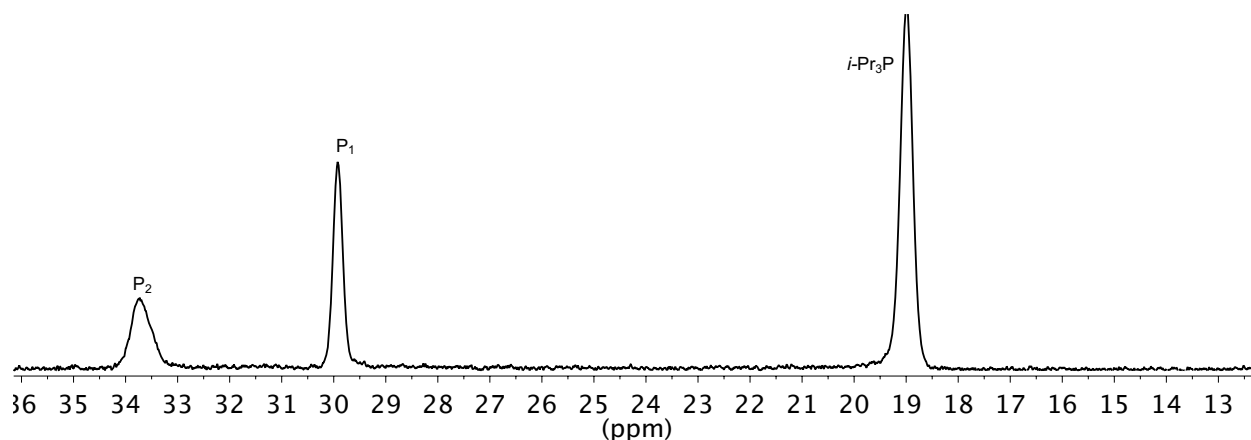
Figure 54. ^{31}P NMR spectrum of reaction mixture of complex **70** and **121.**

4.4.2. Investigations of [(i-Pr₃P)(4-FC₆H₄)Pd(OH)]₂ with 4-Fluorophenylboronic acid esters

The successful formation of Pd-O-B linkages with arylboronic acid **58** and dimethoxy ester **106** led to the investigation of whether some of the most common arylboronic esters (catechol, pinacol, and neopentyl etc.) utilized in the Suzuki-Miyaura reaction could also form stable, pre-transmetalation complexes.[116] Furthermore, the characterization of dimethyoxy ester Pd-O-B linkage **105** was investigated in pure THF.

The addition of a THF solution of dimethyoxy ester **106** (1.0 equiv/Pd) to a THF solution of **86** at −78 °C followed by warming to −55 °C resulted in the formation of two new complexes in a ratio of 60:40 by the observation of two new sets of ^{19}F NMR signals in a near 1:1 ratio. The first set of signals was assigned to complex **105** −121.58 ppm (F_a) and −118.85 ppm (F_b). The second set of signals was tentatively assigned as complex **125** −121.13 ppm (F_c) and −118.72 ppm (F_d) (Scheme 51, Figure 55). The observation of the two complexes in a 60:40 ratio is believed to be due to the kinetic binding of the boronic ester with the dimeric palladium complex as it exists in a 60:40 ratio typically. Furthermore, the ^{19}F NMR chemical shifts for complex **105** in THF/CH$_3$OH were measured to be −121.01 ppm (F_a) and −118.33 ppm (F_b) suggesting a solvent effect for the measurement of these chemical shifts. Moreover, this complex formed cross-coupling product **73** readily at this temperature. The ability to form two dimethyoxy ester Pd-O-B linkages in THF led us to investigate more typical alkyl ester used in the Suzuki-Miyaura reaction such as isopropyl ester **126**.

Scheme 51
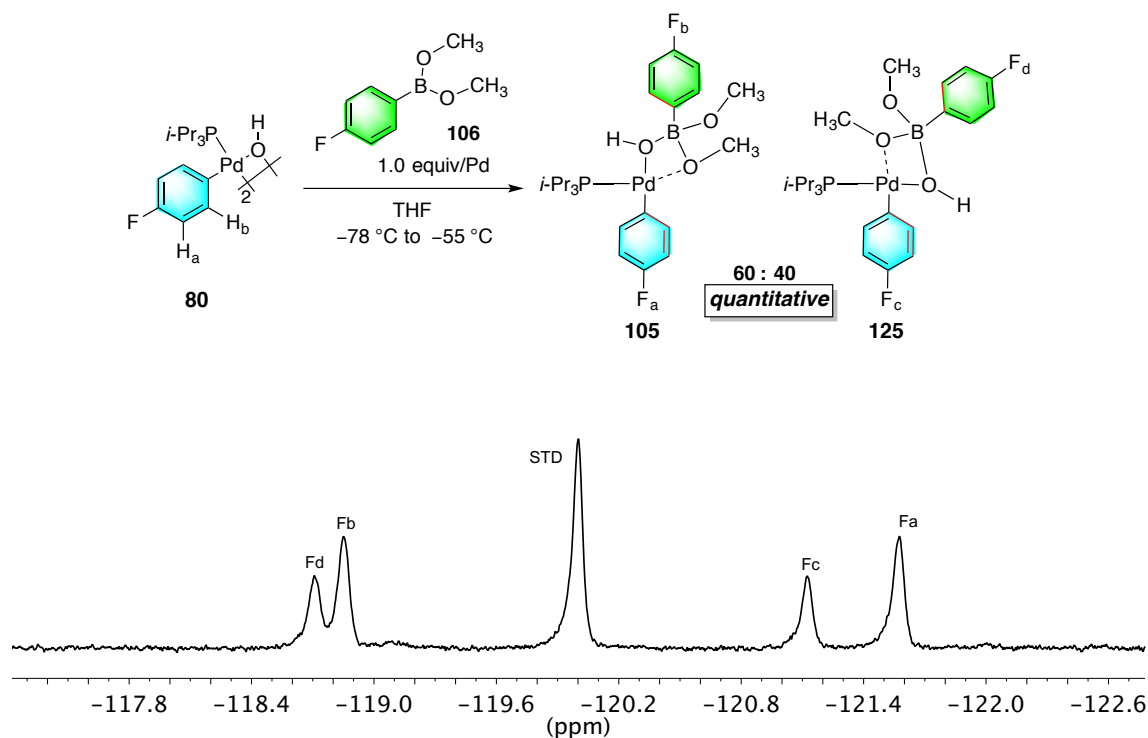
Figure 55. ^{19}F NMR spectrum of complex **105** and **125**.

Combining 1.0 equiv/Pd of isopropyl ester **126** with [(i-Pr$_3$P)(4-FC$_6$H$_4$)Pd(OH)]$_2$ (**80**) in THF at −78 °C followed by warming to −55 °C resulted in the observation of a ~75% conversion

of the starting materials to two new species in a c.a. 1:1 ratio by ^{19}F NMR spectroscopy. The first set of signals was assigned to complex **127** at −123.49 ppm (F_a) and −114.98 ppm (F_b). The second set of signals was tentatively assigned as complex **128** −123.10 ppm (F_c) and −114.35 ppm (F_d). Interestingly, allowing the reaction mixture to sit at −55 °C for ~1 h did not result in any further incorporation of the ester into the dimeric palladium complex. Warming the sample to −30 °C resulted in the formation of cross-coupling product **73**. The incomplete consumption of starting materials suggests that the system is at equilibrium. The isopropyl groups are bulkier and more electron rich than the dimethyl ester suggesting that both steric and electronic parameters are involved in the formation of pre-transmetalation intermediates. This led us to investigate cyclic aryl boronate esters because both sterics and electronics (ie Lewis acidity of the boron atom) can be easily tuned.

Scheme 52
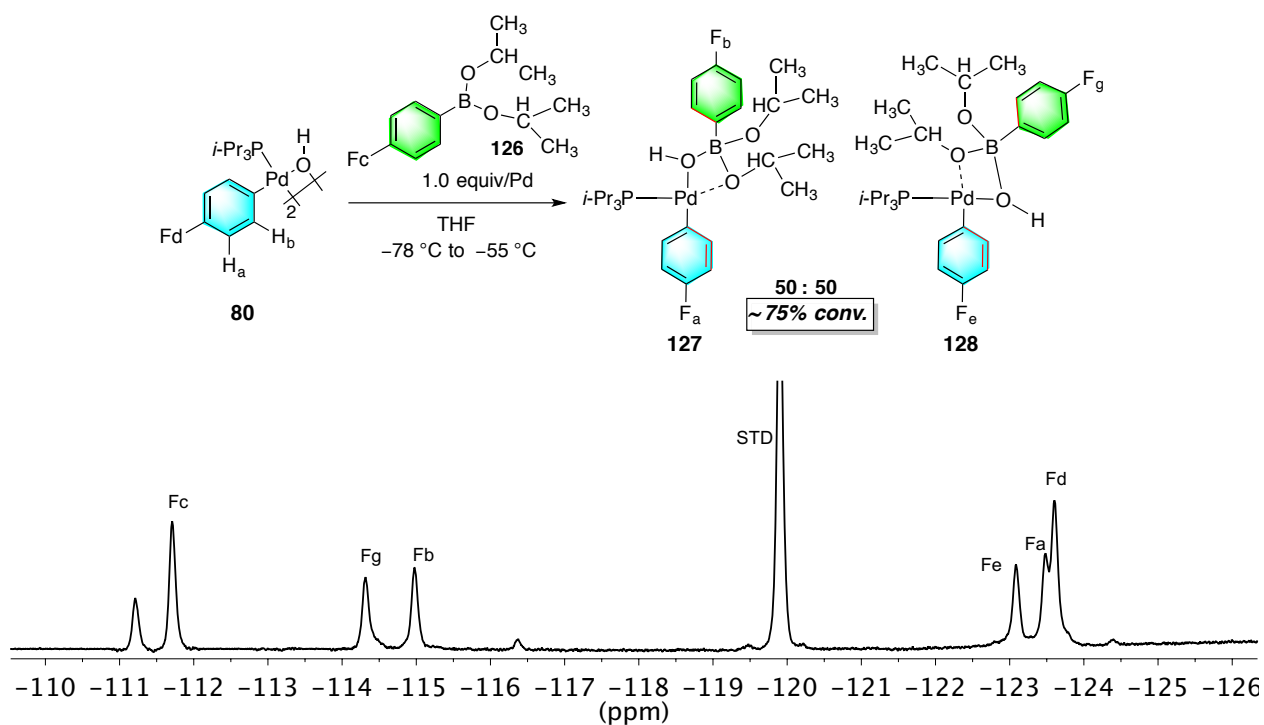
Figure 56. ^{19}F NMR spectrum of reaction mixture of **127** and **128**.

4.4.3. Investigations of [(i-Pr₃P)(4-FC₆H₄)Pd(OH)]₂ with cyclic 4-Fluorophenylboronic acid esters

The addition of a THF-d_8 solution of catechol ester **121** (1.0 equiv/Pd) to a THF-d_8 solution of **80** at −78 °C followed by warming to −55 °C produced complex **121** in quantitative yield by[1]H NMR spectroscopy (Scheme 53, Figure 57). It should be noted that this reaction was extremely sensitive to water and thus the THF-d_8 was freshly distilled over NaK prior to each experiment and the catechol ester **121** was freshly sublimed. The use of extensive 1D and 2D NMR techniques at −55 °C lead to the structure elucidation of the newly formed species as complex **121** containing a Pd−O−B linkage.

Scheme 53
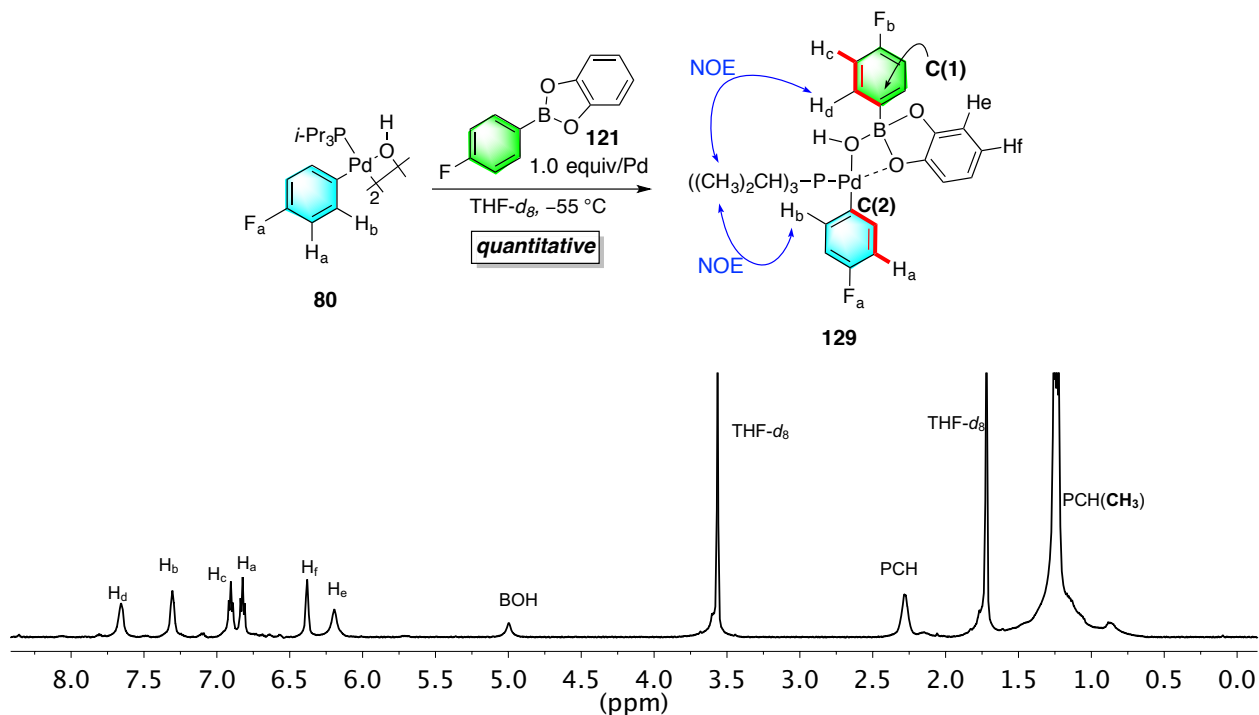
Figure 57. ^{1}H NMR spectrum of complex **129.**

The bonding connectivity of the new Pd−O−B linkage was established by the observation of NOE cross peaks between H_b, and H_d with the methyl hydrogens on the *i*-Pr₃P group. This interaction reveals that both aryl residues were proximal to the phosphines and thus established the presence of a Pd-O-B linkage. Additionally, no NOE cross peaks were observed between the

89

catechol hydrogens and the *i*-Pr$_3$P methyl groups because they are computationally predicted to be *trans* (Figure 58). Furthermore, the two possible isomers differ by ~2.5 kcal/mol signifying a greater thermodynamic stability for one complex over the other, suggesting the system is under thermodynamic control.

0.0 kcal/mol   **2.5 kcal/mol**
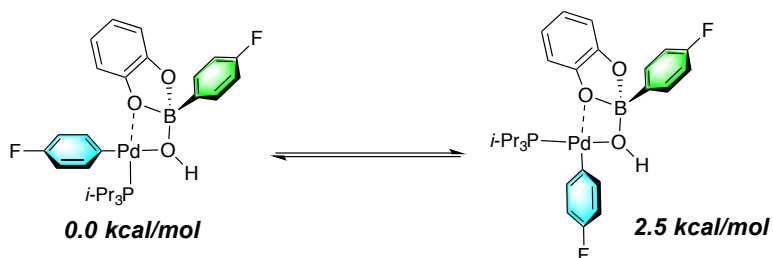
Figure 58. Ground state calculation of two possible intermediates.

The identity of the carbons bound to the boron and palladium atoms C(1) and C(2) were revealed in the HMBC (^{1}H-^{13}C) spectrum by the observation of cross peaks between the H$_c$ and H$_a$ hydrogens with the ^{13}C signals at 144.52 ppm (C(1)) and 136.85 ppm (C(2)) respectively (red bonds) (Figure 59).
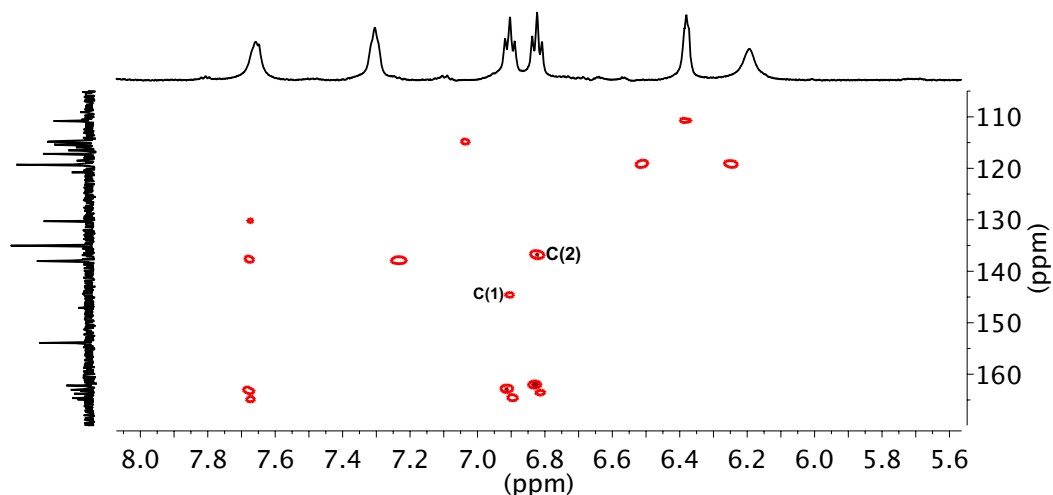
Figure 59. gHMBC spectrum of complex **129**.

Furthermore, the ^{11}B NMR spectrum displayed a signal at 12 ppm, well within the tetracoordinate regime (Figure 60). Interestingly, the broad ^{11}B NMR signal suggests that rapid exchange is present as evident by the observation of only one of two possible isomers by NMR spectroscopy.
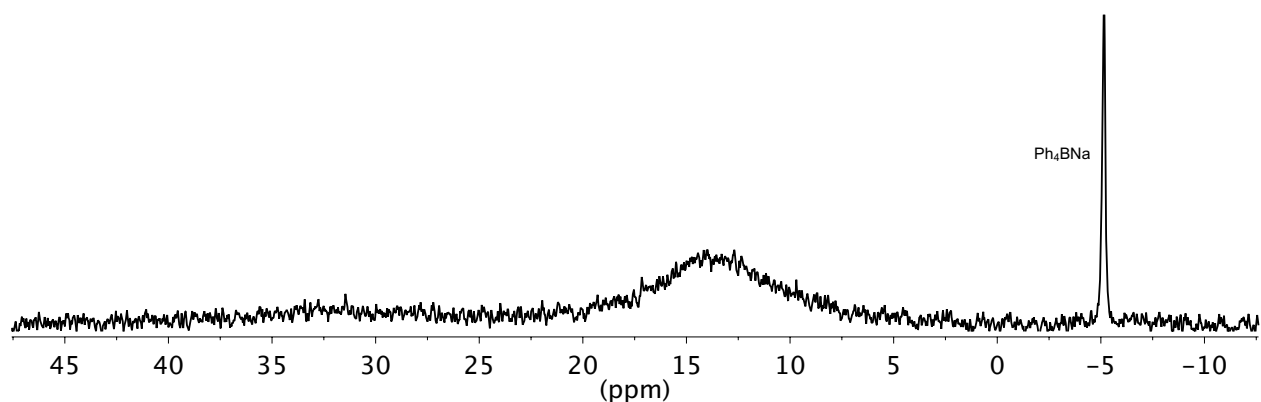
Figure 60. ^{11}B NMR spectrum of complex **129**.

Additionally, at −55 °C the ^{19}F NMR signals for (F$_a$) and (F$_b$) were observed as broad singlets with values of −120.77 ppm and −117.43 ppm respectively. This broadening is believed to be an effect of exchange or a rocking motion imparted by the catechol ring rotation (Figure 61).
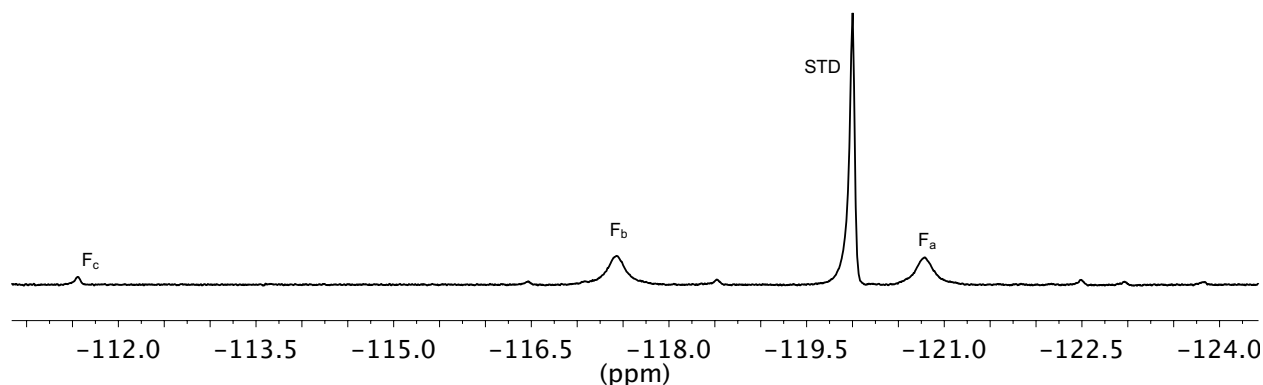
Figure 61. ^{19}F NMR spectrum of complex **129**.

The smooth formation of a Pd-O-B linkage with catechol ester **121** led us to investigate the steric and electronic steric parameters on the formation of Pd-O-B linkages with 5-membered ring boronic esters. Therefore, upon addition of 2.0 equiv of pinacol ester **119** to complex **80** at −78 °C followed by warming to −55 °C in THF resulted in no complex formation by ^{19}F NMR spectroscopy (Scheme 54, Figure 62). Even upon warming to −30 °C no complexation was observed. Furthermore, the ^{19}F NMR signals remained as sharp singlets indicating that no dynamic process was evident (Figure 62). The lack of formation of a Pd-O-B linkage is possibly due to the steric bulk imparted by the methyl substitutions on the pinacol ester. Therefore, our next line of investigations involved the glycol ester **131**.

Scheme 54
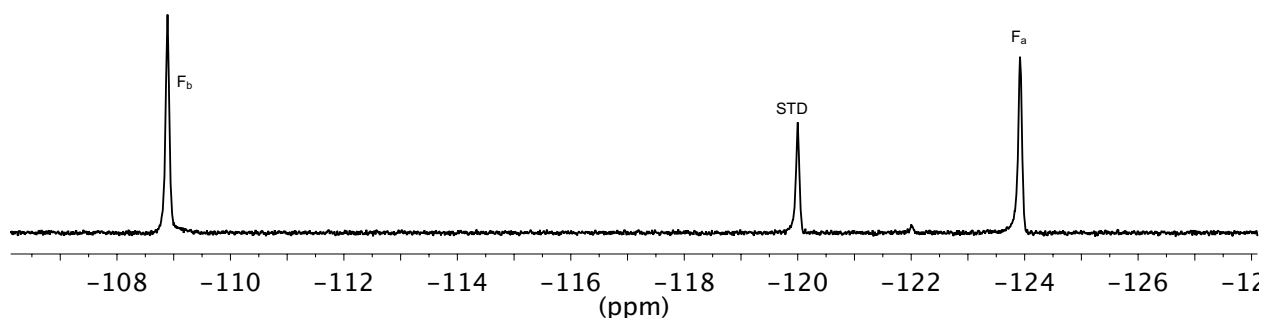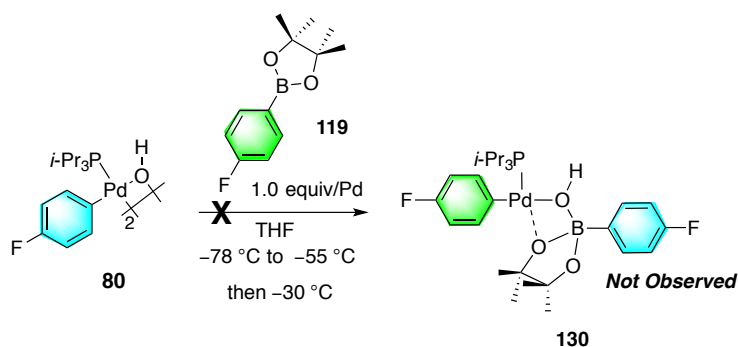
Figure 62. ^{19}F NMR spectrum of complex **80** and pinacol ester **119**.

Addition of a THF solution of glycol ester **131** (1.0 equiv/Pd) to dimeric complex [(*i*-Pr$_3$P)(4-FC$_6$H$_4$)Pd(OH)]$_2$ (**80**) in THF-d_8 at −78 °C followed by warming to −55 °C resulted in the conversion of the starting materials to two new complexes by ^{19}F NMR spectroscopy in a ~90:10 ratio (Scheme 55, Figure 64). The major complex **132** displayed ^{19}F NMR signals at −121.65 ppm and −118.70 for F$_a$ and F$_b$ respectively. The minor complex **131** displayed ^{19}F NMR signals at −121.97 ppm and −119.16 for F$_g$ and F$_e$ respectively.

Scheme 55
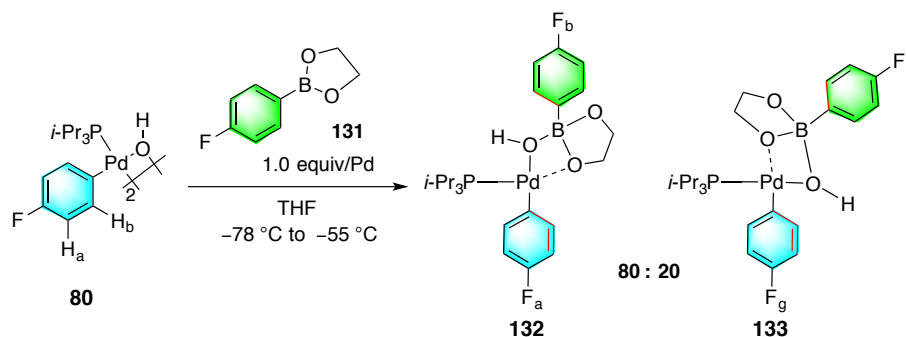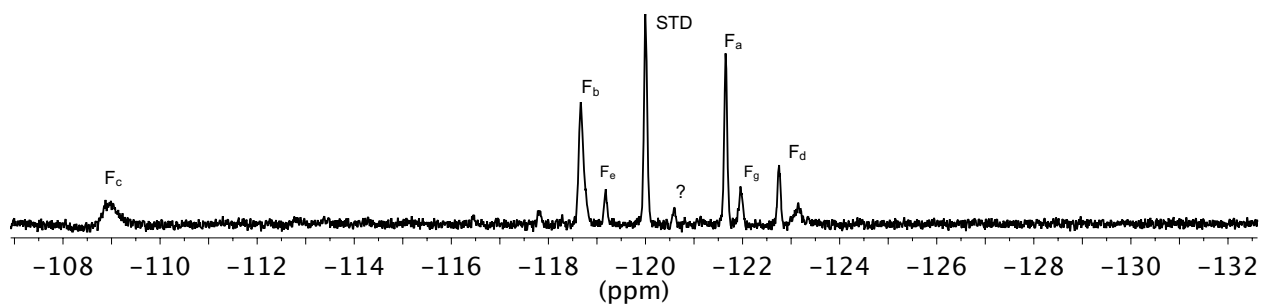
Figure 63. ^{19}F NMR spectrum of complex **132** and **127.**

These complexes are most likely the result of two different isomers as depicted in Figure 64. The observation of two complexes is supported by the calculated ground states that only differ by 1.5 kcal/mol indicating that both isomers could be observed experimentally (Figure 64).
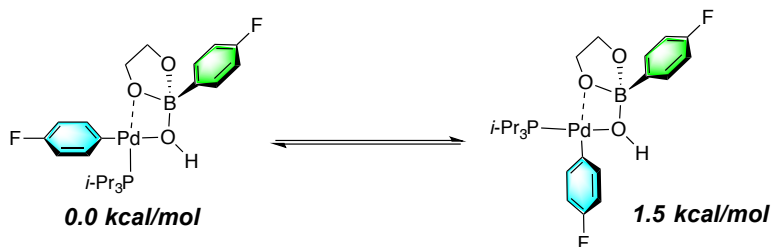
Figure 64. Ground state calculation for complex **132** and **133**.

The observation of two complexes with the glycol ester and not the catechol ester is most likely not the result of the Lewis acidity of the boron atom, but the increased Lewis basicity of the oxygen atoms. This is a difficult parameter to probe because the boron and oxygen atoms interact with one another. However, upon binding the boron atom with Pd-OH should increase the Lewis basicity of the oxygen atoms making them stronger binders to palladium. As outlined in chapter 3 the necessity of an empty coordination site on palladium is essential to induce transmetalation. Therefore, the next line of investigation involved the development of electron deficient boronate esters.

On this note we prepared 2-hydroxy-2-methyl propanoic acid boronate ester **134** by condensing the propanoic acid with 4-fluorophenylboronic acid **58** using a dean stark apparatus packed with 3 Å molecular sieves (Scheme 56).

Scheme 56
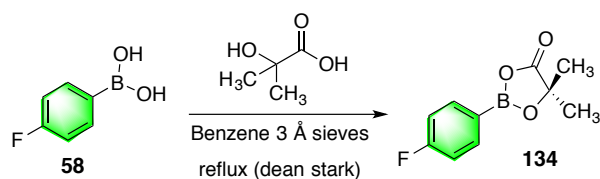
Combination of ester **134** (1.0 equiv/Pd) to dimeric complex **80** in THF at −78 °C followed by warming to −55 °C resulted in two new broad signals in the ^{19}F NMR spectrum at −117.56 and −121.07 ppm which were assigned to complex **135** (Figure 65). The broadness of the signals in Pd-O-B linkage **135** is suspected to be the result of a rapid equilibrium between complex **135** and the staring materials.

Scheme 57
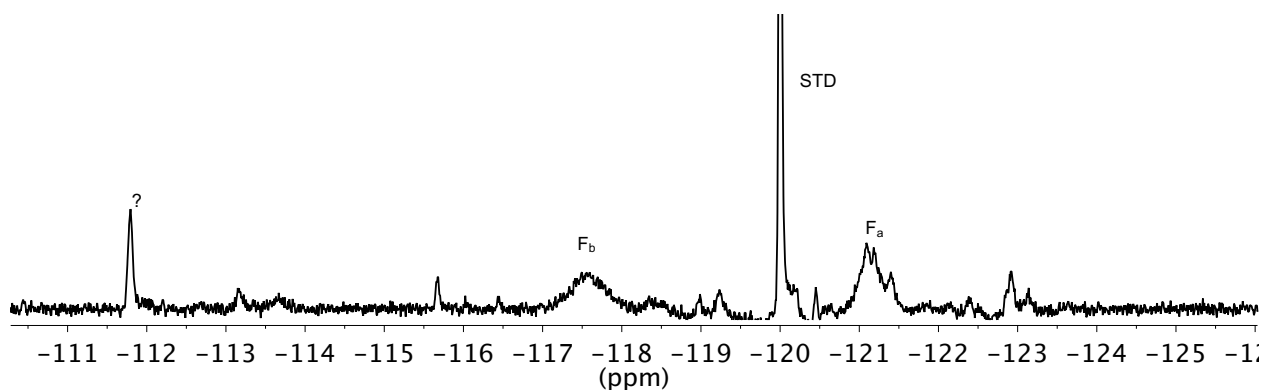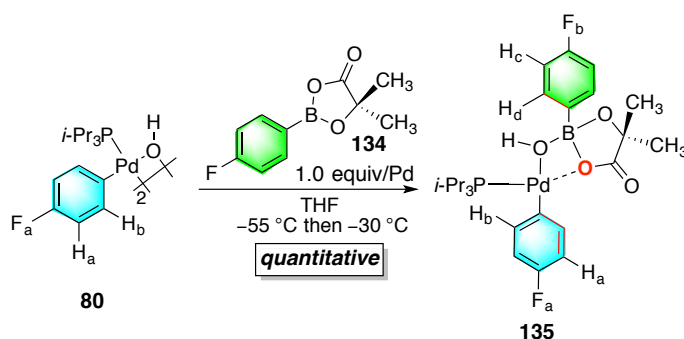
Figure 65. ^{19}F NMR spectrum of complex **135**.

Finally, neopentyl ester **117** was investigated. Addition of a THF solution of neopentyl ester **117** (1.0 equiv/Pd) to dimeric complex [(*i*-Pr₃P)(4-FC₆H₄)Pd(OH)]₂ (**80**) in THF at −78 °C followed by warming to −55 °C resulted in no change in the ¹⁹F NMR spectrum. Even upon warming to −30 °C no Pd-O-B linkage was observed (Scheme 58). The lack of intermediate formation with pinacol **119** and neopentyl **117** esters **117** with **80** suggests that both sterics and electronics play a role in the formation of intermediate complexes.

Scheme 58
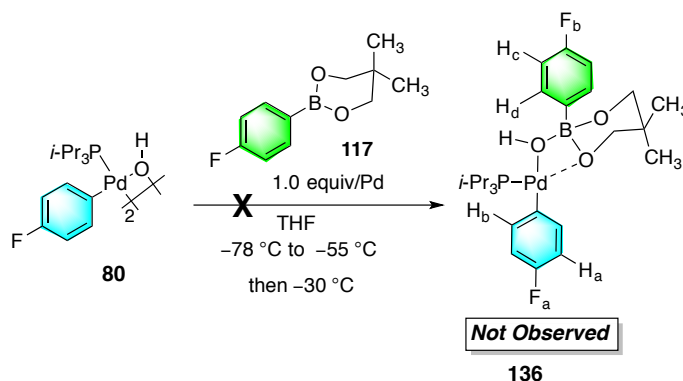
4.5 Kinetic Analysis of Aryl Group Transfer from Pd-O-B Complexes

Catechol ester complex **129** was prepared as described in Section 4.4.2. by the addition of a THF solution of **121** (1.0 equiv/Pd) to a THF solution of **80** at −78 °C. To establish the kinetic behavior, the sample was warmed to −30 °C and the ¹⁹F NMR signals for both **129** and **73** were monitored (Scheme 59). First order plots of [**129**] and [**73**] *versus* time were fitted using functions [A]=[A]₀e^{−kt} and [P]=[A]₀(1−e^{−kt}) respectively, where [A] is the concentration of **129**, [A]₀ is the initial concentration of **129**, [P] is the concentration of **73**, k is the rate constant, and t is time. These functions provided accurate values for k (the observed kinetic constant) for the decay of **129** ($2.74 \pm 0.32 \times 10^{-3}$ s⁻¹) and the formation of **73** ($2.60 \pm 0.17 \times 10^{-3}$ s⁻¹) (Figure 66, Table 10). Interestingly, the measured rate of transfer is approximately 4.5 times faster than arylboronic acid **58** suggesting that the coordination site on palladium is easily accessed by breakage of the less electron rich ester Pd-O-B bond. Furthermore, the experimentally measured Gibbs free energy of 16.99 ± 0.06 kcal/mol is in good agreement with the calculated Gibbs free energy 17.7 kcal/mol

indicating that complex **129** is most likely the complex that is transferring its organic group. Moreover, the similarity of rates for appearance of **73** and consumption of **129** suggests that transmetalation is the rate-determining step for this process. This led to a series of kinetic investigations with various arylboronate esters.

Scheme 59
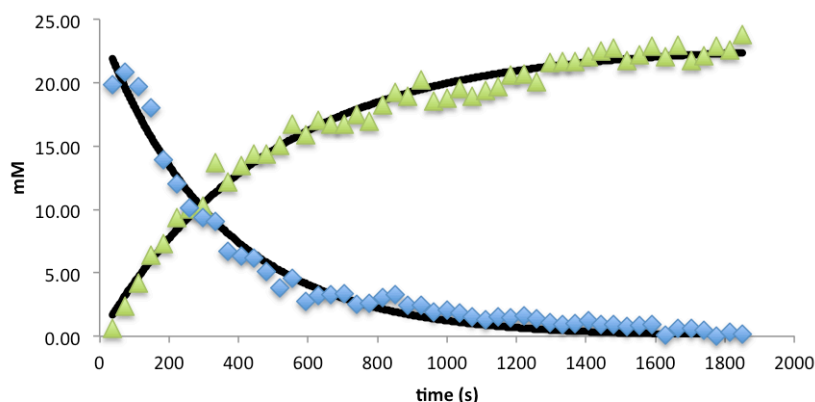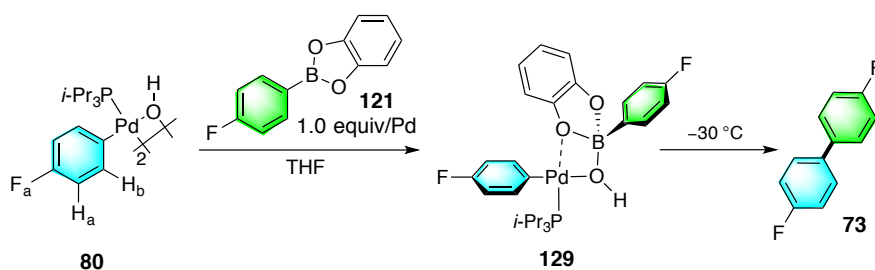
Figure 66. Decay of complex **129** and formation of **73** at −30 °C.

Glycol ester complex **132** was prepared by the addition of a THF solution of **80** (1.0 equiv/Pd) to a THF solution of **131** at −78 °C. To establish the kinetic behavior, the sample was warmed to −30 °C and the ^{19}F NMR signal for the formation of cross coupling product **73** was monitored and found to provide a first order rate constant of $k = 2.60 \pm 0.17 \times 10^{-3}$ s^{-1}. Furthermore, the experimentally measured Gibbs free energy of 16.22 ± 0.1 kcal/mol is in good agreement with the calculated Gibbs free energy 15.9 kcal/mol. The decay of complex **132** was not monitored because of signal broadening and enhanced rate of its decay. Unlike the catechol ester complex **129** the glycol ester was found to transfer its aryl group ~23 times faster than the arylboronic acid **58** and ~5 times faster than the catechol ester **129** indicating that the *ipso* carbon bound to the boron atom in the catechol ester was less nucleophilic than the glycol ester as it

contains an electron withdrawing entity. Interestingly, the dimethyoxy ester complex **106** displayed similar magnitudes for aryl group transfer as the glycol ester complex **132** suggesting that the alkyl substituents are playing similar roles (entry 4).

Attempts to measure rates for the formation of cross-coupling product from pinacol ester **119** (Figure 68) and neopently ester **117** resulted in sigmoidal kinetics that could not be fitted using a first order decay. Furthermore, the S-shaped curves could not be fitted with a first order auto-catalytic equation **1** as described earlier suggesting that this process was more complicated than other complexes. However, the pinacol ester did react over ~5.5 h to form cross-coupling product **73** where the arylboronic acid **58** complex takes roughly 45 min to fully form cross coupling product **73**. Similarly, the neopentyl ester also took longer to form (~1.5 h) cross-coupling product **73**. We suspected that the formation of cross coupling product was inhibited in esters **117** and **119** due to the increased sterics. Because the pinacol and neopently esters did not form an observable intermediate, it is not surprising that they exhibit different reactivity profiles.
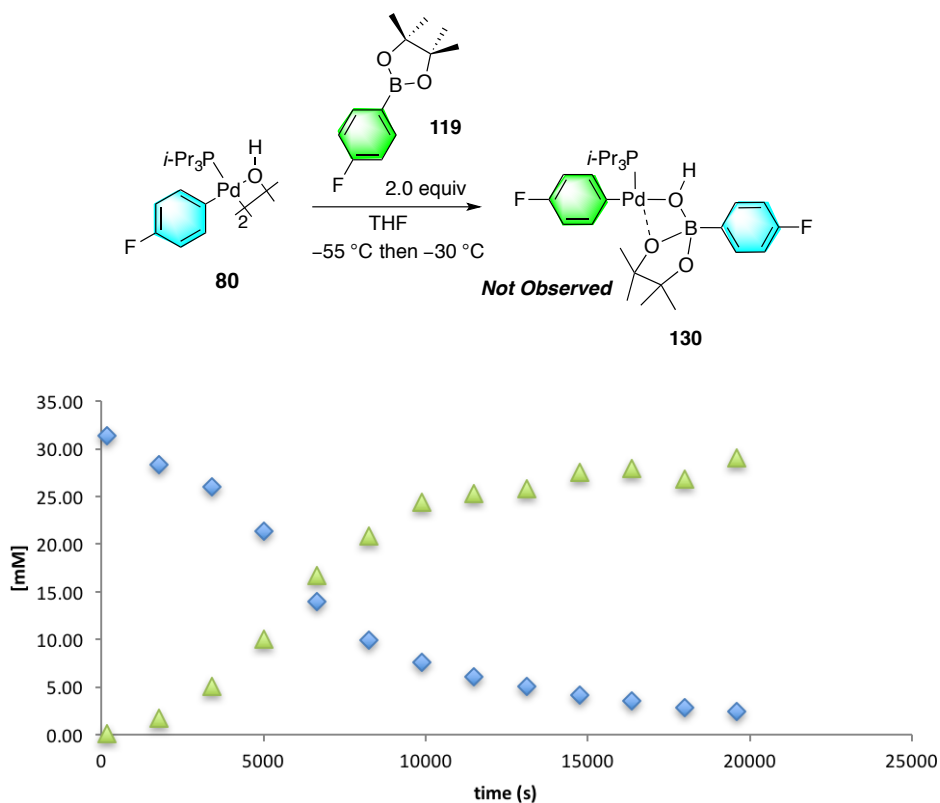
Figure 67. Decay of complex **80** and formation of **73**.

Next, ester **134** was reacted with complex **80** at –78 °C followed by warming to –30 °C where the formation of cross-coupling product **73** could be monitored. A first order rate constant was obtained $2.26 \pm 0.31 \times 10^{-4}$ s^{-1}. While this complex was slower (k_{rel} = 0.39) than the arylboronic acid **58** it was considerably faster than the pinacol ester **119**.

Combining these results, we suspected that the driving force for the transmetalation event is centered on the ability to access an empty coordination site on the palladium atom. Therefore, the oxygen atoms bound to the aryl boron substrate needs to have low electron donation ability which should allow for rapid transmetalation. This led the investigation to oxalic acid arylboronate ester **132** which should allow for rapid transmetalation at low temperature.

Combination of oxalic acid ester **137** with complex **80** at –78 °C in THF resulted in cross-coupling product instantly. In attempts to measure the rate for cross-coupling product **73** the rapid injection NMR apparatus was charged with the oxalic ester **137** in THF followed by lowering into an NMR tube containing complex **80** spinning inside the bore of the magnet at –100 °C. Upon injection of ester **137** into the solution of **80** at –100 °C only cross-coupling product **73** was detected after the first data set (9 s), (Scheme 60). This suggests that this reaction is instantaneous under these conditions. From these data the rate of the transmetalation event follows the trend **137** >> **131** > **106** > **72** > **121** for B-aryl coupling partner.

Scheme 60

64 s

45 s

36 s

After Injection

27 s

Injection

F_c

18 s

Before Injection

9 s

STD

F_a

99
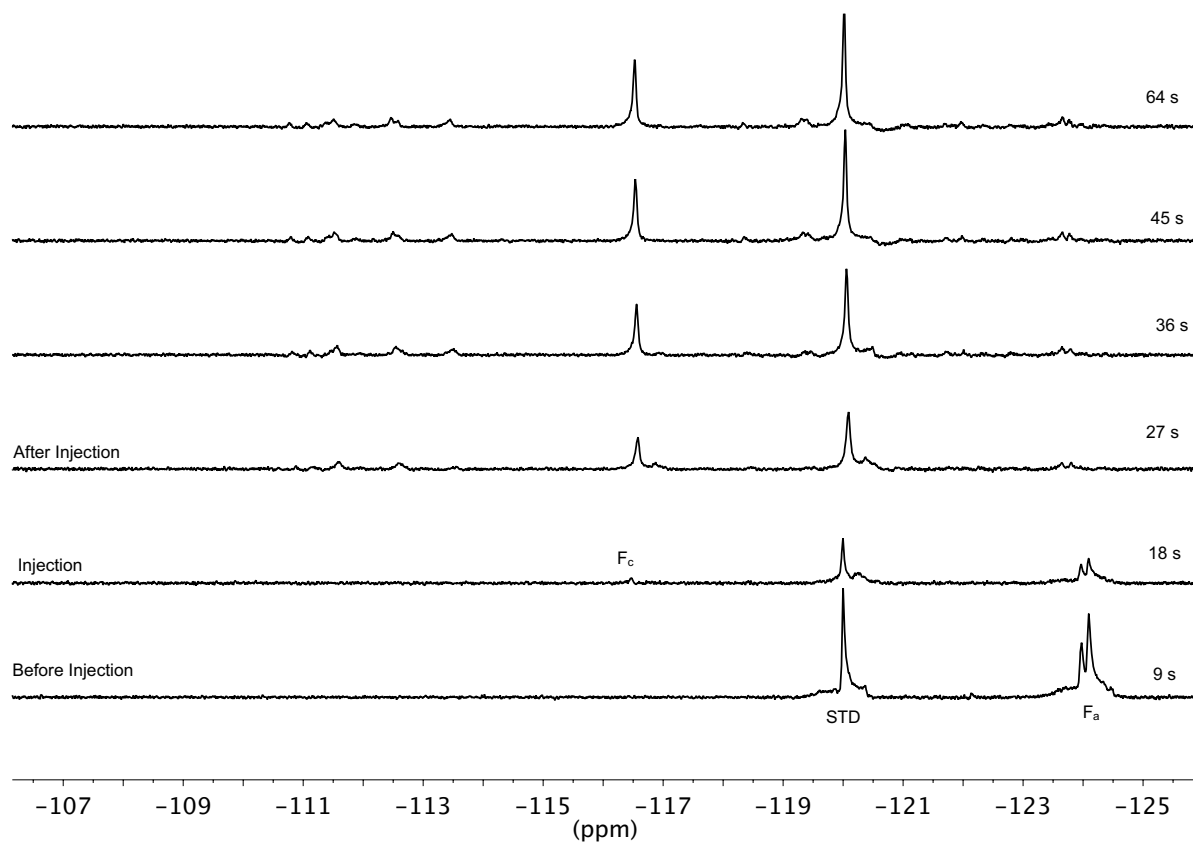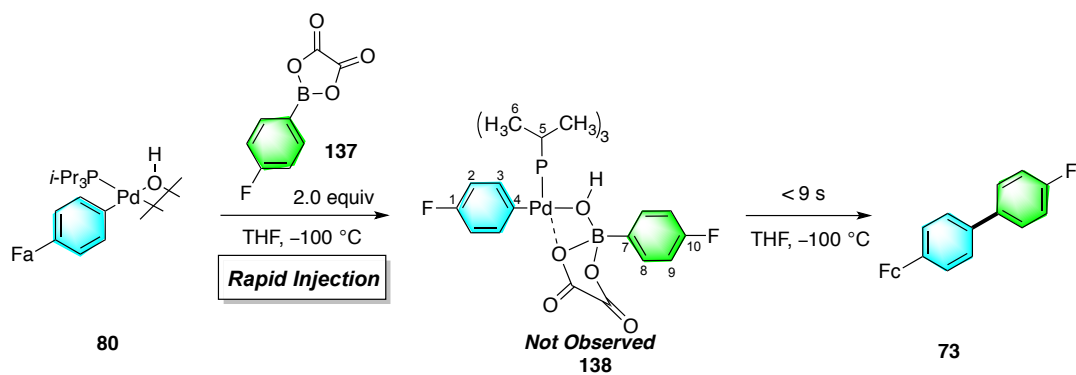
Table 10. Rate data for boronate esters
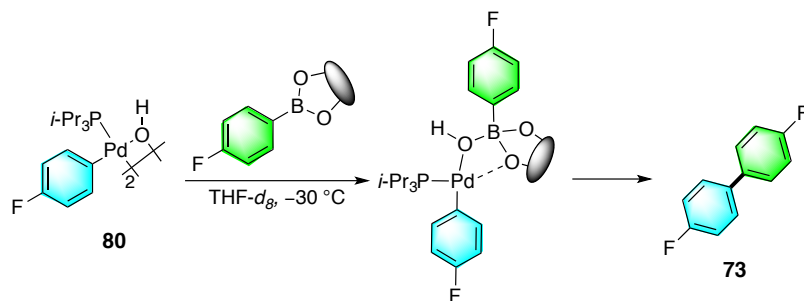
Entry	substrate		complex	decay k, 10^{-3} s^{-1}	form k, 10^{-3} s^{-1}	k_{rel}
1	B(OH)₂	**58**	**86**	0.759 ± 0.058	0.578 ± 0.013	1.00
2[b]		**72**	**87**	–	5.39 ± 0.07	9.33
4	B(OCH₃)₂	**106**	**105**	–	12.4 ± 0.2	21.45
5		**121**	**129**	2.74 ± 0.32	2.60 ± 0.17	4.49
6		**131**	**132**	–	13.3 ± 0.7	23.01
7		**134**	**135**	–	0.226 ± 0.031	0.39
8[c]		**119**	**120**	–	–	–
9[c]		**117**	**118**	–	–	–
10[c]		**137**	**138**	–	–	–

[a] Average of triplicate runs. [b] No intermediate was detected

100

4.6 Computational Analysis

4.6.1 Computational analysis of Complex *129*

The energy profile for the catechol ester complex **129** was computed in a similar manner as 8-B-4 complex **86** (Figure 68). In this case, the ground state is unsymmetrical creating two possible structures *129-React-TA* (2.5 kcal/mol) and *129-React-TP* (0 kcal/mol) that contain one hydroxyl group and an ester oxygen bound to the palladium center creating an energy difference of 2.5 kcal/mol. The dissociation of the ester oxygen in *129-React-TA* and *129-React-TP* have activation barriers of 14.9 and 15.7 kcal/mol respectively that led to two T-shaped complexes *129-inter-TA* and *129-inter-TP* that differ by 1.2 kcal/mol, favoring *129-inter-TP* which subsequently underwent transmetalation. Similarly, because of the steric repulsion created by the bulky *i*-Pr$_3$P ligand, the transfer of the B-aryl group from the *TA* isomer (*129-TS-TA*) also possessed a significantly higher activation barrier than the *TP* isomer (*129-TS-TP*) by 9.4 kcal/mol (Figure 68). The experimental activation barrier, $\Delta G^{\neq} = 17.0 \pm 2$ kcal/mol, is within error of the calculated transition state *129-TS-TP* ($\Delta G^{\neq} = 17.7$). After the transmetalation event, the immediate product is either *129-Prod-Trans* or *129-Prod-Cis* diarylpalladium complex with the boron moiety coordinated *trans* to *i*-Pr$_3$P or the 4-fluorophenyl group, indicating an early transition state (Figure 69). After dissociation of the boron moiety, the reductive elimination proceeds from two different diarylpalladium complexes (*Pd-Prod-Trans* and *Pd-Prod-Cis*). Here again the species *Pd-Prod-Cis* is created in a configuration immediately disposed to rapid reductive elimination where as species *Pd-Prod-Trans* must isomerize to achieve a favorable disposition of substituents.
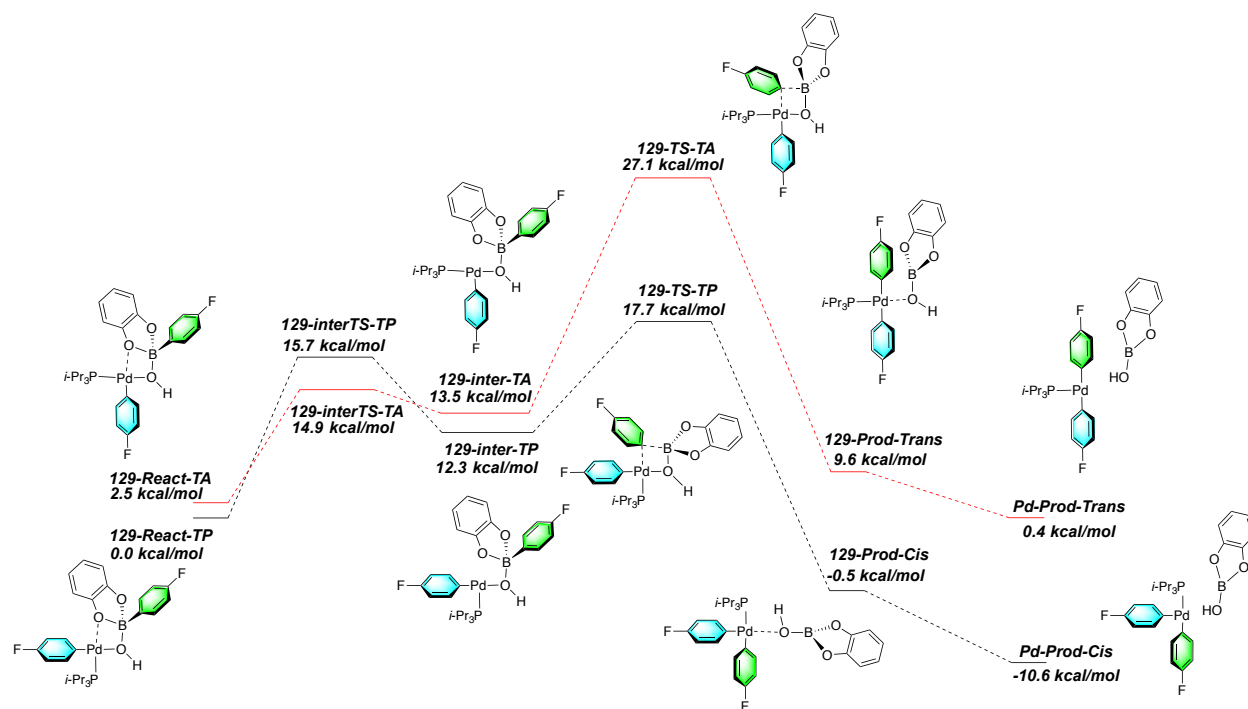
Figure 68. Energy profile for the transmetalation of **129**. Energies are single point solvation energies (THF) using M062X/6-31G(d) on the B3LYP/6-31G(d) optimized structures.
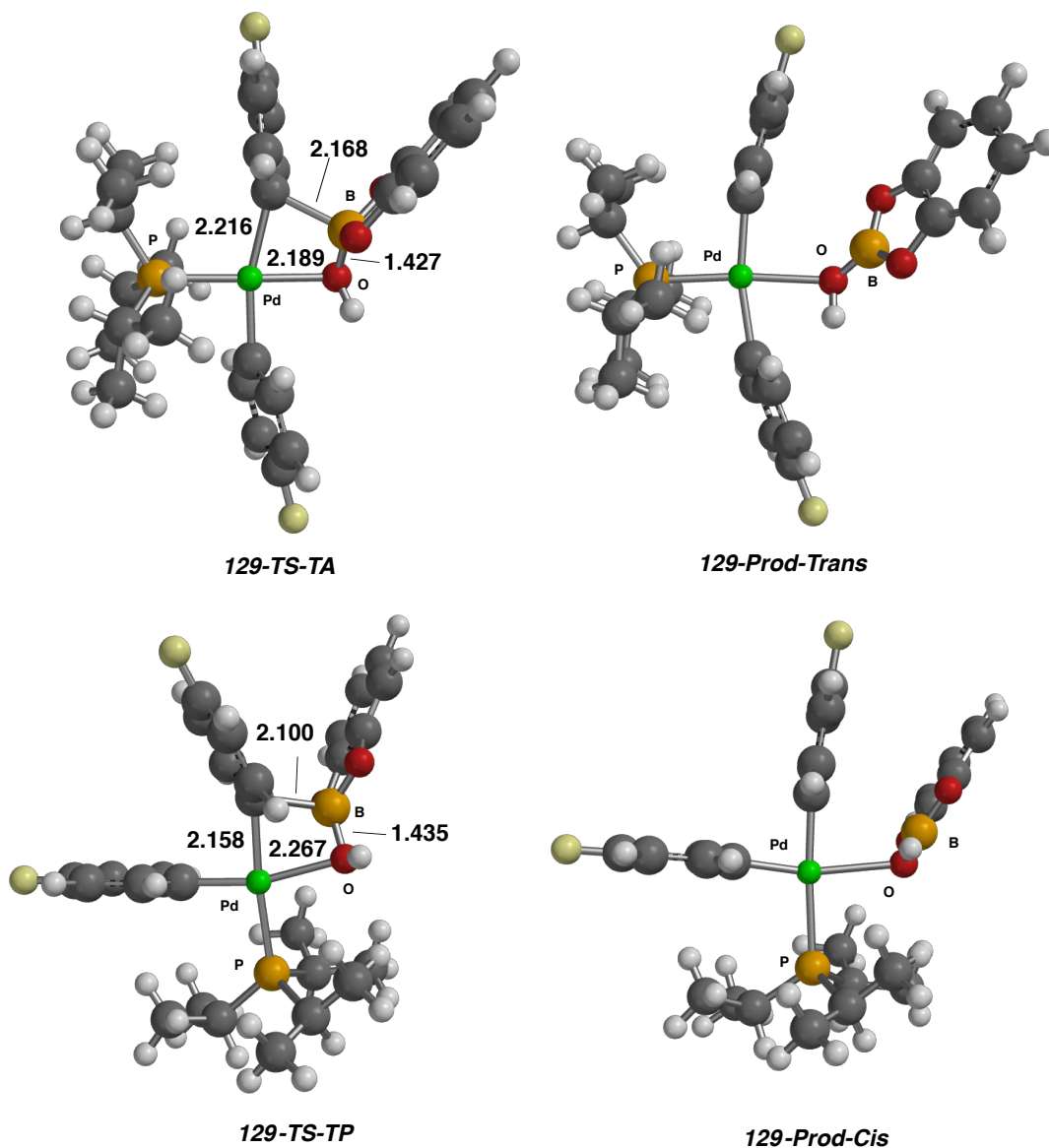
Figure 69. Energy profile for the transmetalation of **129**. Energies are single point solvation energies (THF) using M062X/6-31G(d) on the B3LYP/6-31G(d) optimized structures.

4.6.2. Computational analysis of Complex 132

The energy profile for the glycol ester complex **132** was computed in a similar manner as 8-B-4 catechol ester complex **129** (Figure 70). [This profile has not been fully calculated at this time.] In this case, the ground state is unsymmetrical creating two possible structures *132-React-TA* (1.5 kcal/mol) and *132-React-TP* (0 kcal/mol) that contain one hydroxyl group and an ester oxygen bound to the palladium center creating an energy difference of 1.5 kcal/mol. The

dissociation of the ester oxygen in132-*React-TA* and **132-*React-TP*** have activation barriers of 12.9.0 and 14.1 kcal/mol respectively that led to two T-shaped complexes **132-*inter-TA*** and **132-*inter-TP*** that are currently being calculated. Similarly, because of the steric repulsion created by the bulky *i*-Pr₃P ligand, the transfer of the B-aryl group from the *TA* isomer (**132-*TS-TA***) also possessed a significantly higher activation barrier than the *TP* isomer (**132-*TS-TP***) by 9.2 kcal/mol (Figure 69). Interestingly, unlike the catechol ester complex the experimental activation barrier, $\Delta G^{\neq} = 16.22 \pm 0.1$ kcal/mol, is within error of the calculated transition state **132-*TS-TP*** ($\Delta G^{\neq} = 15.9$ kcal/mol). The remainder or this energy profile is currently being calculated (Figure 70).
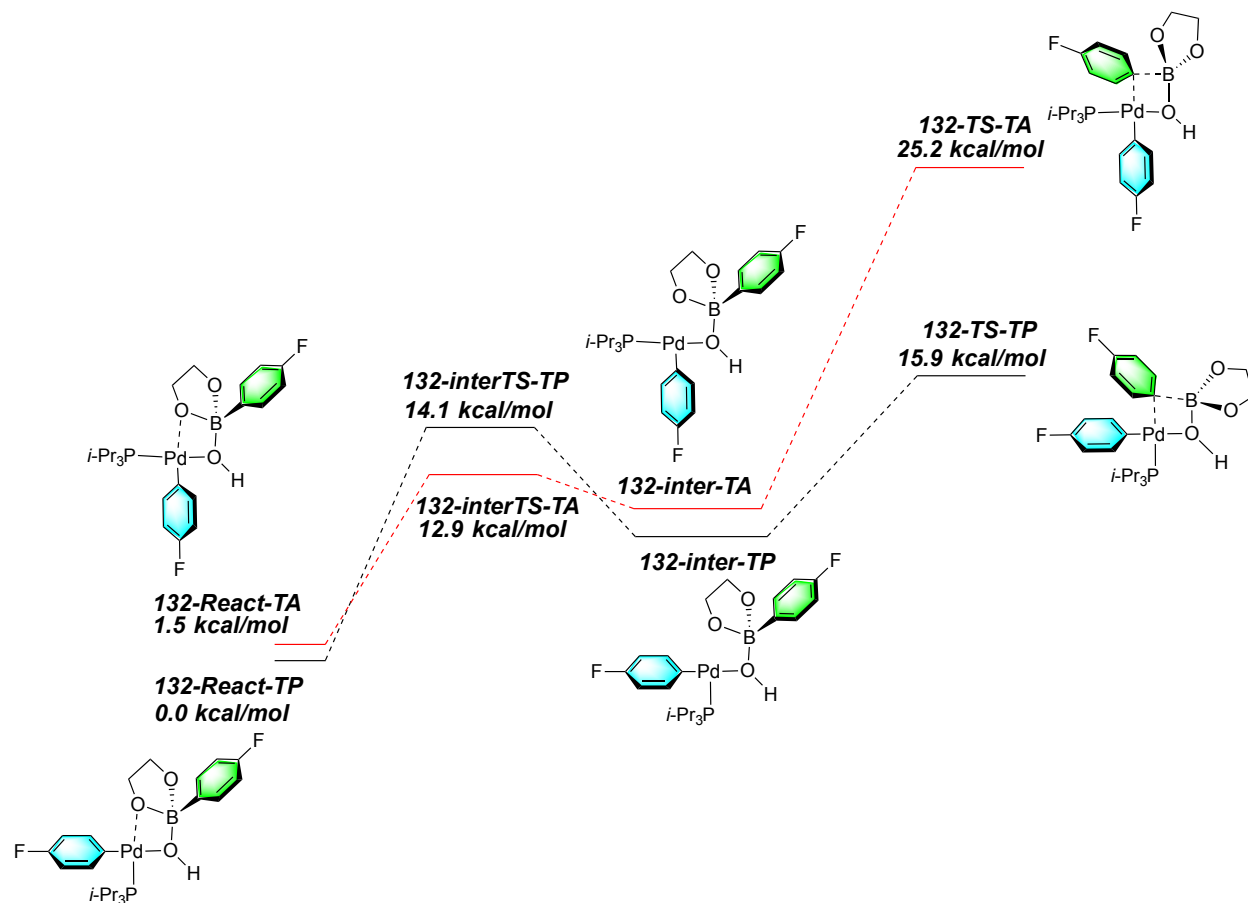
Figure 70. Energy profile for the transmetalation of **132**. Energies are single point solvation energies (THF) using M062X/6-31G(d) on the B3LYP/6-31G(d) optimized structures.

Table 11. Gibbs free energy comparison for cross-coupled product formation. [A]
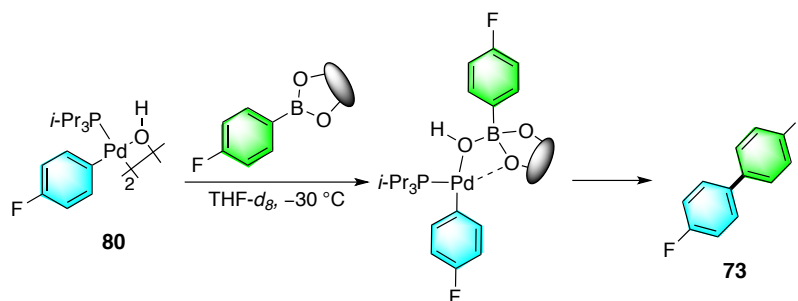
entry	Complex	$\Delta G^{\ne}_{243.15}$ kcal/mol (measured[a])	$\Delta G^{\ne}_{243.15}$ kcal/mol (calculated)
1[b]	**83**	17.7 ± 1.1	18.6
2	**129**	16.99 ± 0.06	17.7
3	**132**	16.22 ± 0.1	15.9

[a] Average of triplicate runs. [b] Full Eyring analysis

4.7 Conclusions

The combination of low temperature and rapid injection NMR spectroscopic analysis has allowed the unambiguous demonstration that under anhydrous conditions boronic esters form Pd-O-B linkages prior to the transmetalation event in the Suzuki-Miyaura cross-coupling reaction. Structures of the intermediates identified were assigned by NMR spectroscopy with the NOE and HMBC experiments being crucial in determining the bonding connectivity. Furthermore, a series of structural, kinetic and computational investigations revealed that the esters can transmetalate directly without a prior hydrolysis step. Furthermore, depending on the ester used, dramatic rate enhancements for the transfer of the B-aryl groups were observed. Overall, the critical feature that enables the transfer of the organic fragment from boron to palladium is the availability of an empty coordination site on the palladium atom. The importance of a coordinatively unsaturated palladium atom was revealed by both the calculation profiles and the electron deficient oxalic acid ester **137.** The impacts of these results are currently being transferred to catalytic process and will be reported in due course.

CHAPTER 5: Platinum Investigations of Pt-O-B Linkages

Building on the literature precedents outlined in chapter 2 our initial investigations were centered on making fluorine labeled Pt-O-B linkages that could be isolated and serve as NMR standards which if detected allow for a fleeting Pd-O-B linkage to be assigned.[52] Therefore, our preliminary studies comprised the investigation of fluorine labeled *trans*-$(Ph_3P)_2(4\text{-}FC_6H_4)Pt(I)$ (**139**) with arylboronic acids. However, for this to be a viable route an efficient synthesis of complex **139** was needed. Platinum dichloride was dissolved in molten Ph_3P (80 °C) which allowed for the synthesis of *cis*-$(Ph_3P)_2PtCl_2$.[117] This platinum complex was converted to $(Ph_3P)_4Pt^0$ by reduction with aqueous KOH in ethanol in the presence of Ph_3P whereupon a yellow solid was obtained.[117] The fluorine labeled *trans*-$(Ph_3P)_2(4\text{-}FC_6H_4)Pt(I)$ was then prepared by the oxidative addition of 4-fluoroiodobenzene with $(Ph_3P)_4Pt^0$ yielding 0.216 g, 88% (Figure 71).
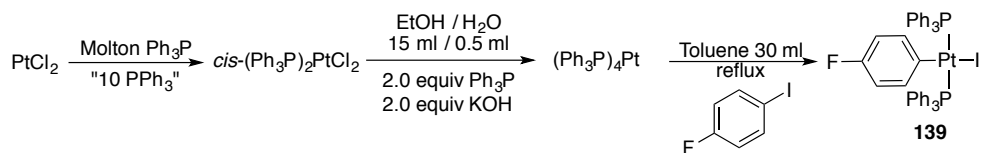
Figure 71. Synthesis of complex **139**.

However, following the reaction conditions outlined by Osakada et. al.[52] utilizing Ag_2O the isolation of a pre-transmetalation intermediate **140** was not possible, furthermore the isolation of **3a** resulted in failure (Figure 72).
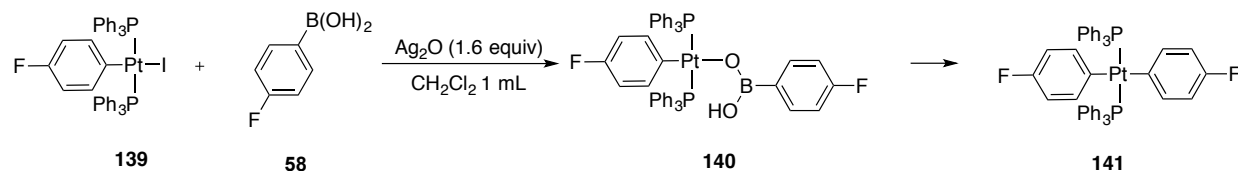
Figure 72. Attempts at the synthesis of complex **140**.

Concurrently, during the investigation outlined above the synthesis of the fluorine labeled analog dimethylphenylphosphino platinum hydroxide *trans*-$(Me_2PPh)_2(4\text{-}FC_6H_4)Pt(I)$ (**142**) was commenced. Interestingly, this synthesis was not as trivial as the one outlined above for complex **140**. Upon mixing K_2PtCl_4 with 1,5-cyclooctadiene in aqueous propanol with a catalytic amount of $SnCl_2$, $CODPtCl_2$ was prepared.[118] Performing a Finkelstein reaction with potassium iodide in acetone converted the dichloride to $CODPtI_2$.[118] A double addition with *bis*-4-

fluorophenylmagnesium afforded the *cis*-CODPtAryl$_2$ complex **142**.[118] A ligand exchange reaction was performed with dimethylphenylphosphine in DCM to yield *cis*-(PhPMe$_2$)$_2$PtAryl$_2$ **143**. Refluxing the material in methanol with excess methyl iodide yielded the *trans*-(Me$_2$PPh)$_2$(4-FC$_6$H$_4$)Pt(I) (**144**).[119] However, it was difficult to isolate the complex in high purity due to the observation of Pt(IV) complexes. This line of investigation was abandoned due to the corresponding *trans*-(Me$_2$PPh)$_2$(4-FC$_6$H$_4$)Pd(OH) **145** complex is reported to[120] be unstable and the observation of Pd-O-B linkages as outlined in Chapter 2. [120]
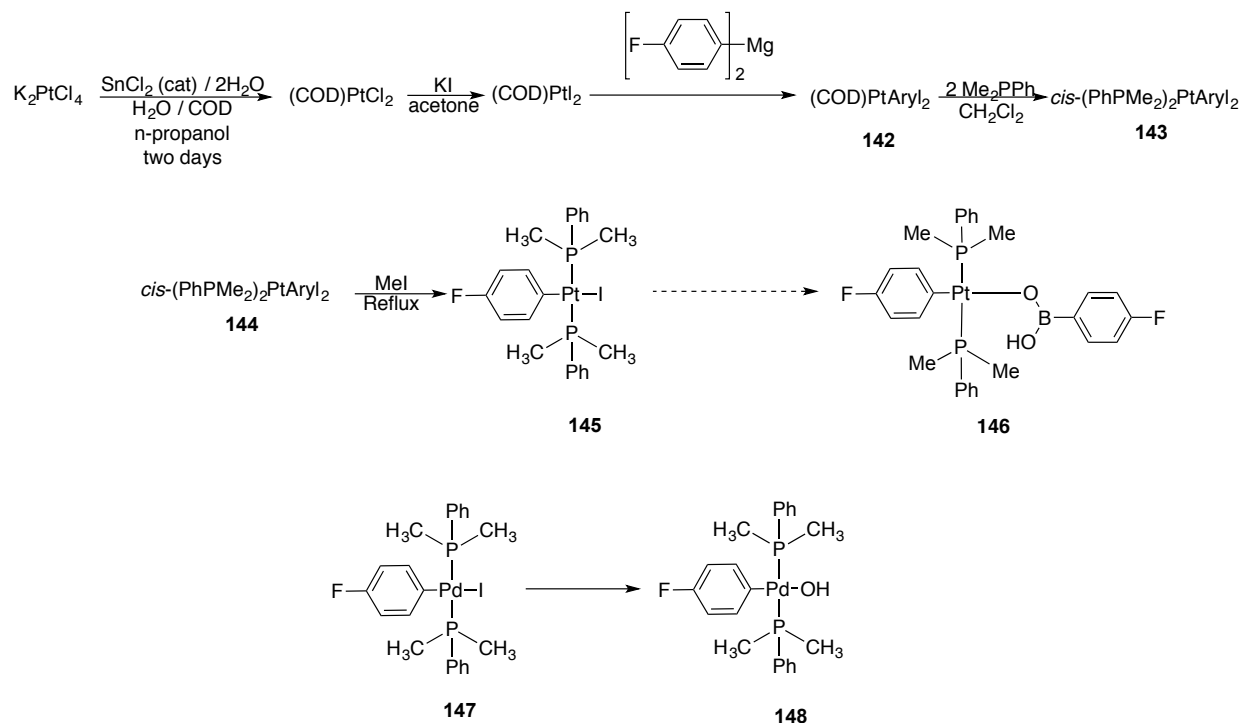
Figure 73. Attempts at the synthesis of complex **145.**

Experimental for Platinum investigations of Pt-O-B Linkages

Table of Contents   *Page*

General Experimental

Reactions were performed using glassware that had been flame-dried under vacuum or oven-dried (210 $^{\circ}$C) overnight. All reactions were conducted under an inert atmosphere using argon connected to a drying tube equipped with phosphorous pentoxide, calcium sulfate, and sodium hydroxide. Solvents used for extraction were reagent grade. Reaction solvents tetrahydrofuran (Fisher, HPLC grade), diethyl ether (Fisher, HPLC grade), toluene (Fisher, HPLC grade), hexane (Fisher, HPLC grade), and methylene chloride (Fisher, HPLC grade) were dried by percolation through two columns packed with neutral alumina under positive pressure of argon (solvent dispersion system method). Benzene (ACS grade) and pentane (ACS grade) were distilled over sodium while methanol (ACS grade) was distilled over magnesium.

Commercial reagents were purified by distillation or recrystallization prior to use unless otherwise noted. Tetrafluoroboric acid diethyl ether complex, cesium hydroxide monohydrate, isopropylmagnesium chloride solution (2M in THF), triphenylphosphine, thallium formate and trichlorophosphine, pinacol, 2-hydroxyisobutyric acid were all purchased from Aldrich. Palladium chloride was purchased from Pressure Chemical. Platinum chloride and potassium tetrachloroplatinum were purchased from Strem. Sodium tetraphenylboron was purchased from Mallinkrodt Chemical. 4-Fluorophenylboronic acid, 1,4-fluoroiodobenzene, 1,1'-bis(diphenylphosphino)ferrocene, and 1,4-difluorobenzene were all purchased from Oakwood Products. The following compounds were prepared by literature methods *bis*-4-fluorophenylmagnesium. [121]

^{1}H, ^{13}C, ^{19}F, and ^{31}P, spectra were recorded on a Varian Unity, Agilent, or Bruker Avance 600 MHz spectrometers (^{1}H, 151 MHz; ^{13}C, 565 MHz; ^{19}F, 243 MHz; ^{31}P, 193 MHz). ^{11}B NMR spectra were reordered on a Varian Unity 400 MHz (^{11}B NMR, 129 MHz).

Spectra are referenced to residual chloroform (7.26 ppm, ^{1}H; 77.00 ppm, ^{13}C), residual THF (1.72 ppm, ^{1}H; 68.21 ppm, ^{13}C), 1,4-difluorobenzene (−120.00 ppm, ^{19}F), Ph$_4$BNa (−6.14 ppm, ^{11}B), triisopropylphosphine (19.00 ppm, ^{31}P), and external HBF$_4$•OEt$_2$ (0.00 ppm, ^{11}B). Chemical shifts are reported in ppm, multiplicities are indicated by s (singlet), d (doublet), t (triplet), q (quartet), p (pentet), h (hextet), m (multiplet) and br (broad). Coupling constants, *J*, are reported in Hertz.

Experiment 1: Preparation of *trans*-(Ph₃P)₂Pt(4-FC₆H₄)(I) (139).
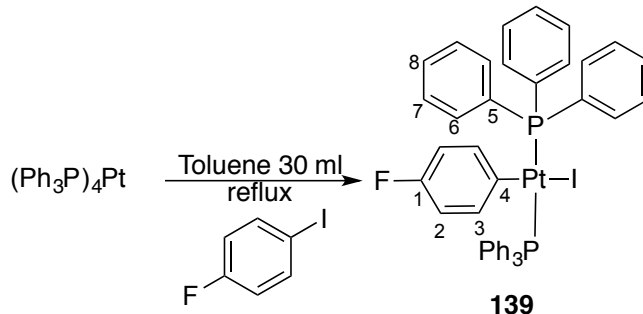
A flame-dried, 100-mL, Schlenk flask was charged with (Ph₃P)₄Pt (0.324 g, 1.33 mmol, 1.0 equiv) inside the glovebox followed by 40 mL of toluene. The vessel was taken out of the dry box and the contents were transferred to a round bottom flask equipped with a reflux condenser and stir bar under nitrogen followed by 1,4-fluoroiodobenene (0.354 g, 1.6 mmol, 1.2 equiv). The reaction was refluxed overnight. The following day the solvent was removed *via* roto evaporation. Then hexanes were added to precipitate the product which was collected 0.216 g, 88%.

Data for **139**:

¹H NMR:	(600 MHz, THF-d_8)
	7.52 (m, 12 HC(7)), 7.31 (m, 6 HC(8)), 7.22 (m, 6 HC(6)), 6.53 (dt, ^3J(Pt-H) = 57 Hz, 2 HC(4)), 5.89 (dd, ^3J(H-H) = 7 Hz, 2 HC(2
¹⁹F NMR:	(565 MHz, THF-d_8)
	−126.24 (s, FC(1))
³¹P NMR:	(243 MHz, THF-d_8)
	22.34 (d, ^3J(Pt-H) = 3026 Hz, , 2 P(Pd))
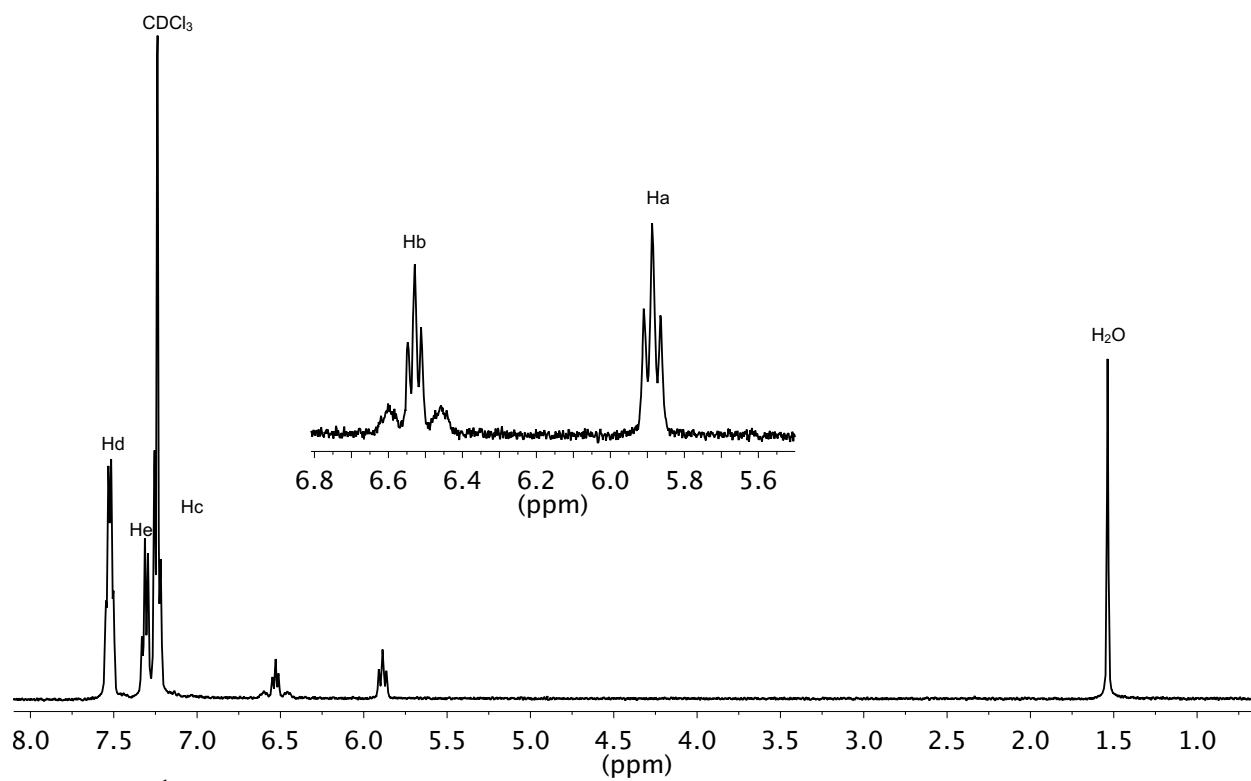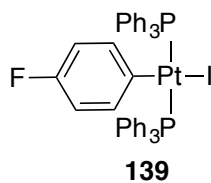
Figure 74. ^{1}H NMR spectrum of **139**, referenced to CDCl$_3$ (7.2 ppm).
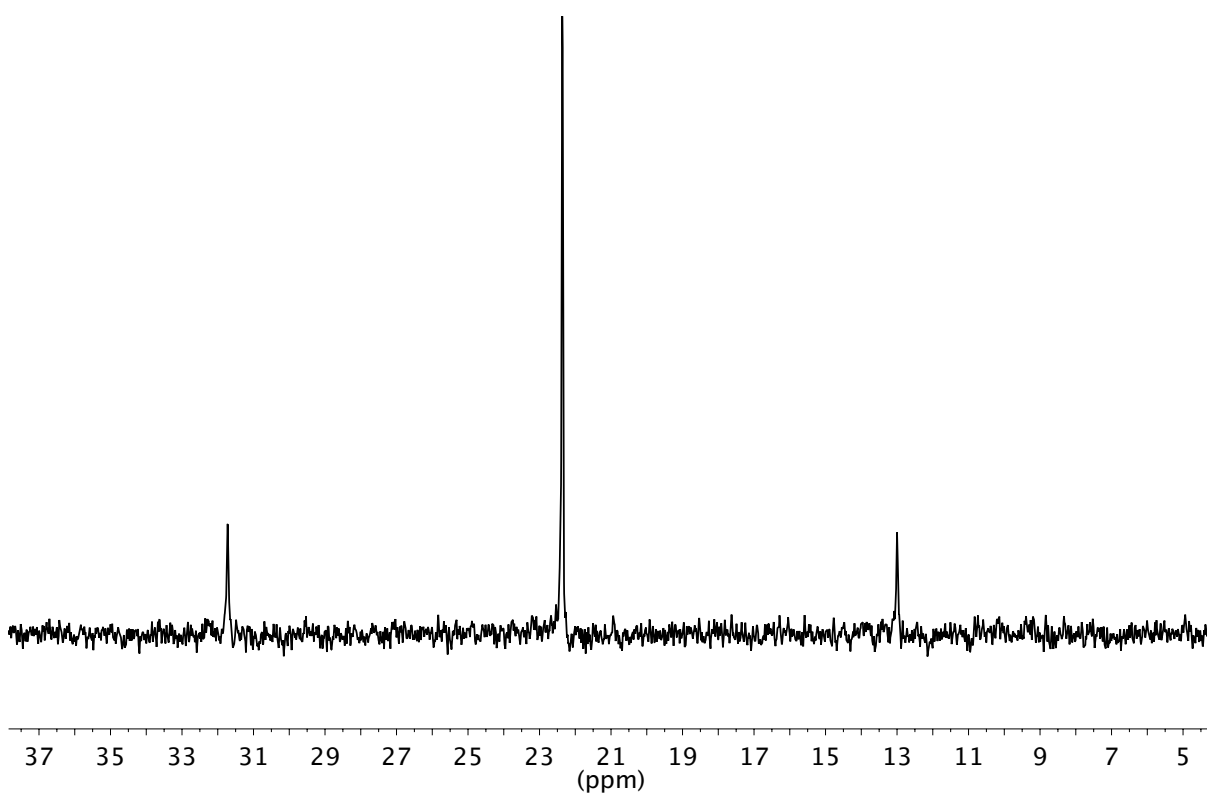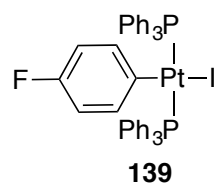
Figure 75. ^{31}P NMR spectrum of **139**.
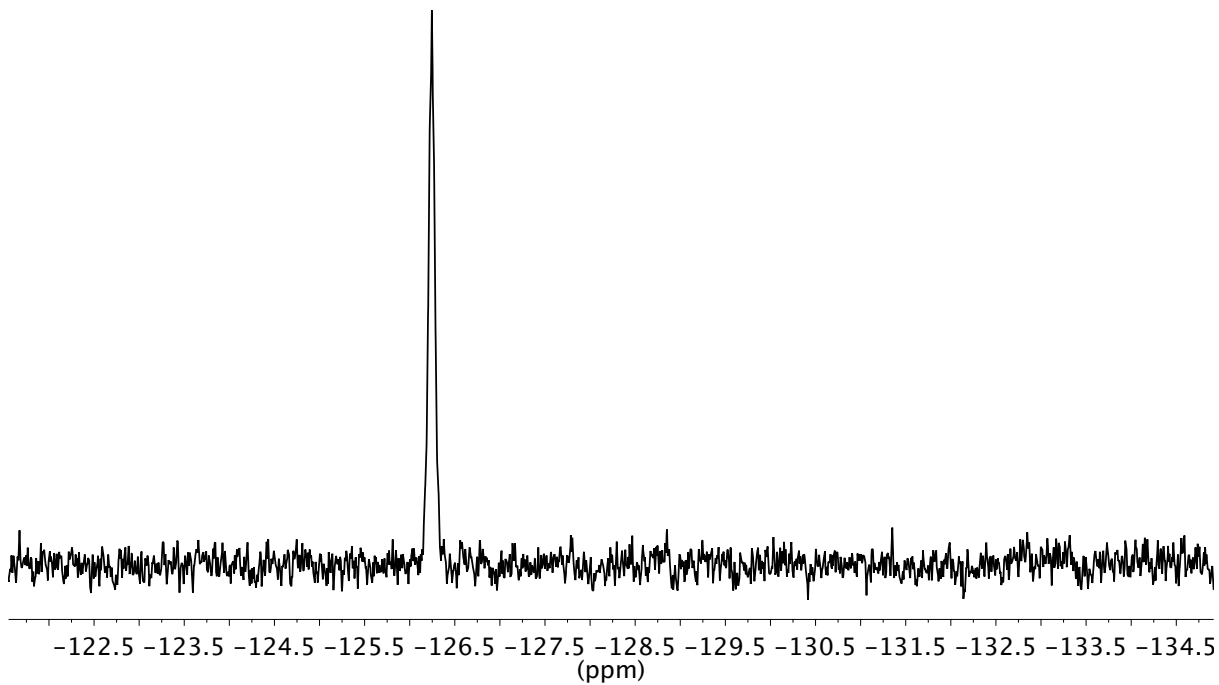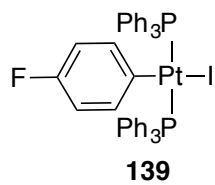
Figure 76. ^{19}F NMR spectrum of **139**.

Experiment 2: Attempts to prepare (140).
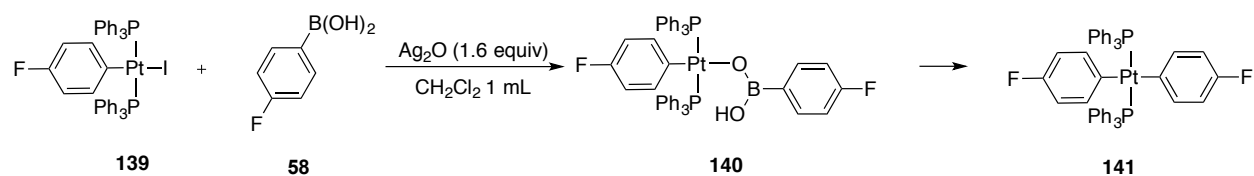
A flame-dried, 5-mL, Schlenk flask was charged with *trans*-(Ph₃P)₂Pt(4-FC₆H₄)(I) (50 mg, 47 μmol, 1.0 equiv) followed by 2 mL of DCM. Then 4-fluorophenyl boronic acid **58** (7.8 mg, 57 μmol, 1.2 equiv) and Ag₂O (11 mg, 75 μmol, 1.6 equiv) were added and the reaction was stirred for 3 h followed by solvent removal to ~1 mL. Then ether (~5 mL) was added and the flask was placed in the freezer. This resulted in powder that was collected and found to contain multiple products.

Experiment 3: Preparation of *cis*-(COD)Pt(4-FC$_6$H$_4$)$_2$ (142).

142
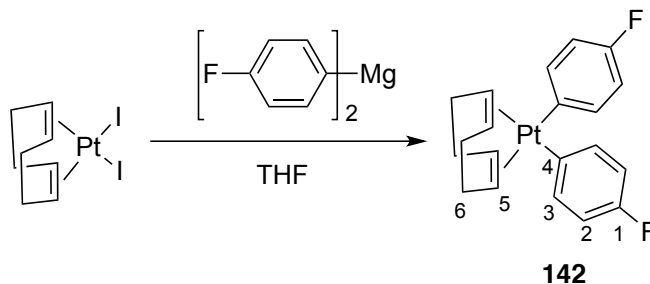
A flame-dried, 5-mL, Schlenk flask was charged with *cis*-(COD)Pt(I)$_2$ (75 mg, 134 μmol, 1.0 equiv) followed by 2 mL of THF inside the glovebox. Then *bis*-4-fluorophenylmagnesium (28 mg, 402 μmol, 3.0 equiv) was added as a powder. The reaction vessel was removed from the glove box and placed under nitrogen and allowed to stir overnight. The next morning ice chips were added to the flask. Once dissolved the THF was removed by roto evaporation leaving water and a white solid behind. The solid was collected and washed with water yielding 46 mg, 70%.

Data for **142**:

^{1}H NMR: (600 MHz, CDCl$_3$)

7.12 (dt, ^3J(Pt-H) = 108 Hz, 4 HC(4)), 6.73 (m, 4 HC(8)), 5.06 (dt, ^3J(Pt-H) = 31 Hz, 4 HC(4)), 2.50 (m, 4 HC(8)),

^{19}F NMR: (565 MHz, THF-d_8)

−122.06 (s, FC(1))
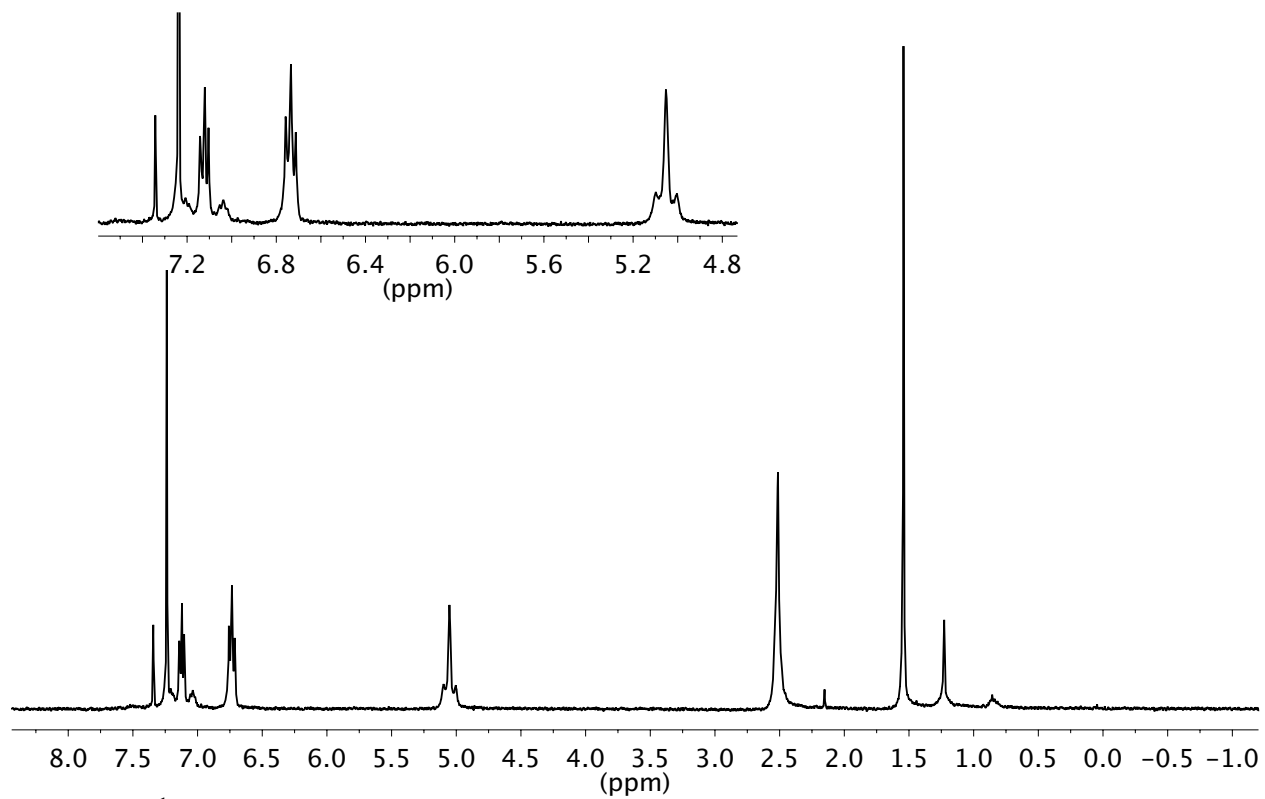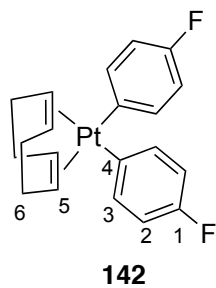
Figure 77. ^{1}H NMR spectrum of **142**, referenced to CDCl$_3$ (7.2 ppm).
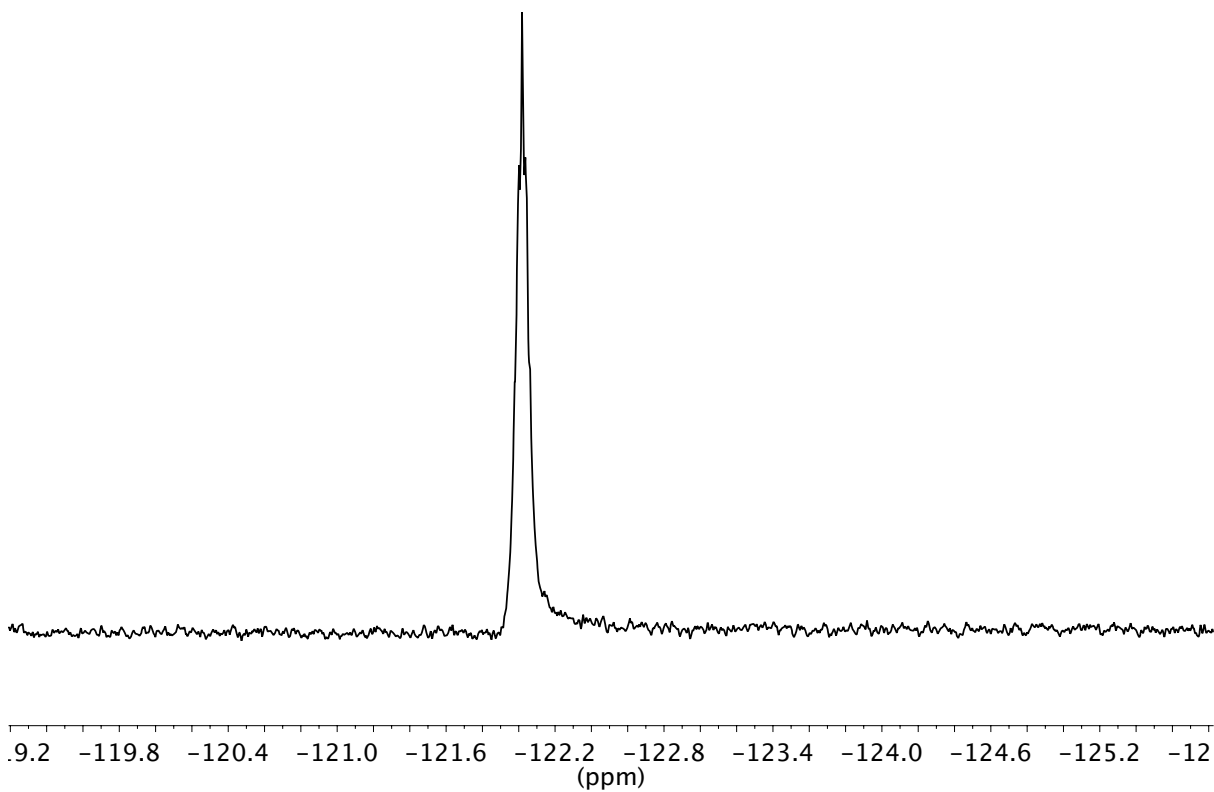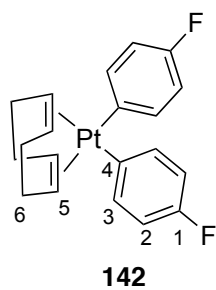
Figure 78. ^{19}F NMR spectrum of **142.**

Experiment 4: Preparation of *cis*-(Me₂PPh)Pt(4-FC₆H₄)₂ (144).
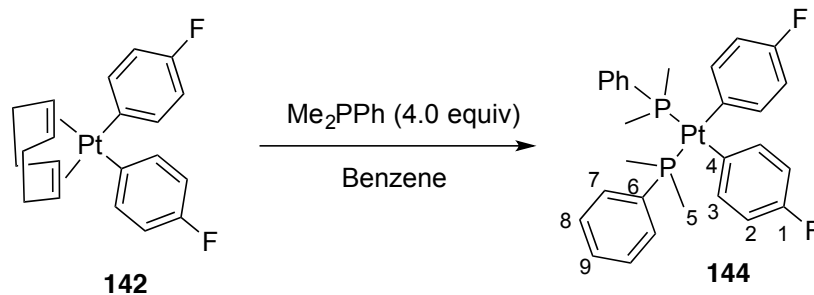
A flame-dried, 25-mL, Schlenk flask was charged with *cis*-(COD)Pt(Aryl2)₂ (126 mg, 0.26 mmol, 1.0 equiv) followed by 5 mL of benzene inside the glovebox. Then Me₂(Ph)P (0.145 mg, 1.04 mmol, 4.0 equiv) was added followed by capping the vessel. The reaction was allowed to stir overnight. The following morning the solvent was removed by roto-evaporation. The powder was collected and washed with pentane yielding 0.162 mg, 94%.

Data for **144**:

¹H NMR:	(600 MHz, CD₂Cl₂)
	7.45 (m, 4 HC(7-9, 3)), 7.36 (m, 4 HC(7-9, 3)), 6.70 (d, 4 HC(2)), 1.13 (m, 4 HC(5)),
¹⁹F NMR:	(565 MHz, CD₂Cl₂)
	−25.24 (s, FC(1))
³¹P NMR:	(243 MHz, CD₂Cl₂)
	−14.18 (d, ³J(Pt-H) = 1791 Hz, , 2 P(Pd))
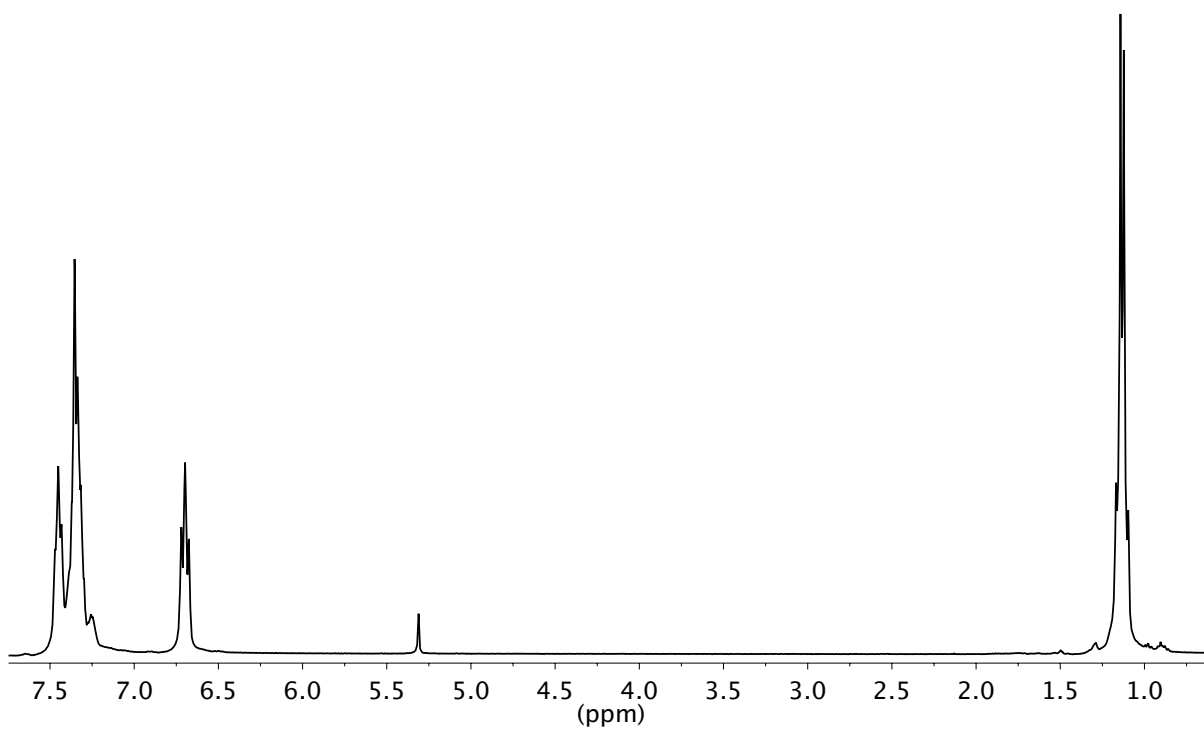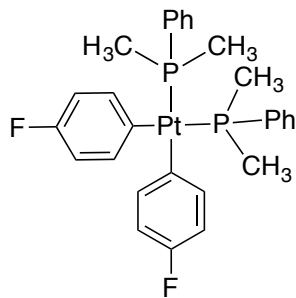
Figure 79. ^{1}H NMR spectrum of **144**, referenced to DCM (5.3 ppm).
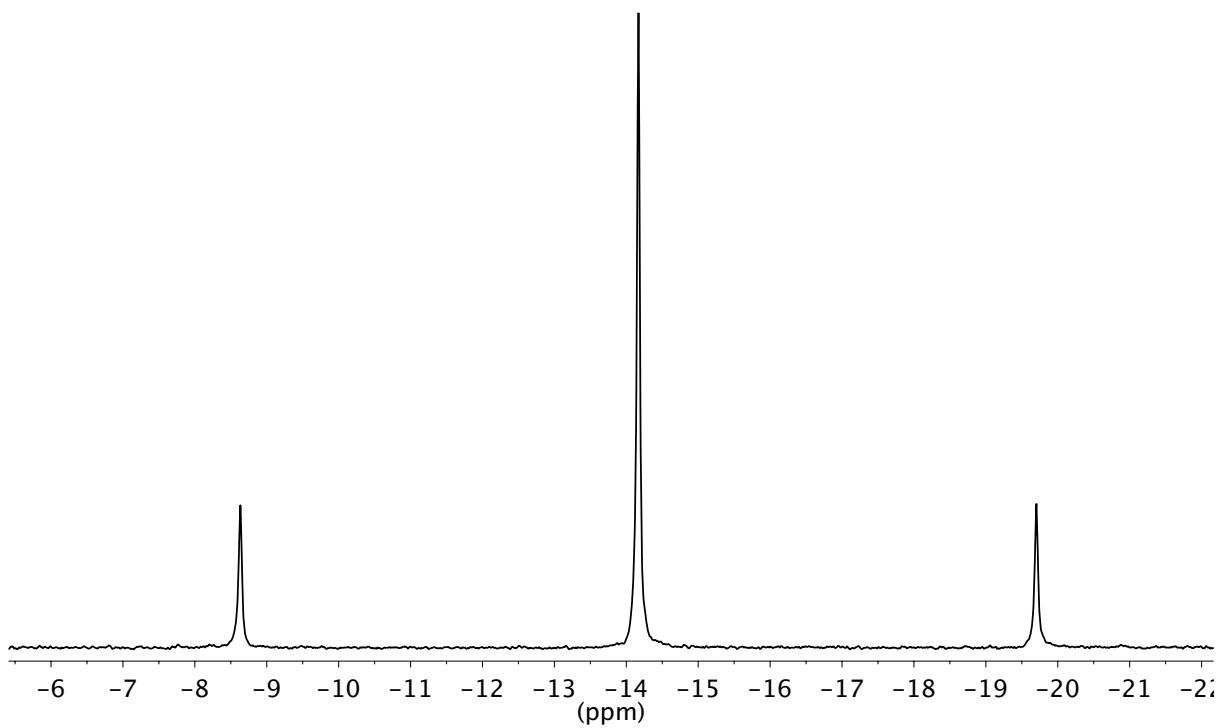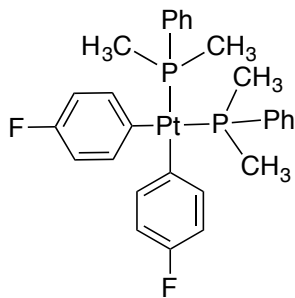
Figure 80. [13]P NMR spectrum of **144.**
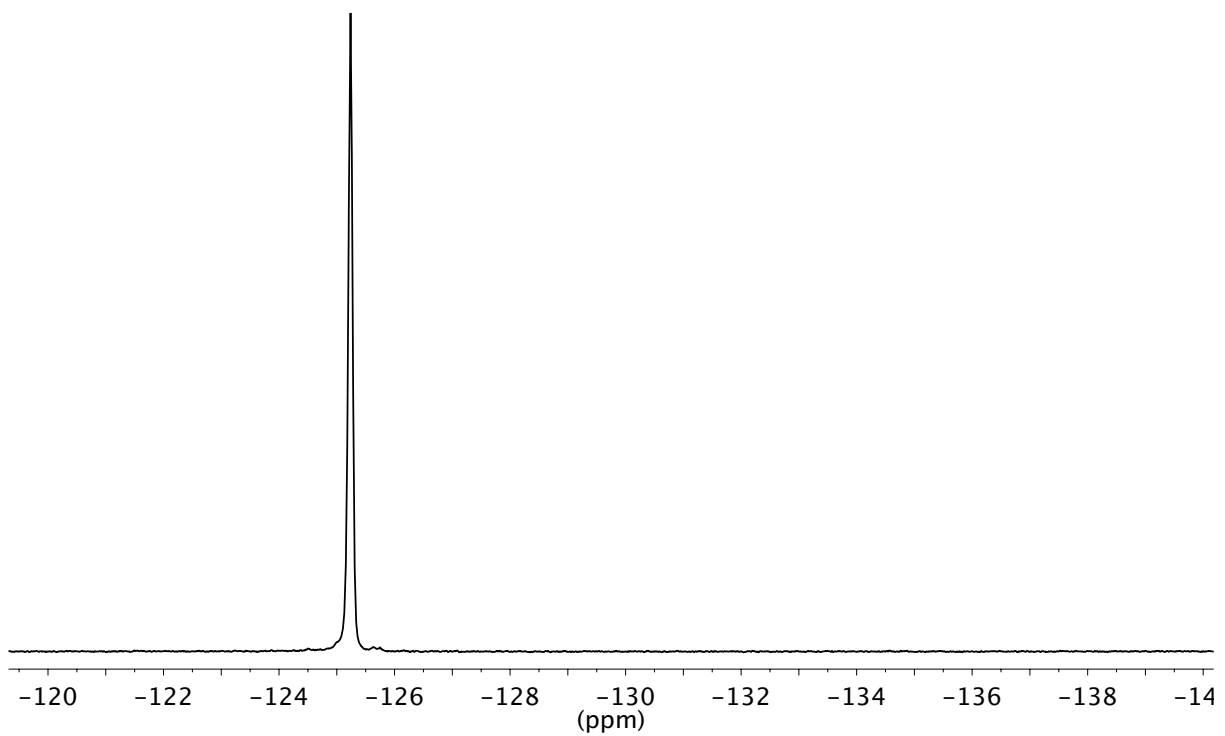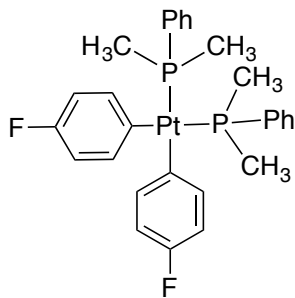
Figure 81. ^{19}F NMR spectrum of **144.**

Experiment 5: Preparation of *trans*-(Ph₃P)₂Pt(4-FC₆H₄)I (147).

144   **147**
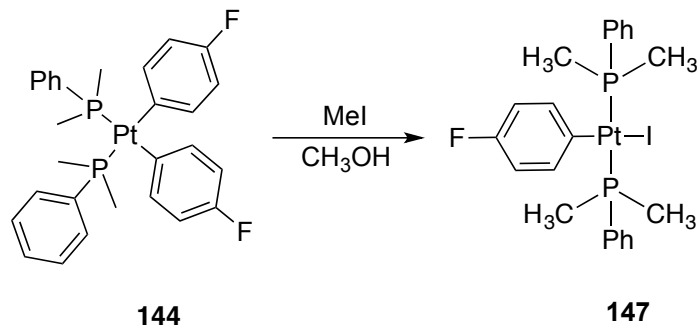
A flame-dried, 5-mL, round bottom flask / reflux condenser combo flask was charged with *trans*-(PhPMe₂)₂Pt(4-FC₆H₄)(I) (20 mg, 30 μmol, 1.0 equiv) followed by 2 mL of methanol and chloroform followed by methyl iodide (10 μL, 150 μmol, 5.0 equiv). The reaction was refluxed for 5 h where 3 complexes were present by ^{31}P NMR spectroscopy. The starting material was converted to **147** major and two platinum IV complexes.
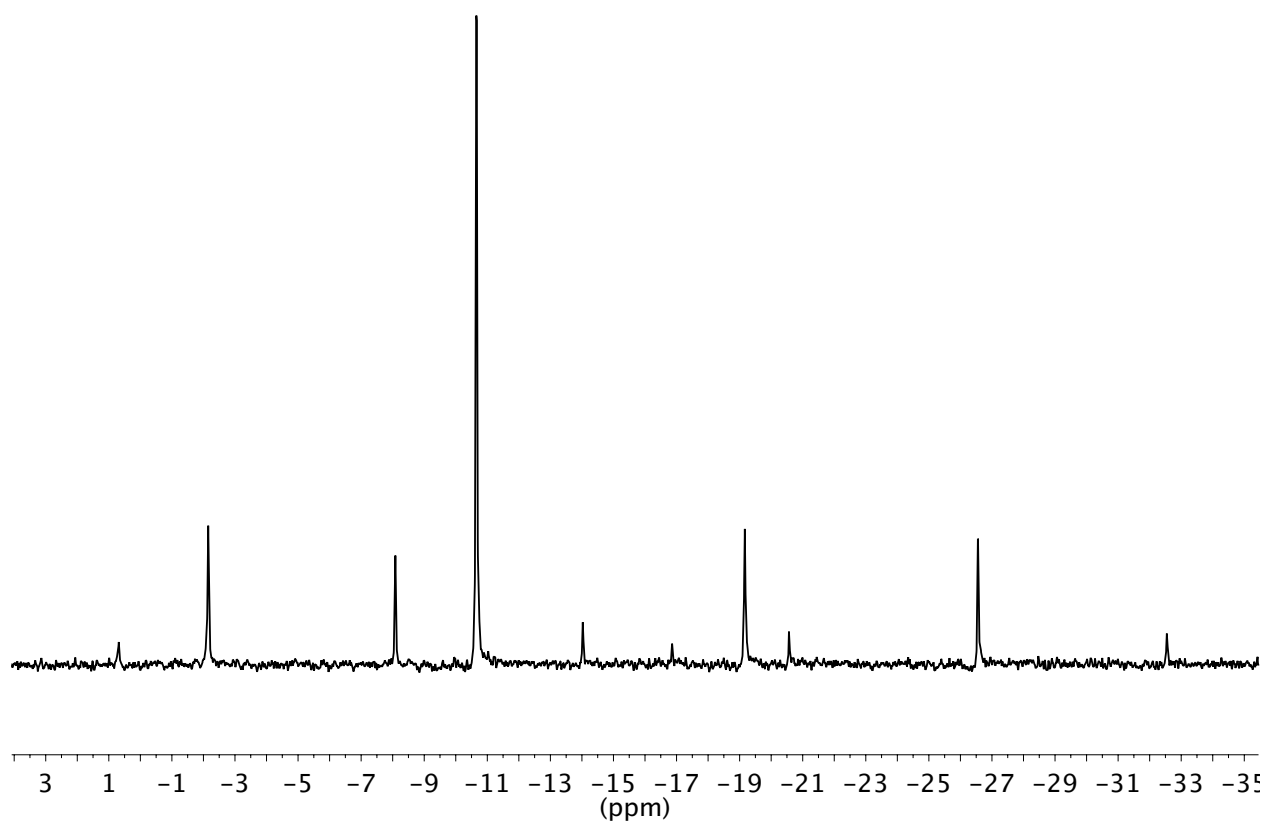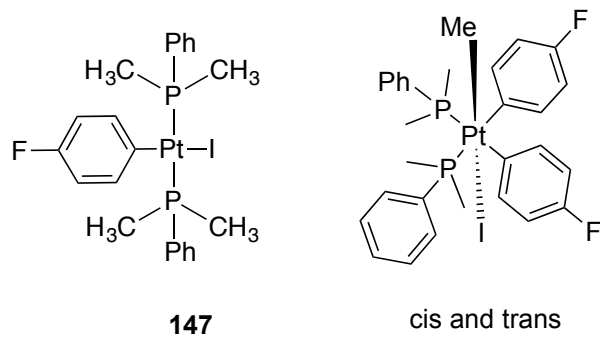
Figure 82. ^{13}P NMR spectrum of **147** and platinum IV complexes.

CHAPTER 6: Experimental for Chapter 2

Table of Contents *Page*

General Experimental *125*

Chemical Shift Summary Tables *126*

General Experimental

Reactions were performed using glassware that had been flame-dried under vacuum or oven-dried (210 ^{o}C) overnight. All reactions were conducted under an inert atmosphere using argon connected to a drying tube equipped with phosphorous pentoxide, calcium sulfate, and sodium hydroxide. Solvents used for extraction were reagent grade. Reaction solvents tetrahydrofuran (Fisher, HPLC grade), diethyl ether (Fisher, HPLC grade), toluene (Fisher, HPLC grade), hexane (Fisher, HPLC grade), and methylene chloride (Fisher, HPLC grade) were dried by percolation through two columns packed with neutral alumina under positive pressure of argon (solvent dispersion system method). Benzene (ACS grade) and pentane (ACS grade) were distilled over sodium while methanol (ACS grade) was distilled over magnesium.

Commercial reagents were purified by distillation or recrystallization prior to use unless otherwise noted. Tetrafluoroboric acid diethyl ether complex, cesium hydroxide monohydrate, isopropylmagnesium chloride solution (2M in THF), triphenylphosphine, thallium formate and trichlorophosphine, pinacol, 2-hydroxyisobutyric acid were all purchased from Aldrich. Palladium chloride was purchased from Pressure Chemical. Sodium tetraphenylboron was purchased from Mallinkrodt Chemical. 4-Fluorophenylboronic acid, 1,4-fluoroiodobenzene, 1,1'-bis(diphenylphosphino)ferrocene, and 1,4-difluorobenzene were all purchased from Oakwood Products. The following compounds were prepared by literature methods, 4-fluorophenylboroxine,[122] potassium 4-fluorophenyltrihydroxyboronate,[123] bromo(4-fluorophenyl)(tri-*tert*-butylphosphine)palladium[124] and allylcyclopentyl-palladium(II).[125]

^{1}H, ^{13}C, ^{19}F, and ^{31}P, spectra were recorded on a Varian Unity, Agilent, or Bruker Avance 600 MHz spectrometers (^{1}H, 151 MHz; ^{13}C, 565 MHz; ^{19}F, 243 MHz; ^{31}P, 193 MHz). ^{11}B NMR spectra were reordered on a Varian Unity 400 MHz (^{11}B NMR, 129 MHz).

Spectra are referenced to residual chloroform (7.26 ppm, ^{1}H; 77.00 ppm, ^{13}C), residual THF (1.72 ppm, ^{1}H; 68.21 ppm, ^{13}C), 1,4-difluorobenzene (−120.00 ppm, ^{19}F), Ph$_4$BNa (−6.14 ppm, ^{11}B), triisopropylphosphine (19.00 ppm, ^{31}P), and external HBF$_4$•OEt$_2$ (0.00 ppm, ^{11}B). Chemical shifts are reported in ppm, multiplicities are indicated by s (singlet), d (doublet), t (triplet), q (quartet), p (pentet), h (hextet), m (multiplet) and br (broad). Coupling constants, *J*, are reported in Hertz.

Notes: Thallium compounds are extremely toxic and therefore extra precaution should be taken when handling such compounds, especially when cleaning glassware.

Chemical Shift Summary Table
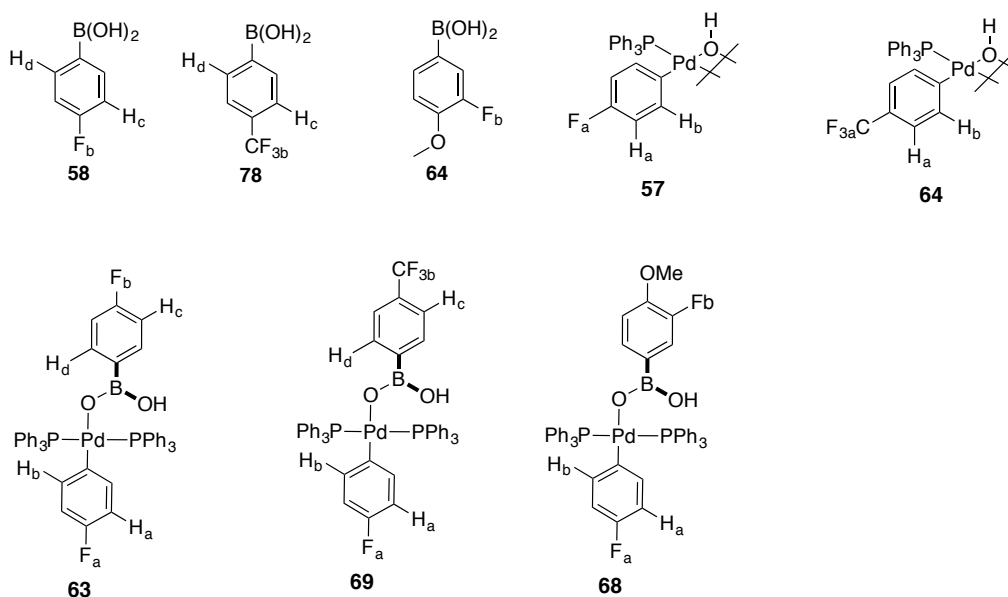
Table 12. ^{19}F, and ^{31}P NMR chemical shifts (ppm) for starting materials, products and complexes

Entry	complex	^{31}P	^{19}F$_a$	^{19}F$_b$
1	**58**	−	−	−111.21
2	**57**	34.83	−123.79	−
3	**63**	20.60	−125.40	−116.74
4	**58**	−	−	−111.21
5	**64**	34.64	−62.18	−
6	**69**	21.11	−61.10	−118.50
7	**66**	−	−	−139.39
8	**57**	34.83	−123.79	−
9	**68**	19.95	−126.47	−141.31

Chemical Shift Summary Table

58   **78**   **84**   **79**   **106**

70   **70**   **76**   **80**   **90**

109   **57**   **103**   **107**

71   **105**   **107**

58   **104**   **111**
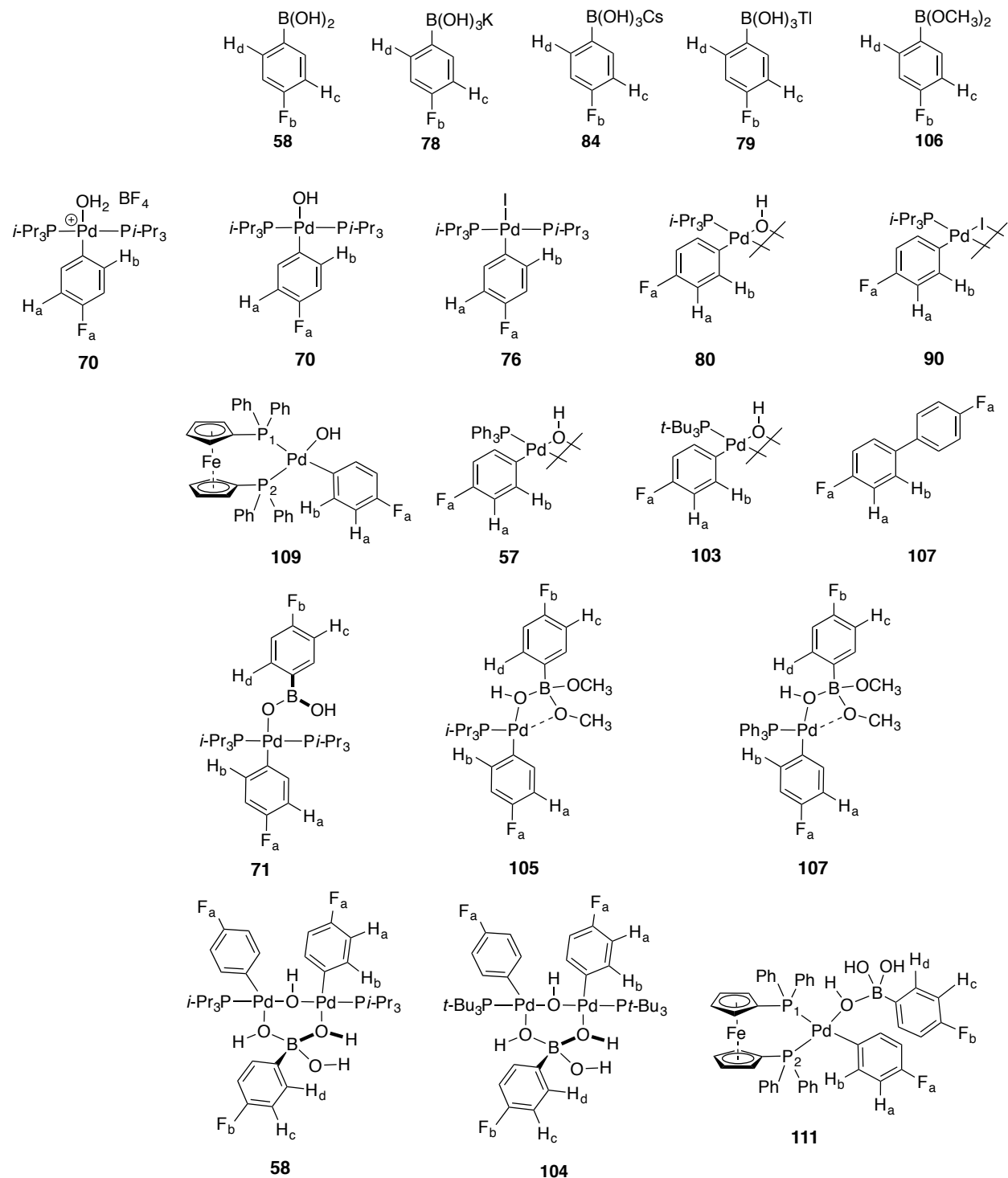
Table 13. ^{1}H, ^{19}F, ^{11}B and ^{31}P NMR chemical shifts (ppm) for starting materials, products and complexe

Entry	complex	^{11}B	^{31}P	^{19}F$_a$	^{19}F$_b$	^{1}H$_a$	^{1}H$_b$	^{1}H$_c$	^{1}H$_d$	^{1}HO
1	**70**	−	33.00	−124.68	−	6.64	7.35	−	−	3.60
2	**58**	29	−	−	−111.21	−	−	7.04	7.86	7.06
3[a]	**71**	29	29.98	−123.77	−115.75	6.71	7.45	6.88	7.76	4.47
4	**76**	−	30.36	−122.52	−	6.73	7.28	−	−	−
5	**79**	4	−	−	−118.41	−	−	6.79	7.43	3.74
6[b]	**71**	N.D.	29.02	−123.72	−115.73	N.D	N.D	N.D	N.D	N.D.
7[c]	**71**	28	29.98	−123.76	−115.74	6.72	7.46	6.88	7.78	4.48
8	**80**	−	45.55	−122.61	−	6.67	7.36	−	−	−1.74
9[d]	**88**	Broad	45.62	−123.67	−113.40	6.74	7.41	7.04	7.86	10.22
10	**90**	−	43.99	−123.25	−	6.66	7.35	−	−	−
11[e]	**88**	N.D.	46.12	−123.59	−113.36	6.72	7.39	7.06	7.87	10.21
12	**103**	−	75.68	−125.18	−	6.58	7.30	−	−	−2.23
13	**104**	N.D.	N.D.	N.D.	N.D.	6.76	7.46, 7.28	6.76	7.13	9.51
14	**106**	28	−		−111.38			7.08	7.67	−
15	**107**	9	51.00	−121.01	−118.33	6.85	7.45	6.95	7.68	4.02
16[g]	**107**	−	−	−	−	6.84	7.46	6.92	7.70	4.01
17	**58**	−	34.83	−123.79	−	6.33	6.92	−	−	−1.78
18	**106**	10	34.86	−121.09	−118.16	6.60	7.05	6.99	7.76	4.14
19	**109**	−	28.42(P1) 8.96(P2)	−123.63	−	6.93	6.34	−	−	0.45
20	**111**	N.D.	33.06(P1) 11.47(P2)	−122.35	−116.47	7.08	6.97	6.45	6.97	N.D.
21	**73**	−	−	−116.45	−	7.65	7.21	−	−	−

[a] 6-B-3 complex **71** was prepared from **70** and **58**. [b] 6-B-3 complex **71** was prepared from **76** and **71**. [c] 6-B-3 complex **71** was prepared from **70** and **76**. [d] Complex **88** was prepared from **80** and **90**. [e] Complex **88** was prepared from **90** and **79**. [f] Complex **107** was prepared from **80** and **58** in THF/CH$_3$OH. [g] Complex **107** was prepared from **80** and **106** in THF/CH$_3$OH.

Experiment 6: Reaction of Ph₃P complex 57 with 47 and 4.0 equiv of Ph₃P.
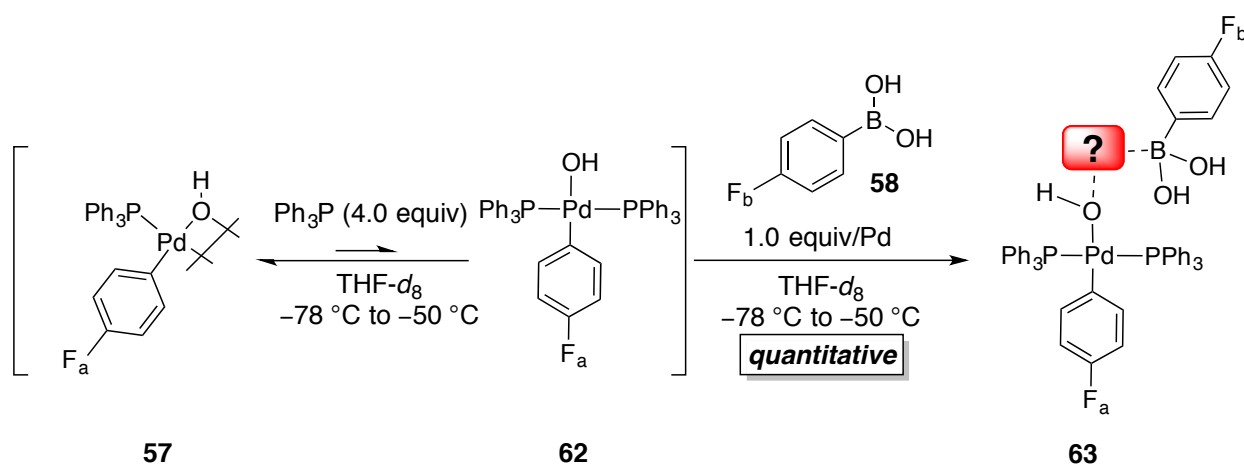
A 1-mL volumetric flask was charged with 4-fluorophenylboroxine (88 mg, 240 μmol, 1.0 equiv) followed by H₂O (13 μL, 722 μmol, 3.0 equiv). Then ~0.5 mL of THF-d_8 was added followed by sonication until the solid had dissolved. Once dissolved the flask was filled to the mark with THF-d_8 yielding a 4-fluorophenylboronic acid solution (0.72 M).

An oven dried, 5-mm, NMR tube as charged with [(Ph₃P)Pd(4-FC₆H₄)(μ-OH)]₂ (9.60 mg, 10 μmol, 1.0 equiv), sublimed Ph₃P (10.5 mg, 40 μmol, 4.0 equiv) and 500 μL of THF-d_8 followed by shaking until dissolved. The tube was placed into a −78 °C dry-ice acetone bath followed by the addition of 4-fluorophenylboronic acid solution (28 μL, 20 μmol, 2.0 equiv). The tube was vortexed (not shaken) quickly wiped with a Kimwipe and placed into the probe of the NMR spectrometer pre-cooled to −50 °C. The complex could not be characterized by standard techniques due to the messy aromatic region. However, the structure was assigned by analogy to complex **51** which has been fully characterized.

Data for **63**:

¹⁹F NMR: (565 MHz, THF-d_8)

−116.74 (s, FC(12)), −125.40 (s, FC(1))

³¹P NMR: (243 MHz, THF-d_8)

20.60 (s, 2 P(Pd))

63
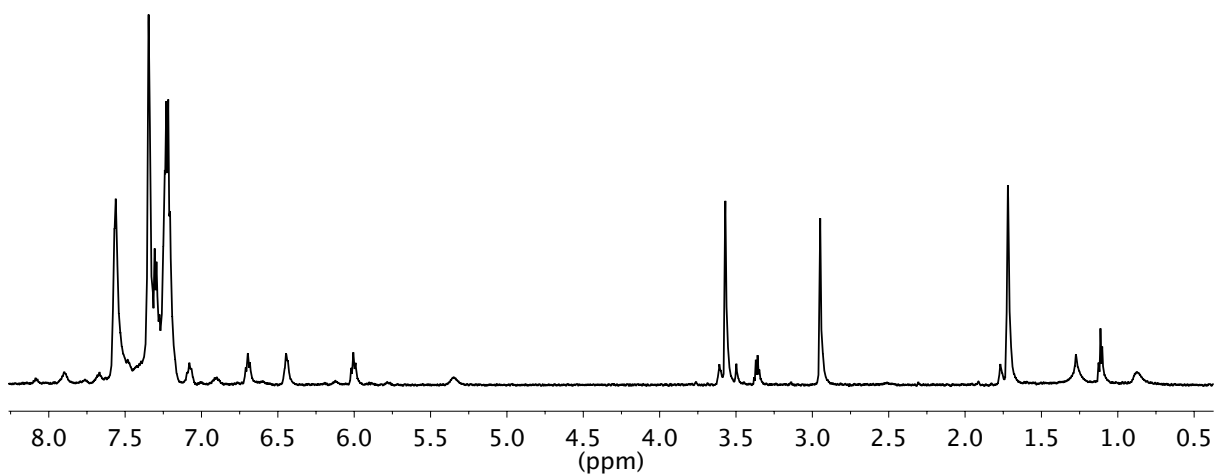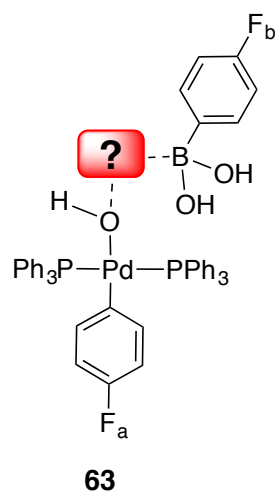
Figure 83. ^{1}H NMR spectrum of **63** at -50 °C, referenced to THF-d_8 (1.72 ppm).
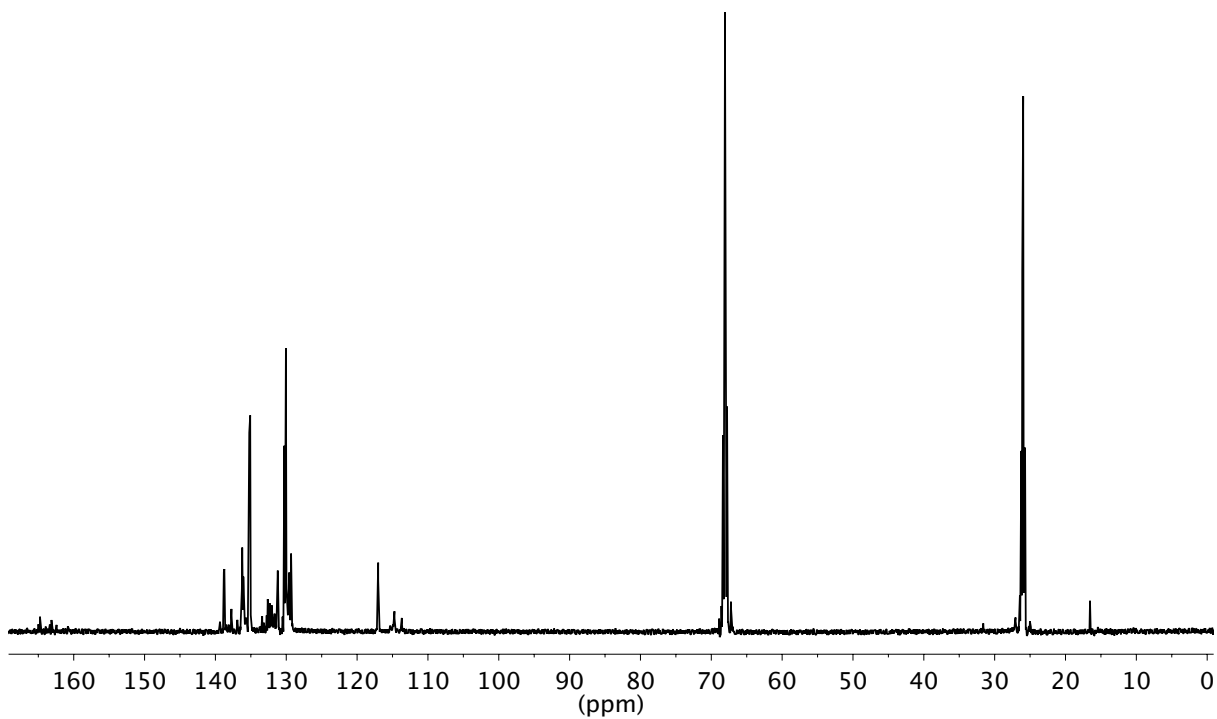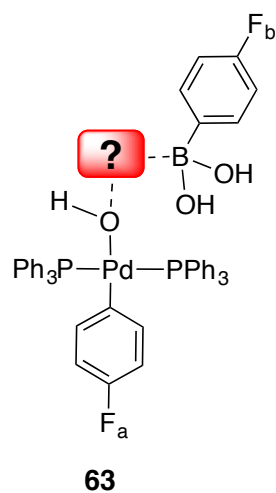
Figure 84. ^{13}C NMR spectrum of **63** at −50 °C, referenced to THF-d_8 (68.21 ppm).
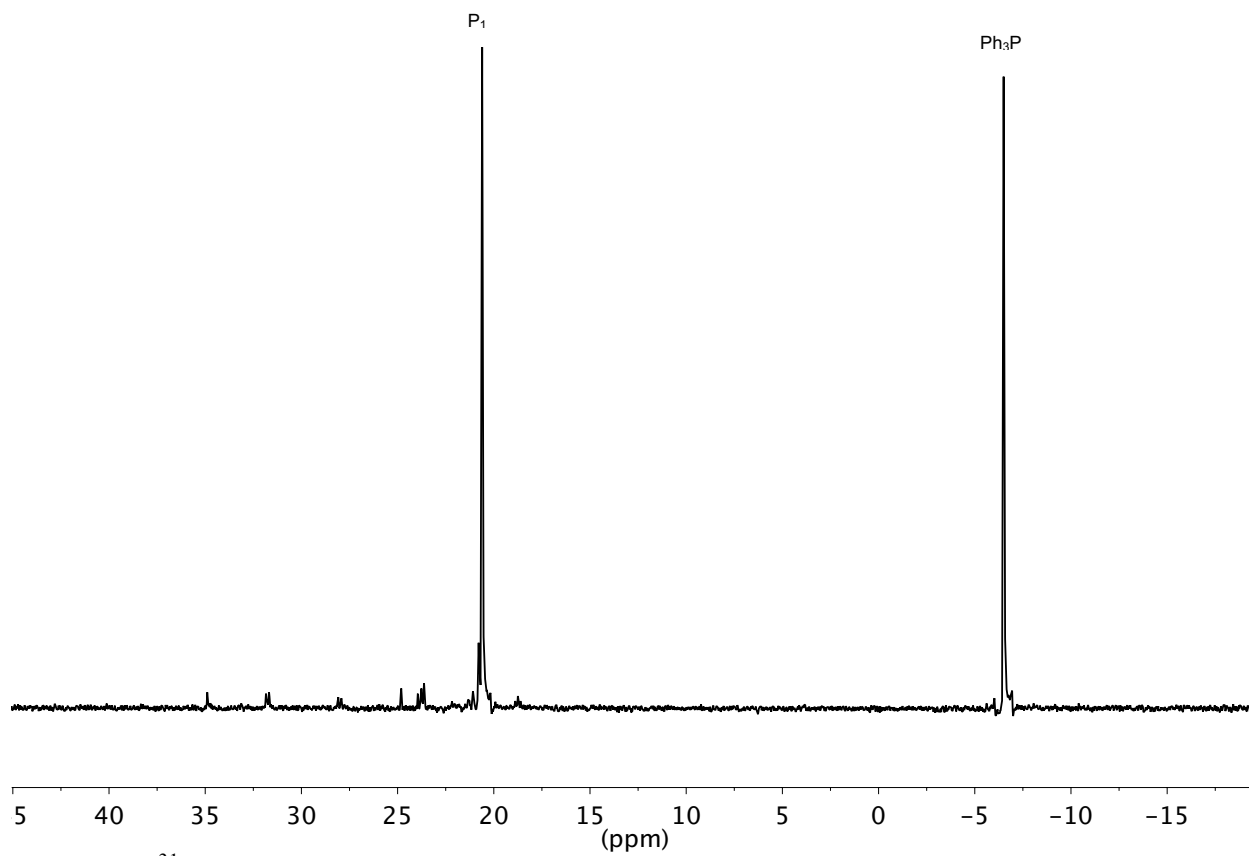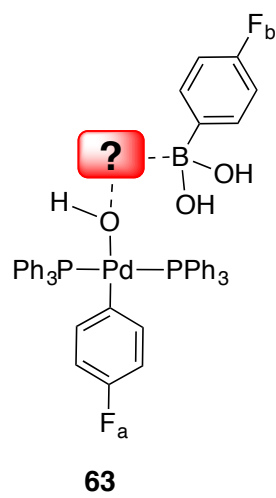
Figure 85. ^{31}P NMR spectrum of **63** at −50 °C, referenced to Ph$_3$P (−6.5 ppm).

132

63
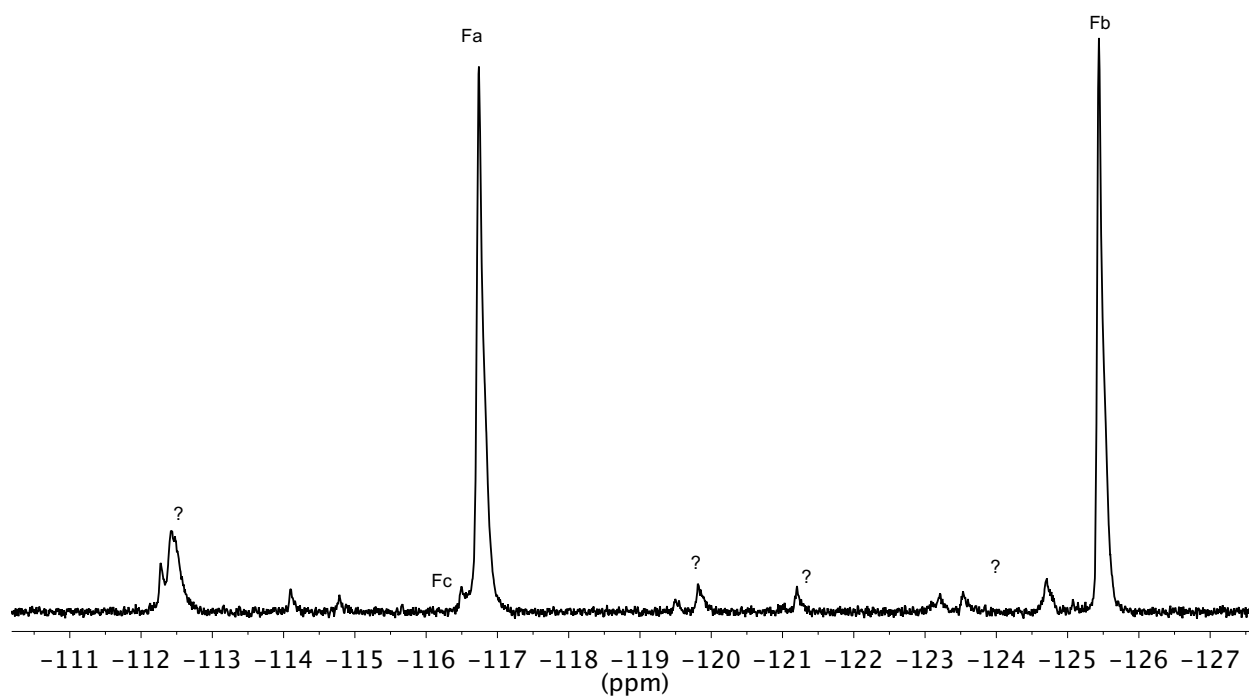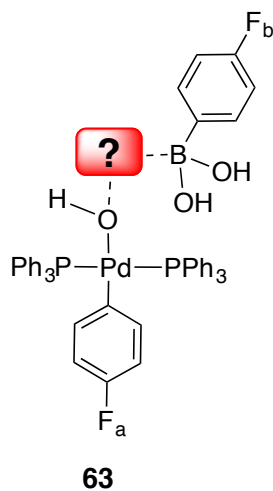
Figure 86. ^{19}F NMR spectrum of **63** at −50 °C, referenced to cross-coupled product **73** (−116.45 ppm).

Experiment 7: Reaction of Ph₃P complex 57 with 65 and 3.0 equiv of Ph₃P.

A dram vial was charged with 4-trifluoromethylphenylboronic acid (6 mg, 240 μmol, 1.0 equiv) followed by 100 μL of THF-d_8.

An oven dried, 5-mm, NMR tube as charged with [(Ph₃P)Pd(4-FC₆H₄)(μ-OH)]₂ (14.4 mg, 15 μmol, 1.0 equiv), sublimed Ph₃P (12 mg, 45 μmol, 3.0 equiv) and 500 μL of THF-d_8 followed by shaking until dissolved. The tube was placed into a −78 °C dry-ice acetone bath followed by the addition of 4-trifluoromethylphenylboronic acid solution (100 μL, 30 μmol, 2.0 equiv). The tube was shaken quickly wiped with a Kimwipe and placed into the probe of the NMR spectrometer pre-cooled to −50 °C. The complex could not be characterized by standard techniques due to the messy aromatic region. However, the structure was assigned by analogy to complex **71** which has been fully characterized.

Data for **67**:

¹⁹F NMR:	(565 MHz, THF-d_8)
	−62.18 (s, FC(12)), −125.48 (s, FC(1))
³¹P NMR:	(243 MHz, THF-d_8)
	21.30 (s, 2 P(Pd))

Figure 87. ^{19}F NMR spectrum of **67** at −40 °C, referenced to excess **57** (−123.79 ppm).

135
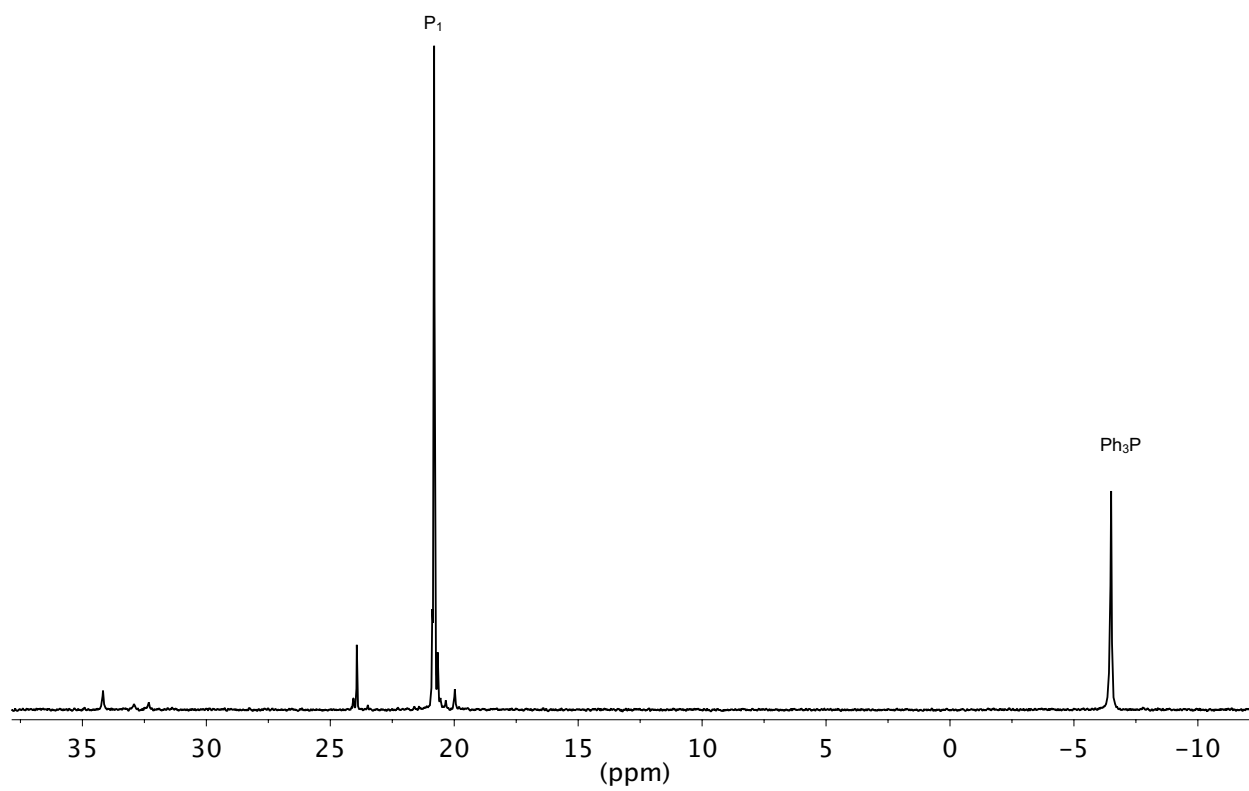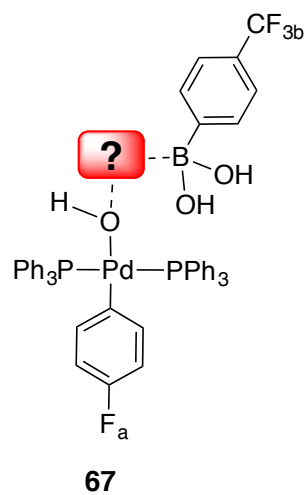
Figure 88. ^{31}P NMR spectrum of **67** at −40 °C, referenced to Ph$_3$P (−6.5 ppm).

136

Experiment 8: Reaction of Ph₃P complex 57 with 66 and 3.0 equiv of Ph₃P.
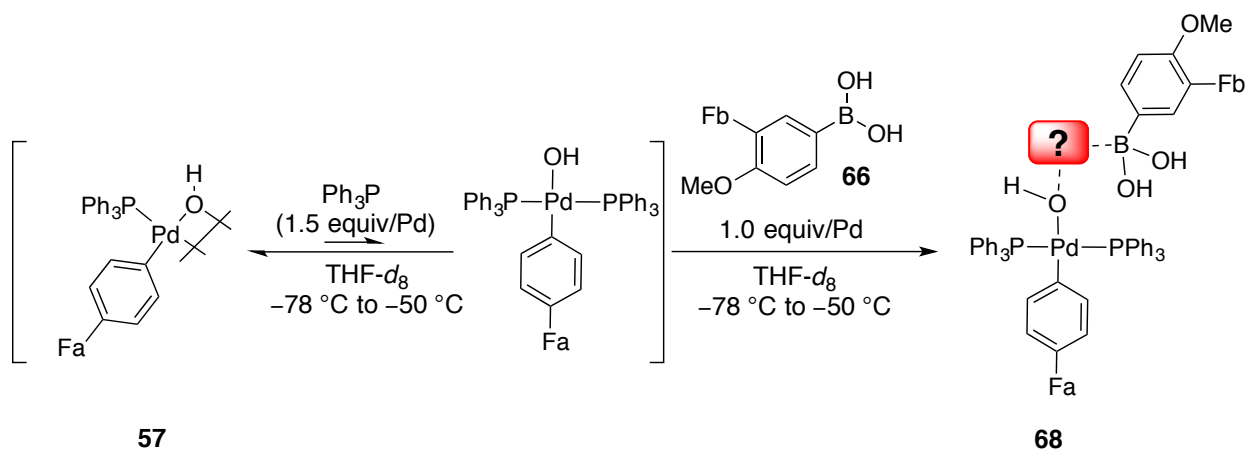
A 1-mL volumetric flask was charged with 4-methyoxy-3-fluorophenylboroxine (151 mg, 331 μmol, 1.0 equiv) followed by H₂O (18 μL, 993 μmol, 3.0 equiv). Then ~0.5 mL of THF-d_8 was added followed by sonication until the solid had dissolved. Once dissolved the flask was filled to the mark with THF yielding a 4-fluorophenylboronic acid solution (1.0 M).

An oven dried, 5-mm, NMR tube as charged with [(Ph₃P)Pd(4-CF₃C₆H₄)(μ-OH)]₂ (6.0 mg, 6.25 μmol, 1.0 equiv), sublimed Ph₃P (9.8 mg, 19 μmol, 3.0 equiv) and 500 μL of THF followed by shaking until dissolved. The tube was placed into a −78 °C dry-ice acetone bath followed by the addition of 4-fluorophenylboronic acid solution (13 μL, 13 μmol, 2.0 equiv). The tube was shaken quickly wiped with a Kimwipe and placed into the probe of the NMR spectrometer pre-cooled to −50 °C. The sample was then warmed to −40 °C

Data for **68**:

¹⁹F NMR: (565 MHz, THF-d_8)

−141.31 (s, FC(12)), −126.47 (s, FC(1))

³¹P NMR: (243 MHz, THF-d_8)

19.95 (s, 2 P(Pd))
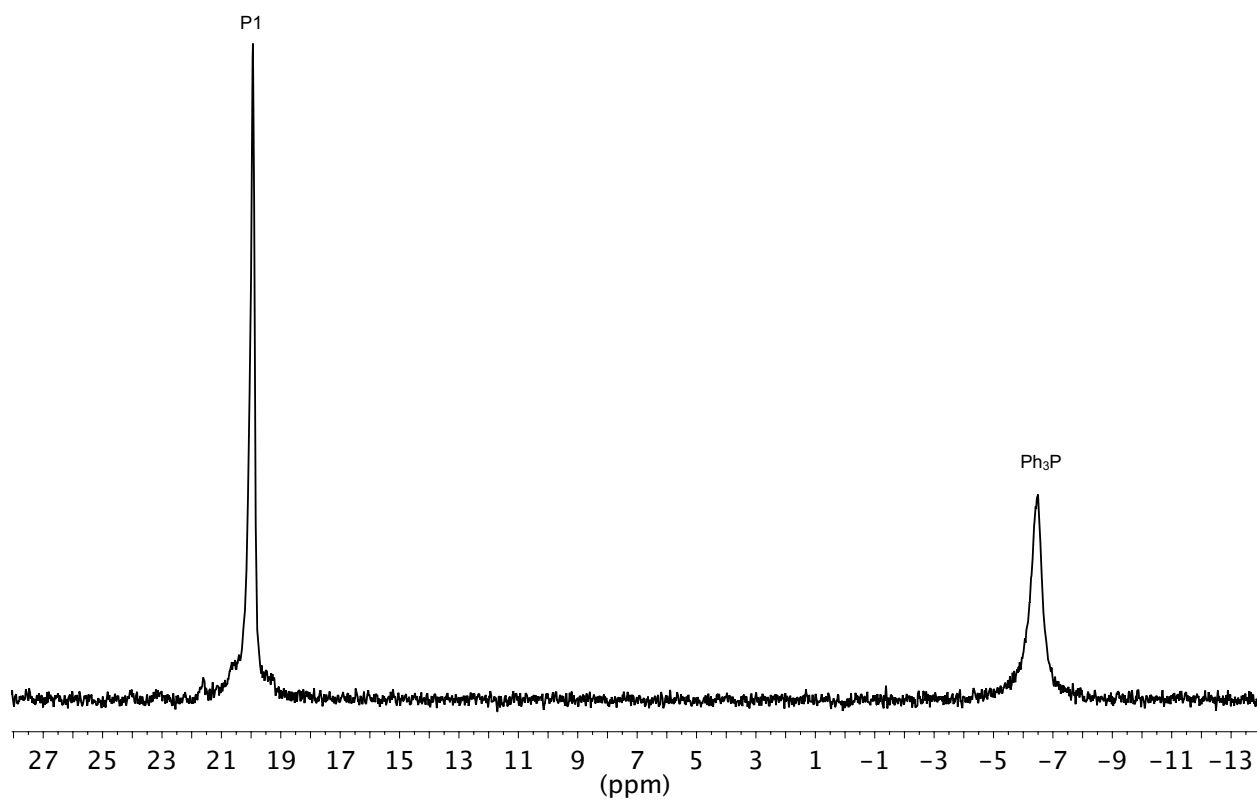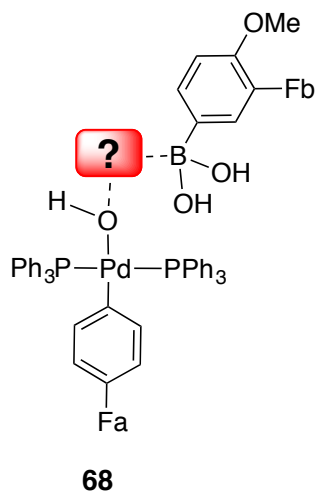
Figure 89. ^{31}P NMR spectrum of **68** at −40 °C, referenced to Ph$_3$P (−6.5 ppm).
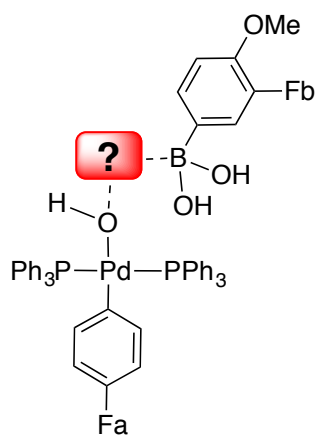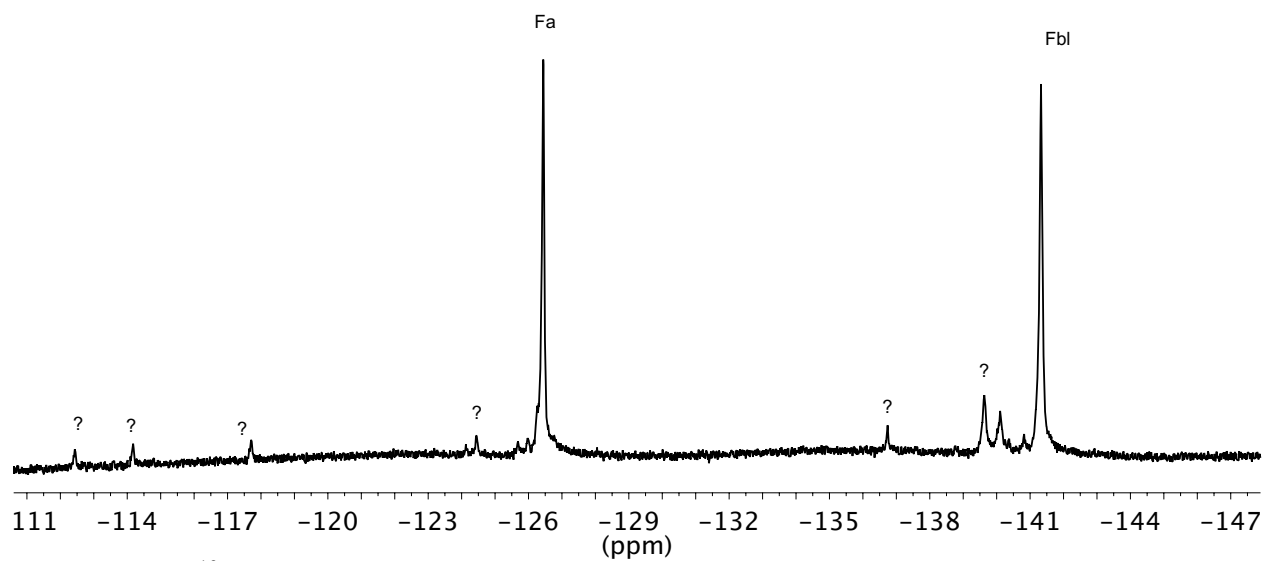
Figure 90. ^{19}F NMR spectrum of **68** at −40 °C, referenced to externally to 4-trifluoromethylbenzene (−63.72 ppm).

Experiment 9: Reaction of Ph₃P complex 64 with 58 and 2.0 equiv of Ph₃P.

64   69
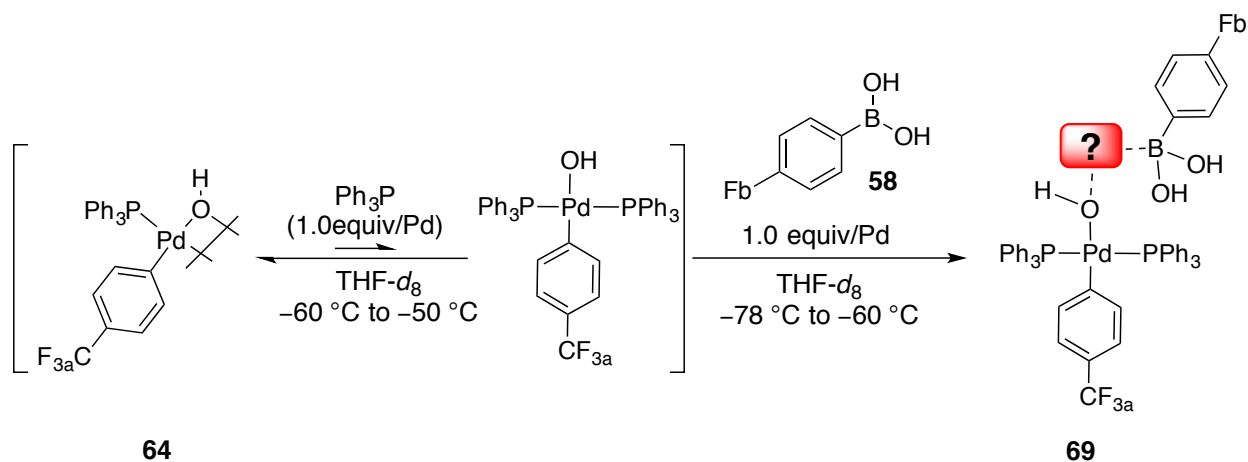
A dram vial was charged with with 4-fluorophenylboronic acid- (3.0 mg, 20 μmol) followed by 50 μL of THF.

An oven dried, 5-mm, NMR tube as charged with [(Ph₃P)Pd(4-CF₃C₆H₄)(μ-OH)]₂ (10 mg, 10.0 μmol, 1.0 equiv), sublimed Ph₃P (5.3 mg, 10 μmol, 2.0 equiv) and 500 μL of THF followed by shaking until dissolved. The tube was placed into a −78 °C dry-ice acetone bath followed by the addition of 4-fluorophenylboronic acid solution (50 μL, 20 μmol, 2.0 equiv). The tube was shaken quickly wiped with a Kimwipe and placed into the probe of the NMR spectrometer pre-cooled to −50 °C. The sample was then warmed to −40 °C where the observation of a new complex was observed.

Data for **69**:

^{19}F NMR: (565 MHz, THF-d_8)

        −118.50 (s, FC(12)), −61.10 (s, FC(1))

^{31}P NMR: (243 MHz, THF-d_8)

        21.11 (s, 2 P(Pd))

64 **58** **69**
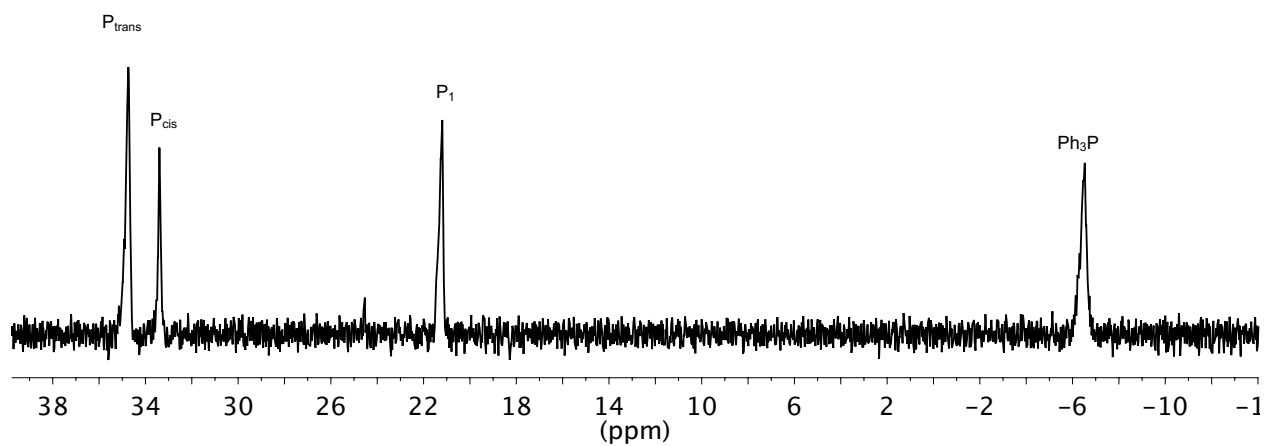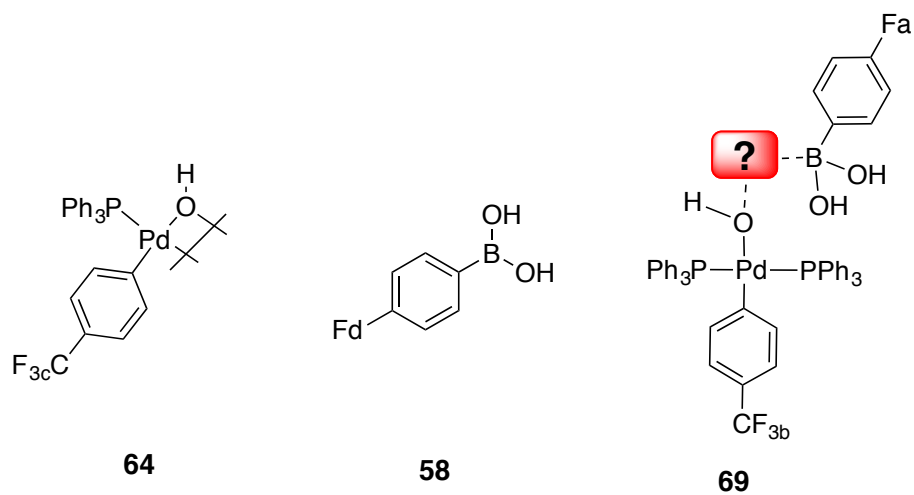
Figure 91. ^{31}P NMR spectrum of **68** at −60 °C, referenced to Ph$_3$P (−6.5 ppm).
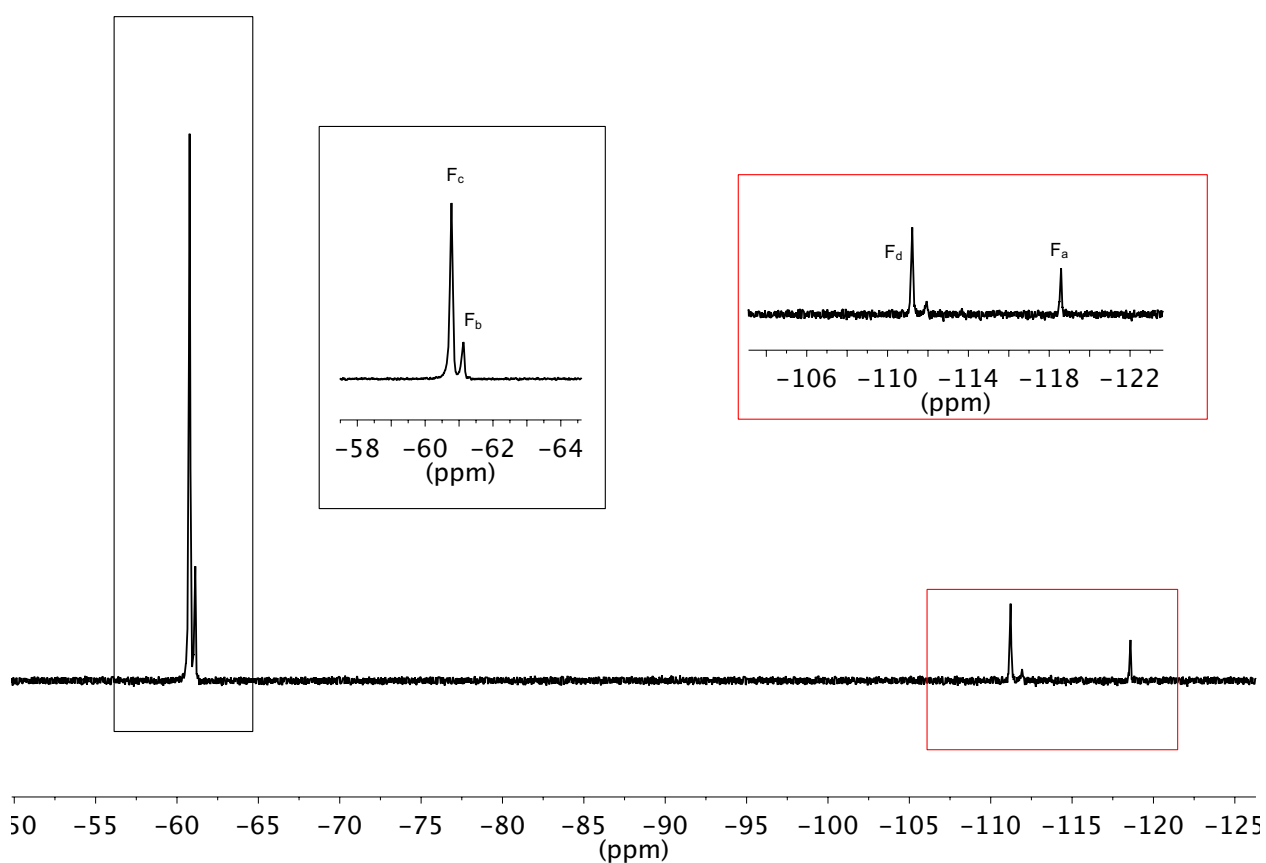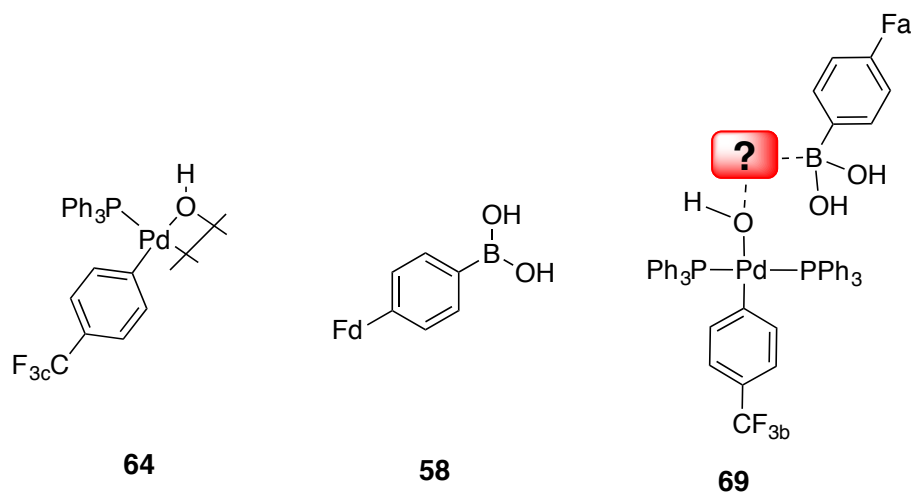
Figure 92. ^{19}F NMR spectrum of **68** at −40 °C, referenced to excess **58** (−111.21 ppm).

Experiment 10: Preparation of 6-B-3 complex 71 from 70 and 58.
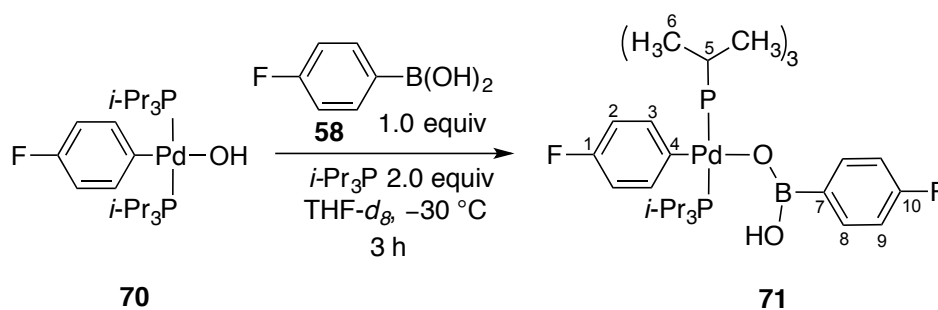
A flame dried, 1.0 mL volumetric flask was charged with 4-fluorophenylboroxine (26 mg, 71 μmol, 1.0 equiv), H_2O (4 μL, 222 μmol, 3.1 equiv) and filled to the mark with freshly distilled (NaK) THF-d_8 generating a 4-fluorophenylboronic acid solution (0.21 M).

An oven-dried, 5-mm, quartz NMR tube was taken into the glove box and both *trans*-(*i*-Pr$_3$P)$_2$Pd(4-FC$_6$H$_4$)(OH) (10.8 mg, 20 μmol, 1.0 equiv) and *i*-Pr$_3$P (7.6 μL, 40 μmol, 2.0 equiv) were added, followed by the addition of 500 μL of freshly distilled (NaK) THF-d_8. The tube was capped with a septum and Teflon taped followed by removal from the glove box. The tube was shaken and placed into a −78 °C dry-ice acetone bath followed by the addition of 95 μL (20 μmol, 0.21 M, 1.0 equiv) of the freshly prepared 4-fluorophenylboronic acid solution (above). The tube was shaken and quickly cleaned with a Kimwipe then placed into the probe of the NMR spectrometer pre-cooled to −30 °C. After ~3 h the reaction was found to be at completion and the complex was characterized by 1D and 2D NMR experiments at −30 °C. (This reaction was performed multiple times where no reaction was observed between **70** and **57** at −60 °C). The following day the sample was placed into a −78 °C dry-ice acetone bath followed by the addition of internal standards 1,4-difluorobenzene (0.5 μL, 5 μmol, 0.25 equiv) and Ph$_4$BNa (2.0 mg, 6 μmol, 0.3 equiv) as a 100 μL THF-d_8 solution to reference the ^{19}F and ^{11}B NMR spectra.

Data for **71:**

^{1}H NMR: (600 MHz, THF-d_8)

7.76 (dd, ^3J(H-H) = 7 Hz, 2 HC(8)), 7.45 (dd, ^3J(H-H) = 7 Hz, 2 HC(3)), 6.88 (m, 2 HC(9)), 6.71 (m, 2 CH(2)), 4.47 (s, HO), 2.15 (m, 6 HC(5)), 1.23 (m, 36 HC(6))

^{13}C NMR: (151 MHz, THF-d_8)

165.77, 164.16 (d, ^1J(F-C) = 244 Hz, 1 C(10)), 162.60, 161.02 (d, ^1J(F-C) = 241 Hz, 1 C(1)), 141.59 (t, ^2J(P-C) = 4 Hz, 1 C(4)), 140.84 (m, 2 C(3)), 138.68 (s, 1

C(7)), 137.90 (d, ^3J(F-C) = 8 Hz, 2 C(8)), 114.77 (d, ^2J(F-C) = 14 Hz, 2 C(9)), 114.65 (d, ^2J(F-C) = 14 Hz, 2 C(2)), 25.38 (t, J = 10 Hz, 6 C(5)), 20.88 (s, 12 C(6))

^{19}F NMR: (565 MHz, THF-d_8)

−115.75 (s, FC(10)), −123.77 (s, FC(1))

^{31}P NMR: (243 MHz, THF-d_8)

29.98 (s, 2 P(Pd))

^{11}B NMR: (129 MHz, THF-d_8)

29 ppm (br, B(O))
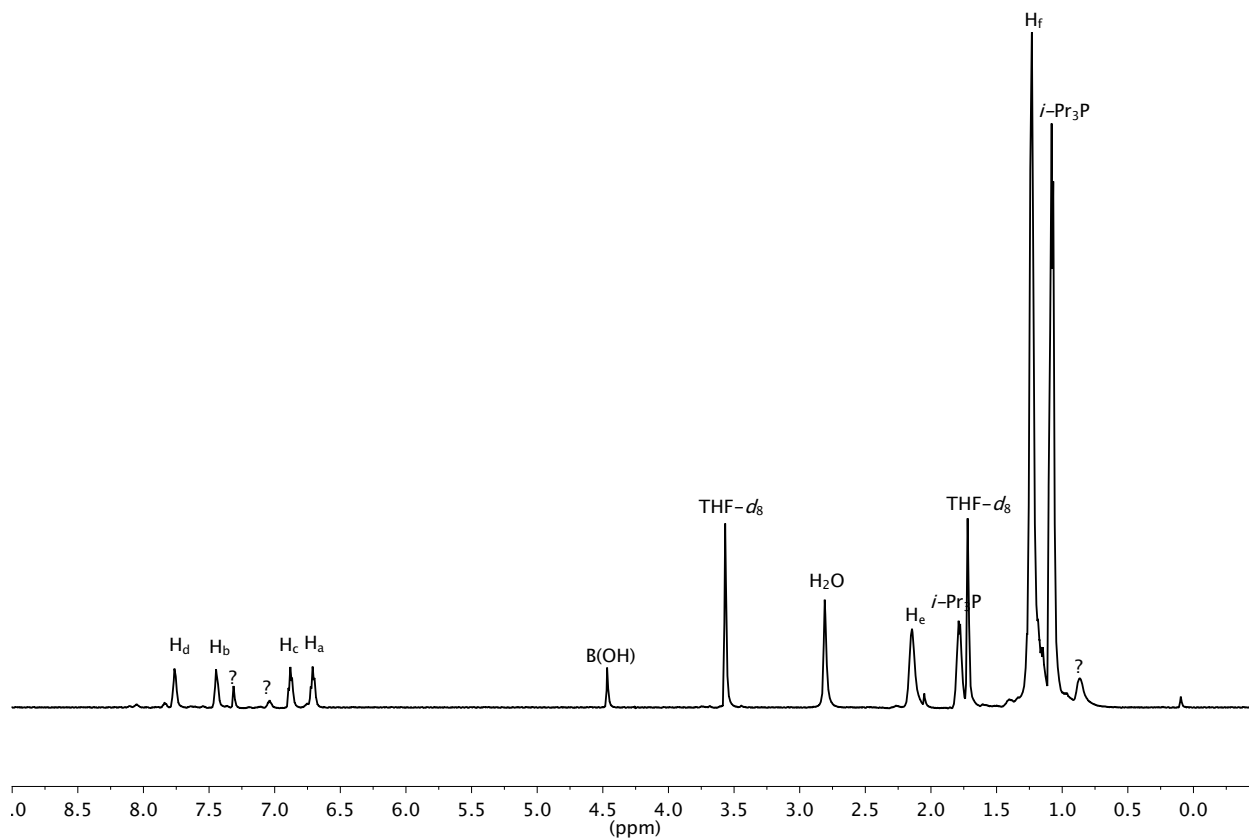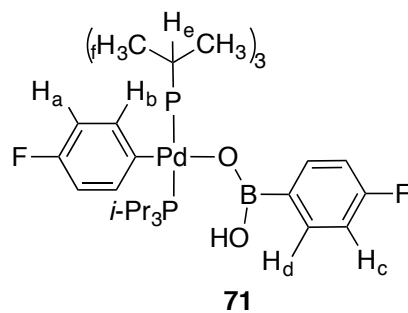
Figure 93. ^{1}H NMR spectrum of **71** at −30 °C, referenced to THF-d_8 (1.72 ppm).
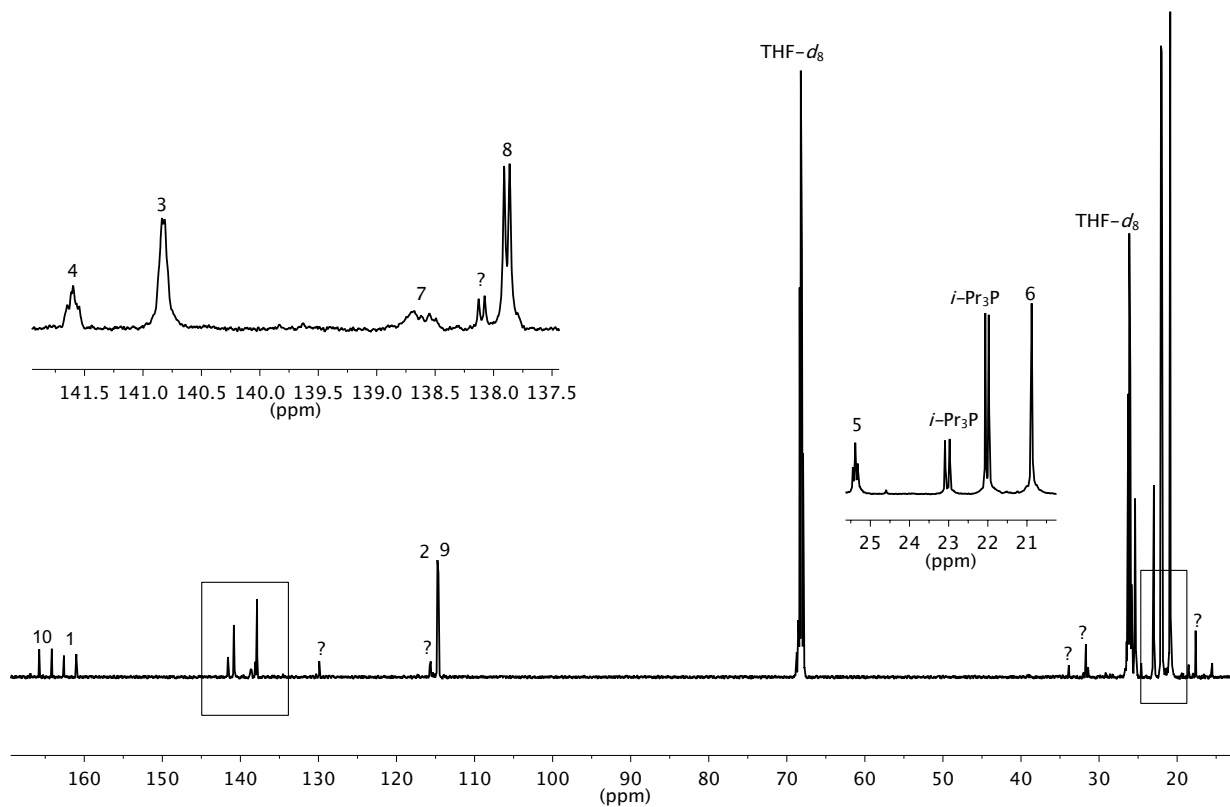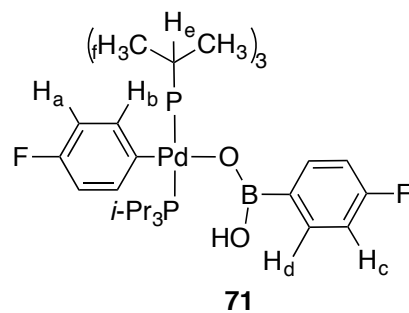
Figure 94. ^{13}C NMR spectrum of **71** at -30 °C, referenced to THF-d_8 (68.21 ppm).

146
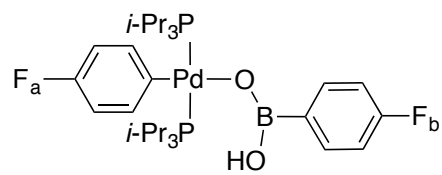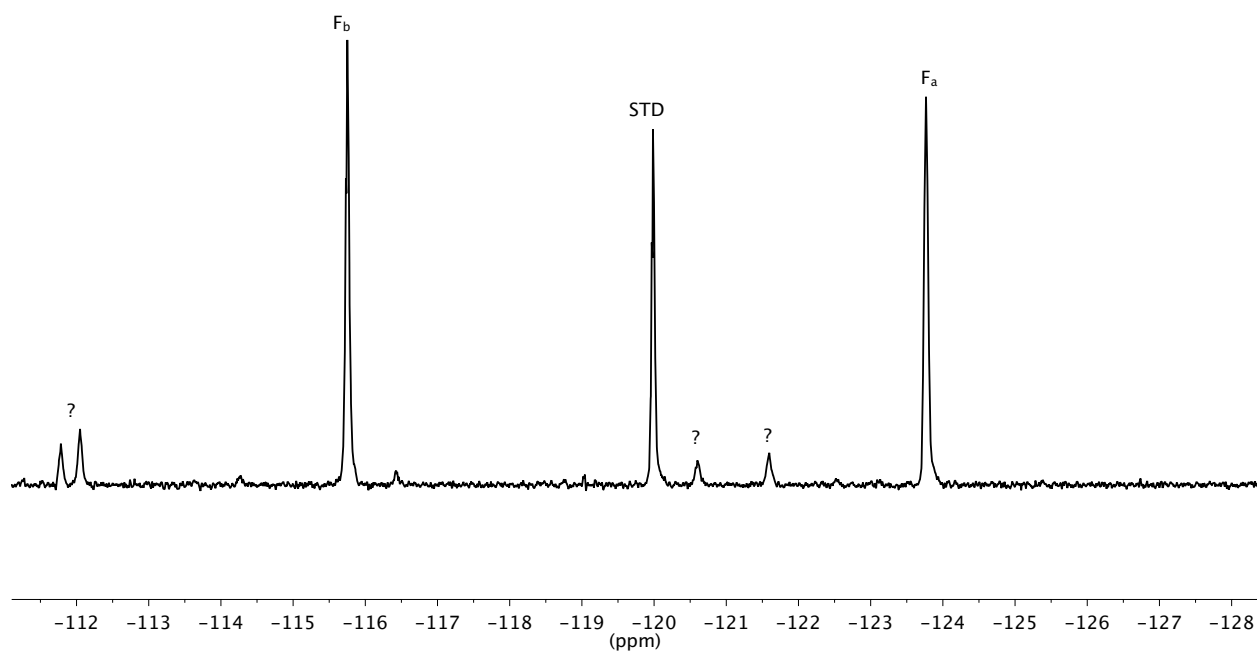
Figure 95. ^{19}F NMR spectrum of **71** at −30 °C, referenced to 1,4-difluorobenzene (−120.00 ppm).
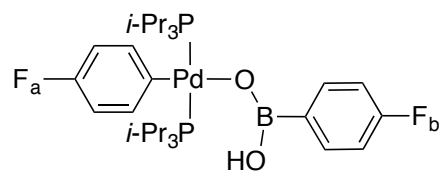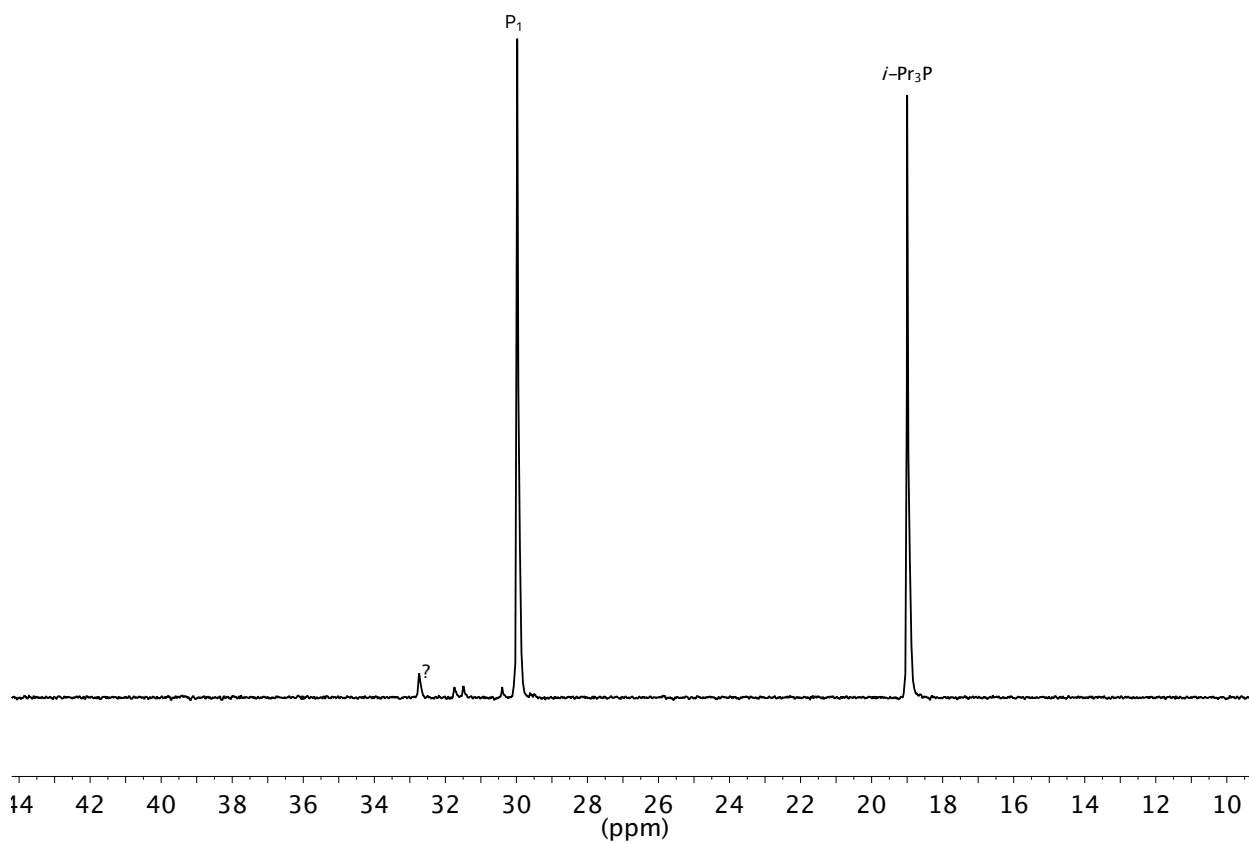
Figure 96. ^{31}P NMR spectrum of **71** at −30 °C, referenced to i-Pr$_3$P (19.00 ppm).

148
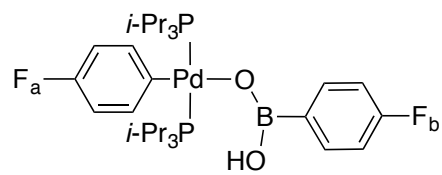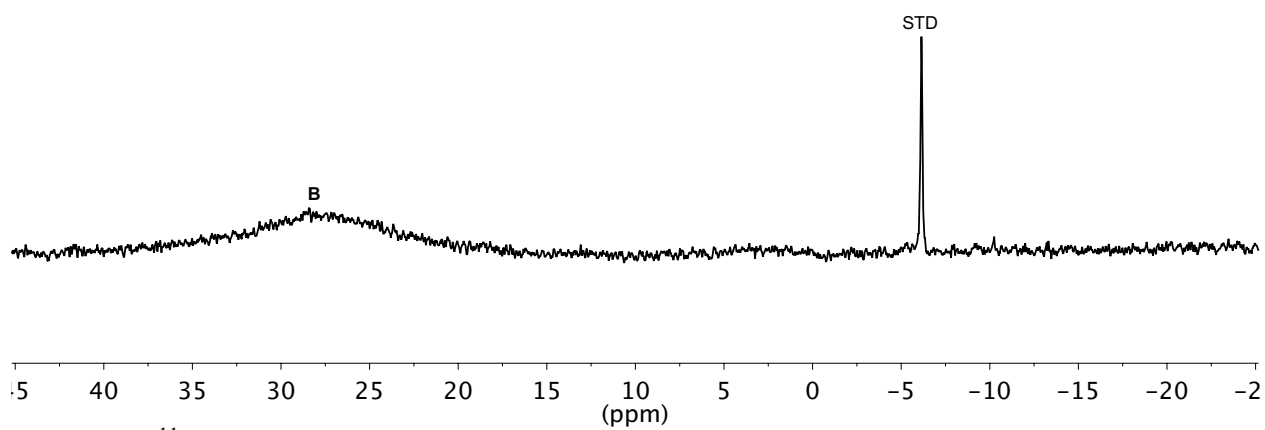
Figure 97. ^{11}B NMR spectrum of **71** at −30 °C, referenced to Ph$_4$BNa (−6.14 ppm).
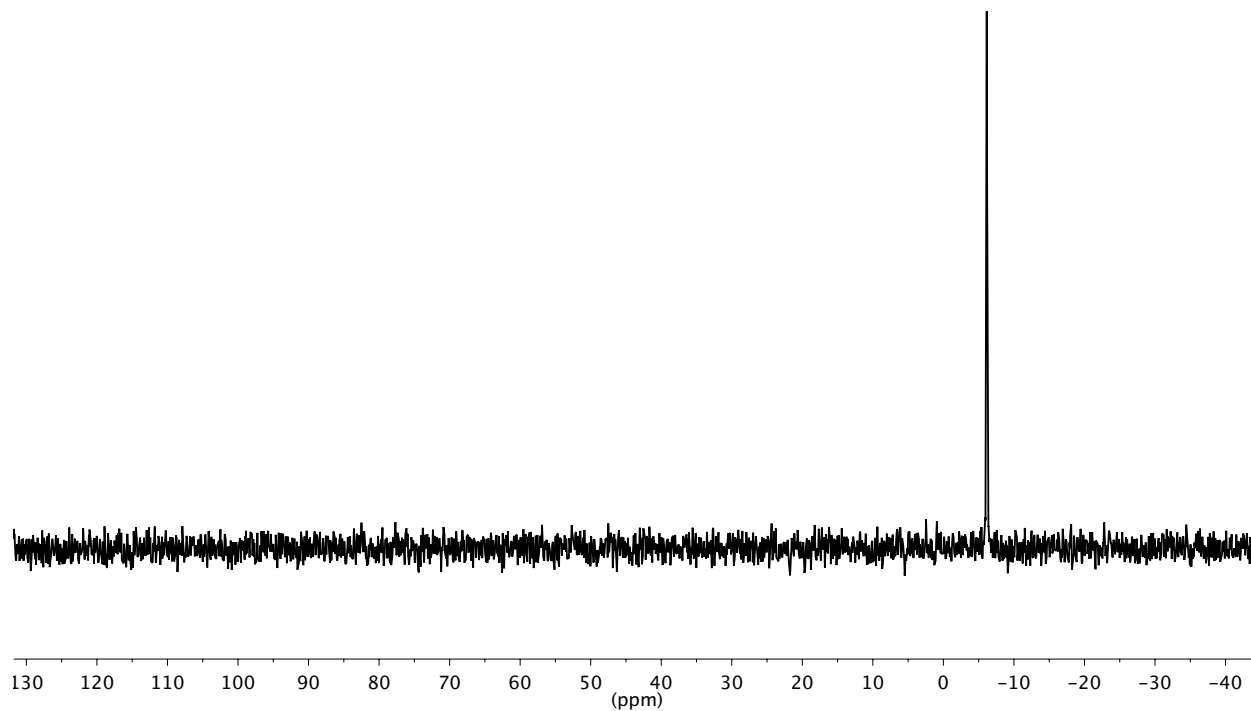
Figure 98. ^{11}B NMR background spectrum of Ph$_4$BNa (-6.14 ppm) in THF.
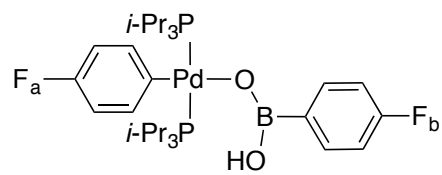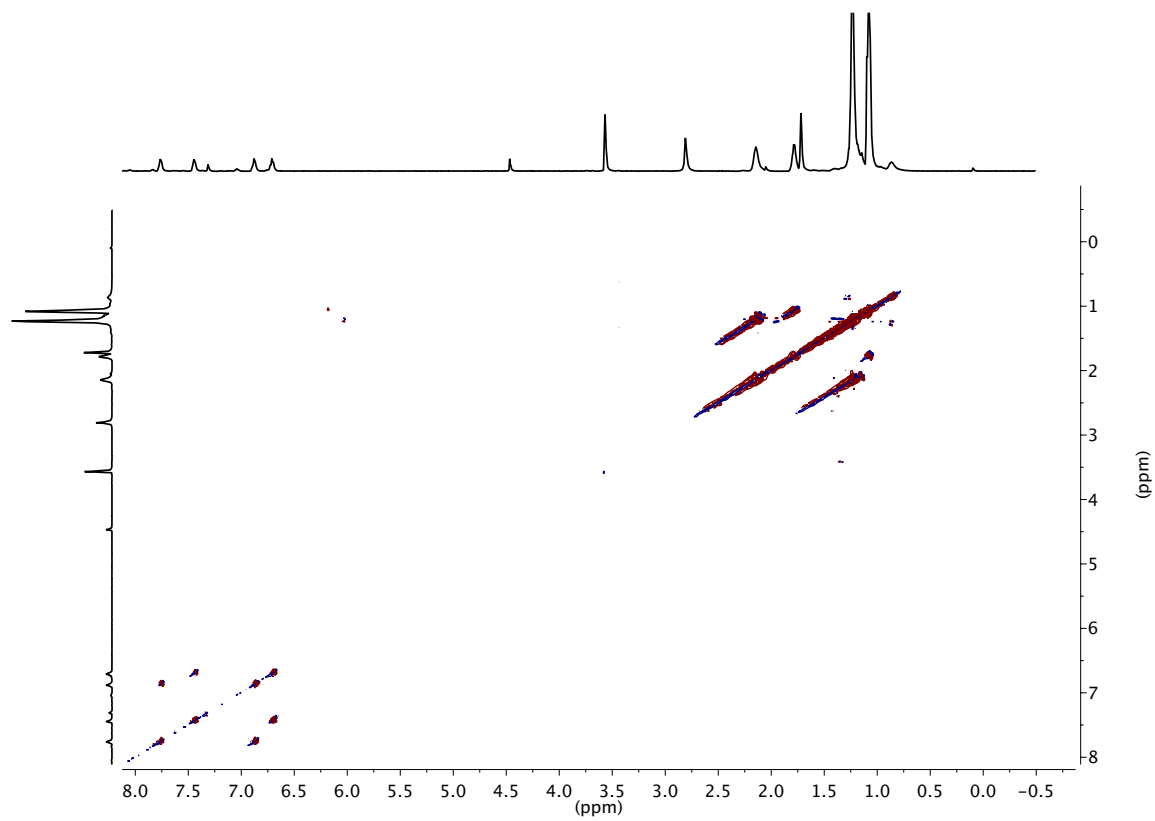
Figure 99. dgfCOSY spectrum of **71** at −30 °C, referenced to THF-d_8 (1.72 ppm).
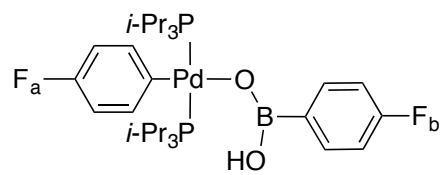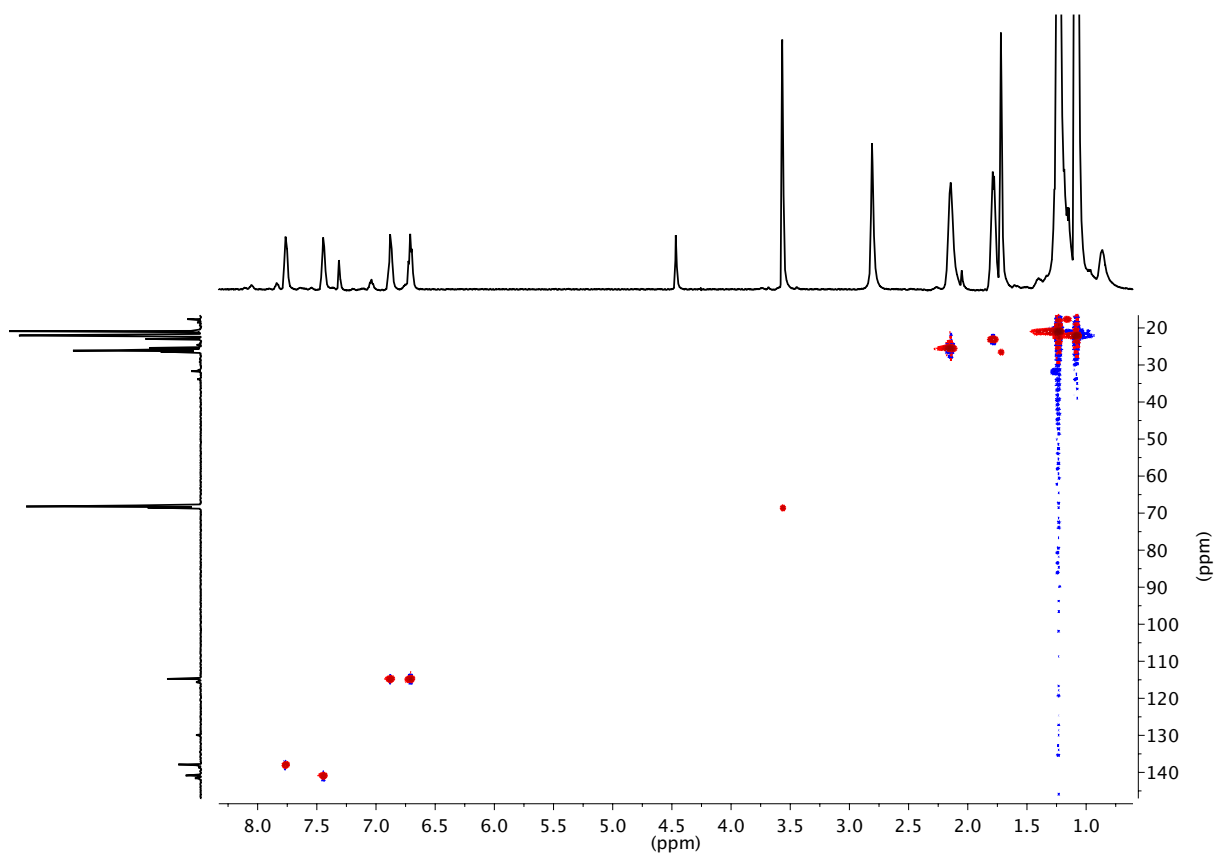
Figure 100. gHSQC spectrum of **71** at −30 °C, referenced to THF-d_8 (1.72 and 68.21 ppm).
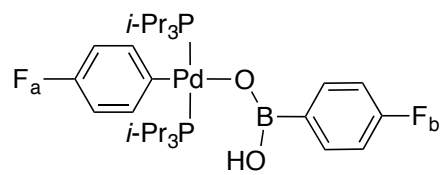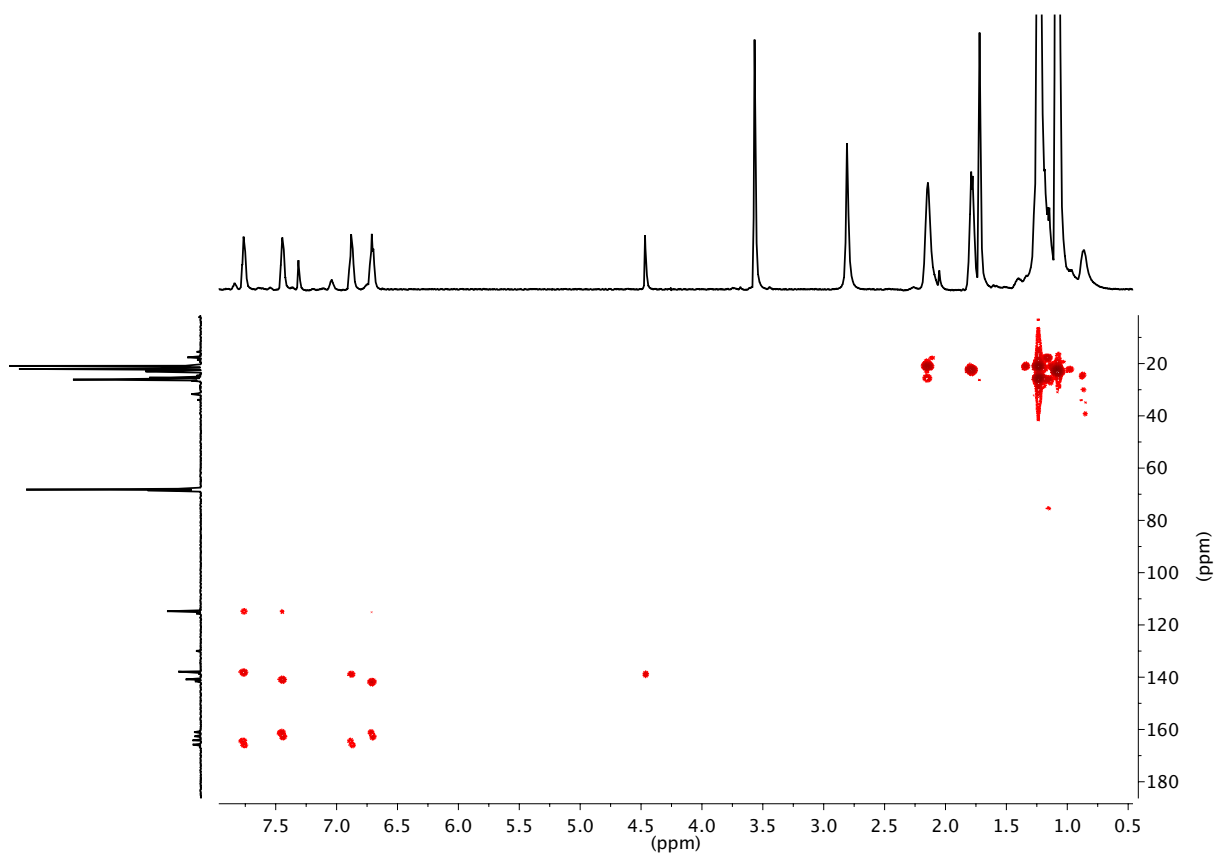
Figure 101. gHMBC spectrum of **71** at −30 °C, referenced to THF-d_8 (1.72 and 68.21 ppm).
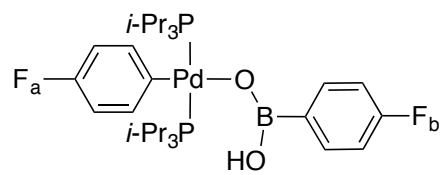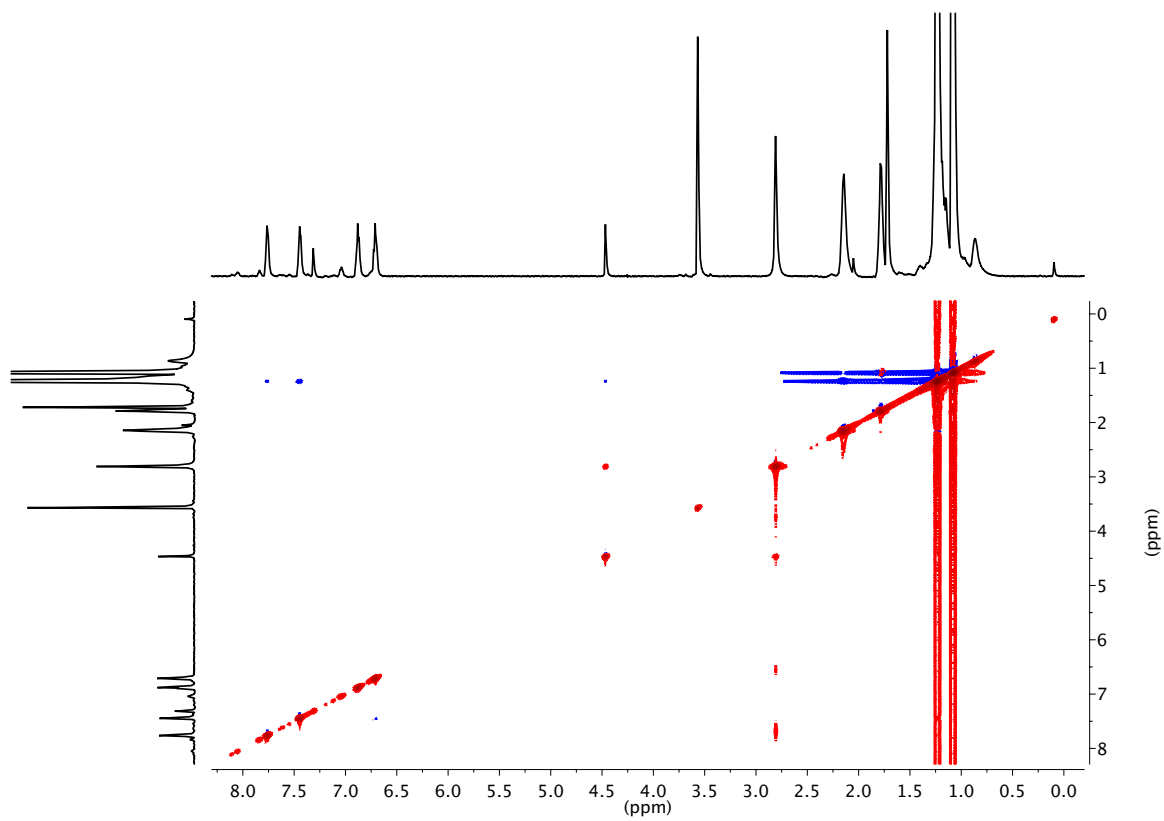
Figure 102. NOESY spectrum of **71** at −30 °C, referenced to THF-d_8 (1.72 ppm).

Experiment 11: Preparation of 6-B-3 complex 71 from 70 and 72.
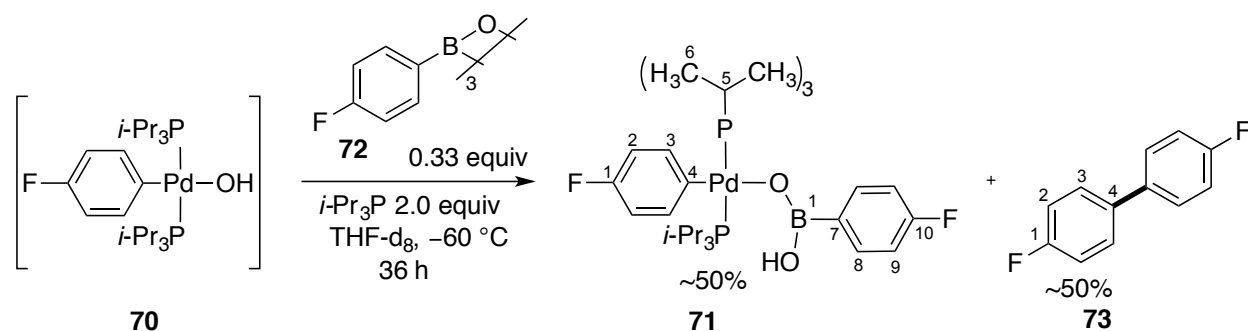
An oven-dried, 5-mm, quartz NMR tube was taken into the glove box and both [(i-Pr$_3$P)Pd(4-FC$_6$H$_4$)(μ-OH)]$_2$ (7.58 mg, 10 μmol, 1.0 equiv) and i-Pr$_3$P (8 μL, 40 μmol, 4.0 equiv) were added, followed by the addition of 500 μL of freshly distilled (NaK) THF-d_8. The tube was capped with a septum and Teflon taped, then shaken. After ~24 h the formation of *trans*-(i-Pr$_3$P)$_2$Pd(4-FC$_6$H$_4$)(OH) was observed and the tube was shaken and placed into a −78 °C dry-ice acetone bath followed by the addition of 4-fluorophenylboroxine 2.5 mg (6.8 μmol, 0.68 equiv) as a solid. The tube was shaken, and quickly cleaned with a Kimwipe and placed into the probe of the NMR spectrometer pre-cooled to −60 °C. After ~36 h a ~50% conversion to both cross-coupling product **73** and complex **71** was observed. The species were confirmed by characterization at −30 °C by 1D and 2D NMR experiments. (Internal standards 1,4-difluorobenzene (0.5 μL, 5 μmol) and Ph$_4$BNa (2 mg, 6 μmol) were added as a THF-d_8 solution at the end of the experiment to reference the ^{19}F and ^{11}B NMR spectra.)

Data for **71**:

^{1}H NMR: (600 MHz, THF-d_8)

7.78 (dd, ^3J(H-H) = 6 Hz, 2 HC(8)), 7.46 (dd, ^3J(H-H) = 6 Hz, 2 HC(3)), 6.88 (m, 2 HC(9)), 6.72 (m, 2 CH(2)), 4.48 (s, HO), 2.15 (m, 6 HC(5)), 1.24 (m, 36 HC(6))

^{13}C NMR: (151 MHz, THF-d_8)

165.77, 164.18 (d, ^1J(F-C) = 245 Hz, 1 C(10)), 162.59, 161.01 (d, ^1J(F-C) = 240 Hz, 1 C(1)), 141.52 (t, ^2J(P-C) = 4 Hz, 2 C(4)), 140.82 (m, 2 C(3)), 137.75 (s, 2 C(7)), 137.95 (d, ^3J(F-C) = 8 Hz, 2 C(8)), 114.76 (d, ^2J(F-C) = 14 Hz, 2 C(9)), 114.64 (d, ^2J(F-C) = 14 Hz, 2 C(2)), 25.37 (t, J = 9 Hz, 6 C(5)), 20.87 (s, 12 C(6))

^{19}F NMR: (565 MHz, THF-d_8)

−115.74 (s, FC(10)), −123.76 (s, FC(1))

<u>^{31}P NMR:</u>　　(243 MHz, THF-d_8)

　　　　29.98 (s, 2 P(Pd))

<u>^{11}B NMR:</u>　　(129 MHz, THF-d_8)

　　　　28 ppm (br, 1 B(O)
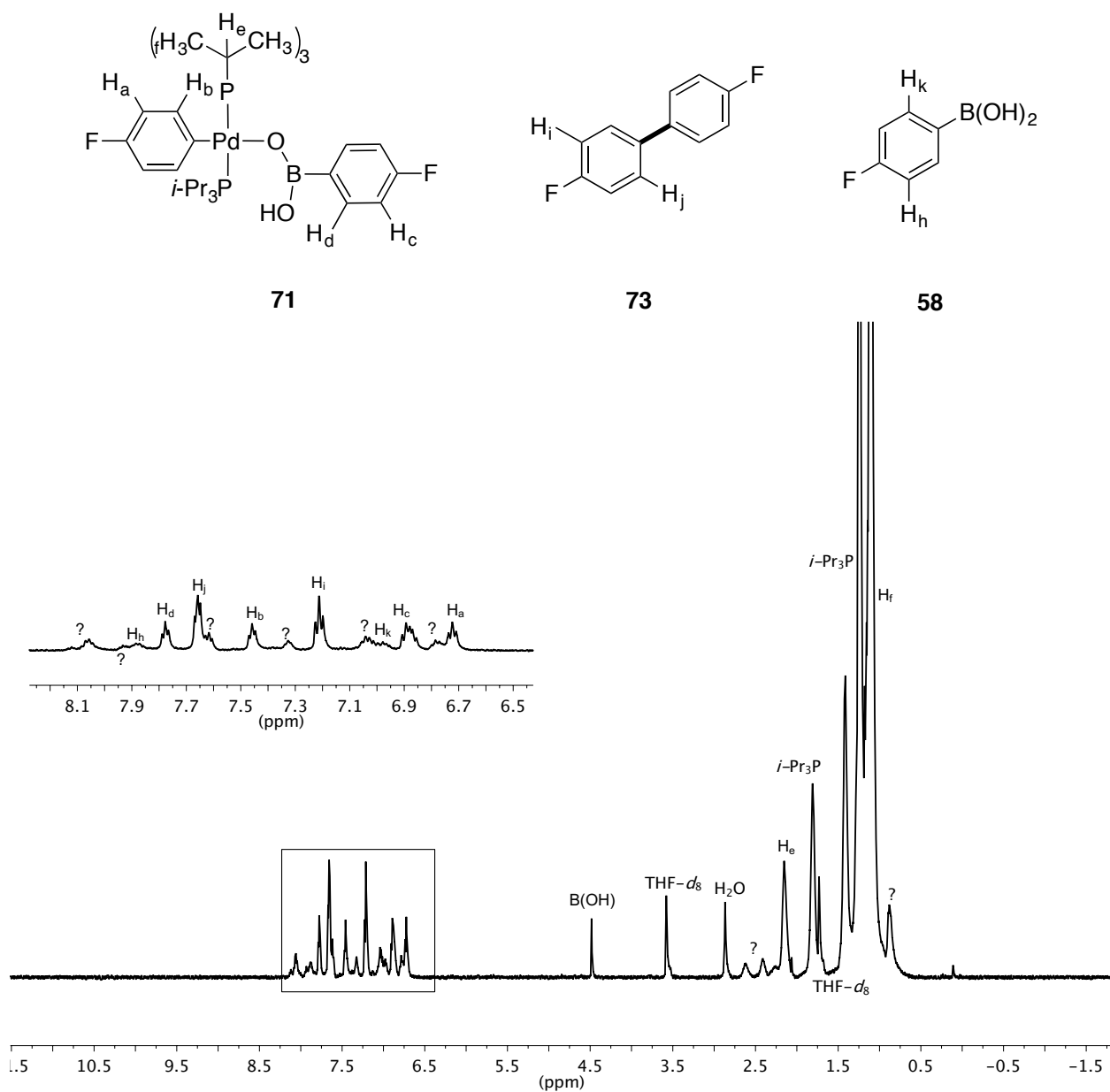
Figure 103. ^{1}H NMR spectrum of **71** and **73** at −30 °C, referenced to THF-d_8 (1.72 ppm).

157
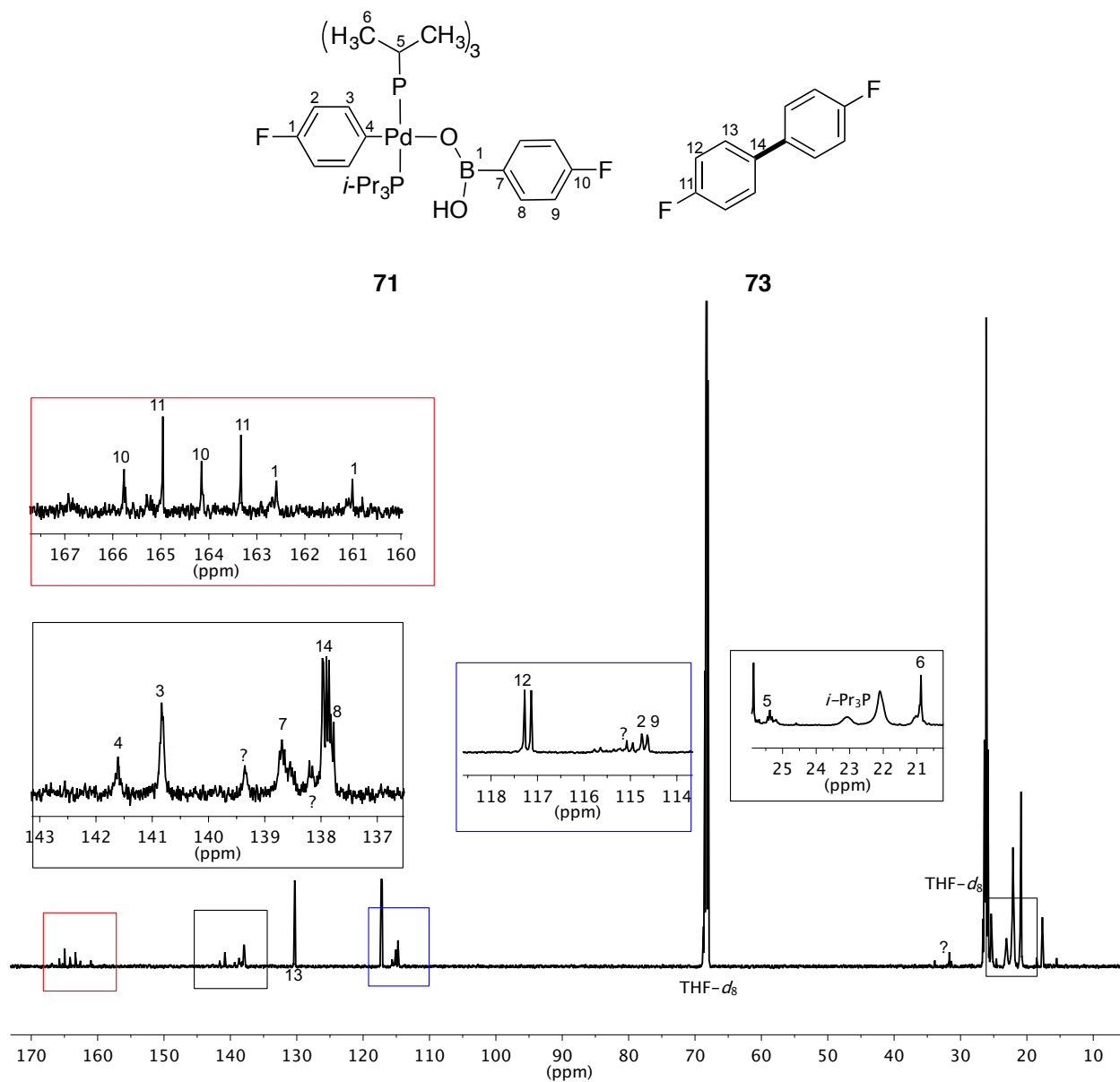
Figure 104. ^{13}C NMR spectrum of **71** and **73** at −30 °C, referenced to THF-d_8 (68.21 ppm).
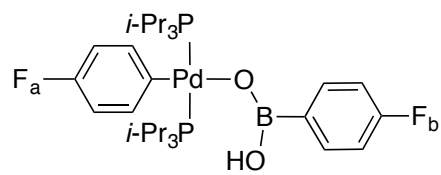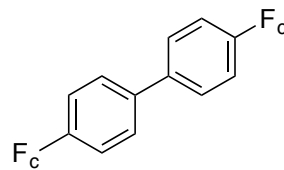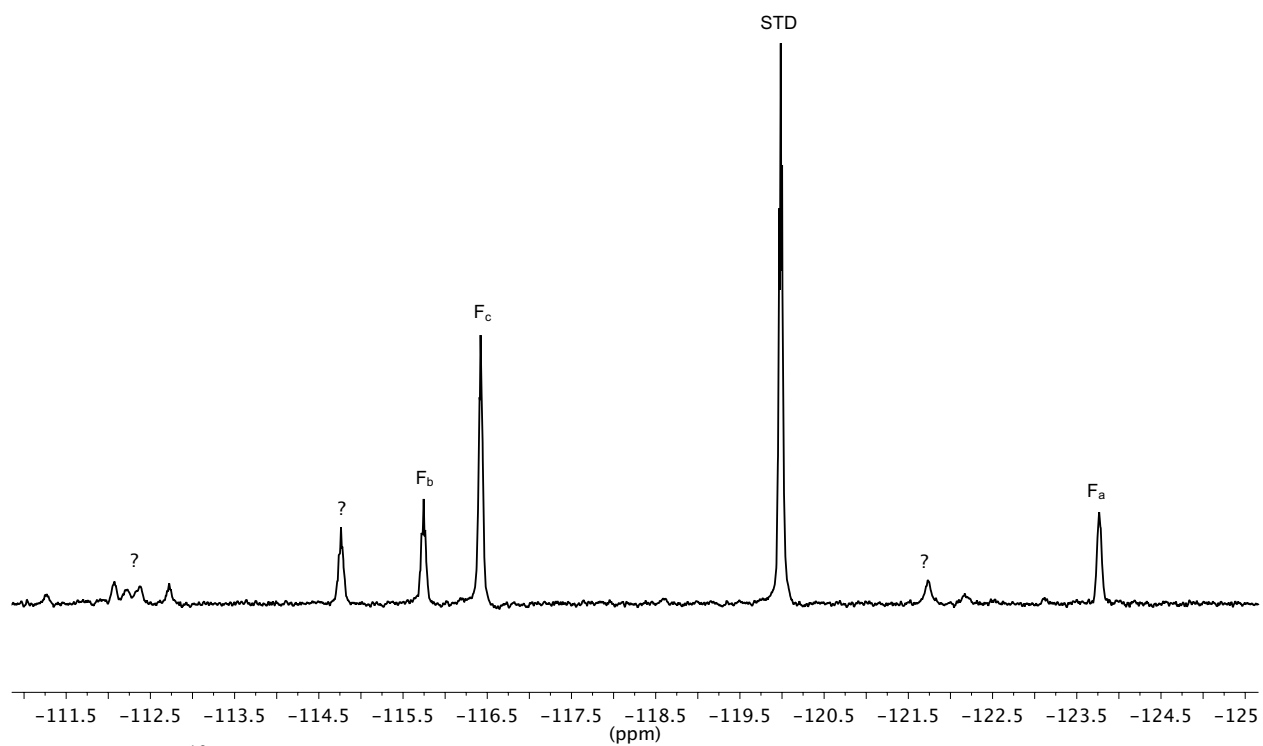
Figure 105. ^{19}F NMR spectrum of **71** and **73** at −30 °C, referenced to 1,4-difluorobenzene (−120.00 ppm).

159
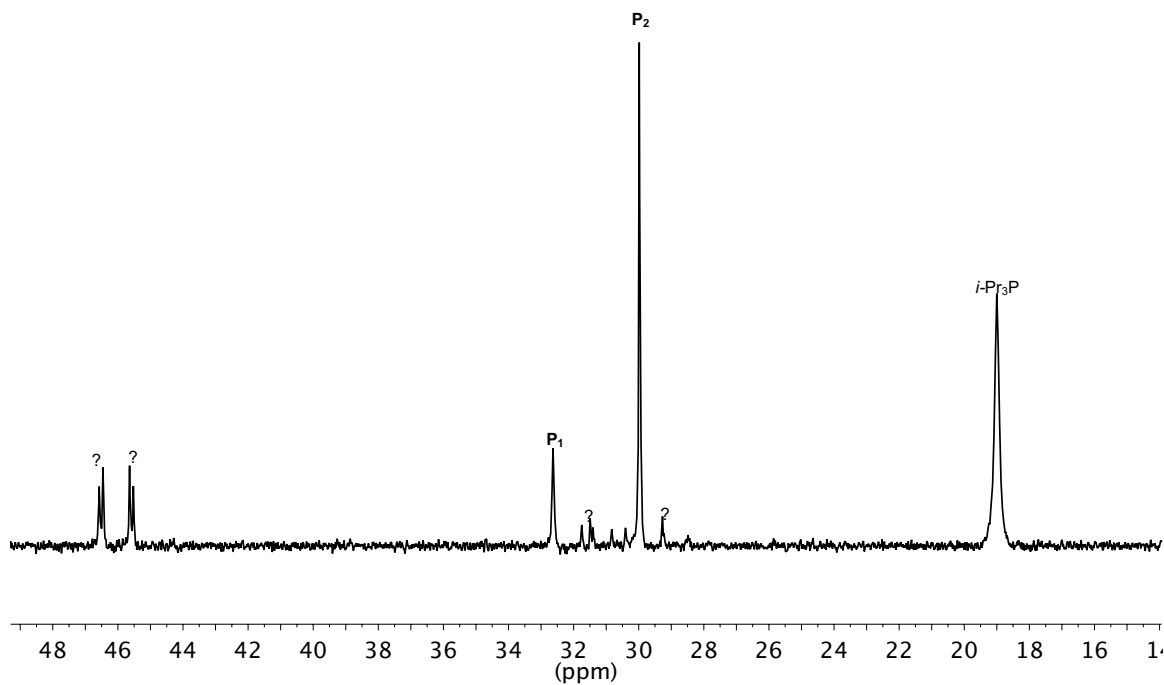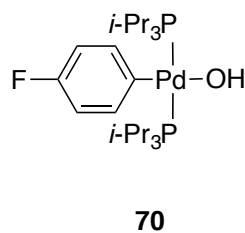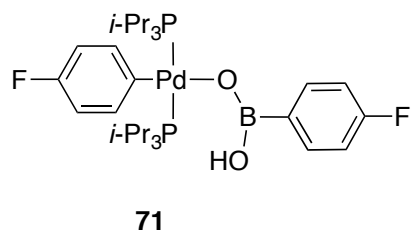
Figure 106. ^{31}P NMR spectrum of **70** and **71** at −30 °C, referenced to i-Pr$_3$P (19.00 ppm).
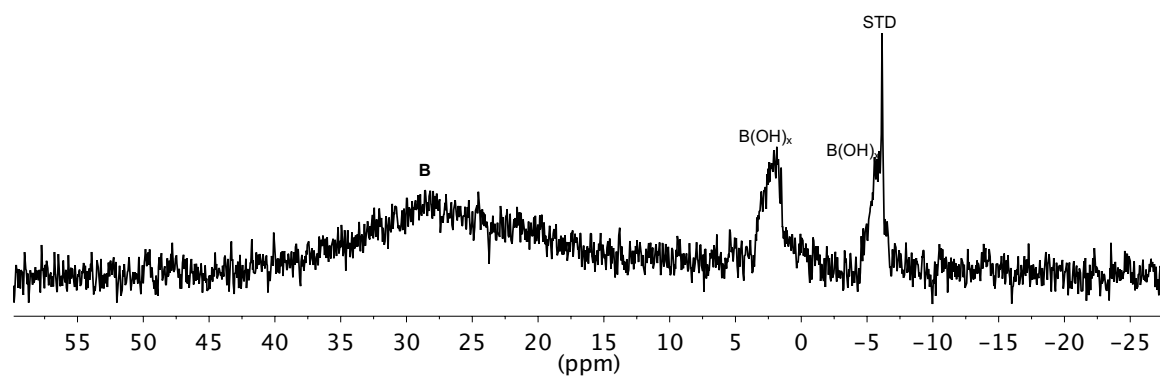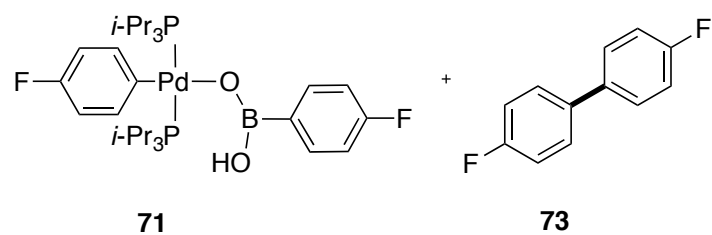
Figure 107. ^{11}B NMR spectrum of **71** and **73** at −30 °C, referenced to Ph$_4$BNa (−6.14 ppm).

161
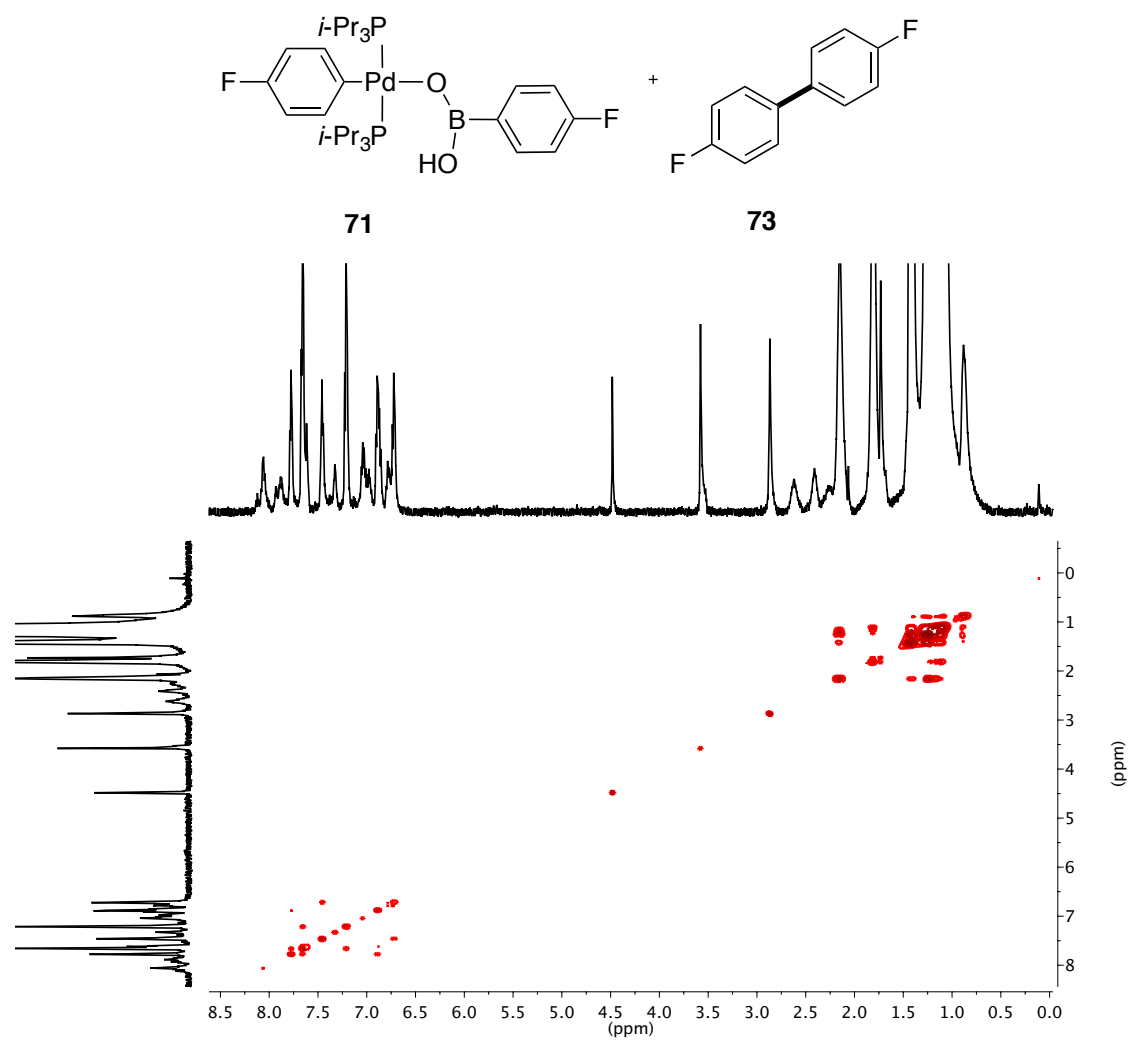
Figure 108. gCOSY spectrum of **71** and **73** at −30 °C, referenced to THF-d_8 (1.72 ppm).
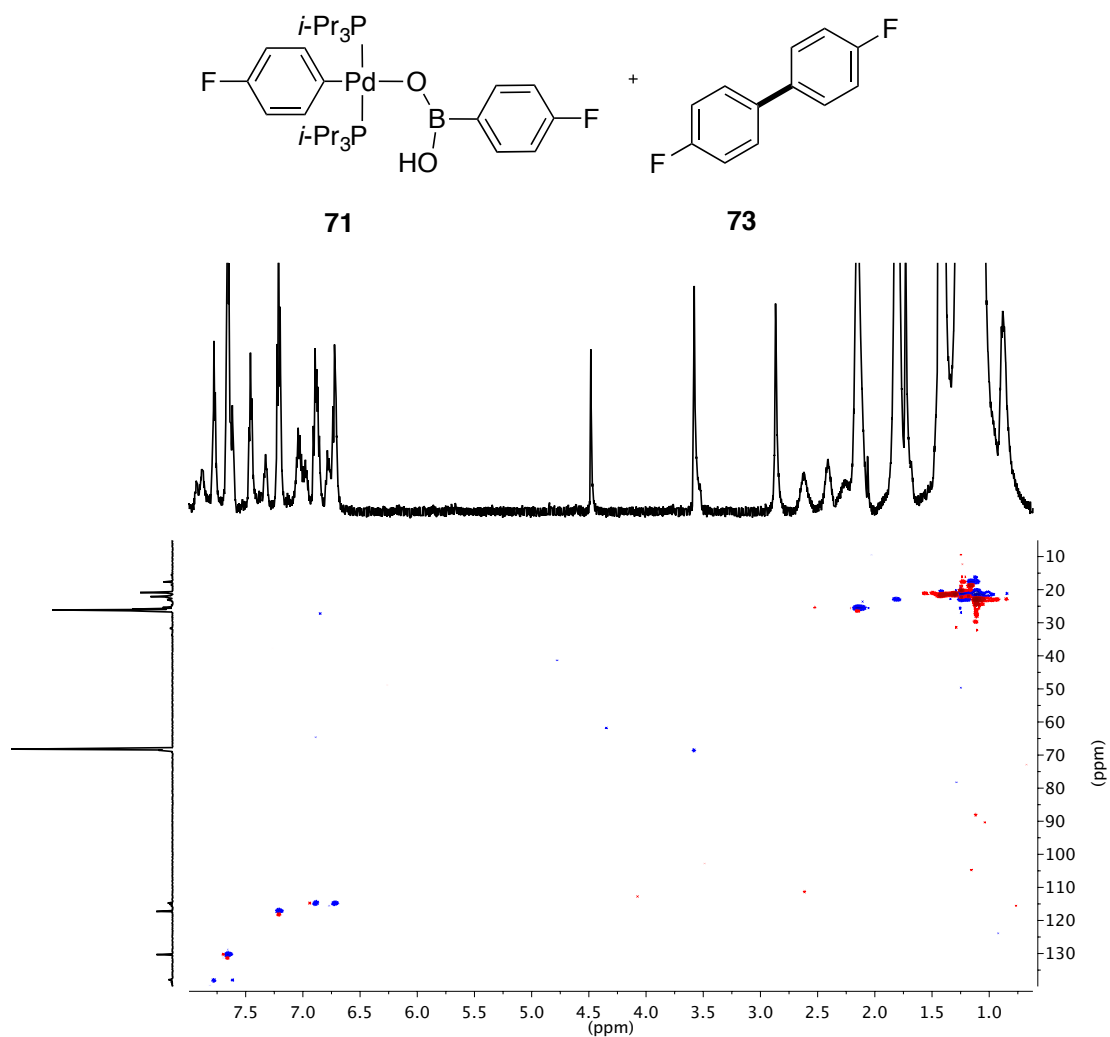
Figure 109. gHSQC spectrum of **71** and **73** at −30 °C, referenced to THF-d_8 (1.72 and 68.21 ppm).
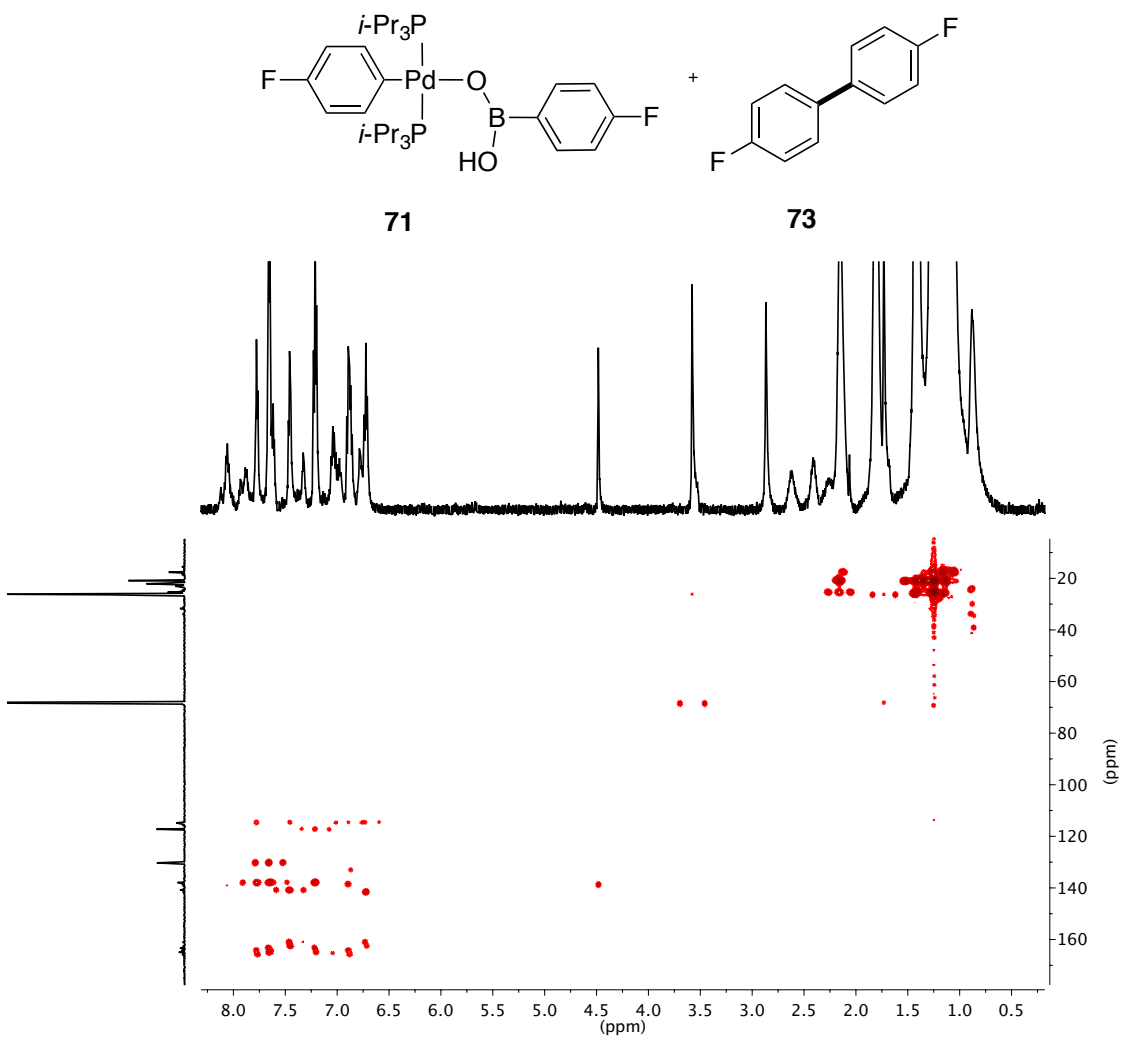
Figure 110. gHMBC spectrum of **71** and **73** at −30 °C, referenced to THF-d_8 (1.72 and 68.21 ppm).
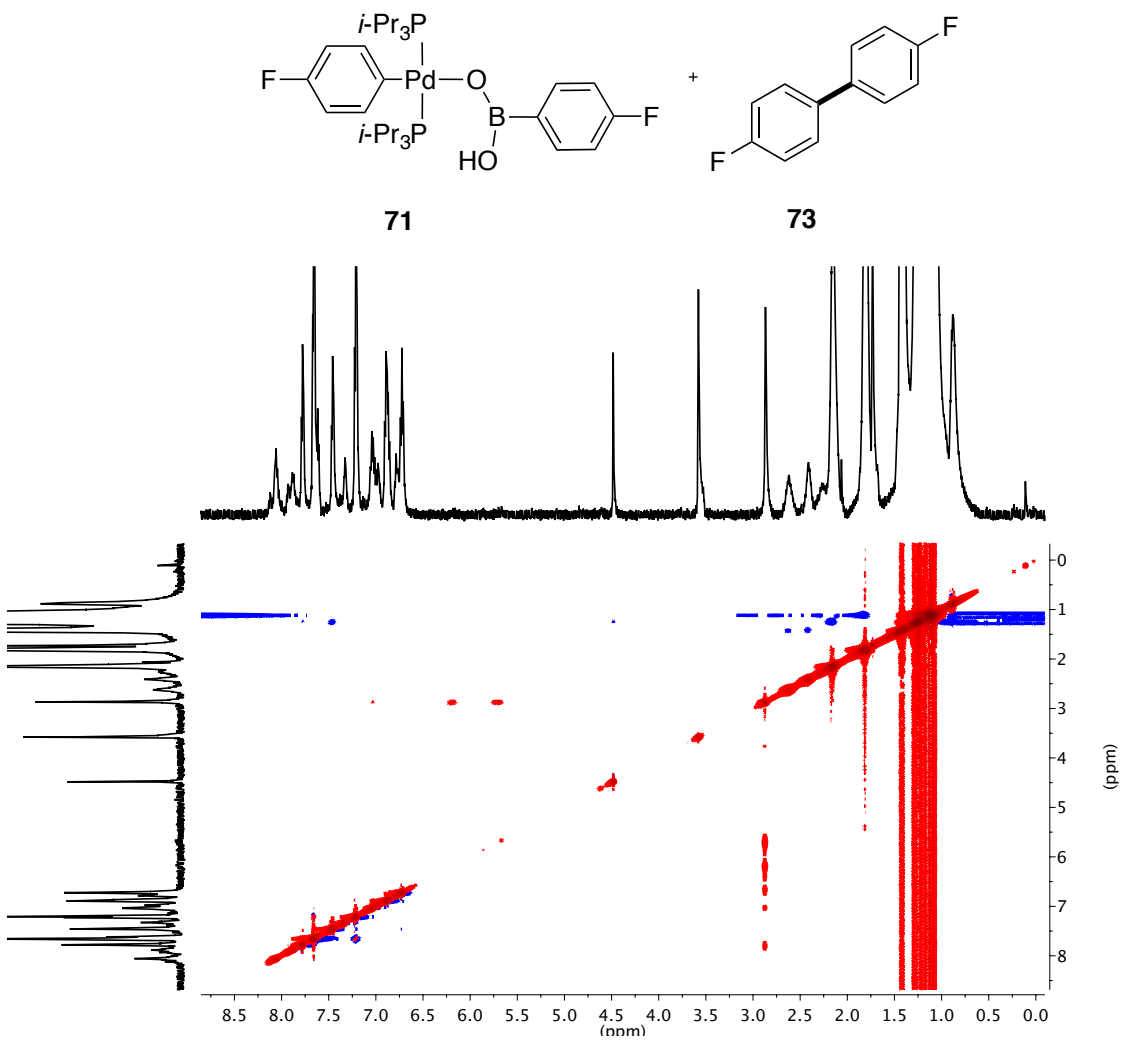
Figure 111. NOESY spectrum of **71** and **73** at −30 °C, referenced to THF-d_8 (1.72 ppm).

Experiment 12: Reaction of 76 with potassium arylboronate 78.
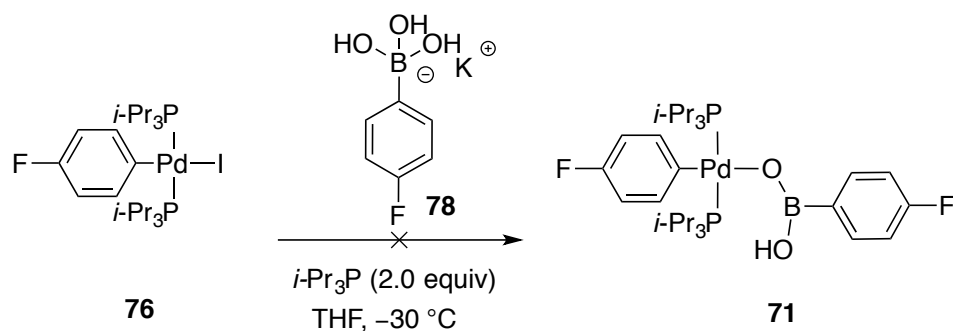
An oven-dried, 5-mm, NMR tube was taken into the glove box and potassium 4-fluorophenylboronate (17.6 mg, 90 μmol, 3.0 equiv), 1,4-difluorobenzene (0.5 μL, 5.0 μmol, 0.16 equiv) and i-Pr$_3$P (11.6 μL, 60 μmol, 2.0 equiv) were added, followed by the addition of 500 μL of THF (SDS). The tube was capped with a septum and Teflon taped followed by removal from the glove box. The tube was shaken and sonicated for ~5 min until a fine suspension was observed.

A 2-dram vial was charged with $trans$-(i-Pr$_3$P)$_2$Pd(4-FC$_6$H$_4$)(I) (19.4 mg, 30 μmol, 1.0 equiv) and 200 μL of THF (SDS). The vial was capped and sonicated until the solid had dissolved ~2-3 min.

The potassium boronate solution was placed into a −78 °C dry-ice acetone bath followed by the addition of 200 μL (30 μmol, 1.0 equiv) of the freshly prepared $trans$-(i-Pr$_3$P)$_2$Pd(4-FC$_6$H$_4$)(I) solution. The tube was shaken and quickly cleaned with a Kimwipe then placed into the probe of the NMR spectrometer pre-cooled to −30 °C. After ~3 h no reaction was observed thus the sample was warmed in 10 degree intervals until 20 °C at which point the tube was removed and shaken violently followed by placement into the probe at 30 °C where no reaction was observed.
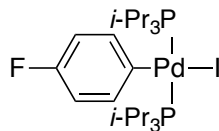
76
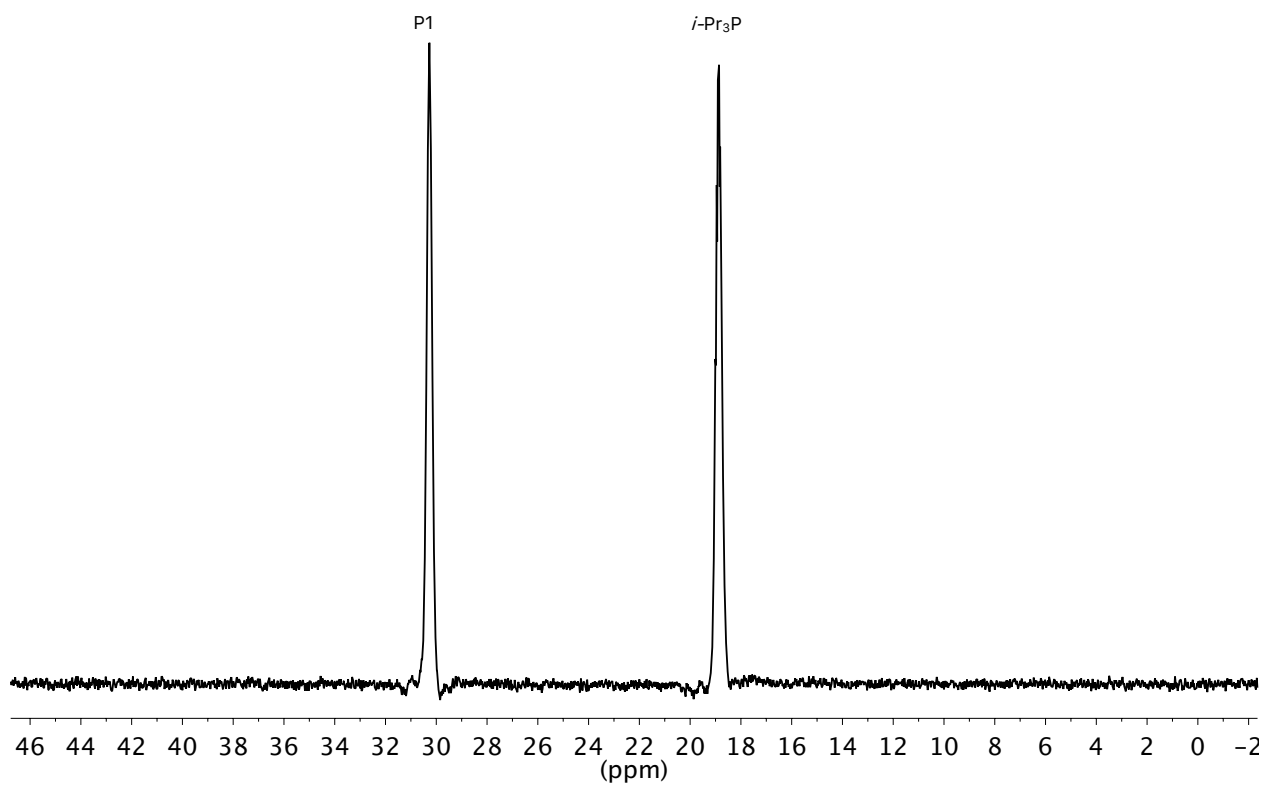
Figure 112. ^{31}P NMR spectrum of reaction mixture of **76** with **78** at −30 °C, referenced to *i*-Pr$_3$P (19.00 ppm).

167

76

Figure 113. ^{19}F NMR spectrum of reaction mixture of **76** with **78** at −30 °C (bottom) and 30 °C top, referenced to 1,4-difluorobenzene (−120.00 ppm).

Experiment 13: Preparation of 6-B-3 complex 71 from 76 and 79.
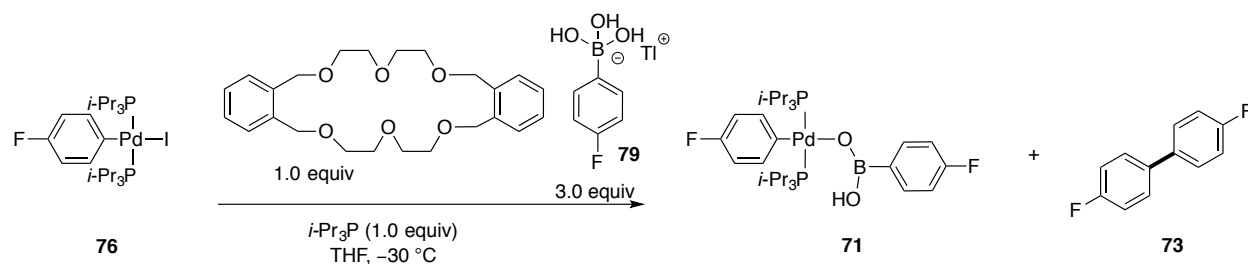
An oven-dried, 5-mm, NMR tube was taken into the glove box and both thallium 4-fluorophenylboronate (33.0 mg, 90 µmol, 3.0 equiv), dibenzo-22-crown-6 (12.5 mg, 30 µmol, 1.0 equiv), 1,4-difluorobenzene (0.5 µL, 5.0 µmol, 0.16 equiv) and i-Pr$_3$P (5.8 µL, 30 µmol, 1.0 equiv) were added, followed by the addition of 450 µL of THF (SDS). The tube was capped with a septum and Teflon taped followed by removal from the glove box. The tube was shaken and sonicated for ~5 min until a fine suspension was observed.

A 2-dram vial was charged with $trans$-(i-Pr$_3$P)$_2$Pd(4-FC$_6$H$_4$)(I) (19.4 mg, 30 µmol, 1.0 equiv) and 200 µL of THF (SDS). The vial was capped and sonicated until the solid had dissolved ~5 min.

The thallium boronate solution was placed into a −78 °C dry-ice acetone bath followed by the addition of 200 µL (30 µmol, 1.0 equiv) of the freshly prepared $trans$-(i-Pr$_3$P)$_2$Pd(4-FC$_6$H$_4$)(I) solution. The tube was shaken and quickly cleaned with a Kimwipe then placed into the probe of the NMR spectrometer pre-cooled to −30 °C. After ~3 h the observation of ~30% conversion to cross-coupling product **73** and ~10% conversion to 6-B-3 complex **71** was observed.
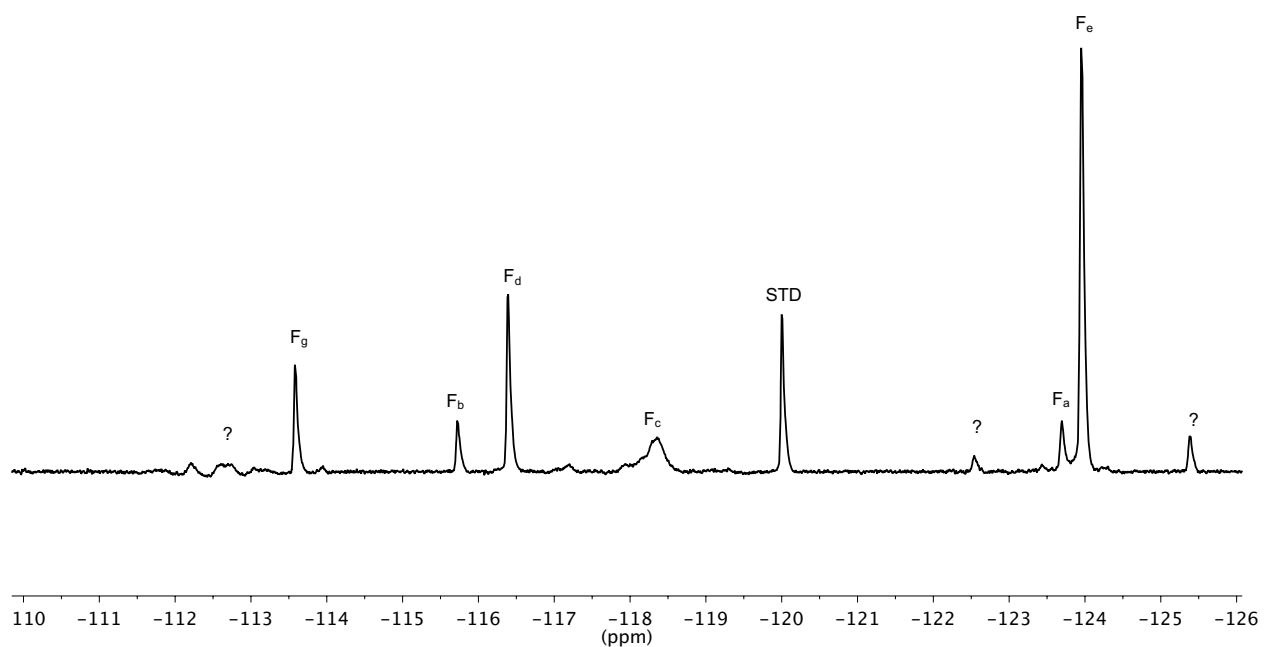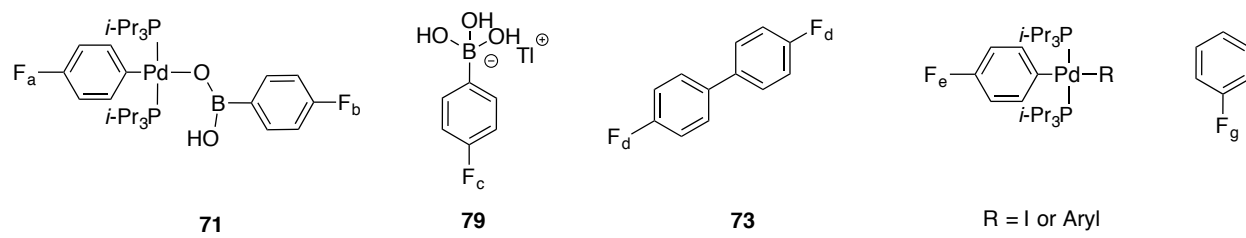
Figure 114. ^{19}F NMR spectrum of **71** at −30 °C, referenced to 1,4-difluorobenzene (−120.00 ppm).
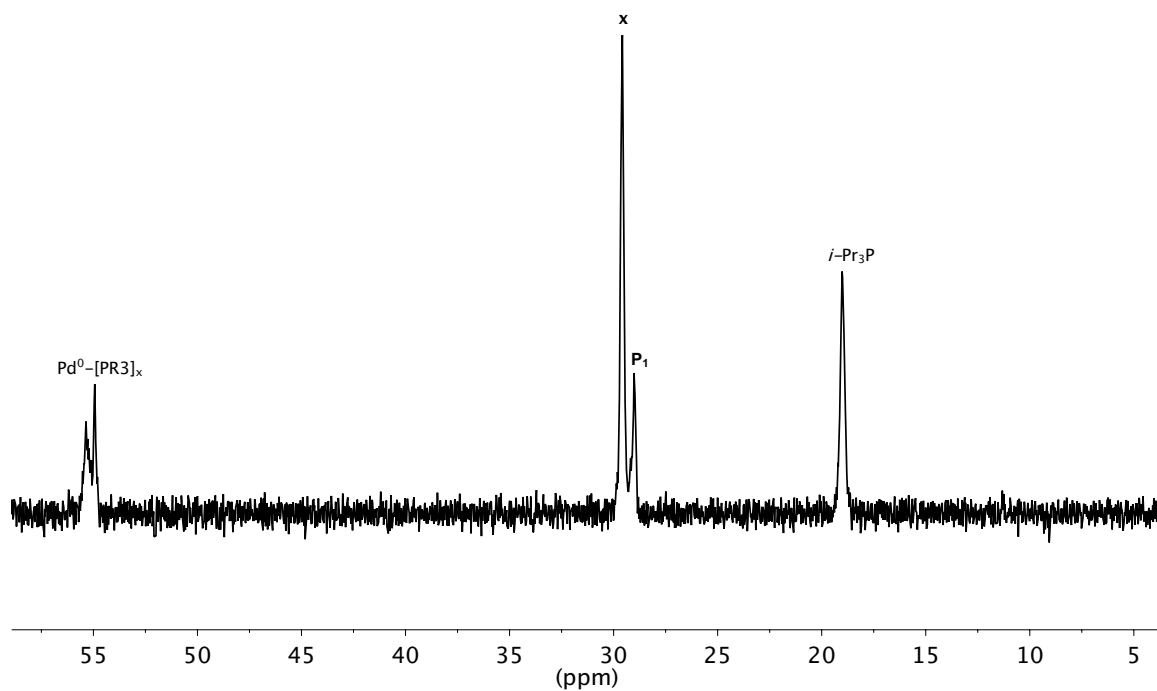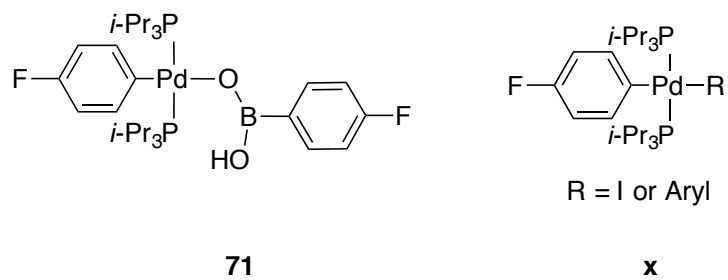
Figure 115. ^{31}P NMR spectrum of **71** at −30 °C, referenced to *i*-Pr$_3$P (19.00 ppm).

Experiment 14: Preparation of 6-B-3 complex 75 from 74 and 58.

A 1-mL volumetric flask was charged with 4-fluorophenylboroxine (88 mg, 240 μmol, 1.0 equiv) followed by H_2O (13 μL, 722 μmol, 3.0 equiv). Then ~0.5 mL of THF-d_8 was added followed by sonication until the solid had dissolved. Once dissolved the flask was filled to the mark with THF-d_8 yielding a 4-fluorophenylboronic acid solution (0.72 M).

An oven dried, 5-mm, NMR tube as charged with [(i-Pr$_3$P)Pd(aryl)(μ-OH)]$_2$ (8.22 mg, 11 μmol, 1.0 equiv), i-Pr$_3$P (8 μL, 28 μmol, 2.5 equiv) and 500 μL of THF-d_8 followed by shaking until dissolved. The tube was placed into a −78 °C dry-ice acetone bath followed by the addition of 4-fluorophenylboronic acid solution (31 μL, 22 μmol, 2.0 equiv). The tube was vortexed (not shaken) quickly wiped with a Kimwipe and placed into the probe of the NMR spectrometer pre-cooled to −30 °C. The complex ^{1}H and ^{31}P NMR spectra could be analyzed however the ^{13}C NMR spectrum could not be analyzed due to failed HSQC and HETCOR experiments. However, the structure was assigned by analogy to complex **xx** which has been fully characterized.

Data for **75:**

^{1}H NMR: (600 MHz, THF-d_8)

7.93 (s, 1 HC(2)), 7.85 (m, 1 HC(10)), 7.84 (m, 2 HC(15)), 7.65 (d, ^3J(H-H) = 8 Hz 1 CH(4)), 7.58 (d, ^3J(H-H) = 7 Hz 1 CH(7)), 7.43 (d, ^3J(H-H) = 7 Hz 1 CH(9)), 7.31 (dd, ^3J(H-H) = 7 Hz, 1 CH(5)), 7.24 (dd, ^3J(H-H) = 7 Hz, 1 CH(6)), 6.92 (dd, ^3J(H-H) = 7 Hz, 1 CH(14)), 4.16 (s, HO), 2.22 (m, 6 HC(11)), 1.15 (m, 36 HC(12))

^{31}P NMR: (243 MHz, THF-d_8)

28.51 (s, 2 P(Pd))
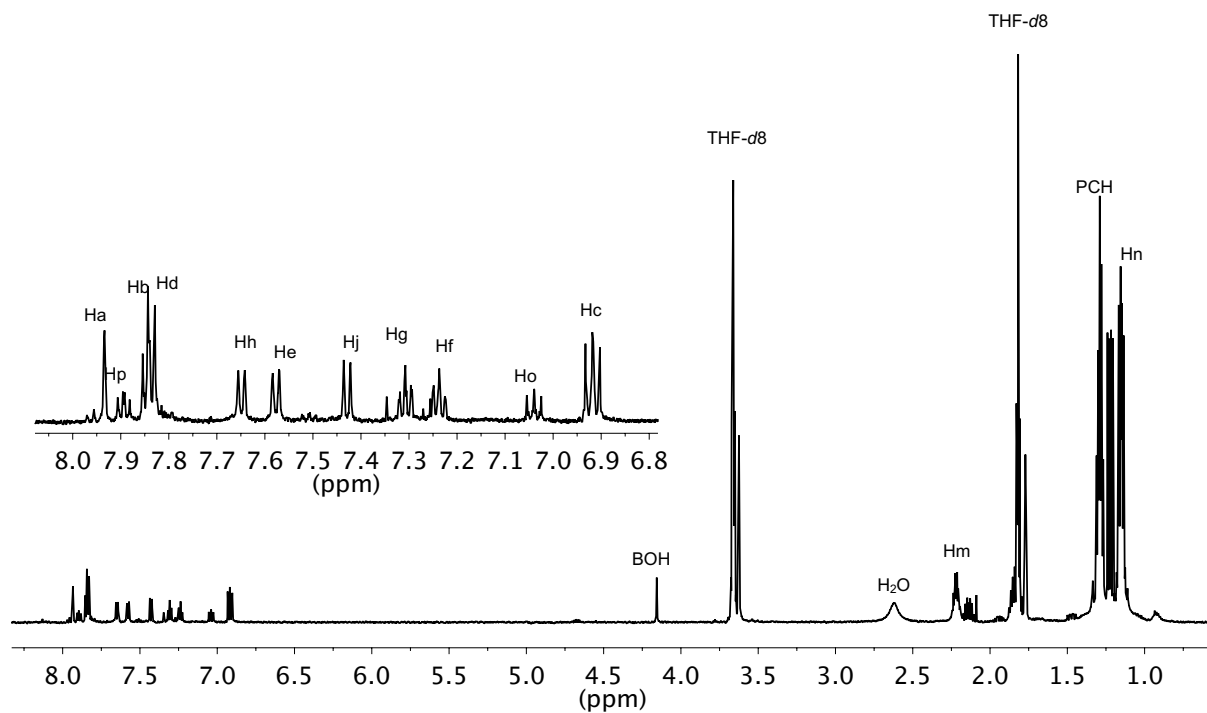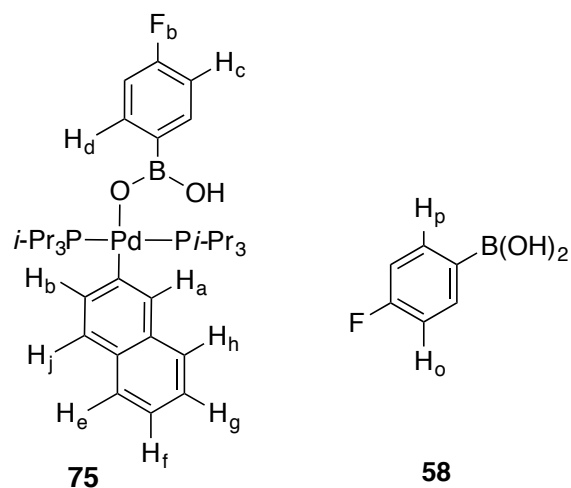
Figure 116. ¹H NMR spectrum of **75** at −30 °C, referenced to THF-d_8 (1.72 ppm).
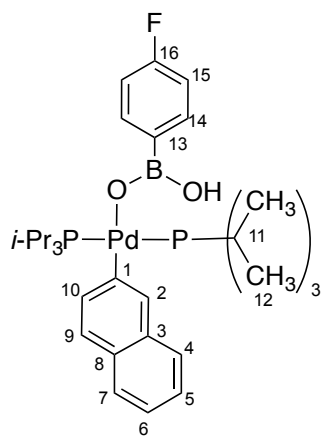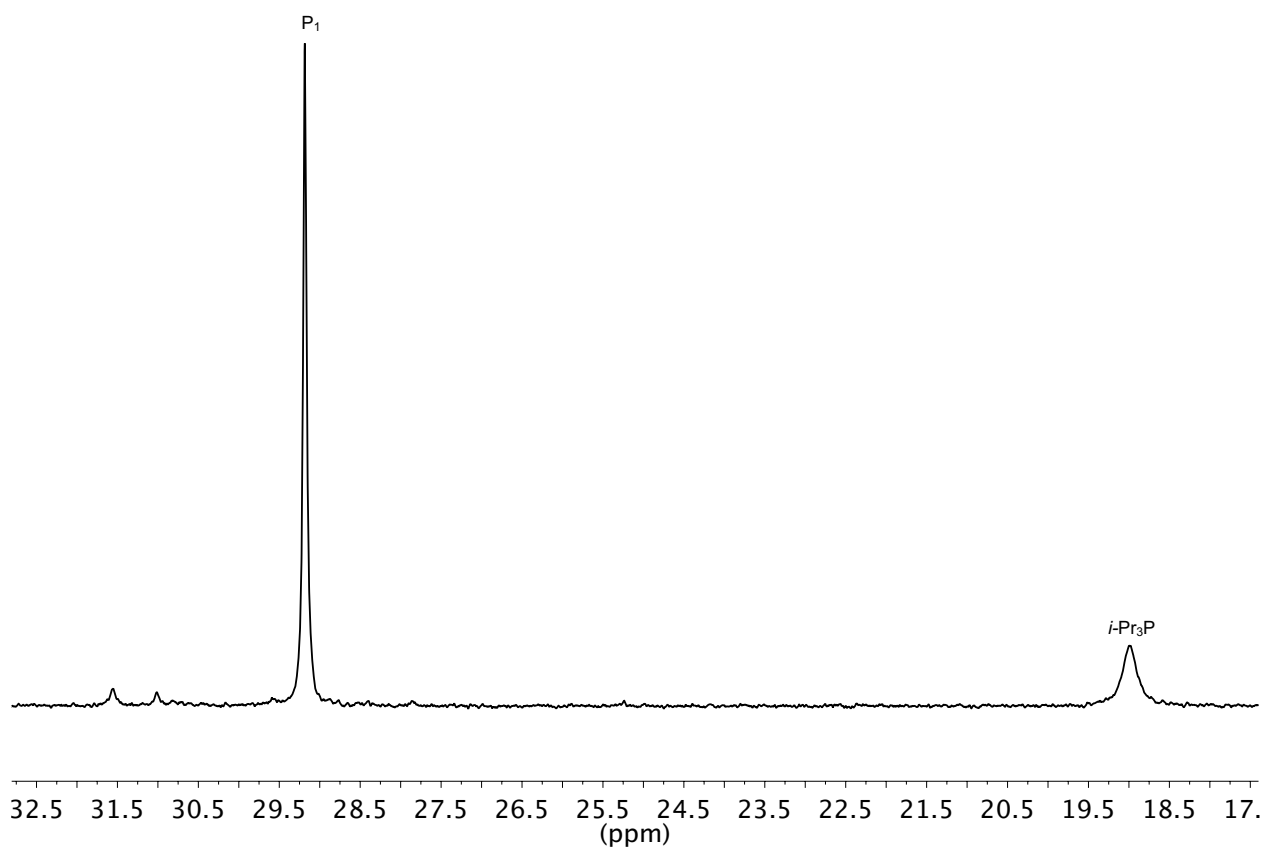
Figure 117. ^{31}P NMR spectrum of **75** at −30 °C, referenced to *i*-Pr$_3$P (19.00 ppm).

Experiment 15: Preparation of cationic complex 81
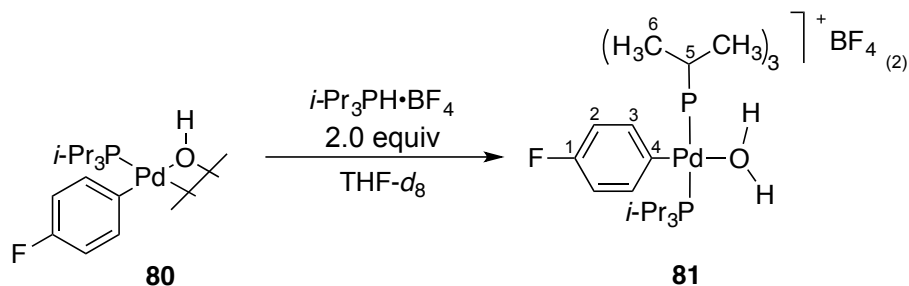
In the glove box, an oven-dried, 5-mm NMR tube was charged with [(i-Pr$_3$P)Pd(4-FC$_6$H$_4$)(μ-OH)]$_2$ (**80**) (11 mg, 15 μmol, 1.0 equiv), and i-Pr$_3$PH•BF$_4$ (7.5 mg, 30 μmol, 2.0 equiv) followed by 600 μL of THF-d_8. The tube was capped with a septum and removed from the box followed by sonication for ~5 min and shaken vigorously.

Data for **81**:

^{1}H NMR: (600 MHz, THF-d_8)

7.36 (dd, ^3J(F-H) = 7 Hz, ^3J(H-H) = 6 Hz, 2 HC(3)), 6.80 (dd, ^2J(F-H) = 6 Hz), ^3J(H-H) = 6 Hz, 2 HC(2)), 5.00 (s, HO(1)), 2.05 (m, 6 HC(5)), 1.27 (m, 36 HC(6))

^{19}F NMR: (565 MHz, THF-d_8)

−122.49 (s, FC(1)), −152.00 (s, BF$_4$)

^{31}P NMR: (242 MHz, THF-d_8)

33.02 (s, 2 P(Pd)))
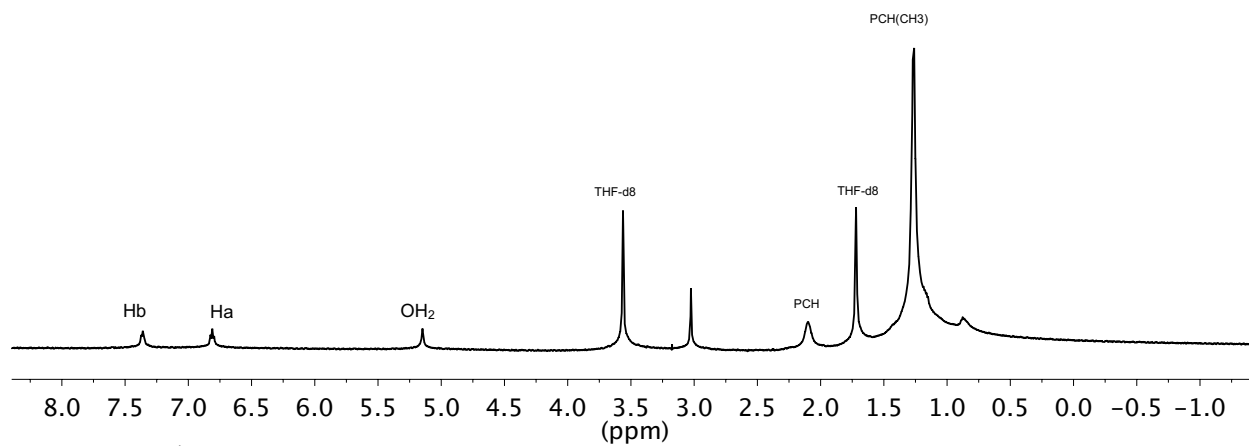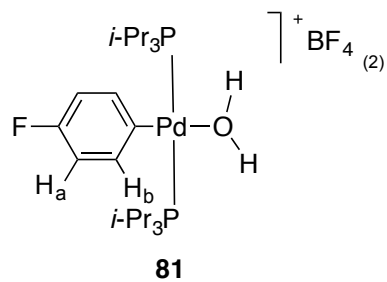
Figure 118. ^{1}H NMR spectrum of **81** at −30 °C, referenced to THF-d_8 (1.72 ppm).
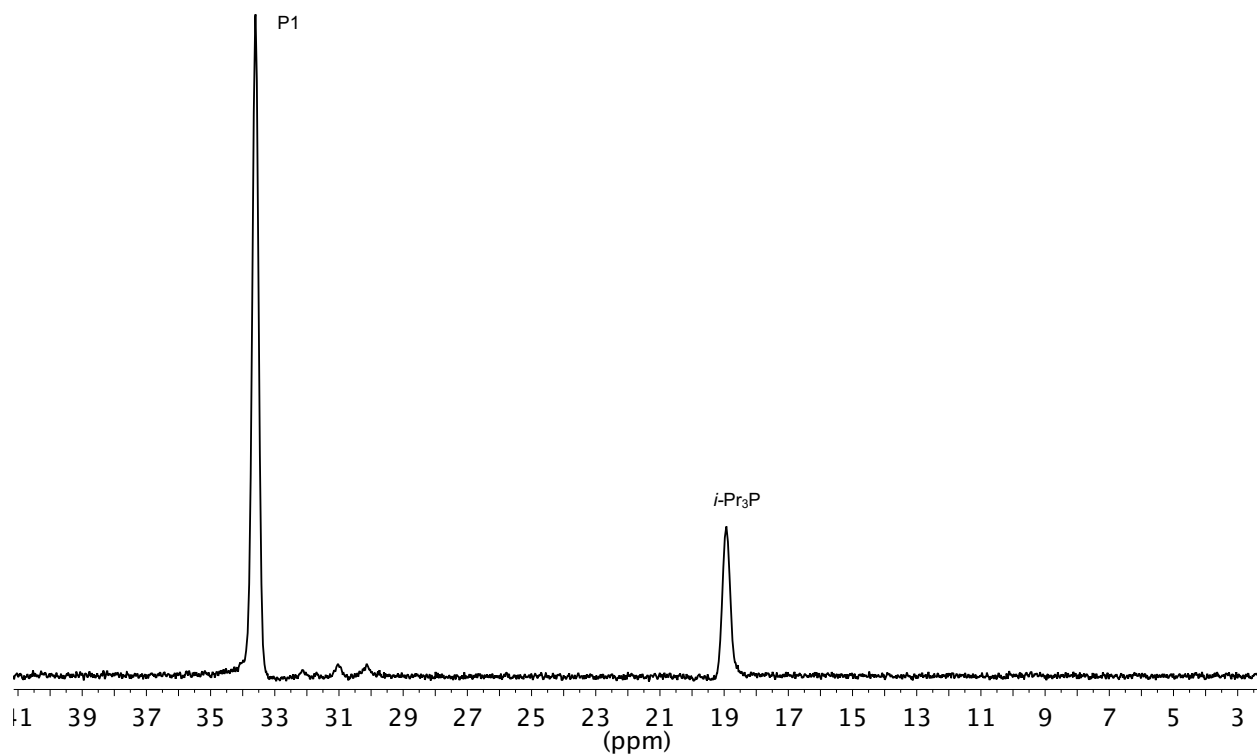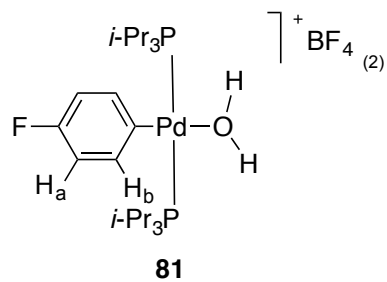
Figure 119. ^{31}P NMR spectrum of **81** at −30 °C, referenced to i-Pr$_3$P (19.00 ppm).
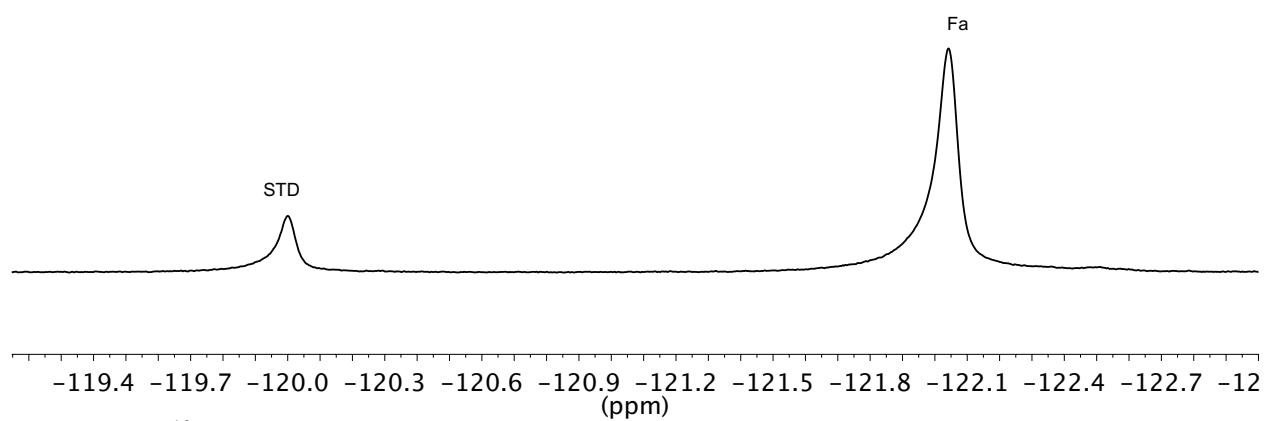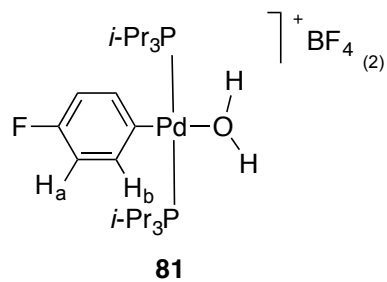
Figure 120. ^{19}F NMR spectrum of **81** at −30 °C, referenced to 1,4-difluorobenzene (−120.00 ppm).

Experiment 16: Addition of 81 to 82.
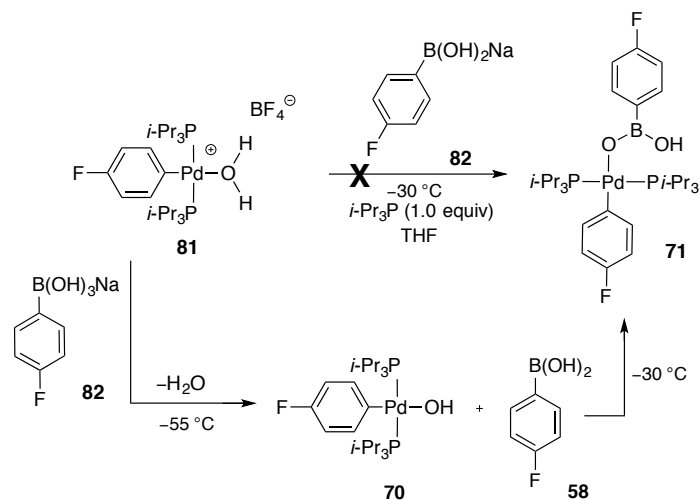
A dram vial was charged with sodium 4-fluorophenyltrihydroxyborate (6 mg, 33.3 μmol, 2.2 equiv) followed by 200 μL of THF.

An oven-dried, 5-mm, NMR tube was taken into the glove box and both [(*i*-Pr$_3$P)Pd(4-FC$_6$H$_4$)(μ-OH)]$_2$ (11.4 mg, 15 μmol, 1.0 equiv), *i*-Pr$_3$P (5 μL, 26 μmol, 2 equiv), 1,4-difluorobenzene (0.5 μL) and *i*-Pr$_3$P•HBF$_4$ (7.4 mg, 30 μmol, 2.0 equiv) were added, followed by the addition of 400 μL of THF. The tube was capped with a septum and Teflon taped, then placed in an ice bath in the sonicator for ~5 min. The tube was transferred to a dry-ice bath followed by the addition of the sodium boronate solution. The sample was placed into the NMR set to −55 °C for ~5 h. The observation of **71**, **70**, and **58** were observed by ^{19}F NMR spectroscopy demonstrating that the aqua complex **81** was being deprotonated.
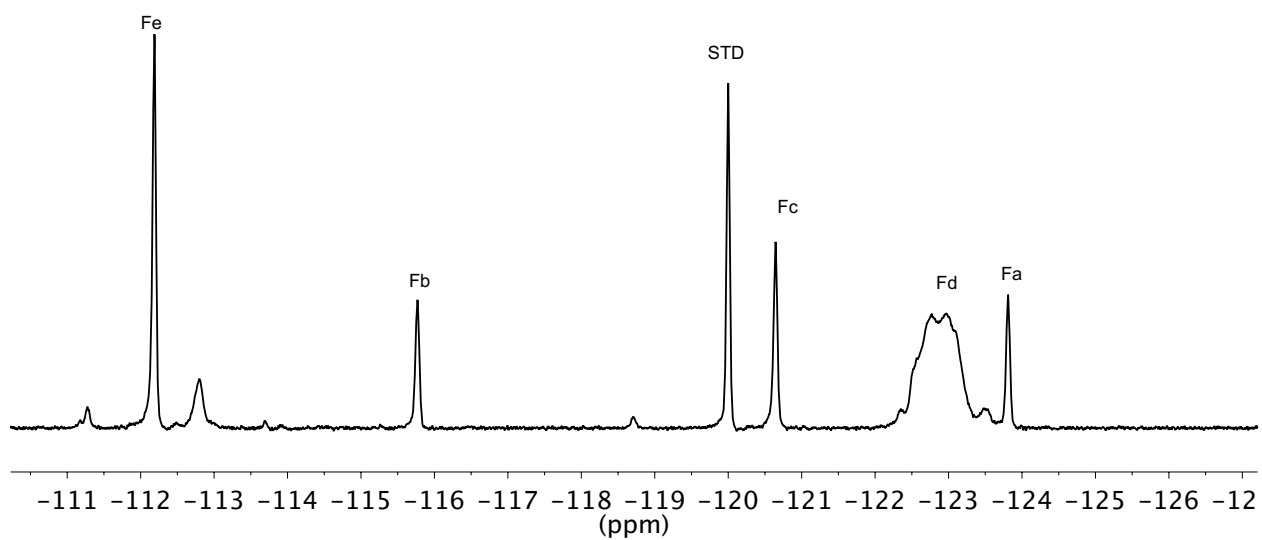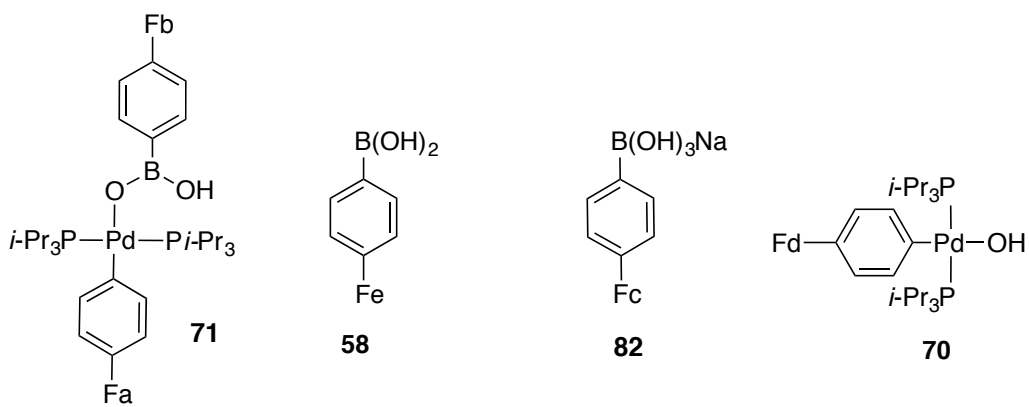
Figure 121. ^{19}F NMR spectrum of reaction mixture between **81** and **82** at −55 °C, referenced to 1,4-difluorobenzene (−120.00 ppm).
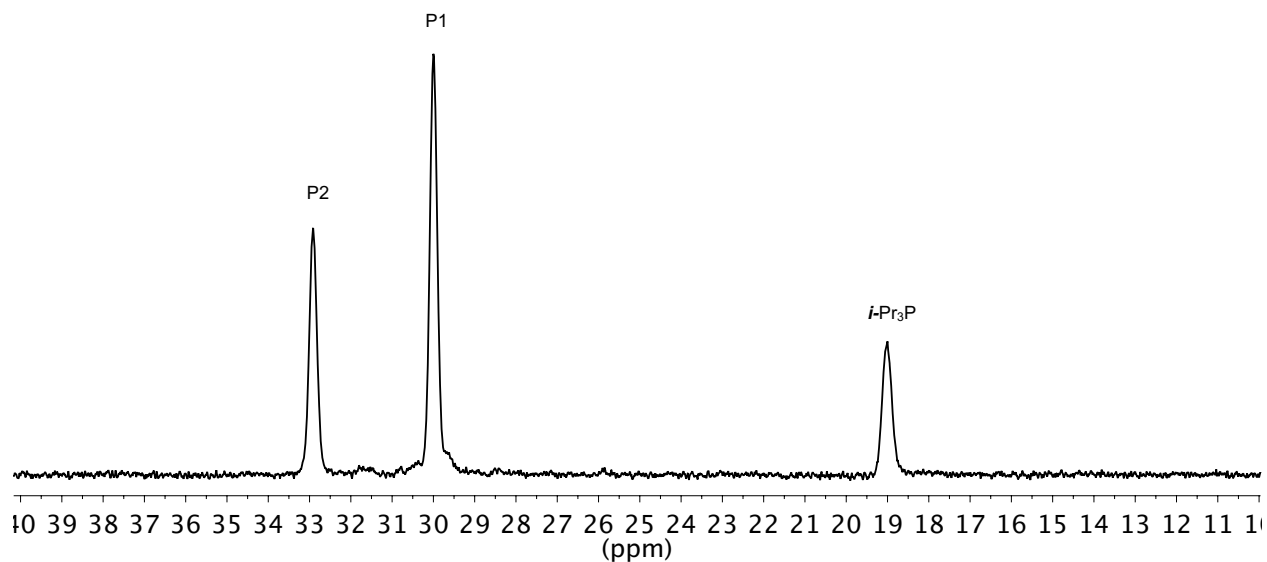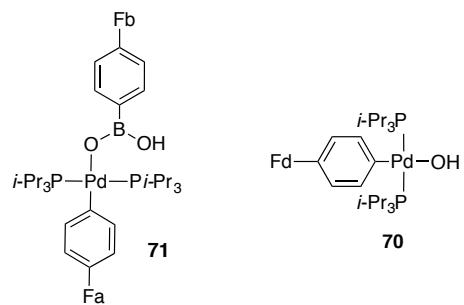
Figure 122. ^{31}P NMR spectrum of reaction mixture between **81** and **82** at −55 °C, referenced to *i*-Pr$_3$P (19.00 ppm).

Experiment 17: Formation of 6-B-3 complex 71 in THF/H$_2$O
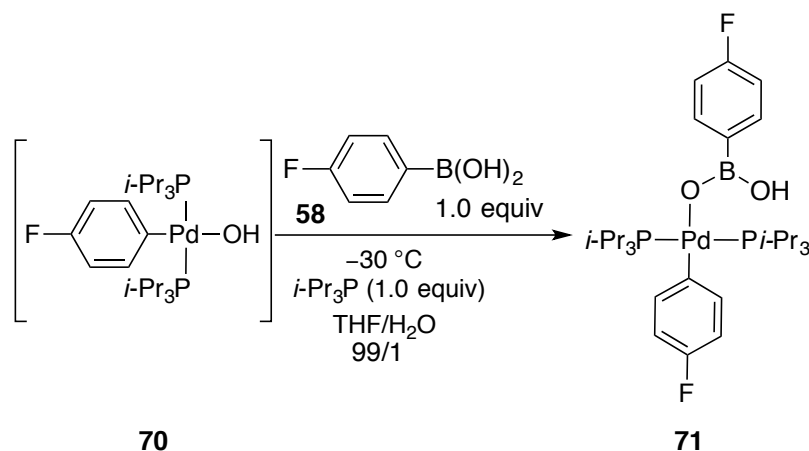
An oven-dried, 5-mm, quartz NMR tube was taken into the glove box and [(*i*-Pr$_3$P)Pd(4-FC$_6$H$_4$)(OH)]$_2$ (7.58 mg, 10 μmol, 1.0 equiv), *i*-Pr$_3$P (5.75 μL, 30 μmol, 3.0 equiv), 1,4-difluorobenzene (0.5 μL, 5 μmol), and NaBPh$_4$ (2.0 mg, 8 μmol) were added, followed by the addition of 500 μL of freshly distilled THF. The tube was capped with a septum and Teflon taped then removed from the glove box. Then H$_2$O (6 μL) was added and the tube was shaken and placed into a −78 °C dry-ice acetone bath followed by the addition of 95 μL (20 μmol, 0.21 M) of the freshly prepared 4-fluorophenylboronic acid stock solution. The tube was shaken and quickly wiped with a Kimwipe then placed into the probe of the NMR spectrometer pre-cooled to −30 °C. No new species were observed by NMR spectroscopy at −30 °C other than complex **71**. The experiment was stopped after ~50% conversion with the lack of new species (8-B-4) being present.
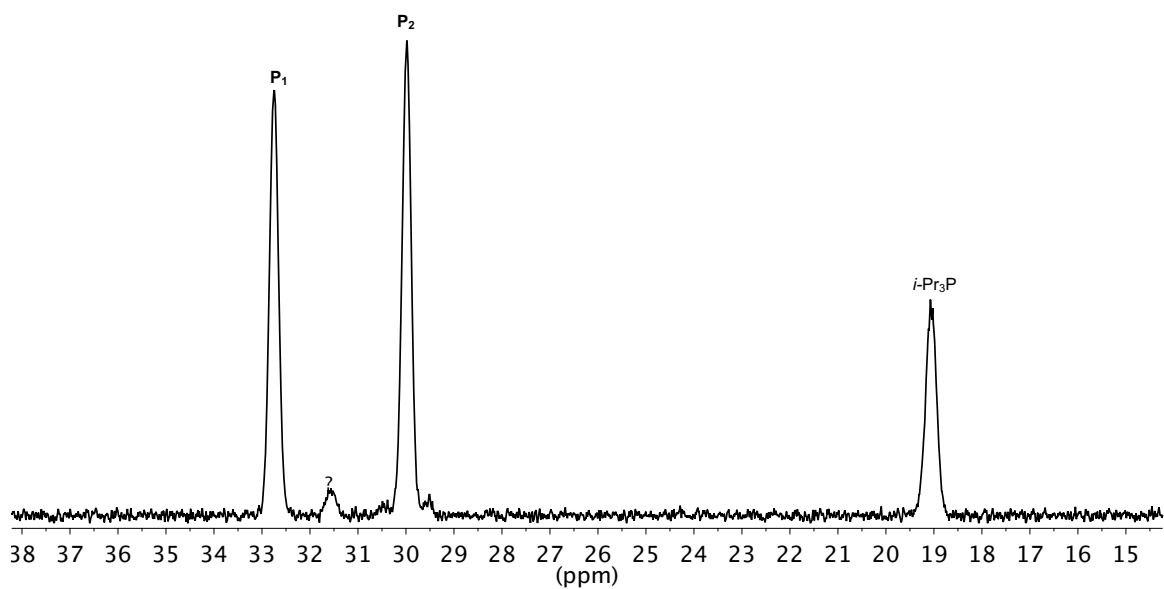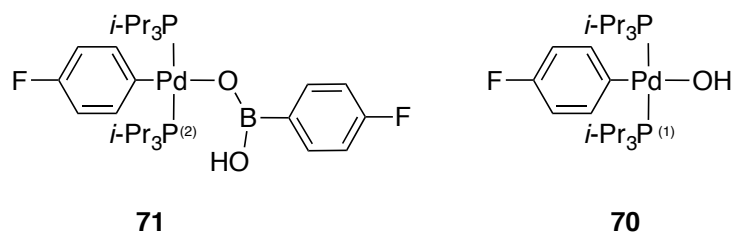
Figure 123. ^{31}P NMR spectrum of **71** at −30 °C, referenced to i-Pr$_3$P (19.00 ppm).
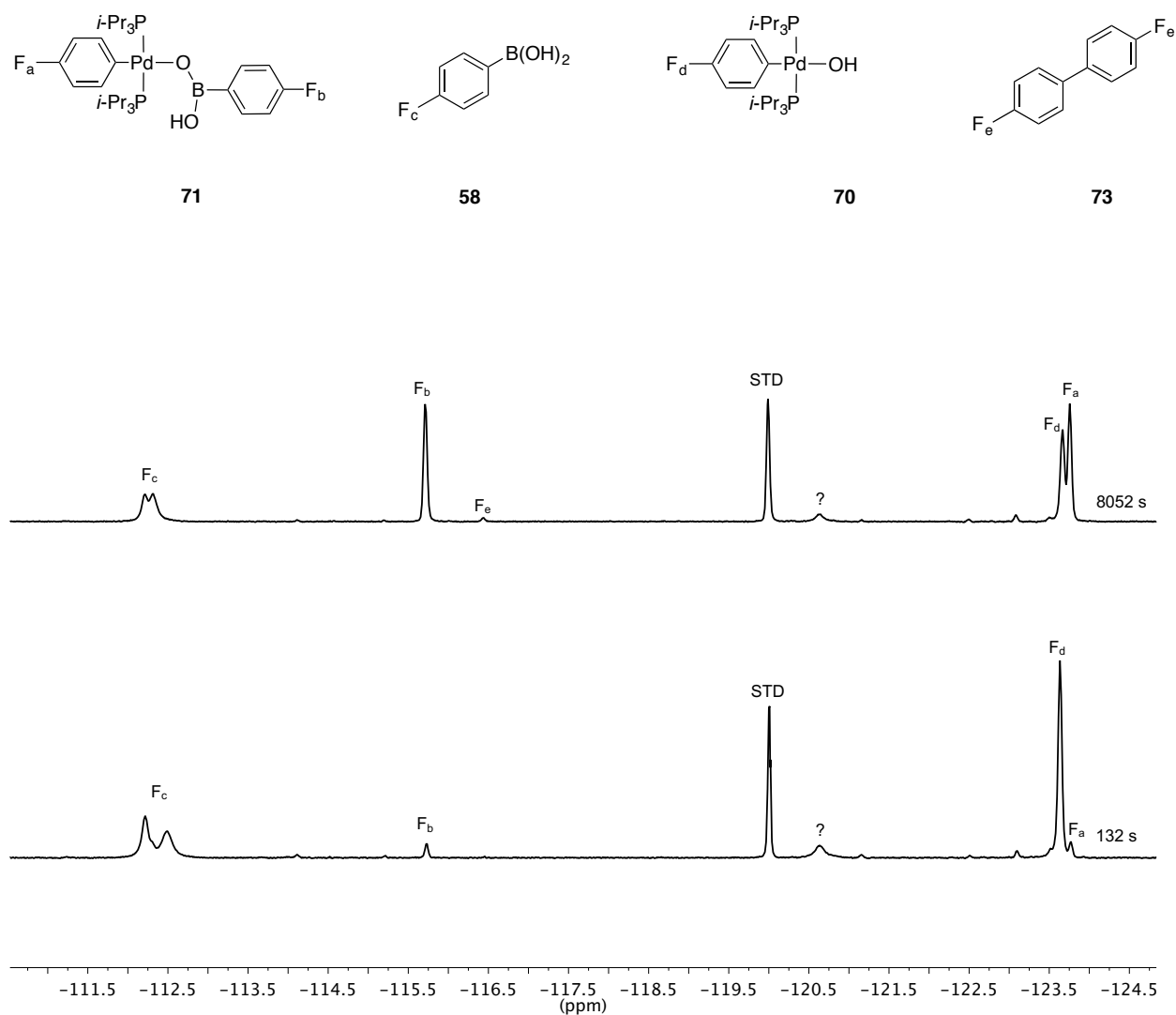
Figure 124. ^{19}F NMR spectra of **71** at −30 °C, referenced to 1,4-difluorobenzene (−120.00 ppm).

184
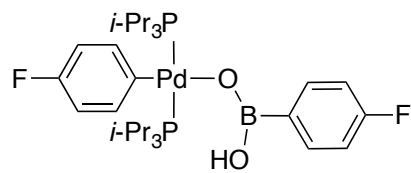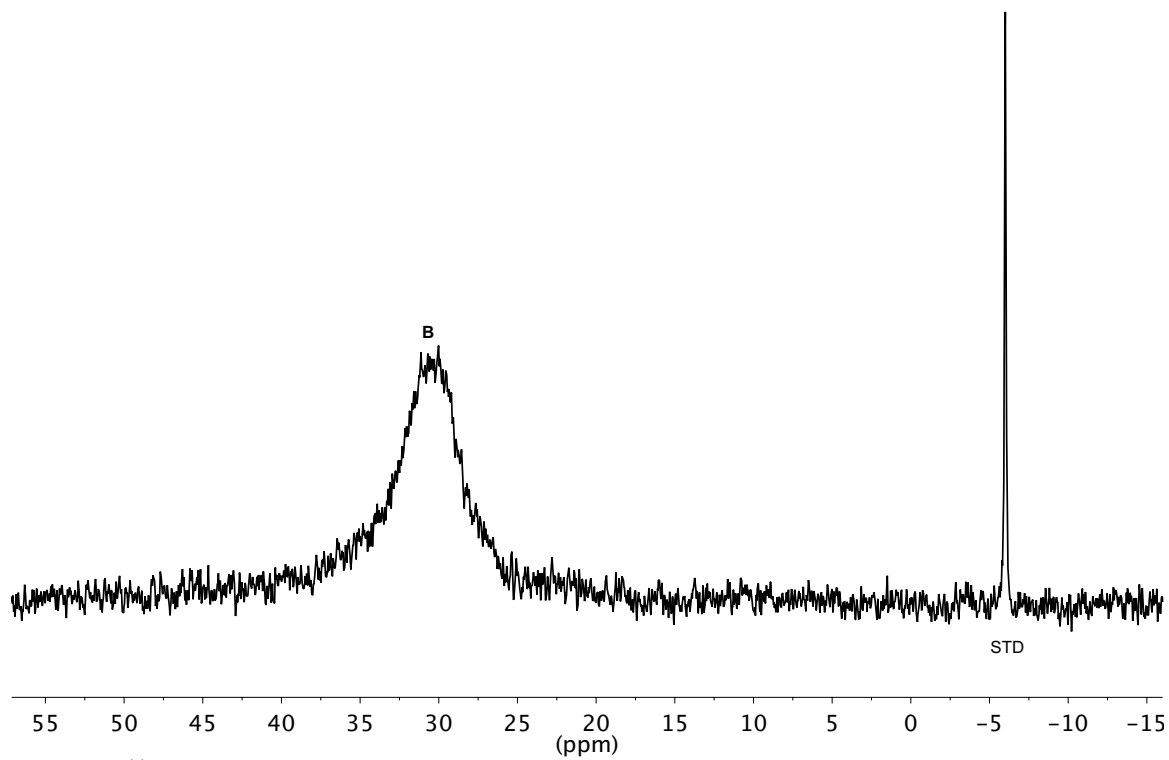
Figure 125. ^{11}B NMR spectrum of **71** at −30 °C, referenced to Ph$_4$BNa (−6.14 ppm).

Experiment 18: Addition of CsOH•H₂O to 6-B-3 complex 71 in THF/CH₃OH.
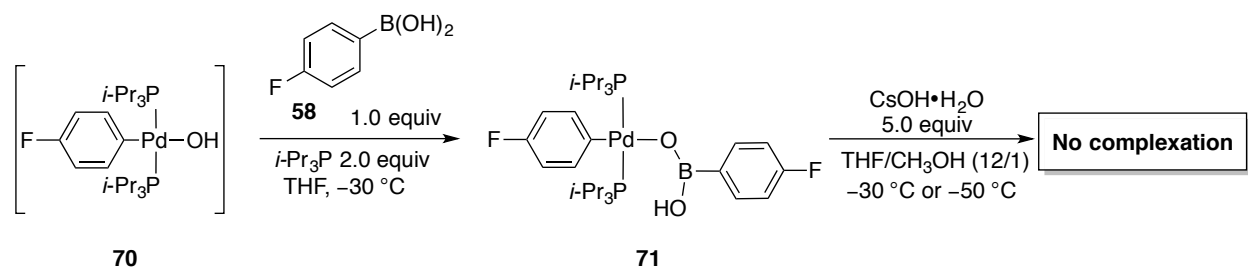
A flame dried, 1.0 mL volumetric flask was charged with 4-fluorophenylboroxine (77 mg, 210 μmol 1.0 equiv), H_2O (11 μL, 631 μmol, 3.0 equiv) followed by ~0.5 mL THF. The flask was sonicated for ~1-2 min then filled to the mark with THF (0.63 M).

An oven-dried, 5-mm, quartz NMR tube was taken into the glove box and [(*i*-Pr₃P)Pd(4-FC₆H₄)(OH)]₂ (7.58 mg, 10 μmol, 1.0 equiv), *i*-Pr₃P (8 μL, 40 μmol, 4.0 equiv), and 1,4-difluorobenzene (0.5 μL, 5 μmol) were added, followed by the addition of 500 μL of THF (SDS). The tube was capped with a septum, Teflon taped, and removed from the glove box. The tube was shaken and placed into a −78 °C dry-ice acetone bath followed by the addition of 32 μL (20 μmol, 0.63 M) of the freshly prepared 4-fluorophenylboronic acid solution. The tube was shaken and quickly wiped with a Kimwipe then placed into the probe of the NMR spectrometer pre-cooled to −30 °C for 14.5 h (overnight). The following day the tube was removed and placed into a −78 °C dry-ice acetone bath followed by the addition of CsOH•H₂O (16 mg, 0.1 mmol, 10 equiv) dissolved in 50 μL of CH₃OH. The tube was vortexed followed by the addition of NaBPh₄ (1 mg, 4 μmol, 0.4 equiv) and 1,4-difluorobenzene dissolved in 50 μL of THF (SDS). The tube was placed into the NMR spectrometer pre-cooled to either −30 °C or −50 °C. The ^{19}F, ^{31}P and ^{11}B NMR chemical shifts had no significant change, however, unbound boronic acid species (always traces from formation) generated small amounts of boronates that are detected *via* NMR spectroscopy. Upon warming to room temperature the formation of **70** and **84** was observed. The complex was characterized *via* 1D NMR experiments over a course of similar experiments.
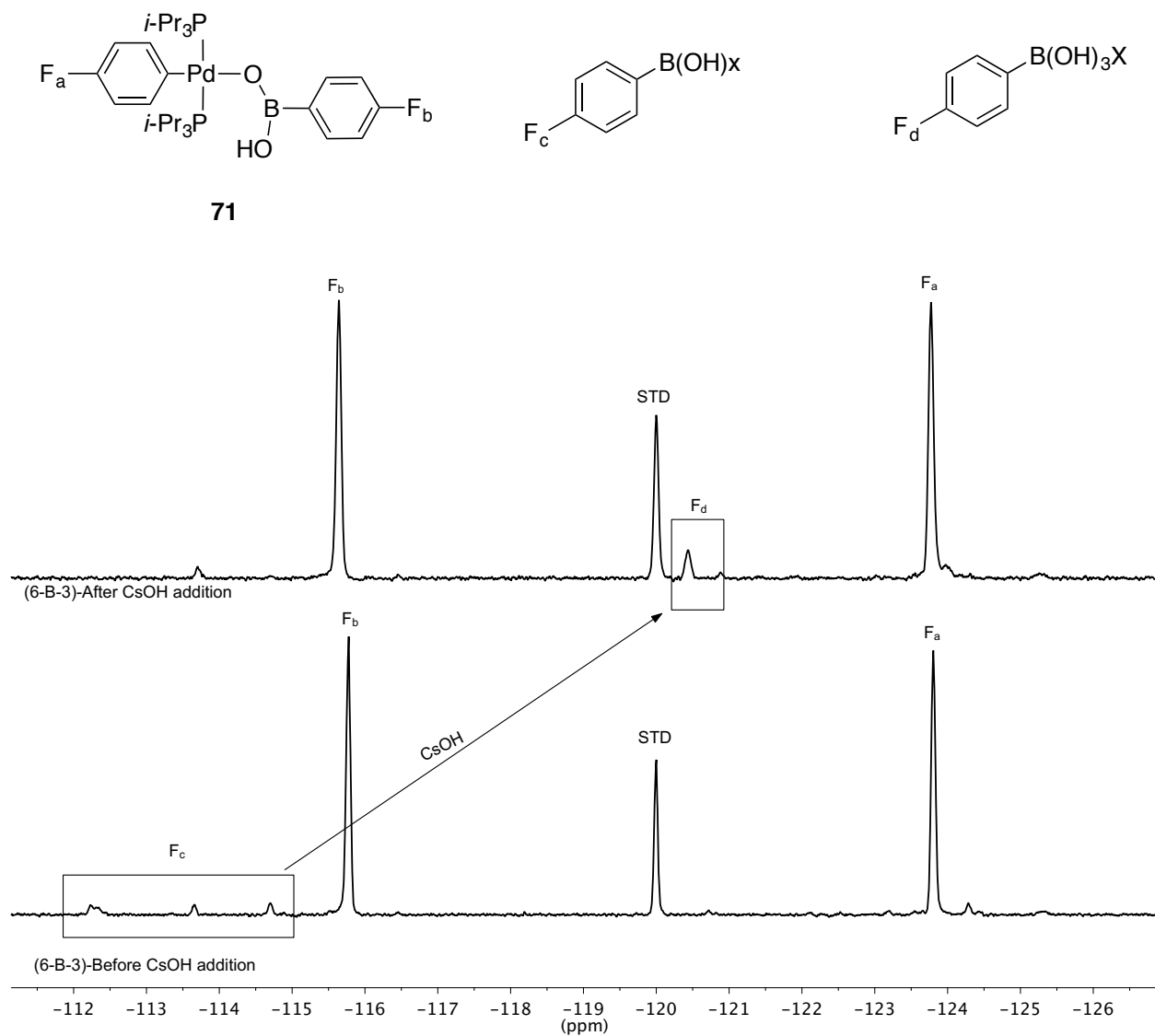
Figure 126. ^{19}F NMR spectra of **71** with (top) and without (bottom) CsOH•H$_2$O at −50 °C, referenced to 1,4-difluorobenzene (−120.00 ppm).

71

(6-B-3)-After CsOH addition

(6-B-3)-Before CsOH addition
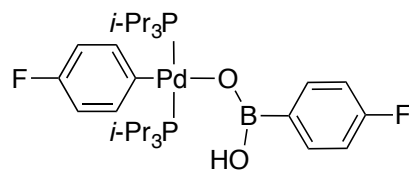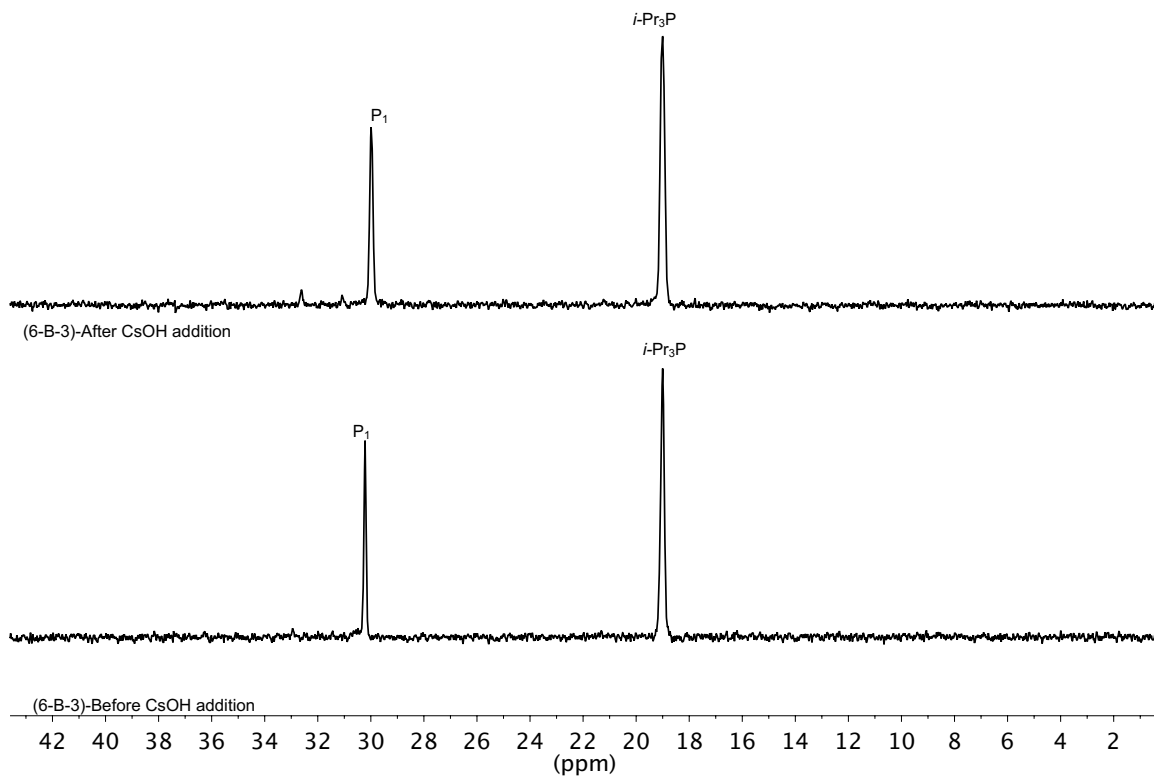
Figure 127. ^{31}P NMR spectra of **71** with (top) and without (bottom) CsOH•H$_2$O at −50 °C, referenced to *i*-Pr$_3$P (19.00 ppm).

188
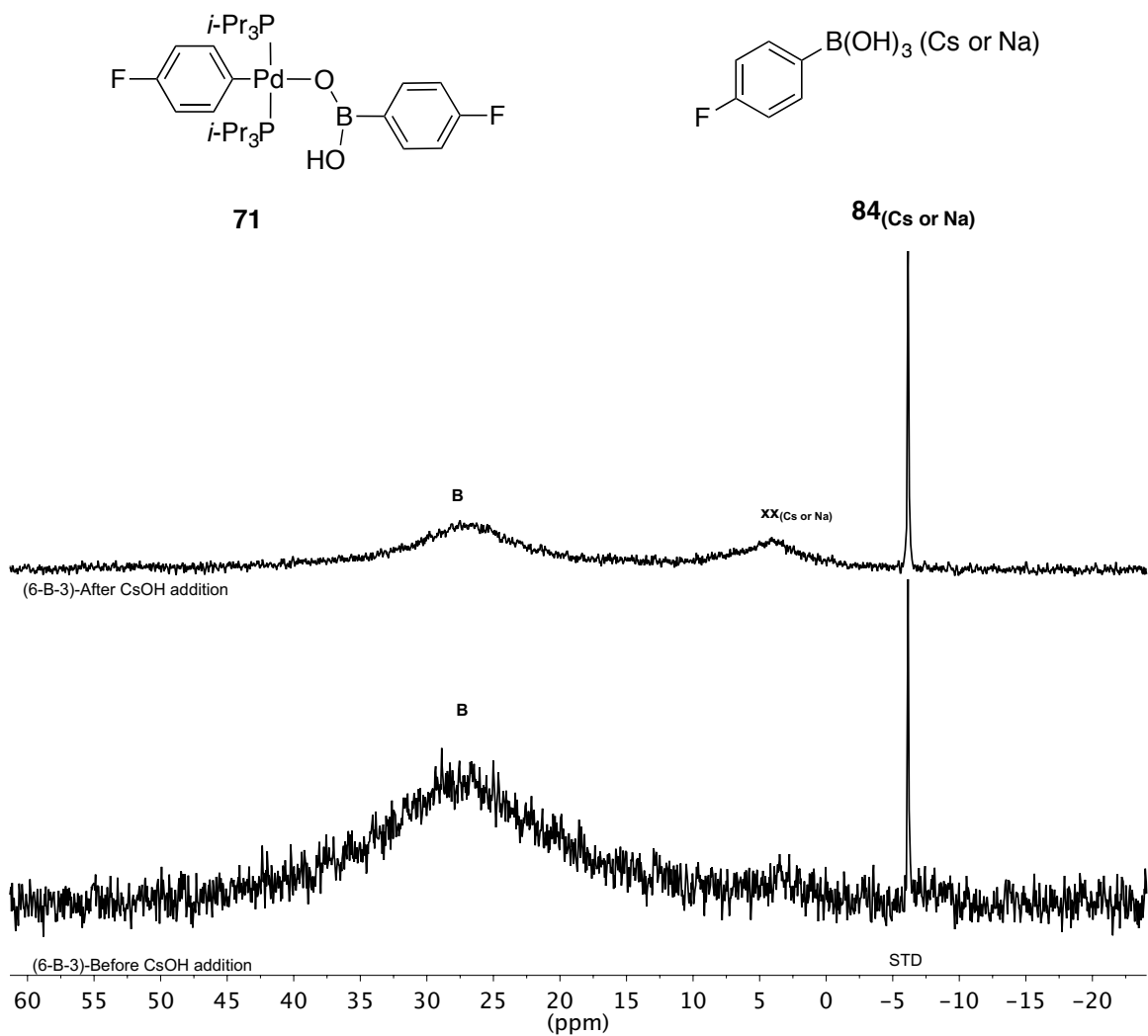
Figure 128. ^{11}B NMR spectra of **71** with (top) and without (bottom) CsOH•H$_2$O at −50 °C, referenced to Ph$_4$BNa (−6.14 ppm) in THF.

Figure 129. ^{19}F NMR spectra of **71** with (top) and without (bottom) CsOH•H$_2$O at −30 °C, referenced to 1,4-difluorobenzene (−120.00 ppm).
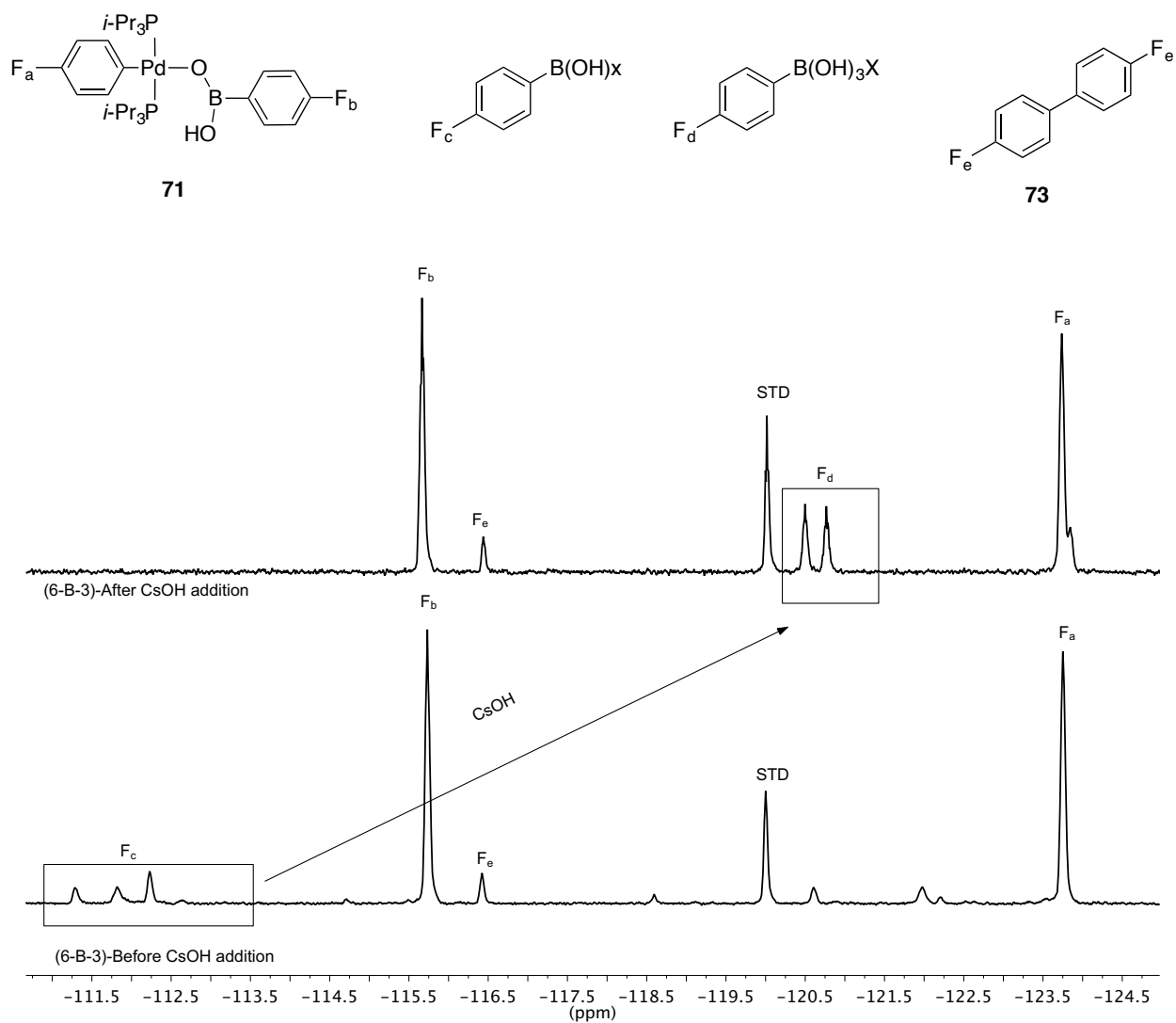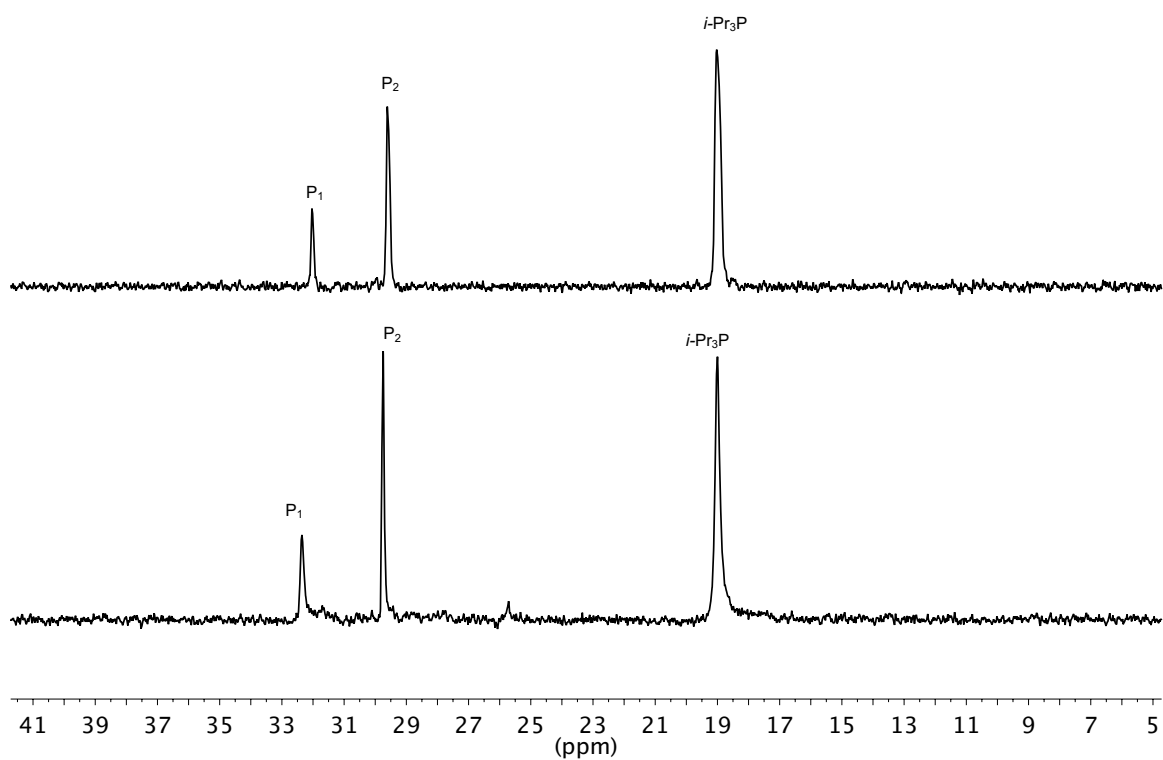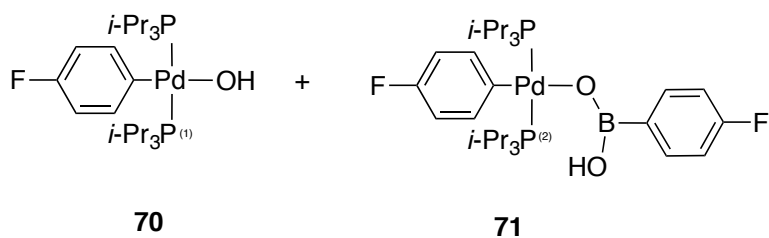
Figure 130. ^{31}P NMR spectra of **71** with (top) and without (bottom) CsOH•H_2O at −30 °C, referenced to *i*-Pr_3P (19.00 ppm).

Figure 131. ^{19}F NMR spectra of **71** with CsOH•H$_2$O at 20 °C and −30 °C (top, middle) and without (bottom) CsOH•H$_2$O at −30 °C, referenced to 1,4-difluorobenzene (−120.00 ppm).
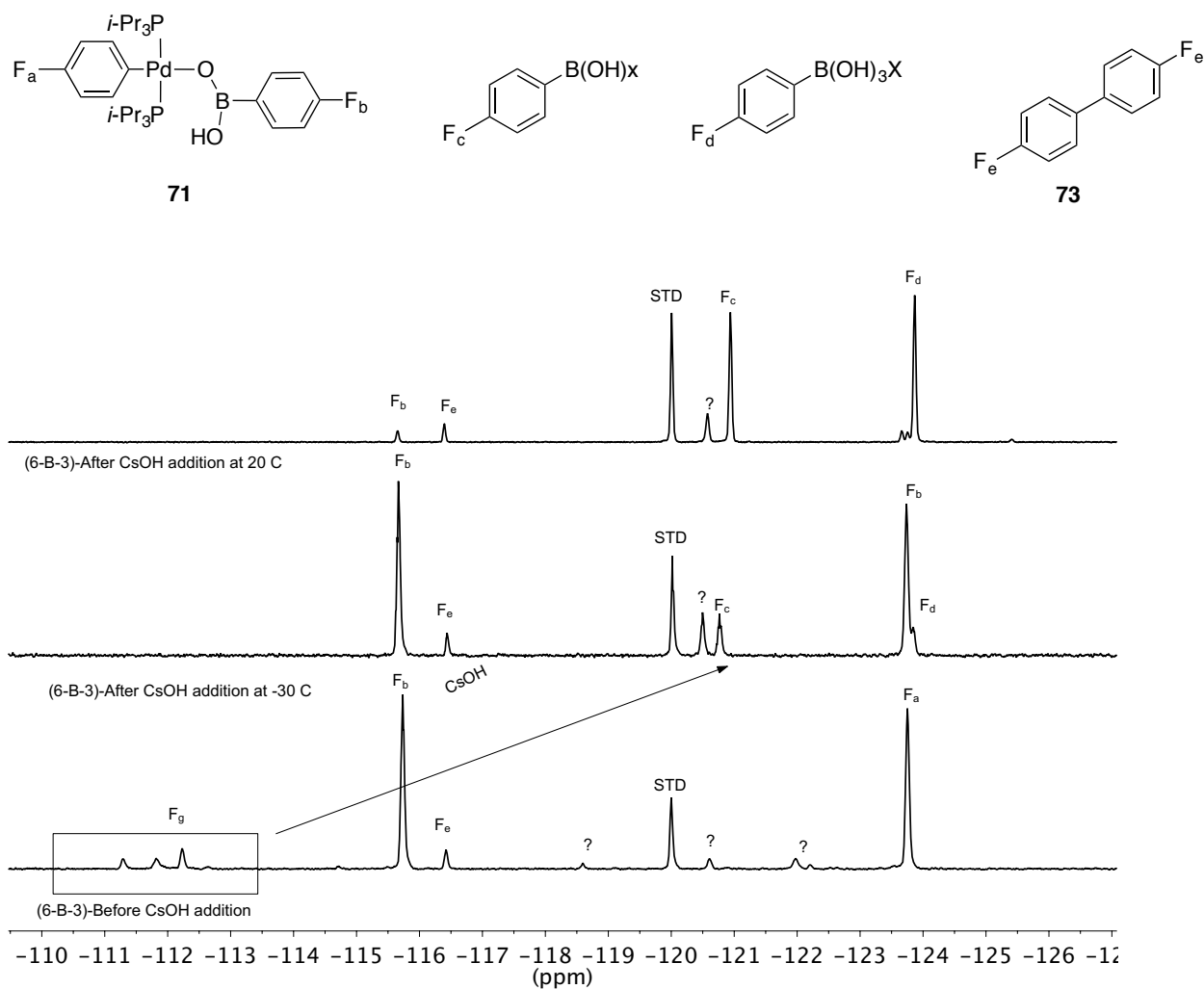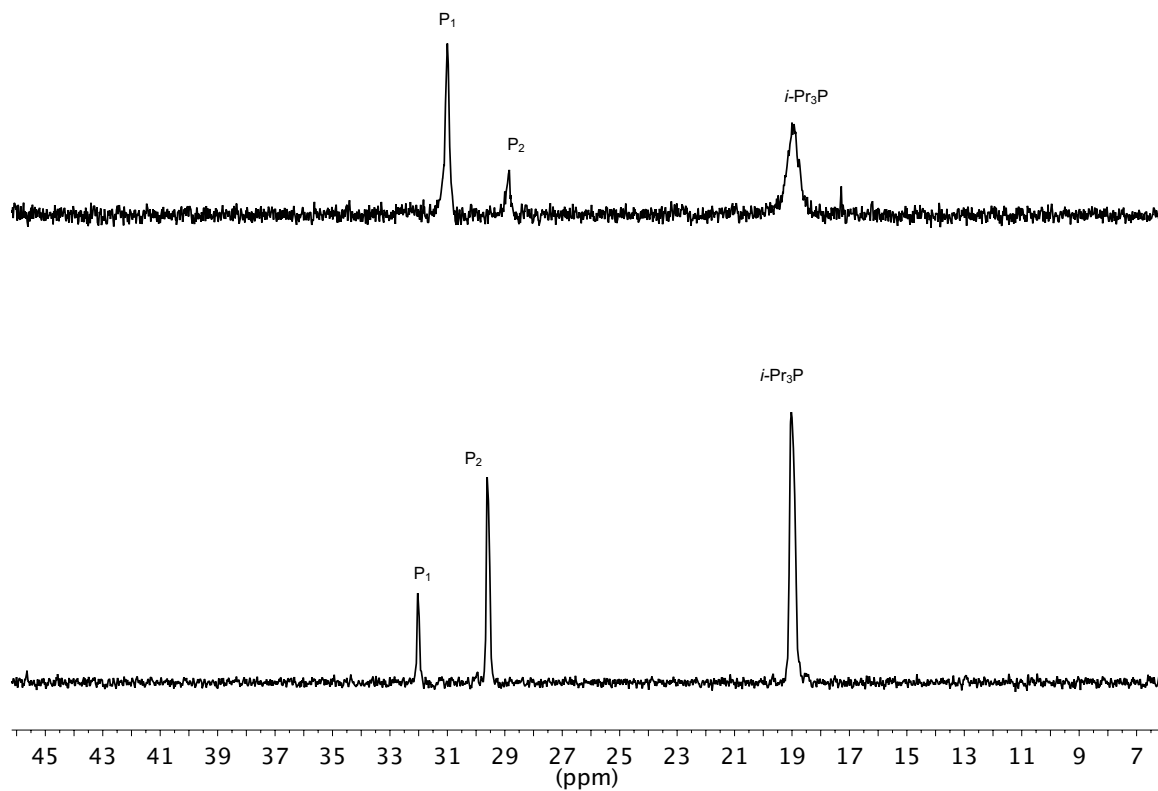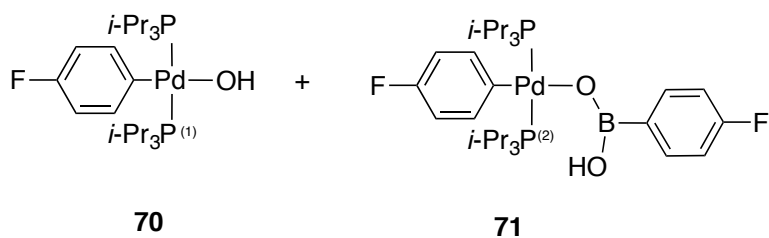
Figure 132. ^{31}P NMR spectra of **71** with (top) and without (bottom) CsOH•H$_2$O at 20 °C, referenced to *i*-Pr$_3$P (19.00 ppm).

Figure 133. ^{11}B NMR spectra of **71** with (top) and without (bottom) CsOH•H$_2$O at 20 °C, referenced to Ph$_4$BNa (−6.14 ppm) in THF.

Experiment 19: Preparation of *i*-Pr₃P complex 88 from 80 and 1.0 equiv of 58.
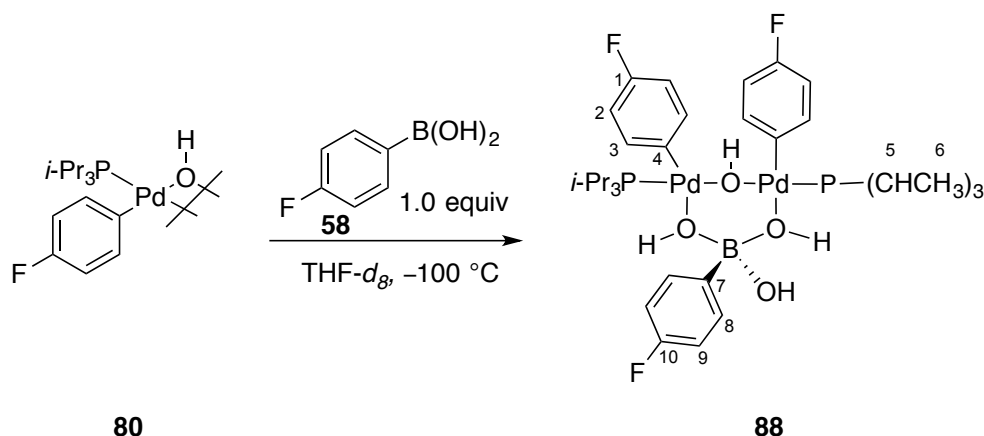
An oven dried, 5-mm, NMR tube was charged with 4-fluorophenylboroxine (20 mg, 182 μmol, 1.0 equiv), H_2O (6.5 μL, 564 μmol, 3.1 equiv) followed by 500 μL of freshly distilled (NaK) THF-d_8 (0.33 M). The tube was capped with a septum and Teflon tapped.

An oven-dried, 5-mm, NMR tube was taken into the glove box and [(*i*-Pr₃P)Pd(4-FC₆H₄)(μ-OH)]₂ (7.58 mg, 10 μmol, 1.0 equiv) was added, followed by the addition of 500 μL of freshly distilled THF-d_8 (NaK). The tube was shaken and placed into a −78 °C dry-ice acetone bath followed by the addition of the freshly prepared 4-fluorophenylboronic acid solution (33 μL, 10 μmol, 1.0 equiv). The tube was vortexed (not shaken) quickly wiped with a Kimwipe and placed into the probe of the NMR spectrometer pre-cooled to −60 °C. After a few minutes the sample was cooled to −100 °C where the complex was observed. The complex was characterized *via* 1D NMR experiments over a course of multiple experiments.

Data for **88**:

¹H NMR: (600 MHz, THF-d_8)

10.22 (s, HO), 7.86 (m, 2 HC(8)), 7.41 (m, 4 HC(3)), 7.04 (dd, 8 Hz, 2 HC(9)), 6.74 (m, 4 CH(2)), 2.27 (br, 6 HC(5)), 1.26 (br, 36 HC(6))

¹⁹F NMR: (565 MHz, THF-d_8)

−113.40 (s, FC(10)), −123.67 (s, 2 FC(1))

³¹P NMR: (243 MHz, THF-d_8)

45.62 (s, 2 P(Pd))
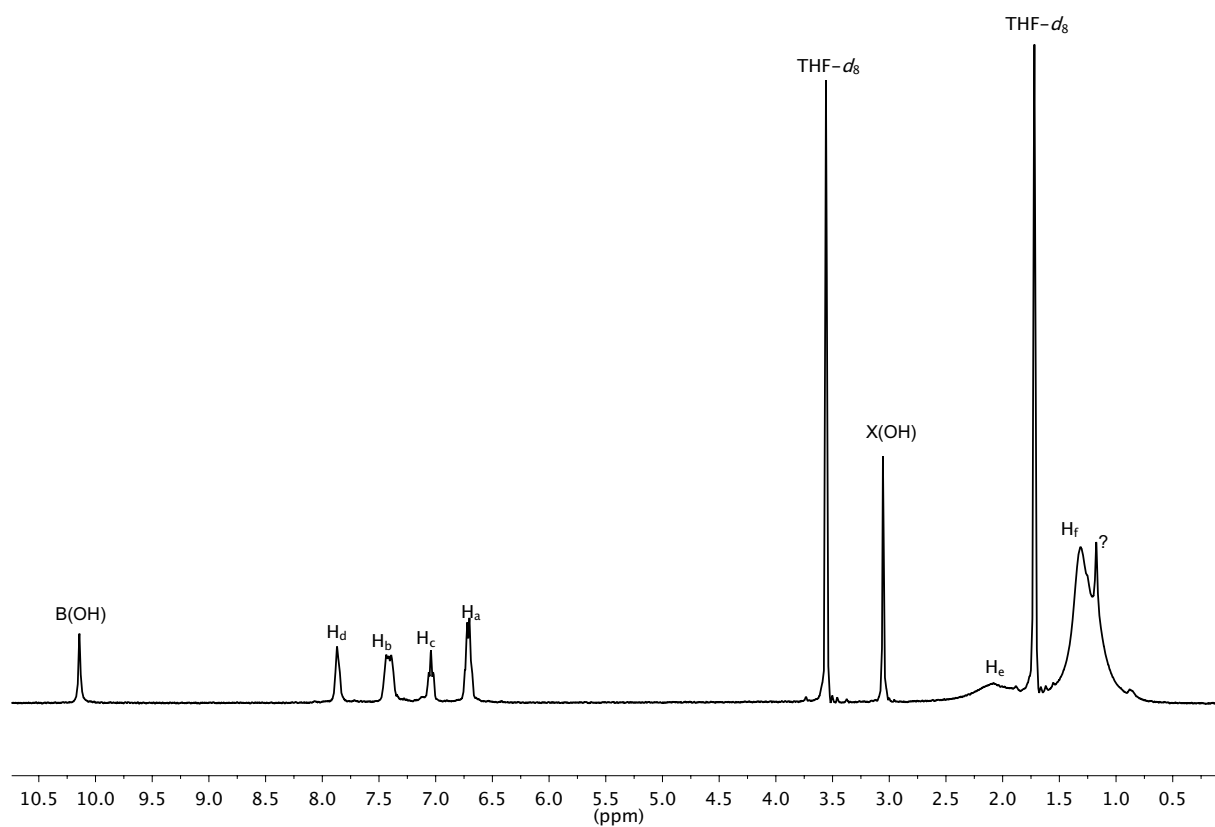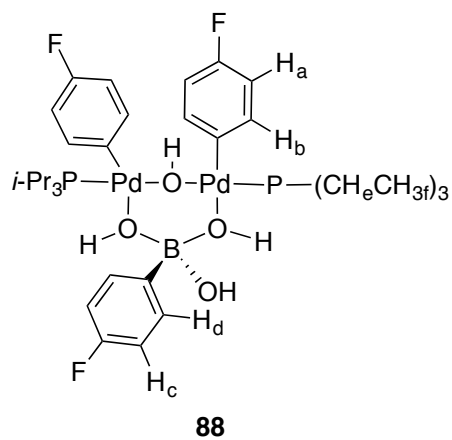
Figure 134. ^1H NMR spectrum of **88** at -100 °C, referenced to THF-d_8 (1.72 ppm).
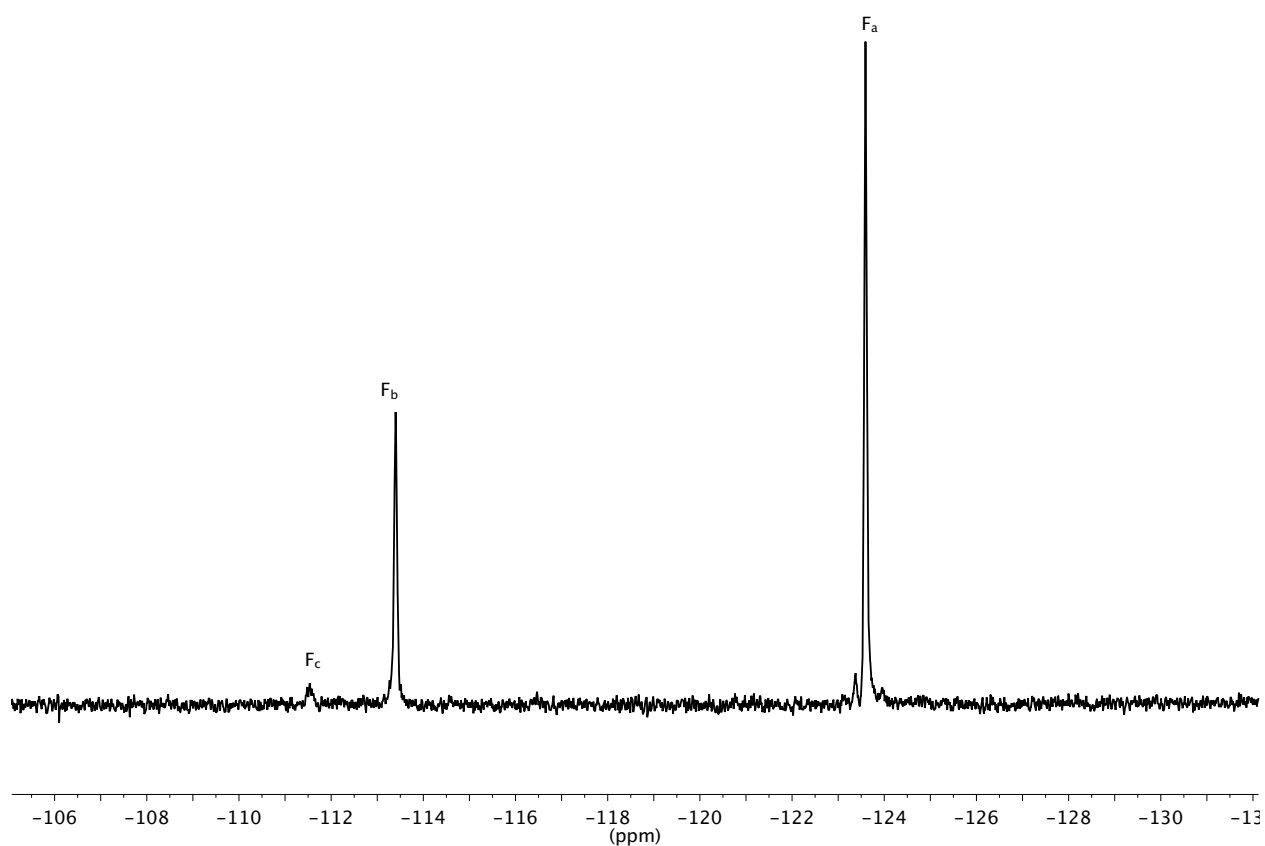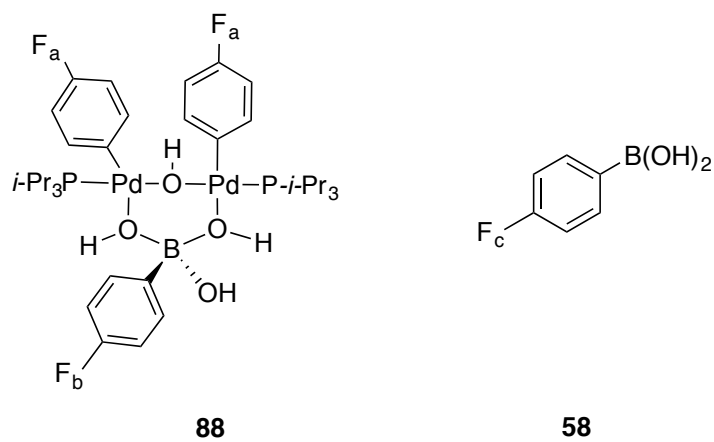
Figure 135. ^{19}F NMR spectrum of **88** at −100 °C, externally referenced to 1,4-difluorobenzene (−120.00 ppm).
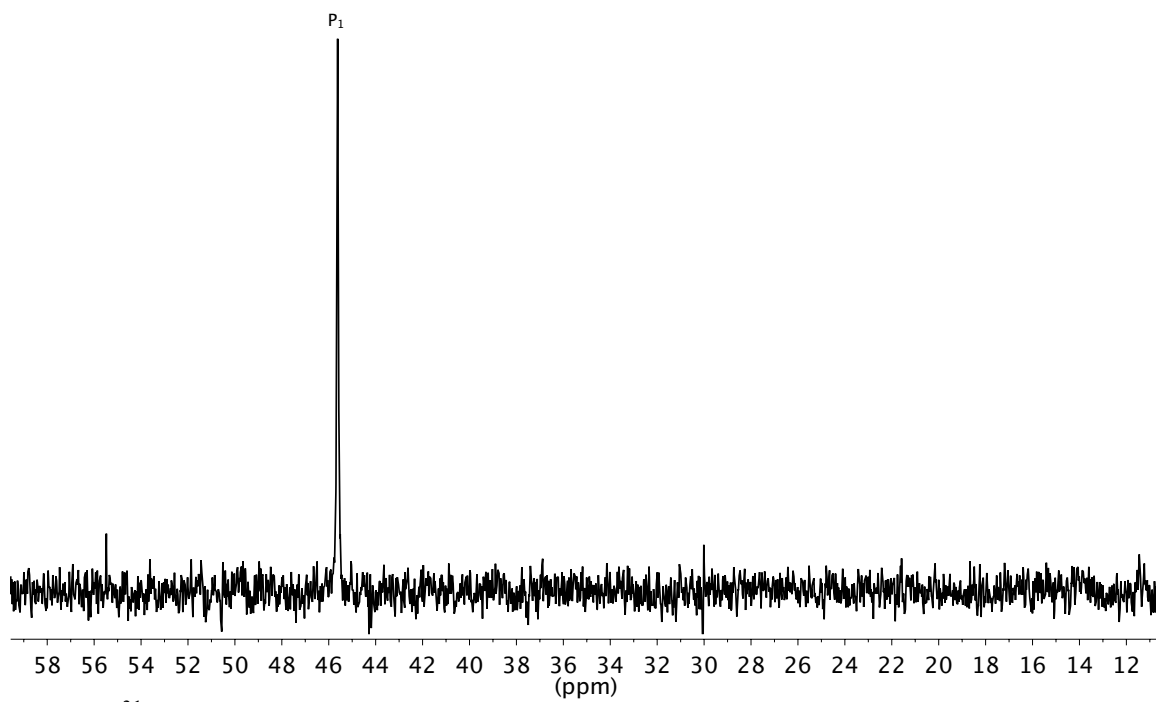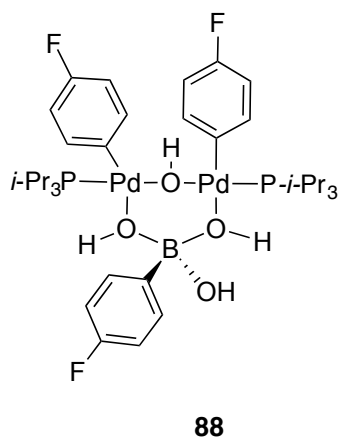
Figure 136. ^{31}P NMR spectrum of **88** at $-100\,°C$, externally referenced to $[(i\text{-}Pr_3P)Pd(4\text{-}FC_6H_4)(\mu\text{-}OH)]_2$ (45.55 ppm).

88
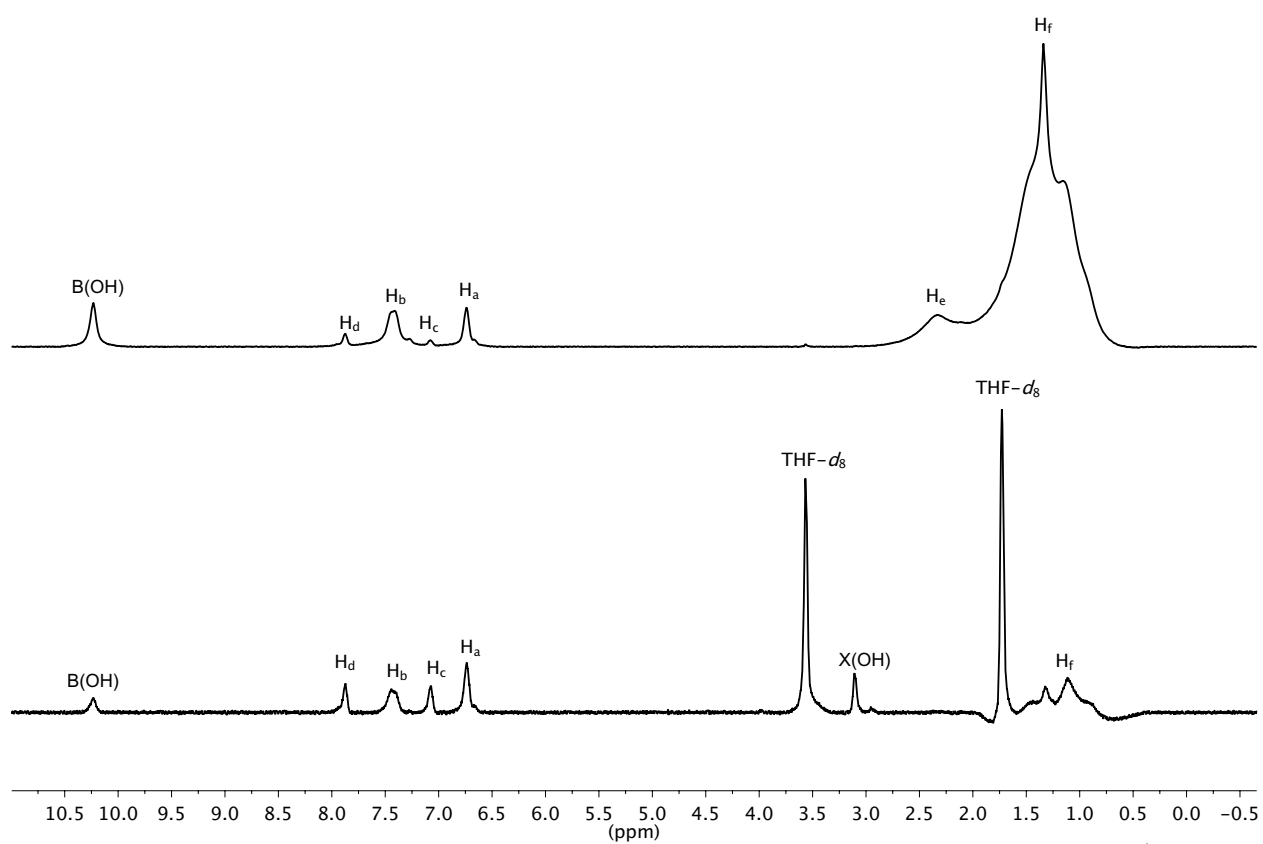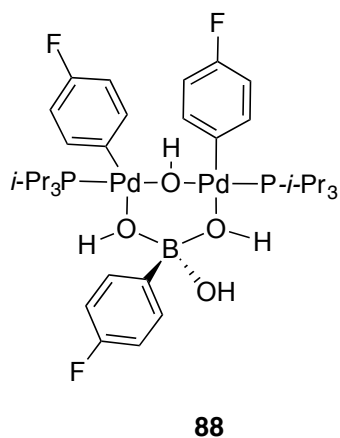
Figure 137. 1D-Phase cycled NOE spectrum (CH_3 irradiated at 1.26 ppm) (top) and ^{1}H NMR spectrum (bottom) at −100 °C, referenced to THF-d_8 (1.72 ppm).

Experiment 20: Preparation of *i*-Pr₃P complex 88 with 2.0 equiv of 58.

80   **88**   **58**
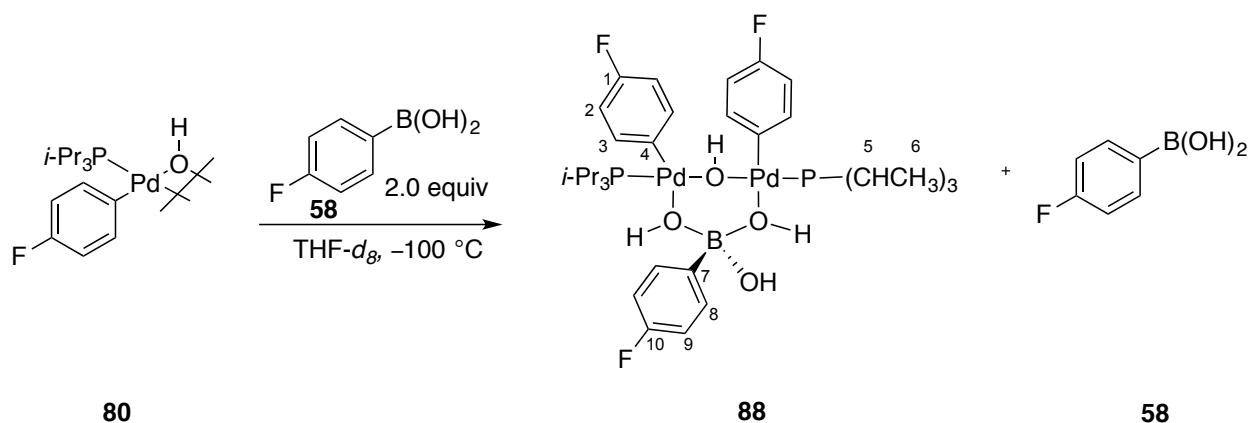
An oven dried, 1.0 mL volumetric flask was charged with 4-fluorophenylboroxine (66.5 mg, 182 μmol 1.0 equiv), H₂O (10 μL, 564 μmol, 3.1 equiv) and filled to the mark with freshly distilled (NaK) THF-d_8 (0.56 M).

An oven-dried, 5-mm, NMR tube was taken into the glove box and [(*i*-Pr₃P)Pd(4-FC₆H₄)(μ-OH)]₂ (11.8 mg, 16 μmol, 1.0 equiv) was added, followed by the addition of 500 μL of freshly distilled THF-d_8 (NaK). The tube was shaken and placed into a −78 °C dry-ice acetone bath followed by the addition of the freshly prepared 4-fluorophenylboronic acid solution (57 μL, 32 μmol, 2.0 eqiuv). The tube was vortexed (not shaken), quickly wiped with a Kimwipe and placed into the probe of the NMR spectrometer pre-cooled to −50 °C. After a few minutes the sample was cooled to −100 °C and complex **63** was observed. The complex was characterized *via* 1D and 2D NMR experiments over a course of experiments. Using internal standards 1,4-difluorobenzene (0.5 μL, 5 μmol, 0.25 equiv) and Ph₄BNa (2.0 mg, 6 μmol, 0.3 equiv) ¹⁹F and ¹¹B NMR chemical shifts were recorded.

Data for **88**:

¹H NMR: (600 MHz, THF-d_8)

10.25 (s, HO), 7.86 (m, 2 HC(8)), 7.42 (m, 4 HC(3)), 7.07 (dd, 8 Hz, 2 HC(9)), 6.72 (m, 4 CH(2)), 2.27 (broad, 6 HC(5)), 1.26 (broad, 36 HC(6))

¹³C NMR: (151 MHz, THF-d_8)

167.00, 165.01 (d, ^1J(F-C) = 248 Hz, 1 C(10)), 166.59, 164.64 (d, ^1J(F-C) = 244 Hz, 2 C(1)), 144.94 (m, 2 C(4)), 138.30 (m, 4 C(3)), 137.14 (s, 2, C(8), 135.38 (m, 1 C(7), 115.19 (s, 2 C(9)), 114.62 (m, 4 C(2)), 25.96 (b, 6 C(5)), 19.68 (b, 12 C(6))

¹⁹F NMR: (565 MHz, THF-d_8)

−113.43 (s, FC(10)), −123.65 (s, 2 FC(1)),

<u>^{31}P NMR:</u>   (243 MHz, THF-d_8)

45.62 (s, 2 P(Pd))

<u>^{11}B NMR:</u>   (129 MHz, THF-d_8)

Br (B(O))
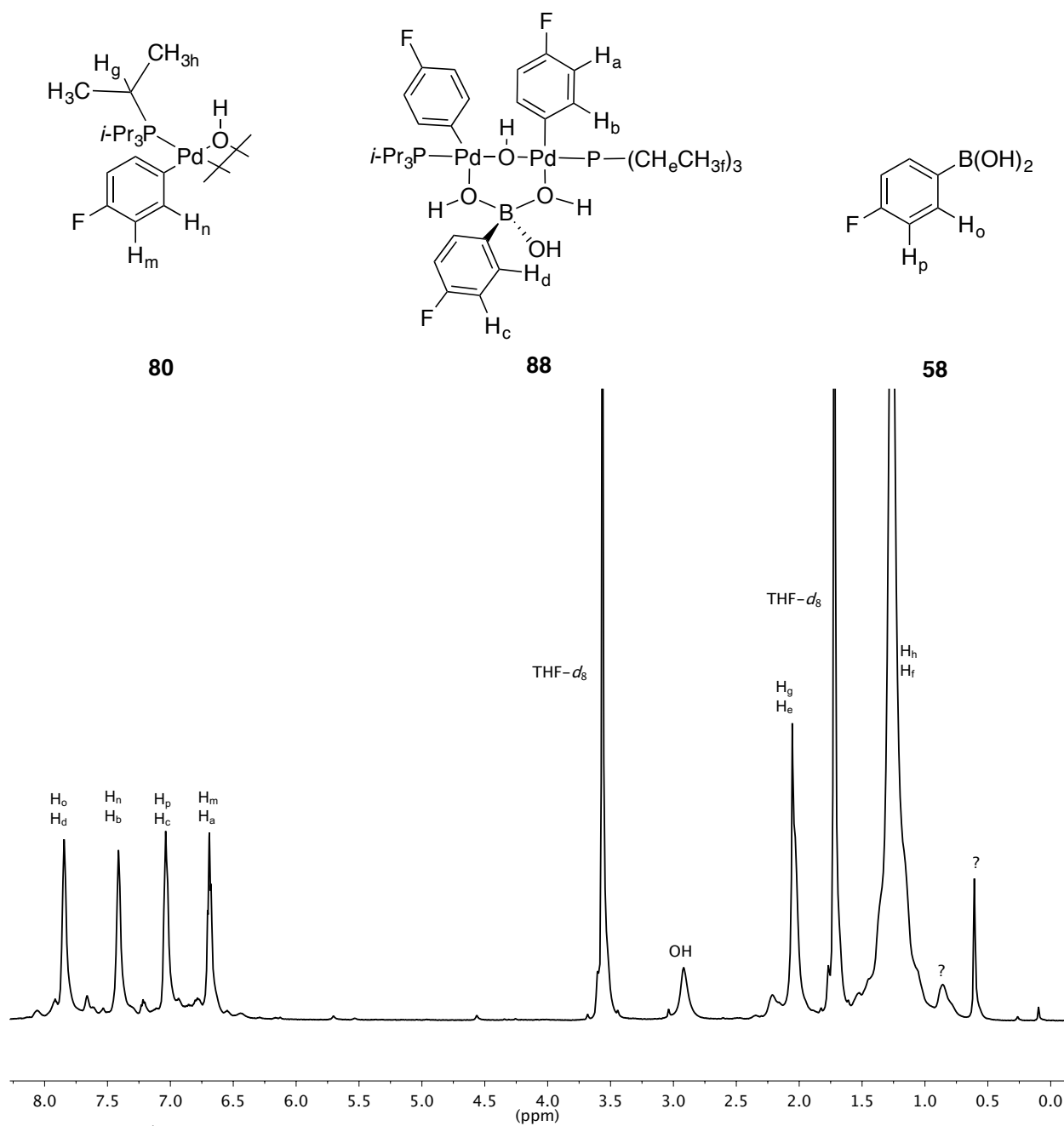
Figure 138. ^{1}H NMR spectrum of **80** and **58** at $-50\ °C$, referenced to THF-d_8 (1.72 ppm).
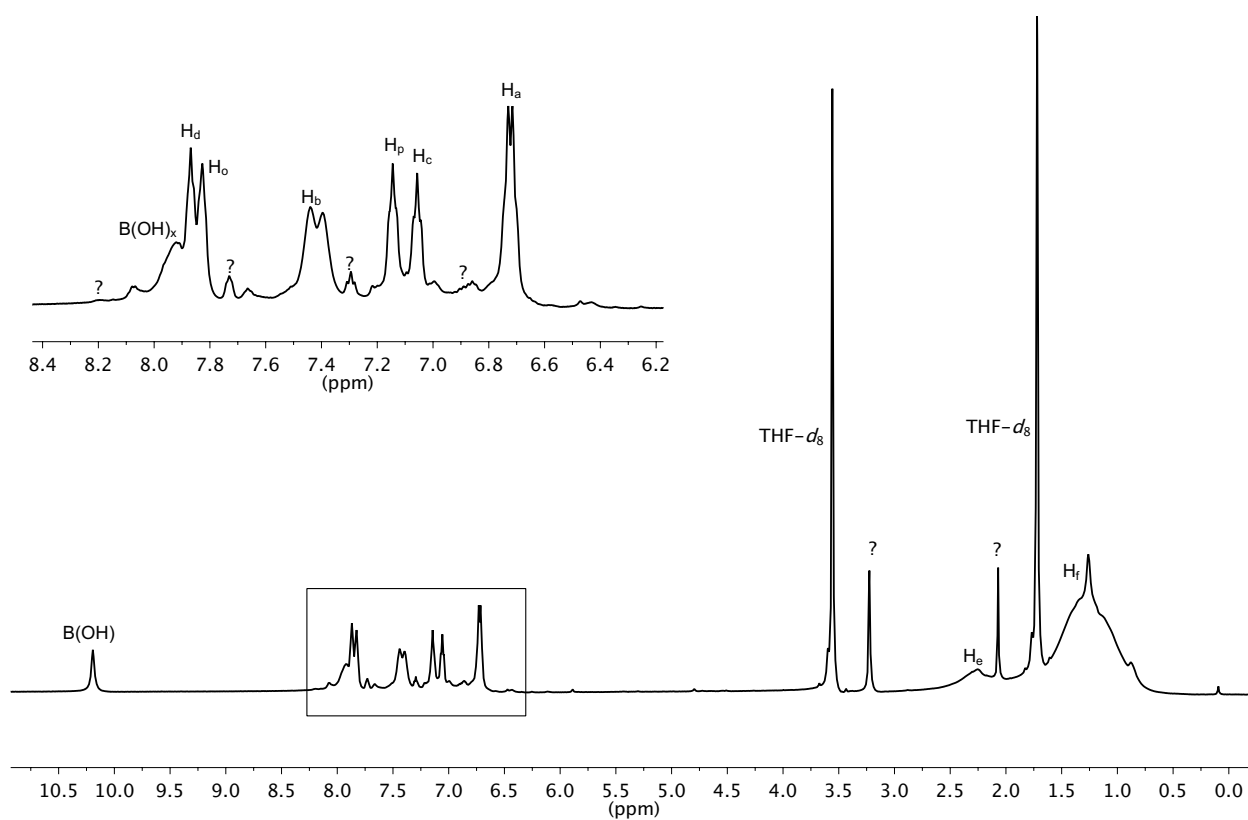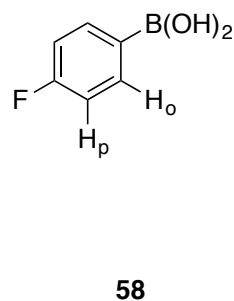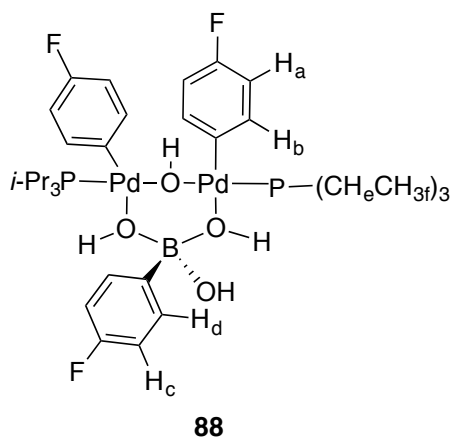
Figure 139. ^{1}H NMR spectrum of **88** and **58** at −100 °C, referenced to THF-d_8 (1.72 ppm).

Figure 140.. ^{13}C NMR spectrum of **58** and **88** at −100 °C, referenced to THF-d_8 (68.21 ppm).
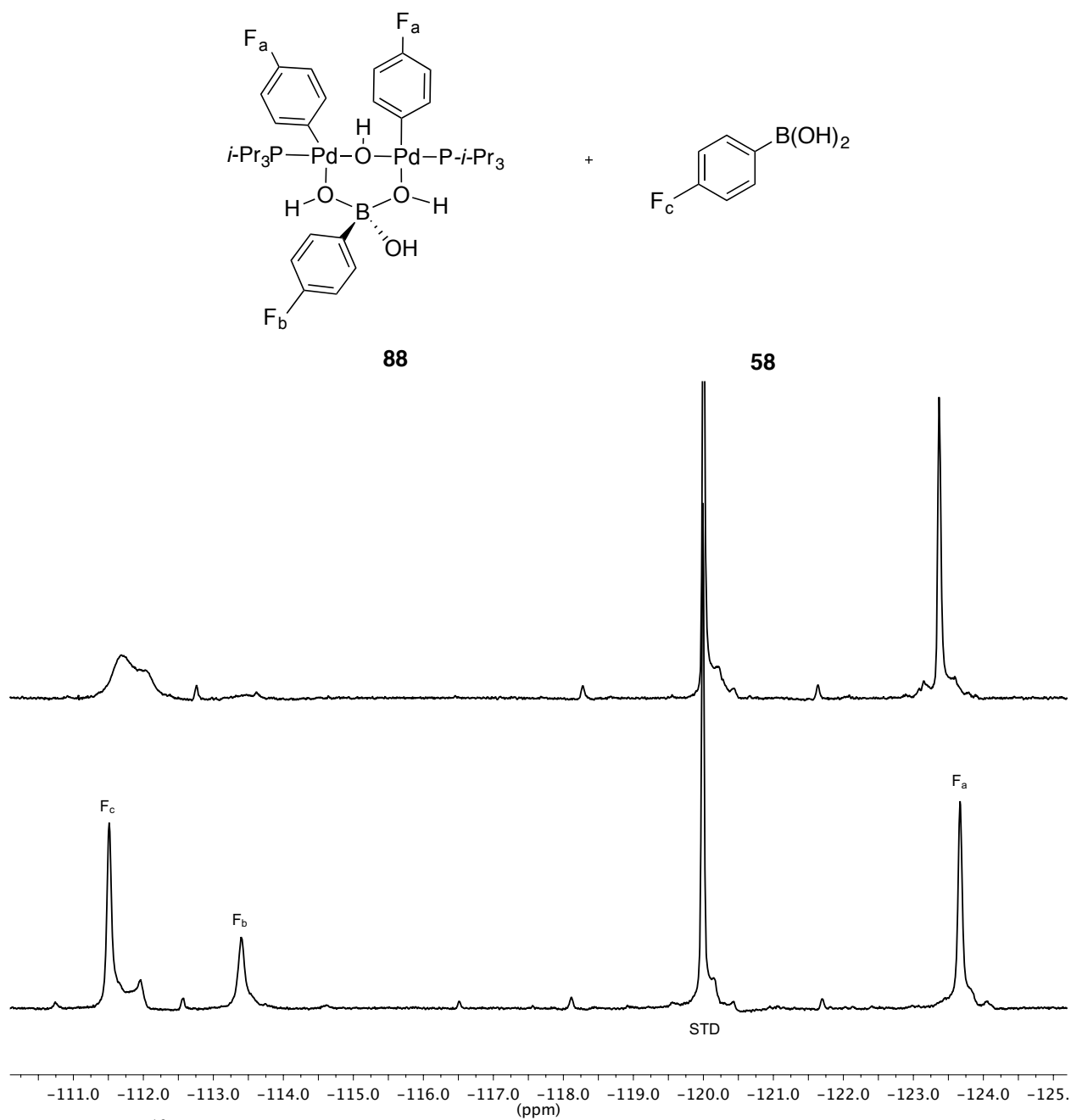
Figure 141. ^{19}F NMR spectra of **88** and **58** at −50 °C (top) and −100 °C (bottom), referenced to 1,4-difluorobenzene (−120.00 ppm).

205

88   **58**
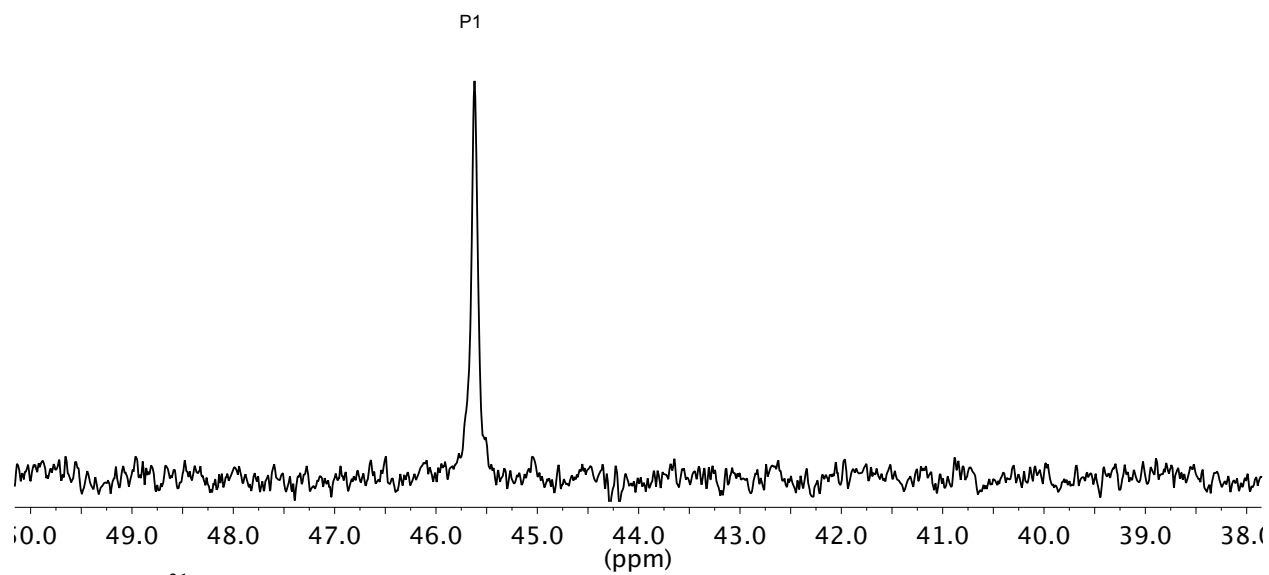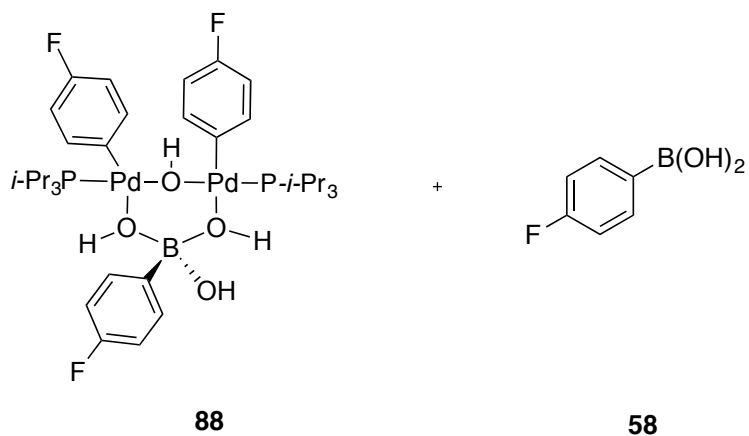
Figure 142. ^{31}P NMR spectrum of **88** at −100 °C, externally referenced to [(i-Pr$_3$P)Pd(4-FC$_6$H$_4$)(μ-OH)]$_2$ (45.55 ppm).
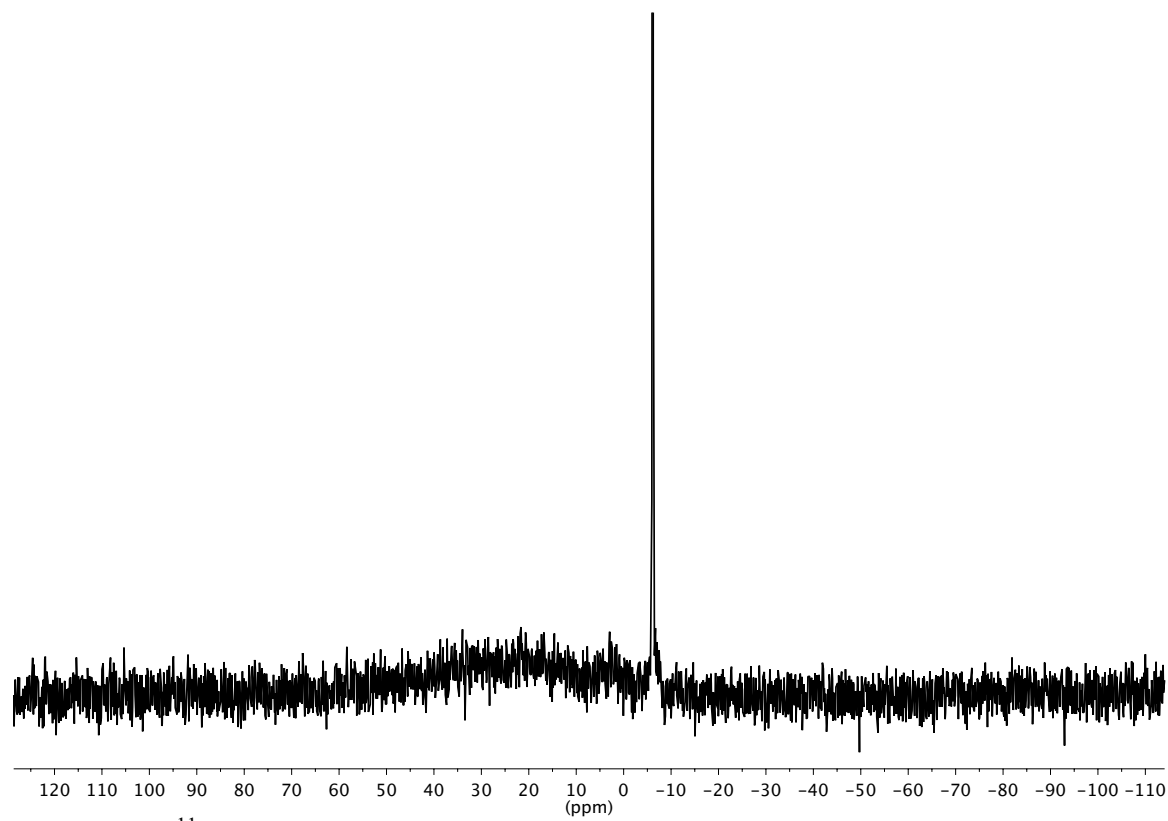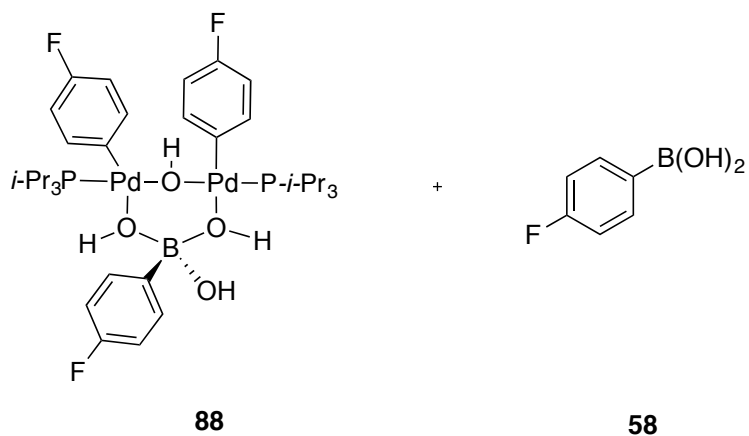
Figure 143. ^{11}B NMR spectrum of **88** and **58** at -100 °C, referenced to Ph$_4$BNa (-6.14 ppm).
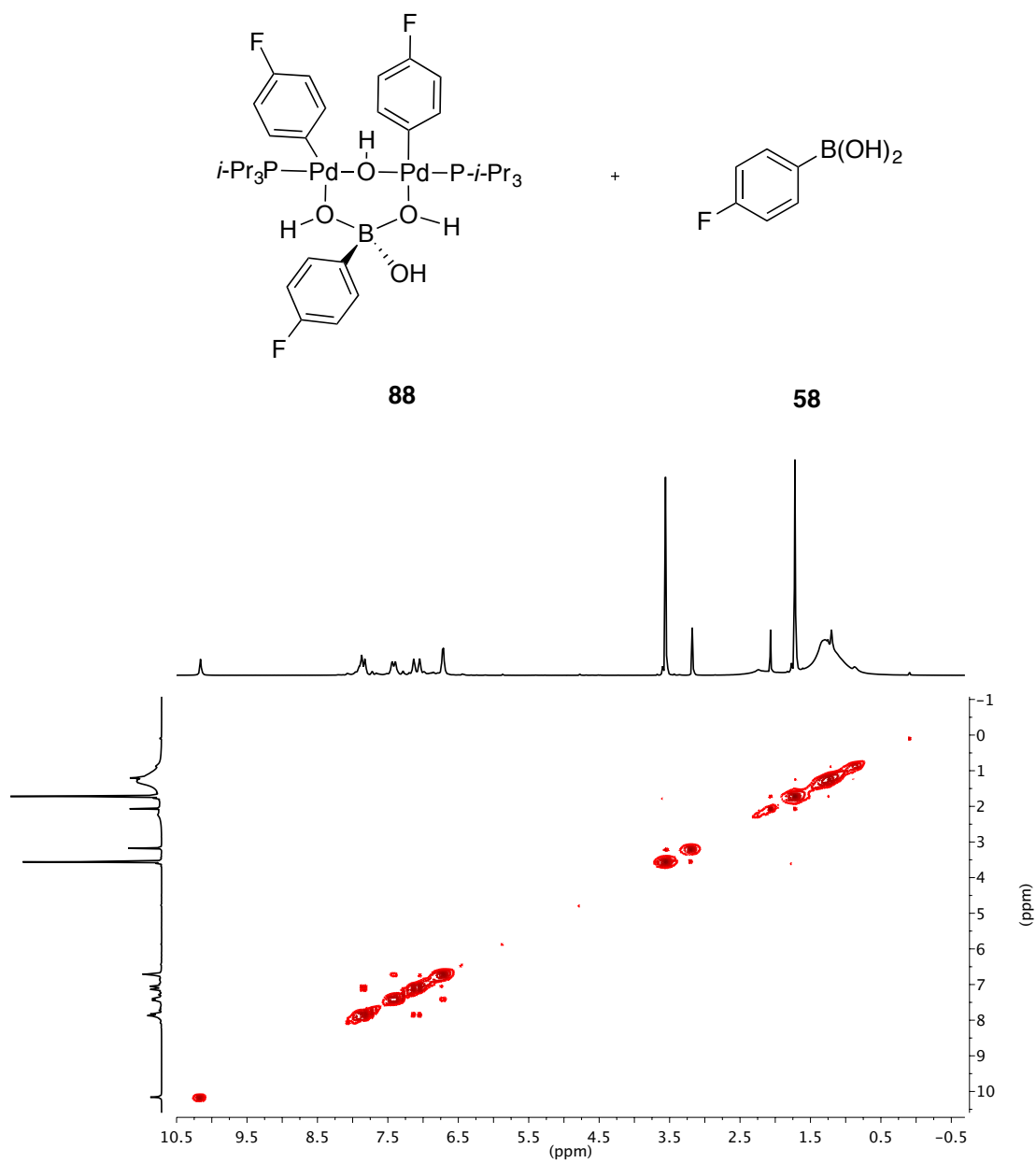
Figure 144. COSY spectrum of **88** and **58** at −100 °C, referenced to THF-d_8 (1.72 ppm).

Figure 145. gHSQC spectrum of **88** and **58** at −100 °C, referenced to THF-d_8 (1.72 and 68.21 ppm).
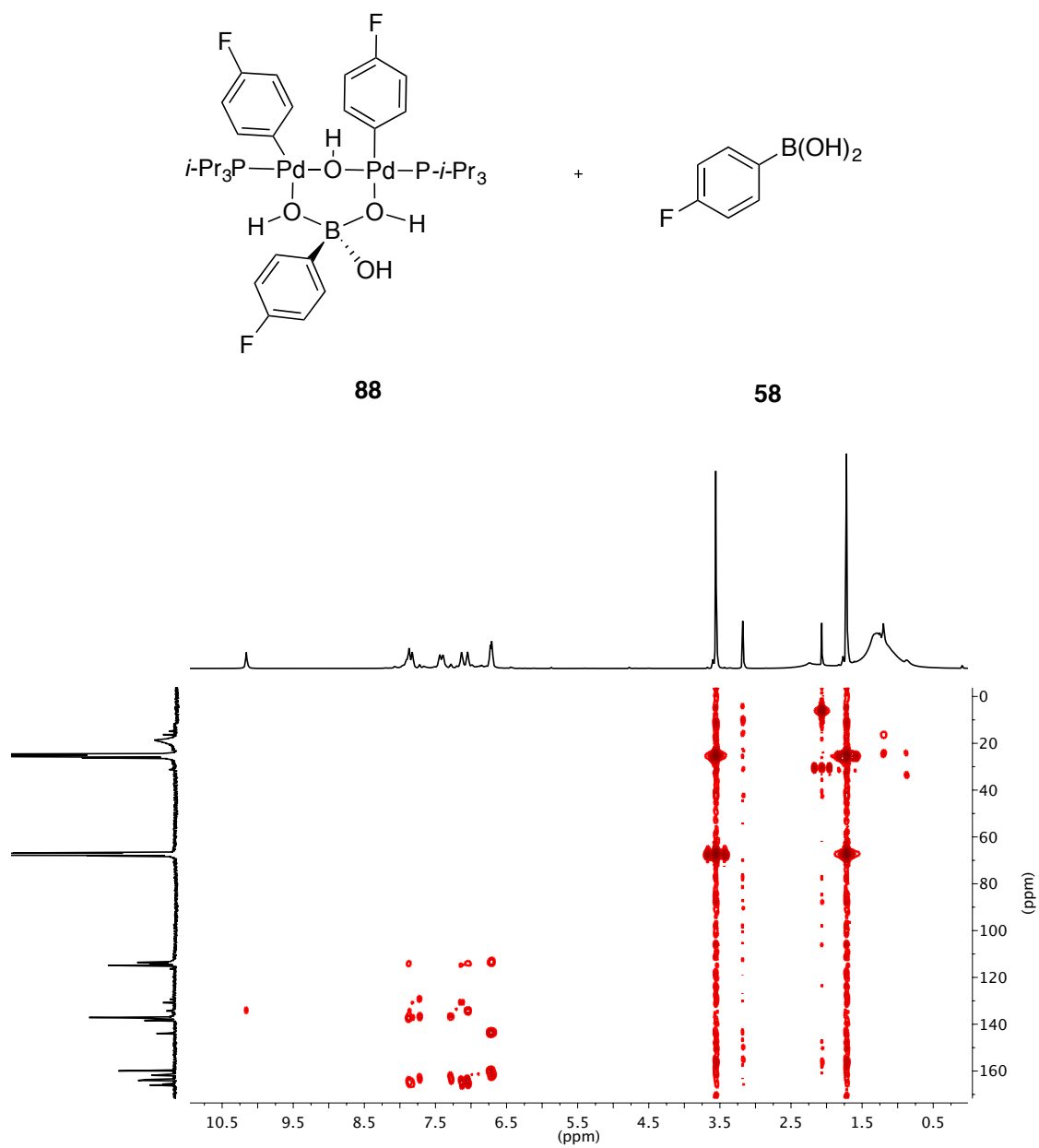
Figure 146. gHMBC spectrum of **88** and **58** at −100 °C, referenced to THF-d_8 (1.72 and 68.21 ppm).
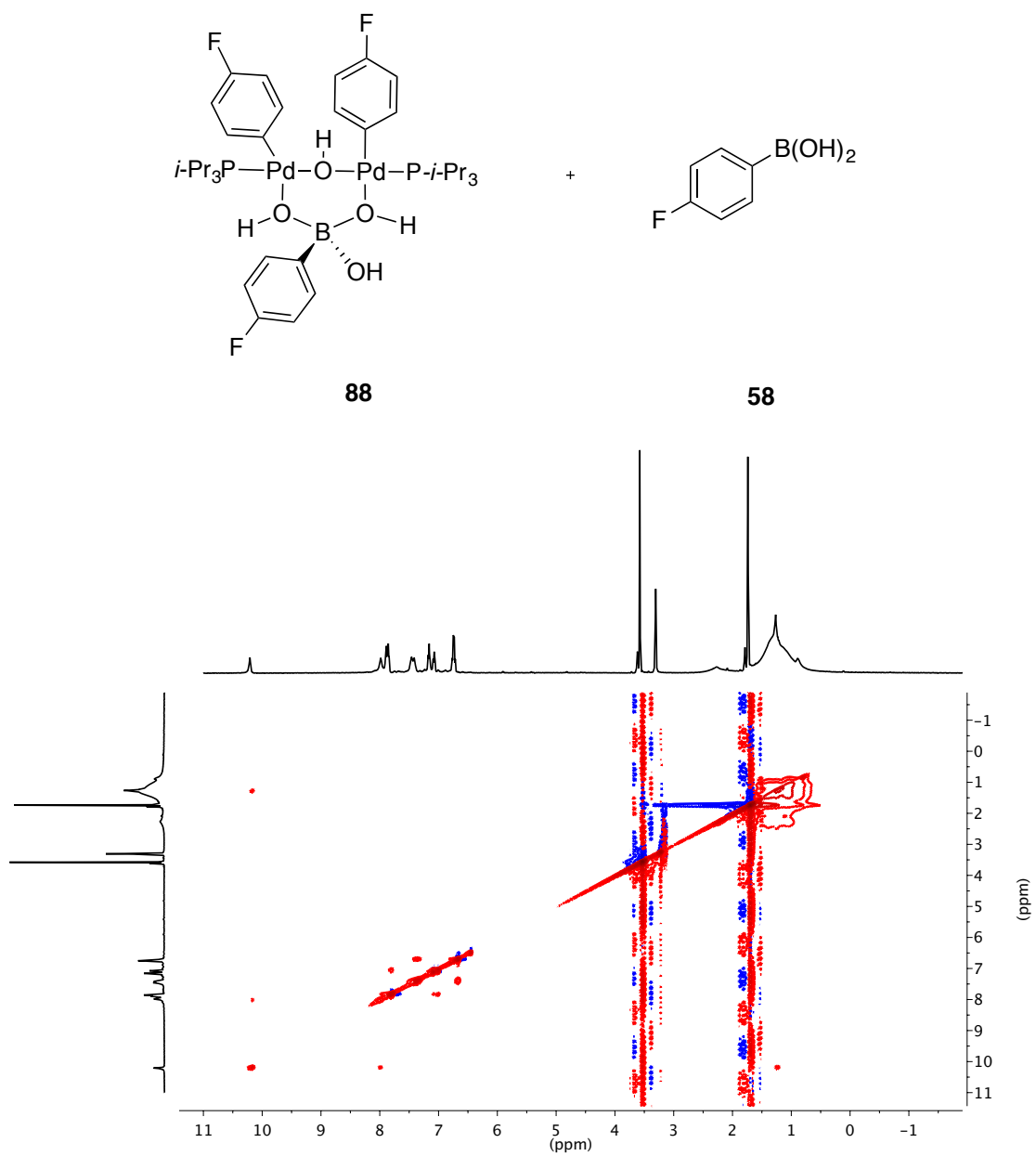
Figure 147. NOESY/EXSY spectrum of **58** and **88** at −100 °C, referenced to THF-d_8 (1.72 ppm).

Experiment 21: Preparation of *i*-Pr₃P complex 88 with 4.0 equiv of 58.

80   88   58
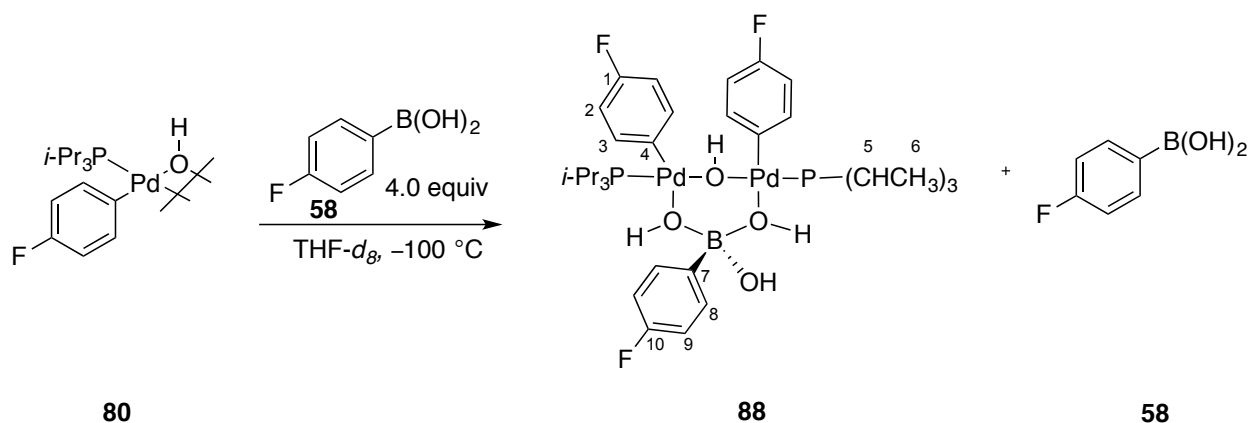
An oven dried, 2-dram vial was charged with 4-fluorophenylboroxine (7.4 mg, 20 μmol 1.0 equiv), H_2O (1 μL, 55 μmol, 5.5 equiv) followed by 100 μL THF-d_8. The vial was shaken until the solid had dissolved.

An oven-dried, 5-mm, NMR tube was taken into the glove box and [(*i*-Pr₃P)Pd(4-FC₆H₄)(μ-OH)]₂ (11.4 mg, 15 μmol, 1.0 equiv) was added, followed by the addition of 500 μL of THF-d_8. The tube was shaken and placed into a −78 °C dry-ice acetone bath followed by the addition of the freshly prepared 4-fluorophenylboronic acid solution (100 μL, 60 μmol, 4.0 eqiuv). The tube was vortexed (not shaken) quickly wiped with a Kimwipe and palced into the probe of the NMR spectrometer pre-cooled to −50 °C. After a few minutes the sample was cooled to −100 °C where complex **88** was observed. The complex was monitored *via* ¹H NMR spectroscopy.
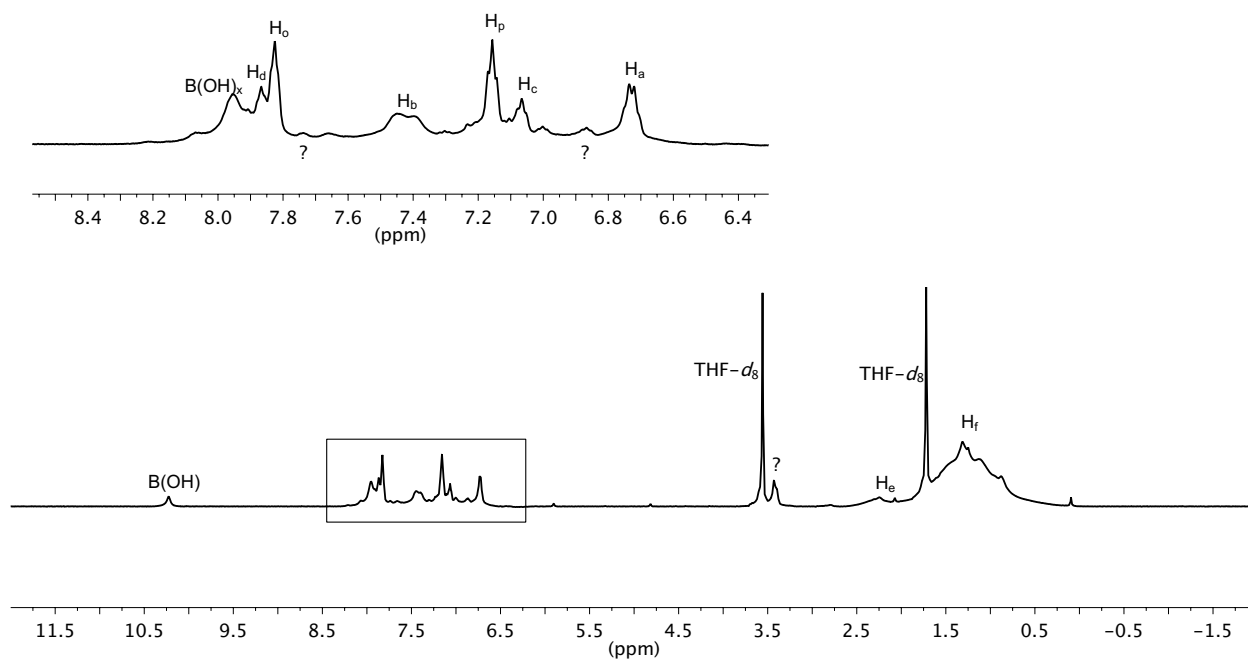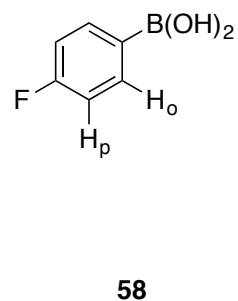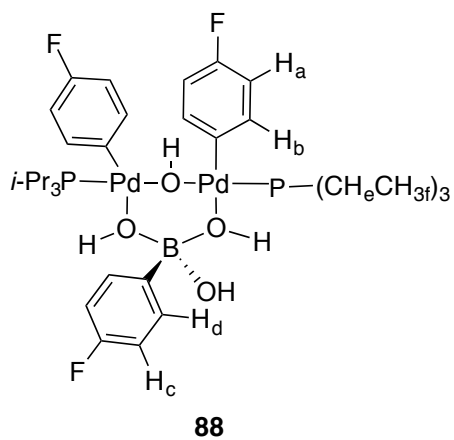
Figure 148. ^{1}H NMR spectrum of **88** and **58** at −100 °C, referenced to THF-d_8 (1.72 ppm).

213

Variable temperature Eyring analysis for *i*-Pr₃P complex 88 with 1.0 equiv of 58
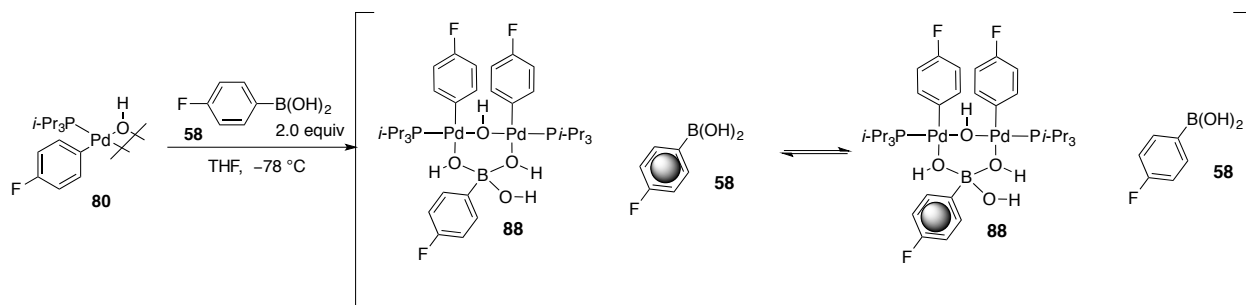
An approximate coalescence temperature (T_c) was measured at –40 °C by the signals merging with the baseline. The rate constant k_c at coalescence was measured using $k_c = \pi\Delta v/\sqrt{2}$, where Δv is the maximum chemical shift difference (1068 Hz) between **88** and **58** at −100 °C. Using the Eyring equation $\Delta G_e^{\neq} = -RT_c\ln(k_c\hbar/k_BT_c)$ where R is the gas constant, k_B is Boltzmann constant, $\hbar$ is Planck's constant, the activation of exchange was measured to be approximately $\Delta G_e^{\neq} = 11$ kcal/mol.
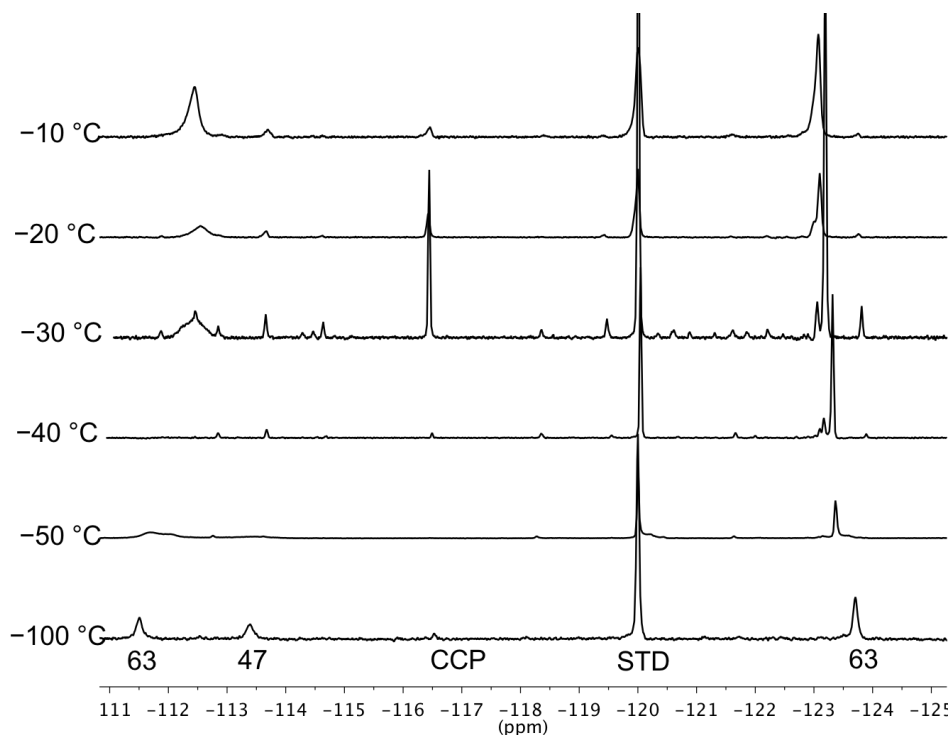
Figure 149. Eyring analysis of exchange at various temperatures, referenced to 1,4-difluorobenzene (−120 ppm).

214

Experiment 22: Reaction of 90 with thallium arylboronate 79.
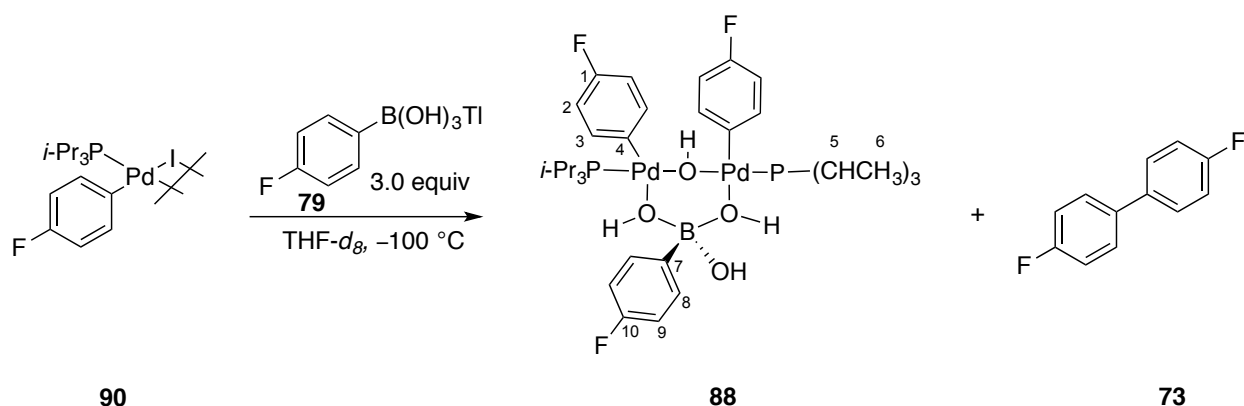
An oven-dried, 5-mm, NMR tube was charged with [(i-Pr$_3$P)Pd(4-FC$_6$H$_4$)(μ-I)]$_2$ (9.76 mg, 10 μmol, 1.0 equiv) followed by the addition of 400 μL of THF-d_8 (NaK).

An oven dried, 5-mm, NMR tube as charged with thallium 4-fluorophenylboronate (11 mg, 30 μmol 3.0 equiv) and 200 THF-d_8 (NaK) and sonicated for ~2 min. The tube was placed into a −78 °C dry-ice acetone bath followed by the addition of the freshly prepared [(i-Pr$_3$P)Pd(4-FC$_6$H$_4$)(μ-I)]$_2$ solution (400 μL). The tube was vortexed (not shaken) quickly wiped with a Kimwipe and placed into the probe of the NMR spectrometer pre-cooled to −50 °C. After ~1 h the sample was characteristic of complex **88** at −50 °C which was confirmed by cooling the spectrometer to −100 °C where ^{1}H, and ^{19}F NMR spectra were collected.

Data for **88**:

^{1}H NMR: (500 MHz, THF-d_8)

10.21 (s, HO), 7.87 (m, 2 HC(8)), 7.39 (m, 4 HC(3)), 7.06 (dd, 8 Hz, 2 HC(9)), 6.72 (m, 4 CH(2)), 2.28 (broad, 3 HC(5)), 1.26 (broad, 18 HC(6))

^{19}F NMR: (565 MHz, THF-d_8)

−113.36 (s, FC(10)), −123.59 (s, 2 FC(1))

^{31}P NMR: (243 MHz, THF-d_8)

45.12 (s, 2 P(Pd))
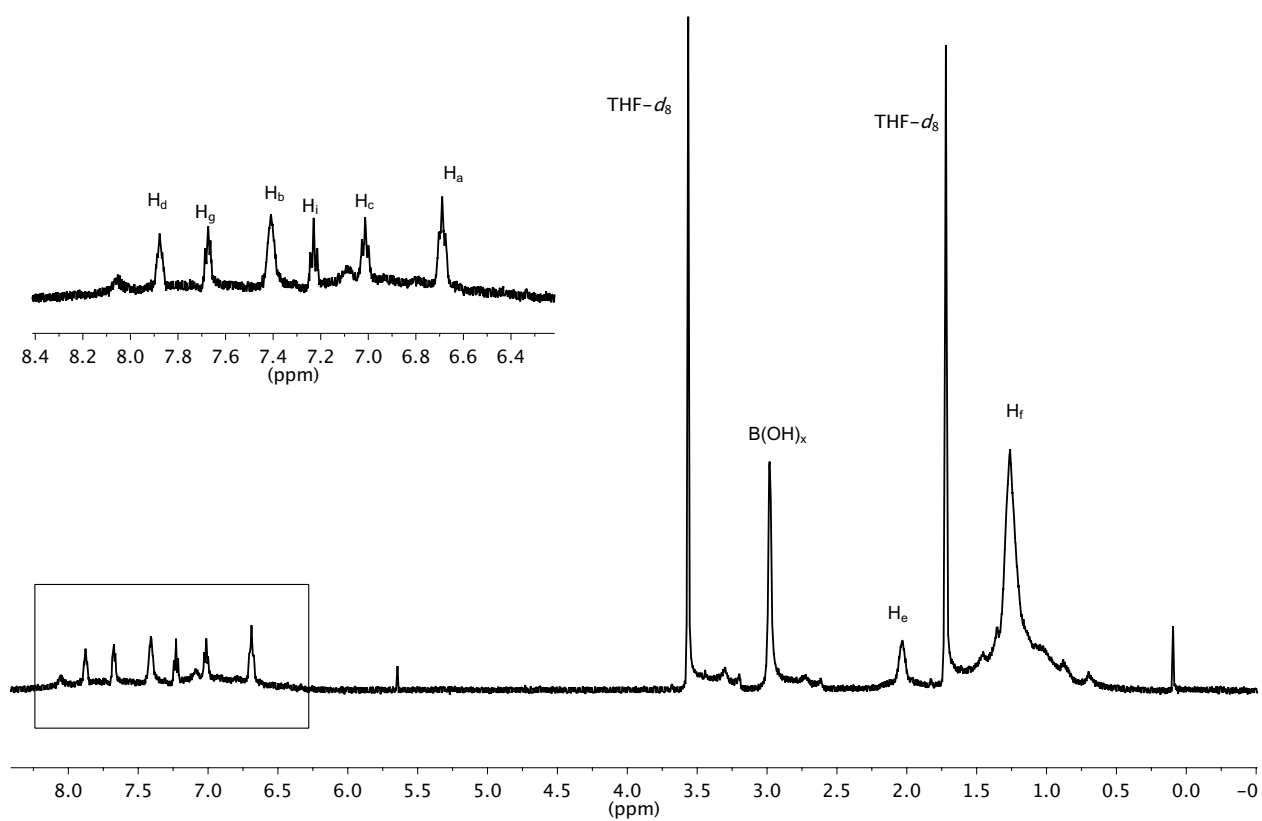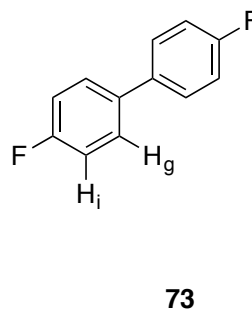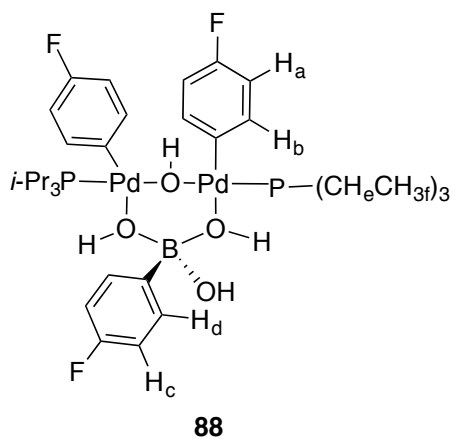
Figure 150. ^{1}H NMR spectrum of **88** at −50 °C, referenced to THF-d_8 (1.72 ppm).
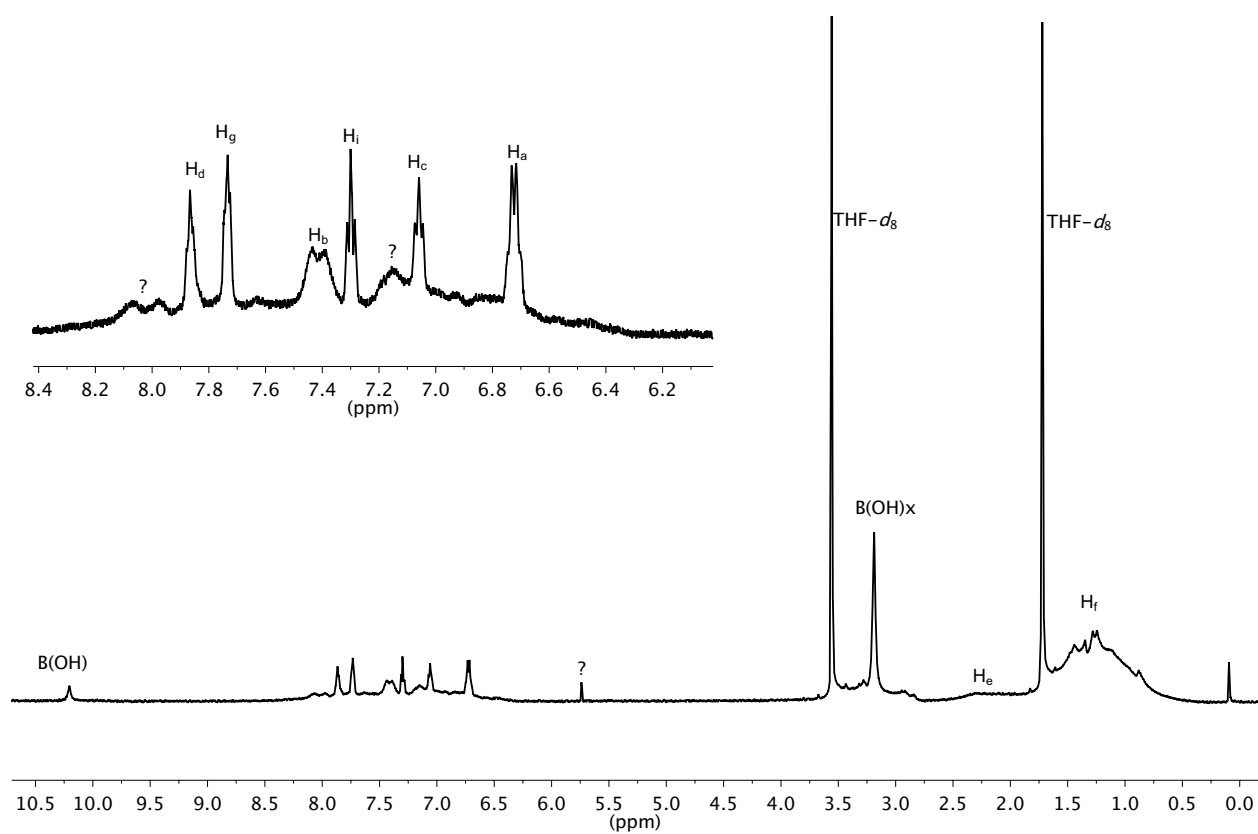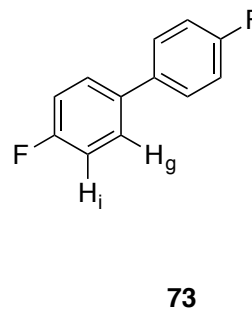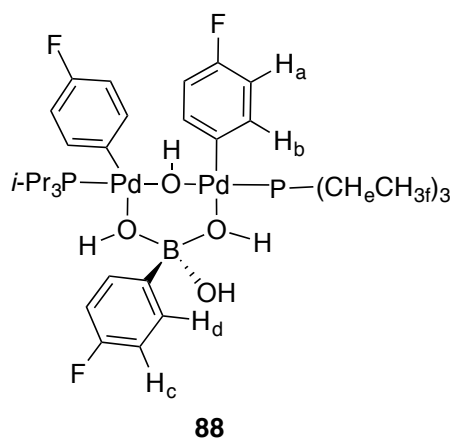
Figure 151. ^{1}H NMR spectrum of **88** at −100 °C, referenced to THF-d_8 (1.72 ppm).

217

88

73
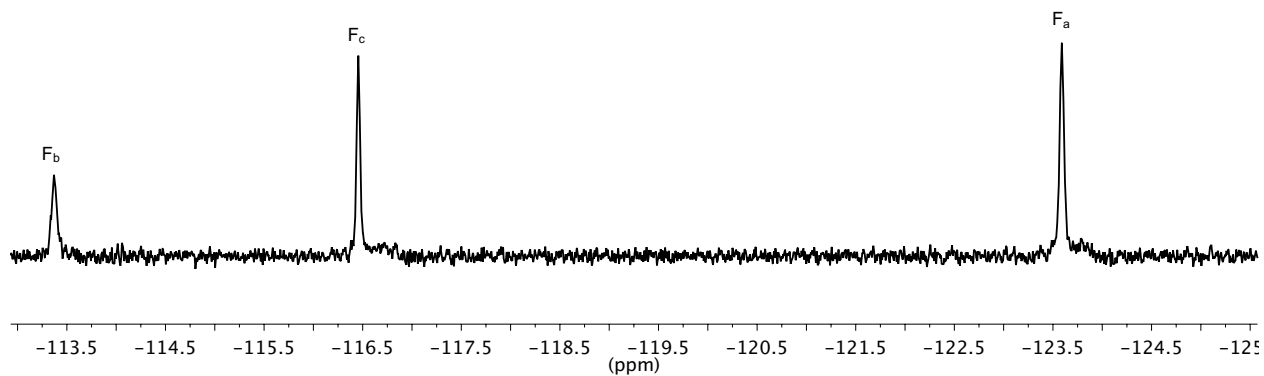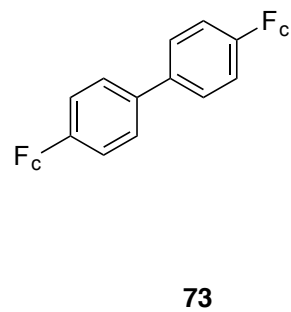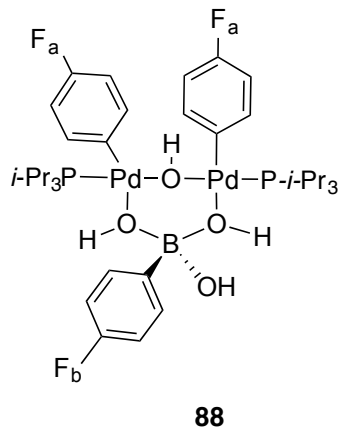
Figure 152. ^{19}F NMR spectrum of **88** at −100 °C, referenced externally to 1,4-difluorobenzene (−120 ppm).

88
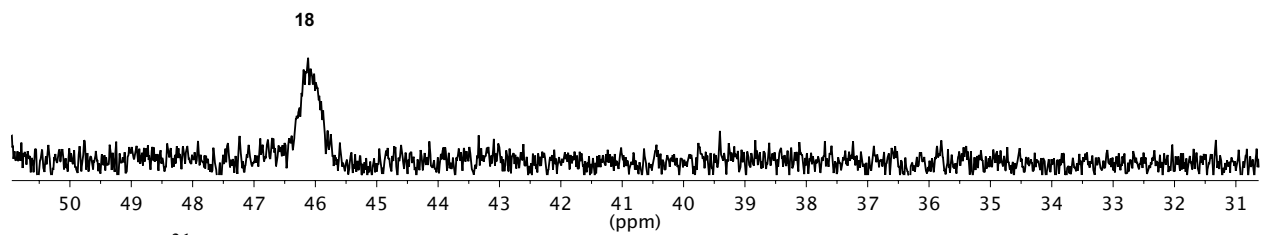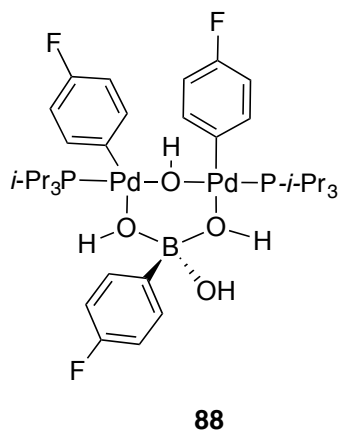
Figure 153. ^{31}P NMR spectrum of **88** at −100 °C, externally referenced to [(*i*-Pr$_3$P)Pd(4-FC$_6$H$_4$)(μ-OH)]$_2$ (45.55 ppm).

Experiment 23: Preparation of *i*-Pr$_3$P complex 94 with 2.0 equiv of 58.

An oven dried, vial was charged with 4-trifluoromethylphenylboroxine (86 mg, 167 µmol 1.0 equiv), H$_2$O (9 µL, 500 µmol, 3.1 equiv) and 500 µL of THF to generate a 1 M solution. The solution was transfer to an NMR tube and capped with a septum.

An oven-dried, 5-mm, NMR tube was taken into the glove box and [(*i*-Pr$_3$P)Pd(4-CF$_3$C$_6$H$_4$)(µ-OH)]$_2$ (8.6 mg, 10 µmol, 1.0 equiv) was added, followed by the addition of 500 µL of freshly distilled THF-d_8 (NaK). The tube was shaken and placed into a −78 °C dry-ice acetone bath followed by the addition of the freshly prepared 4-trifluoromethylboronic acid solution (20 µL, 20 µmol, 2.0 eqiuv). The tube was vortexed (not shaken), quickly wiped with a Kimwipe and placed into the probe of the NMR spectrometer pre-cooled to −50 °C. After a few minutes the sample was cooled to −100 °C and complex **94** was observed. The signals were not well separated in the ^{1}H NMR spectrum.

Data for **94**:

^{19}F NMR:　　(565 MHz, THF-d_8)

　　−113.18 (s, FC(10)), −61.69 (s, 2 FC(1)),
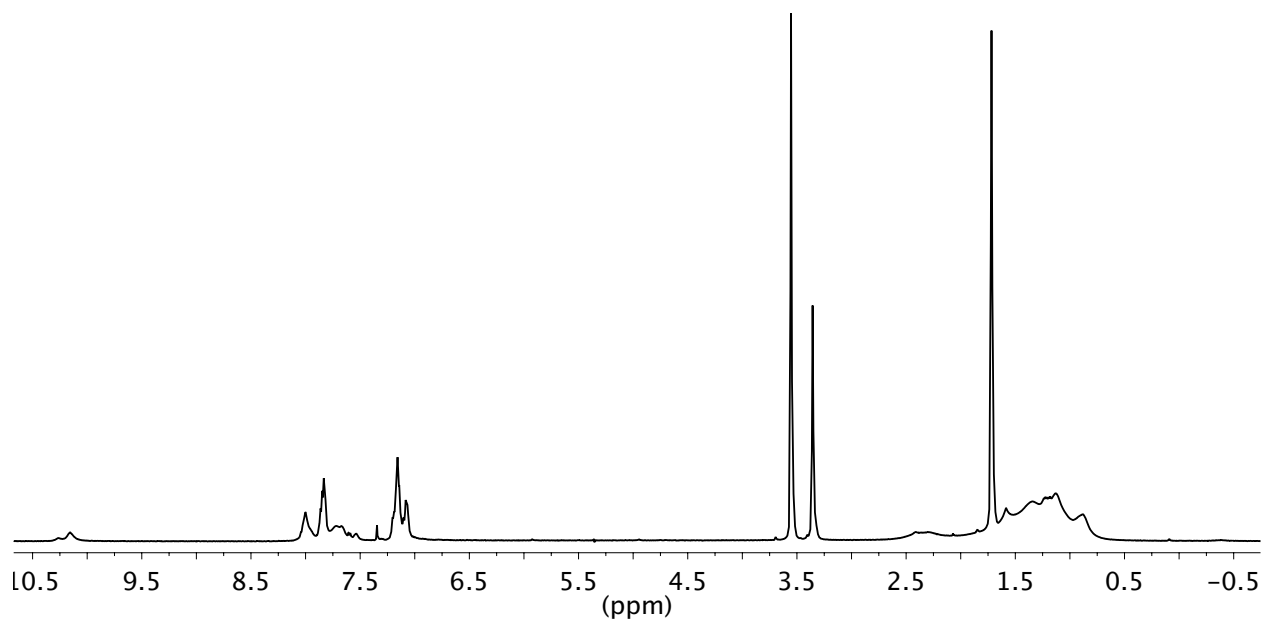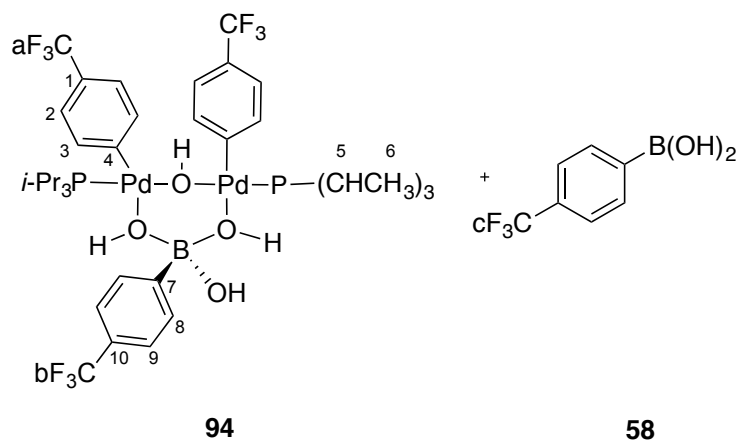
Figure 154. ^{1}H NMR spectrum of **94** and **58** at −100 °C, referenced externally to 1,4-difluorobenzene (−120.00 ppm).

Figure 155. ^{19}F NMR spectrum of **94** and **58** at −100 °C, referenced to **58** (−111.21 ppm).

Experiment 24: Preparation of *i*-Pr$_3$P complex 94 with 2.0 equiv of 58.
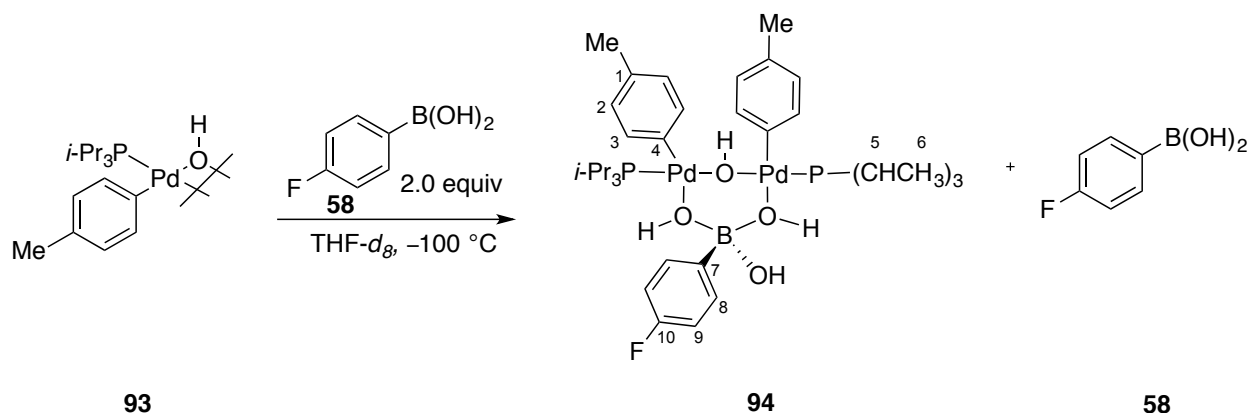
An oven dried, 1.0 mL volumetric flask was charged with 4-fluorophenylboroxine (65 mg, 182 µmol 1.0 equiv), H$_2$O (10 µL, 564 µmol, 3.1 equiv) and filled to the mark with freshly distilled (NaK) THF-d_8 (0.56 M).

An oven-dried, 5-mm, NMR tube was taken into the glove box and [(*i*-Pr$_3$P)Pd(4-MeC$_6$H$_4$)(µ-OH)]$_2$ (11.3 mg, 15 µmol, 1.0 equiv) was added, followed by the addition of 500 µL of freshly distilled THF-d_8 (NaK). The tube was shaken and placed into a −78 °C dry-ice acetone bath followed by the addition of the freshly prepared 4-fluorophenyllboronic acid solution (54 µL, 30 µmol, 2.0 eqiuv). The tube was vortexed (not shaken), quickly wiped with a Kimwipe and placed into the probe of the NMR spectrometer pre-cooled to −50 °C. After a few minutes the sample was cooled to −100 °C and complex **9** was observed. The signals were not well separated in the ^{1}H NMR spectrum.
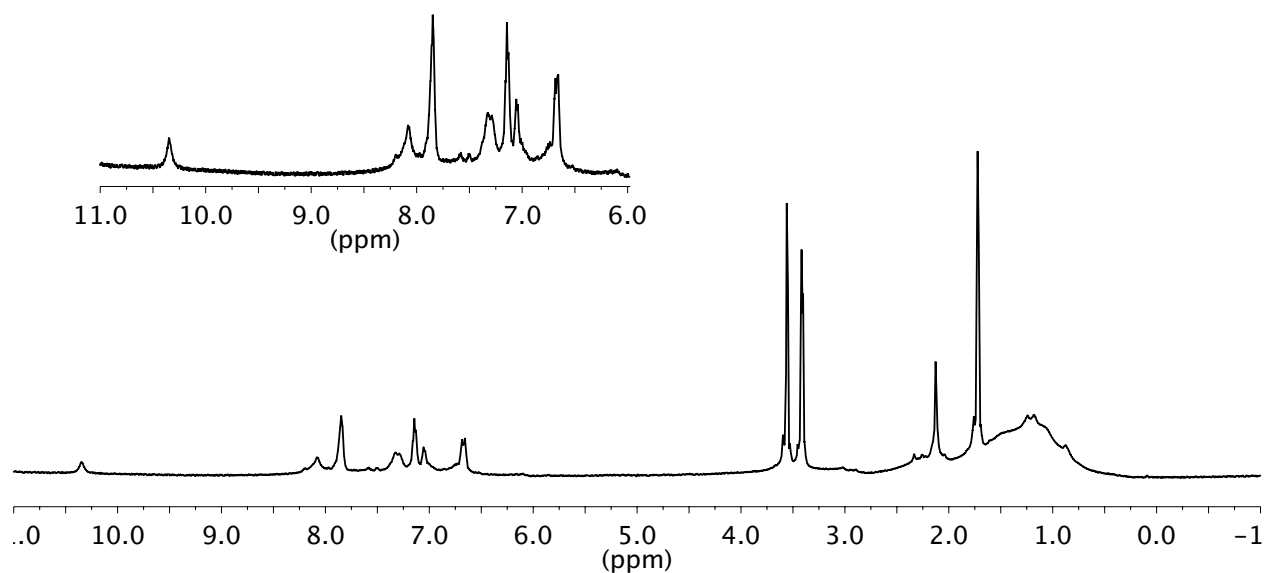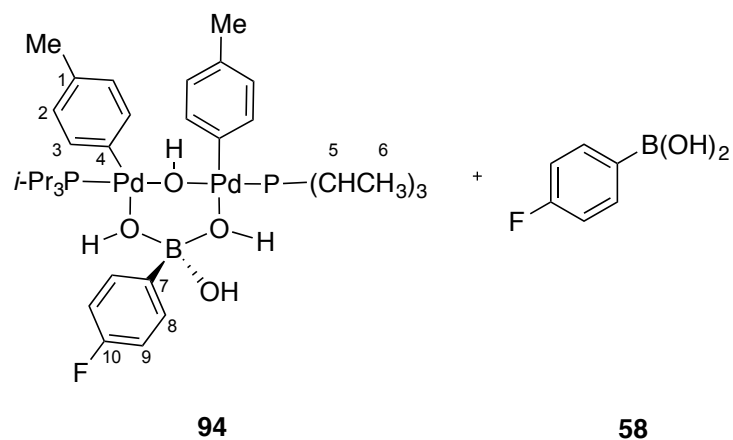
Figure 156. ^{1}H NMR spectrum of **96** and **58** at −100 °C, referenced to THF-d_8 (−120.00 ppm).

224

Experiment 25: Preparation of *i*-Pr₃P complex 97 with 2.0 equiv of 65.

64   **97**   **65**

An oven dried, vial was charged with 4-trifluoromethylphenylboroxine (86 mg, 167 μmol 1.0 equiv), H₂O (9 μL, 500 μmol, 3.1 equiv) and 500 μL of THF to generate a 1 M solution. The solution was transfer to an NMR tube and capped with a septum.

An oven-dried, 5-mm, NMR tube was taken into the glove box and [(*i*-Pr₃P)Pd(4-CF₃C₆H₄)(μ-OH)]₂ (13.0 mg, 15 μmol, 1.0 equiv) was added, followed by the addition of 500 μL of freshly distilled THF-*d₈* (NaK). The tube was shaken and placed into a −78 °C dry-ice acetone bath followed by the addition of the freshly prepared 4-trifluoromethylboronic acid solution (30 μL, 30 μmol, 2.0 eqiuv). The tube was vortexed (not shaken), quickly wiped with a Kimwipe and placed into the probe of the NMR spectrometer pre-cooled to −50 °C. After a few minutes the sample was cooled to −100 °C and complex **97** was observed. The signals were not well separated in the ¹H NMR spectrum.

Data for **97**:

¹⁹F NMR: (565 MHz, THF-*d₈*)

    −60.81 (s, FC(10)), −61.45 (s, 2 FC(1)),
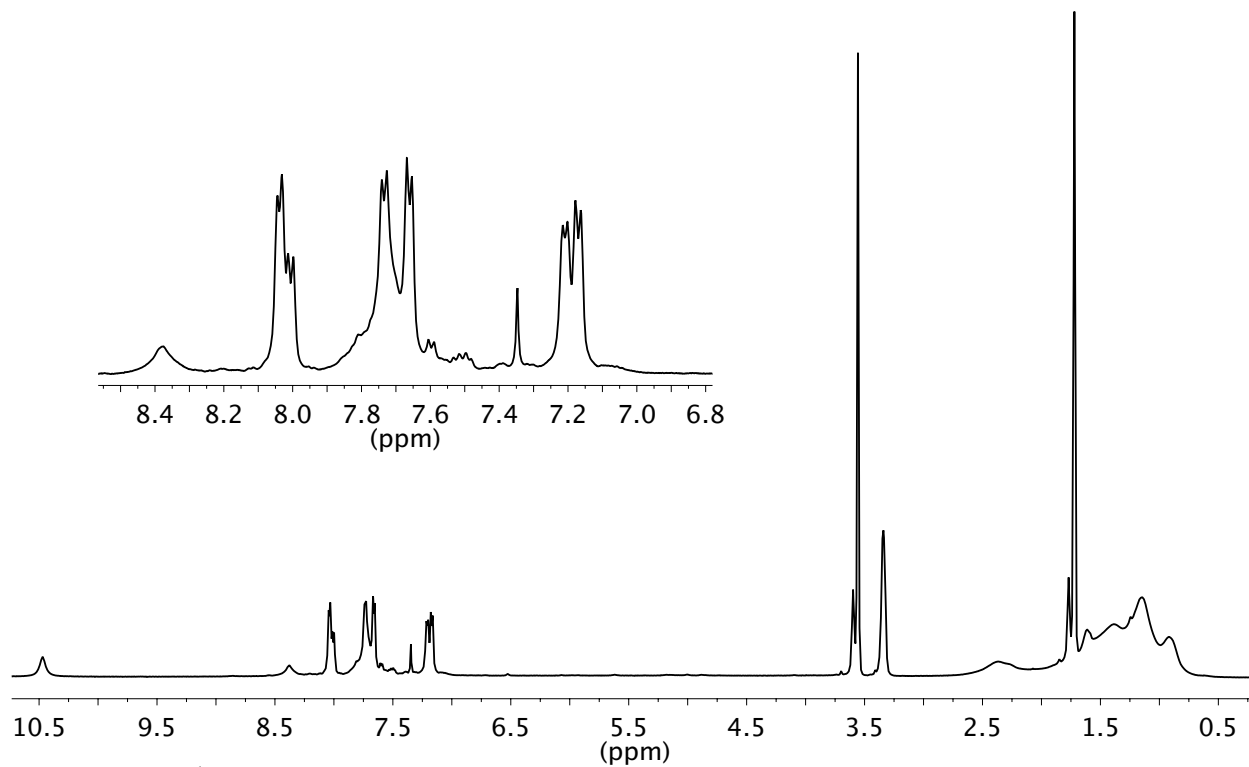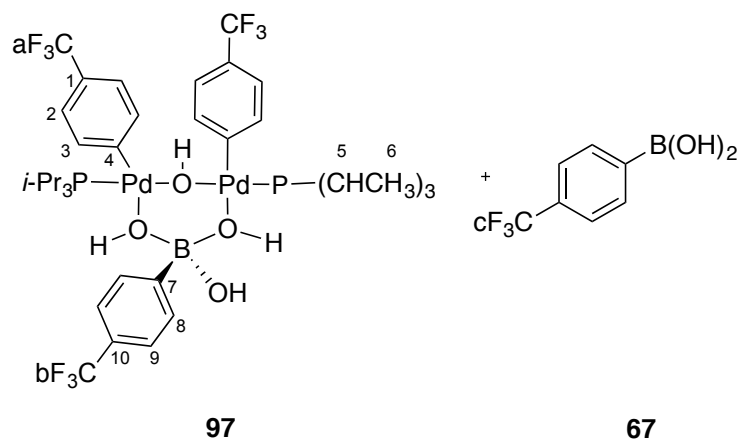
Figure 157. ^{1}H NMR spectrum of **97** and **65** at −100 °C, referenced externally to 1,4-difluorobenzene (−120.00 ppm).
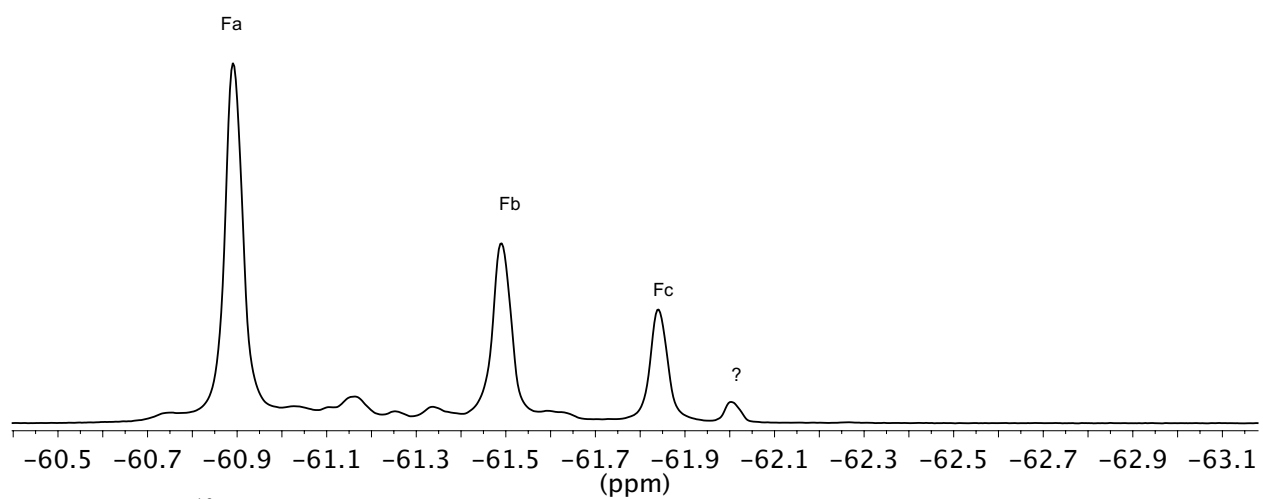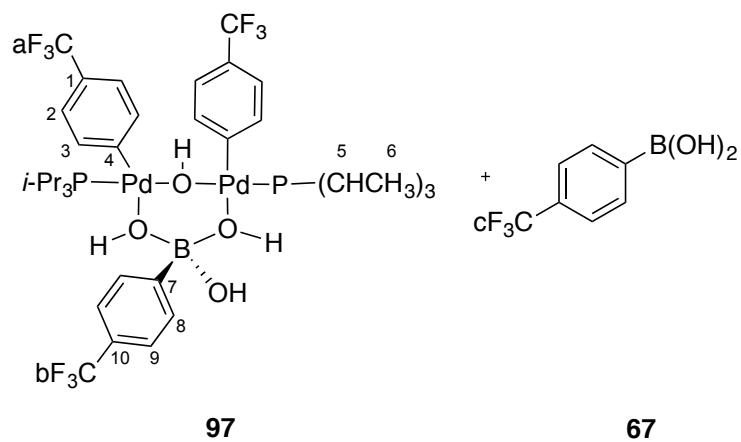
Figure 158. ^{19}F NMR spectrum of **97** and **67** at −100 °C, referenced externally to 1,4-difluorobenzene (−120.00 ppm).

Experiment 26: Preparation of *i*-Pr$_3$P complex 80 with 2.0 equiv of 66.

80   **98**   **66**
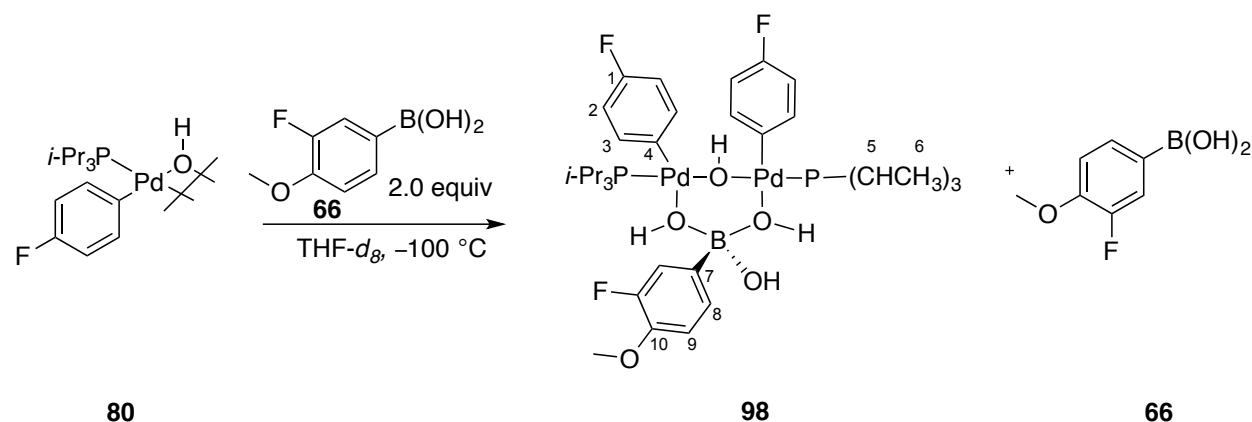
A dram vial was charged with 4-methyoxy-3-fluorophenylboroxine (4.56 mg, 10 µmol, 1.0 equiv) followed by H$_2$O (0.5 µL, 30 µmol, 3.0 equiv). Then 100 µL of THF-*d*$_8$ was added followed by sonication until the solid had dissolved.

An oven-dried, 5-mm, NMR tube was taken into the glove box and [(*i*-Pr$_3$P)Pd(4-MeC$_6$H$_4$)(µ-OH)]$_2$ (11.5 mg, 15 µmol, 1.0 equiv) was added, followed by the addition of 500 µL of freshly distilled THF-*d*$_8$ (NaK). The tube was shaken and placed into a −78 °C dry-ice acetone bath followed by the addition of the freshly prepared 4-fluorophenyllboronic acid solution (100 µL, 30 µmol, 2.0 eqiuv). The tube was vortexed (not shaken), quickly wiped with a Kimwipe and placed into the probe of the NMR spectrometer pre-cooled to −50 °C. After a few minutes the sample was cooled to −100 °C and complex **98** was observed. The signals were not well separated in the ^{1}H NMR spectrum.

Data for **94**:

^{19}F NMR: (565 MHz, THF-*d*$_8$)

−140.29 (s, FC(10)), −124.1 (s, 2 FC(1)),
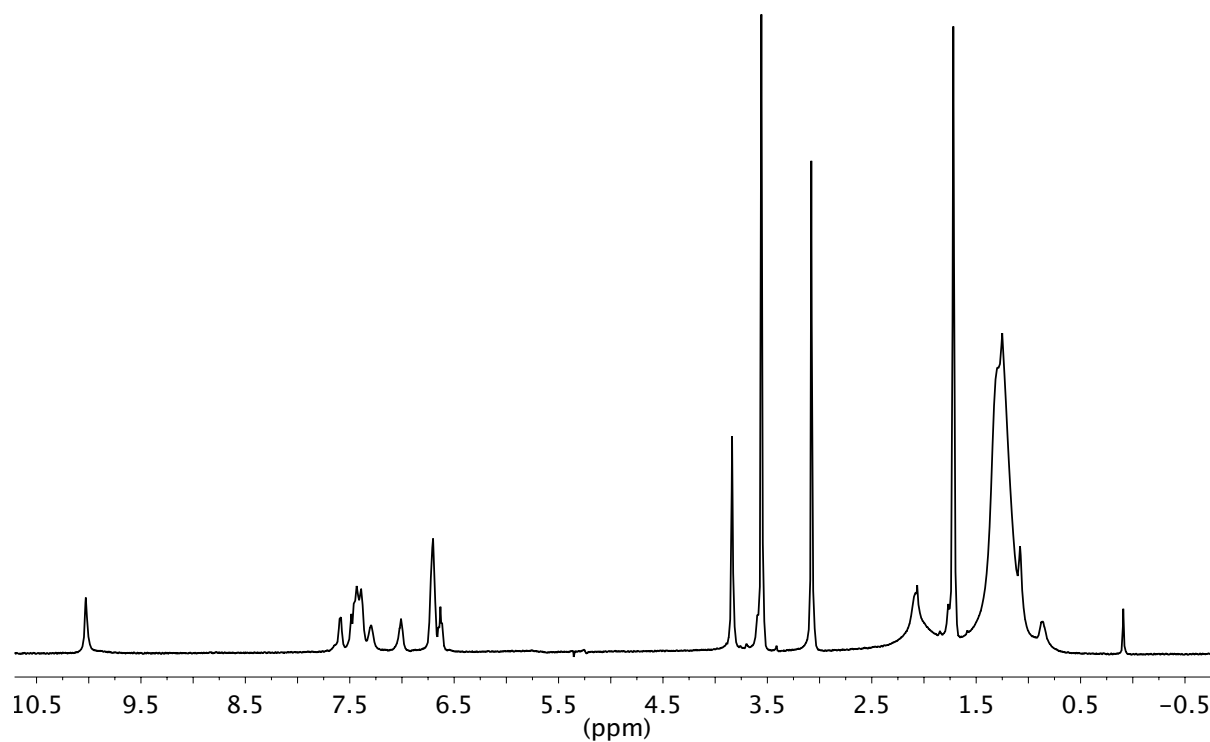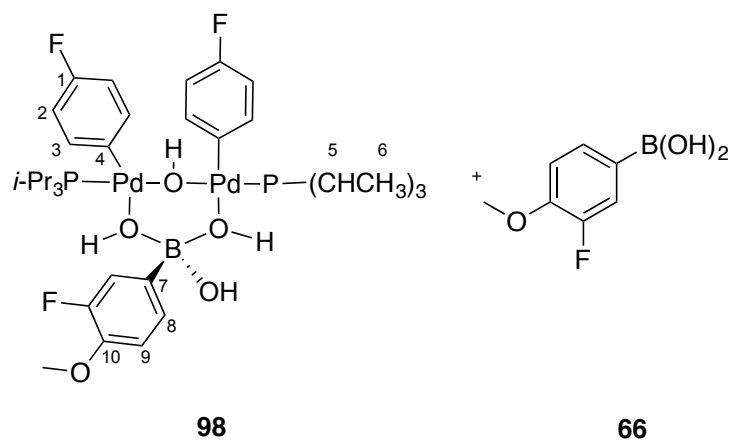
Figure 159. ^{1}H NMR spectrum of **96** and **58** at −100 °C, referenced to THF-d_8 (−120.00 ppm).

229

98

66

Figure 160. ^{19}F NMR spectrum of **98** and **66** at −100 °C, referenced externally to 1,4-difluorobenzene (−120.00 ppm).

Experiment 27: Preparation of t-Bu₃P complex 104 from 103 with 2.0 equiv of 58.

103   **04**
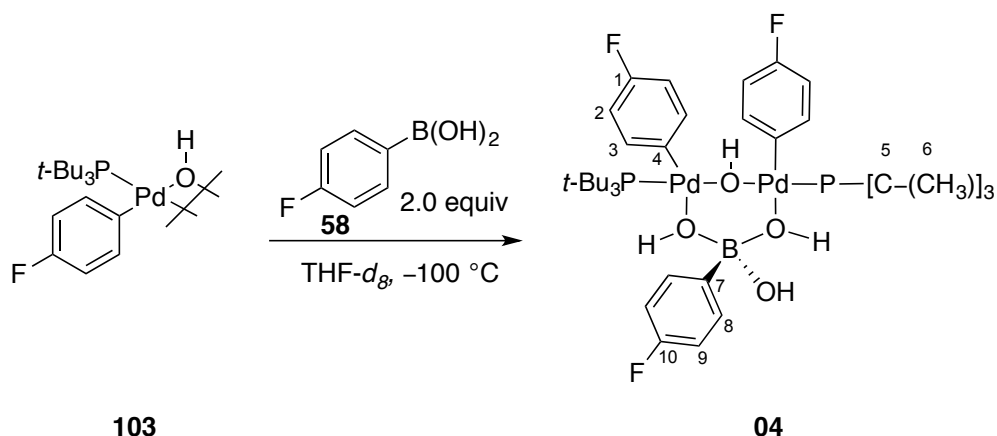
An flame dried vial was charged with 4-fluorophenylboroxine (2.5 mg, 6.8 μmol, 2.0 equiv), H_2O (0.6 μL, 20 μmol, 3.1 equiv) followed by 100 μL of freshly distilled (NaK) THF-d_8 .The tube was capped with a septum and Teflon tapped.

An oven-dried, 5-mm, NMR tube was taken into the glove box and [(t-Bu₃P)Pd(4-FC₆H₄)(μ-OH)]₂ (6.8 mg, 8.2 μmol, 1.0 equiv) was added, followed by the addition of 500 μL of freshly distilled THF-d_8 (NaK). The tube was shaken and placed into a −78 °C dry-ice acetone bath followed by the addition of the freshly prepared 4-fluorophenylboronic acid solution. The tube was vortexed (not shaken) quickly wiped with a Kimwipe and placed into the probe of the NMR spectrometer pre-cooled to −60 °C. After a few minutes the sample was cooled to −100 °C where the complex was observed.

Using the Eyring equation $\Delta G_e^{\neq} = -RT_c \ln(k_c \hbar / k_B T_c)$ where R is the gas constant, k_B is Boltzmann constant, $\hbar$ is Planck's constant, the barrier to rotation about the Pd-Aryl bond was measured to be approximately $\Delta G_r^{\neq} = 10$ kcal/mol. The coalescence temperature (T_c) was measured approximately at –75 °C by the signals broadening and separating over a 10 °C difference. The rate constant k_c at coalescence was measured using $k_c = \pi \Delta v / \sqrt{2}$, where Δv is the maximum chemical shift difference (101 Hz) between H_a and $H_{a'}$ at −100 °C.

Data for **104**:

¹H NMR: (600 MHz, THF-d_8)

9.51 (s, HO), 7.84 (m, 2 HC(8)), 7.46, 7.28 (m, 4 HC(3)), 7.13 (dd, 8 Hz, 2 HC(9)), 6.76 (m, 4 CH(2)), 1.32 (br, 54 HC(6))

Figure 161. ^{1}H NMR spectrum of **104** at −100 °C, referenced to THF-d_8 (1.72 ppm).
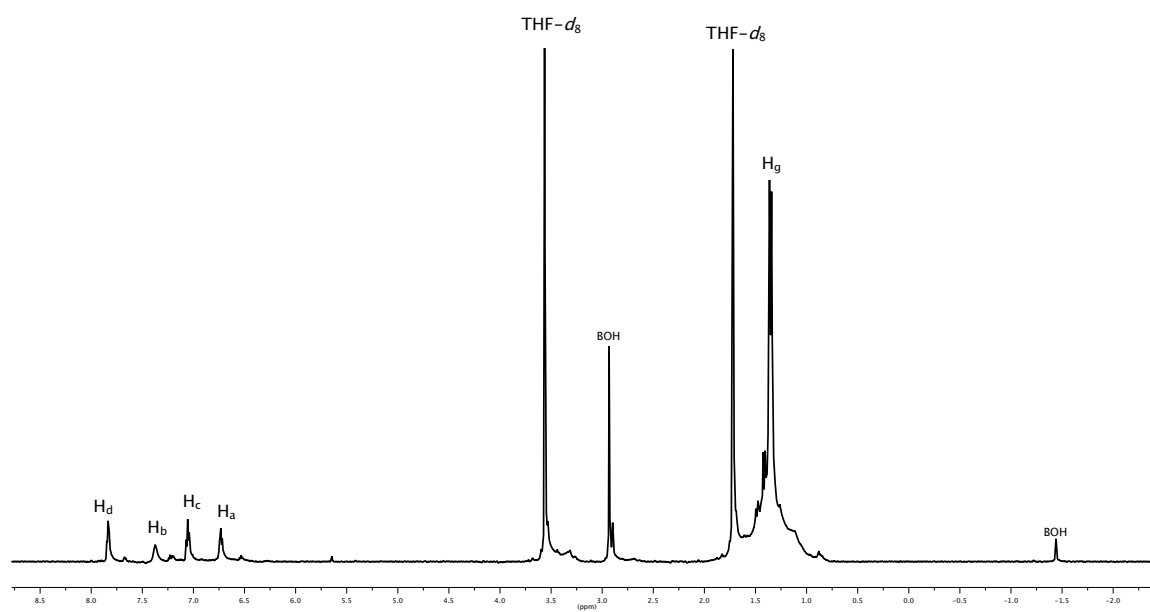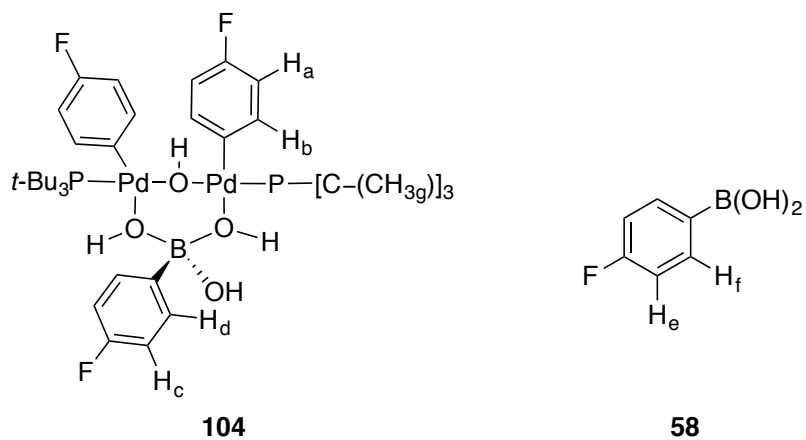
Figure 162. ^{1}H NMR spectrum of **104** at −60 °C, referenced to THF-d_8 (1.72 ppm).

233
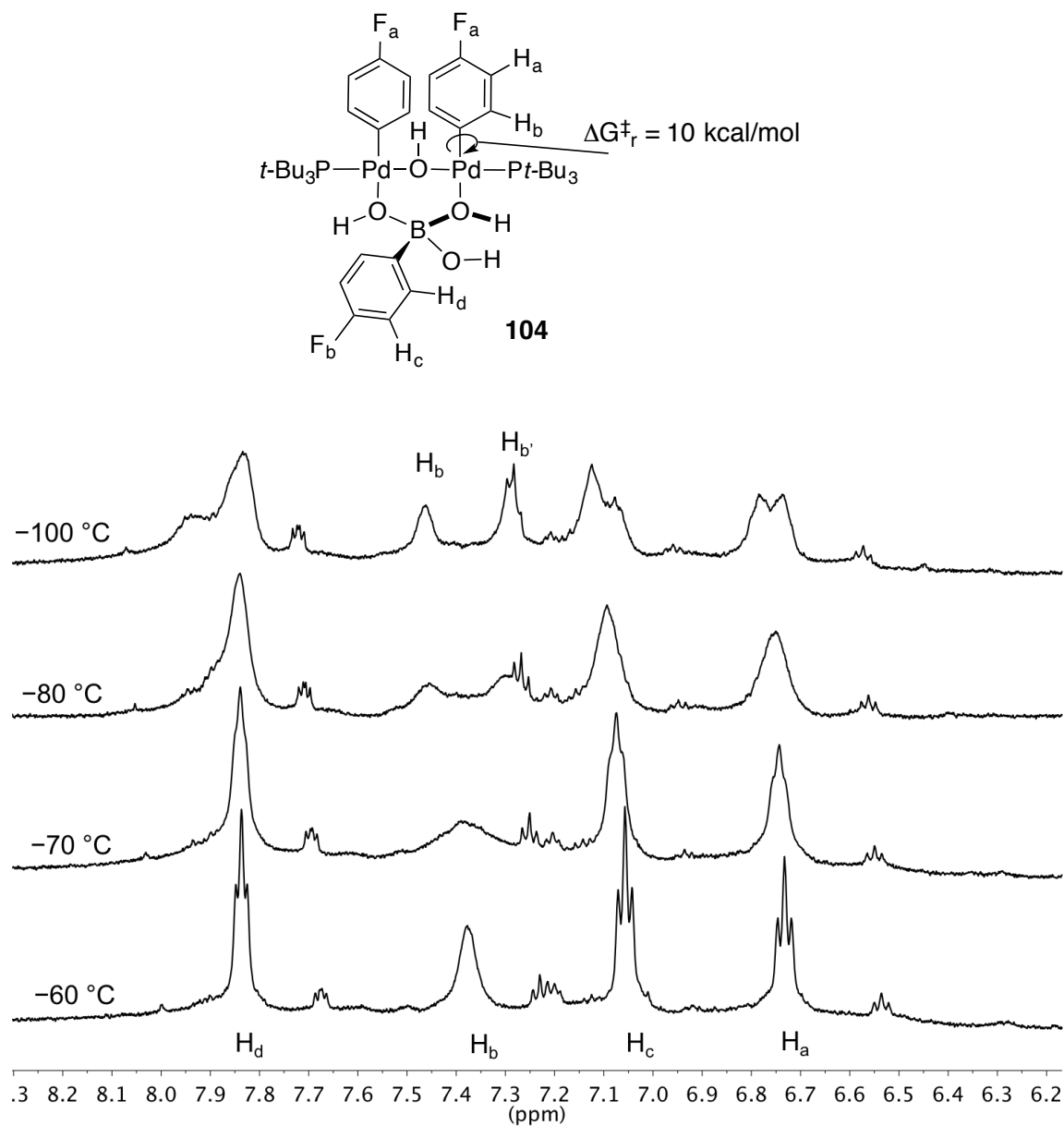
Figure 163. ^{1}H NMR spectrum of **104** over a range of temperatures, referenced to THF-d_8 (1.72 ppm).

Experiment 28: RI-NMR addition of CH₃OH to complex 105.
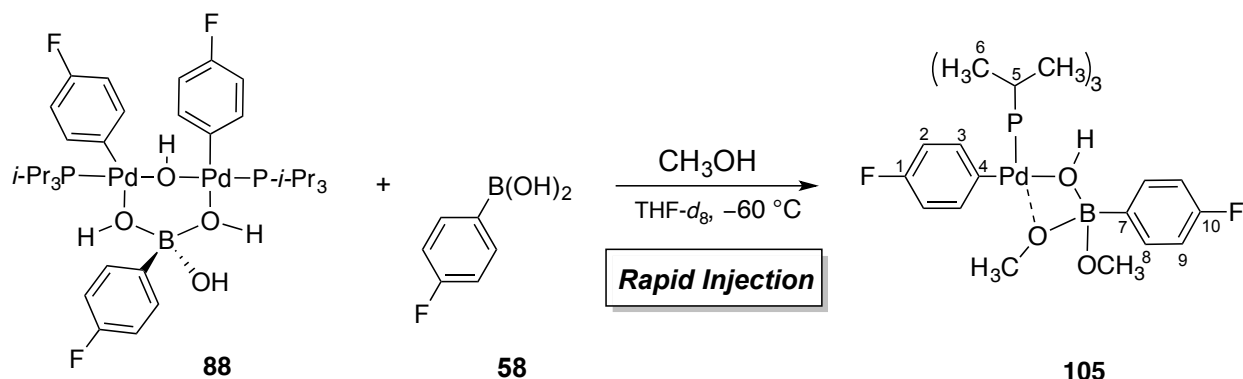
An oven-dried, 5-mm, NMR tube was charged with 4-fluorophenylboroxine (63.1 mg, 172 μmol, 1.0 equiv) and H_2O (9.5, 172 μmol, 3.1 equiv) followed by the addition of 750 μL of THF-d_8 yielding a 4-fluorophenylboronic acid solution (0.69 M).

An oven dried, 5-mm, NMR tube as charged with [(i-Pr₃P)Pd(4-FC₆H₄)(μ-OH)]₂ (7.58 mg, 10 μmol, 1.0 equiv) and THF-d_8 (500 μL) then sonicated for ~2 min. The tube was placed into a −78 °C dry-ice acetone bath followed by the addition of 4-fluorophenylboronic acid solution (29 μL, 20 μmol, 2.0 equiv). The tube was vortexed (not shaken) quickly wiped with a Kimwipe and placed into the probe of the NMR spectrometer pre-cooled to −60 °C with the cap off. The sample was warmed to −50 °C for ~10 min followed by cooling to −60 °C. Then CH₃OH (30 μL, 741 μmol, 37 equiv) was injected at a rate of 10 μL per sec. The injector was used to mix the sample followed by data collection. The formation of complex **105** was monitored by ¹H NMR by collecting a spectrum every 6 min.
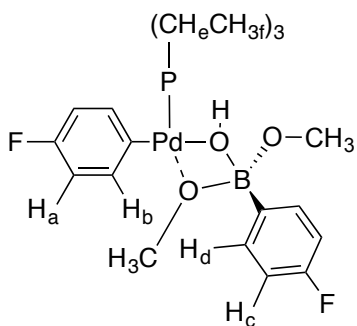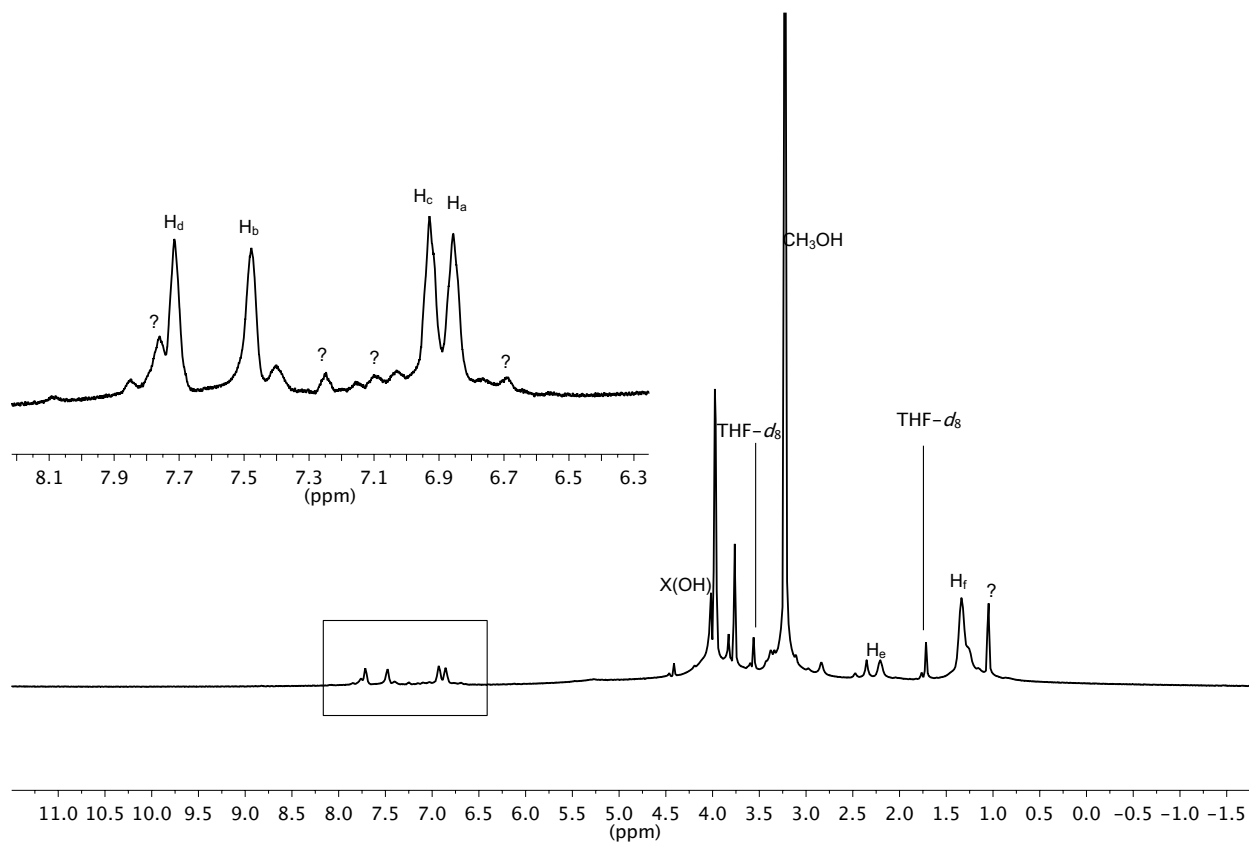
Figure 164. ^{1}H NMR spectrum of **105** at −60 °C, referenced to THF-d_8 (1.72 ppm).
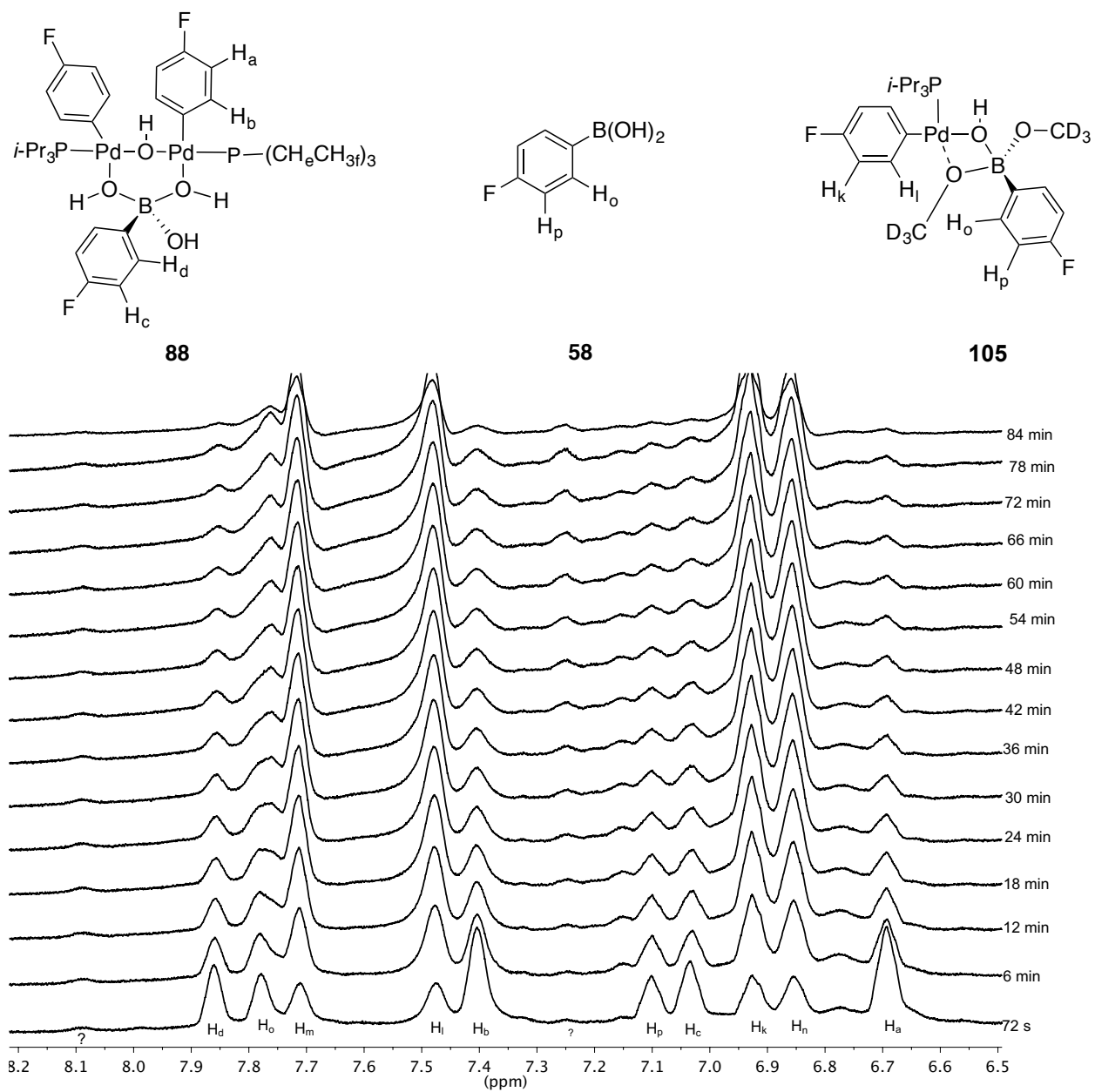
Figure 165. ^{1}H NMR spectra (RI-NMR) of **105** at −60 °C, referenced to THF-d_8 (1.72 ppm).

237

Experiment 29: Addition of CD$_3$OD to *i*-Pr$_3$P complex 105.
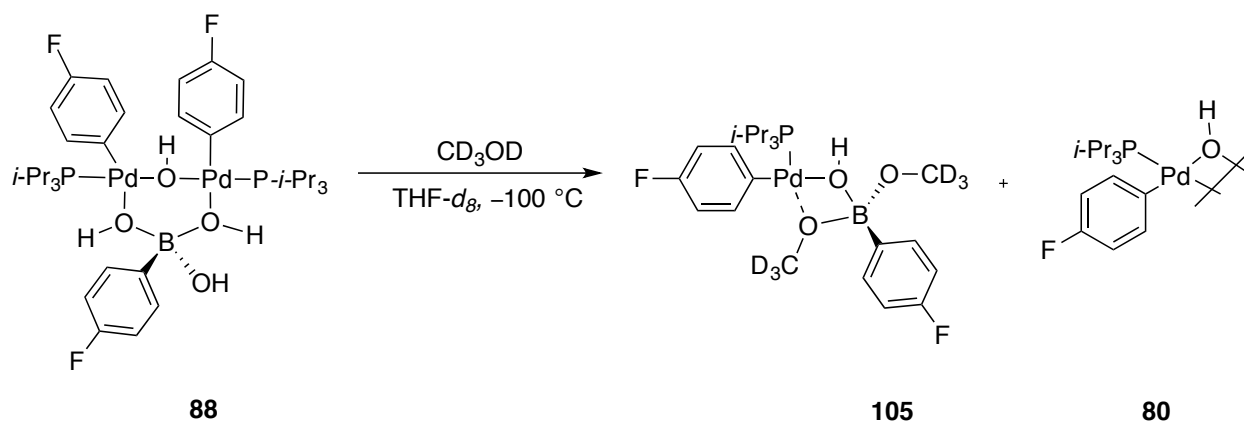
The sample from Experiment 8 was removed from the spectrometer and placed into a −78 °C dry-ice acetone bath followed by the addition of 100 μL of CD$_3$OD. The tube was vortexed (not shaken), quickly wiped with a Kimwipe, and placed into the probe of the NMR spectrometer pre-cooled to −60 °C. After cooling the NMR spectrometer to −100 °C, a new complex **105** was observed and [(*i*-Pr$_3$P)Pd(4-FC$_6$H$_4$)(μ-OH)]$_2$ **80** in a ratio of 1 : 0.5. The complex was observed *via* 1D NMR.
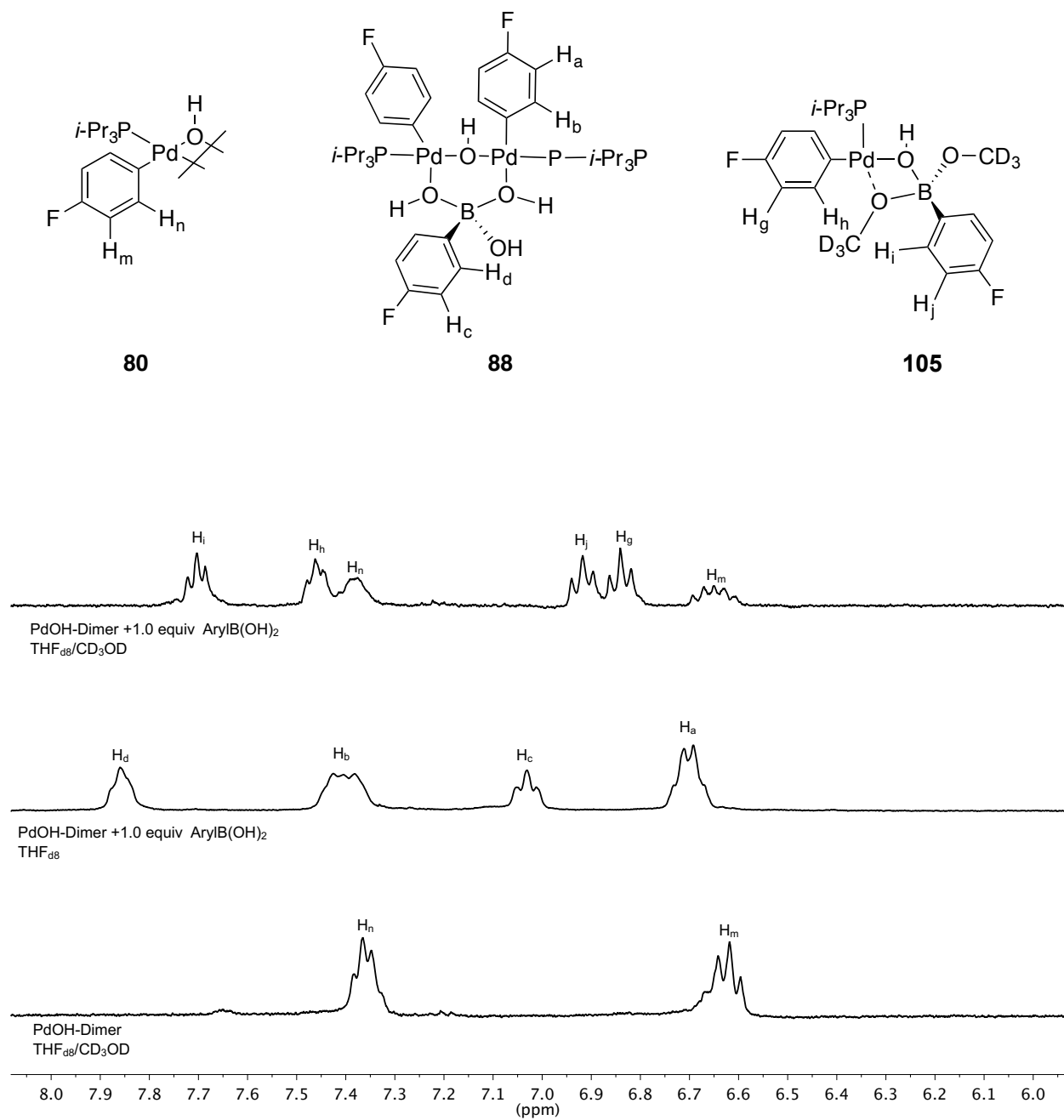
Figure 166. ^{1}H NMR spectra at -100 °C, referenced to THF-d_8 (1.72 ppm).

Experiment 30: Preparation of 8-B-4 complex 105 in THF/CD$_3$OH/D from 88 and 58.
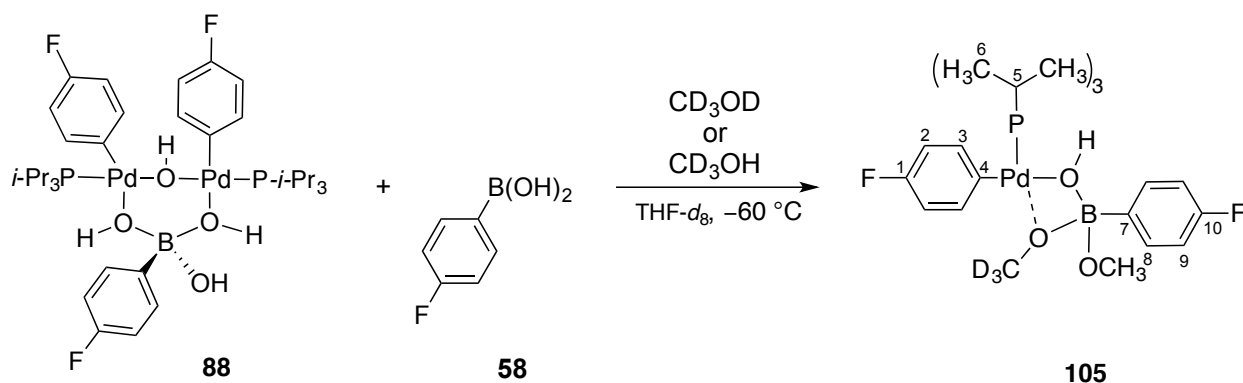
An oven-dried, 5-mm, NMR tube was charged with 4-fluorophenylboroxine (44 mg, 120 µmol, 1.0 equiv) and H$_2$O (6.5 µL, 172 µmol, 3.1 equiv) followed by the addition of 500 µL of THF-d_8 yielding a 4-fluorophenylboronic acid solution (0.72 M).

An oven dried, 5-mm, NMR tube as charged with [(i-Pr$_3$P)Pd(4-FC$_6$H$_4$)(µ-OH)]$_2$ (7.58 mg, 10 µmol, 1.0 equiv) and 500 THF-d_8 followed by sonication for ~2 min. The tube was placed into a −78 °C dry-ice acetone bath followed by the addition of 4-fluorophenylboronic acid solution (28 µL, 20 µmol, 2.0 equiv). The tube was vortexed (not shaken) quickly cleaned with a Kimwipe and placed into the −78 °C bath. Then CD$_3$OD (60 µL, 1.48 mmol, 74 equiv) was added *via* syringe. The tube was vortexed (not shaken) quickly wiped with a Kimwipe and placed into the probe of the NMR spectrometer pre-cooled to −60 °C. The sample was found to be stable for ~8 h at −60 °C. The complex was characterized *via* 1D and 2D NMR experiments over a course of multiple experiments using either CD$_3$OH or CD$_3$OD.

Data for **105**:

^{1}H NMR: (600 MHz, THF-d_8)

7.68 (m, 2 HC(8)), 7.45 (m, 2 HC(3)), 6.95 (m, 2 HC(9)), 6.85 (m, 2 CH(2)), 4.48 (broad, HO), 2.20 (m, 6 HC(5)), 1.32 (m, 36 HC(6))

^{13}C NMR: (151 MHz, THF-d_8)

164.44, 162.85 (d, ^1J(F-C) = 241 Hz, 1 C(10)), 163.42, 161.83 (d, ^1J(F-C) = 240 Hz, 1 C(1)), 143.38 (m, 1 C(4)), 139.56 (m, 1 C(7)), 137.17 (m, 2 C(3)), 135.91 (m, 2 C(8)) , 115.97, 115.84 (d, ^2J(F-C) = 20 Hz, 2 C(9), 114.85, 114.71 (d, ^2J(F-C) = 18 Hz, 2 C(2)), 25.71 (UD, 3 C(5)), 20.18 (s, 6 C(6))

<u>^{19}F NMR:</u>   (565 MHz, THF-d_8)

−118.33 (s, FC(10)), −121.01 (s, FC(1)),

<u>^{31}P NMR:</u>   (243 MHz, THF-d_8)

51.00 (s, 1 P(Pd))

<u>^{11}B NMR:</u>   (129 MHz, THF-d_8)

9 ppm (br, 1 B(O))
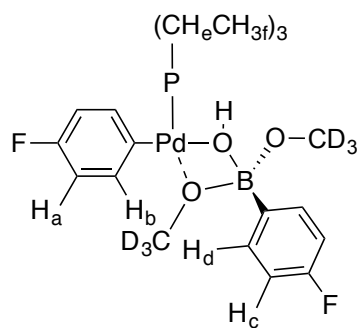
105
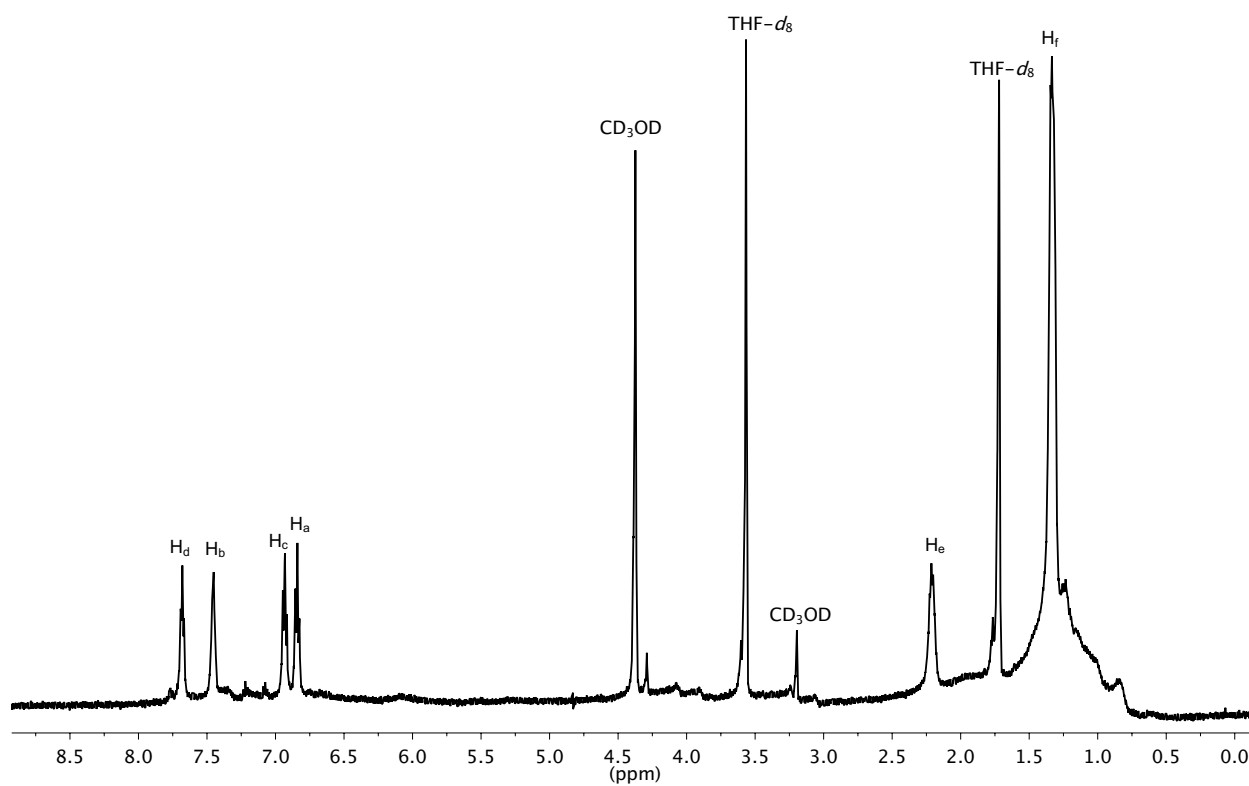
Figure 167. ^{1}H NMR spectrum of **105** at −60 °C, referenced to THF-d_8 (1.72 ppm).
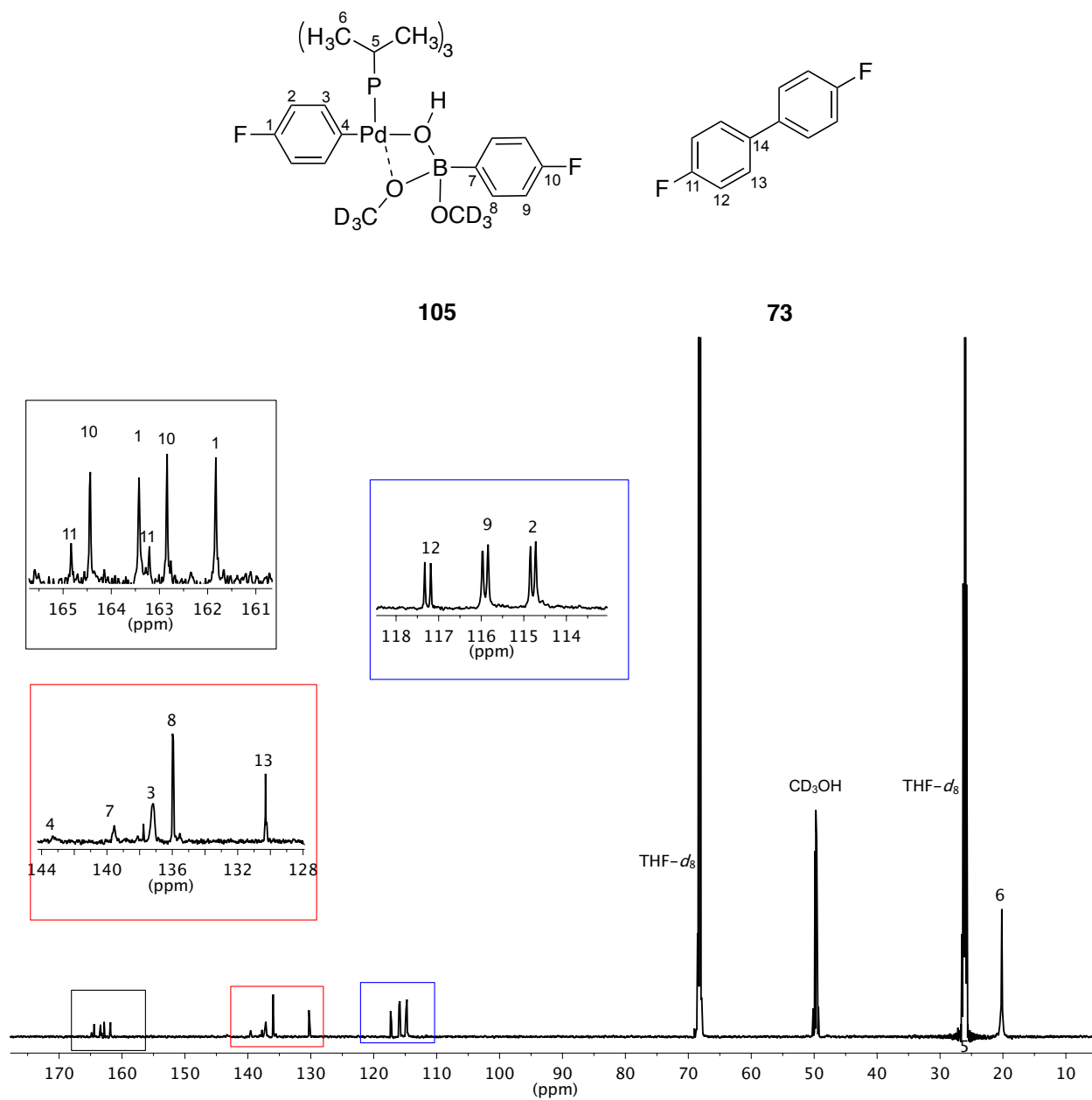
Figure 168. ¹³C NMR spectrum of **105** at −60 °C, referenced to THF-d_8 (68.21 ppm).
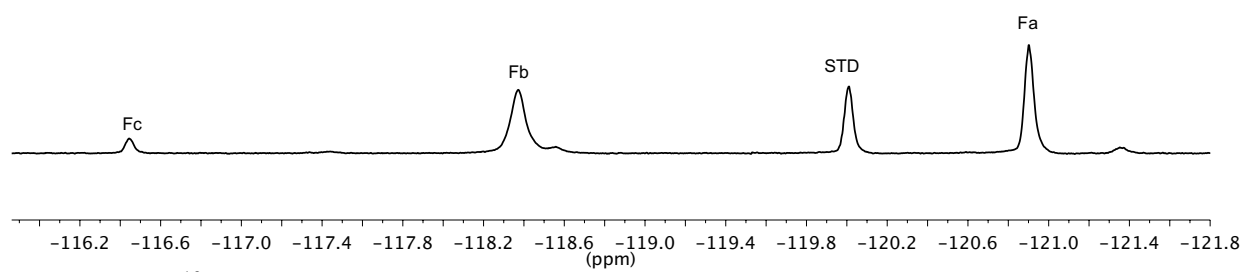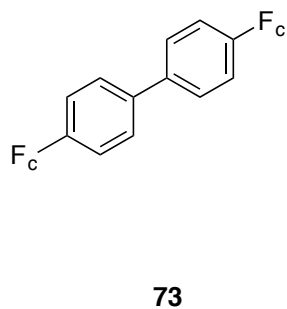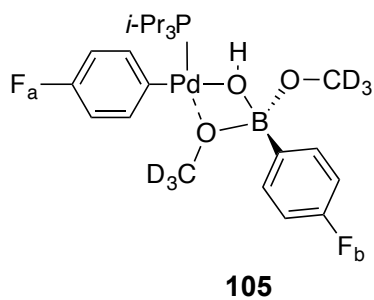
Figure 169. ^{19}F NMR spectrum of **105** at −60 °C, referenced to 1,4-difluorobenzene (−120.00 ppm).

244
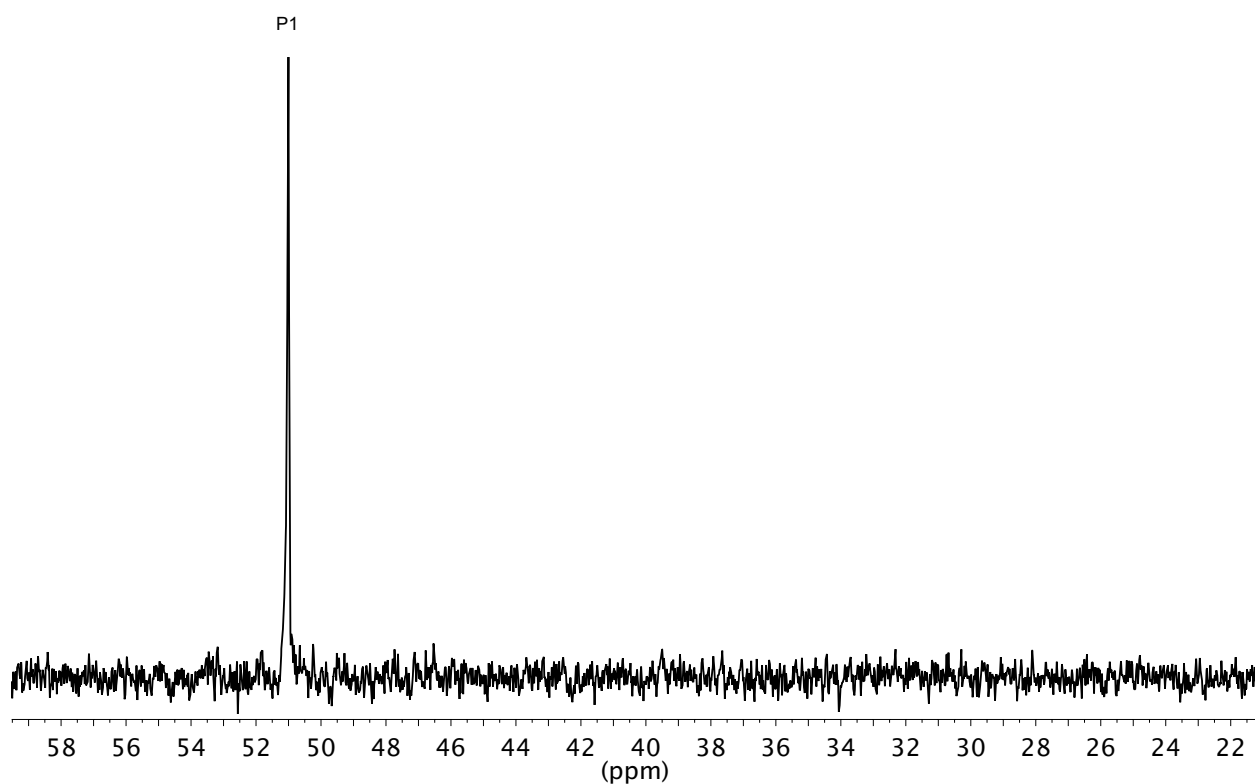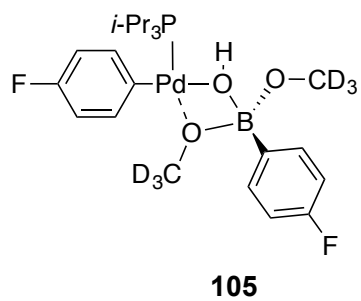
Figure 170. ^{31}P NMR spectrum of **105** at −60 °C, externally referenced to *i*-Pr$_3$P (19.00 ppm).
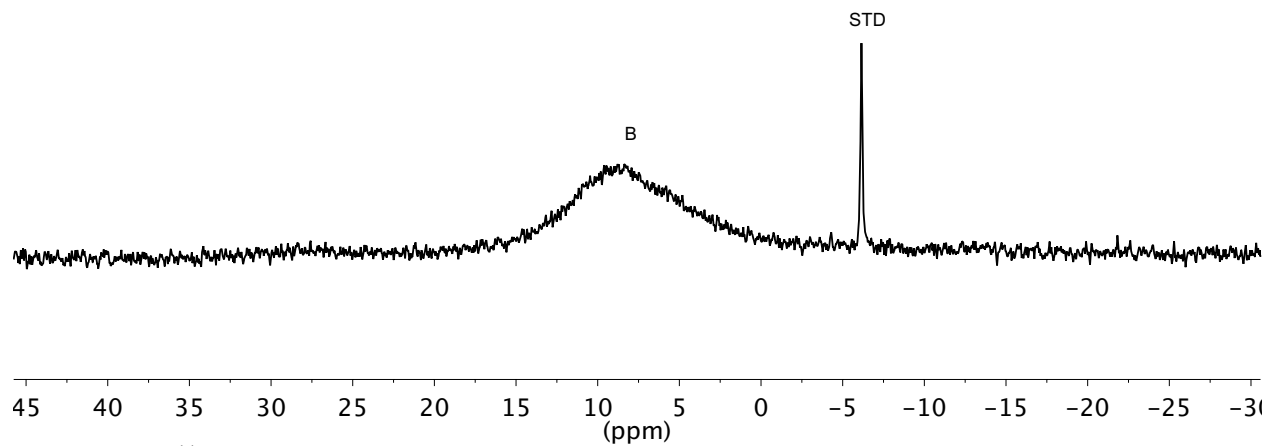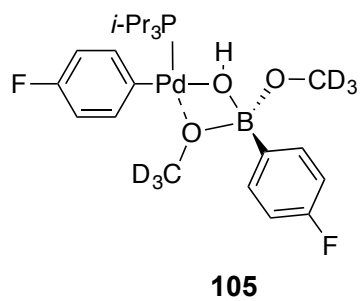
Figure 171. ^{11}B NMR spectrum of **105** at −60 °C, referenced to Ph$_4$BNa (−6.14 ppm).
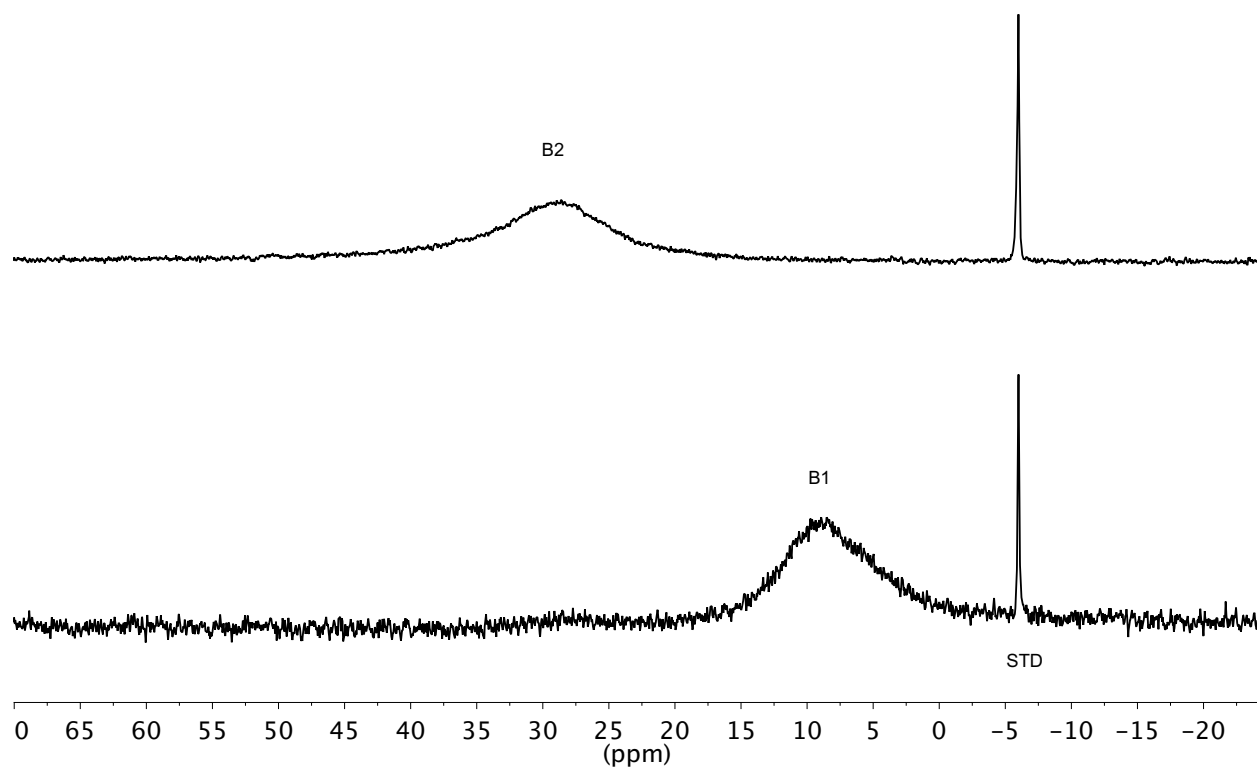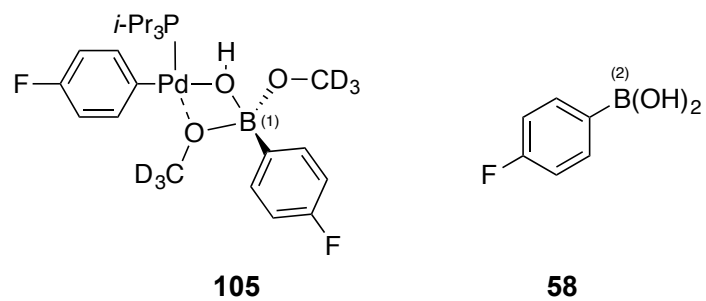
Figure 172. ^{11}B NMR spectra of **58** (top) and **105** (bottom) at −60 °C, referenced to Ph$_4$BNa (−6.14 ppm).
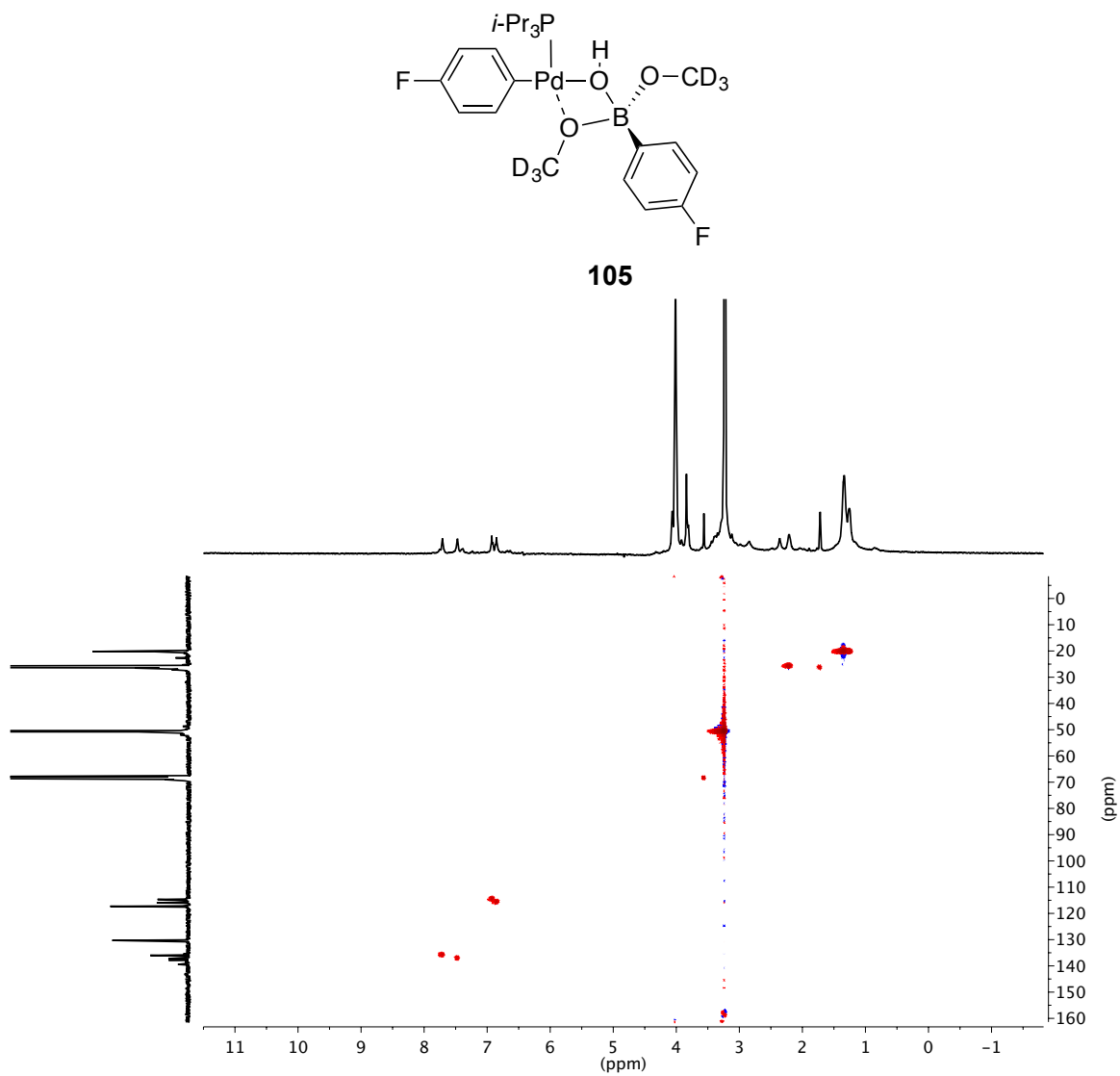
Figure 173. gHSQC spectrum of **105** at −60 °C, referenced to THF-d_8 (1.72 and 68.21 ppm).
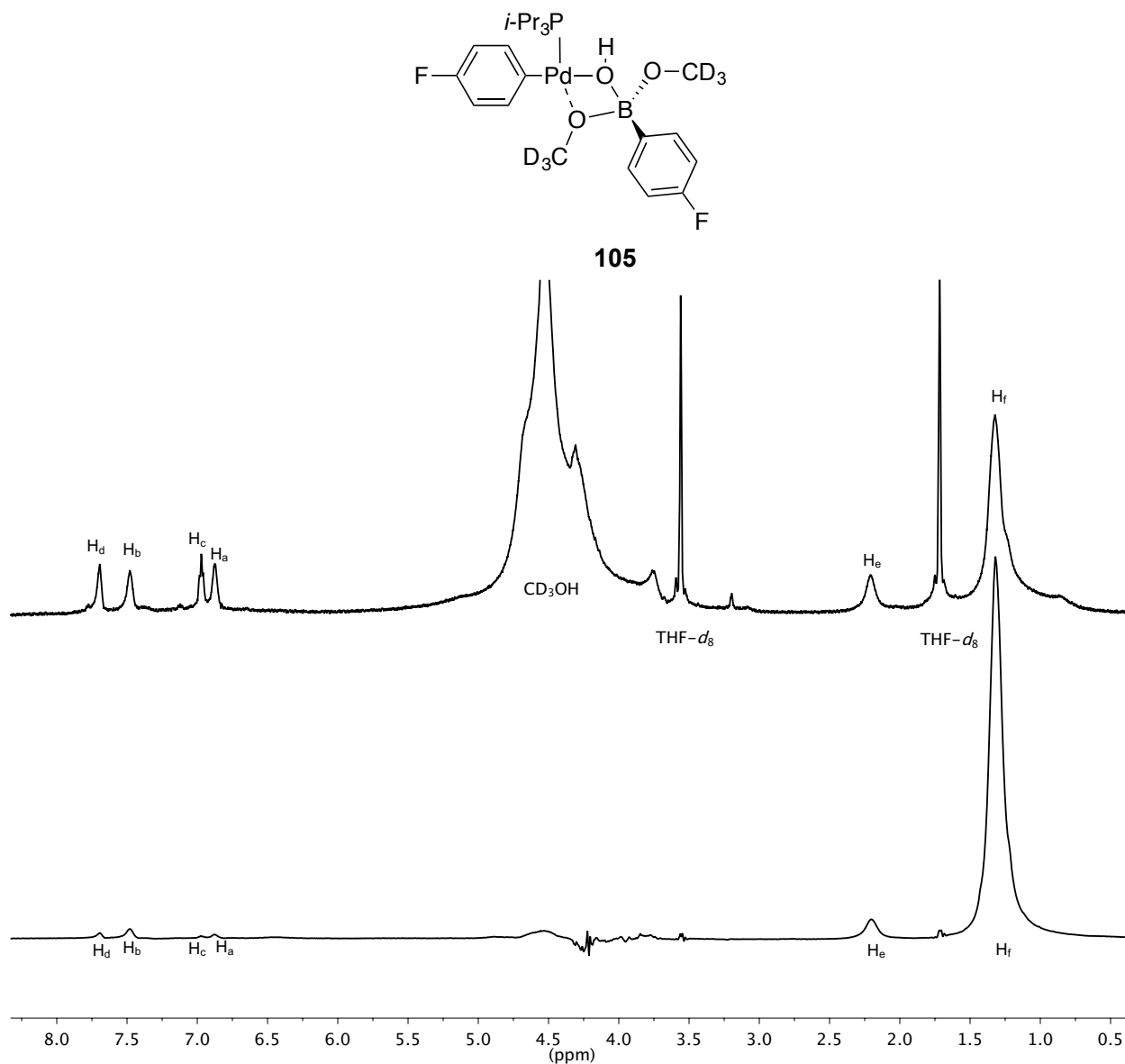
Figure 174. 1D-Phase cycled NOE spectrum at −90 °C (CH$_3$ irradiated at 1.32) (bottom) and ^{1}H NMR spectrum (top) at −90 °C, referenced to THF-d_8 (1.72 ppm).
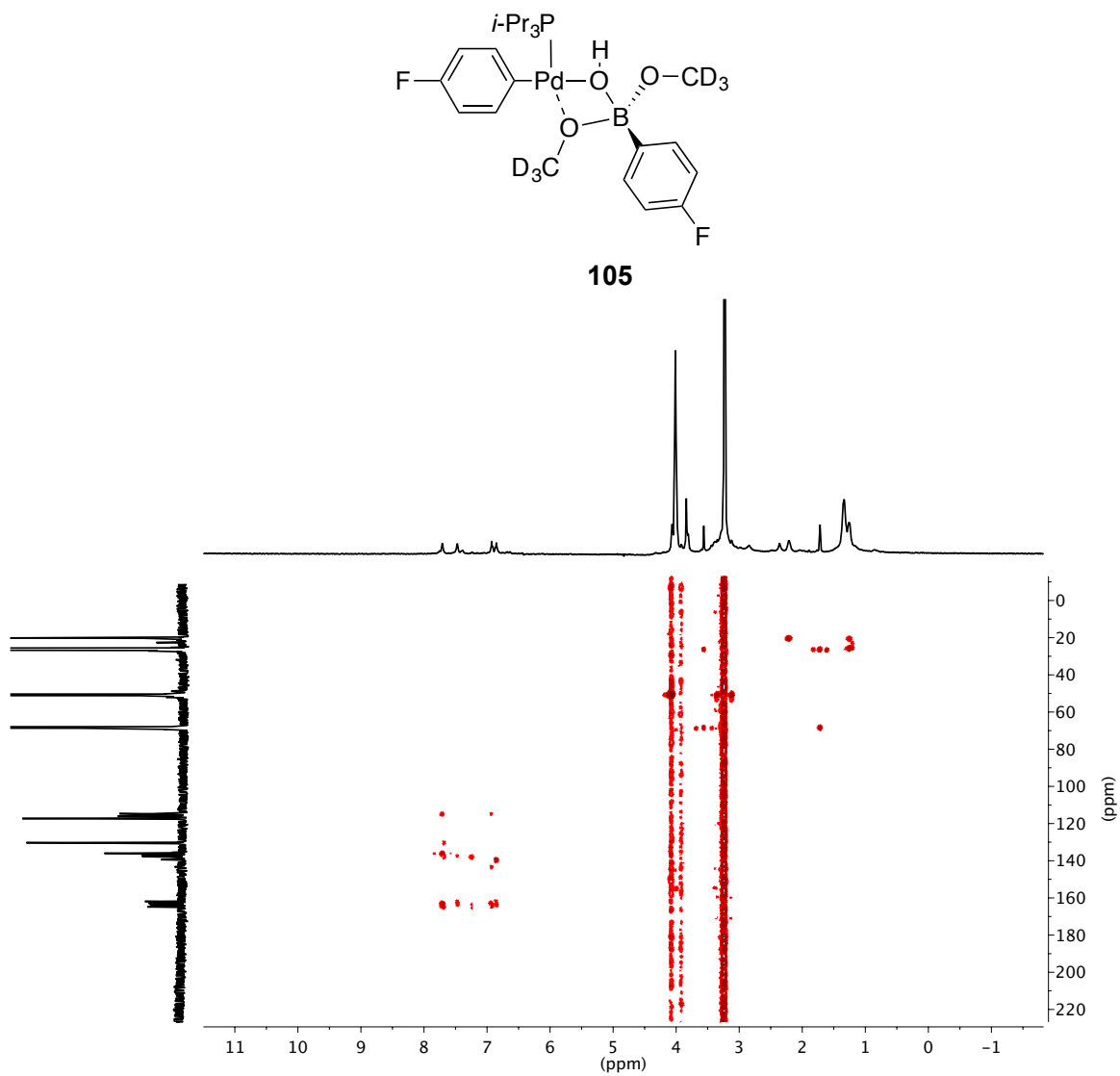
Figure 175. gHMBC spectrum of **105** at −60 °C, referenced to THF-d_8 (1.72 and 68.21 ppm).

Experiment 31: Preparation of 8-B-4 complex 105 in THF/CD₃OD from 80 and 106.

80   **105**
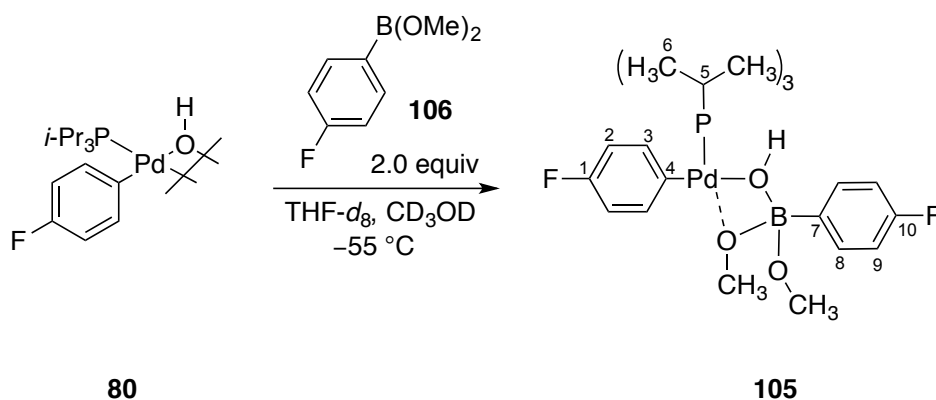
An oven-dried, 5-mm, NMR tube was charged with dimethyl 4-fluorophenylboronate (60.5 mg, 360 μmol, 1.0 equiv) followed by the addition of 500 μL of THF-d_8 yielding a dimethyl 4-fluorophenylboronate solution (0.72 M).

An oven dried, 5-mm, NMR tube as charged with [(*i*-Pr₃P)Pd(4-FC₆H₄)(μ-OH)]₂ (7.58 mg, 10 μmol, 1.0 equiv) and 500 THF-d_8 followed by sonication for ~2 min. The tube was placed into a −78 °C dry-ice acetone bath followed by the addition of dimethyl 4-fluorophenylboronate solution (28 μL, 20 μmol, 2.0 equiv). The tube was vortexed (not shaken) quickly cleaned with a Kimwipe and placed into the −78 °C bath. Then CD₃OD (60 μL, 1.48 mmol, 74 equiv) was added *via* syringe. The tube was vortexed (not shaken) quickly wiped with a Kimwipe and placed into the probe of the NMR spectrometer pre-cooled to −55 °C. The complex was characterized *via* 1D and 2D NMR experiments over a course of multiple experiments using either CD₃OH or CD₃OD. The solvents were dried and checked by Karl Fisher titration. Either THF-d_8 or THF were distilled over (NaK) and placed over 3 Å molecular sieves, which was found to contain 10 ug/mL of H₂O. Either CH₃OH or CD₃OD was placed over 3 Å molecular sieves for 3 days, which led to 12 μg/mL of H₂O.

Data for **105**:

<u>¹H NMR:</u>   (600 MHz, THF-d_8)

7.70 (m, 2 HC(8)), 7.46 (m, 2 HC(3)), 6.92 (m, 2 HC(9)), 6.84 (m, 2 CH(2)), 2.21 (m, 6 HC(5)), 1.34 (m, 36 HC(6))

<u>¹³C NMR:</u>   (151 MHz, THF-d_8)

164.45, 162.85 (d, ^1J(F-C) = 241 Hz, 1 C(10)), 163.47, 161.87 (d, ^1J(F-C) = 240 Hz, 1 C(1)), 139.17 (m, 1 C(7)), 137.81 (m, 2 C(3)), 135.95 (m, 2 C(8)), 115.94,

115.81 (d, ^2J(F-C) = 18 Hz, 2 C(9)), 114.79, 114.67 (d, ^2J(F-C) = 18 Hz, 2 C(2)), 25.71 (UD, 3 C(5)), 20.19 (s, 6 C(6))
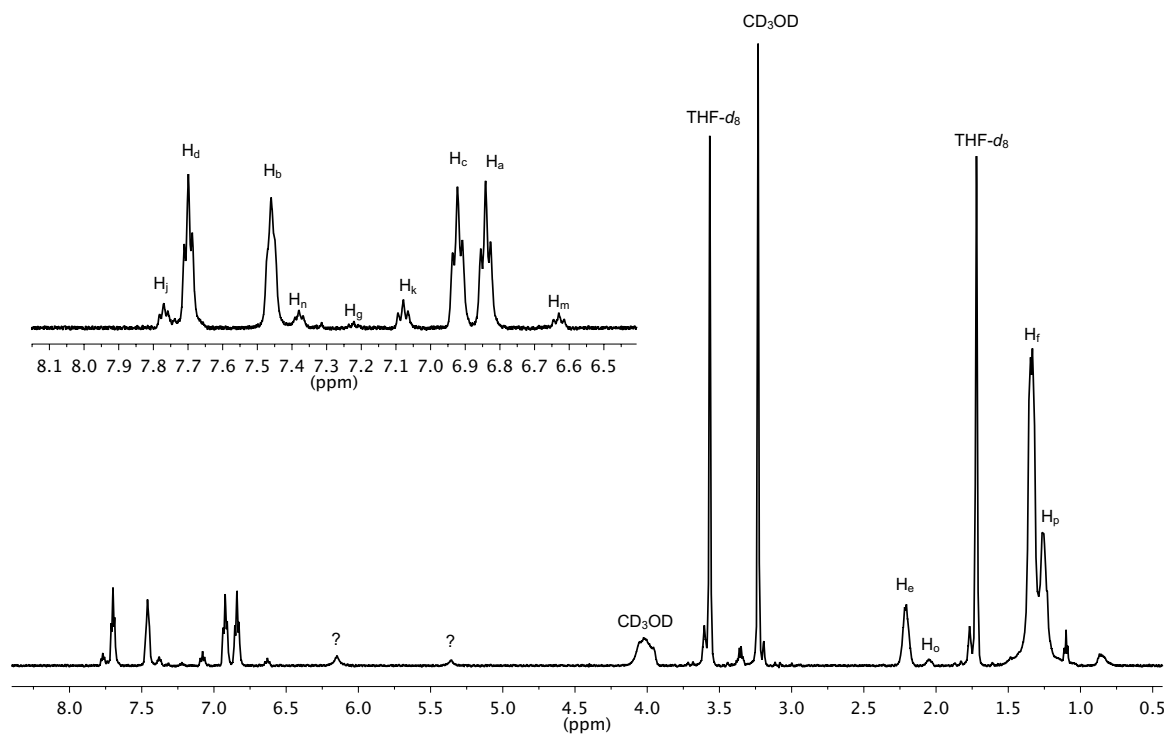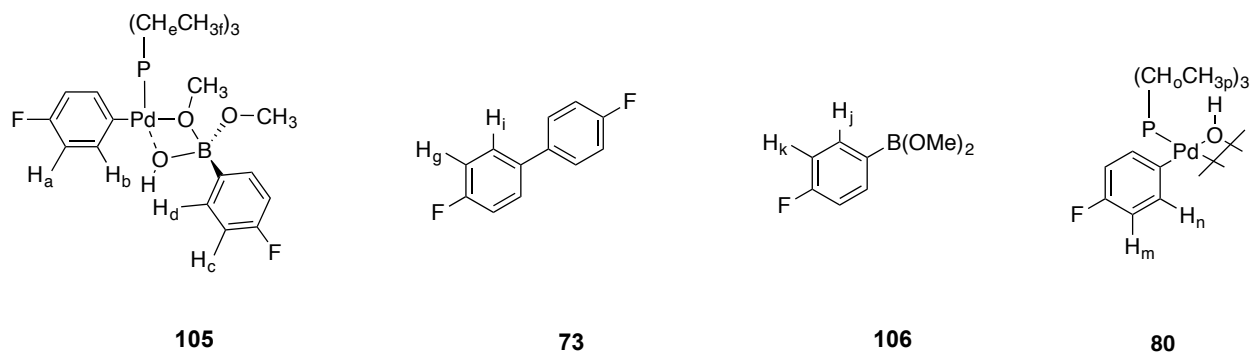
Figure 176. ^{1}H NMR spectrum of **105** at −55 °C, referenced to THF-d_8 (1.72 ppm).

253
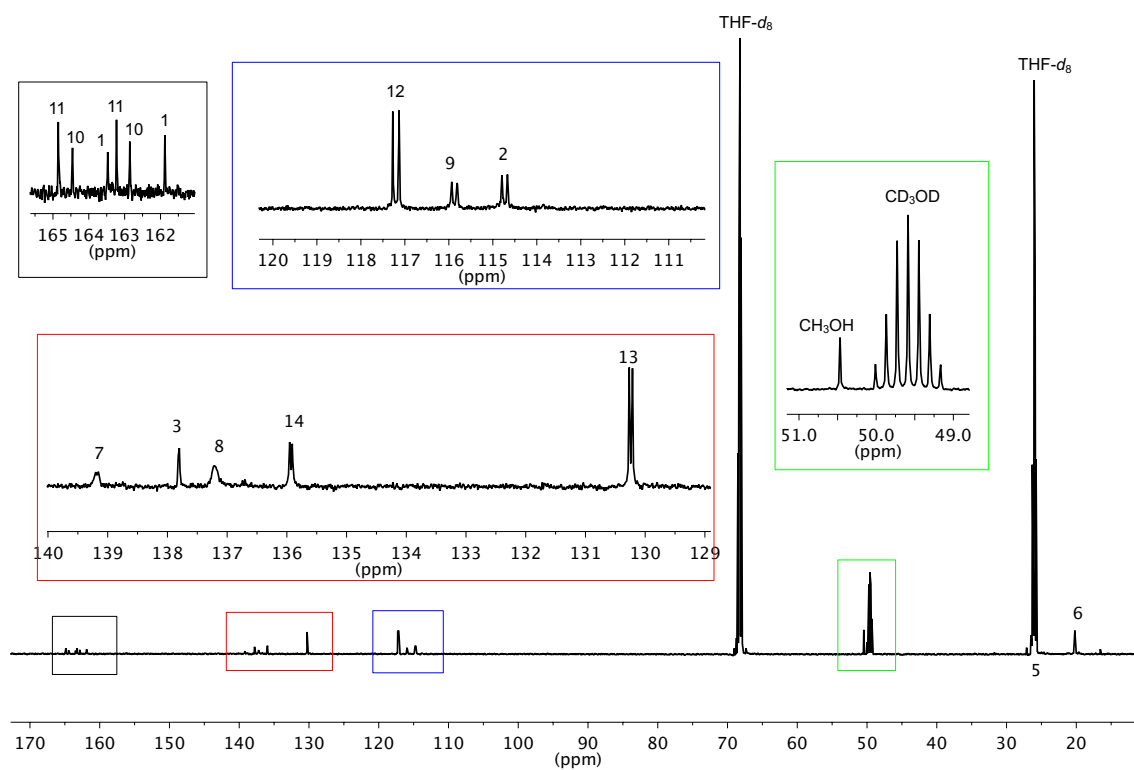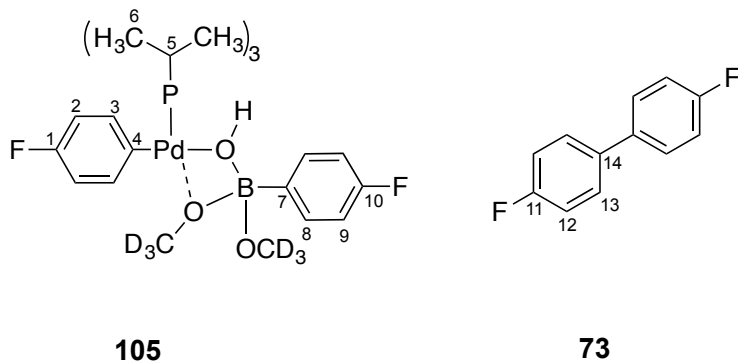
Figure 177. ^{13}C NMR spectrum of **105** at −55°C, referenced to THF-d_8 (68.21 ppm).
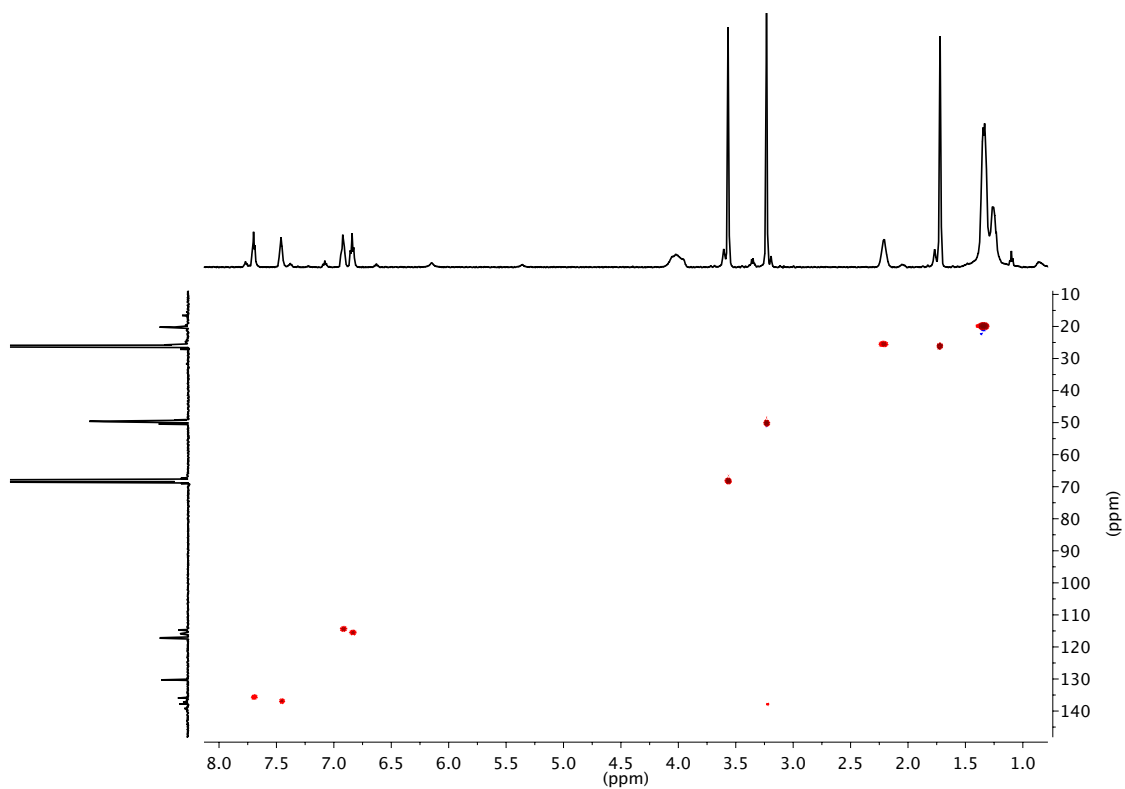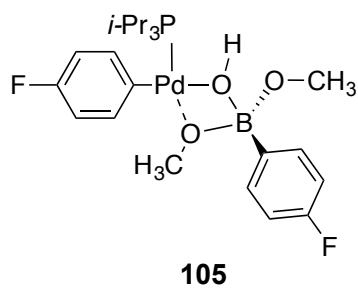
Figure 178. gHSQC spectrum of **105** at −55°C, referenced to THF-d_8 (1.72 and 68.21 ppm).

Experiment 32: Preparation of Ph₃P 8-B-4 complex 107 from 57 and 58

57 **107**

A 1-mL volumetric flask was charged with 4-fluorophenylboroxine (88 mg, 240 μmol) followed by H₂O (13 μL, 722 μmol, 3.0 equiv). Then ~0.5 mL of THF-d_8 was added followed by sonication until the solid had dissolved. Once dissolved the flask was filled to the mark with THF-d_8 yielding a 4-fluorophenylboronic acid solution (0.72 M).

An oven dried, 5-mm, NMR tube as charged with [(Ph₃P)Pd(4-FC₆H₄)(μ-OH)]₂ (9.60 mg, 10 μmol, 1.0 equiv) and 500 THF-d_8 followed by sonication for ~2 min. The tube was placed into a −78 °C dry-ice acetone bath followed by the addition of 4-fluorophenylboronic acid solution (28 μL, 20 μmol, 2.0 equiv). The tube was vortexed (not shaken) quickly cleaned with a Kimwipe and placed into the −78 °C bath. Then CD₃OD (60 μL, 1.48 mmol, 74 equiv) was added *via* syringe. The tube was vortexed (not shaken) quickly wiped with a Kimwipe and placed into the probe of the NMR spectrometer pre-cooled to −55 °C. The sample was found to form cross-coupling product over ~2 h at −55 °C. The complex was characterized *via* 1D and 2D NMR experiments over a course of multiple experiments using CD₃OD.

Data for **107**:

¹H NMR: (600 MHz, THF-d_8)

7.76 (m, 2 HC(10)), 7.53 (m, 3 HC(8)), 7.51 (m, 6 HC(6)), 7.45 (m, 6 CH(7)), 7.05 (m, 2 CH(3)), 6.99 (m, 2 CH(11)), 6.60 (m, 2 CH(2)) 4.14 (broad, HO)

¹³C NMR: (151 MHz, THF-d_8)

164.57, 162.95 (d, ^1J(F-C) = 243 Hz, 1 C(12)), 163.49, 161.91 (d, ^1J(F-C) = 242 Hz, 1 C(1)), 140.93 (m, 1 C(4)), 136.54 (m, 2 C(3)), 135.97 (m, 2 C(10)), 135.84, 135.76 (d, ^2J(P-C) = 12 Hz, 6 C(6)), 133.14 (m, 3 C(8)), 130.58, 130.50 (d, ^3J(P-C) = 7 Hz, 6 C(7)), 116.11, 116.00 (d, ^2J(F-C) = 17 Hz, 2 C(2), 114.91, 114.79 (d,

256

Experiment 32: Preparation of Ph₃P 8-B-4 complex 107 from 57 and 58

57 **107**

A 1-mL volumetric flask was charged with 4-fluorophenylboroxine (88 mg, 240 μmol) followed by H₂O (13 μL, 722 μmol, 3.0 equiv). Then ~0.5 mL of THF-d_8 was added followed by sonication until the solid had dissolved. Once dissolved the flask was filled to the mark with THF-d_8 yielding a 4-fluorophenylboronic acid solution (0.72 M).

An oven dried, 5-mm, NMR tube as charged with [(Ph₃P)Pd(4-FC₆H₄)(μ-OH)]₂ (9.60 mg, 10 μmol, 1.0 equiv) and 500 THF-d_8 followed by sonication for ~2 min. The tube was placed into a −78 °C dry-ice acetone bath followed by the addition of 4-fluorophenylboronic acid solution (28 μL, 20 μmol, 2.0 equiv). The tube was vortexed (not shaken) quickly cleaned with a Kimwipe and placed into the −78 °C bath. Then CD₃OD (60 μL, 1.48 mmol, 74 equiv) was added *via* syringe. The tube was vortexed (not shaken) quickly wiped with a Kimwipe and placed into the probe of the NMR spectrometer pre-cooled to −55 °C. The sample was found to form cross-coupling product over ~2 h at −55 °C. The complex was characterized *via* 1D and 2D NMR experiments over a course of multiple experiments using CD₃OD.

Data for **107**:

¹H NMR: (600 MHz, THF-d_8)

7.76 (m, 2 HC(10)), 7.53 (m, 3 HC(8)), 7.51 (m, 6 HC(6)), 7.45 (m, 6 CH(7)), 7.05 (m, 2 CH(3)), 6.99 (m, 2 CH(11)), 6.60 (m, 2 CH(2)) 4.14 (broad, HO)

¹³C NMR: (151 MHz, THF-d_8)

164.57, 162.95 (d, ^1J(F-C) = 243 Hz, 1 C(12)), 163.49, 161.91 (d, ^1J(F-C) = 242 Hz, 1 C(1)), 140.93 (m, 1 C(4)), 136.54 (m, 2 C(3)), 135.97 (m, 2 C(10)), 135.84, 135.76 (d, ^2J(P-C) = 12 Hz, 6 C(6)), 133.14 (m, 3 C(8)), 130.58, 130.50 (d, ^3J(P-C) = 7 Hz, 6 C(7)), 116.11, 116.00 (d, ^2J(F-C) = 17 Hz, 2 C(2), 114.91, 114.79 (d,

^2J(F-C) = 17 Hz, 2 C(11)) [Carbons 5 and 9 could not be determined]

<u>^{19}F NMR:</u>   (565 MHz, THF-d_8)

−118.16 (s, FC(10)), −121.09 (s, FC(1)),

<u>^{31}P NMR:</u>   (243 MHz, THF-d_8)

34.86 (s, 1 P(Pd))

<u>^{11}B NMR:</u>   (129 MHz, THF-d_8)

10 ppm (br, 1 B(O))
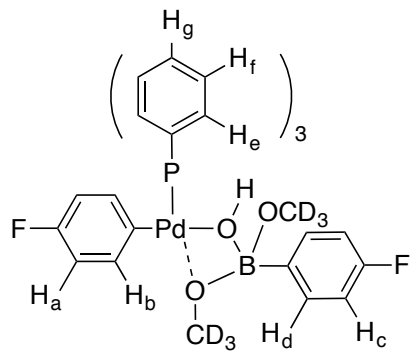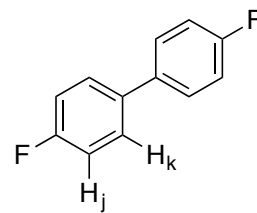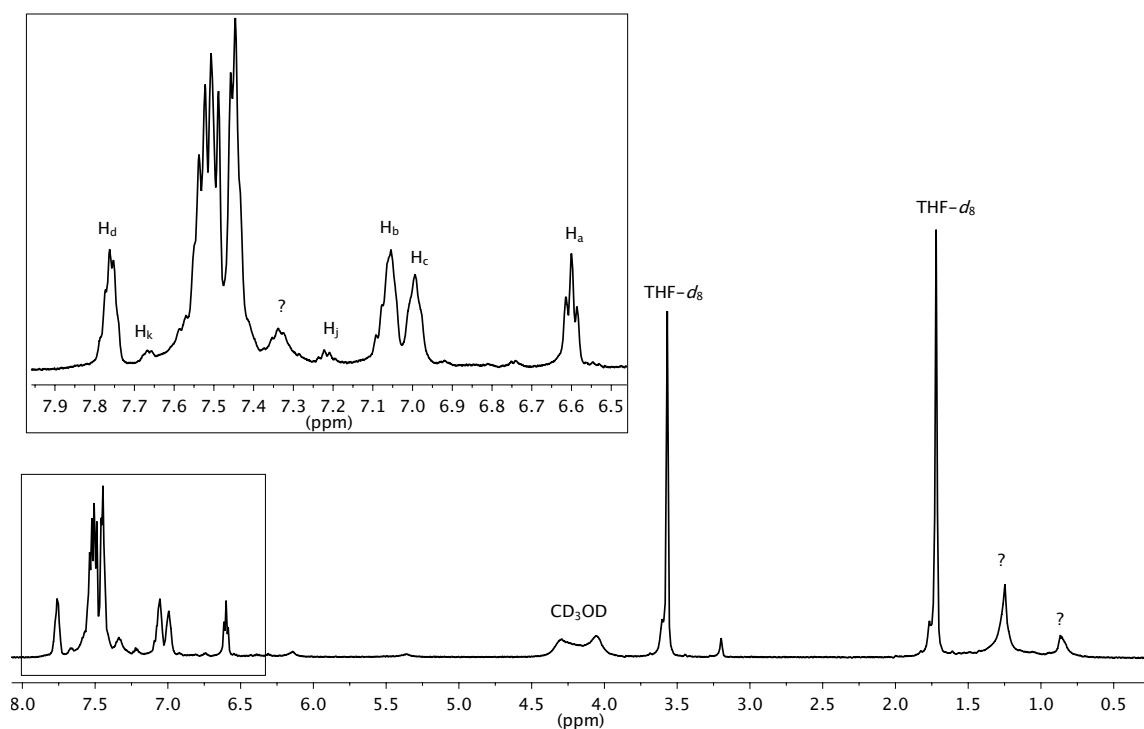
Figure 179. ^{1}H NMR spectrum of **107** at −55 °C, referenced to THF-d_8 (1.72 ppm).
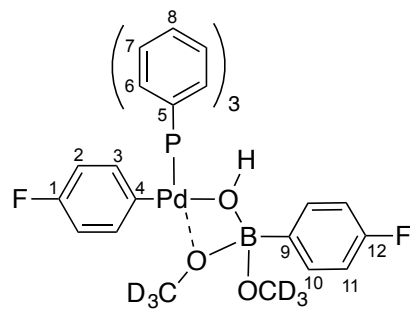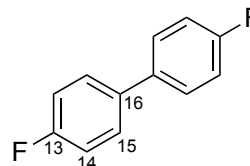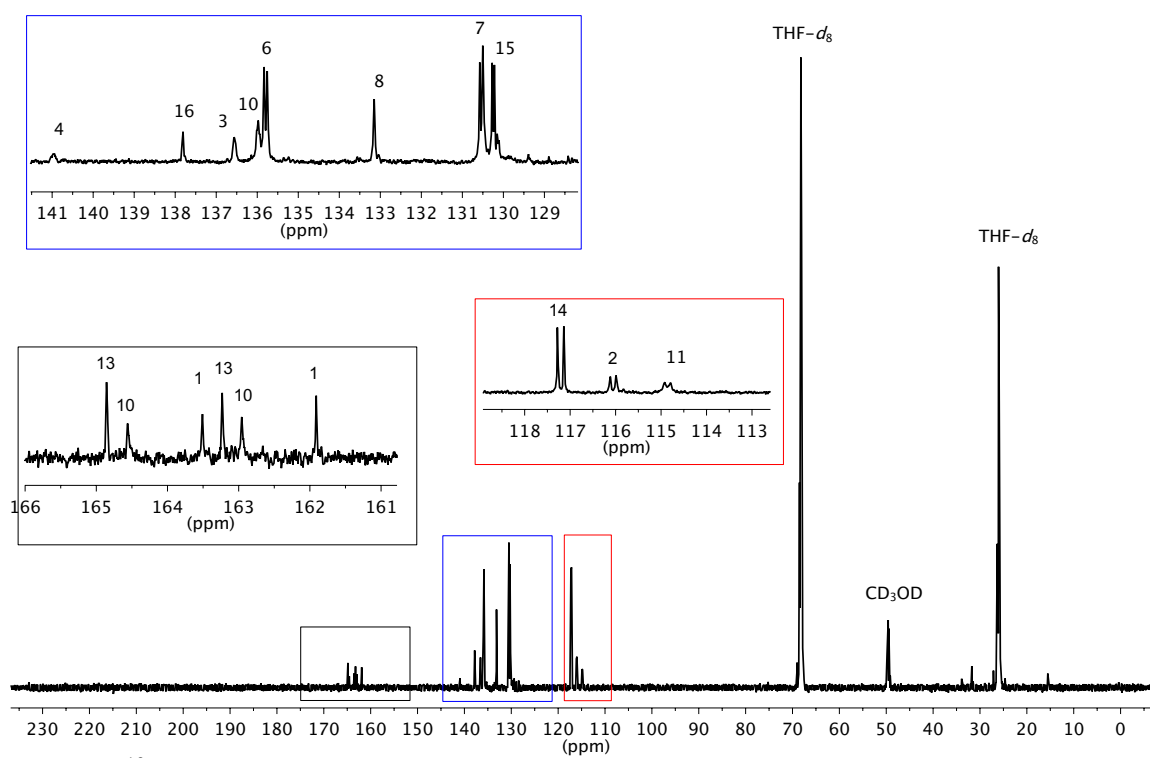
Figure 180. ^{13}C NMR spectrum of **107** at −55 °C, referenced to THF-d_8 (68.21 ppm).
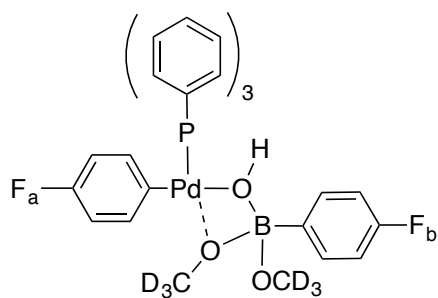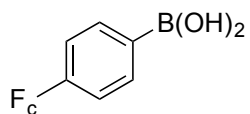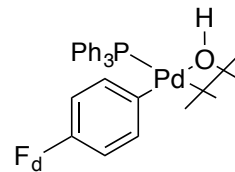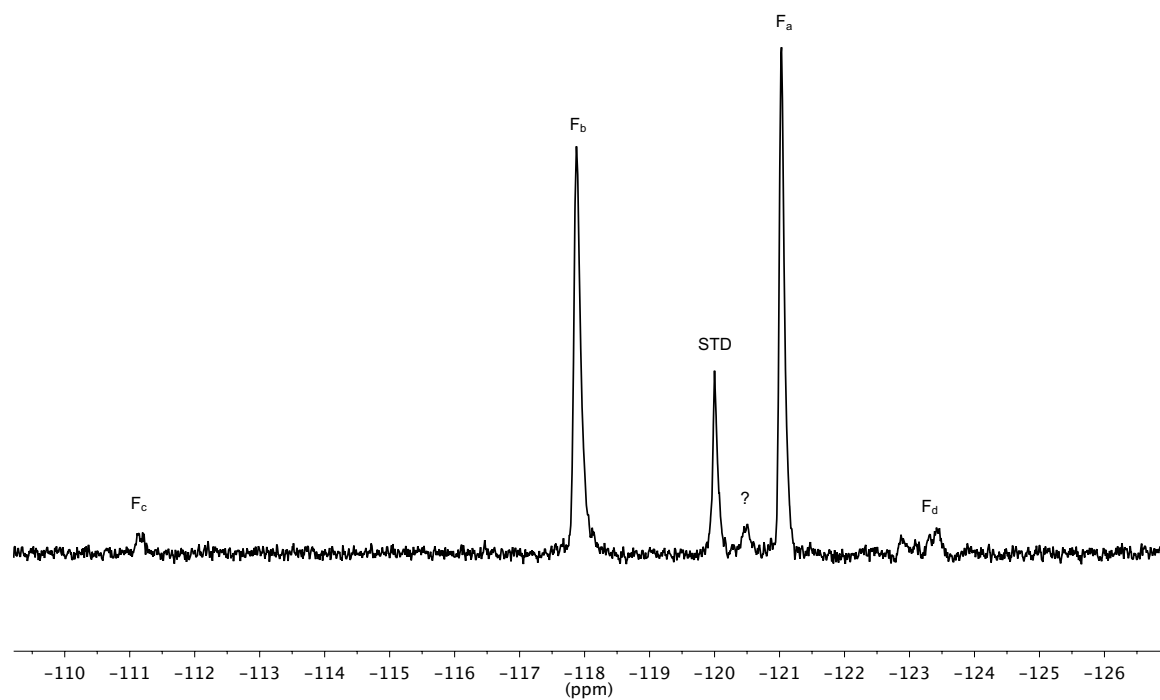
Figure 181. ^{19}F NMR spectrum of **107** at −55 °C, referenced to 1,4-difluorobenzene (−120.00 ppm).
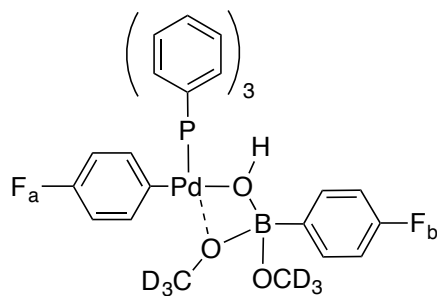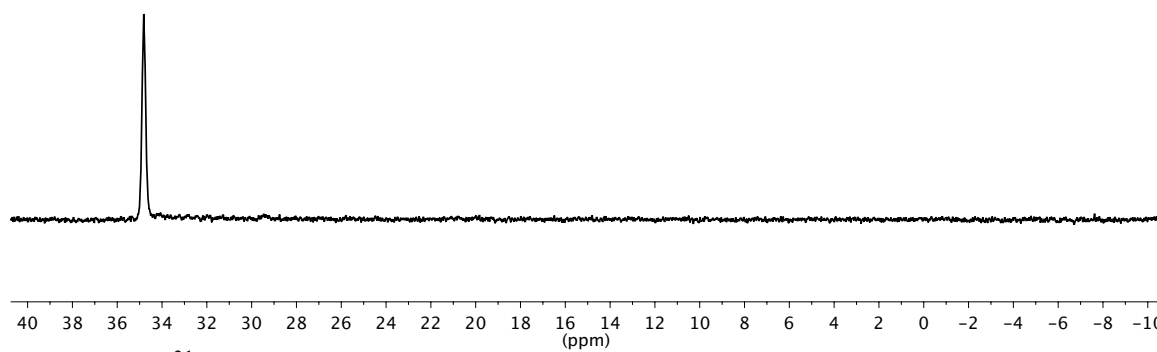
Figure 182. ^{31}P NMR spectrum of **107** at −55 °C, externally referenced to i-Pr$_3$P (19.00 ppm).
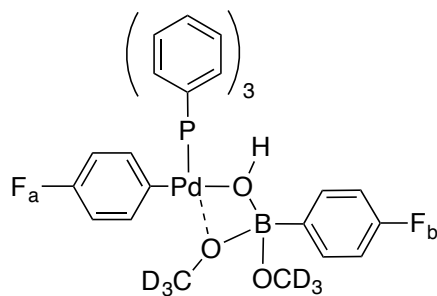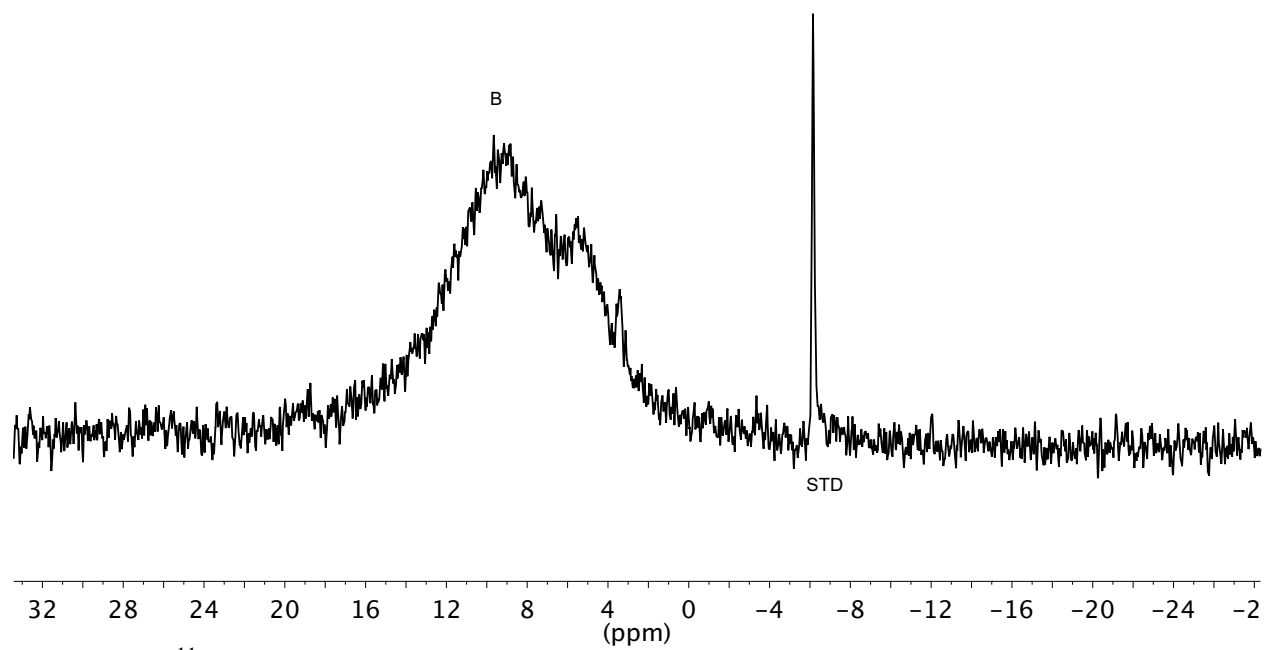
Figure 183. ^{11}B NMR spectrum of **107** at −55 °C, referenced to Ph$_4$BNa (−6.14 ppm).
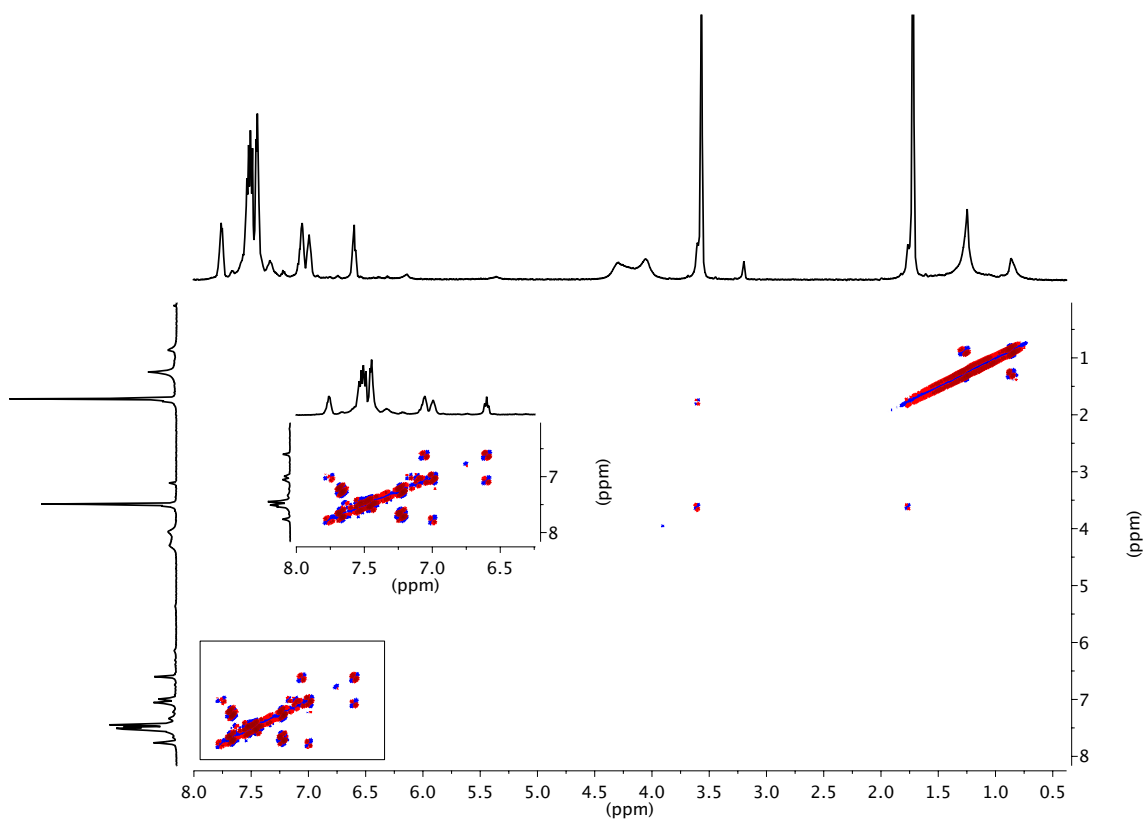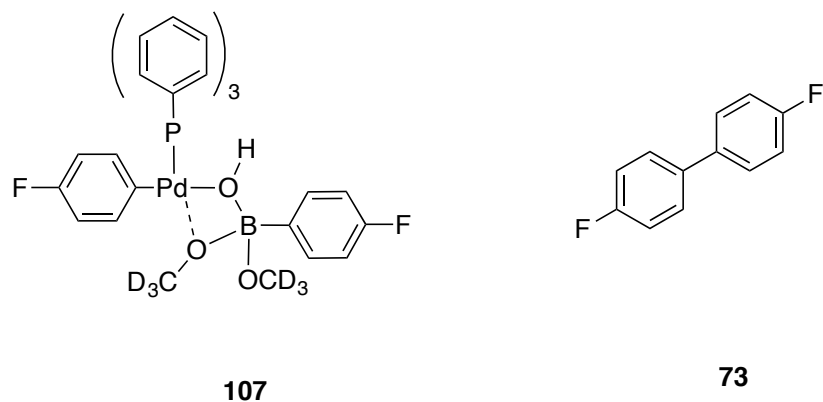
Figure 184. dgfCOSY spectrum of **107** at −55 °C, referenced to THF-d_8 (1.72 ppm).
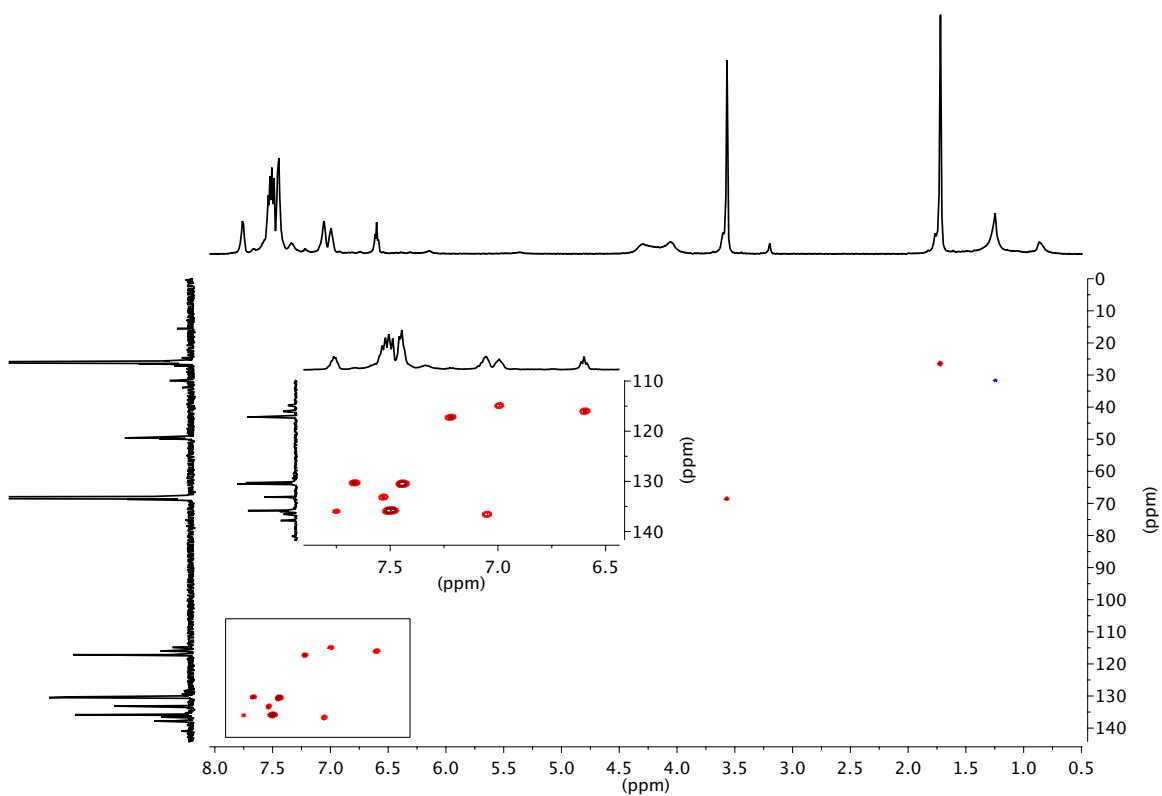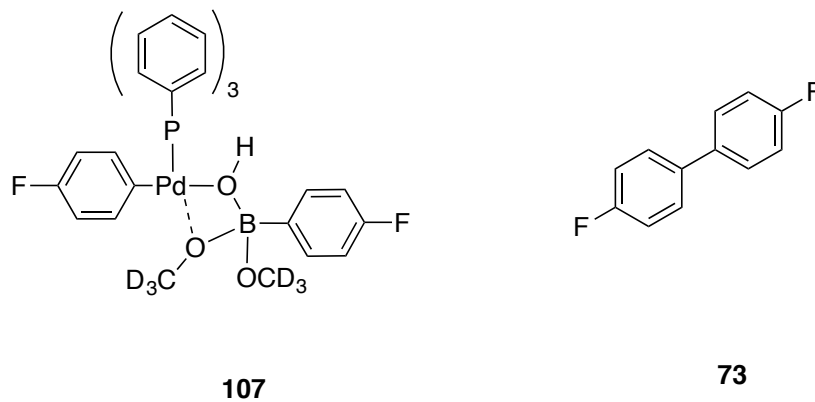
Figure 185. gHSQC spectrum of **107** at −55 °C, referenced to THF-d_8 (1.72 and 68.21 ppm).
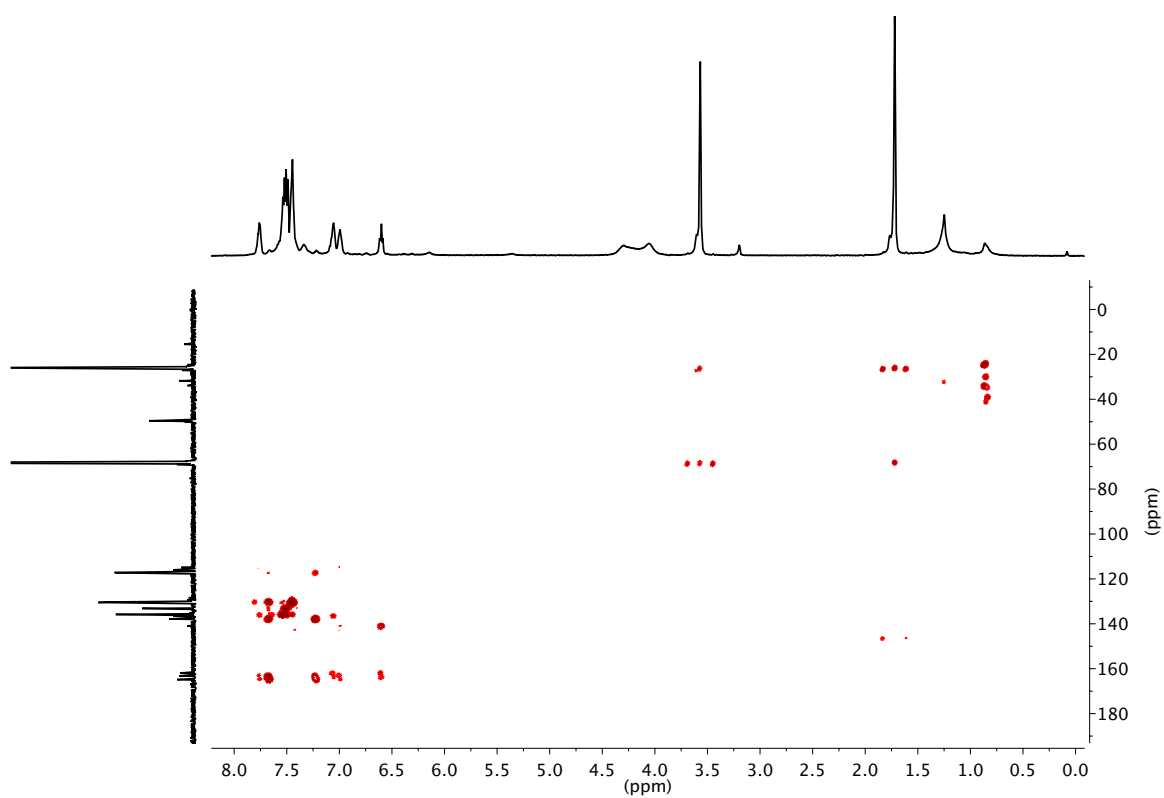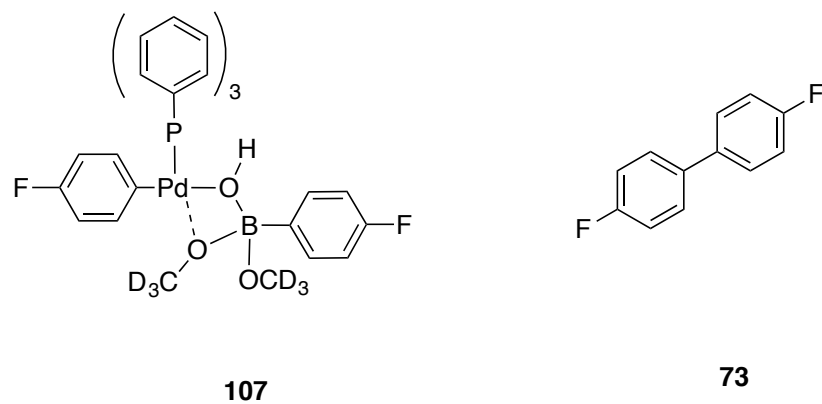
Figure 186. gHMBC spectrum of **107** at −55 °C, referenced to THF-d_8 (1.72 and 68.21 ppm).

Experiment 33: Preparation of DPPF 8-B-4 complex 109 from 58 and 111.
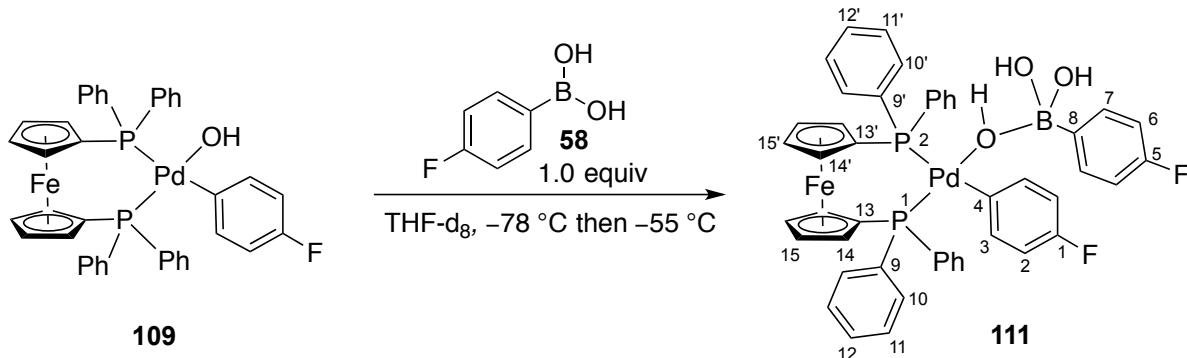
A flame dried, 1.0 mL volumetric flask was charged with 4-fluorophenylboroxine (26 mg, 71 μmol 1.0 equiv), H$_2$O (4 μL, 222 μmol, 3.3 equiv) and filled to the mark with freshly distilled (NaK) THF-d_8 (0.21 M).

An oven dried, 5-mm, NMR tube as charged with (DPPF)Pd(4-FC$_6$H$_4$)(OH) (15.5 mg, 20 μmol, 1.0 equiv) and THF-d_8 (500 μL) followed by heating gently with warm tap water until the solid had dissolved. The tube was placed into a −78 °C dry-ice acetone bath followed by the addition of 4-fluorophenylboronic acid solution (95 μL, 20 μmol, 2.0 equiv). The tube was vortexed (not shaken) quickly cleaned with a Kimwipe and placed into the −78 °C bath. The tube was then placed into the probe of the NMR spectrometer pre-cooled to −55 °C. The sample was found to be stable for over 24 h at −55 °C. The complex was characterized *via* 1D and 2D NMR experiments over a course of multiple experiments.

Data for **111**:

^{1}H NMR: (600 MHz, THF-d_8)

8.19 (m, 4 HC(10')), 7.42 (m, 4 HC(12 and 12')), 7.41 (m, 4 HC(11')), 7.34 (m, 4 HC(11)), 7.12 (m, 4 HC(10)), 7.08 (m, 2 HC(3)), 6.97 (m, 2 HC(7)), 6.45 (m, 2 HC(6)), 6.38 (m, 2 HC(2)), 4.94 (m, 2 HC(15)), 4.67 (m, 2 HC(14)), 4.28 (m, 2 HC(15')), 3.50 (m, 2 HC(14'))

^{13}C NMR: (151 MHz, THF-d_8)

165.23, 163.62 (d, ^1J(F-C) = 243 Hz, 1 FC(5)), 162.65, 161.25 (d, ^1J(F-C) = 238 Hz, 1 FC(1)), 154.35, 153.47 (dd, ^2J(P-C) = 133 and 10 Hz, 1 HC(4)) 137.68 (d, ^3J(F-C) = 9 Hz, 2 C(7)), 135.84, (m, 1 BC(8)), 136.79, 136.70 (d, ^2J(P-C) = 15 Hz, 4 HC(10')) 132.00 (m, 4 HC(12 and 12')), 131.85 (m, 4 HC(11)), 130.02, 129.95 (d, ^3J(P-C) = 10 Hz, 4 HC(11')), 129.58, 129.51 (d, ^2J(P-C) = 12 Hz, 4 HC(10)),

78.52 to 78.14 (m, 2 PC(13 and 13')), 76.13, 76.07 (d, ^2J(P-C) = 8 Hz, 2 HC(14')), 75.43 (m, 2 HC(14)), 74.71, 74.44 (d, ^3J(P-C) = 40 Hz, 2 HC(15')), 73.95 (m, 2 HC(15))

^{19}F NMR: (565 MHz, THF-d_8)

−116.47 (s, FC(5)), −122.35 (s, FC(1))

^{31}P NMR: (243 MHz, THF-d_8)

33.14, 32.98 (d, ^2J(P-P) = 36 Hz, 1 P(1)), 11.54, 11.41 (d, ^2J(P-P) = 36 Hz, 1 P(2))

^{11}B NMR: (129 MHz, THF-d_8)

Cannot determine

Figure 187. ^{1}H NMR spectrum of **111** at −55 °C, referenced to THF-d_8 (1.72 ppm).
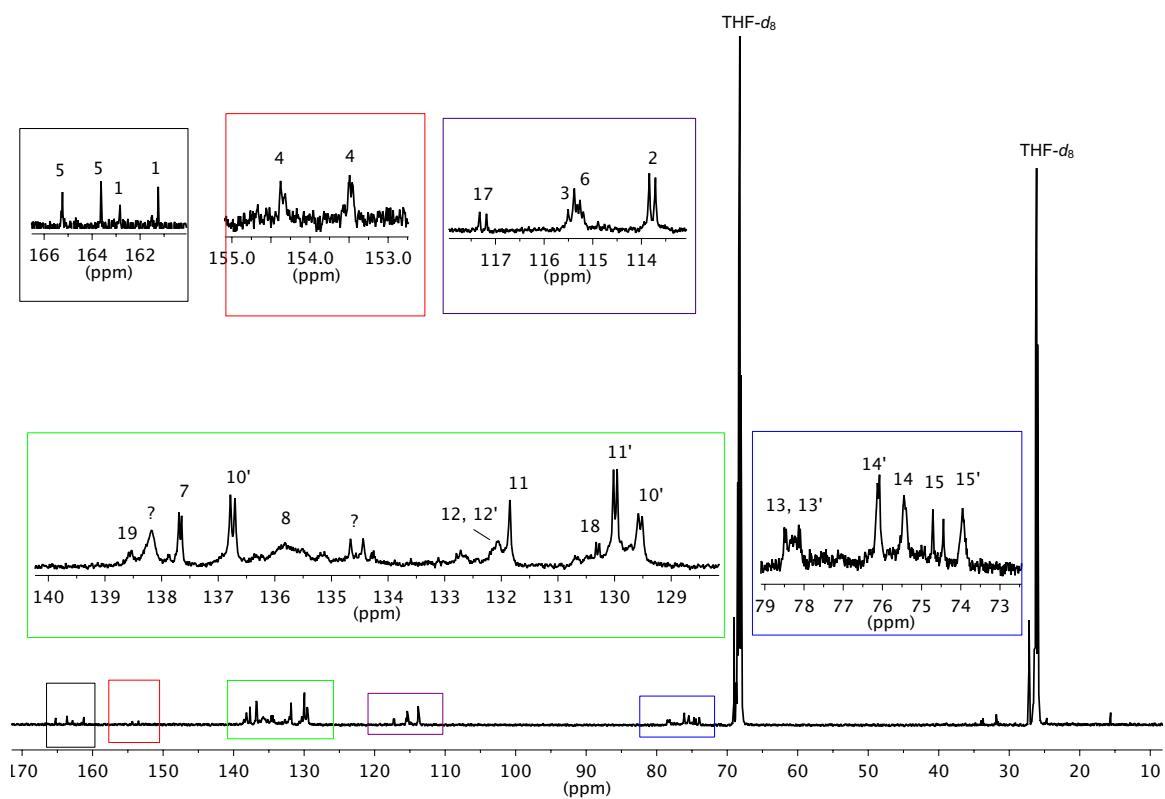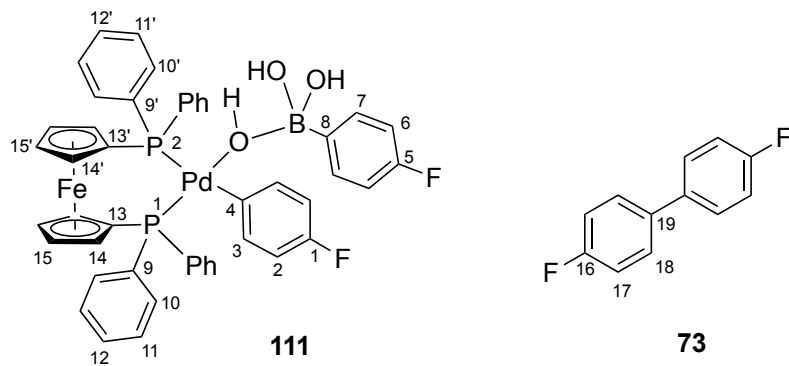
Figure 188. ^{13}C NMR spectrum of **111** at −55 °C, referenced to THF-d_8 (68.21 ppm).
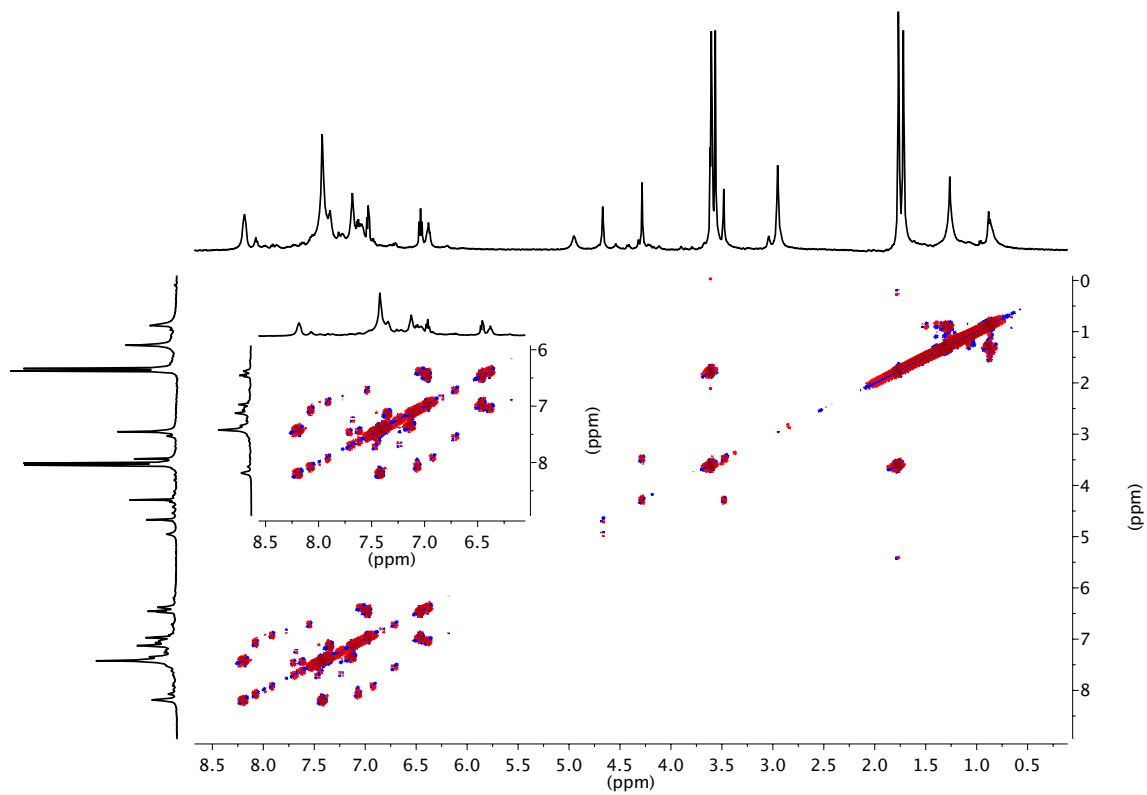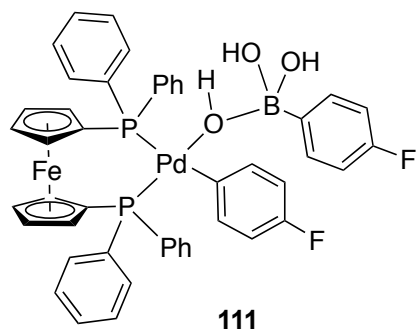
Figure 189. COSY NMR spectrum of **111** at −55 °C, referenced to THF-d_8 (1.72 ppm).
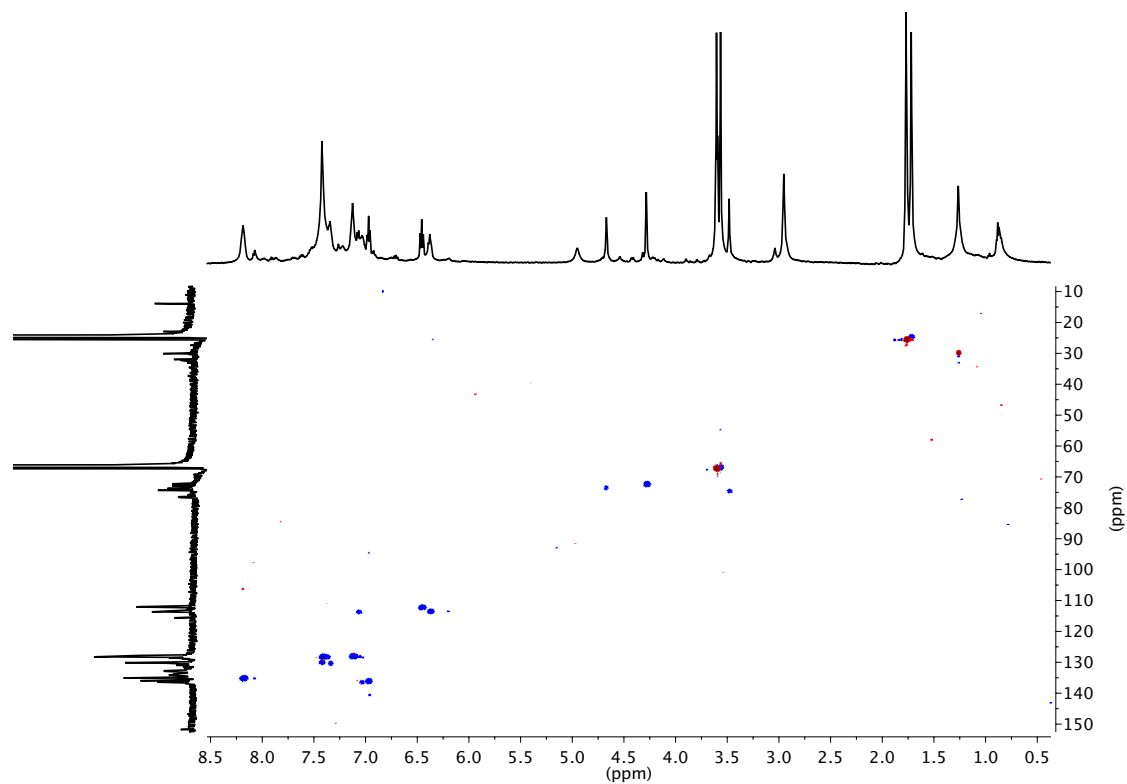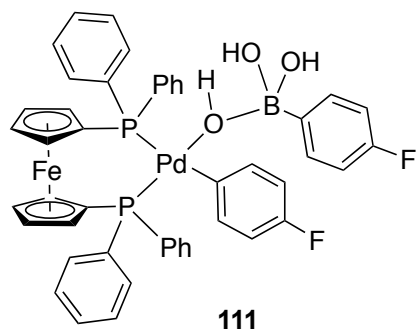
Figure 190. gHSQC spectrum of **111** at −55 °C, referenced to THF-d_8 (1.72 and 68.21 ppm).
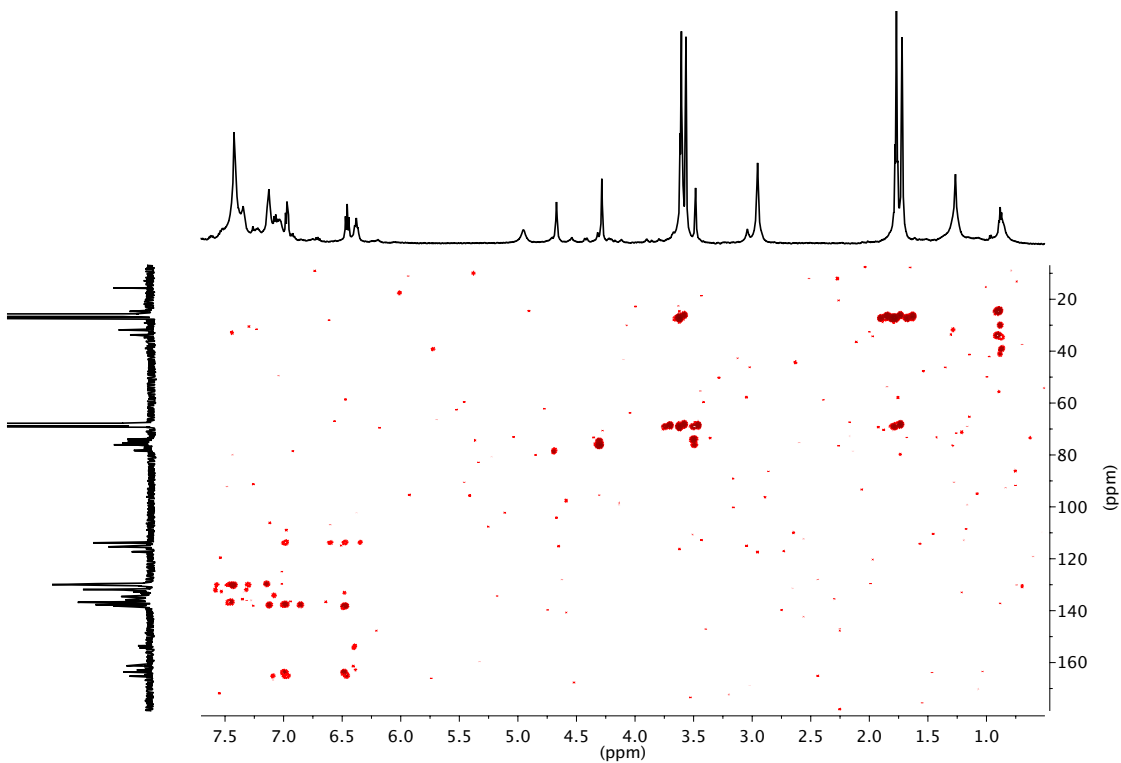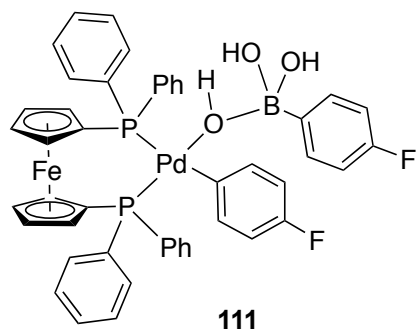
Figure 191. gHMBC spectrum of **111** at −55 °C, referenced to THF-d_8 (1.72 and 68.21 ppm).
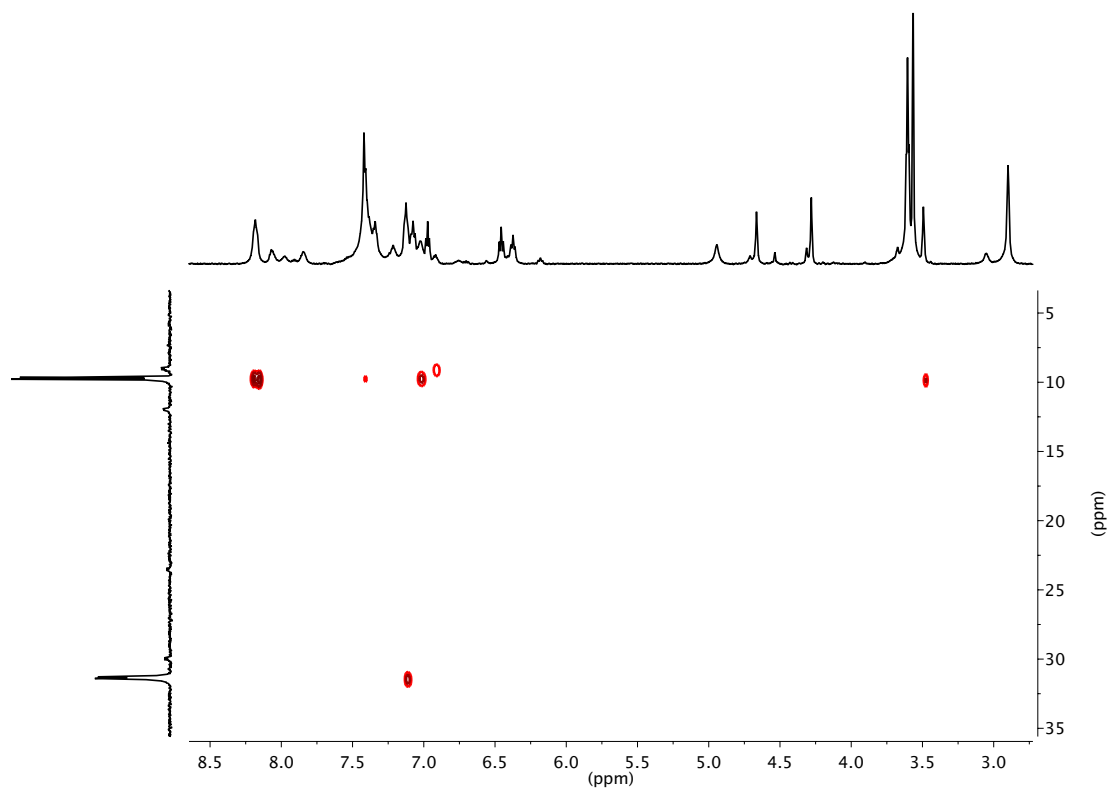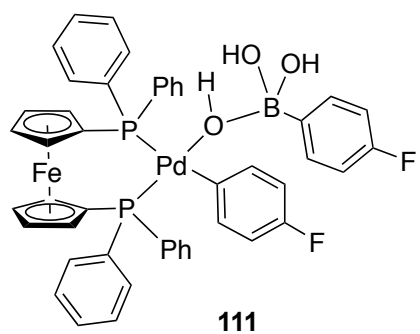
Figure 192. gHMBC (^{1}H-^{31}P) spectrum of **111** at −55 °C, referenced to THF-d_8 (1.72).
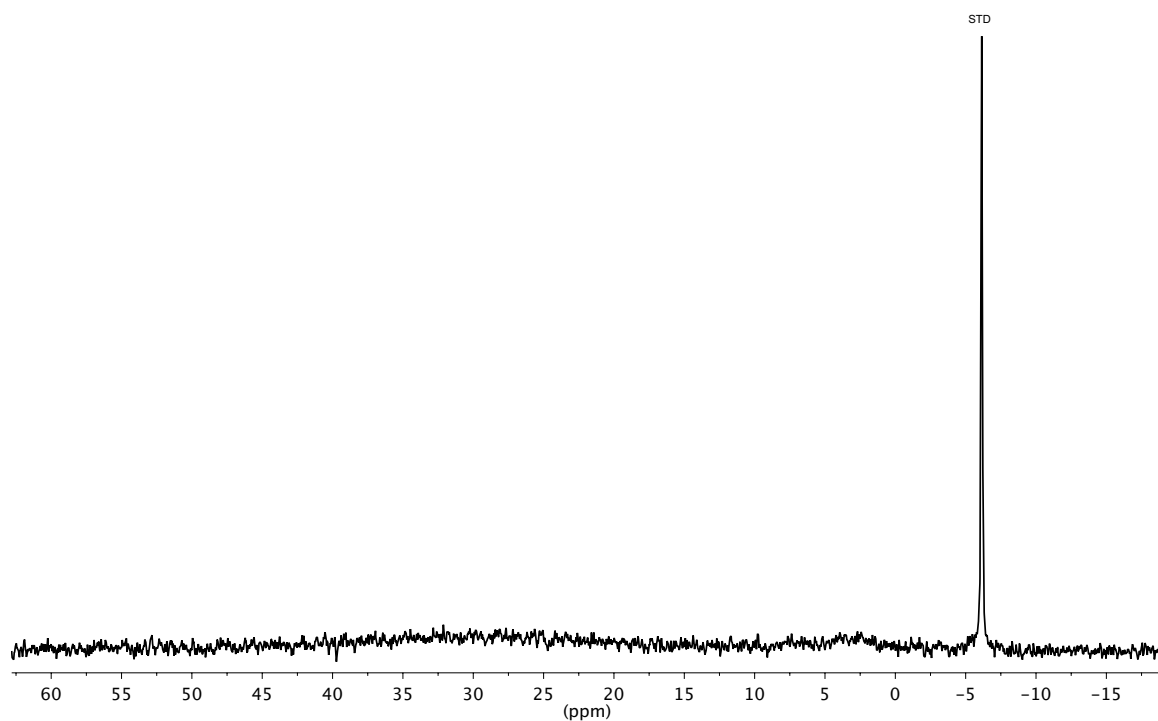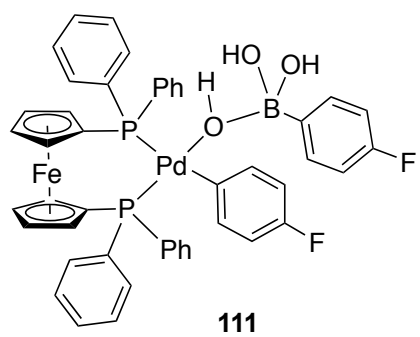
Figure 193. ^{11}B NMR spectrum of **111** at −55 °C, referenced to Ph$_4$BNa (−6.14 ppm).

274
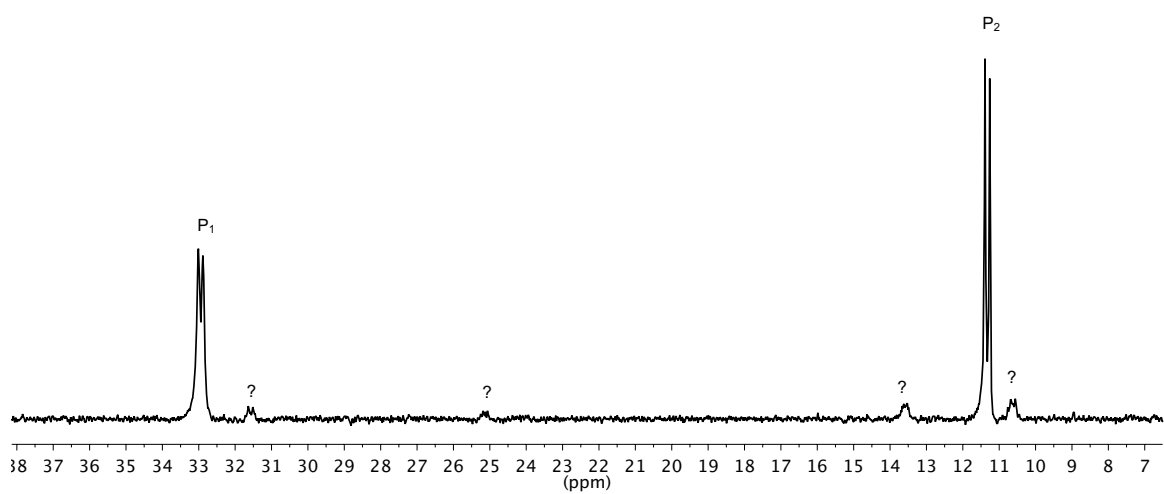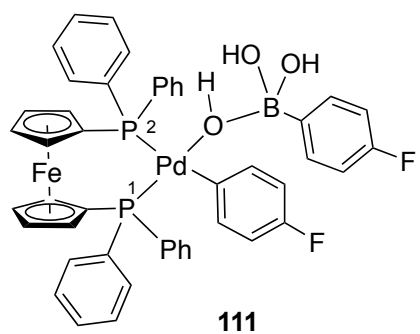
Figure 194. ^{31}P NMR spectrum of **111** at −55 °C, externally referenced to Ph$_3$P (−6.00 ppm).
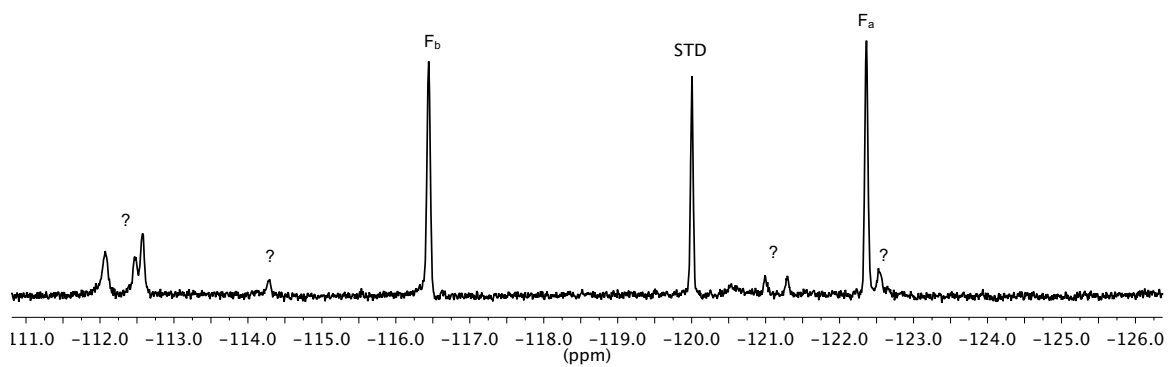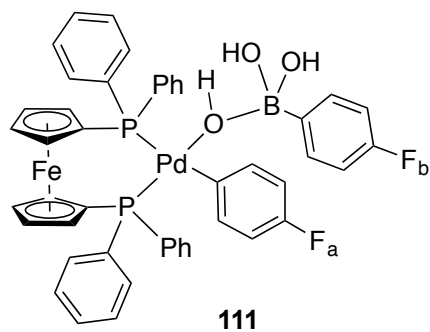
Figure 195. ^{19}F NMR spectrum of **111** at −55 °C, referenced to 1,4-difluorobenzene (−120.00 ppm).

Experiment 34: Preparation of *trans*-bis-(triisopropylphosphine)palladium dichloride
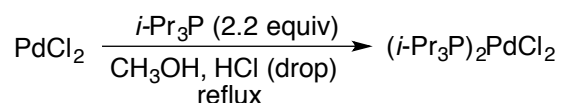
$$PdCl_2 \xrightarrow[\substack{CH_3OH, HCl \text{ (drop)} \\ reflux}]{i\text{-}Pr_3P \text{ (2.2 equiv)}} (i\text{-}Pr_3P)_2PdCl_2$$

trans-Bis-(triisopropylphosphine)palladium dichloride was prepared by modifying a procedure by Badshah and co-workers.[126] A 500-mL, three-necked, round-bottomed flask was charged with a magnetic stir bar, $PdCl_2$ (1.00 g, 5.7 mmol, 1.0 equiv) and fitted with a reflux condenser. The apparatus was purged for ~10 min with argon followed by the addition of 200 mL of freshly distilled methanol (Mg) and a drop of glacial HCl. The solution was heated to reflux for 30 min (deep red solution was observed), then $i\text{-}Pr_3P$ (2.4 mL, 12.54 mmol, 2.2 equiv) was added at once *via* syringe. A canary yellow solid was observed instantly. After the addition, the suspension was heated to reflux for 7 h, then cooled to room temperature overnight (~12 h). A yellow solid was collected on a glass frit. The solid was dissolved in dichloromethane (~200 mL) followed by extraction in triplicate with water (50 mL). The organic layer was dried with $MgSO_4$ until flocculent, followed by gravity filtration. The solvent was removed by rotary-evaporation (30 mm Hg, 30 °C). The solid was collected over a glass-fritted funnel and was washed with ether (100-150 mL) yielding 2.67 g (81%) of a canary yellow solid, which was used without further purification. The spectra matched those previously reported by Grushin and Alper.[127]

Experiment 35: Preparation of *trans*-bis-(triphenylphosphine)palladium dichloride
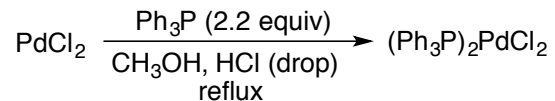
$$PdCl_2 \xrightarrow[\substack{CH_3OH, HCl \text{ (drop)} \\ \text{reflux}}]{Ph_3P \text{ (2.2 equiv)}} (Ph_3P)_2PdCl_2$$

trans-Bis-(triphenylphosphine)palladium dichloride was prepared by modifying a procedure by Badshah and co-workers. A 500-mL, round-bottomed flask was charged with a magnetic stir bar, PdCl$_2$ (1.0 g, 5.7 mmol, 1.0 equiv) and 150 mL of methanol was added followed by fitting with a reflux condenser. Then ~0.5 mL of HCl was added and the mixture was refluxed for 40 min (deep red solution was observed), then Ph$_3$P (3.3 g, 12.6 mmol, 2.2 equiv) was added at once *via* a funnel dissolved in 25 mL of acetone. A canary yellow solid was observed instantly. After the addition, the suspension was heated to reflux for 4 h, then cooled to room temperature overnight (~12 h). A yellow solid was collected on a glass frit. The solid was dissolved in hot chloroform (~200 mL) followed by extraction with water (100 mL). The organic layer was dried with MgSO$_4$ until flocculent, followed by gravity filtration. The solvent was removed by rotary-evaporation (30 mm Hg, 30 °C). The solid was collected over a glass-fritted funnel and was washed with a small amount of acetone (~10 mL) yielding 3.50 g (88%) of a canary yellow solid, which was used without further purification. The spectra matched those previously reported by Grushin and Alper.

Experiment 36: Preparation of [(*i*-Pr₃P)Pd(4-FC₆H₄)(μ-OH)]₂ 90

Compound **90** was synthesized by a modification of a procedure by Grushin and Alper as described below *(51)*. A 100-mL, round-bottomed flask was charged with a magnetic stir bar, (*i*-Pr₃P)₂PdCl₂ (0.5 g, 1.0 mmol, 1.0 equiv) and KOH (10 g, 178 mmol, 178 equiv). Then 1,4-iodofluorobenzene (0.88 g, 4.0 mmol, 4.0 equiv) was added *via* syringe. The flask was fitted with a reflux condenser and purged with high purity argon for ~5 min followed by addition of 10 mL of degassed benzene and 5 mL of degassed H₂O. The mixture was stirred vigorously for ~12 h at reflux, during which time the reaction mixture turned from light yellow to deep red after ~1 hour. After 12 h, the water layer was removed *via* syringe and 5 mL of H₂O and KOH (10 g, 178 mmol, 178 equiv) were added and the mixture was stirred for another 3 hour at reflux. The organic layer was separated and filtered through glass wool (remove Pd-Black). The organic layer was extracted with H₂O (5 mL X 5) separated and the solvent was removed under reduced pressure. THF (1 mL) was added to the flask followed by ~10 mL hexanes and the solution was placed into the freezer for ~15 hours. The following day a white precipitate had formed and was collected on a glass-fritted funnel followed by dissolving with THF (~15 mL). The solution was filtered through a syringe filter (0.20 μm) followed by removing the THF at reduced pressure. Then 10 mL of hexane was added while stirring and a white precipitate was observed over 30 min. The solid was collected on a glass frit followed by washing with 200 mL of hexanes. The precipitate was then dried under high vacuum (4 mm Hg) yielding 102 mg (27 %) of a white solid. A mixture of *trans* / *cis* isomers were observed in a ratio of 3:2.

Data for *trans* **90**:

¹H NMR: (600 MHz, THF-*d*₈)

7.36 (m, 4 HC(3)), 6.67 (m, 4 HC(2)), 1.92 (m. 6 HC(5)), 1.24 (m. 6 HC(36)), −1.74 (s, 2 (OH))

¹³C NMR: (151 MHz, THF-*d*₈)

162.69, 161.11 (d, ¹*J*(F-C) = 241 Hz, 2 C(1)), 147.15 (m, 2 C(4)), 139.15, (m, 6

C(3)), 114.48, 114.35 (d, ^1J(F-C) = 18 Hz, 4 C(2)), 24.36 (m, 6 C(5)), 19.69 (m, 12 C(6))

^{19}F NMR: (565 MHz, THF-d_8)

   −122.61 (s, FC(1))

^{31}P NMR: (243 MHz, THF-d_8)

   45.55 (s, P(Pd))

Data for *cis* **90**:

^{1}H NMR: (600 MHz, THF-d_8)

   7.31 (m, 4 HC(3)), 6.62 (m, 4 HC(2)), 2.03 (m. 6 HC(5)), 1.24 (m. 6 HC(36))

   −1.55 (s, 2 (OH))

^{13}C NMR: (151 MHz, THF-d_8)

   162.82, 161.24 (d, ^1J(F-C) = 239 Hz, 2 C(1)), 145.40 (m, 2 C(4)), 139.83, (m, 6 C(3)), 114.40, 114.28 (d, ^1J(F-C) = 18 Hz, 4 C(2)), 24.16 (m, 6 C(5)), 19.73 (m, 12 C(6))

^{19}F NMR: (565 MHz, THF-d_8)

   −122.82 (s, FC(1))

^{31}P NMR: (243 MHz, THF-d_8)

   45.55 (s, P(Pd))
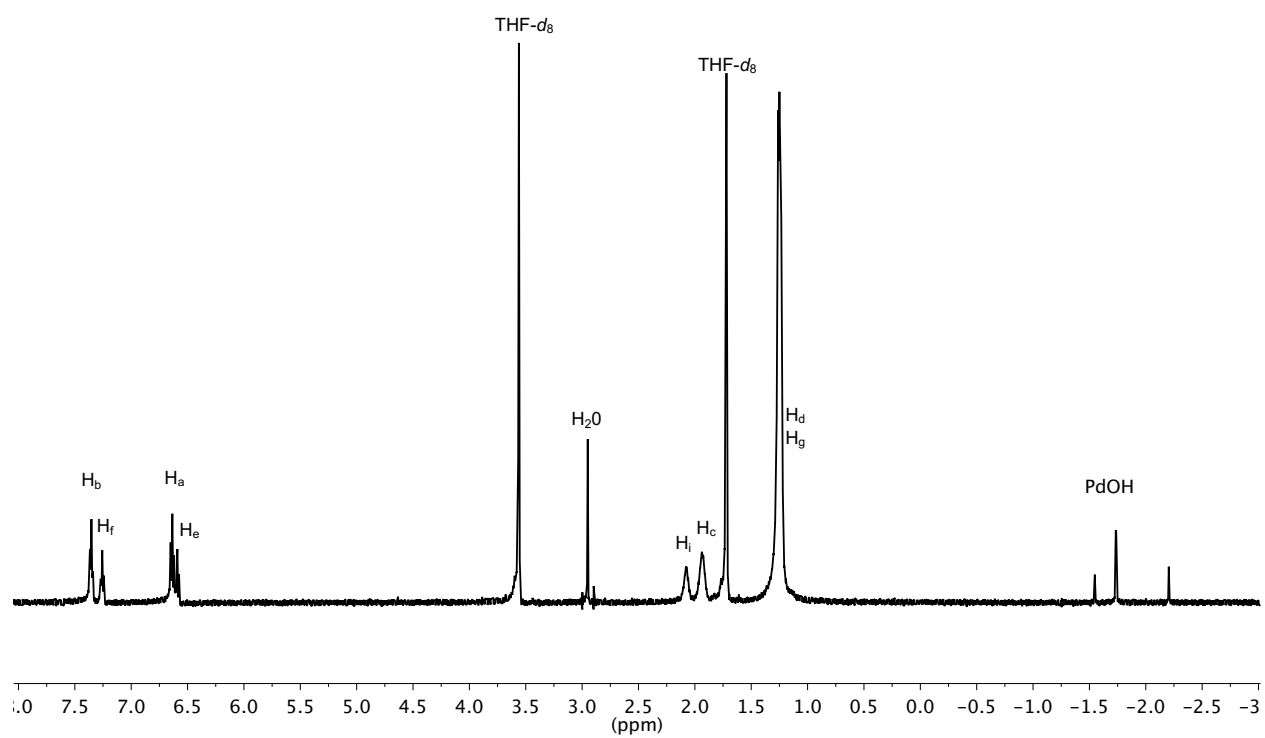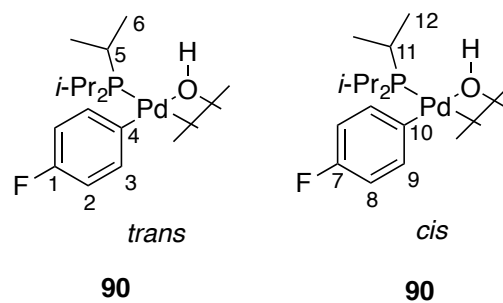
Figure 196. ¹H NMR spectrum of **90** at −30 °C, referenced to THF-d_8 (1.72 ppm).
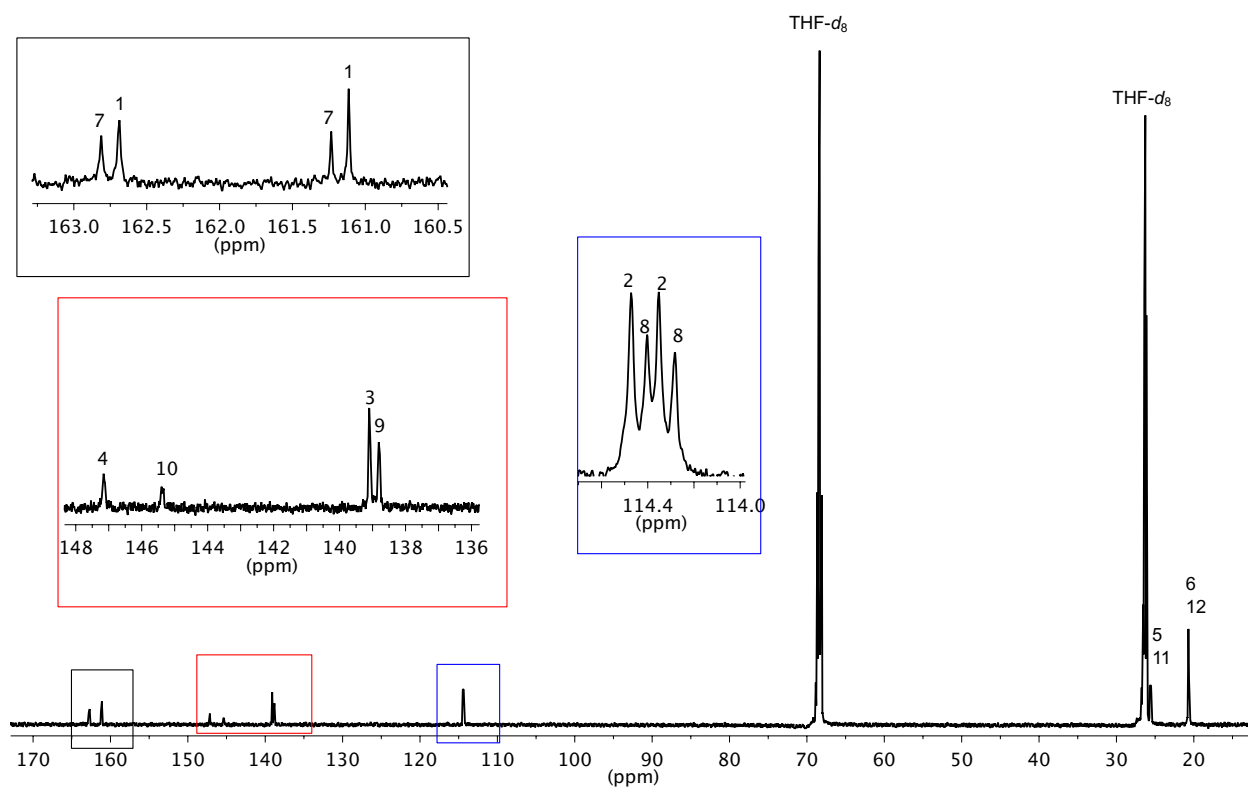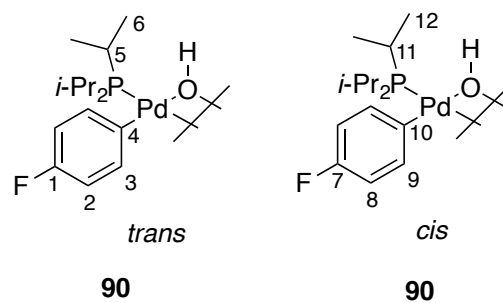
Figure 197. ^{13}C NMR spectrum of **90** at −30 °C, referenced to THF-d_8 (68.21 ppm).
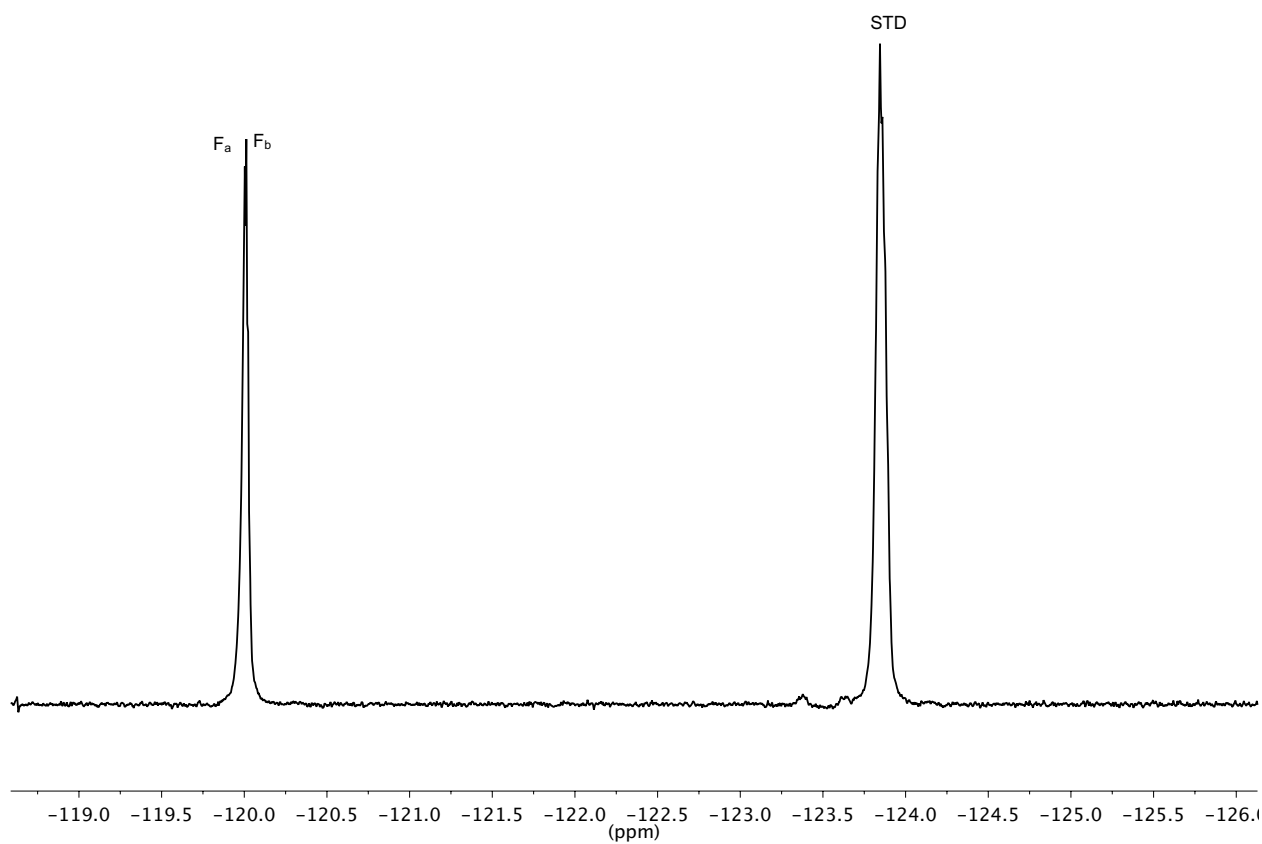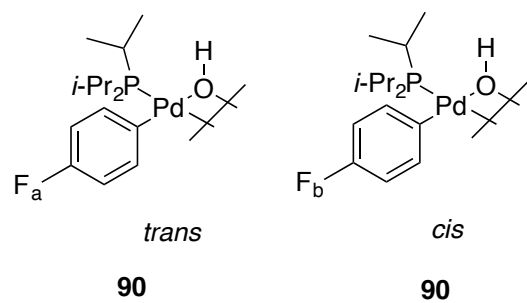
Figure 198. ^{19}F NMR spectrum of **90** at $-30\,°C$, referenced to 1,4-difluorobenzene (-120.00 ppm).
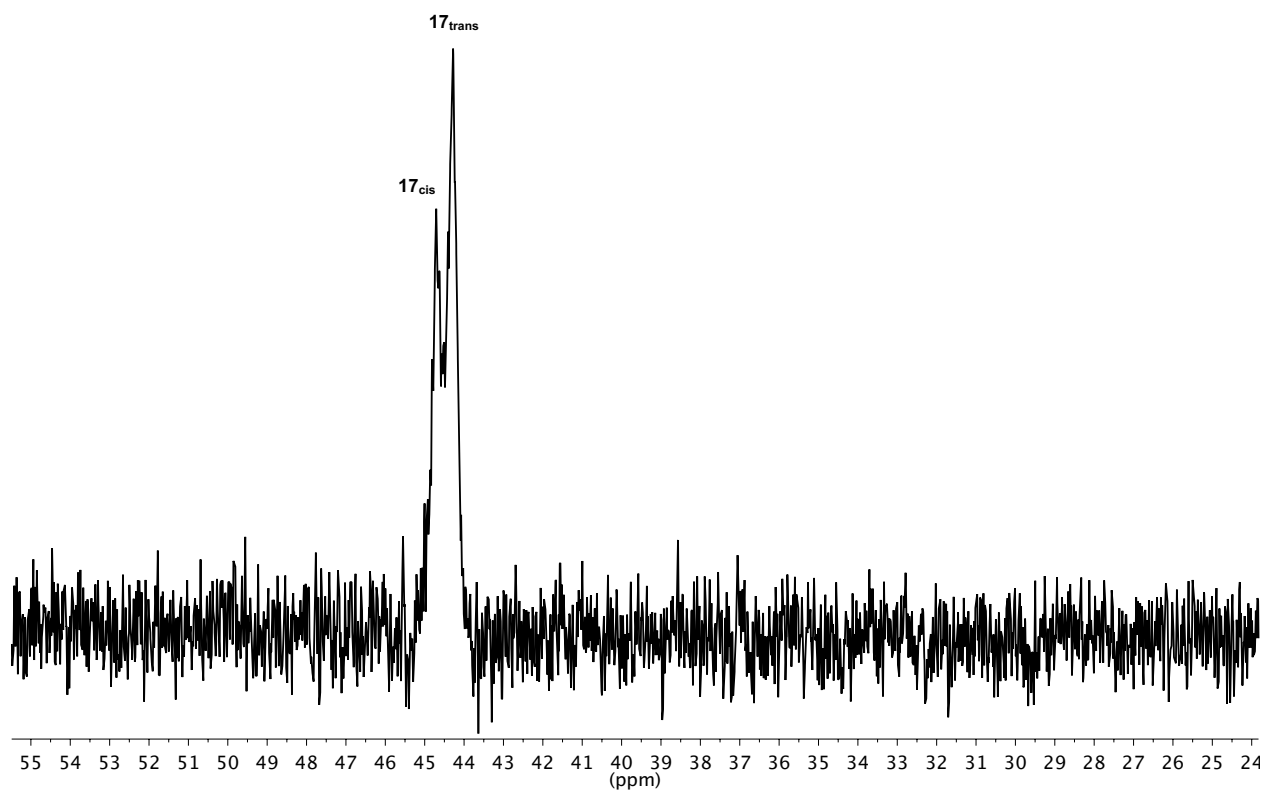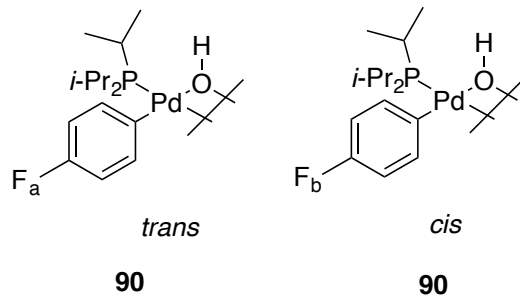
Figure 199. ^{31}P NMR spectrum of **90** at −30 °C, externally referenced to *i*-Pr$_3$P (19.00 ppm).

Experiment 37: Preparation of [(*t*-Bu₃P)Pd(4-FC₆H₄)(μ-OH)]₂ (103)
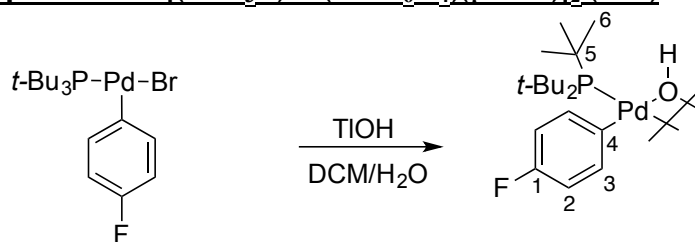
103

A scintillation vial was charged with (4-C₆H₄)*t*-Bu₃PPd-Br (50 mg, 0.1 mmol, 1.0 equiv) and a magnetic stir bar. Then TlOH (120 mg, 6.48 mmol, 64.8 equiv) was placed into a 2ⁿᵈ scintillation vial and dissolved with H₂O (2 mL) *via* pipette. While stirring the palladium bromide solution the thallium hydroxide solution was added dropwise by pipette where a white precipitate was observed. The mixture was stirred for ~5 min followed by decanting the DCM layer by syringe. The TlBr was removed by passing the DCM solution through a 0.2 micron syringe filter. The DCM was removed by rotary evaporation yielding 10.2 mg, 17% of an off white solid.

Data for *trans*-**103**:

¹H NMR: (600 MHz, THF-*d*₈)

7.30 (m, 4 HC(3)), 6.58 (m, 4 HC(2)), 1.39, 1.36 (d, ³*J*(P-H) = 12 Hz, 54 C(1)), −2.23 (s, 2 (OH))

¹³C NMR: (151 MHz, THF-*d*₈)

162.85, 161.27 (d, ¹*J*(F-C) = 239 Hz, 2 C(1)), 143.11 (m, 2 C(4)), 138.64, 138.46 (d, , ³*J*(F-C) = 28 Hz, 4 C(3)), 114.13 (m, 4 C(2)), 41.30, 41.23 (d, ¹*J*(P-C) = 11 Hz, 6 C(5)), 34.06 (b, 18 C(6))

¹⁹F NMR: (565 MHz, THF-*d*₈)

−125.18 (s, FC(1))

³¹P NMR: (243 MHz, THF-*d*₈)

75.68 (s, P(Pd))

Data for *cis*-**103**:

¹H NMR: (600 MHz, THF-d_8)

        7.18 (m, 4 HC(3)), 6.49 (m, 4 HC(2)), 1.46, 1.43 (d, ^3J(P-H) = 12 Hz, 54 C(1)),

        −2.56, −3.19 (s, 2 (OH))

¹³C NMR: (151 MHz, THF-d_8)

        162.85, 161.27 (d, ^1J(F-C) = 239 Hz, 2 C(1)), 143.11 (m, 2 C(4)), 139.72, 139.54

        (d, ^3J(F-C) = 28 Hz, 4 C(3)), 113.87 (m, 4 C(2)), 41.40, 41.33 (d, ^1J(P-C) = 11 Hz,

        6 C(5)), 34.06 (b, 18 C(6))

¹⁹F NMR: (565 MHz, THF-d_8)

    −125.02 (s, FC(1))

³¹P NMR: (243 MHz, THF-d_8)

    74.71 (s, P(Pd))
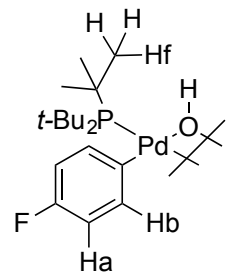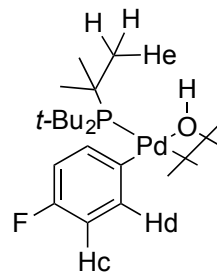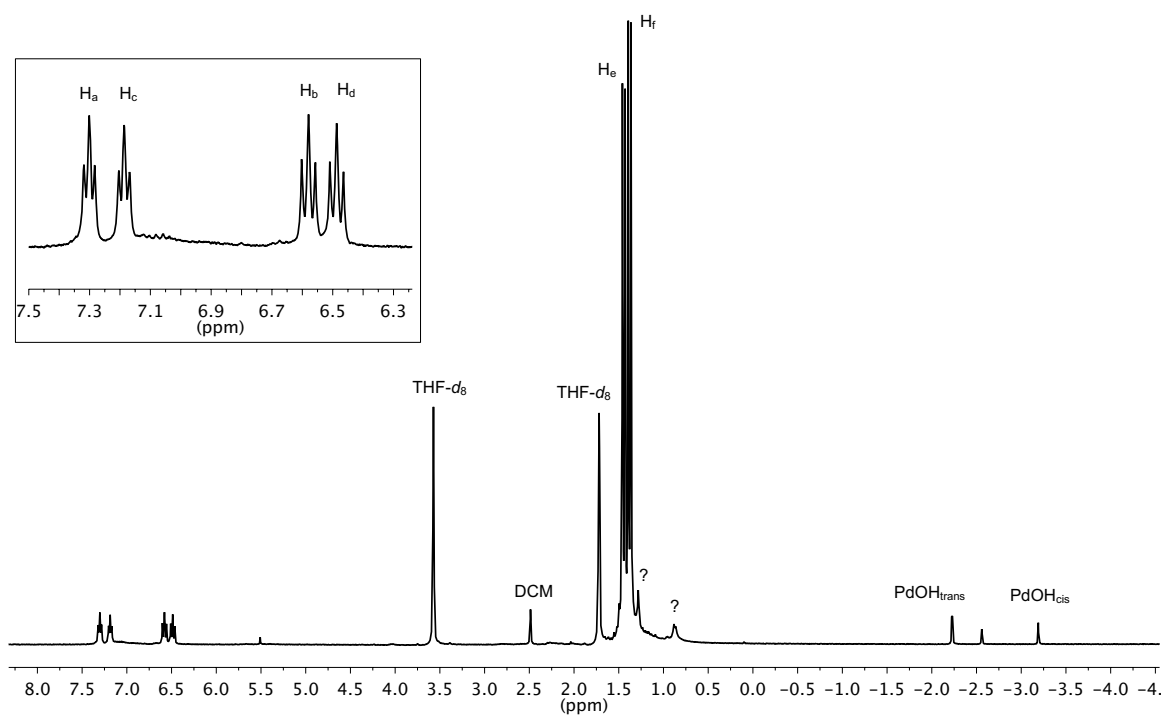
Figure 200. ¹H NMR spectrum of **103** at −50 °C, referenced to THF-d_8 (1.72 ppm).
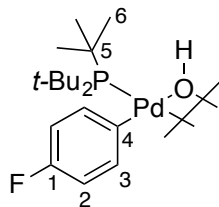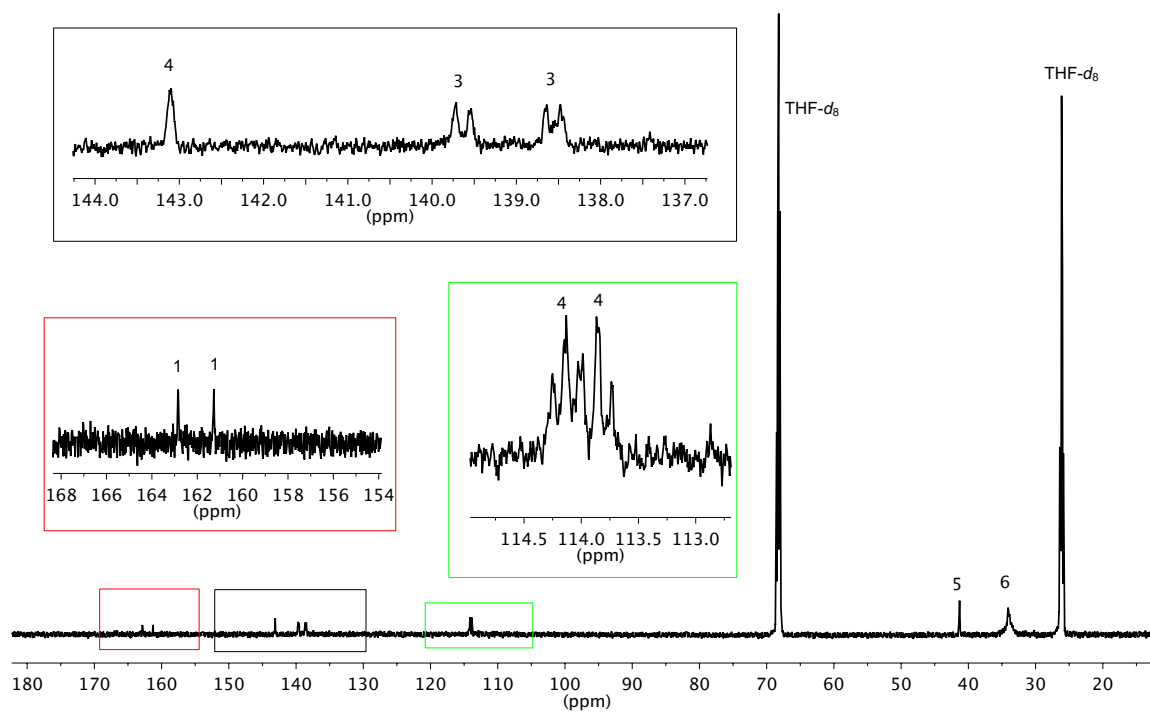
Figure 201. ^{13}C NMR spectrum of **103** at −50 °C, referenced to THF-d_8 (68.21 ppm).
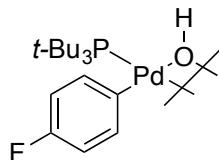
103
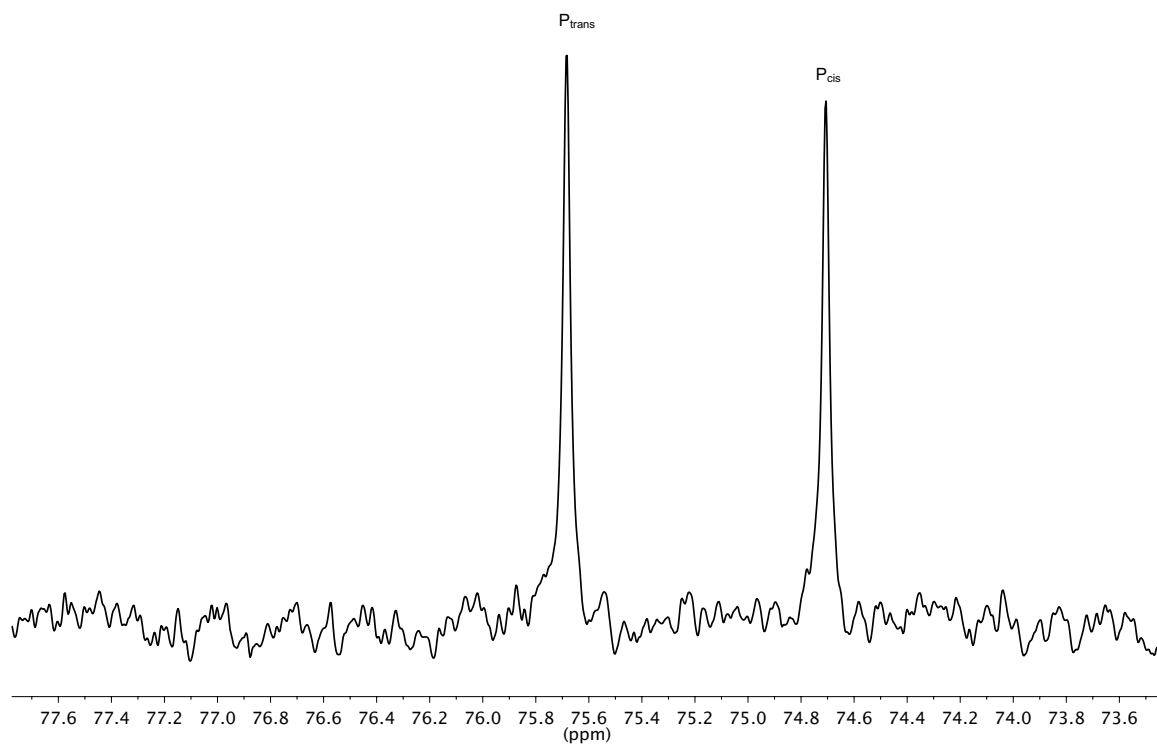
Figure 202. ^{31}P NMR spectrum of **103** at −30 °C, externally referenced to *i*-Pr$_3$P (19.00 ppm).
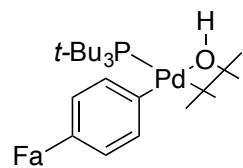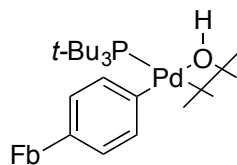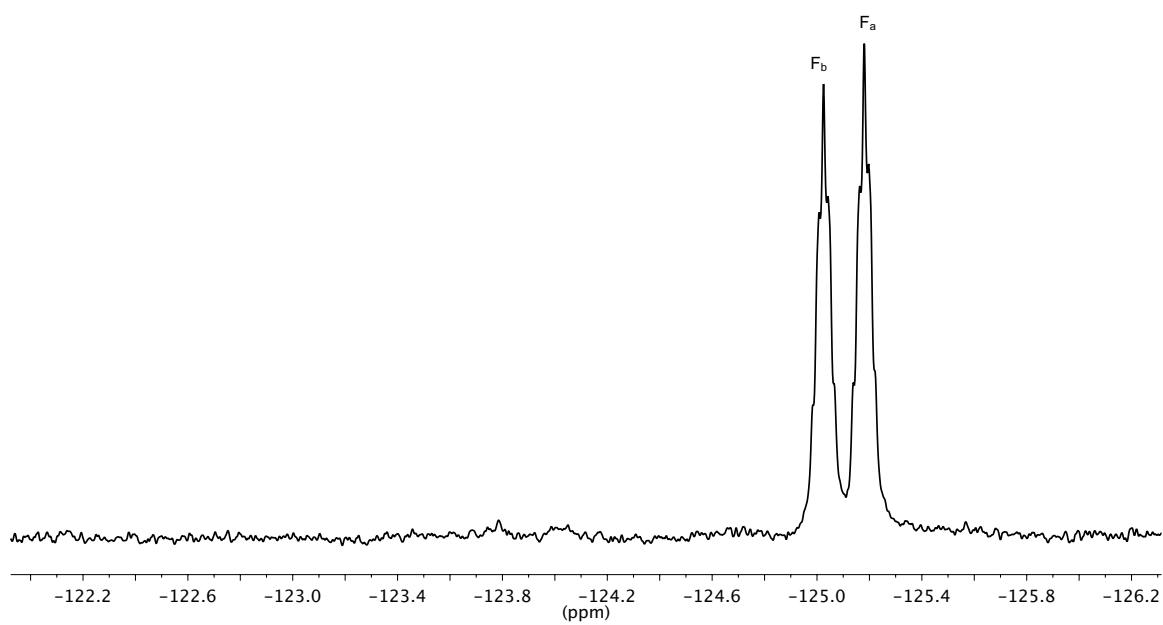
Figure 203. ^{19}F NMR spectrum of **103** at −30 °C, referenced externally to 1,4-difluorobenzene (−120.00 ppm).

Experiment 38: Preparation of [(Ph$_3$P)Pd(4-FC$_6$H$_4$)(μ-OH)]$_2$ (57) from 59
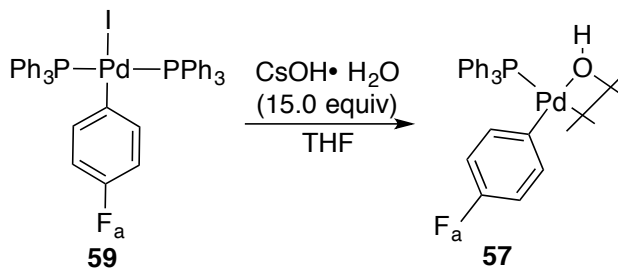
A 250-mL, Schlenk flask was charged with *trans*-(Ph$_3$P)$_2$Pd(C$_6$H$_4$F)I (0.523 g, 0.614 mmol) and a magnetic stir bar followed by placement into the glovebox. Then THF (40 mL) was added followed by CsOH•H$_2$O (1.5 g, 9.0 mmol, 15 equiv). The reaction was filtered through glass wool followed by removal of the THF. Then freshly distilled CHCl$_3$ was added ~3 mL followed by freshly distilled pentane ~5 mL. The flask was placed into the freezer and allowed to sit overnight. The following day ~16 h white needles and black cube crystals were observed. The contents were collected on a filter paper followed by separating the crystals by hand yielding 87 mg, 30%. Spectra matched those described in the following experiment.

Experiment 39: Preparation of [(Ph$_3$P)Pd(4-FC$_6$H$_4$)(μ-OH)]$_2$ (57)
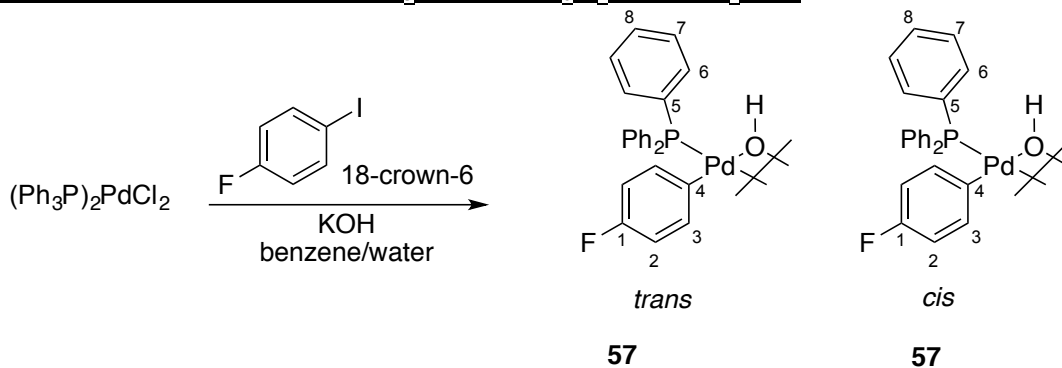
Compound **46** was synthesized by a modification of a procedure by Grushin and Alper as described below. A 100-mL, round-bottomed flask was charged with a magnetic stir bar, (Ph$_3$P)$_2$PdCl$_2$ (0.5 g, 1.0 mmol, 1.0 equiv), KOH (10 g, 178 mmol, 178 equiv) and a chip of 18-crown-6. Then 1,4-iodofluorobenzene (0.88 g, 4.0 mmol, 4.0 equiv) was added *via* syringe. The flask was fitted with a reflux condenser and purged with argon for ~5 min followed by addition of 25 mL of degassed benzene and 5 mL of degassed H$_2$O. The mixture was stirred vigorously for ~6 h at 80 °C, during which time the reaction mixture turned from yellow to deep red then slowly changed to a colorless solution with a white precipitate (Ph$_3$PO). The organic layer was separated

and filtered through glass wool (remove Pd-Black and Ph₃PO). The organic layer was extracted with H_2O (5 mL X 5) separated and the solvent was removed under reduced pressure. THF (1 mL) was added to the flask followed by ~10 mL ether and the solution was placed into the freezer for ~12 hours (overnight). The following day a white precipitate had formed and was collected on a glass-fritted funnel followed by dissolving with THF (~15 mL). The solution was filtered through a syringe filter (0.20 μm) followed by removing the THF at reduced pressure. The solid was collected on a glass frit followed by washing with 250 mL of ether. The precipitate was then dried under high vacuum (4 mm Hg) yielding 192 mg (56 %) of a white solid. A mixture of *trans / cis* isomers were observed.

Data for *trans* **57**:

¹H NMR: (600 MHz, THF-d_8)

7.53 (m, 6 HC(7)), 7.37 (m, 6 HC(8)), 7.29 (m, 6 CH(6)), 6.92 (m, 2 CH(3)), 6.33 (m, 2 CH(2)), −1.78 (broad, HO)

¹³C NMR: (151 MHz, THF-d_8)

162.79, 161.22 (d, ${}^1J$(F-C) = 239 Hz, 1 C(1)), 145.54, 145.50 (d, ${}^2J$(P-C) = 5 Hz, 1 C(4)), 138.24 (m, 2 C(3)), 135.94 (m, 6 C(7)), 133.09, 132.76 (d, ${}^1J$(P-C) = 50 Hz, 3 C(5)), 132.02 (m, 3 C(8)), 129.88 (m, 6 C(6)), 114.57, 114.44 (d, ${}^2J$(F-C) = 19 Hz, 2 C(2))

¹⁹F NMR: (565 MHz, THF-d_8)

−123.79 (s, FC(1))

³¹P NMR: (243 MHz, THF-d_8)

34.83 (s, 1 P(Pd))

Data for *cis* **57**

¹H NMR: (600 MHz, THF-d_8)

7.53 (m, 6 HC(7)), 7.43 (m, 3 HC(8)), 7.29 (m, 6 CH(6)), 6.86 (m, 2 CH(3)), 6.32 (m, 2 CH(2)), −0.56, 0.11 (broad, HO)

¹³C NMR: (151 MHz, THF-d_8)

162.84, 161.25 (d, ${}^1J$(F-C) = 239 Hz, 1 C(1)), 144.73, 144.69 (d, ${}^2J$(P-C) = 6 Hz, 1 C(4)), 138.24 (m, 2 C(3)), 135.94 (m, 6 C(7)), 132.79, 132.45 (d, ${}^1J$(P-C) = 49 Hz,

3 C(5)), 131.92 (m, 3 C(8)), 129.88 (m, 6 C(6)), 114.25, 114.13 (d, ^2J(F-C) = 18 Hz, 2 C(2))

<u>^{19}F NMR:</u>   (565 MHz, THF-d_8)

−123.93 (s, FC(1))

<u>^{31}P NMR:</u>   (243 MHz, THF-d_8)

33.52 (s, 1 P(Pd))
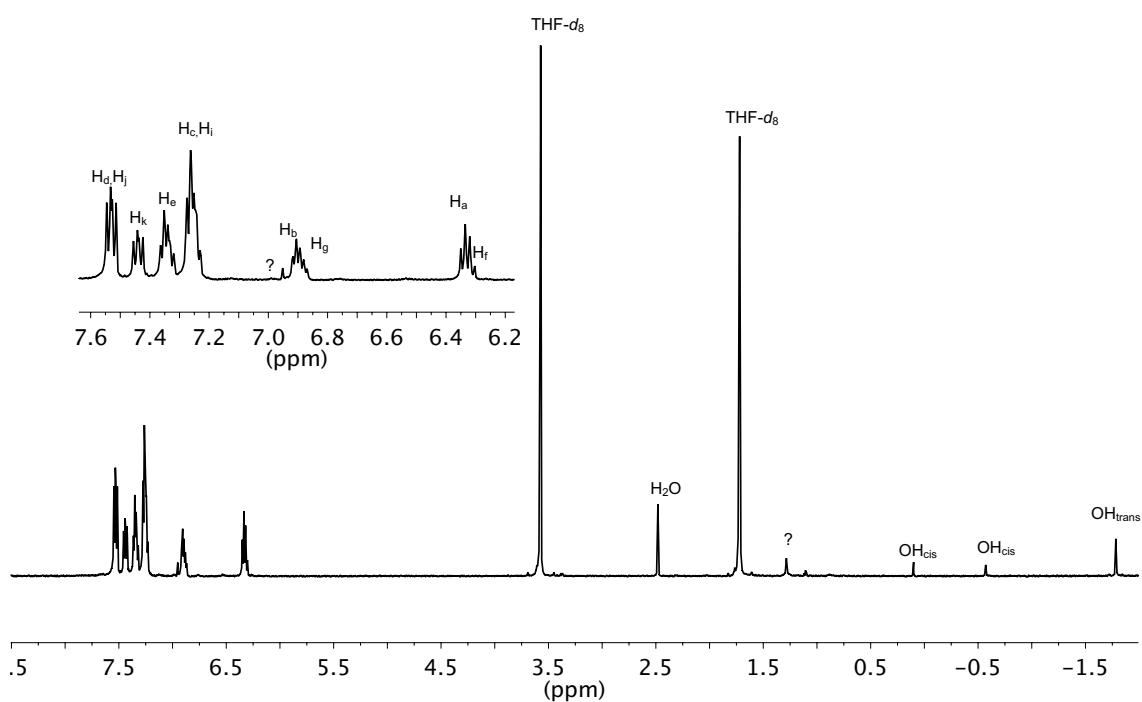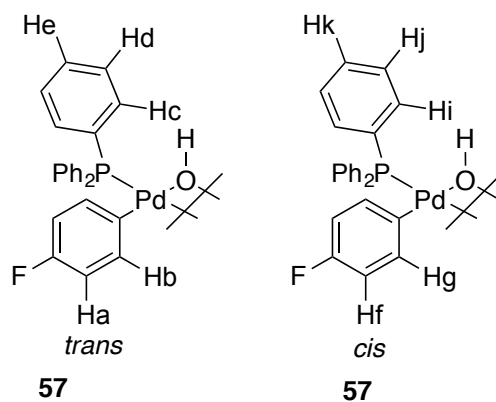
Figure 204. ^{1}H NMR spectrum of **57** at −55 °C, referenced to THF-d_8 (1.72 ppm).
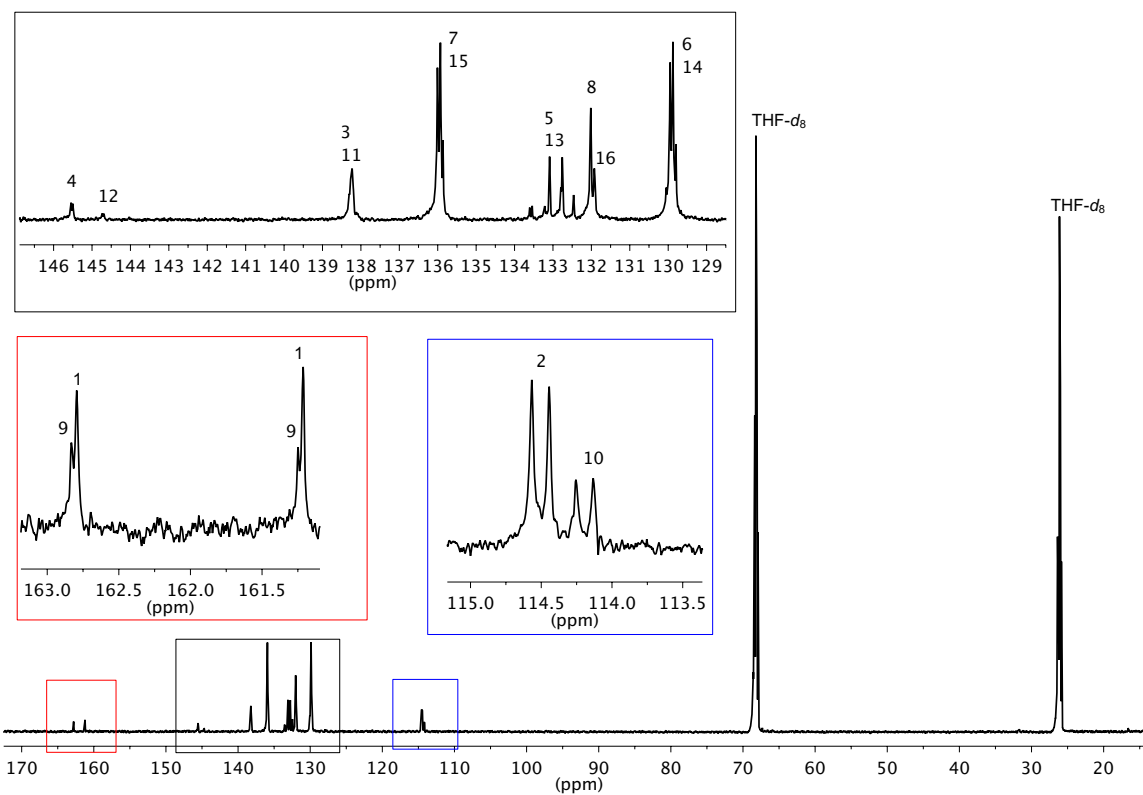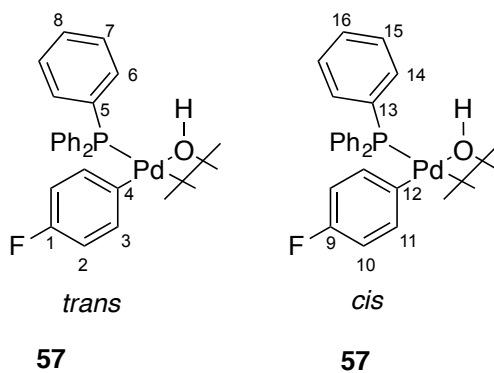
Figure 205. ^{13}C NMR spectrum of **57** at −55 °C, referenced to THF-d_8 (68.21 ppm).
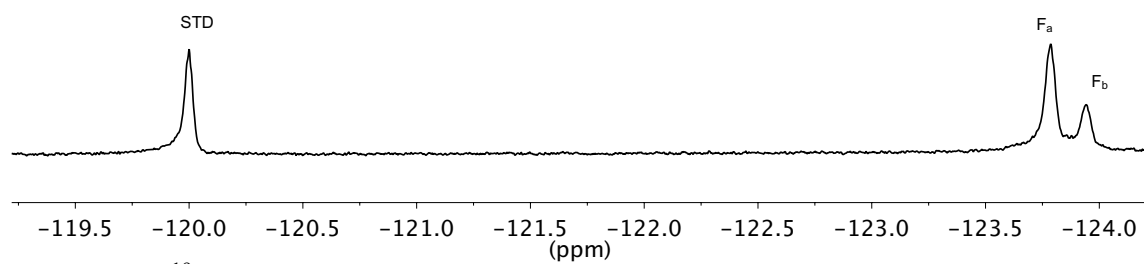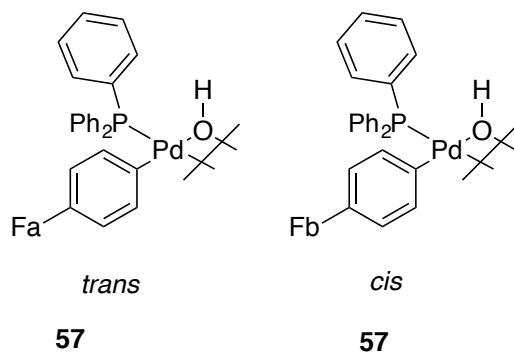
Figure 206. ^{19}F NMR spectrum of **57** at −55 °C, referenced to 1,4-difluorobenzene (−120.00 ppm).
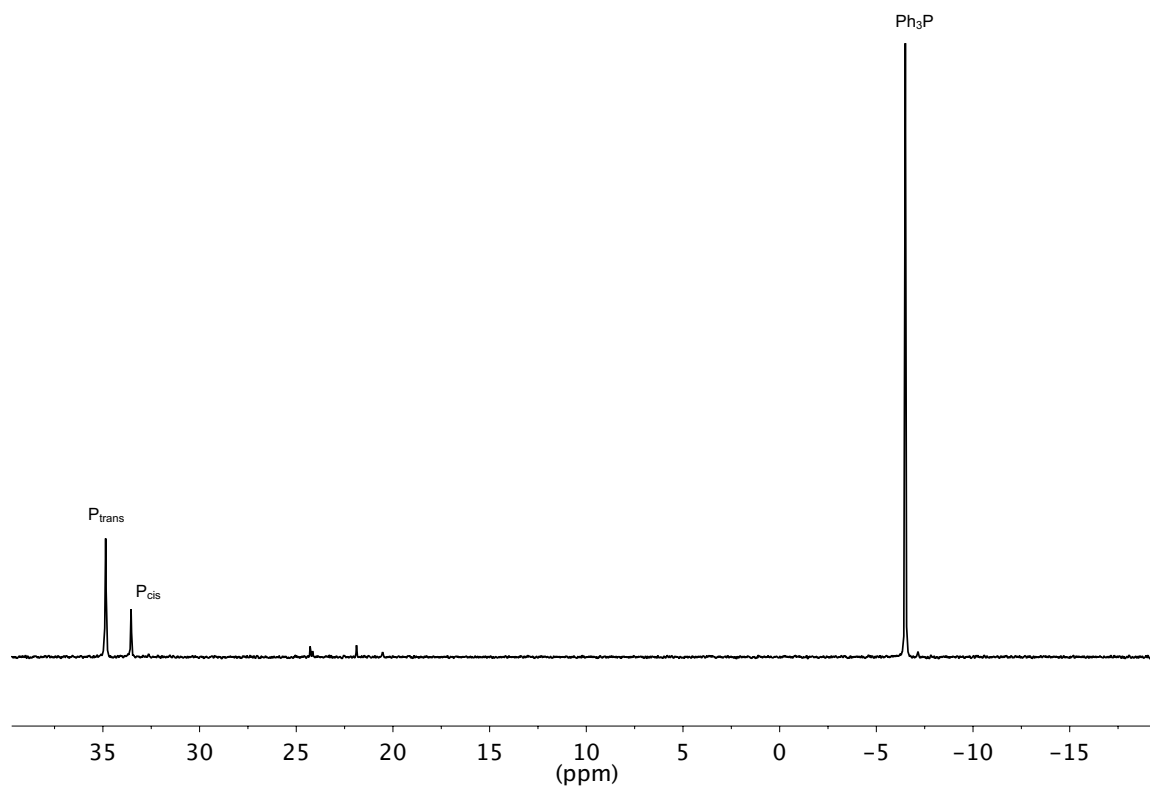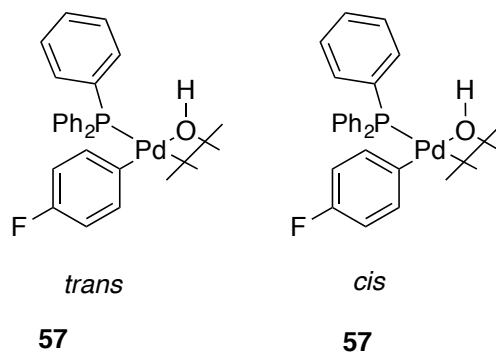
Figure 207. ^{31}P NMR spectrum of **57** at −55 °C, externally referenced to Ph$_3$P (−6.5 ppm).

Experiment 40: Preparation of *trans*-(*i*-Pr₃P)₂Pd(4-FC₆H₄)(OH) (70).
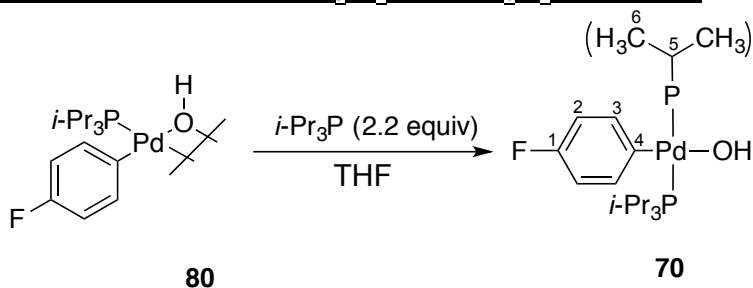
Compound **6** was synthesized by a modification of a procedure by Grushin and Alper *(51)*. A flame-dried, 25-mL, round-bottomed flask was charged with **17** (30 mg, 40 µmol, 1.0 equiv) and a magnetic stir bar. The vessel was taken into the dry box and *i*-Pr₃P (18 µL, 78 µmol, 2.2 equiv) was added followed by 3 mL of freshly-distilled, degassed THF. The flask was capped with a septum and the solution was stirred for 30 min, followed by solvent removal under reduced pressure. The tan solid was dissolved in 3 mL of pentane, capped and placed into the freezer at −27 °C. Colorless crystals were observed ~16 h later. The crystals were collected and washed with cold (−27 °C) pentane (2 mL) followed by drying under high vacuum (3 mm Hg) over night yielding 31.2 mg (72%) of compound **70** as colorless crystals.

Data for **70**:

^{1}H NMR: (600 MHz, THF-d_8)

7.35 (dd, ^3J(H-H) = 7 Hz, 2 HC(3)), 6.64 (dd, ^3J(H-H) = 7 Hz, 2 HC(2)), 3.60 (s, HO), 2.17 (m, 6 HC(5)), 1.23 (m, 36 HC(6))

^{13}C NMR: (151 MHz, THF-d_8)

161.90, 160.38 (d, ^1J(F-C) = 243 Hz, 1 C(1)), 148.07 (m, 1 C(4)), 140.81 (d, ^3J(F-C) = 5 Hz, 3 C(3)), 114.40, 114.29 (d, ^2J(F-C) = 17 Hz, 2 C(2)), 24.73 (t, J = 10 Hz, 6 C(5)), 20.82 (s, 12 C(6))

^{19}F NMR: (565 MHz, THF-d_8)

−124.68 (s, FC(1))

^{31}P NMR: (243 MHz, THF-d_8)

33.00 (s, 2 P(Pd))
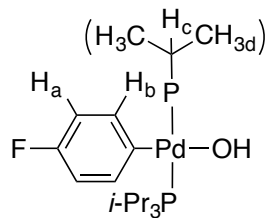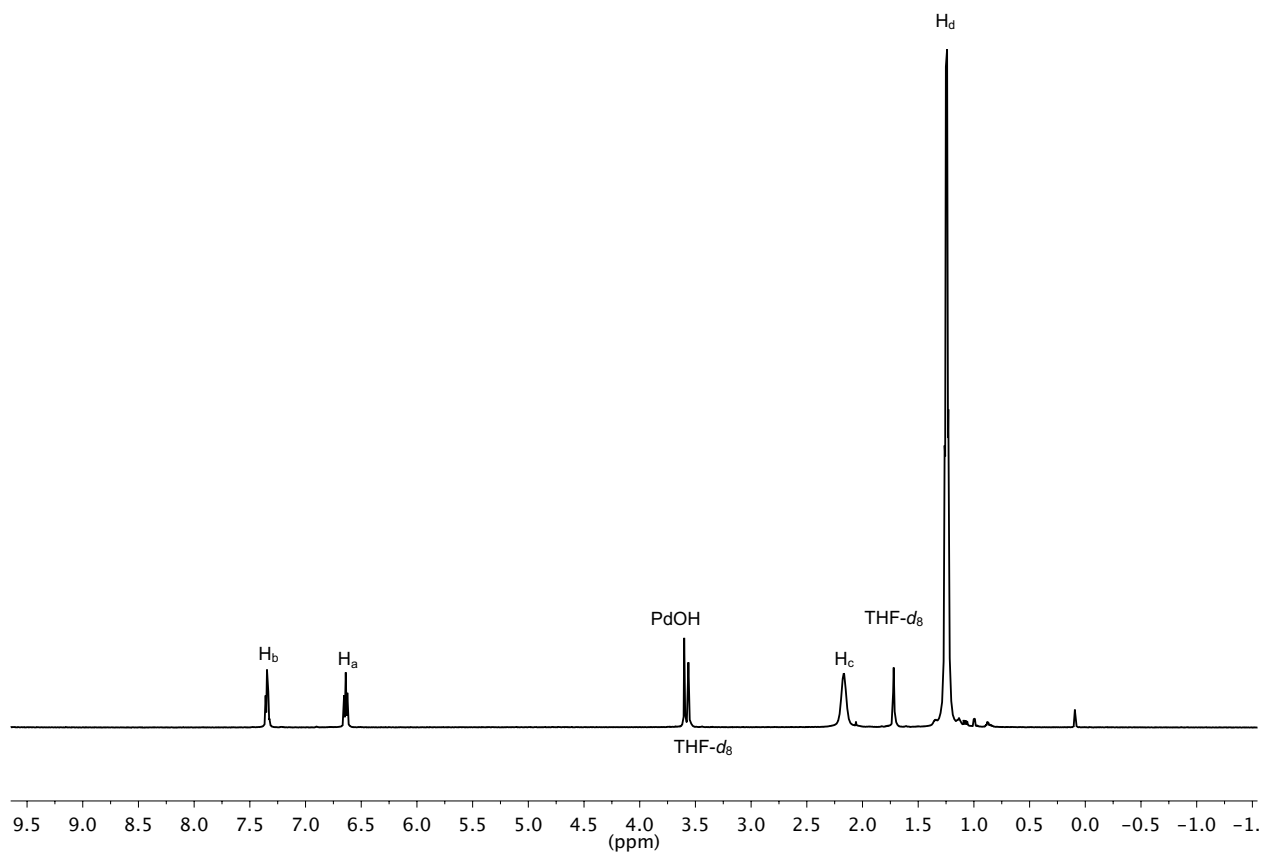
Figure 208. ^{1}H NMR spectrum of **70** at −30 °C, referenced to residual THF (1.72 ppm).
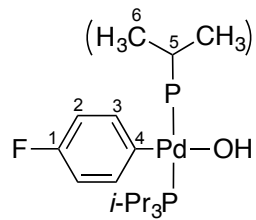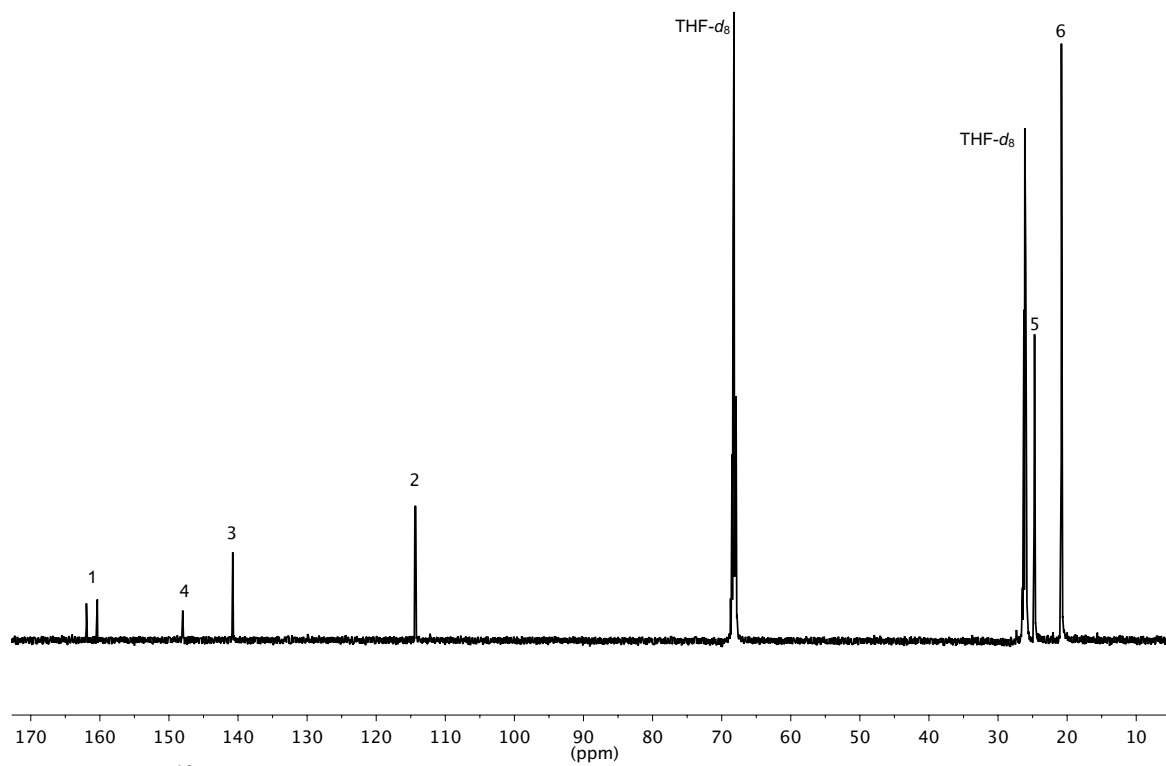
Figure 209. ^{13}C NMR spectrum of **70** at −30 °C, referenced to THF-d_8 (68.29 ppm).
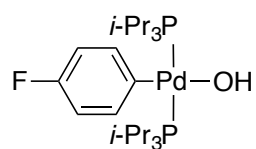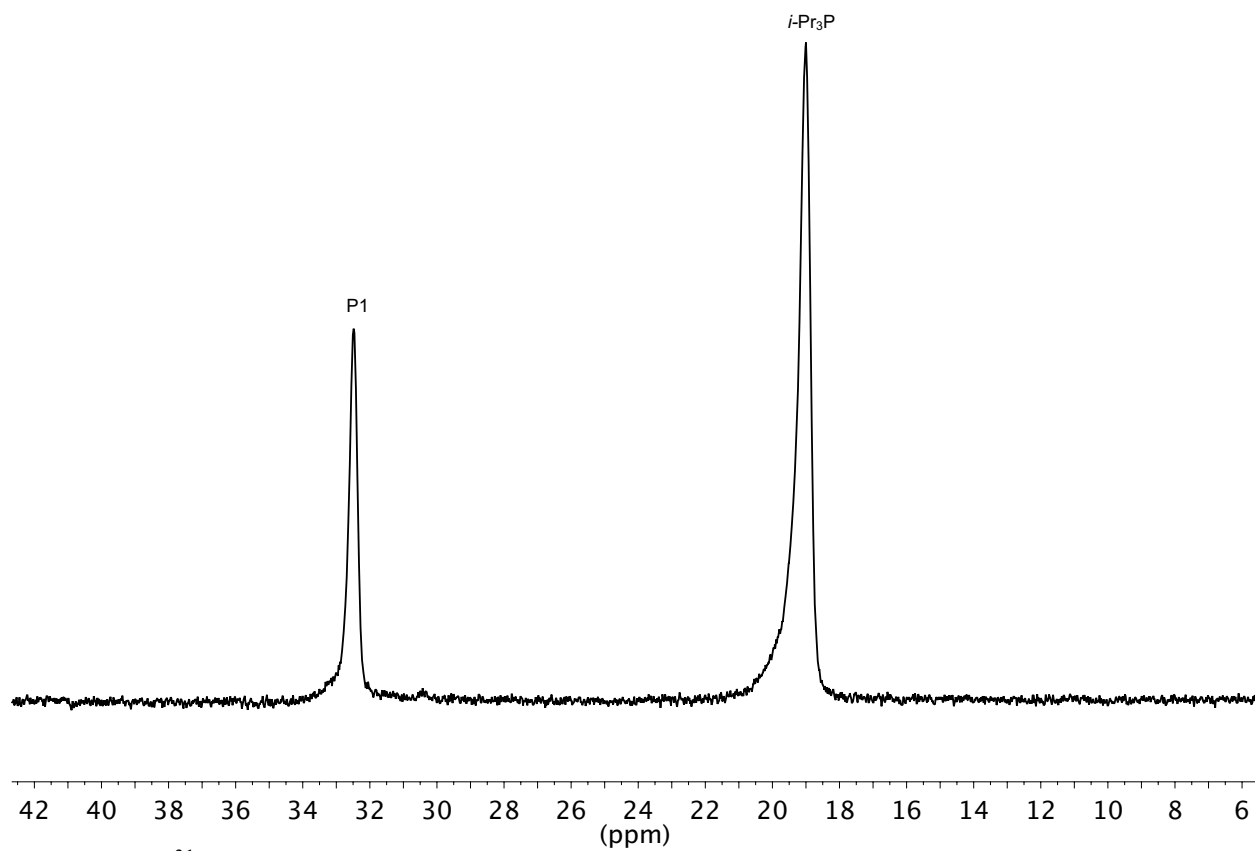
Figure 210. ^{31}P NMR spectrum of **70** at −30 °C, referenced to *i*-Pr$_3$P (19.00 ppm).
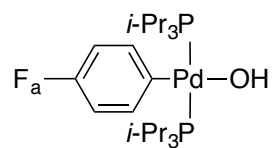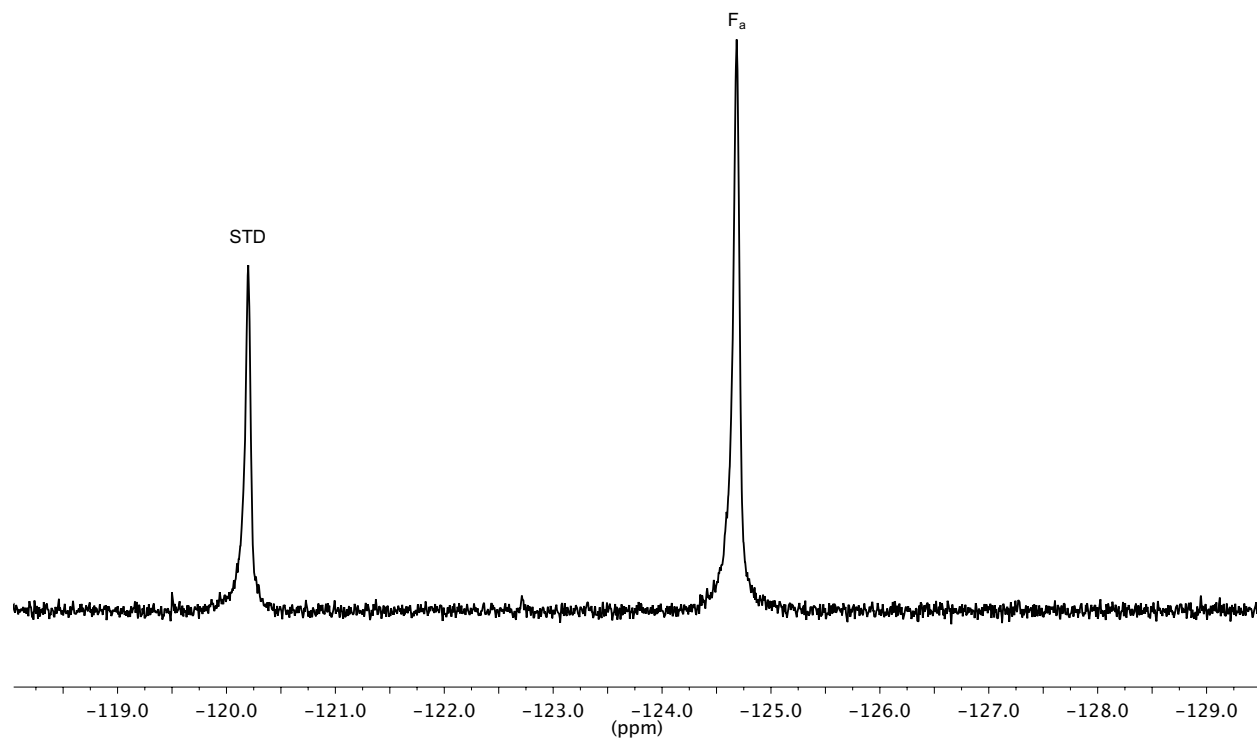
Figure 211. ¹⁹F NMR spectrum of **70** at −30 °C, externally referenced to 1,4-difluorobenzene (−120.00 ppm).

Experiment 41: Preparation of DPPF complex 109
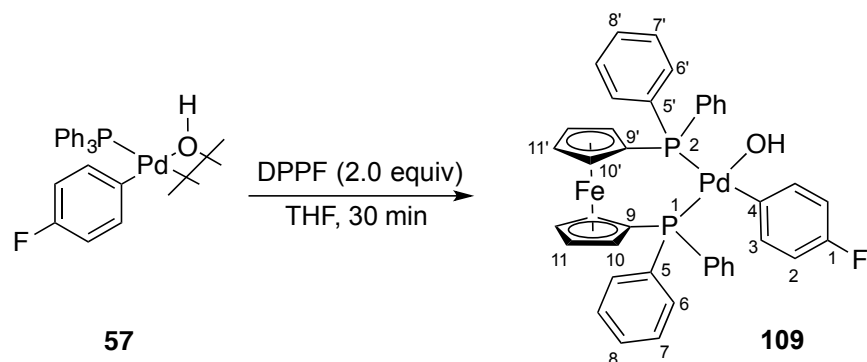
A flame dried, 25 mL Schlenk flask was charged with $[(Ph_3P)Pd(4\text{-}FC_6H_4)(\mu\text{-}OH)]_2$ (50 mg, 52 μmol, 1.0 equiv), DPPF (58 mg, 104 μmol, 2.0 equiv), stir bar and transferred into the glovebox. THF (5 mL) was added and the reaction was allowed to stir for 30 min. While stirring hexane (5 mL) was added *via* syringe and the vessel was capped with a septum and placed in the freezer (~12 h). Bright yellow crystals were observed which were collected on a glass frit and dried under high vacuum yielding 53 mg 66% of orange crystals.

Data for **109**:

^{1}H NMR: (600 MHz, THF-d_8)

8.29 (m, 4 HC(6')), 7.42 (m, 4 HC(7')), 7.39 (m, 4 HC(7)), 7.33 (m, 2 HC(8')), 7.30 (m, 2 HC(8)), 7.14 (m, 4 HC(6)), 6.93 (m, 2 HC(3)), 6.34 (m, 2 HC(2)), 4.68 (m, 2 HC(10)), 4.53 (m, 2 HC(11)), 4.28 (m, 2 HC(11')), 3.67 (m, 2 HC(10'), 0.45 (t, ^3J(P-C) = 7 Hz, OH)

^{13}C NMR: (151 MHz, THF-d_8)

162.52, 160.95 (d, ^1J(F-C) = 238 Hz, 1 C(1)), 160.90, 160.04 (dd, ^2J(P-C) = 132 and 9 Hz, 1 C(4)), 137.30 (m, 2 C(3)), 136.00 (m, 4 C(6')), 135.91 (m, 4 C(8 and 8')), 131.50 (m, 4 C(7')), 129.47 (m, 4 C(7)), 129.30 (m, 4 C(6)), 114.59 (m, 2 C(2)), 78.76, 78.49 (d, ^1J(P-C) = 42 Hz, 1 C(9)), 77.49, (m, 2 C(10)), 76.04 (m, 2 C(10')), 75.54, 75.27 (d, ^1J(P-C) = 39 Hz, 1 C(9')), 75.01 (m, 2 C(11)), 73.88 (m, 2 C((11')) [carbons 5 and 5' could not be determined]

^{19}F NMR: (565 MHz, THF-d_8)

−123.63 (s, FC(1))

<u>^{31}P NMR:</u>   (243 MHz, THF-d_8)

28.50, 28.35 (d, ^2J(P-P) = 30 Hz, 1 P(1)), 9.08, 8.83 (d, ^2J(P-P) = 30 Hz, 1 P(2))
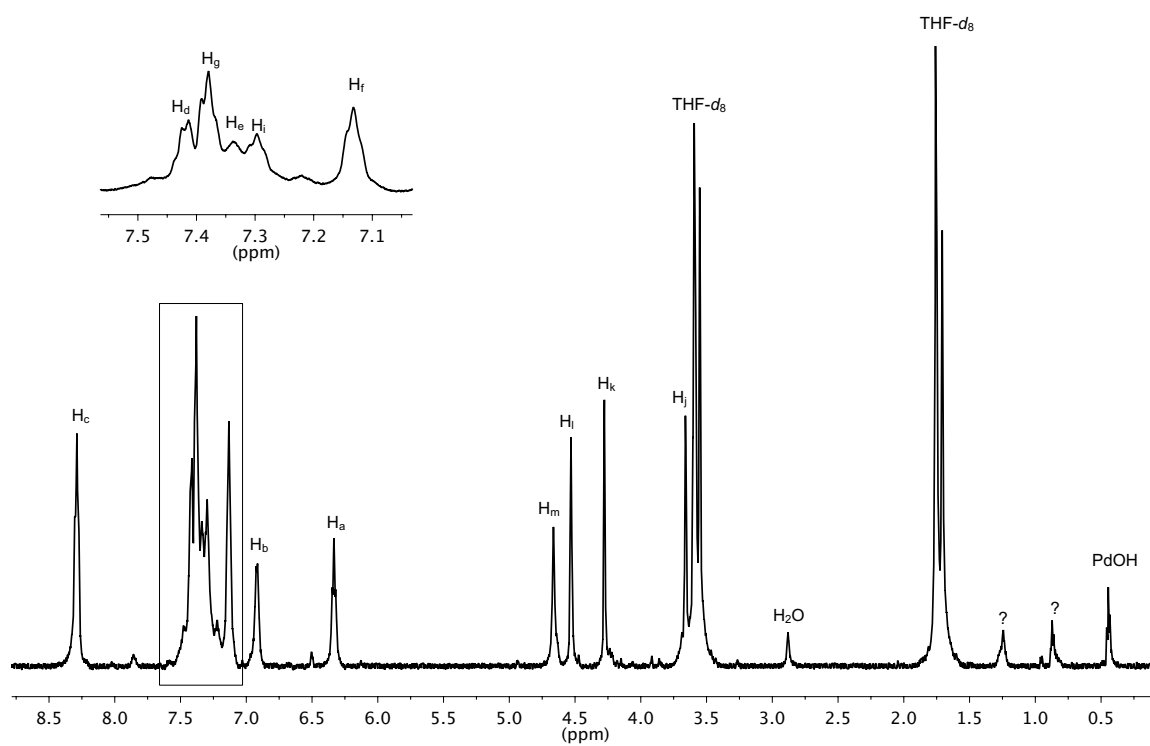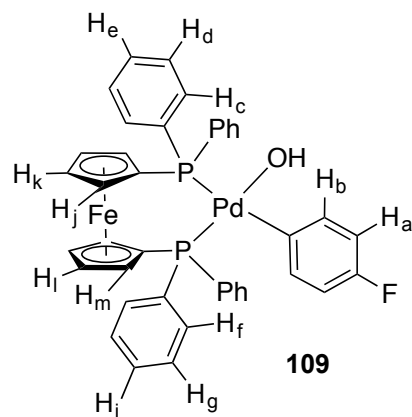
Figure 212. ^{1}H NMR spectrum of **109** at −55 °C, referenced to THF-d_8 (1.72 ppm).
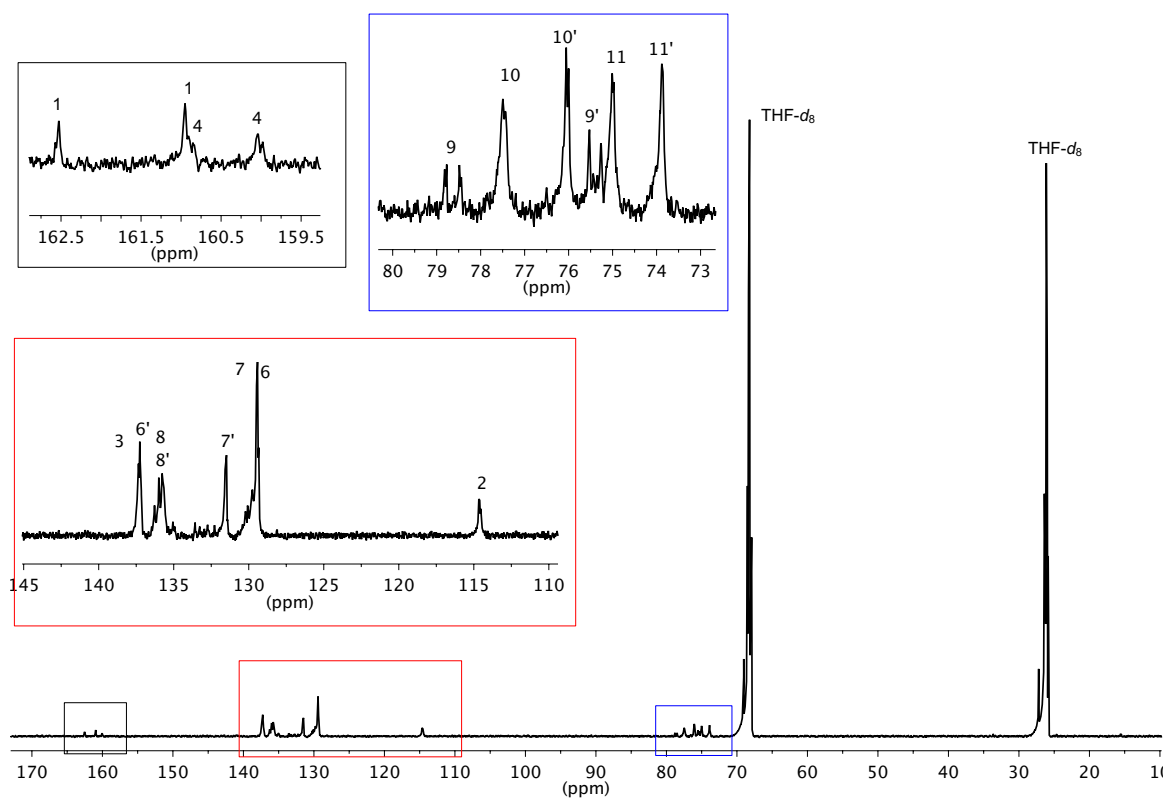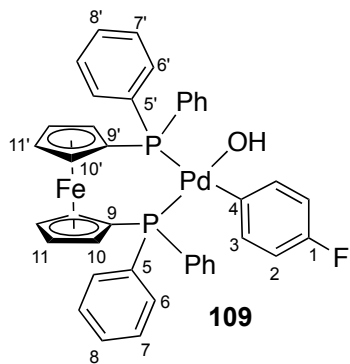
Figure 213. ^{13}C NMR spectrum of **109** at −55 °C, referenced to THF-d_8 (68.21 ppm).
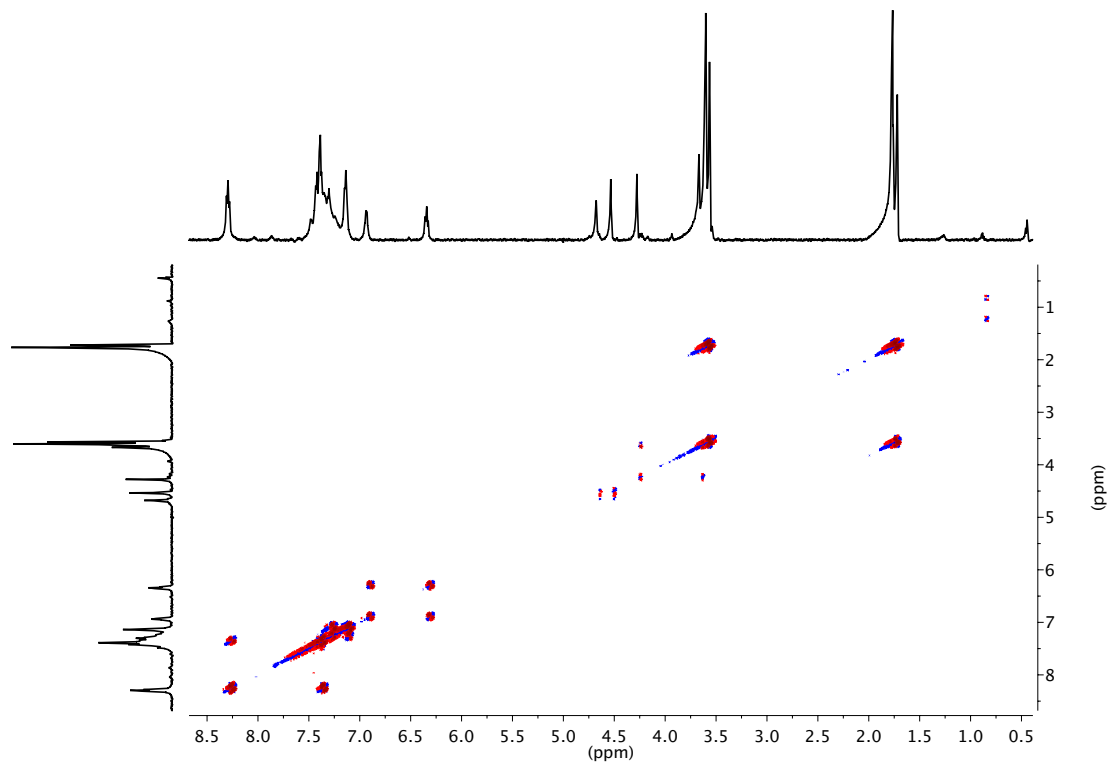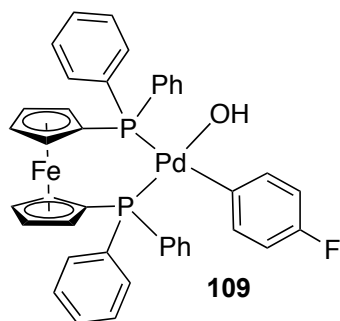
Figure 214. dqfCOSY spectrum of **109** at −55 °C, referenced to THF-d_8 (1.72 ppm).
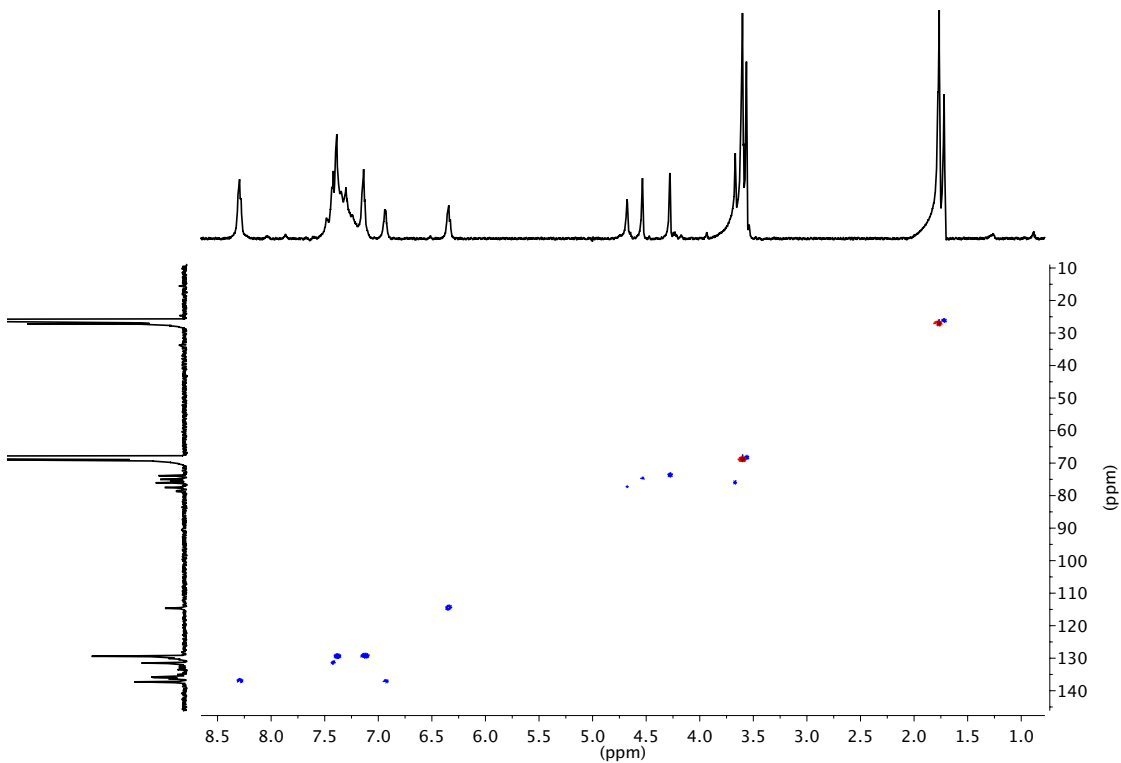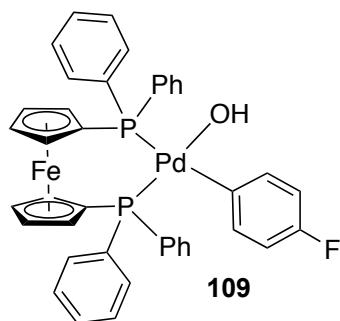
Figure 215. gHSQC spectrum of **109** at −55 °C, referenced to THF-d_8 (1.72 and 68.21 ppm).
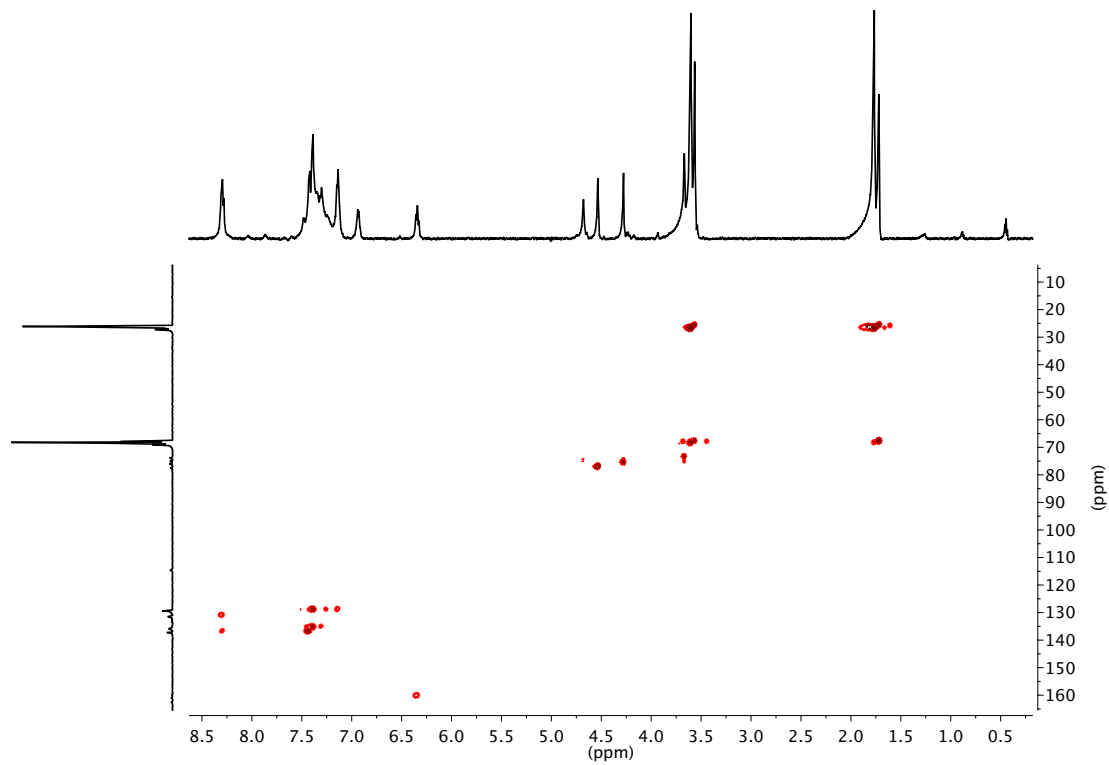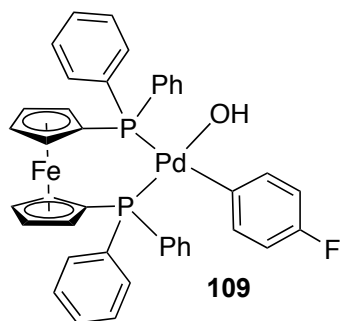
Figure 216. gHMBC spectrum of **109** at −55 °C, referenced to THF-d_8 (1.72 and 68.21 ppm).
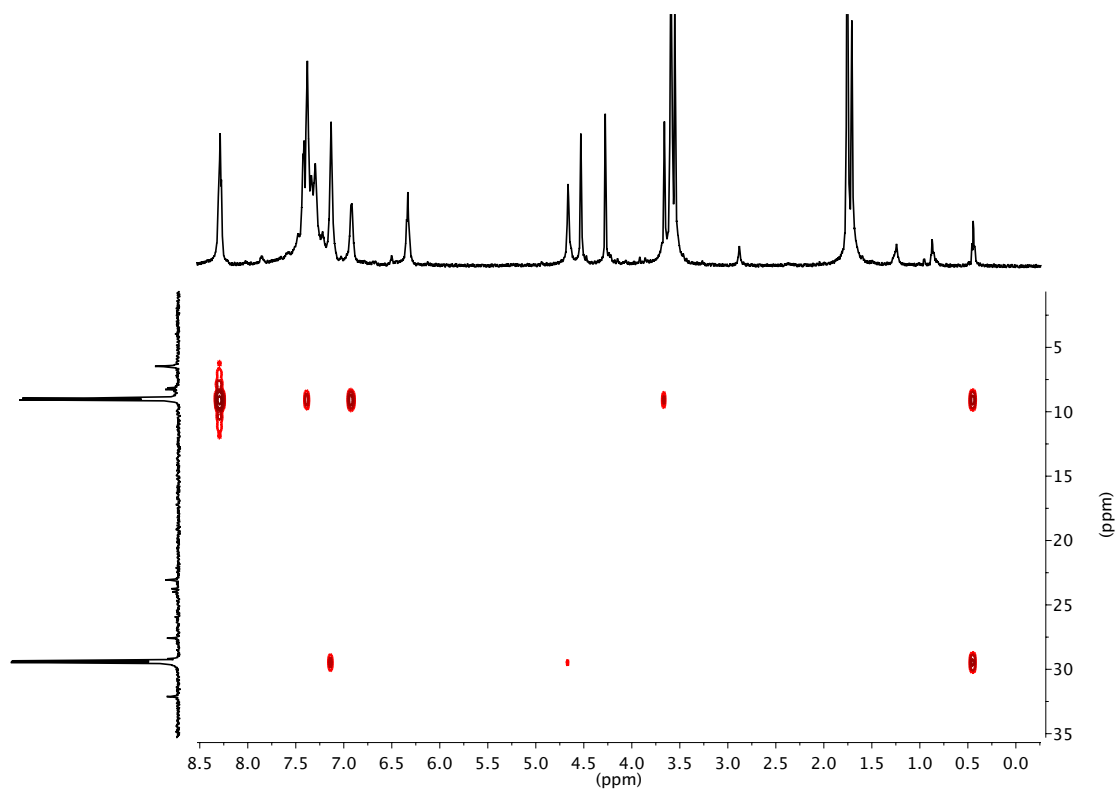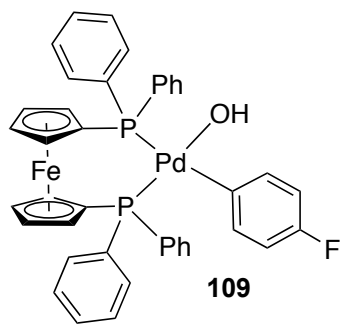
Figure 217. gHMBC (^{1}H-^{31}P) spectrum of **109** at −55 °C, referenced to THF-d_8 (1.72).
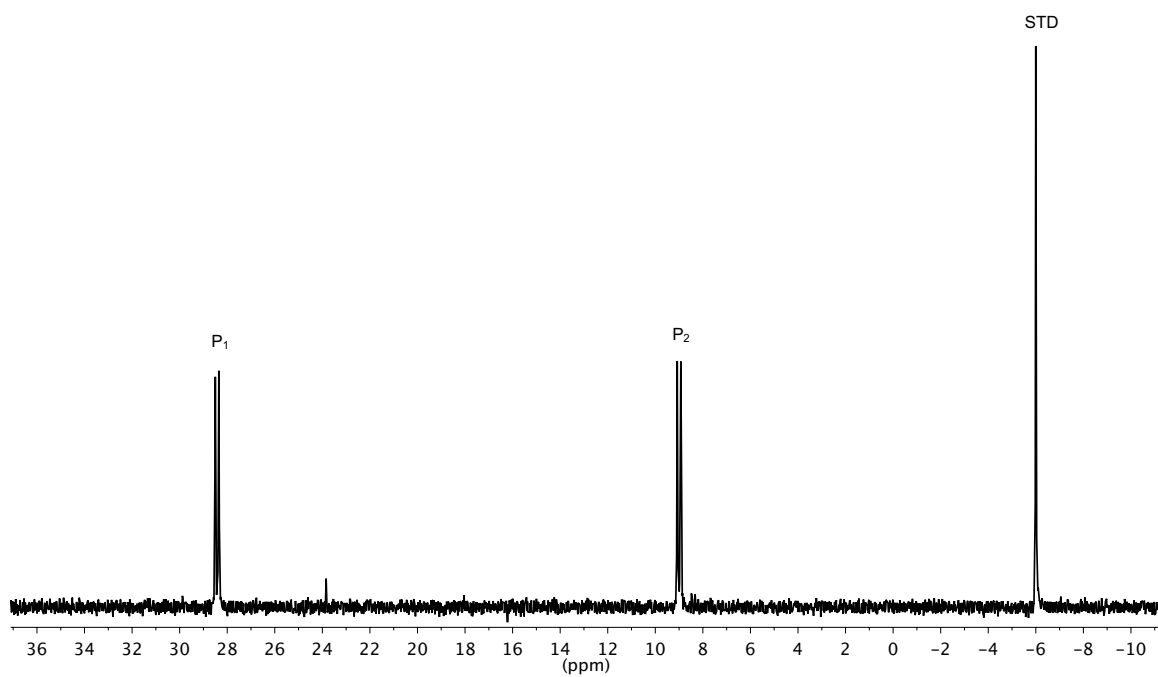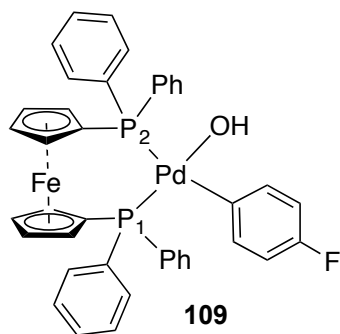
Figure 218. ^{31}P NMR spectrum of **109** at −55 °C, referenced to Ph$_3$P (−6.00 ppm).
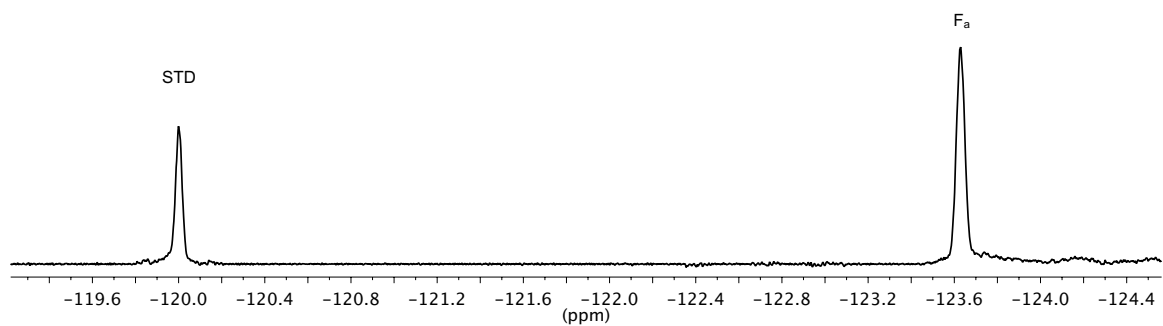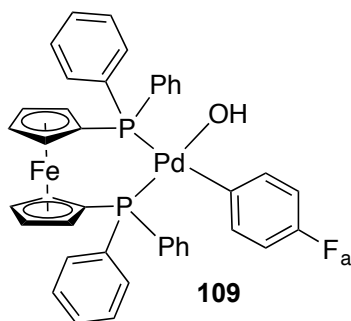
Figure 219. ^{19}F NMR spectrum of **109** at −55 °C, referenced to 1,4-difluorobenzene (−120.00 ppm).

Experiment 42: Preparation of [(*i*-Pr₃P)Pd(4-FC₆H₄)(μ-I)]₂ (90)
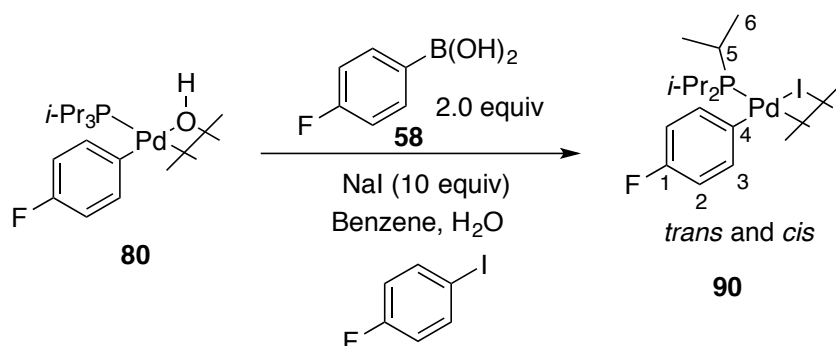
A 2-dram vial was charged with 4-fluorophenylboroxine (16 mg, 44 μmol 1.0 equiv), H₂O (3 μL, 132 μmol, 3.0 equiv) and ~1 mL of THF.

A 25-mL, flame dried Schlenk flask was charged with a magnetic stir bar, [(*i*-Pr₃P)Pd(4-FC₆H₄)(μ-OH)]₂ (80 mg, 0.106 mmol, 1.0 equiv) and NaI (0.159 g, 1.06 mmol, 10 equiv). The flask was fitted with a septum and purged with argon for 5 min followed by addition of 5 mL of benzene, 4-fluoroiodobenzene (2 mL, 17.4 mmol, 164 equiv) and 2 mL of degassed H₂O. The mixture was degassed for ~5 min followed by the addition of the 4-fluorophenylboronic acid solution at once. The mixture was stirred vigorously for 1 h at 50 °C, during which time the reaction mixture turned from colorless to deep red. After 1 h, the benzene layer was separated and filtered through glass wool followed by benzene removal *via* rotary-evaporation (30 mm Hg, 30 °C). The remaining liquid was charged with 10 mL of hexanes and placed in the freezer overnight yielding a red-brown precipitate. The solid was collected on a glass frit followed by recrystallization with dichloromethane/hexanes affording a red microcrystalline solid (46 mg, 45%). The compound was found to exist as *trans* and *cis* isomers (55:445) in solution. The ^{1}H and ^{13}C chemicals shifts are indistinguishable.

Data for **90**:

^{1}H NMR: (600 MHz, THF-d_8)

7.35 (m, 2 HC(3)), 6.66 (m, 2 HC(2)), 2.22 (m. 3 HC(5)), 1.31 (m. 6 HC(18))

^{13}C NMR: (151 MHz, THF-d_8)

162.84, 161.26 (d, ^1J(F-C) = 244 Hz, 2 C(1)), 146.67 (m, 2 C(4)), 139.13, (m, 6 C(3)), 115.25, 115.13 (d, ^1J(F-C) = 20 Hz, 4 C(2)), 27.64 (m, 6 C(5)), 21.17 (m, 12 C(6))

^{19}F NMR: (565 MHz, THF-d_8)

−123.15 *(cis)* (s, FC(1)) and −123.25 *(trans)* (s, FC(1))

<u>^{31}P NMR:</u>   (243 MHz, THF-d_8)

  43.99 *(trans)* (s, P(Pd)) and 41.29 *(cis)* (s, P(Pd))
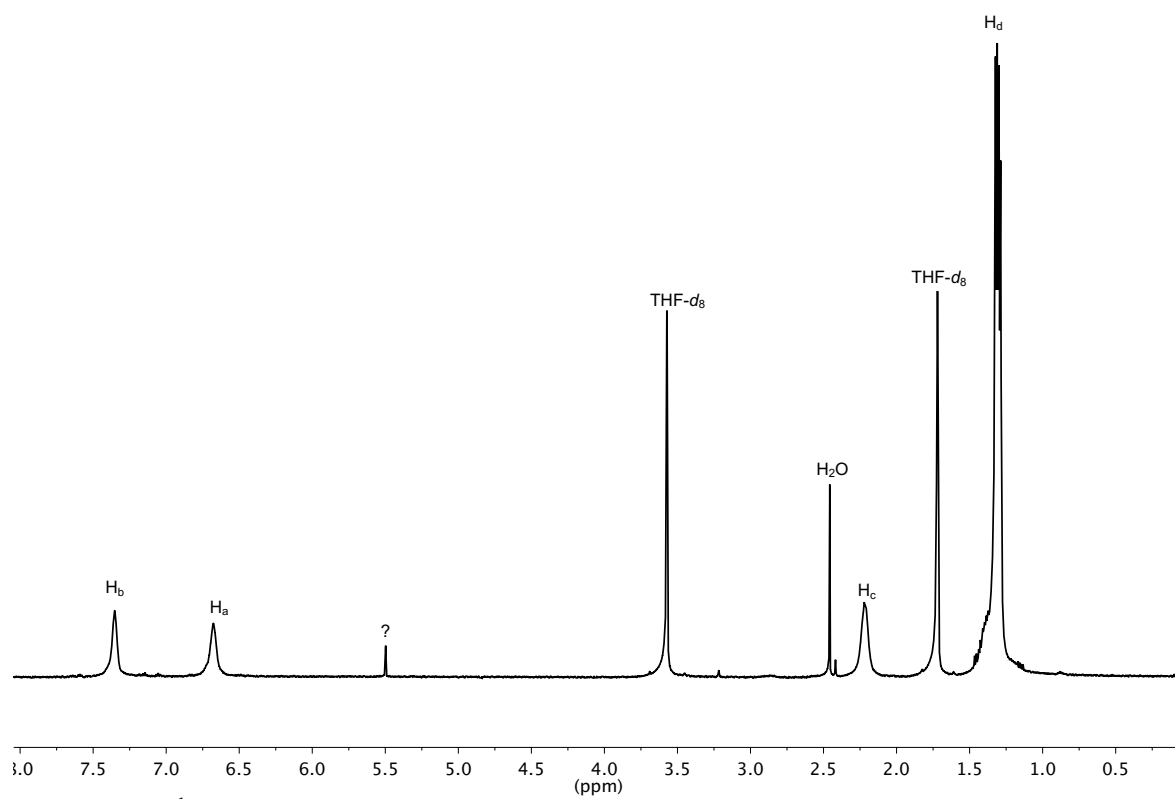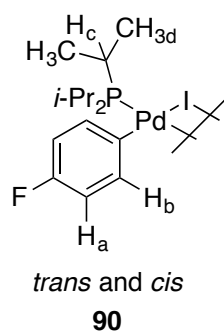
Figure 220. ^{1}H NMR spectrum of **90** at -30 °C, referenced to THF-d_8 (1.72 ppm).

315
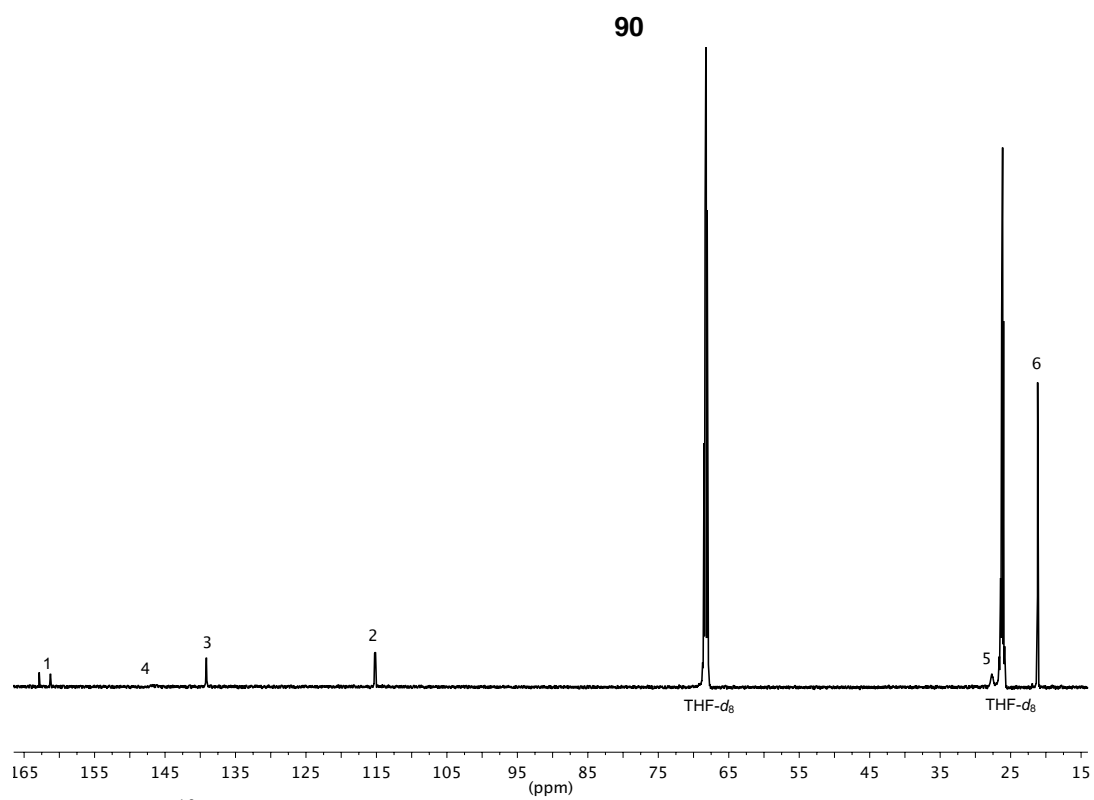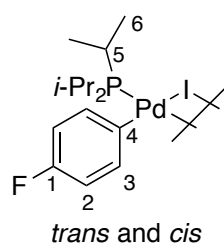
Figure 221. ^{13}C NMR spectrum of **90** at $-30\ °C$, referenced to THF-d_8 (68.21 ppm).
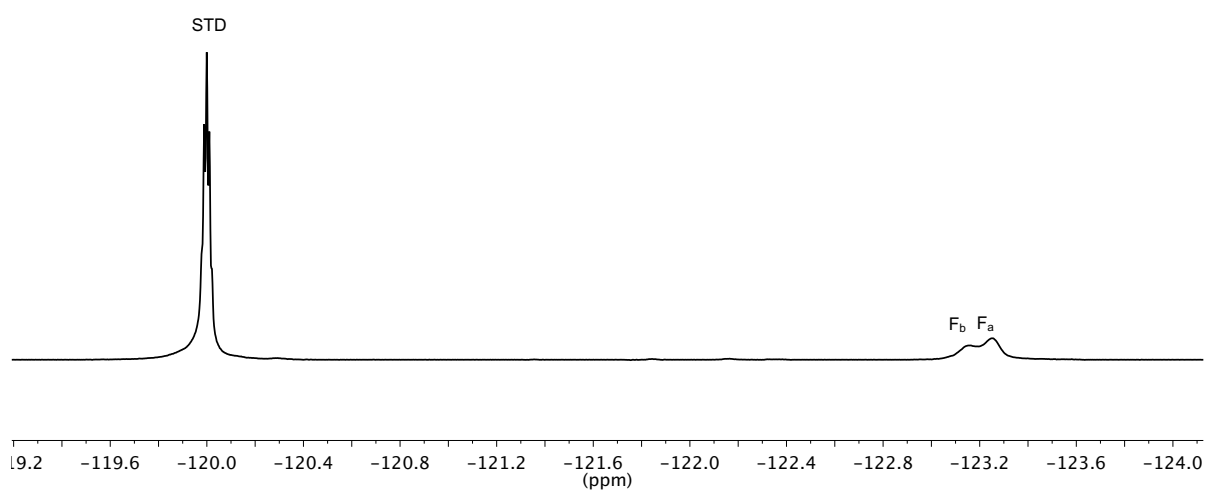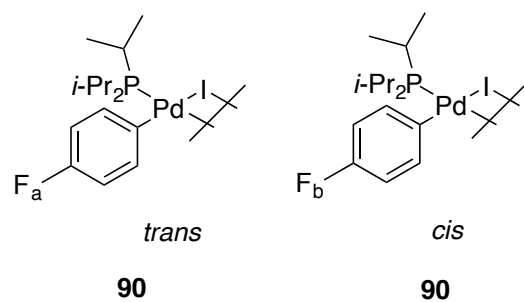
Figure 222. ^{19}F NMR spectrum of **90** at −30 °C, referenced to 1,4-difluorobenzene (−120.00 ppm).
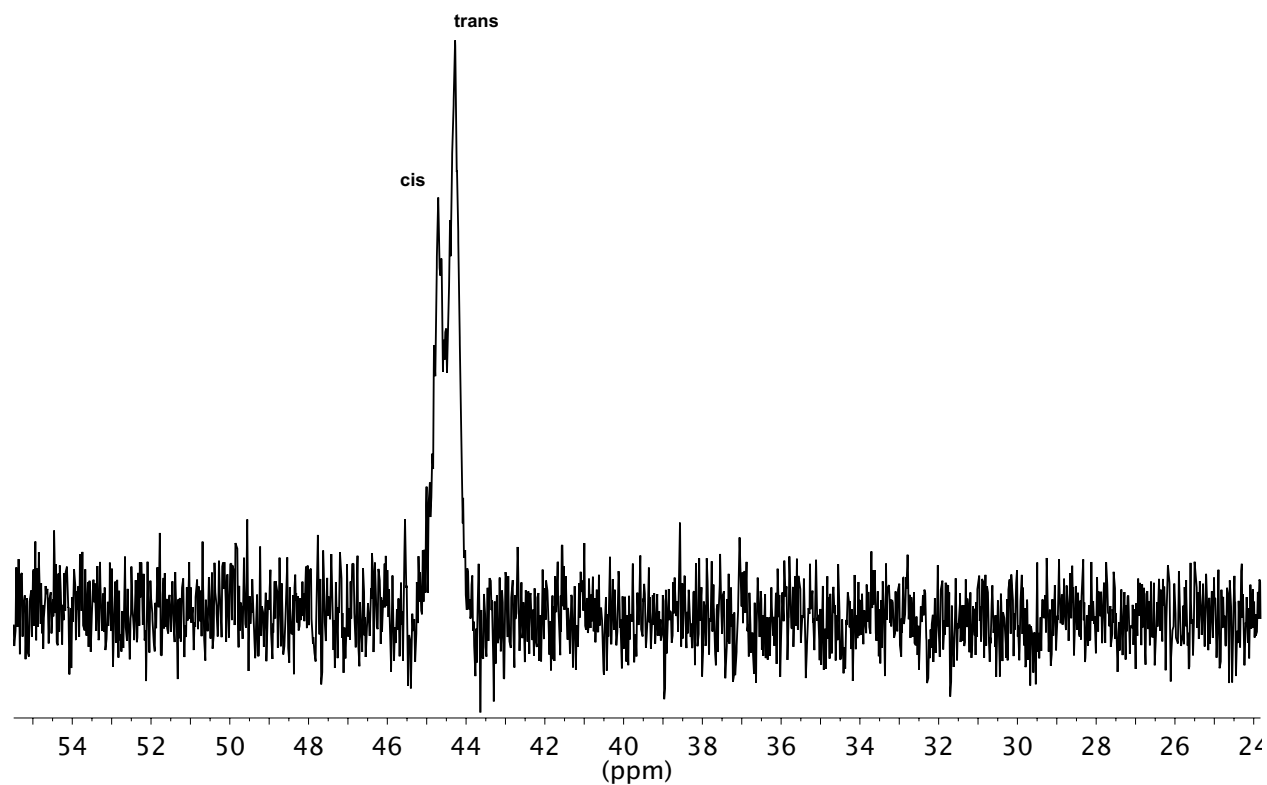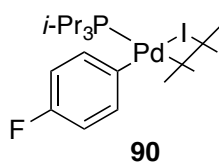
Figure 223. ^{31}P NMR spectrum of **90** at −30 °C, externally referenced to i-Pr$_3$P (19.00 ppm).

Experiment 43: Preparation of *trans*-(*i*-Pr₃P)₂Pd(4-FC₆H₄)(I) (76)
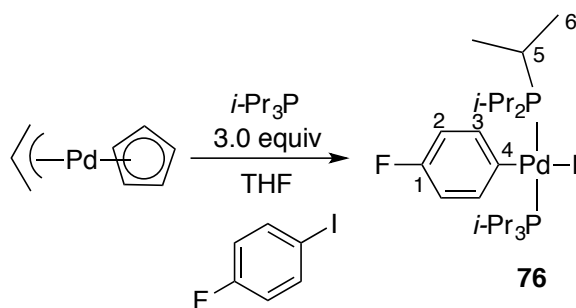
Inside the glove box an 25-mL, oven dried round bottom flask was charged with a magnetic stir bar, allylCpPd (0.212 g, 1 mmol, 1.0 equiv) and 10 mL of THF. Once stirring was started *i*-Pr₃P (0.483 g, 3 mmol, 3.0 equiv) was added at once *via* syringe. It was allowed to stir for ~5 min followed by the addition of 4-fluoroiodobenzene (2 mL, 17.4 mmol, 17.4 equiv) at once. The deep red solution turned to a light orange color after ~30 s. The reaction was allowed to stir overnight (~15 h). The following day the THF was removed under reduced pressure. The flask was removed from the glove box and pentane (~10 mL) was added followed by placement for ~2 h in an acetone bath cooled to −35 °C, yielding yellow crystals (0.416 g, 64%).

Data for **76**:

^{1}H NMR: (600 MHz, THF-d_8)

7.36 (m, 2 HC(3)), 6.76 (m, 2 HC(2)), 2.49 (m. 6 HC(5)), 1.24 (m. 36 HC(6))

^{13}C NMR: (151 MHz, THF-d_8)

163.03, 161.42 (d, ^1J(F-C) = 242 Hz, 2 C(1)), 145.49 (m, 2 C(4)), 141.10, (m, 6 C(3)), 115.18, 115.06 (d, ^1J(F-C) = 18 Hz, 4 C(2)), 27.86 (t, J(P-C) = 10 Hz, 6 C(5)), 21.58 (m, 12 C(6))

^{19}F NMR: (565 MHz, THF-d_8)

−122.52 (s, FC(1))

^{31}P NMR: (243 MHz, THF-d_8)

30.36 (s, P(Pd))
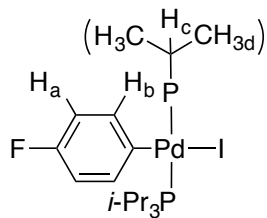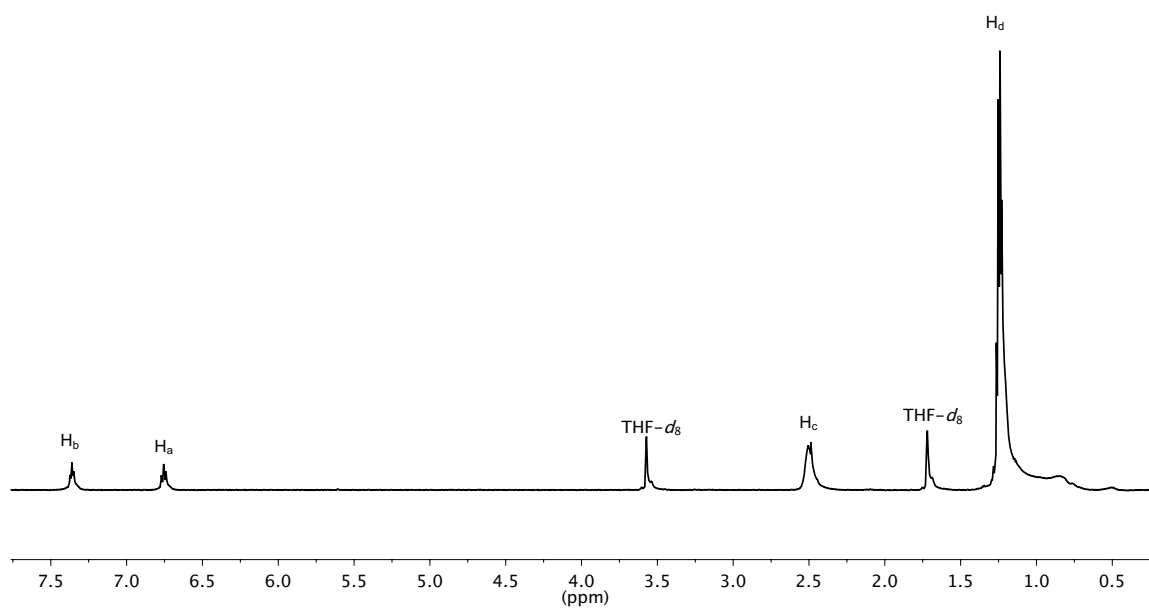
Figure 224. ¹H NMR spectrum of **76** at −30 °C, referenced to THF-d_8 (1.72 ppm).
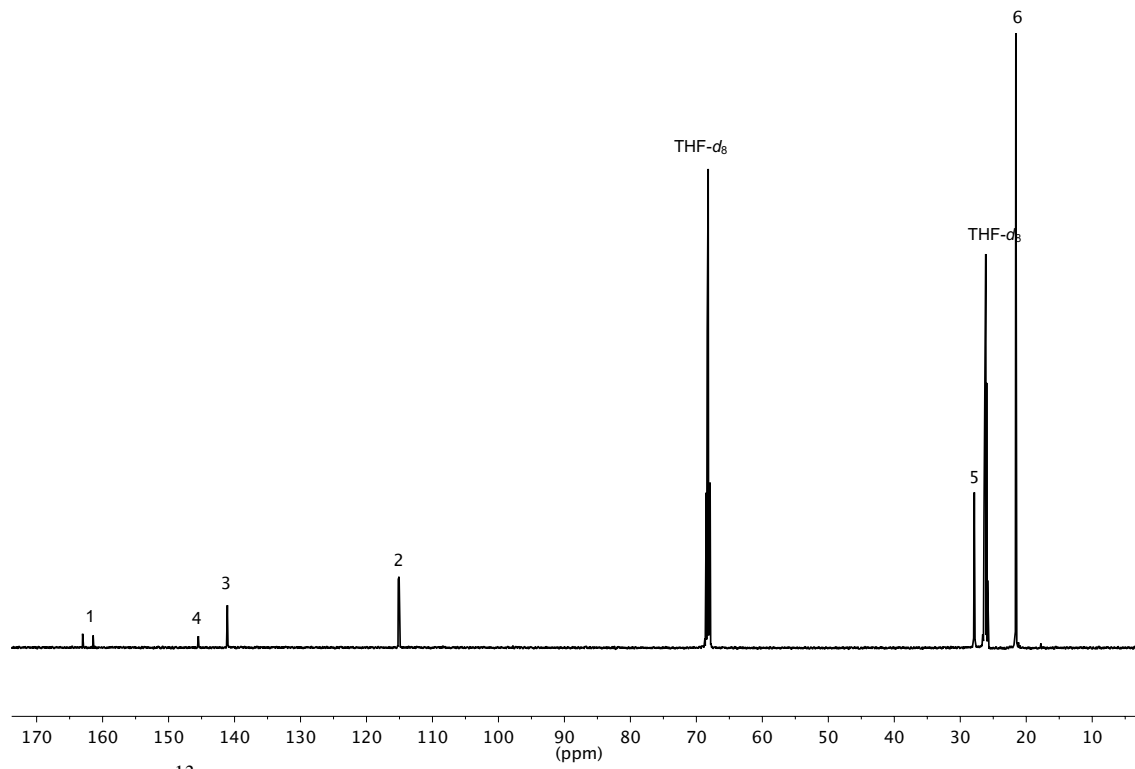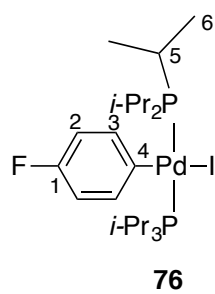
Figure 225. ^{13}C NMR spectrum of **76** at −30 °C, referenced to THF-d_8 (68.21 ppm).
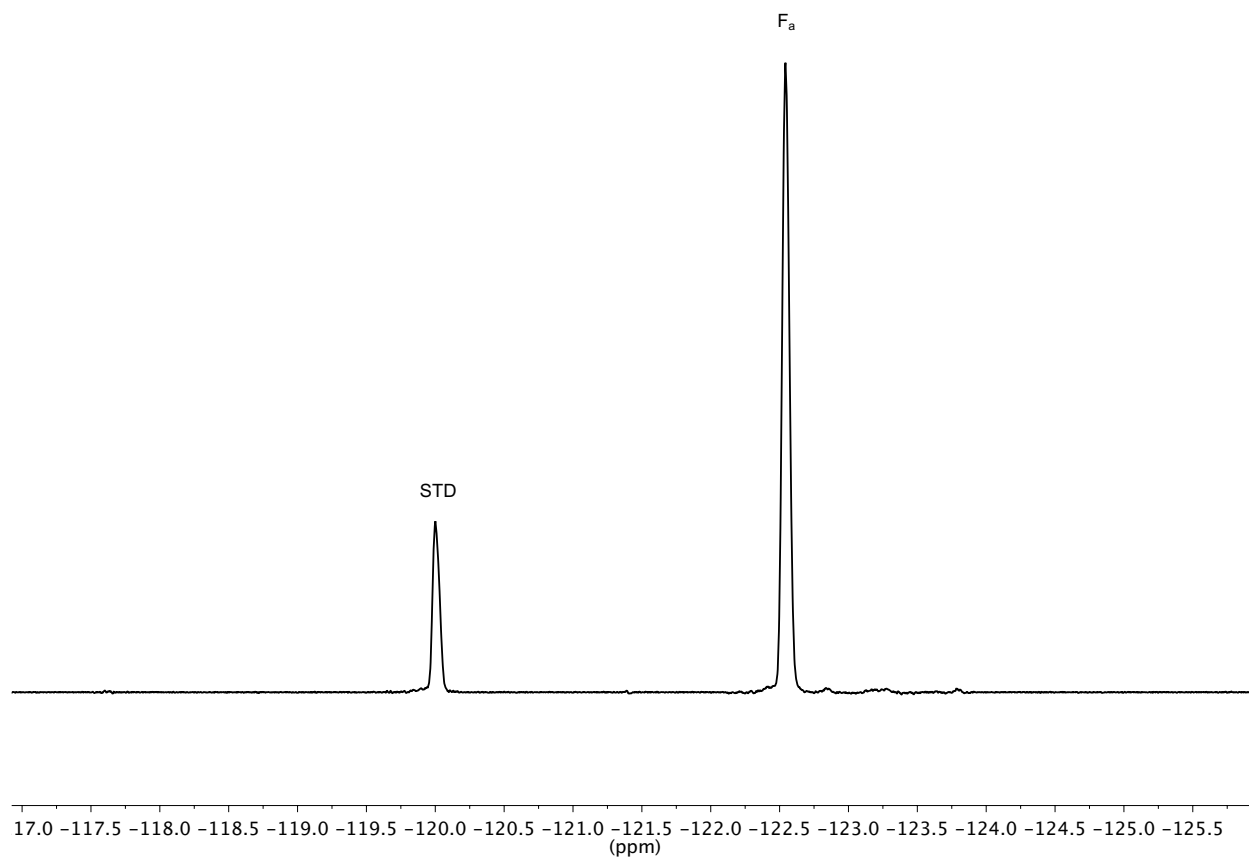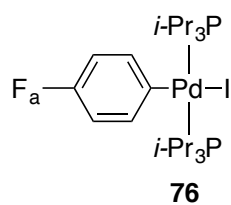
Figure 226. ^{19}F NMR spectrum of **76** at $-30\ °C$, referenced to 1,4-difluorobenzene $(-120.00\ ppm)$.
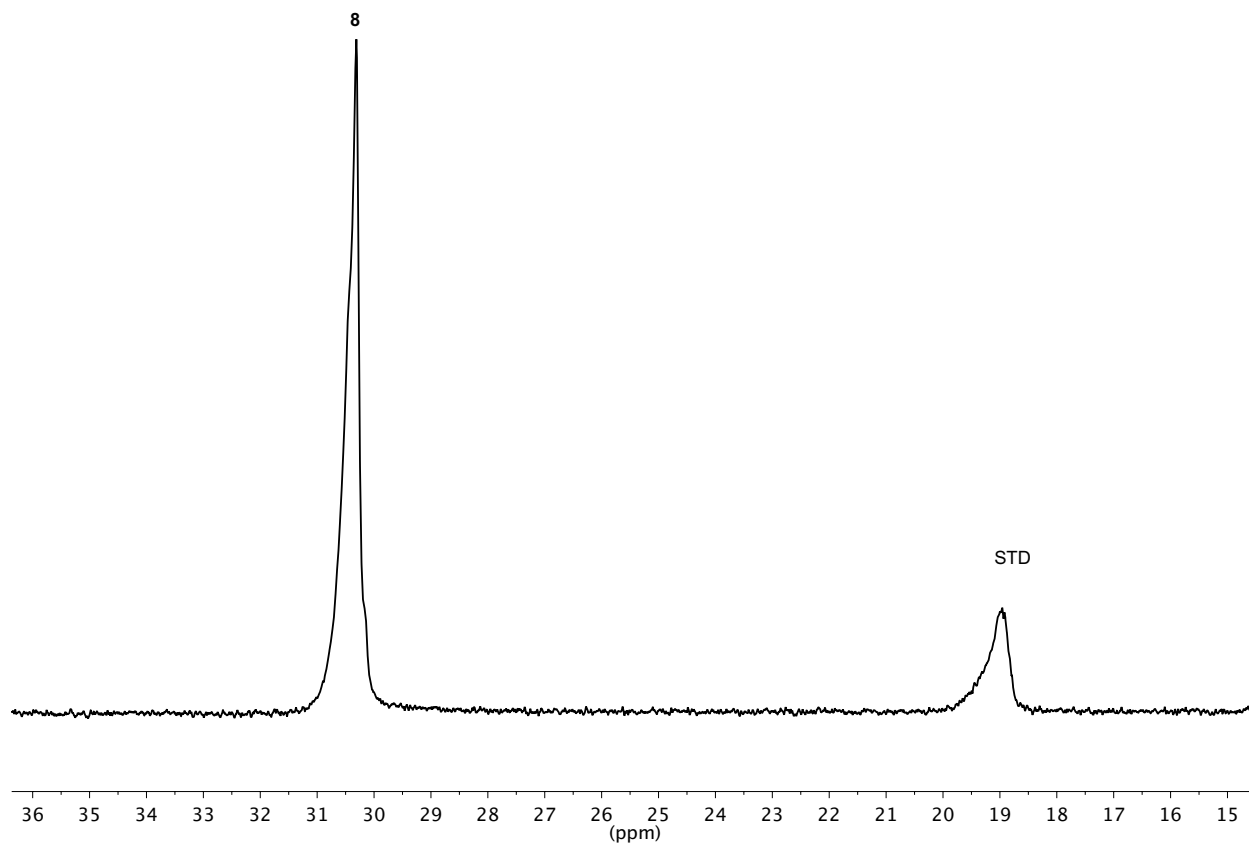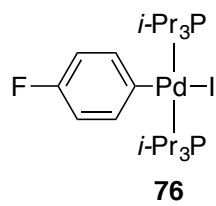
Figure 227. ^{31}P NMR spectrum of **76** at $-30\ ^\circ C$, referenced to i-Pr_3P (19.00 ppm).

323

Experiment 44: Formation of cross-coupling product 73 and (*i*-Pr₃P)₂Pd.
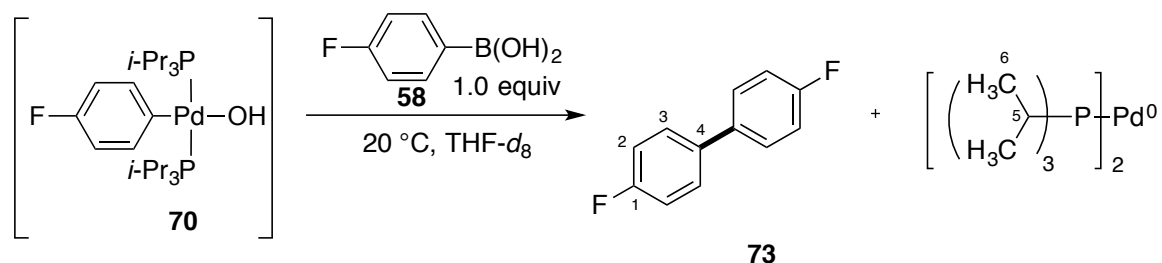
A flame-dried, 2-dram vial was charged with 4-fluorophenylboroxine (2.5 mg, 6.8 μmol, 0.68 equiv), and H₂O (0.4 μL, 22 μmol, 1.1 equiv) followed by dissolving with THF-d_8 (100 μL, Na/K distilled).

An oven dried, 5-mm, NMR tube was taken into the glove box and charged with [(*i*-Pr₃P)Pd(4-FC₆H₄)(μ-OH)]₂ (7.58 mg, 10.0 μmol, 1.0 equiv), and *i*-Pr₃P (3.8 μL, 20 μmol, 2.0 equiv) followed by THF-d_8 (500 μL, NaK distilled). The tube was capped with a septum and Teflon taped and shaken until the solid had dissolved. Then 4-fluorophenylboronic acid (100 μL, 20 μmol) was added *via* a μL glass syringe. The NMR tube was shaken and wiped with a Kimwipe and placed into the NMR probe set to 20 °C. The reaction was allowed to take place over ~10 min, followed by the collection of spectra at −30 °C. (1,4-Difluorobenzene (0.1 μL) was added at the end of the experiment to obtain a referenced fluorine spectrum.)

Data for **73**:

^{1}H NMR: (600 MHz, THF-d_8)

7.65 (m, 4 HC(3)), 7.21 (dd, ^4J(F-H) = 9 Hz, 4 HC(2)),

^{13}C NMR: (151 MHz, THF-d_8)

165.41, 163.41 (d, ^1J(F-C) = 238 Hz, 2 C(1)), 138.05. 138.03 (d, ^1J(F-C) = 3 Hz, 2 C(4)), 130.39, 130.33 (d, ^1J(F-C) = 8 Hz, 4 C(3)), 117.36, 117.21 (d, ^1J(F-C) = 21 Hz, 4 C(2))

^{19}F NMR: (565 MHz, THF-d_8)

−116.45 (s, FC(1))

Data for (*i*-Pr₃P)₂Pd:

^{1}H NMR: (600 MHz, THF-d_8)

1.90 (m, 6 HC(5)), 1.20 m, 36 HC(6))

<u>13C NMR:</u>   (151 MHz, THF-d_8)

25.61, (t, J(P-C) = 6 Hz, 6 C(5)), 17.66, (m, 12 C(6)),

<u>31P NMR:</u>   (243 MHz, THF-d_8)

53.43 (s, 2 P(Pd))
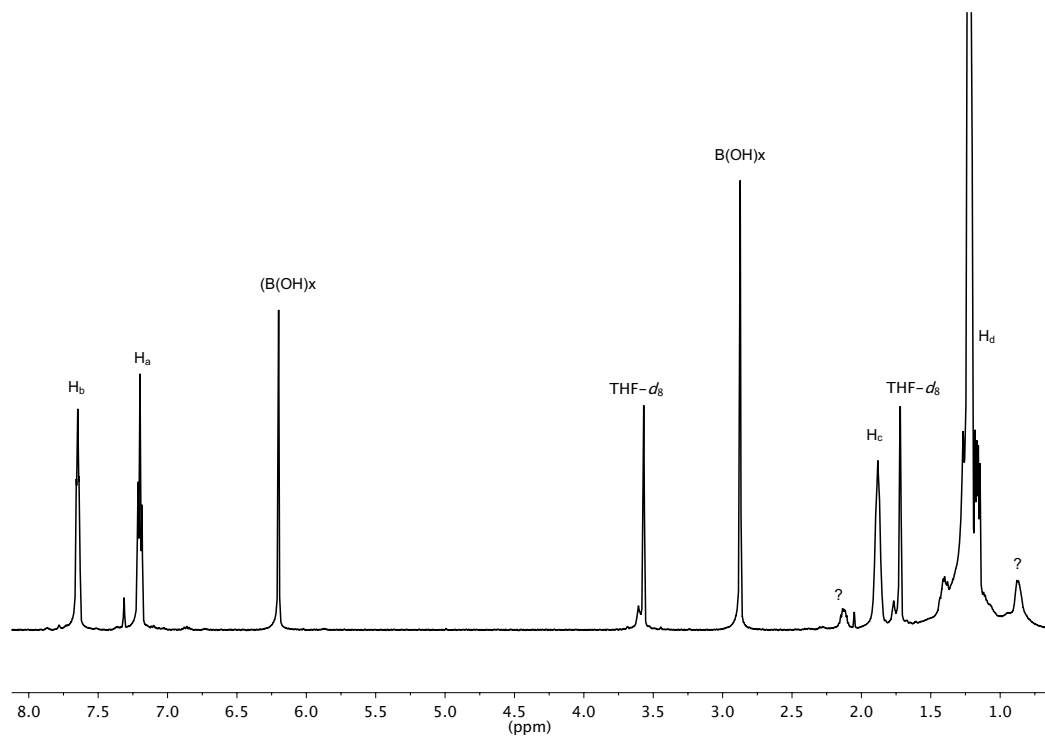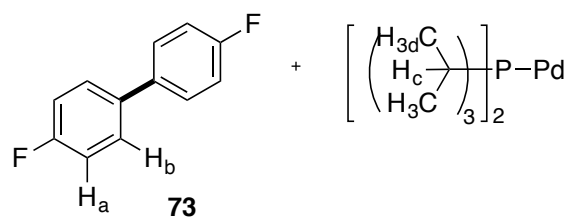
Figure 228. ^{1}H NMR spectrum of **73** and 1.0 equiv of [*i*-Pr$_3$P]$_2$Pd^0 at −30 °C, referenced to THF-d_8 (1.72 ppm).
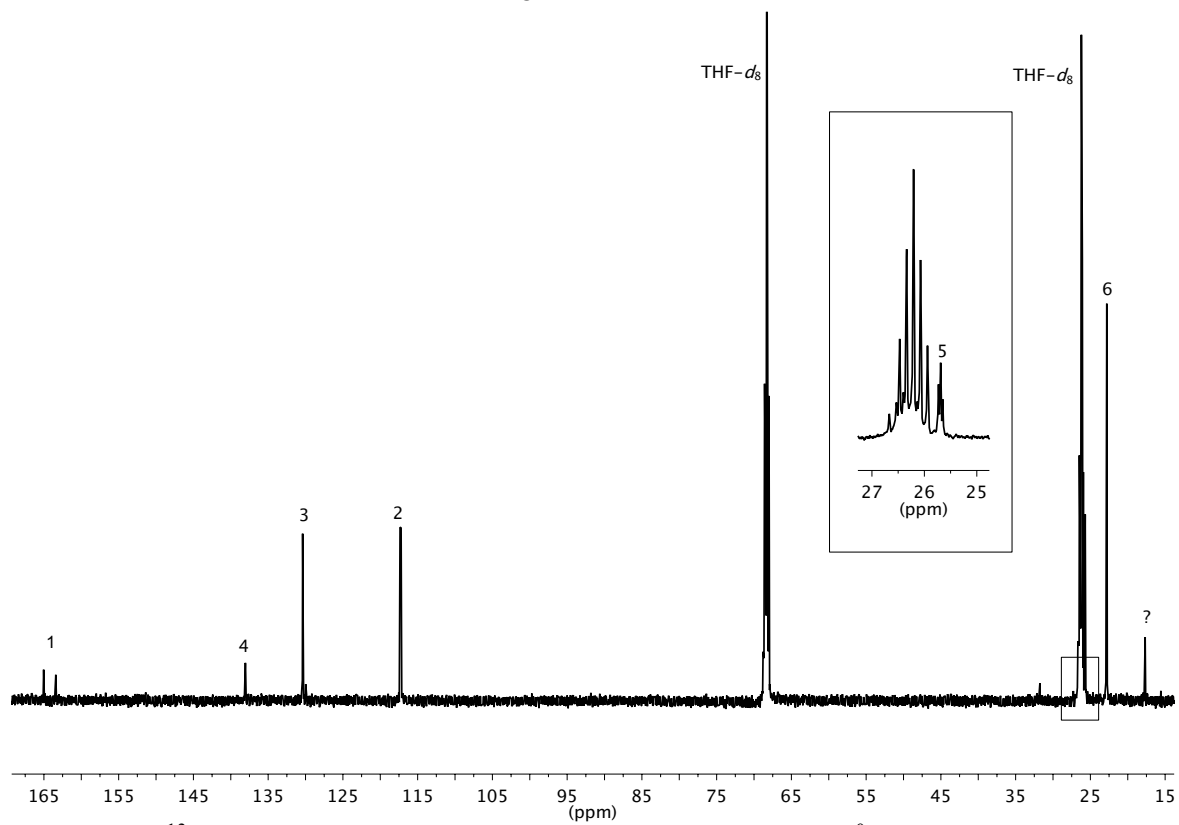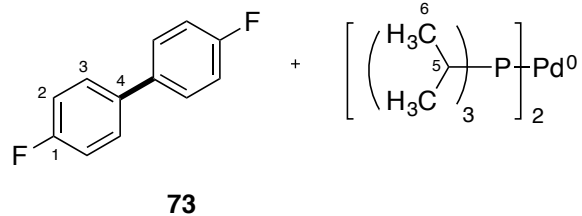
Figure 229. ^{13}C NMR spectrum of **73** and 1.0 equiv of $[i\text{-Pr}_3\text{P}]_2\text{Pd}^0$ at $-30\ °\text{C}$, referenced to THF-d_8 (68.21 ppm).
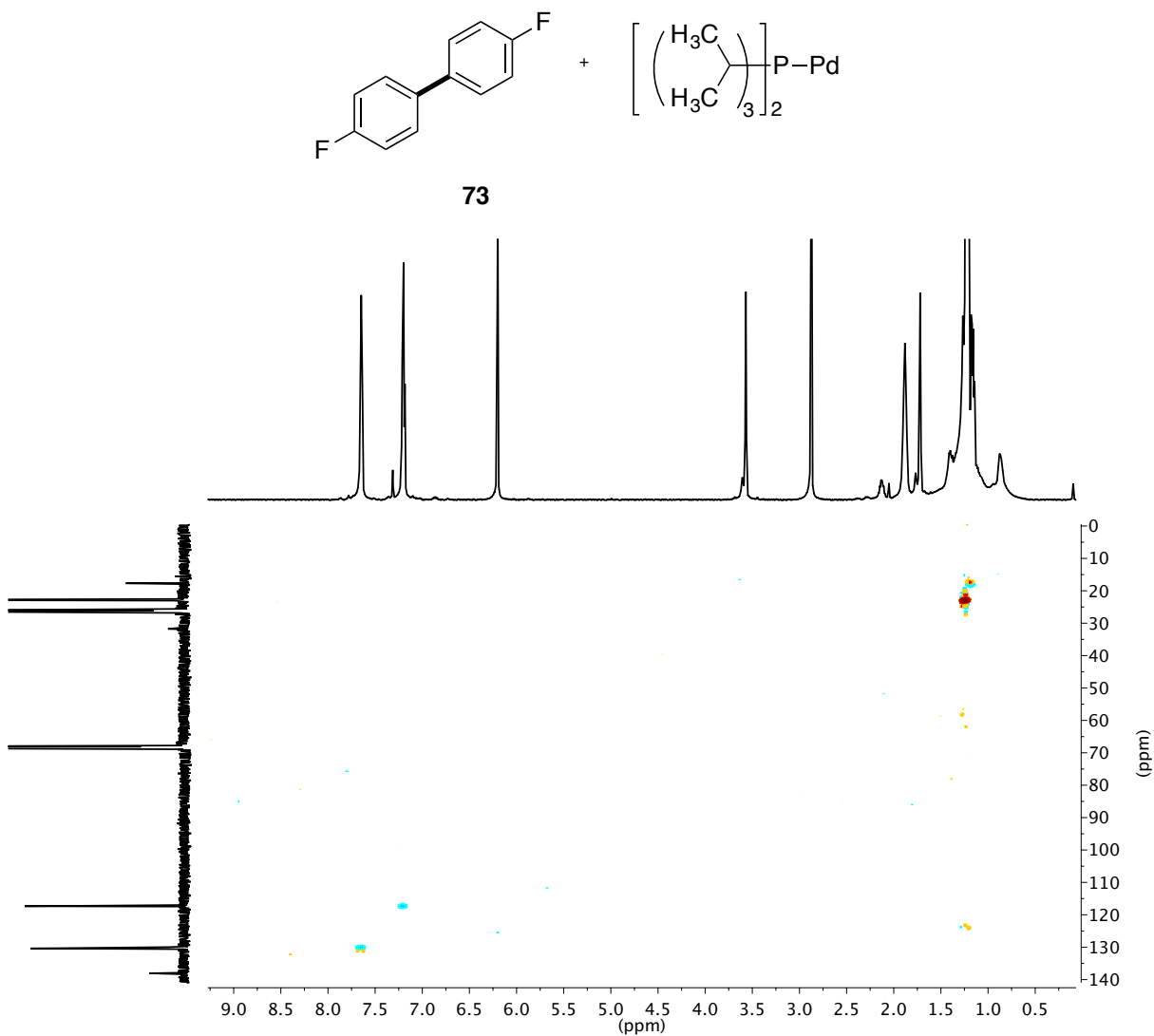
Figure 230. gHMQC spectrum of **73** and 1.0 equiv of [*i*-Pr$_3$P]$_2$Pd^0 at −30 °C, referenced to residual THF (1.72 ppm) and THF-*d*$_8$ (68.21 ppm).
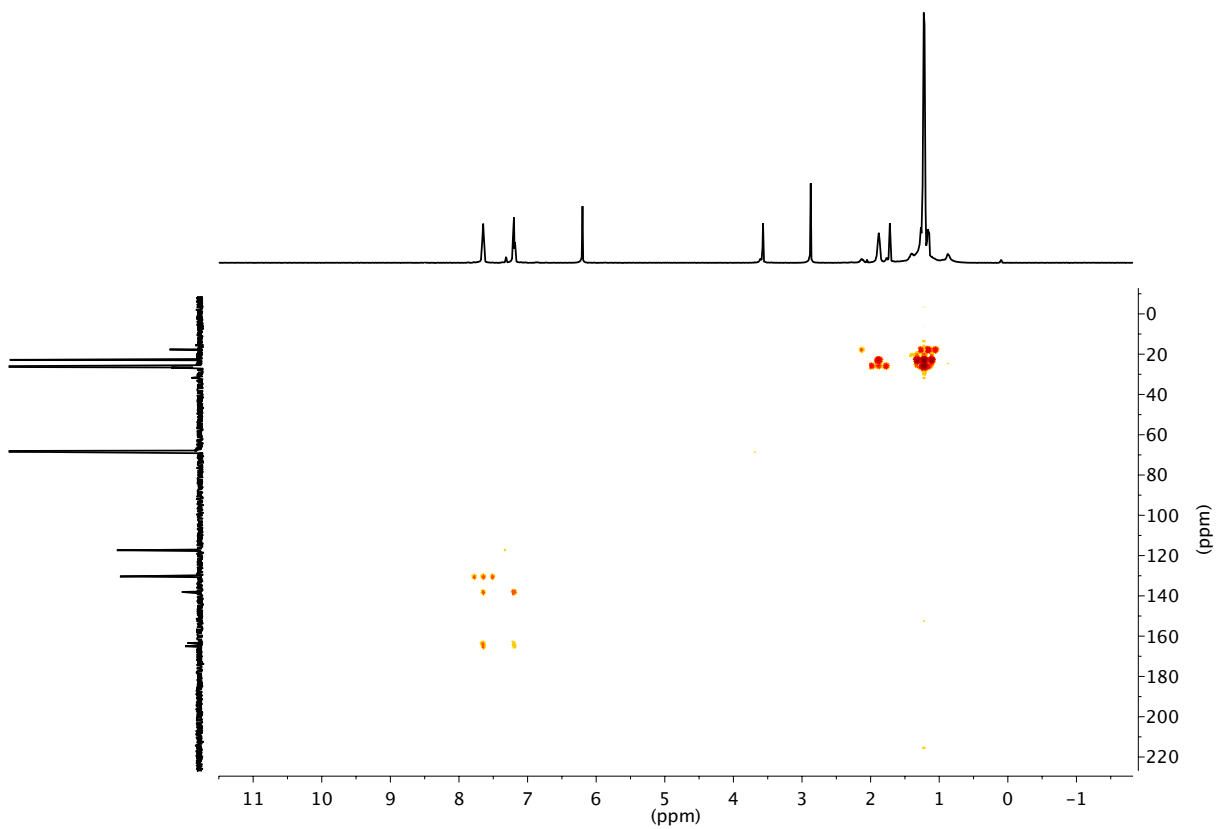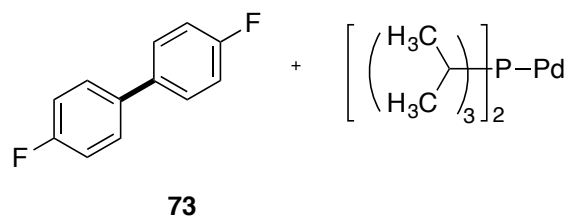
Figure 231. gHMBC spectrum of **73** and 1.0 equiv of [i-Pr$_3$P]$_2$Pd^0 at −30 °C, referenced to residual THF (1.72 ppm) and THF-d_8 (68.21 ppm).
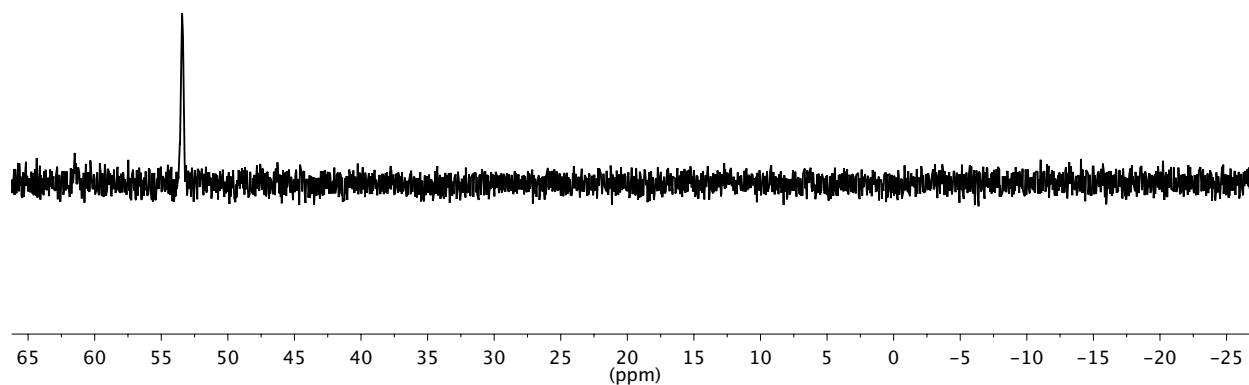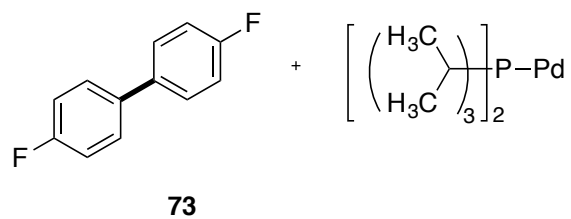
Figure 232. ^{31}P NMR spectrum of **73** and 1.0 equiv of [i-Pr$_3$P]$_2$Pd^0 at −30 °C, referenced externally to i-Pr$_3$P (19.00 ppm).
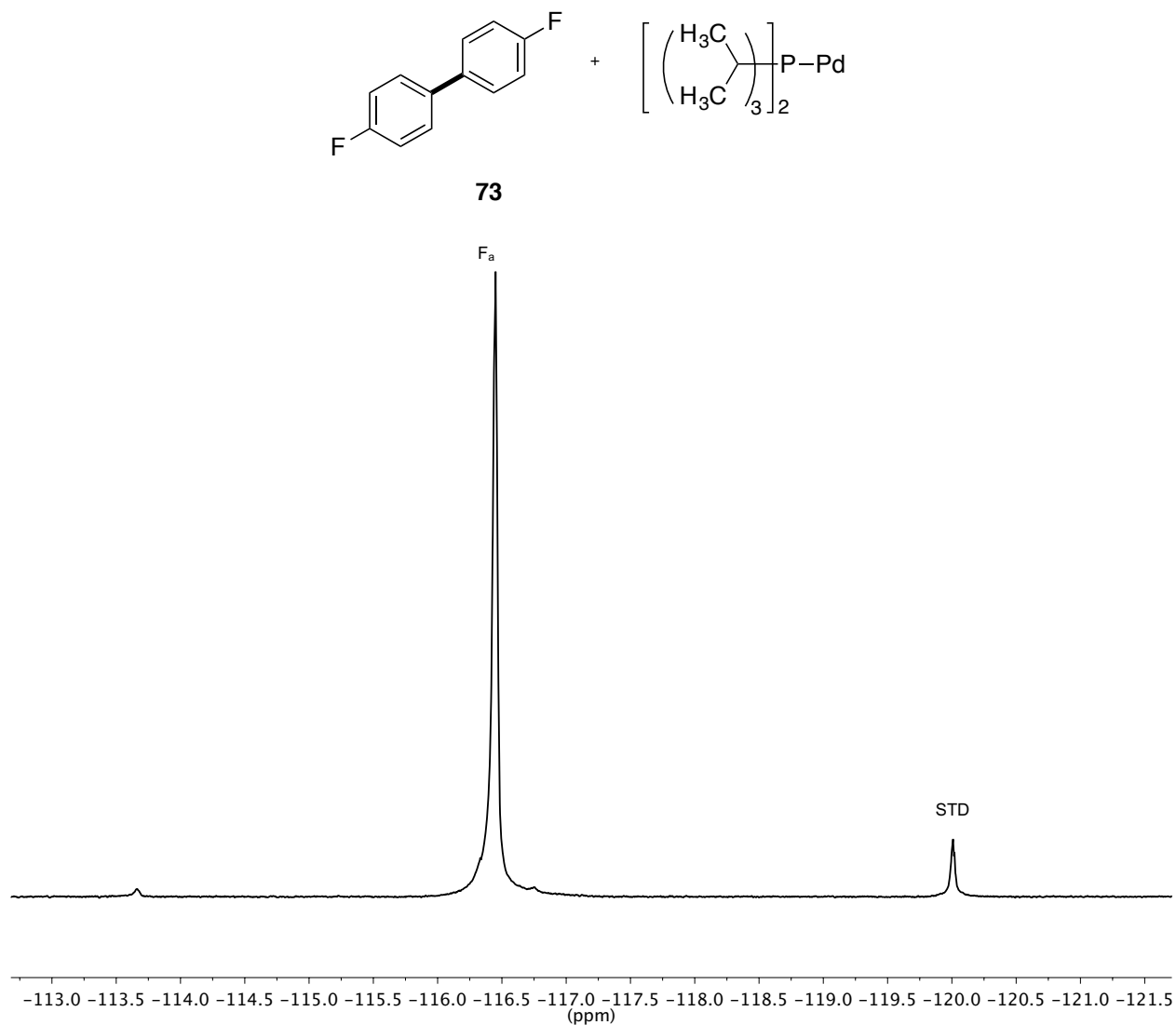
Figure 233. ^{19}F NMR spectrum of **73** and 1.0 equiv of [i-Pr$_3$P]$_2$Pd^0 at −30 °C, referenced to 1,4-difluorobenzene (−120.00 ppm).

Experiment 45: Preparation of (*i*-Pr₃P)₃Pd
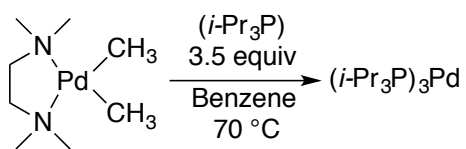
A flame dried, 100 mL Schlenk flask was charged with [TMEDA]PdMe₂ (400 mg, 1.6 mmol, 1.0 equiv), stir bar and capped with a septum followed by an evacuation purge cycle in triplicate with argon. Then 25 mL of benzene (Na) was added along with *i*-Pr₃P (1.07 g 3.5 equiv, 5.6 mmol) followed by heating to 70 °C and stirring for 2 h where the reaction was found to be at completion by ^{1}H and ^{31}P NMR. The benzene was removed by high vacuum while gently heating with a heat gun. Then the vessel was placed into the glove box and 10 mL of pentane was added dissolving the solid. The flask was placed into the freezer (−25 °C) and colorless crystals were observed yielding (210 mg, 22%). In solution the compound exists as (*i*-Pr₃P)₂Pd along with unbound *i*-Pr₃P which matched the previously published spectra.[128]

Experiment 46: Preparation of thallium 4-fluorophenylboronate (79).
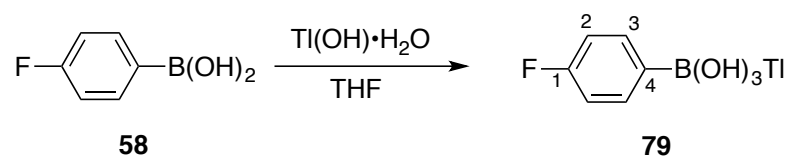
A scintillation vial was charged with thallium hydroxide (0.442 g, 2.0 mmol, 1.0 equiv) and a magnetic stir bar. Then 4-fluorophenylboronic acid (0.38 g, 2.0 mmol, 1.0 equiv) dissolved in THF (10 mL) was added *via* pipette. Upon stirring a white precipitate was observed. The reaction was allowed to stir for 1 h after which the white solid was collected on a glass fritted funnel yielding 0.61 g, 85%.

Data for **79**:

^{1}H NMR: (600 MHz, THF:CD$_3$OD)

7.43 (t, *J*=6.5 Hz, 2 HC(3)), 6.79 (t, *J*=7.2 Hz, 2 HC(2)), 3.74 (s, 3 (OH))

^{13}C NMR: (151 MHz, THF:CD$_3$OD)

164.14, 162.54 (d, *J*=240 Hz, 1 C(1)), 135.86, 135.81 (d, *J*=7 2 C(3)) 114.17, 114.05 (d, *J*=20 Hz, 4 2 C(2)), (Signals 1 and 4 not determined)

^{19}F NMR: (565 MHz, THF:CD$_3$OD)

−118.41 (s, 1 FC(1))

^{11}B NMR: (193 MHz, D$_2$O)

4 (s, 1 B))
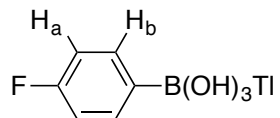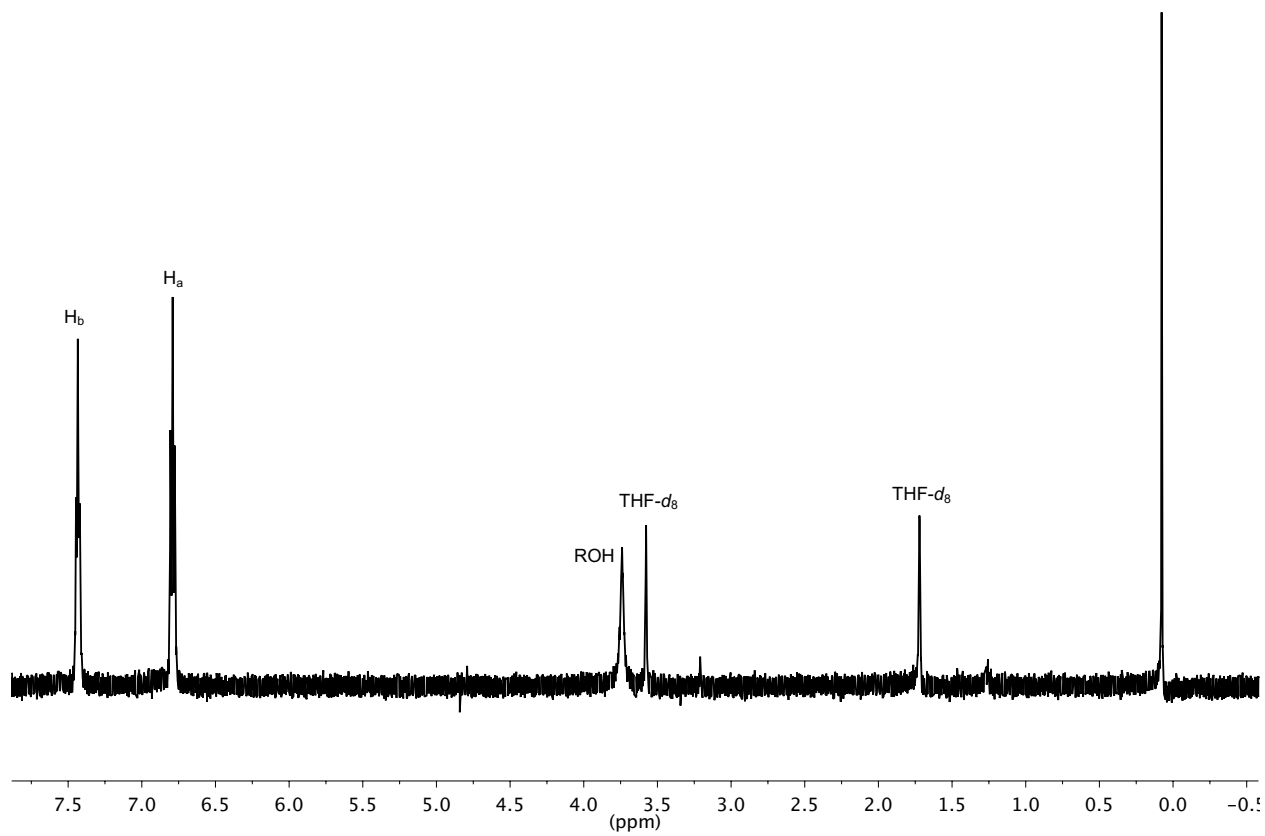
Figure 234. ^{1}H NMR spectrum of **79**, referenced to residual THF$_{d8}$ (1.72 ppm).
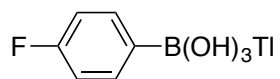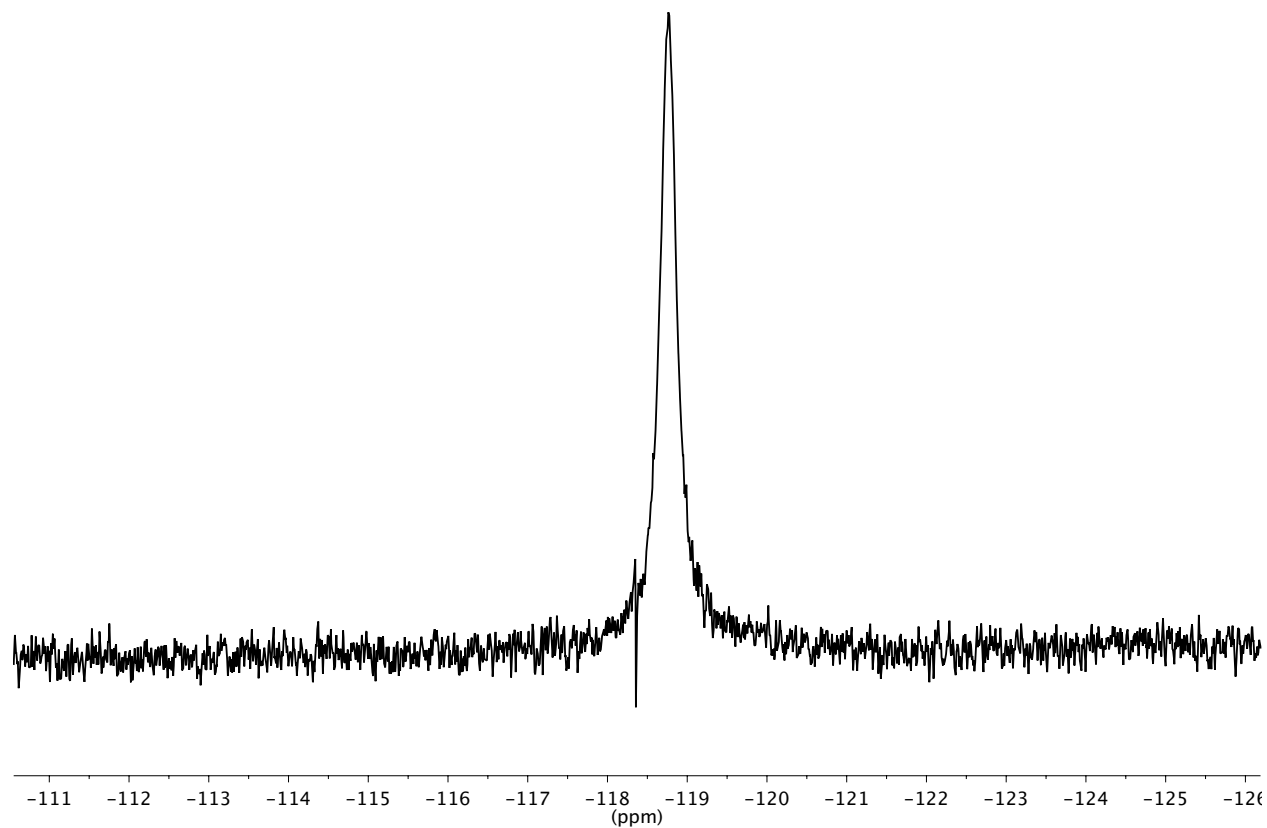
Figure 235. ^{19}F NMR spectrum of **79**, externally referenced to 1,4-difluorobenzene (-120.00 ppm).

F—⟨benzene ring⟩—B(OH)₃Tl
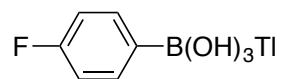
79
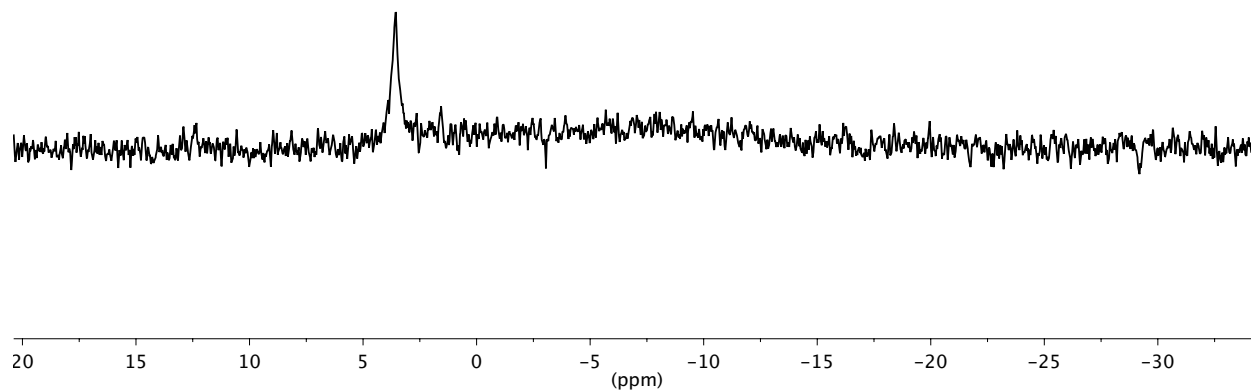
Figure 236. ^{11}B NMR spectrum of **79,** referenced externally to NaBPh$_4$ (−6.14 ppm).
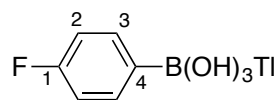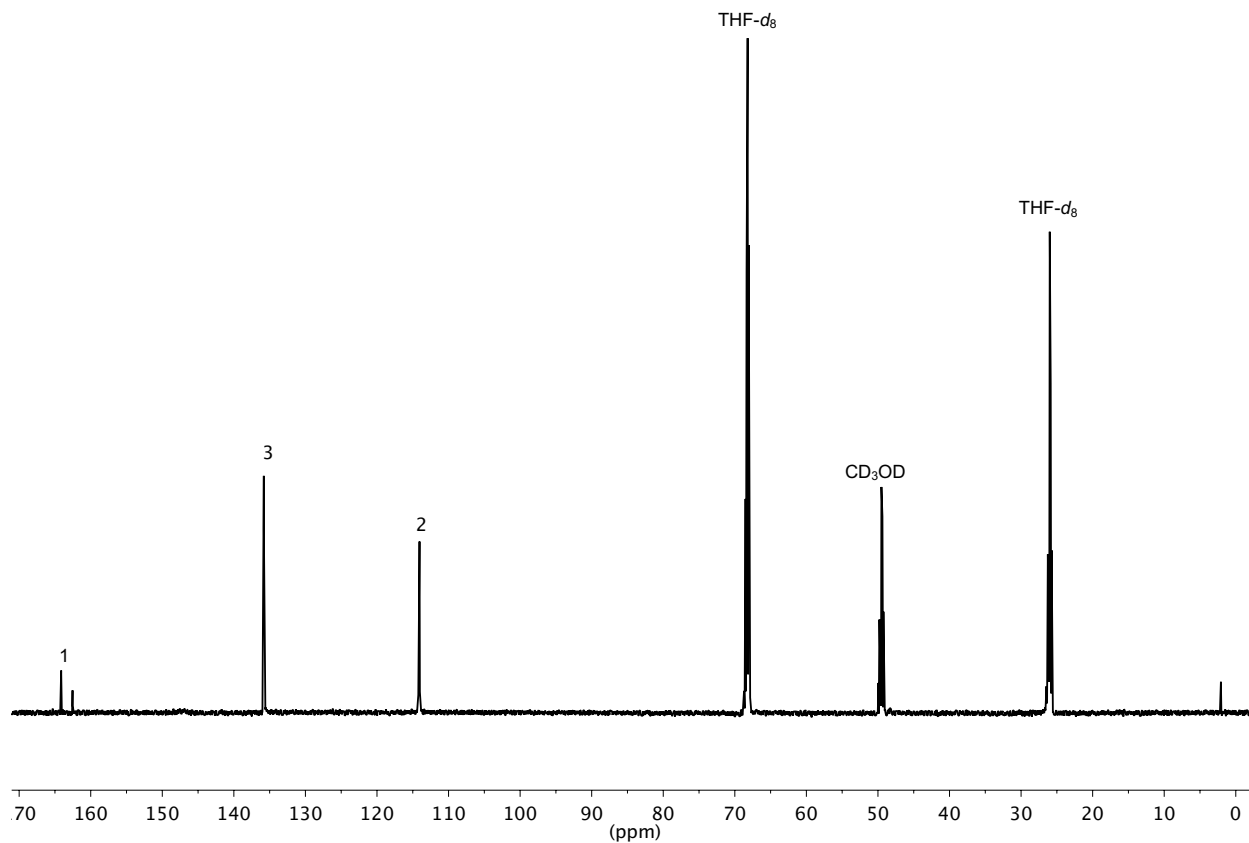
Figure 237. ^{13}C NMR spectrum of **79** at −30 °C, referenced to THF-d_8 (68.29 ppm).

337

Experiment 47: Preparation of 4-fluorophenyldimethyloxyboronate 106.
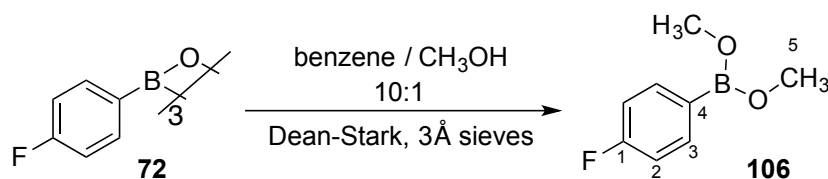
A 500-mL, round-bottomed flask was charged with a magnetic stir bar, 4-fluorophenylboroxine (3.0 g, 8.2 mmol, 1.0 equiv) followed by adding 250 mL of benzene (Na) and 25 mL of CH_3OH (Mg). The flask was fitted with a Dean Stark apparatus filled with 3 Å molecular sieves and submerged into a pre-heated oil bath (120 °C). The reaction was refluxed for 15 h followed by benzene removal *via* rotary-evaporation. The product was distilled under high vacuum at 42 °C yielding 1.2 g, 29% of product as a colorless liquid.

Data for **106**:

^{1}H NMR: (600 MHz, THF-d_8/CD$_3$OD)

  7.67 (m, 2 HC(3)), 7.08 (m, 2 HC(2)), 3.72 (s, 6 HC(5)),

^{13}C NMR: (151 MHz, THF-d_8/CD$_3$OD)

  166.69, 164.80 (d, ^1J(F-C) = 250 Hz, 1 C(1)), 137.99, 137.94 (d, ^3J(F-C) = 8 Hz, 2 C(3), 130.20 (m, 1 C(4)), 116.04, 115.91 (d, ^2J(F-C) = 20 Hz, 2 C(2)), 53.58(m, 2 C(5))

^{19}F NMR: (565 MHz, THF:CD$_3$OD)

  −111.38 (s, 1 FC(1))

^{11}B NMR: (193 MHz, D$_2$O)

  28 (s, 1 B))
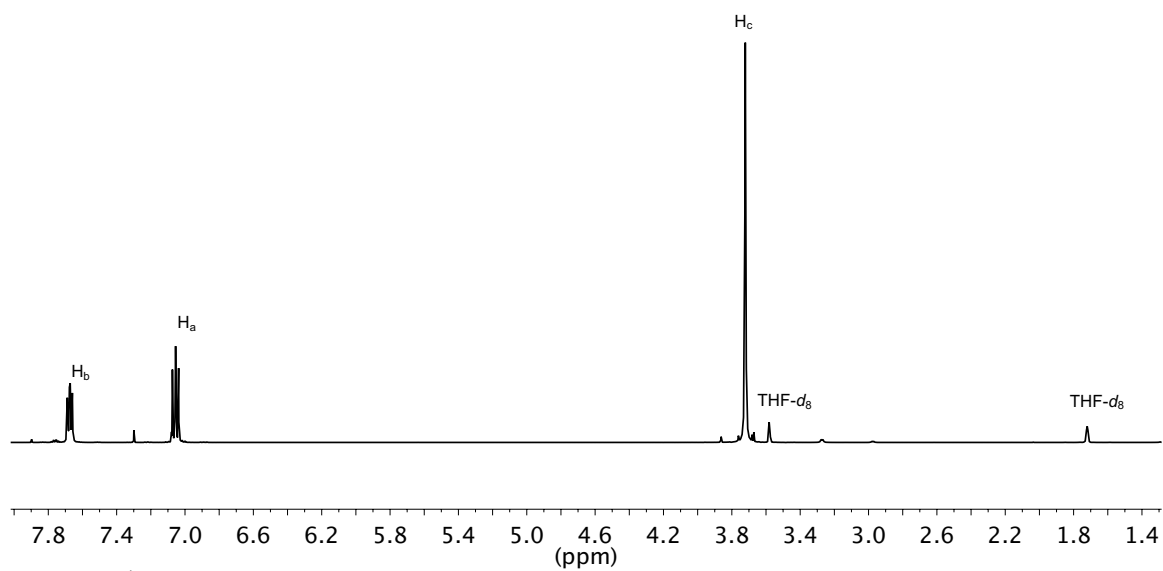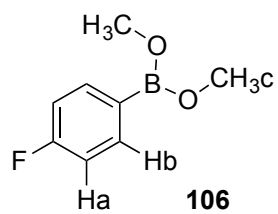
Figure 238. ^{1}H NMR spectrum of **106** at 20 °C, referenced to THF-d_8 (1.72 ppm).
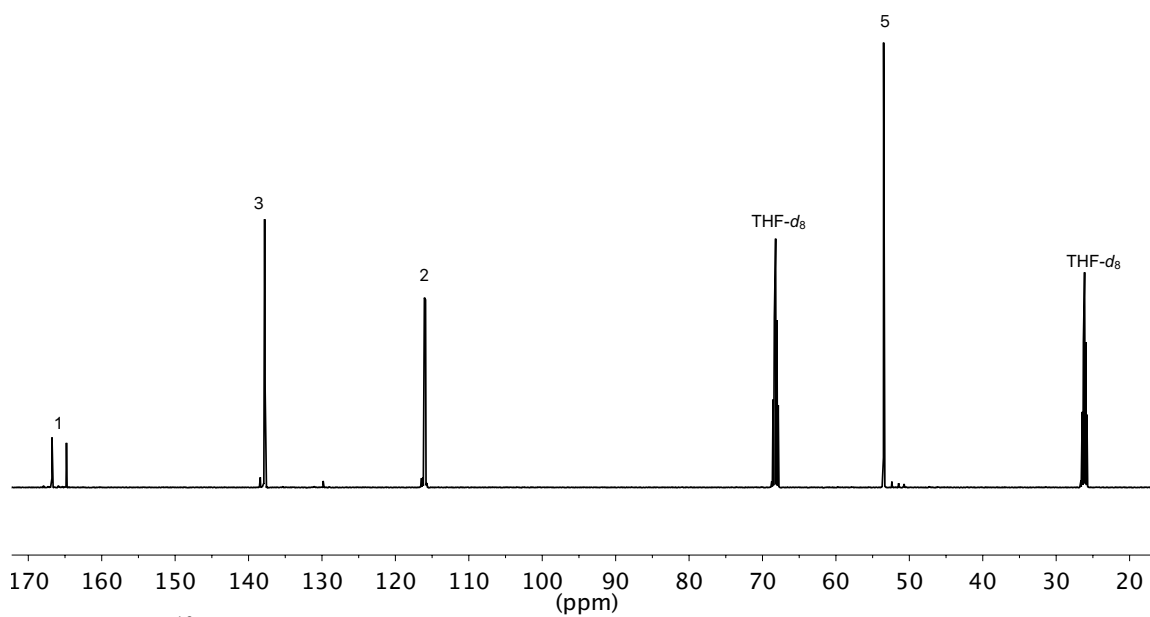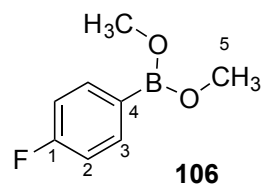
Figure 239. ^{13}C NMR spectrum of **106** at 20°C, referenced to THF-d_8 (68.21 ppm).
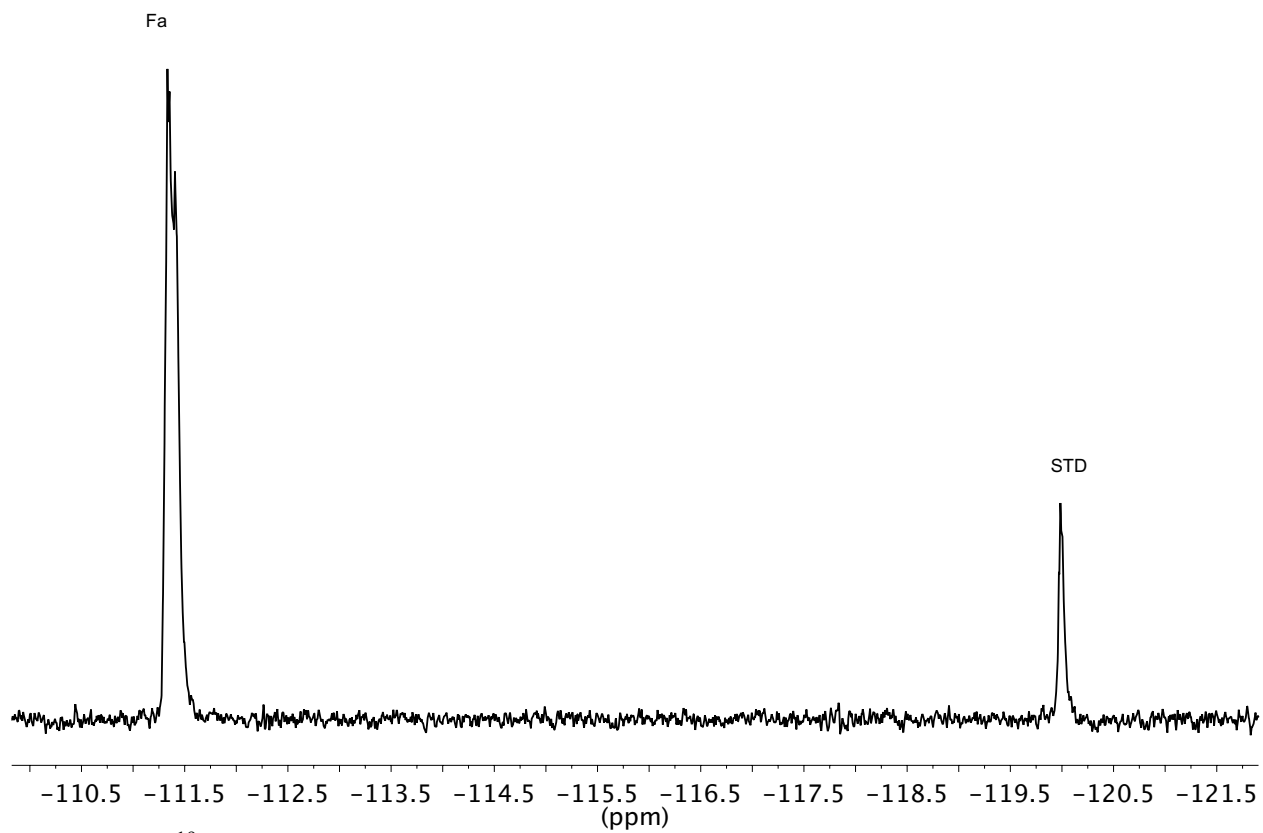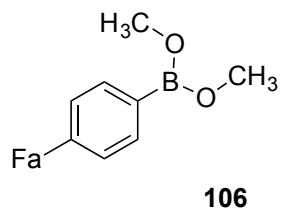
Figure 240. ^{19}F NMR spectrum of **106** at 20°C, referenced to 1,4-difluorobenzene in THF (−120 ppm).
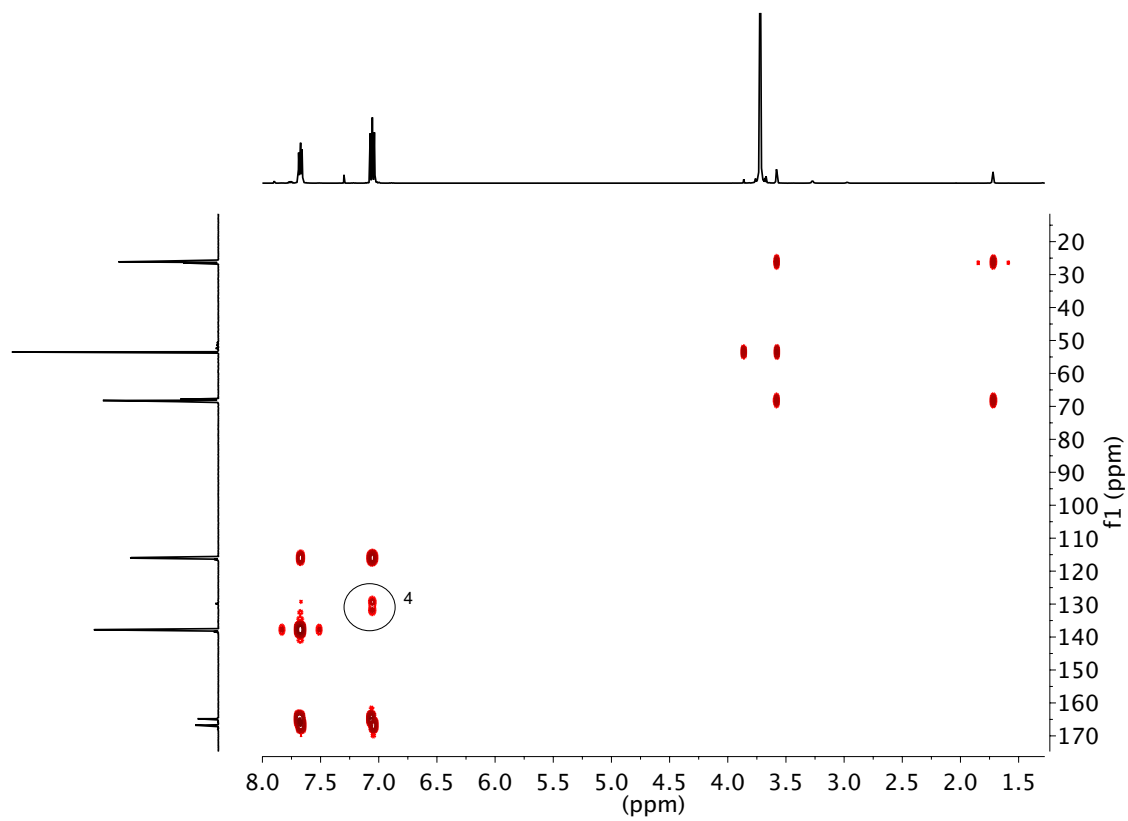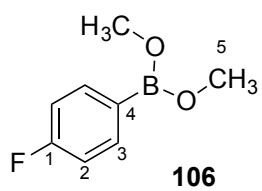
Figure 241. HMBC spectrum of **106** at 20 °C, referenced to THF-d_8 (1.72 and 68.21 ppm).
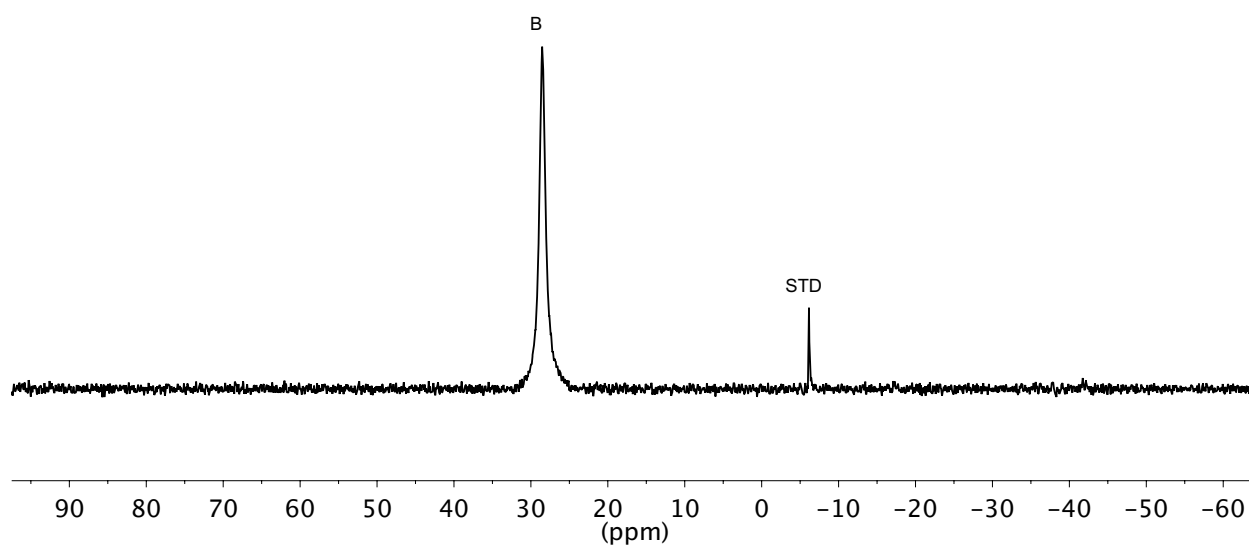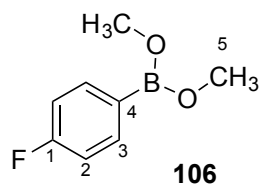
Figure 242. ^{11}B NMR spectrum of **106** at 20°C in THF, referenced to Ph$_4$BNa (−6.15 ppm).

Experiment 48: Preparation of *tri*-isopropylphosphonium tetrafluoroborate
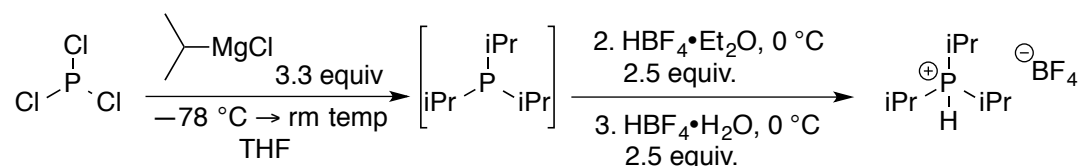
A flame dried, 500-mL round bottom flask fitted with a y-adapter, gas adapter and a septum was purged for ~10 min. The flask was charged with diethyl ether (250 mL) and isopropylmagnesium chloride (111 mL, 1.7 M, 188 mmol, 3.3 equiv) then chilled to an external temperature of −78 °C with a dry-ice acetone bath. The solution was allowed to sit for 10 min for temperature equilibration, followed by the dropwise addition of neat, freshly distilled trichlorophosphine (5.0 mL 57 mmol, 1.0 equiv) over 10 minutes *via* syringe. The solution was allowed to warm to room temperature over night (14 h). The solution was cooled to 0 °C with an ice bath, then ice-chips were added slowly (~15 min) to quench the excess Grignard. Then $HBF_4 \cdot OEt_2$ (22 mL, 140 mmol, 2.5 equiv) and $HBF_4 \cdot OH_2$ (30 mL, 140 mmol, 2.5 equiv, 48 wt%) were added over 20 min *via* pipette. Once the addition was complete 50 mL of water was added followed by extraction in triplicate with dichloromethane (300 mL). The cloudy combined organic layers were dried over $MgSO_4$ until flocculent, followed by gravity filtration. The dichloromethane was removed by reduced pressure (40 mm Hg at 30 °C). The white solid was collected and dissolved in dichloromethane (15 mL) and added dropwise to a stirred solution of diethyl ether (200 mL) yielding a white power 10.25 g, 75%. The spectra matched those previously reported.[129]

Experiment 49: Preparation of *tri*-isopropylphosphine
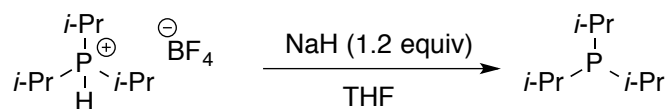
A 500-mL round-bottomed flask with a gas inlet was charged with tri-isopropylphosphonium tetrafluoroborate (8.80 g, 35 mmol, 1.0 equiv) and a magnetic stir bar. The flask was placed into the glove box and washed NaH (1.02 g, 42 mmol, 1.2 equiv) followed by 200 mL of THF. The solution was stirred for 5 h and then it was filtered through dry, activated basic alumina 58 Å (~3 g). The THF was removed by high vacuum (~3 mm Hg) inside the glove box and left for 5 h at which point the THF was removed yielding 4.2 g (74%) of *tri*-isopropylphosphine as a colorless liquid. The spectra matched those previously reported by Olah and co-workers.[130]

Experiment 50: Preparation of thallium hydroxide.
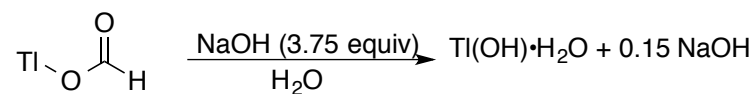
Thallium hydroxide was prepared by a modification of a procedure by Rolfe and co-workers as described below *(52)*. A scintillation vial was charged with thallium formate (1.97 g, 8.0 mmol, 1.0 equiv), water (2 mL) and a magnetic stir bar. Then 3 mL of a freshly prepared 10 M solution of NaOH (30 mmol, 8 equiv) was added *via* pipette. A bright yellow precipitate formed which was collected on a small Büchner funnel. The yellow solid was washed with ice water (2 mL) and collected to afford 0.4469 g (~24%). Using ICP analysis the Na^+, and Tl^+ content was found to be 1.41% and 83.86% respectively which resulted in the molecular formula shown.

Experiment 51: Preparation of dibenzo-22-crown-6.
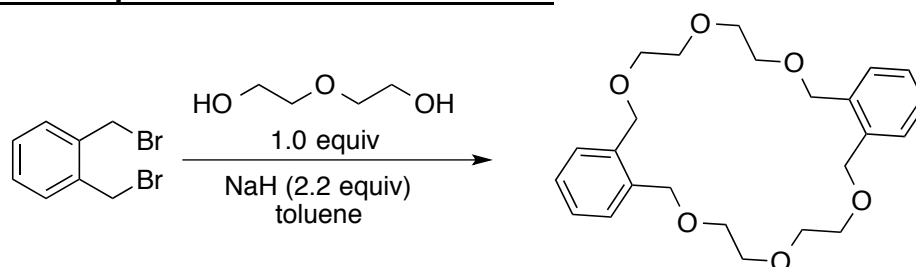
Dibenzo-22-Crown-6 was prepared using a modified procedure by Weber and Ouchi *(32)*. An oven-dried, 1-L, round-bottomed flask was charged with washed NaH (2.16 g, 88 mmol, 2.2 equiv) in the glove box. The flask was capped with a septum and placed under argon. Then 300 mL of toluene (SDS) was added followed by freshly distilled diethylene glycol (4.24 g, 40 mmol, 1.0 equiv). The flask was then placed into an oil bath set to 60 °C and the solution was stirred for 90 min. Then a solution of α,α-dibromo-o-xylene (10.5 g, 40 mmol, 1.0 equiv) in 150 mL of toluene was added at once. The mixture was allowed to stir for 6 h. The flask was removed from the bath and was cooled in a saturated salt bath with an external temperature of 0 °C for 1 h. The solids were removed by filtration through a Celite (5 g) plug followed by toluene removal under vacuum (30 mm Hg, 60 ℃). The remaining oil was purified by column chromatography on neutral alumina (160 g) by eluting with tetrahydrofuran. The fractions were combined and the solvent was removed by rotary-evaporation (30 mm Hg, 40 °C). The yellowish solid was placed under high vacuum overnight (3 mm Hg). The following day the compound was distilled via Kugelrohr (1 × 10^{-4} mm Hg, 250 ℃). A yellow, semi-solid material was collected (562 mg) and the material was dissolved in 5.6 mL of freshly distilled acetonitrile. The solution was placed at −20 °C for 6 h whereupon white crystals formed. The crystals were harvested while cold on a glass-fritted funnel and washed with freshly distilled pentane (3 × 5 mL). (The crystals are soluble at room temperature in CH$_3$CN). The precipitate was then dried under high vacuum (3 mm Hg) at room temperature for 12 h to afford (496 mg, 6%) white crystals. The spectral data for dibenzo-22-Crown-6 matched those previously reported by Weber and Ouchi.

CHAPTER 7: Experimental for Chapter 3

INDEX OF KINETIC EXPERIMENTS:

Experiment 52: Eyring analysis of cross-coupling formation from complex 71 in THF

A 5-mL volumetric flask was charged with 4-fluorophenylboroxine (128 mg, 350 μmol, 1.0 equiv) followed by H_2O (19 μL, 1.05 mmol, 3.0 equiv). Then ~2 mL of THF was added followed by sonication until the solid had dissolved. Once dissolved the flask was filled to the mark with THF (SDS) generating a 0.21 M solution.

A 2-mL volumetric flask was taken into the dry box and charged with [(i-Pr₃P)Pd(4-FC₆H₄)(μ-OH)]₂ (30.8 mg, 41 μmol, 1.0 equiv) and 1,4-difluorobenzene (2.5 μL, 24 μmol) followed by dissolving with THF (SDS) to the 2-mL mark. An oven dried, 5-mm, NMR tube was taken into the dry box and 500 μL of the freshly prepared solution was added. The tube was capped with a septum and Teflon taped. The sample was removed from the glove box and inserted into a −78 °C acetone dry-ice bath followed by the addition of (95 μL, 20.5 μmol, 2.0 equiv) of 4-fluorophenylboronic acid Stock Sol. *via* a 100 μL glass syringe. The NMR tube was vortexed (not shaken), and cleaned with a Kimwipe then placed into the NMR probe set to −10, −20, −30 or −40 °C.

Using the fluorine channel to collect a spectrum every 37 or 162 s, the progress of the reaction was monitored by the decay of the 8-B-4 complex (−123.20 ppm) and formation of cross-coupling product (−116.45 ppm) in comparison with the internal reference 1,4-difluorobenzene (−120.00 ppm). The first order decay and formation profiles were fitted with OrginPro 2015 software using equation 4 and 5 respectively. This procedure was performed three times to obtain an average rate.[131] Then using the Eyring equation 3 $\Delta G^{\ddagger}$, $\Delta H^{\ddagger}$, and $\Delta S^{\ddagger}$ were calculated.

Equation 4.

$$[A] = [A]_0 e^{-kt}$$

Equation 5.

$$[P] = [A]_0 (1 - e^{-kt})$$

Equation 6.

$$\ln\frac{k}{T} = \frac{-\Delta H^{\ddagger}}{R}\frac{1}{T} + \ln\frac{k_B}{h} + \frac{\Delta S^{\ddagger}}{R}$$

Table 14.. Results from the cross-coupling reaction.

Entry	Temp. (K)	k (s^{-1}) (Decay **60**)	k (s^{-1}) (Form **53**)	A_0 [mM] (Decay **71**)	A_0 [mM] (Form **73**)
1	263.15	(7.26 ± 0.03) x 10^{-3}	(4.64 ± 0.02) x 10^{-3}	36.78 ± 1.27	25.51 ± 0.21
2	263.15	(8.02 ± 0.02) x 10^{-3}	(5.01 ± 0.02) x 10^{-3}	31.98 ± 0.76	25.53 ± 0.18
3	263.15	(8.99 ± 0.03) x 10^{-3}	(4.29 ± 0.02) x 10^{-3}	40.05 ± 0.98	27.75 ± 0.26
4	253.15	(3.07 ± 0.05) x 10^{-3}	(2.79 ± 0.02) x 10^{-3}	22.09 ± 0.33	26.20 ± 0.33
5	253.15	(2.44 ± 0.06) x 10^{-3}	(2.45 ± 0.02) x 10^{-3}	22.19 ± 0.51	24.91 ± 0.30
6	253.15	(2.70 ± 0.08) x 10^{-3}	(2.56 ± 0.02) x 10^{-3}	20.71 ± 0.54	25.62 ± 0.33
7	243.15	(8.24 ± 0.09) x 10^{-4}	(6.47 ± 0.02) x 10^{-4}	23.11 ± 0.20	21.34 ± 0.23
8	243.15	(8.47 ± 0.02) x 10^{-4}	(6.00 ± 0.02) x 10^{-4}	21.94 ± 0.24	21.95 ± 0.30
9	243.15	(6.06 ± 0.01) x 10^{-4}	(4.85 ± 0.02) x 10^{-4}	24.13 ± 0.29	21.49 ± 0.34
10	233.15	(1.33 ± 0.03) x 10^{-4}	(2.00 ± 0.04) x 10^{-4}	21.49 ± 0.24	18.98 ± 0.16
11	233.15	(1.59 ± 0.03) x 10^{-4}	(1.67 ± 0.03) x 10^{-4}	24.98 ± 0.33	21.21 ± 0.18
12	233.15	(1.25 ± 0.01) x 10^{-4}	(1.39 ± 0.03) x 10^{-4}	26.27 ± 0.16	20.12 ± 0.18

Table 15.. Averages of results from the cross-coupling reaction.

Entry	T (K)	k (s^{-1}) (Avg. decay **71**)	k (s^{-1}) (Avg. form **73**)
1	263.15	(8.09 ± 0.86) x 10^{-3}	(4.65 ± 0.36) x 10^{-3}
2	253.15	(2.74 ± 0.32) x 10^{-3}	(2.60 ± 0.17) x 10^{-3}
3	243.15	(7.59 ± 0.58) x 10^{-4}	(5.78 ± 0.13) x 10^{-4}
4	233.15	(1.39 ± 0.17) x 10^{-4}	(1.68 ± 0.29) x 10^{-4}

Table 16. Data for Eyring analysis.

Entry	T (K)	k_{avg}-decay (s^{-1})	$\ln(k/T)$	1/T
1	263.15	(8.09 ± 0.86) x 10^{-3}	-10.39	0.00380
2	253.15	(2.74 ± 0.32) x 10^{-3}	-11.43	0.00395
3	243.15	(7.59 ± 0.58) x 10^{-4}	-12.68	0.00411
4	233.15	(1.39 ± 0.17) x 10^{-4}	-14.33	0.00429
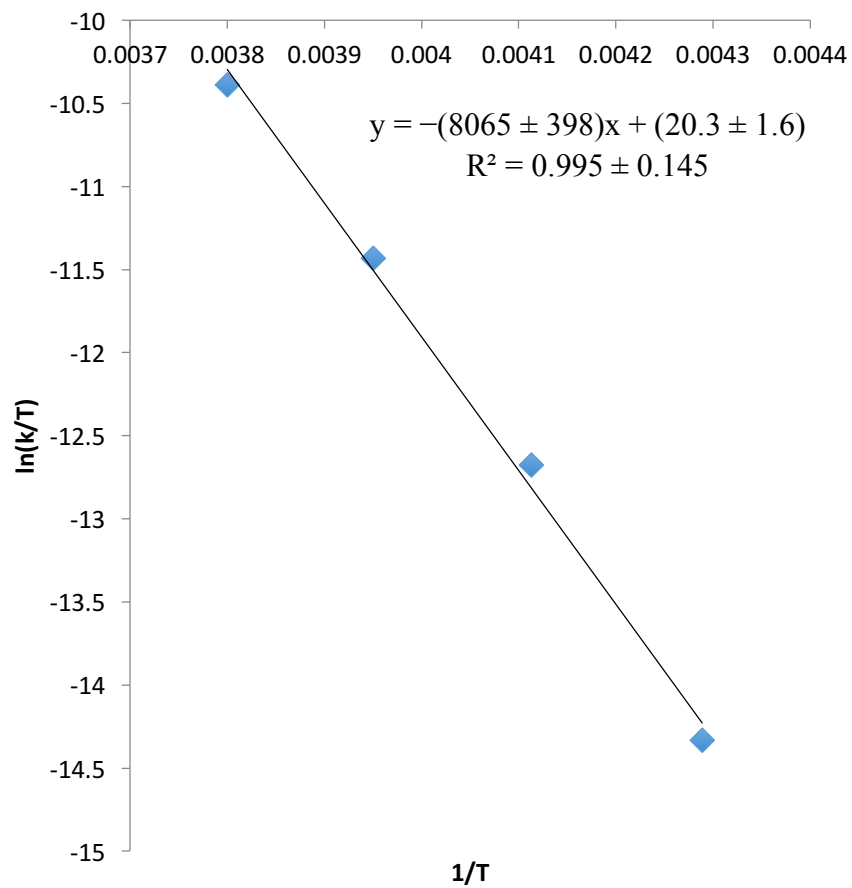
Figure 243. Eyring plot.

Table 17. Results from Eyring analysis.

Entry	Value
$\Delta G^{\ddagger}$	17.7 ± 1.1 (kcal/mol) at -30 °C
$\Delta H^{\ddagger}$	15.98 ± 0.79 (kcal/mol)
$\Delta S^{\ddagger}$	-0.0069 ± 0.0032 (kcal/mol K)
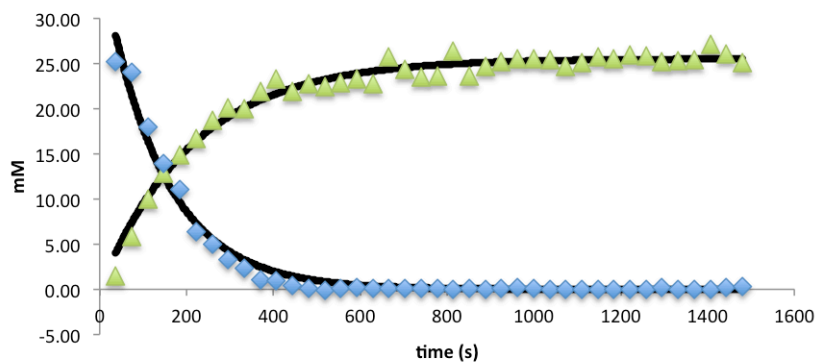
Figure 244. Decay of complex **71** and formation of **73** at −10 °C (Run 1).

Table 18. Data for the decay of complex **71** and formation of **73** at −10 °C (Run 1).

time (s)	Integral IS (−120.00 ppm)	Integral 8-B-4 (−123.20 ppm)	Integral CCP (−116.45 ppm)	[mM] 8-B-4	[mM] CCP
37	1524	1877	216	25.17	1.45
74	1286	1509	738	23.98	5.87
111	1264	1109	1237	17.95	10.01
148	1277	873	1605	13.97	12.84
185	1318	713	1925	11.06	14.93
222	1255	391	2055	6.37	16.73
259	1277	310	2341	4.96	18.73
296	1274	206	2499	3.30	20.04
333	1283	147	2515	2.35	20.04
370	1295	66	2772	1.04	21.87
407	1242	58	2831	0.96	23.30
444	1289	23	2757	0.37	21.86
481	1305	4	2905	0.07	22.74
518	1299	-5	2847	-0.08	22.41
555	1294	6	2886	0.10	22.80
592	1261	16	2880	0.26	23.33
629	1290	9	2874	0.15	22.78
666	1214	8	3053	0.13	25.69
703	1265	5	3011	0.08	24.32
740	1292	6	2966	0.09	23.46
777	1288	3	2980	0.05	23.64
814	1222	1	3148	0.02	26.32
851	1329	9	3061	0.14	23.55
888	1259	2	3040	0.03	24.68
925	1294	5	3187	0.07	25.17

Table 18. (cont.)

962	1261	12	3147	0.19	25.50
999	1290	7	3225	0.11	25.54
1036	1287	-3	3202	-0.05	25.44
1073	648	0	1564	0.00	24.66
1110	1507	1	3699	0.01	25.09
1147	1541	-3	3883	-0.03	25.76
1184	1501	0	3751	-0.01	25.55
1221	1485	0	3776	0.00	25.98
1258	1552	1	3920	0.01	25.81
1295	1534	14	3777	0.18	25.16
1332	1539	0	3812	0.01	25.32
1369	1535	3	3819	0.04	25.43
1406	1480	1	3931	0.01	27.14
1443	1565	15	3988	0.20	26.04
1480	1540	20	3779	0.26	25.07
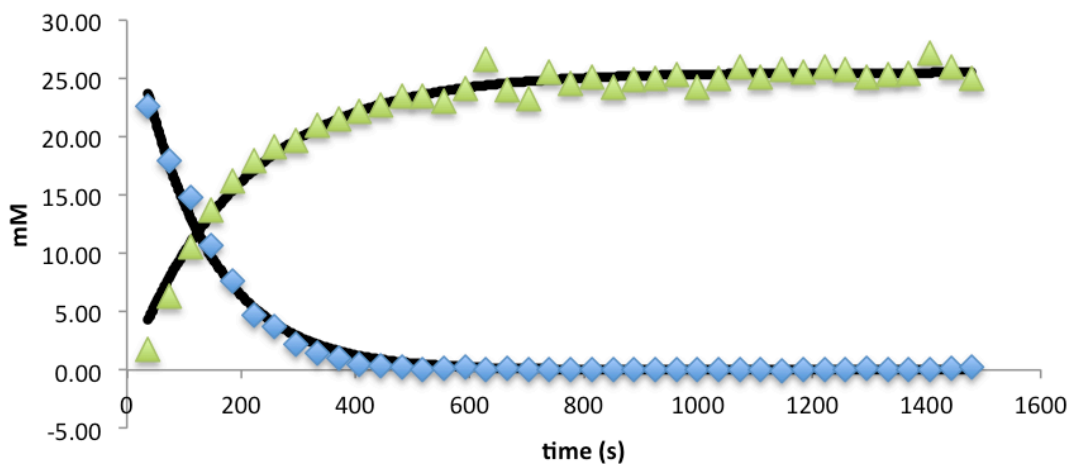
Figure 245. Decay of complex **70** and formation of **73** at −10 °C (Run 2).

Table 19. Data for the decay of complex **70** and formation of **73** at −10 °C (Run 2).

time (s)	Integral IS (−120.00 ppm)	Integral 8-B-4 (−123.20 ppm)	Integral CCP (−116.45 ppm)	[mM] 8-B-4	[mM] CCP
37	1523	1686	270	22.63	1.82
74	1524	1340	950	17.97	6.37
111	1506	1089	1564	14.79	10.62

Table 19. (cont.)

148	1581	826	2119	10.68	13.70
185	1499	561	2382	7.65	16.24
222	1514	352	2658	4.75	17.94
259	1513	273	2838	3.69	19.17
296	1513	161	2909	2.18	19.66
333	1517	109	3118	1.46	21.00
370	1532	77	3233	1.03	21.57
407	1502	35	3268	0.48	22.24
444	1515	23	3365	0.32	22.69
481	1508	20	3468	0.28	23.50
518	1507	5	3460	0.07	23.46
555	1552	8	3505	0.10	23.08
592	1483	18	3505	0.24	24.16
629	1390	2	3624	0.03	26.64
666	1523	8	3574	0.11	23.99
703	1561	2	3560	0.03	23.31
740	1450	0	3619	-0.01	25.51
777	1500	2	3609	0.03	24.59
814	1489	3	3661	0.04	25.12
851	1528	-1	3628	-0.01	24.26
888	1486	2	3624	0.02	24.92
925	1535	5	3751	0.07	24.98
962	1515	1	3757	0.01	25.35
999	1553	5	3689	0.07	24.28
1036	1524	2	3735	0.03	25.04
1073	1472	2	3743	0.03	25.99
1110	1507	1	3699	0.01	25.09
1147	1541	-3	3883	-0.03	25.76
1184	1501	0	3751	-0.01	25.55
1221	1485	0	3776	0.00	25.98
1258	1552	1	3920	0.01	25.81
1295	1534	14	3777	0.18	25.16
1332	1539	0	3812	0.01	25.32
1369	1535	3	3819	0.04	25.43
1406	1480	1	3931	0.01	27.14
1443	1565	15	3988	0.20	26.04
1480	1540	20	3779	0.26	25.07
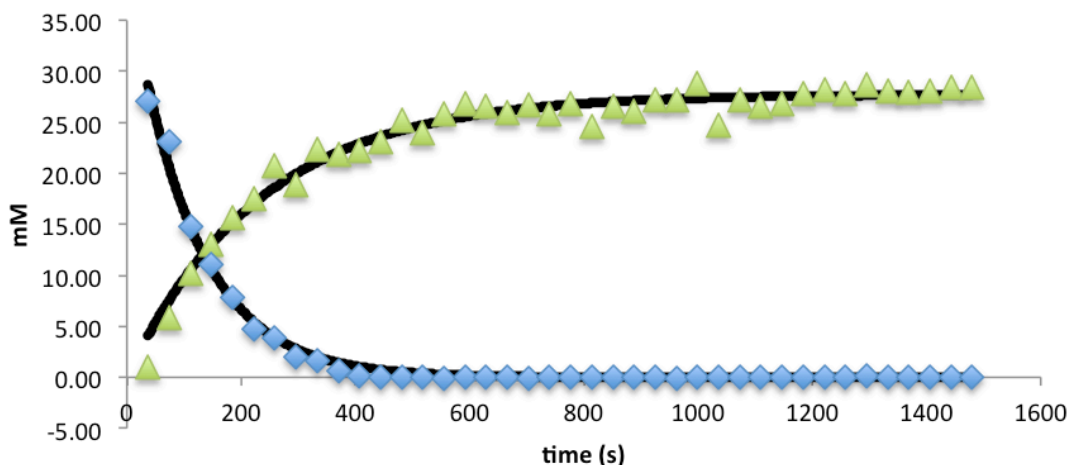
Figure 246. Decay of complex **70** and formation of **73** at −10 °C (Run 3).

Table 20. Data for the decay of complex **71** and formation of **73** at −10 °C (Run 3).

time (s)	Integral IS (−120.00 ppm)	Integral 8-B-4 (−123.20 ppm)	Integral CCP (−116.45 ppm)	[mM] 8-B-4	[mM] CCP
37	1685	2230	164	27.05	0.99
74	1502	1695	864	23.07	5.88
111	1565	1133	1561	14.80	10.20
148	1647	892	2093	11.07	12.99
185	1691	650	2600	7.86	15.71
222	1652	382	2837	4.73	17.55
259	1482	281	3015	3.88	20.80
296	1689	169	3115	2.04	18.85
333	1570	121	3431	1.58	22.34
370	1639	53	3504	0.66	21.85
407	1579	13	3439	0.17	22.25
444	1552	0	3510	0.00	23.11
481	1546	5	3814	0.07	25.21
518	1628	-1	3821	-0.02	23.99
555	1564	-7	3963	-0.09	25.89
592	1501	1	3948	0.01	26.89
629	1537	-1	3995	-0.02	26.57
666	1569	1	3990	0.01	25.99
703	1535	-4	4007	-0.05	26.67
740	1575	1	3986	0.01	25.86
777	1518	-4	3982	-0.05	26.81
814	1560	3	3763	0.04	24.65

Table 20. (cont.)

851	1476	4	3840	0.06	26.59
888	1544	0	3945	0.01	26.11
925	1568	0	4172	0.00	27.19
962	1528	-4	4061	-0.06	27.17
999	1487	-1	4191	-0.02	28.81
1036	1572	1	3804	0.01	24.73
1073	1560	-1	4147	-0.01	27.17
1110	1518	-1	3951	-0.02	26.60
1147	1502	1	3950	0.01	26.88
1184	1571	0	4282	0.00	27.86
1221	1531	-1	4220	-0.01	28.17
1258	1557	-1	4242	-0.02	27.85
1295	1513	9	4239	0.13	28.63
1332	1555	-4	4276	-0.05	28.11
1369	1557	-1	4262	-0.02	27.97
1406	1581	-1	4346	-0.01	28.10
1443	1583	-1	4398	-0.02	28.40
1480	1515	-1	4209	-0.02	28.40
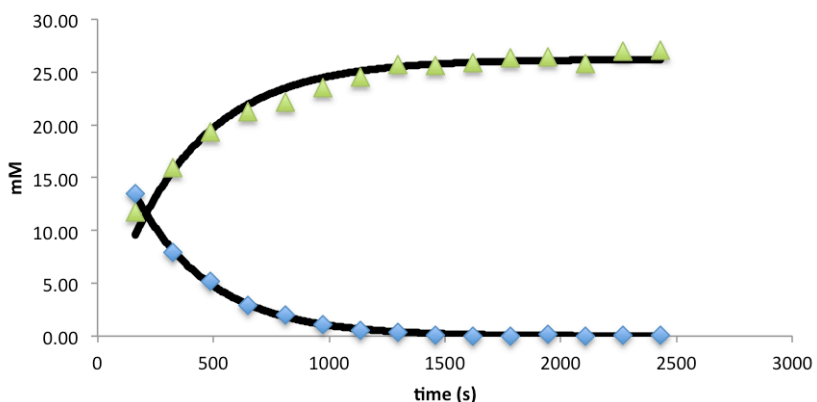
Figure 247. Decay of complex **71** and formation of **73** at −20 °C (Run 1).

Table 21. Data for the decay of complex **71** and formation of **73** at −20 °C (Run 1).

time (s)	Integral IS (−120.00 ppm)	Integral 8-B-4 (−123.20 ppm)	Integral CCP (−116.45 ppm)	[mM] 8-B-4	[mM] CCP
162	847	1123	401	27.10	4.84
324	1076	710	1233	13.48	11.71
486	1103	430	1722	7.96	15.95
648	1140	291	2152	5.22	19.29
810	1103	160	2288	2.96	21.19
972	1114	108	2417	1.98	22.17

Table 21. (cont.)

1134	1121	60	2578	1.10	23.51
1296	1102	31	2647	0.58	24.56
1458	1084	19	2730	0.35	25.73
1620	1103	2	2768	0.05	25.63
1782	1129	2	2862	0.03	25.92
1944	1069	0	2756	0.01	26.36
2106	1083	9	2798	0.16	26.39
2268	1096	2	2767	0.04	25.80
2430	1088	2	2872	0.04	26.99
2592	668	1	1772	0.04	27.11
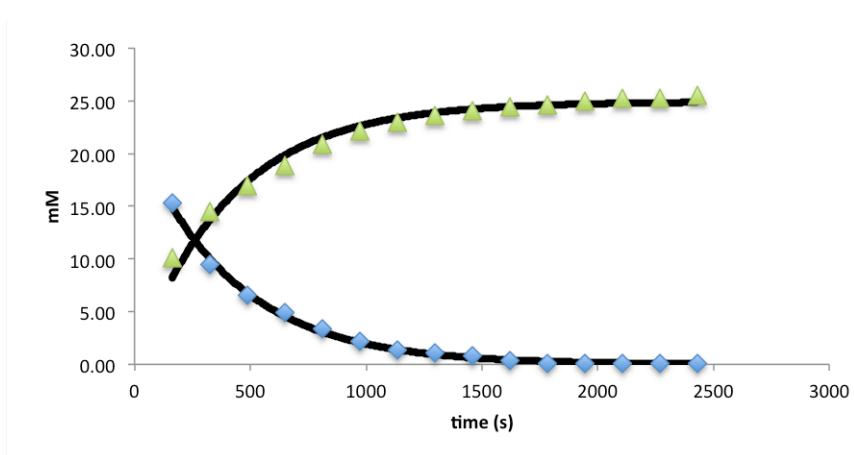
Figure 248. Decay of complex **71** and formation of **73** at −20 °C (Run 2).
Table 22. Data for the decay of complex **70** and formation of **73** at −20 °C (Run 2).

time (s)	Integral IS (−120.00 ppm)	Integral 8-B-4 (−123.20 ppm)	Integral CCP (−116.45 ppm)	[mM] 8-B-4	[mM] CCP
162	987	1122	281	23.25	2.91
324	970	726	957	15.30	10.09
486	979	453	1388	9.45	14.49
648	980	314	1626	6.55	16.96
810	982	236	1813	4.90	18.87
972	973	159	1986	3.34	20.86
1134	975	106	2114	2.23	22.16
1296	981	64	2200	1.34	22.93
1458	983	51	2267	1.06	23.56
1620	983	41	2313	0.85	24.05
1782	982	16	2346	0.34	24.41
1944	986	5	2376	0.11	24.63
2106	975	5	2382	0.11	24.96

Table 22. (cont.)

2268	980	3	2419	0.07	25.23
2430	984	6	2428	0.12	25.21
2592	975	2	2430	0.05	25.48
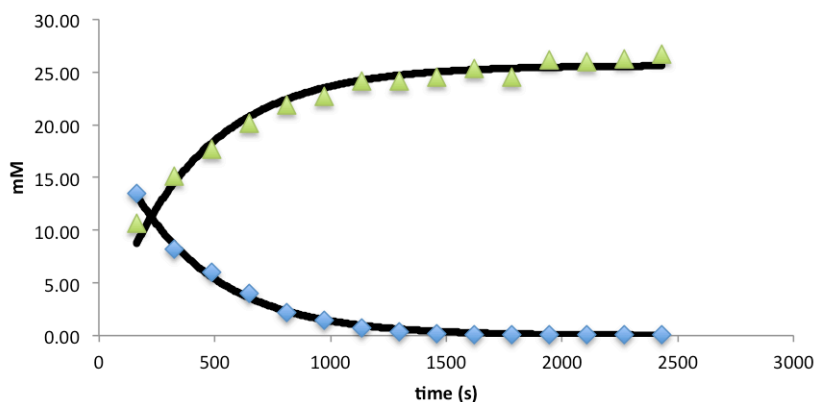
Figure 249. Decay of complex **71** and formation of **73** at −20 °C (Run 3).
Table 23. Data for the decay of complex **71** and formation of **73** at −20 °C (Run 3).

time (s)	Integral IS (−120.00 ppm)	Integral 8-B-4 (−123.20 ppm)	Integral CCP (−116.45 ppm)	[mM] 8-B-4	[mM] CCP
162	801	1253	358	31.95	4.56
324	1209	796	1258	13.45	10.63
486	1210	484	1794	8.17	15.16
648	1195	351	2071	6.00	17.71
810	1202	235	2371	4.00	20.17
972	1185	128	2539	2.21	21.90
1134	1175	86	2606	1.49	22.66
1296	1170	44	2761	0.76	24.12
1458	1195	23	2825	0.39	24.17
1620	1180	9	2826	0.16	24.47
1782	1170	3	2900	0.06	25.34
1944	1198	2	2872	0.04	24.49
2106	1155	4	2957	0.07	26.16
2268	1179	3	2995	0.05	25.96
2430	1182	4	3031	0.06	26.20
2592	1158	4	3021	0.07	26.66
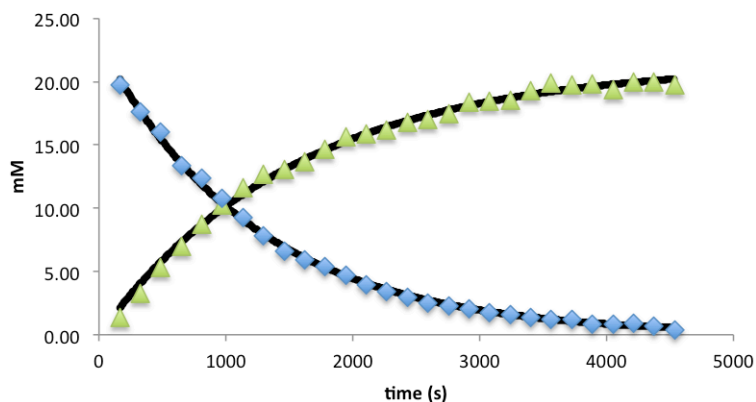
Figure 250. Decay of complex **71** and formation of **73** at −30 °C (Run 1).

Table 24. Data for the decay of complex **71** and formation of **73** at −30 °C (Run 1).

time (s)	Integral IS (−120.00 ppm)	Integral 8-B-4 (−123.20 ppm)	Integral CCP (−116.45 ppm)	[mM] 8-B-4	[mM] CCP
162	4772	4605	653	19.72	1.40
324	4695	4047	1502	17.62	3.27
486	4656	3642	2405	15.99	5.28
648	4853	3180	3315	13.39	6.98
810	4692	2837	3997	12.36	8.71
972	4676	2463	4683	10.77	10.23
1134	4687	2125	5326	9.27	11.61
1296	4720	1812	5860	7.85	12.69
1458	4770	1535	6092	6.58	13.05
1620	4795	1386	6413	5.91	13.67
1782	4738	1255	6798	5.41	14.66
1944	4657	1078	7122	4.73	15.63
2106	4864	947	7563	3.98	15.89
2268	4786	800	7565	3.42	16.15
2430	4802	695	7878	2.96	16.77
2592	4786	593	7964	2.53	17.01
2754	4866	539	8305	2.26	17.44
2916	4713	473	8483	2.05	18.39
3078	4722	408	8531	1.76	18.46
3240	4786	377	8677	1.61	18.53
3402	4673	320	8804	1.40	19.26
3564	4600	267	8954	1.19	19.89
3726	4708	281	9106	1.22	19.77
3888	4731	187	9166	0.81	19.80
4050	4790	192	9076	0.82	19.36

Table 24. (cont.)

4212	4789	211	9348	0.90	19.95
4374	4742	151	9259	0.65	19.96
4536	4714	92	9115	0.40	19.76
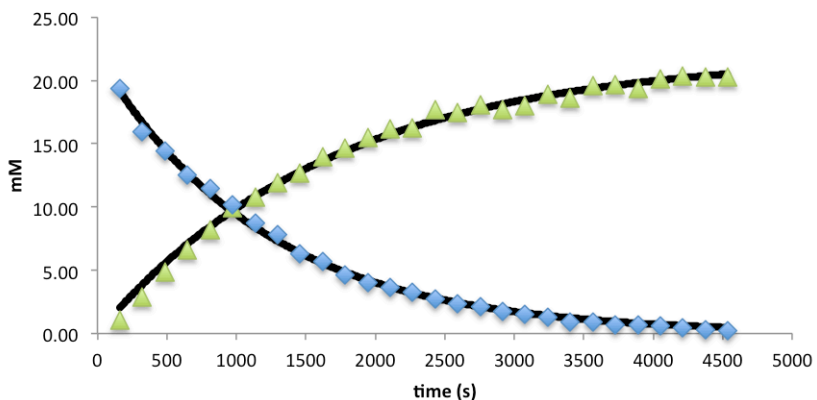
Figure 251. Decay of complex **71** and formation of **73** at −30 °C (Run 2).

Table 25. Data for the decay of complex **71** and formation of **73** at −30 °C (Run 2).

time (s)	Integral IS (−120.00 ppm)	Integral 8-B-4 (−123.20 ppm)	Integral CCP (−116.45 ppm)	[mM] 8-B-4	[mM] CCP
162	4621	4373	479	19.34	1.06
324	4606	3587	1305	15.92	2.90
486	4579	3236	2176	14.44	4.86
648	4625	2837	2990	12.54	6.61
810	4527	2531	3639	11.43	8.21
972	4446	2207	4342	10.14	9.98
1134	4546	1949	4800	8.76	10.79
1296	4519	1723	5284	7.79	11.95
1458	4672	1436	5800	6.28	12.69
1620	4521	1266	6196	5.72	14.01
1782	4633	1054	6633	4.65	14.63
1944	4580	907	6957	4.05	15.52
2106	4575	812	7250	3.63	16.19
2268	4579	725	7298	3.24	16.29
2430	4484	598	7769	2.73	17.71
2592	4662	535	7970	2.35	17.47
2754	4534	464	8011	2.09	18.06
2916	4687	400	8122	1.75	17.71

Table 25. (cont.)

3078	4545	331	8016	1.49	18.03
3240	4505	285	8337	1.29	18.92
3402	4620	209	8401	0.92	18.58
3564	4515	208	8638	0.94	19.55
3726	4599	146	8853	0.65	19.68
3888	4620	153	8768	0.68	19.39
4050	4554	134	8968	0.60	20.13
4212	4539	99	9031	0.45	20.33
4374	4537	68	8991	0.31	20.25
4536	4562	53	9047	0.24	20.27
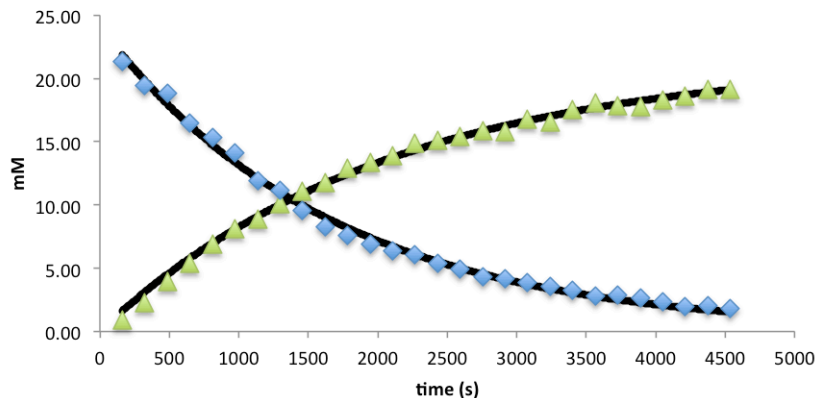
Figure 252. Decay of complex **71** and formation of **73** at −30 °C (Run 3).

Table 26. Data for the decay of complex **71** and formation of **73** at −30 °C (Run 3).

time (s)	Integral IS (−120.00 ppm)	Integral 8-B-4 (−123.20 ppm)	Integral CCP (−116.45 ppm)	[mM] 8-B-4	[mM] CCP
162	4662	4875	416	21.37	0.91
324	4647	4428	1043	19.48	2.29
486	4520	4159	1743	18.81	3.94
648	4645	3736	2452	16.44	5.39
810	4508	3378	3040	15.32	6.89
972	4480	3102	3564	14.15	8.13
1134	4684	2739	4086	11.95	8.91
1296	4573	2497	4520	11.16	10.10
1458	4633	2170	5034	9.57	11.10
1620	4644	1886	5361	8.30	11.80
1782	4586	1705	5800	7.60	12.92

Table 26. (cont.)

1944	4648	1569	6068	6.90	13.34
2106	4596	1434	6239	6.38	13.87
2268	4555	1359	6649	6.10	14.92
2430	4582	1206	6762	5.38	15.08
2592	4475	1083	6745	4.95	15.41
2754	4590	974	7117	4.34	15.85
2916	4676	956	7234	4.18	15.81
3078	4485	856	7369	3.90	16.79
3240	4686	811	7588	3.54	16.55
3402	4553	728	7806	3.27	17.52
3564	4570	622	8093	2.78	18.10
3726	4590	647	8029	2.88	17.88
3888	4623	606	8045	2.68	17.79
4050	4593	531	8211	2.36	18.27
4212	4623	448	8408	1.98	18.59
4374	4500	451	8429	2.05	19.14
4536	4509	409	8432	1.85	19.11
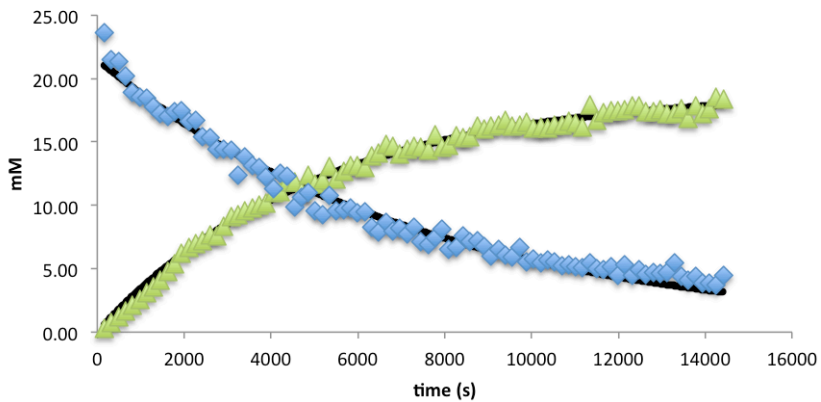
Figure 253. Decay of complex **71** and formation of **73** at −40 °C (Run 1).

Table 27. Data for the decay of complex **71** and formation of **73** at −40 °C (Run 1).

time (s)	Integral IS (−120.00 ppm)	Integral 8-B-4 (−123.20 ppm)	Integral CCP (−116.45 ppm)	[mM] 8-B-4	[mM] CCP
162	1276	1474	38	23.61	0.30
324	1245	1307	95	21.46	0.78
486	1237	1292	146	21.35	1.20
648	1213	1201	198	20.23	1.67
810	1208	1118	248	18.91	2.09
972	1220	1104	312	18.49	2.61
1134	1216	1097	373	18.44	3.14
1296	1222	1062	429	17.77	3.59
1458	1234	1039	493	17.20	4.08
1620	1217	1014	569	17.04	4.78
1782	1172	997	617	17.38	5.38
1944	1143	979	693	17.50	6.19
2106	1149	936	747	16.65	6.64
2268	1134	927	772	16.70	6.96
2430	1188	895	840	15.39	7.22
2592	1156	866	865	15.31	7.65
2754	1216	860	903	14.46	7.59
2916	1201	847	979	14.40	8.33
3078	1185	831	1060	14.32	9.14
3240	1199	726	1089	12.38	9.29
3402	1194	806	1121	13.81	9.60
3564	1181	759	1128	13.14	9.76
3726	1170	744	1146	12.99	10.01
3888	1235	740	1228	12.26	10.17
4050	1212	671	1307	11.31	11.02
4212	1201	738	1303	12.57	11.09
4374	1184	714	1376	12.32	11.88
4536	1218	591	1408	9.91	11.81
4698	1264	659	1368	10.66	11.06
4860	1200	645	1455	10.98	12.39
5022	1225	571	1399	9.53	11.67
5184	1262	574	1485	9.29	12.02
5346	1198	632	1532	10.79	13.07
5508	1279	597	1512	9.54	12.08
5670	1251	589	1555	9.62	12.70
5832	1255	603	1610	9.82	13.11
5994	1239	571	1589	9.42	13.11

Table 27. (cont.)

6156	1236	572	1575	9.46	13.02
6318	1225	495	1668	8.25	13.92
6480	1241	479	1712	7.89	14.10
6642	1200	508	1739	8.66	14.81
6804	1221	477	1750	7.98	14.65
6966	1268	510	1746	8.22	14.07
7128	1180	446	1670	7.73	14.46
7290	1244	505	1787	8.29	14.68
7452	1266	442	1808	7.14	14.60
7614	1264	425	1776	6.87	14.36
7776	1233	449	1877	7.45	15.56
7938	1273	507	1813	8.14	14.55
8100	1250	399	1804	6.52	14.76
8262	1248	409	1888	6.70	15.46
8424	1241	461	1860	7.59	15.31
8586	1277	446	1928	7.15	15.43
8748	1212	429	1924	7.24	16.22
8910	1173	388	1843	6.76	16.05
9072	1259	371	2002	6.02	16.25
9234	1215	387	1941	6.51	16.33
9396	1230	365	2007	6.06	16.67
9558	1231	355	1958	5.89	16.26
9720	1263	412	2018	6.67	16.33
9882	1246	336	2022	5.52	16.59
10044	1266	360	1990	5.80	16.06
10206	1254	338	1986	5.50	16.18
10368	1246	345	1967	5.66	16.13
10530	1249	337	1992	5.52	16.30
10692	1264	322	2017	5.20	16.30
10854	1265	329	2054	5.32	16.60
11016	1230	310	1979	5.15	16.45
11178	1273	316	2015	5.07	16.18
11340	1198	319	2102	5.43	17.93
11502	1244	303	2035	4.98	16.72
11664	1256	305	2133	4.96	17.35
11826	1245	314	2125	5.16	17.45
11988	1232	269	2103	4.47	17.44
12150	1228	317	2106	5.28	17.53
12312	1230	272	2148	4.51	17.85

Table 27 (cont.)

12798	1265	290	2154	4.68	17.41
12960	1248	281	2141	4.60	17.53
13122	1261	292	2122	4.74	17.20
13284	1260	336	2128	5.46	17.26
13446	1241	267	2136	4.39	17.59
13608	1251	252	2064	4.12	16.87
13770	1225	262	2137	4.37	17.82
13932	1265	239	2132	3.87	17.23
14094	1273	242	2198	3.88	17.65
14256	1220	222	2211	3.71	18.53
14418	1236	271	2221	4.48	18.36
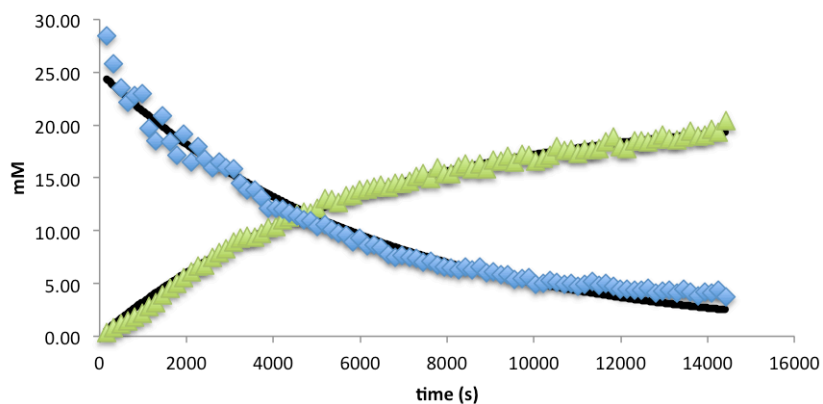
Figure 254. Decay of complex **71** and formation of **73** at −40 °C (Run 2).

Table 28. Data for the decay of complex **71** and formation of **73** at −40 °C (Run 2).

time (s)	Integral IS (−120.00 ppm)	Integral 8-B-4 (−123.20 ppm)	Integral CCP (−116.45 ppm)	[mM] 8-B-4	[mM] CCP
162	1065	1482	38	28.46	0.37
324	1114	1407	85	25.82	0.78
486	1178	1355	135	23.52	1.17
648	1212	1312	173	22.13	1.46
810	1179	1315	212	22.81	1.84
972	1186	1333	251	22.97	2.17
1134	1144	1103	318	19.69	2.84
1296	1176	1064	372	18.49	3.23
1458	1160	1183	447	20.85	3.94

Table 28. (cont.)

1620	1148	1033	508	18.40	4.52
1782	1157	967	563	17.09	4.97
1944	1158	1082	625	19.10	5.51
2106	1148	925	688	16.47	6.12
2268	1138	998	741	17.93	6.66
2430	1206	988	794	16.75	6.73
2592	1160	905	846	15.95	7.46
2754	1154	934	892	16.54	7.90
2916	1167	909	944	15.94	8.27
3078	1143	889	1002	15.90	8.96
3240	1147	814	1045	14.51	9.31
3402	1168	790	1087	13.82	9.51
3564	1174	794	1081	13.82	9.41
3726	1161	745	1107	13.12	9.75
3888	1155	687	1167	12.15	10.32
4050	1157	688	1179	12.15	10.41
4212	1146	675	1240	12.04	11.06
4374	1150	658	1273	11.69	11.31
4536	1157	645	1306	11.39	11.54
4698	1156	625	1326	11.06	11.73
4860	1162	623	1323	10.95	11.63
5022	1158	586	1370	10.34	12.09
5184	1116	575	1424	10.53	13.05
5346	1156	571	1460	10.10	12.91
5508	1160	553	1441	9.74	12.69
5670	1150	538	1500	9.57	13.33
5832	1174	510	1538	8.88	13.40
5994	1148	520	1557	9.25	13.86
6156	1177	491	1605	8.52	13.93
6318	1173	496	1621	8.64	14.13
6480	1168	477	1631	8.35	14.27
6642	1188	448	1638	7.71	14.09
6804	1187	434	1679	7.47	14.46
6966	1175	441	1668	7.67	14.50
7128	1193	435	1713	7.46	14.67
7290	1168	422	1732	7.38	15.15
7452	1174	403	1765	7.01	15.36
7614	1185	412	1728	7.10	14.90
7776	1170	386	1827	6.74	15.96
7938	1175	379	1767	6.60	15.37

Table 28. (cont.)

8100	1175	372	1773	6.48	15.42
8262	1175	364	1841	6.33	16.01
8424	1141	364	1819	6.53	16.30
8586	1144	350	1777	6.26	15.87
8748	1158	370	1847	6.54	16.31
8910	1157	341	1791	6.02	15.82
9072	1147	342	1873	6.10	16.69
9234	1143	328	1854	5.87	16.58
9396	1134	324	1890	5.85	17.03
9558	1189	312	1918	5.36	16.48
9720	1153	309	1940	5.47	17.20
9882	1164	317	1950	5.56	17.12
10044	1179	285	1909	4.94	16.55
10206	1185	293	1953	5.05	16.84
10368	1176	303	1967	5.26	17.09
10530	1142	286	2006	5.12	17.96
10692	1152	278	1978	4.93	17.55
10854	1177	288	2037	5.01	17.69
11016	1179	275	1995	4.77	17.29
11178	1151	278	1988	4.93	17.65
11340	1158	293	1998	5.18	17.64
11502	1178	276	2047	4.79	17.76
11664	1134	279	2040	5.02	18.39
11826	1117	261	2056	4.77	18.82
11988	1170	253	2057	4.42	17.97
12150	1151	250	1998	4.45	17.74
12312	1156	249	2091	4.40	18.49
12474	1155	246	2094	4.36	18.52
12636	1140	252	2058	4.52	18.44
12798	1148	232	2095	4.14	18.66
12960	1136	237	2120	4.26	19.06
13122	1135	240	2074	4.33	18.67
13284	1140	229	2073	4.10	18.59
13446	1143	247	2110	4.42	18.86
13608	1127	230	2140	4.18	19.41
13770	1156	215	2140	3.80	18.92
13932	1127	230	2101	4.16	19.06
14094	1151	228	2211	4.05	19.64
14256	1136	241	2146	4.33	19.31
14418	560	103	1116	3.76	20.38
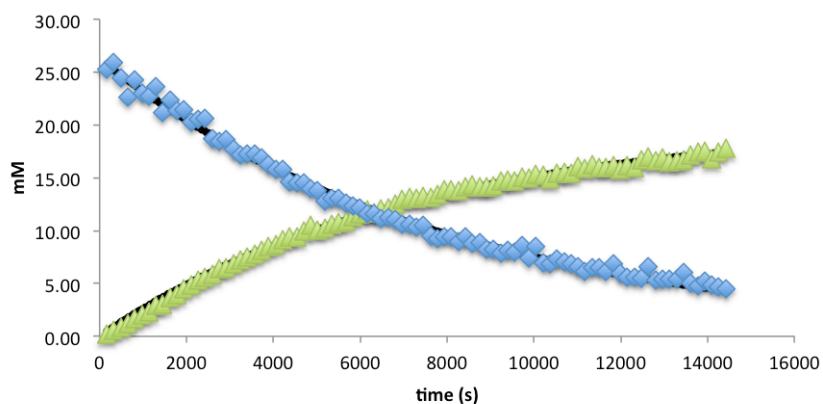
Figure 255. Decay of complex **71** and formation of **73** at −40 °C (Run 3).

Table 29. Data for the decay of complex **71** and formation of **73** at −40 °C (Run 3).

time (s)	Integral IS (−120.00 ppm)	Integral 8-B-4 (−123.20 ppm)	Integral CCP (−116.45 ppm)	[mM] 8-B-4	[mM] CCP
162	1328	1642	28	25.27	0.21
324	1284	1627	68	25.88	0.54
486	1303	1562	111	24.50	0.87
648	1274	1410	148	22.61	1.18
810	1258	1492	203	24.25	1.65
972	1292	1455	262	23.02	2.08
1134	1289	1434	286	22.73	2.26
1296	1281	1479	366	23.60	2.92
1458	1325	1375	396	21.21	3.05
1620	1296	1420	469	22.40	3.69
1782	1300	1356	504	21.33	3.96
1944	1261	1322	551	21.44	4.46
2106	1290	1281	613	20.30	4.85
2268	1284	1288	665	20.51	5.29
2430	1299	1311	704	20.63	5.54
2592	1300	1192	742	18.75	5.83
2754	1305	1175	817	18.41	6.40
2916	1300	1187	825	18.65	6.49
3078	1298	1125	866	17.72	6.82
3240	1305	1096	928	17.16	7.27
3402	1280	1081	934	17.27	7.46
3564	1283	1084	981	17.27	7.82
3726	1290	1065	1023	16.86	8.11
3888	1280	1017	1063	16.24	8.49

367

Table 29. (cont.)

4050	1279	987	1089	15.78	8.70
4212	1258	974	1123	15.82	9.12
4374	1280	917	1177	14.65	9.40
4536	1298	921	1197	14.50	9.43
4698	1287	914	1249	14.52	9.92
4860	1257	857	1291	13.94	10.50
5022	1308	885	1285	13.83	10.04
5184	1321	826	1325	12.78	10.26
5346	1288	826	1334	13.10	10.59
5508	1296	828	1370	13.05	10.80
5670	1302	803	1381	12.60	10.84
5832	1296	783	1441	12.35	11.36
5994	1305	777	1481	12.17	11.60
6156	1283	727	1507	11.58	12.00
6318	1298	735	1482	11.58	11.66
6480	1302	712	1538	11.17	12.08
6642	1289	708	1534	11.23	12.16
6804	1269	685	1556	11.03	12.53
6966	1270	658	1616	10.59	13.00
7128	1276	663	1639	10.63	13.13
7290	1277	645	1629	10.32	13.03
7452	1256	644	1624	10.48	13.22
7614	1305	609	1680	9.53	13.15
7776	1292	584	1693	9.23	13.39
7938	1265	581	1721	9.40	13.90
8100	1268	585	1724	9.44	13.90
8262	1286	561	1739	8.92	13.81
8424	1266	583	1755	9.42	14.17
8586	1288	552	1802	8.75	14.29
8748	1289	558	1788	8.84	14.17
8910	1283	519	1780	8.27	14.19
9072	1318	530	1838	8.21	14.25
9234	1275	489	1837	7.84	14.73
9396	1278	508	1845	8.13	14.75
9558	1286	502	1855	7.97	14.74
9720	1273	534	1873	8.57	15.05
9882	1305	471	1909	7.38	14.95
10044	1273	532	1914	8.54	15.37
10206	1303	445	1941	6.98	15.23
10368	1301	439	1899	6.90	14.92

Table 29. (cont.)

10530	1294	465	1950	7.34	15.40
10692	1295	449	1967	7.08	15.52
10854	1298	433	1961	6.82	15.44
11016	1275	412	2010	6.60	16.11
11178	1299	390	2015	6.13	15.85
11340	1249	397	1991	6.49	16.29
11502	1267	403	1982	6.51	15.99
11664	1282	384	2010	6.12	16.02
11826	1262	425	1999	6.88	16.19
11988	1290	377	1996	5.98	15.82
12150	1301	354	2061	5.57	16.19
12312	1318	359	2054	5.58	15.93
12474	1280	346	2092	5.53	16.70
12636	1270	412	2104	6.63	16.94
12798	1263	330	2048	5.34	16.57
12960	1286	340	2124	5.41	16.88
13122	1269	338	2046	5.44	16.48
13284	1283	339	2085	5.40	16.62
13446	1284	380	2100	6.04	16.71
13608	1279	316	2144	5.06	17.13
13770	1263	296	2149	4.79	17.40
13932	1270	325	2180	5.23	17.55
14094	1289	308	2113	4.89	16.76
14256	1269	291	2168	4.69	17.46
14418	1252	275	2176	4.49	17.76

Experiment 53: Kinetic Measurements for decay of 8-B-4 Ph$_3$P complex 107 in THF/CH$_3$OH at −30 °C

Internal Standard
1,4-Difluorobenzene, 10.22 mM

    A 1-mL volumetric flask was charged with 4-fluorophenylboroxine (77.0 mg, 210 μmol) followed by H$_2$O (11 μL, 3.0 equiv, 631 μmol). Then ~0.5 mL of THF (SDS) was added and sonicated until the solid had dissolved. Once dissolved the flask was filled to the mark with THF (SDS) generating a 0.63 M solution of 4-fluorophenylboronic acid.

    A 2-mL volumetric flask was taken into the dry box and charged with [(*i*-Ph$_3$P)Pd(4-FC$_6$H$_4$)(μ-OH)]$_2$ (39.1 mg, 41 μmol) and 1,4-difluorobenzene (2.5 μL, 24 μmol) followed by dissolving with THF (SDS) to the 2-mL mark. An oven dried, 5-mm, NMR tube was taken into the dry box and 500 μL of the freshly prepared solution was added. The tube was capped with a septum and Teflon taped. The sample was removed from the glove box and inserted into a −78 °C acetone dry-ice bath followed by the addition of the 4-fluorophenylboronic acid solution (35 μL, 20.5 μmol, 2.0 equiv) *via* a 100 μL glass syringe. The NMR tube was vortexed (not shaken) and cleaned with a Kimwipe followed by re-insertion into the −78 °C bath. Then 60 μL of CH$_3$OH (Mg) was added *via* syringe and the tube was vortexed (not shaken) and placed into the NMR probe set to −55 °C. The formation of the 8-B-4 species was observed after ~10-15 min. The tube was removed and placed back into the −78 °C followed by re-insertion into the NMR probe set to −30 °C.

    Using the fluorine channel to collect a spectrum every 37 s the progress of the reaction was monitored by the decay of the 8-B-4 complex (−118.19 ppm) and formation of cross-coupling product (−116.45 ppm) in comparison with the internal reference 1,4-difluorobenzene (−120.00 ppm). The first order decay and formation profiles were fitted with OrginPro 2015 software using equations 3 and 4 respectively. This procedure was performed three times to obtain an average rate.

Table 30. Results from the cross-coupling reaction.

Entry	k (s^{-1}) (Decay 8-B-4)	k (s^{-1}) (Form CCP)	A_0 [mM] (Decay 8-B-4)	A_0 [mM] (Form CCP)
Run 1	$(6.97 \pm 0.11) \times 10^{-3}$	$(7.17 \pm 0.38) \times 10^{-3}$	38.38 ± 0.48	35.17 ± 0.48
Run 2	$(6.34 \pm 0.19) \times 10^{-3}$	$(7.32 \pm 0.62) \times 10^{-3}$	30.45 ± 0.72	34.38 ± 0.75
Run 3	$(6.59 \pm 0.23) \times 10^{-3}$	$(7.86 \pm 0.54) \times 10^{-3}$	38.03 ± 1.04	38.25 ± 0.64

***k* avg. Decay of 8-B-4 = (6.63 ± 0.32) x 10^{-3} s^{-1}**
***k* avg. Formation of CCP = (7.45 ± 0.36) x 10^{-3} s^{-1}**
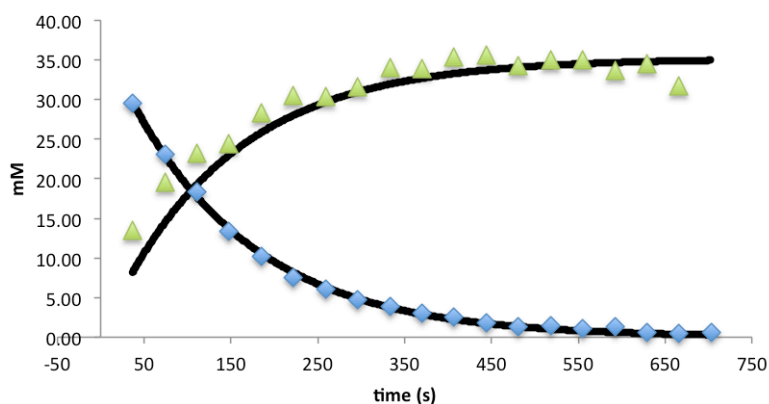
Figure 256. Formation of cross-coupled product from **107** (Run 1).

Table 31. Data for formation of cross-coupled product from **107** (Run 1).

time (s)	Integral IS (-120.00 ppm)	Integral 8-B-4 (-118.19 ppm)	Integral CCP (-116.45 ppm)	[mM] 8-B-4	[mM] CCP
37	1432	2064	1045	29.47	7.46
74	1410	1596	1865	23.13	13.52
111	1390	1247	2653	18.34	19.51
148	1424	933	3236	13.39	23.23
185	1486	743	3557	10.22	24.46
222	1451	534	4019	7.52	28.31
259	1442	429	4296	6.08	30.45
296	1571	367	4678	4.78	30.43
333	1538	296	4760	3.93	31.63
370	1488	221	4960	3.03	34.06
407	1521	191	5046	2.56	33.91
444	1514	131	5244	1.77	35.39
481	1541	104	5365	1.38	35.59
518	1574	115	5282	1.49	34.30

Table 31. (cont.)

555	1578	81	5403	1.05	35.00
592	1575	99	5389	1.28	34.97
629	1565	46	5160	0.61	33.69
666	1613	39	5447	0.50	34.51
703	1632	50	5057	0.62	31.67
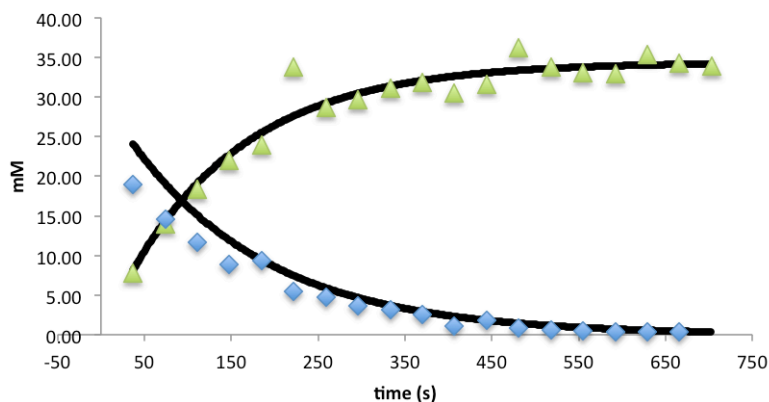
Figure 257. Formation of cross-coupled product from **107** (Run 2).

Table 32. Data for formation of cross-coupled product from **107** (Run 2).

time (s)	Integral IS (−120.00 ppm)	Integral 8-B-4 (−118.19 ppm)	Integral CCP (−116.45 ppm)	[mM] 8-B-4	[mM] CCP
37	1571	1868	1195	24.31	7.78
74	1570	1459	2139	19.00	13.92
111	1582	1133	2842	14.64	18.35
148	1572	894	3392	11.62	22.05
185	1623	700	3799	8.82	23.93
222	1243	571	4111	9.38	33.79
259	1573	424	4408	5.51	28.63
296	1584	369	4601	4.76	29.68
333	1549	277	4720	3.66	31.15
370	1574	238	4909	3.09	31.86
407	1635	206	4884	2.57	30.53
444	1647	89	5085	1.10	31.56
481	1491	129	5279	1.77	36.18
518	1592	65	5267	0.83	33.81
555	1632	51	5282	0.64	33.09
592	1655	34	5324	0.42	32.89

Table 32. (cont.)

629	1562	26	5399	0.35	35.32
666	1607	31	5390	0.39	34.29
703	1631	25	5399	0.31	33.84
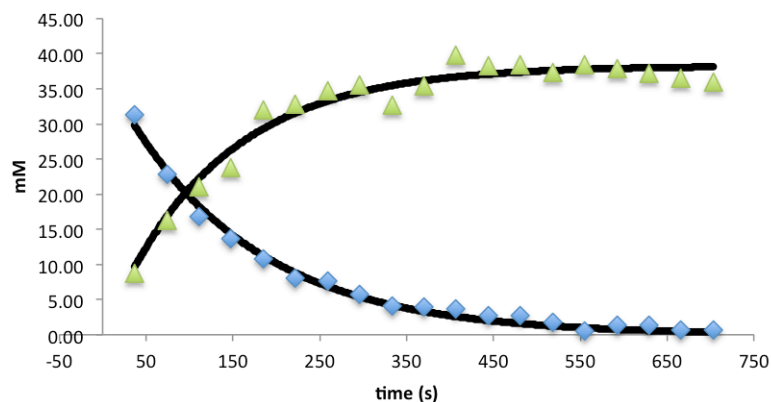
Figure 258. Formation of cross-coupled product from **107** (Run 3).

Table 33. Data for formation of cross-coupled product from **107** (Run 3).

time (s)	Integral IS (−120.00 ppm)	Integral 8-B-4 (−118.19 ppm)	Integral CCP (−116.45 ppm)	[mM] 8-B-4	[mM] CCP
37	1142	1746	971	31.25	8.69
74	1113	1241	1772	22.80	16.27
111	1173	966	2417	16.83	21.06
148	1179	792	2741	13.73	23.75
185	1062	563	3319	10.84	31.96
222	1061	418	3405	8.05	32.79
259	1068	397	3630	7.60	34.75
296	1079	303	3752	5.73	35.55
333	1140	231	3637	4.14	32.61
370	1133	219	3931	3.95	35.44
407	1093	198	4253	3.70	39.77
444	1105	146	4131	2.69	38.22
481	1106	150	4162	2.78	38.45
518	1201	103	4390	1.75	37.36
555	1110	32	4179	0.60	38.47
592	1115	72	4127	1.33	37.81
629	1159	77	4216	1.36	37.17
666	1178	36	4214	0.62	36.55
703	1204	39	4229	0.66	35.89

Experiment 54: Kinetic Measurements for decay of 8-B-4 Ph$_3$P complex 89 in THF at −10 °C

Internal Standard
1,4-Difluorobenzene, 10.22 mM

A 5-mL volumetric flask was charged with 4-fluorophenylboroxine (128 mg, 350 µmol) followed by H$_2$O (19 µL, 3.0 equiv, 1.05 mmol). Then ~2 mL of THF was added followed by sonication until the solid had dissolved. Once dissolved the flask was filled to the mark with THF (SDS) generating a 0.21 M solution.

A 2-mL volumetric flask was taken into the dry box and charged with [(*i*-Ph$_3$P)Pd(4-FC$_6$H$_4$)(µ-OH)]$_2$ (39.1 mg, 41 µmol) and 1,4-difluorobenzene (2.5 µL, 24 µmol) followed by dissolving with THF (SDS) to the 2-mL mark. An oven dried, 5-mm, NMR tube was taken into the dry box and 500 µL of the freshly prepared solution was added. The tube was capped with a septum and Teflon taped. The sample was removed from the glove box and inserted into a −78 °C acetone dry-ice bath followed by the addition of (95 µL, 20.5 µmol, 1.0 equiv) of 4-fluorophenylboronic acid Stock Sol. *via* a 100 µL glass syringe. The NMR tube was vortexed (not shaken), and cleaned with a Kimwipe then placed into the NMR probe set to −10°C.

Using the fluorine channel to collect a spectrum every 25 s the progress of the reaction was monitored by the decay of the 8-B-4 complex (−123.28 ppm) and formation of cross-coupling product (−116.45 ppm) in comparison with the internal reference 1,4-difluorobenzene (−120.00 ppm). The first order decay and formation profiles were fitted with OrginPro 2015 software using equations 3 and 4 respectively. This procedure was performed three times to obtain an average rate.

374

Table 34. Results from the cross-coupling reaction.

Entry	k (s^{-1}) (Decay **89**)	k (s^{-1}) (Form **73**)	A$_0$ [mM] (Decay **89**)	A$_0$ [mM] (Form **73**)
Run 1	$(1.02 \pm 0.05) \times 10^{-2}$	$(1.04 \pm 0.06) \times 10^{-2}$	25.44 ± 0.97	28.65 ± 0.66
Run 2	$(9.14 \pm 0.34) \times 10^{-3}$	$(1.07 \pm 0.13) \times 10^{-2}$	23.77 ± 0.68	27.14 ± 1.10
Run 3	$(1.05 \pm 0.63) \times 10^{-2}$	$(1.08 \pm 0.75) \times 10^{-2}$	23.92 ± 1.15	27.81 ± 2.64

k avg. Decay of 8-B-4 complex 73 = (9.95 ± 0.71) x 10^{-3} s^{-1}
k avg. Formation of CCP 53 = (1.06 ± 0.02) x 10^{-2} s^{-1}
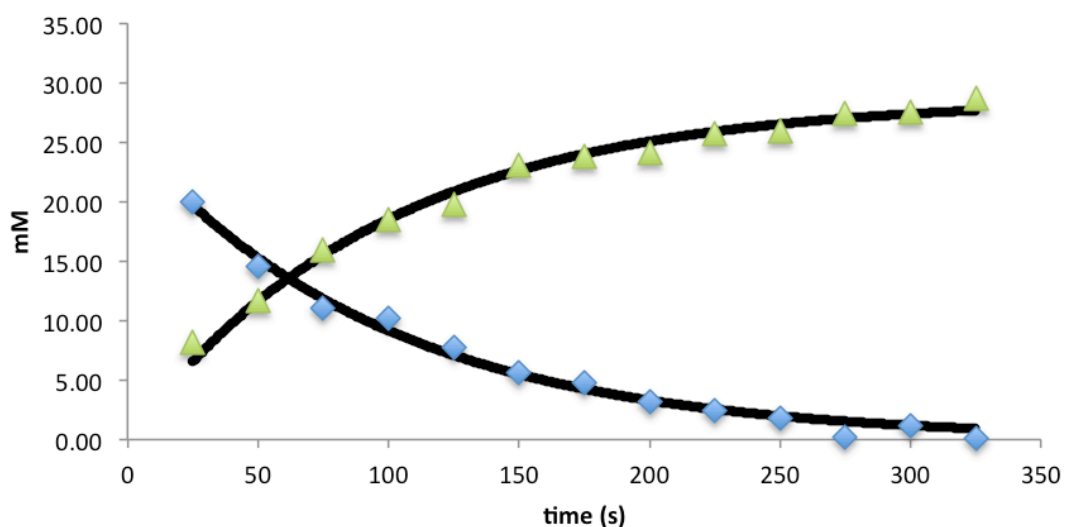
Figure 259. Decay of complex **89** and formation of **73** (Run 1).
Table 35. Data for the decay of complex **89** and formation of **73** (Run 1).

time (s)	Integral IS (-120.00 ppm)	Integral 8-B-4 (-123.28 ppm)	Integral CCP (-116.45 ppm)	[mM] 8-B-4	[mM] CCP
25	535	523	431	19.99	8.22
50	533	380	608	14.57	11.66
75	521	282	814	11.08	15.98
100	528	265	957	10.26	18.52
125	529	202	1023	7.79	19.78
150	519	144	1172	5.68	23.07
175	513	119	1196	4.74	23.84
200	543	84	1279	3.16	24.08
225	543	65	1368	2.45	25.77
250	542	49	1377	1.83	25.97
275	523	5	1400	0.18	27.38
300	539	29	1454	1.11	27.57
325	553	3	1551	0.11	28.68
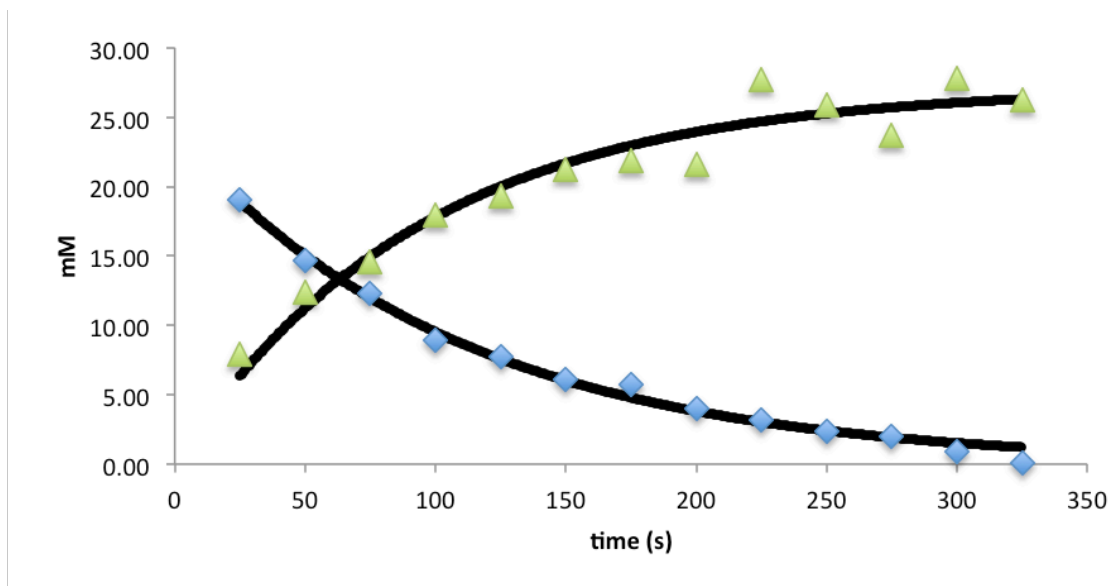
Figure 260. Decay of complex **89** and formation of **73** (Run 2).

Table 36. Data for the decay of complex **89** and formation of **73** (Run 2).

time (s)	Integral IS (−120.00 ppm)	Integral 8-B-4 (−123.28 ppm)	Integral CCP (−116.45 ppm)	[mM] 8-B-4	[mM] CCP
25	547	510	423	19.05	7.90
50	533	383	644	14.70	12.36
75	535	321	762	12.27	14.55
100	547	239	961	8.92	17.96
125	538	204	1019	7.76	19.34
150	532	158	1107	6.09	21.28
175	529	149	1132	5.77	21.90
200	549	107	1160	3.99	21.59
225	522	81	1417	3.18	27.72
250	581	66	1472	2.34	25.90
275	556	54	1291	1.97	23.73
300	526	23	1430	0.89	27.78
325	535	3	1373	0.13	26.23
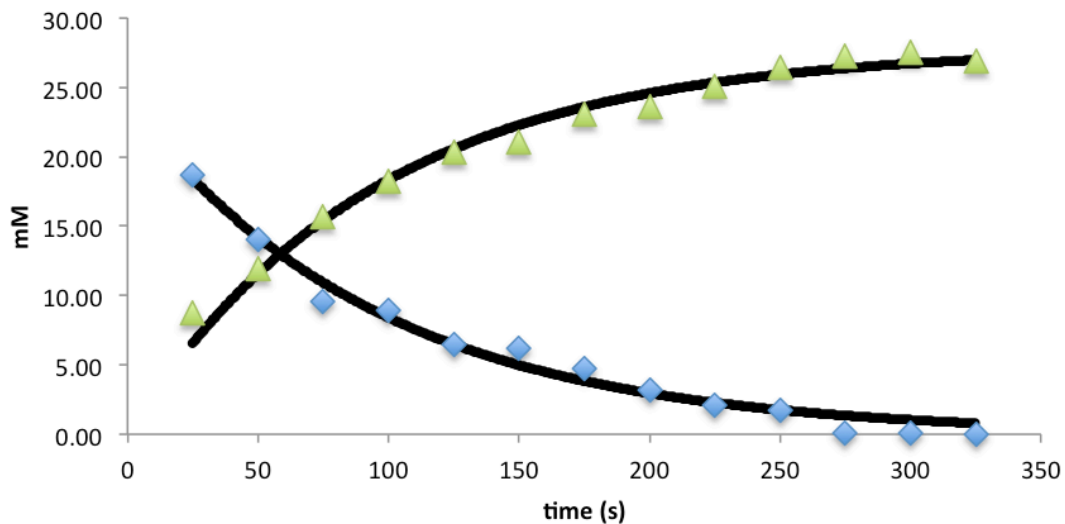
Figure 261. Decay of complex **89** and formation of **73** (Run 3).

Table 37. Data for the decay of complex **89**and formation of **73** (Run 3).

time (s)	Integral IS (−120.00 ppm)	Integral 8-B-4 (−123.28 ppm)	Integral CCP (−116.45 ppm)	[mM] 8-B-4	[mM] CCP
25	538	493	458	18.72	8.71
50	534	367	624	14.05	11.96
75	533	249	816	9.56	15.65
100	534	234	952	8.94	18.21
125	549	174	1094	6.49	20.35
150	547	167	1125	6.24	21.01
175	552	128	1246	4.74	23.06
200	535	83	1236	3.18	23.63
225	547	55	1341	2.06	25.04
250	551	47	1425	1.74	26.44
275	535	3	1427	0.13	27.26
300	532	3	1432	0.11	27.52
325	566	1	1486	0.03	26.85

Experiment 55: Kinetic measurement for decay of 8-B-4 DPPF complex 111 in THF at –10 °C
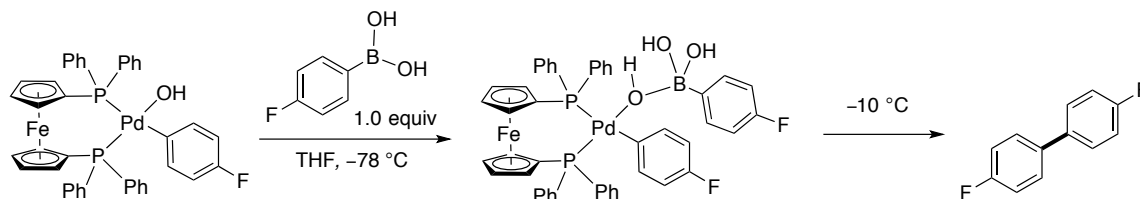
A 5-mL volumetric flask was charged with 4-fluorophenylboroxine (128 mg, 350 μmol, 1.0 equiv) followed by H_2O (19 μL, 1.05 mmol, 3.0 equiv). Then ~2 mL of THF was added followed by sonication until the solid had dissolved. Once dissolved the flask was filled to the mark with THF (SDS) generating a 0.21 M solution.

A 2-mL volumetric flask was taken into the dry box and charged with (dppf)Pd(4-FC_6H_4)(OH) (62 mg, 80.3 μmol, 1.0 equiv) and 1,4-difluorobenzene (2.5 μL, 24 μmol) followed by dissolving with THF (SDS) to the 2-mL mark. An oven dried, 5-mm, NMR tube was taken into the dry box and 500 μL of the freshly prepared solution was added. The tube was capped with a septum and Teflon taped. The sample was removed from the glove box and inserted into a −78 °C acetone dry-ice bath followed by the addition of (95 μL, 20.5 μmol, 1.0 equiv) of 4-fluorophenylboronic acid Stock Sol. *via* a 100 μL glass syringe. The NMR tube was vortexed (not shaken), and cleaned with a Kimwipe then placed into the NMR probe set to −10°C.

Using the fluorine channel to collect a spectrum every 37 or 100 s, the progress of the reaction was monitored by the decay of the 8-B-4 complex (−122.35 ppm) in comparison with the internal reference 1,4-difluorobenzene (−120.00 ppm). [The cross-coupling product could not be monitored due to the 8-B-4 fluorine signal overlapping.] The first order decay profile was fitted with OrginPro 2015 software using equation 3. This procedure was performed three times to obtain an average rate.[131]

Table 38. Results from the cross-coupling reaction.

Entry	k (s^{-1}) (Decay 8-B-4)	A_0 [mM] (Form CCP)
Run 1	$(2.7 \pm 0.2) \times 10^{-3}$	27.98 ± 1.5
Run 2	$(2.78 \pm 0.09) \times 10^{-3}$	31.03 ± 0.72
Run 3	$(2.78 \pm 0.08) \times 10^{-3}$	30.32 ± 0.63

***k* avg. Decay of 8-B-4 = (2.75 ± 0.05) x 10^{-3} s^{-1}**
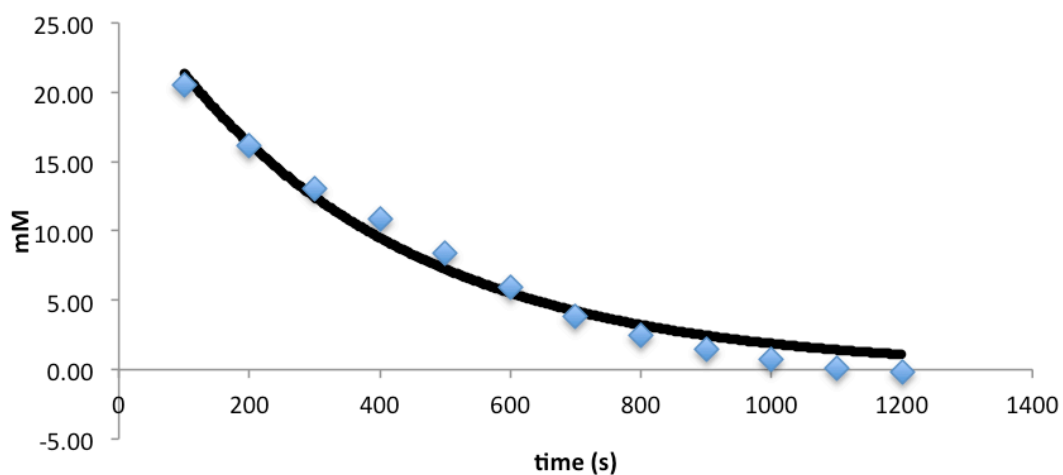
Figure 262. Decay of complex **111** (Run 1).

Table 39. Data for the decay of complex **111** (Run 1).

time (s)	Integral IS (−120.00 ppm)	Integral 8B4 (−117.36 ppm)	[mM] 8-B-4
100	2416	2427	20.53
200	2427	1920	16.17
300	2350	1501	13.05
400	2361	1258	10.89
500	2289	945	8.44
600	2373	691	5.95
700	2416	458	3.87
800	2437	300	2.52
900	2497	182	1.49
1000	2483	85	0.70
1100	2436	11	0.10
1200	321	-2	-0.15

379
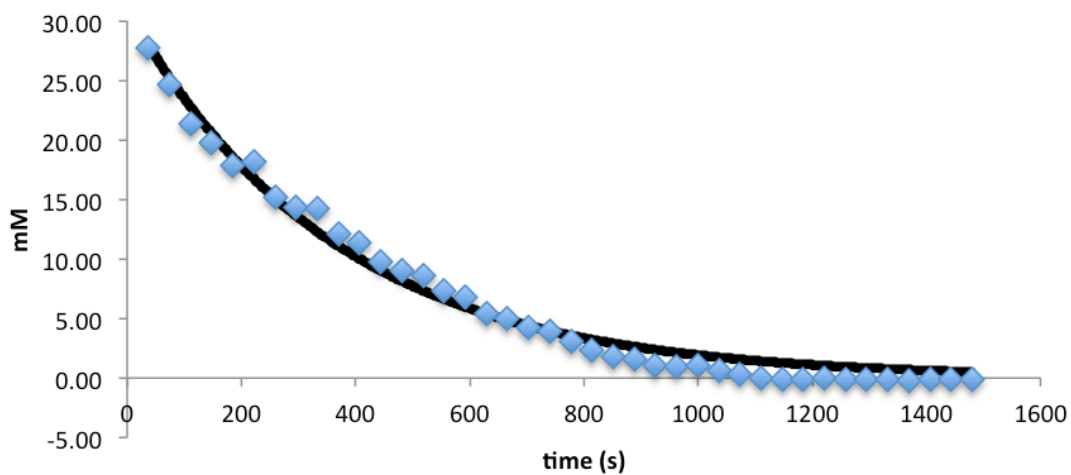
Figure 263. Decay of complex **111** (Run 2).

Table 40. Data for the decay of complex **111** (Run 2).

time (s)	Integral IS (−120.00 ppm)	Integral 8B4 (−117.36 ppm)	[mM] 8-B-4
37	902	1225	27.75
74	916	1104	24.64
111	925	966	21.35
148	903	874	19.79
185	932	814	17.85
222	847	753	18.17
259	935	694	15.18
296	908	640	14.40
333	850	593	14.27
370	888	525	12.09
407	868	482	11.36
444	934	448	9.82
481	936	414	9.04
518	865	363	8.57
555	913	326	7.30
592	850	284	6.82
629	948	252	5.44
666	903	219	4.95

Table 40. (cont.)

703	896	188	4.29
740	936	179	3.91
777	937	140	3.05
814	906	102	2.29
851	947	85	1.83
888	920	74	1.64
925	951	49	1.05
962	891	44	1.00
999	930	46	1.01
1036	929	31	0.68
1073	930	12	0.26
1110	935	-2	-0.04
1147	932	-7	-0.15
1184	929	-4	-0.09
1221	942	-1	-0.02
1258	948	-4	-0.08
1295	871	-3	-0.07
1332	878	-4	-0.10
1369	838	-7	-0.17
1406	966	-4	-0.08
1443	861	-6	-0.14
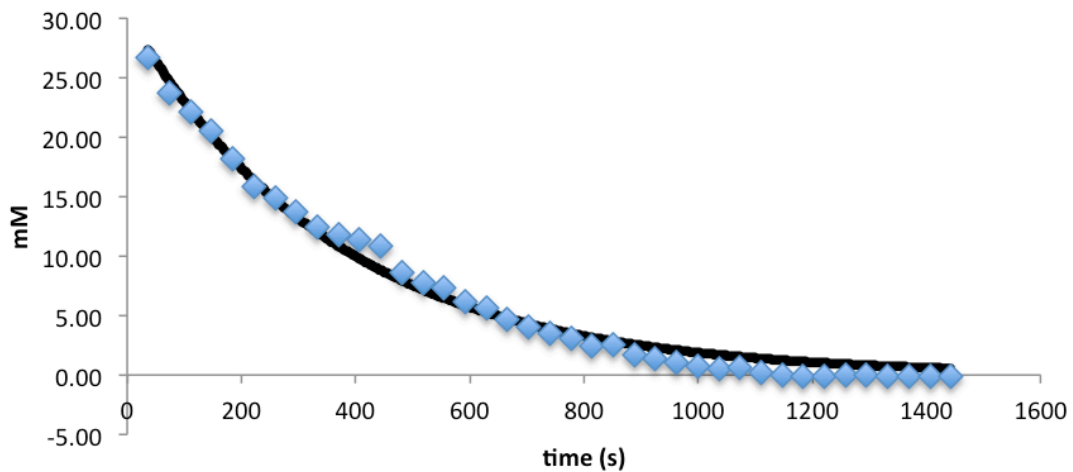
Figure 264. Decay of complex **111** (Run 3).

Table 41. Data for the decay of complex **72** (Run 3).

time (s)	Integral IS (−120.00 ppm)	Integral 8B4 (−117.36 ppm)	[mM] 8-B-4
37	902	1225	26.65
74	916	1104	23.71
111	925	966	22.14
148	903	874	20.46
185	932	814	18.13
222	847	753	15.82
259	935	694	14.93
296	908	640	13.71
333	850	593	12.41
370	888	525	11.84
407	868	482	11.36
444	934	448	10.87
481	936	414	8.61
518	865	363	7.80
555	913	326	7.38
592	850	284	6.19
629	948	252	5.60
666	903	219	4.67
703	896	188	4.03
740	936	179	3.55
777	937	140	3.08
814	906	102	2.49
851	947	85	2.57
888	920	74	1.71
925	951	49	1.34
962	891	44	1.10
999	930	46	0.69
1036	929	31	0.54
1073	930	12	0.59
1110	935	-2	0.20
1147	932	-7	-0.04
1184	929	-4	-0.13
1221	942	-1	-0.10
1258	948	-4	-0.02
1295	871	-3	-0.05
1332	878	-4	-0.08
1369	838	-7	-0.15
1406	966	-4	-0.14

Experiment 56: Kinetic Measurement for decay of 8-B-4 complex 105 in THF/CH₃OH at −30 °C.
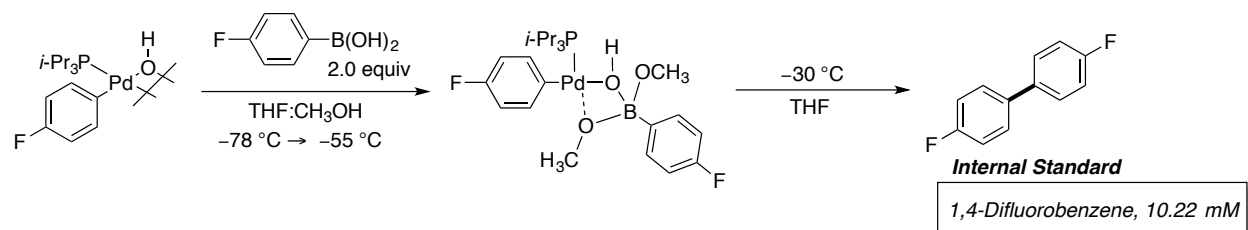
Internal Standard
1,4-Difluorobenzene, 10.22 mM

A 1-mL volumetric flask was charged with 4-fluorophenylboroxine (77.0 mg, 210 μmol, 1.0 equiv) followed by DI-H₂O (11 μL, 631 μmol, 3.0 equiv). Then ~0.5 mL of THF (SDS) was added followed by sonication until the solid had dissolved. Once dissolved the flask was filled to the mark with THF (SDS) generating a 0.63 M solution of 4-fluorophenylboronic acid.

A 2-mL volumetric flask was taken into the dry box and charged with [(*i*-Pr₃P)Pd(4-FC₆H₄)(μ-OH)]₂ (30.8 mg, 41 μmol, 1.0 equiv) and 1,4-difluorobenzene (2.5 μL, 24 μmol) followed by dissolving with THF (SDS) to the 2-mL mark. An oven dried, 5-mm NMR tube was taken into the dry box and 500 μL of the freshly prepared solution was added. The tube was capped with a septum and Teflon taped. The sample was removed from the glove box and inserted into a −78 °C acetone dry-ice bath followed by the addition of (35 μL, 20.5 μmol, 2.0 equiv) of the 4-fluorophenylboronic acid solution *via* a μL glass syringe. The NMR tube was vortexed (not shaken) and cleaned with a Kimwipe followed by re-insertion into the −78 °C bath. Then 60 μL of CH₃OH (Mg) was added *via* syringe and the tube was vortexed (not shaken) followed by placement into the NMR probe set to −55 °C. The formation of the 8-B-4 species was observed after ~10-15 min. The tube was removed and placed back into the −78 °C followed by re-insertion into the NMR probe set to −30 °C.

Using the fluorine channel to collect a spectrum every 37 s the progress of the reaction was monitored by the decay of the 8-B-4 complex fluorine signal (−118.40 ppm) and formation of cross-coupling product fluorine signal (−116.45 ppm) in comparison with the internal reference 1,4-difluorbenzene (−120.00 ppm). The first order decay and formation profiles were fitted with OrginPro 2015 software using equations 3 and 4 respectively. This procedure was performed three times to obtain an average rate.

Table 42. Results from the cross-coupling reaction from the 8-B-4 complex **68** at −30 °C in THF:CH₃OH.

Entry	k (s⁻¹) (Decay **105**)	k (s⁻¹) (Form **73**)	A_0 [mM] (Decay **105**)	A_0 [mM] (Form **73**)
Run 1	$(1.64 \pm 0.03) \times 10^{-3}$	$(1.65 \pm 0.03) \times 10^{-3}$	44.42 ± 0.64	41.42 ± 0.24
Run 2	$(1.32 \pm 0.03) \times 10^{-3}$	$(1.53 \pm 0.06) \times 10^{-3}$	28.58 ± 0.43	32.07 ± 0.44
Run 3	$(1.28 \pm 0.05) \times 10^{-3}$	$(1.47 \pm 0.04) \times 10^{-3}$	31.80 ± 0.53	31.28 ± 0.33

k avg. Decay of 8-B-4 complex 68 = (1.41 ± 0.02) x 10⁻³ s⁻¹
k avg. Formation of 53 = (1.55 ± 0.09) x 10⁻³ s⁻¹
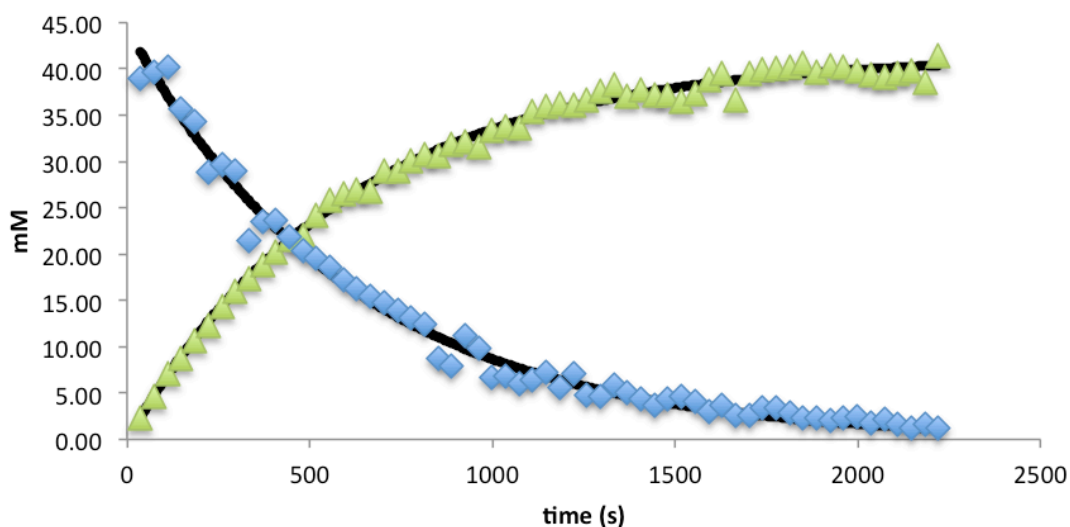
Figure 265. Decay of 8-B-4 complex **105** and formation of cross-coupling product **73** at −30 °C in THF:CH₃OH. (Run 1).

Table 43. Data for decay of 8-B-4 complex **105** and formation of cross-coupling **73** product at −30 °C in THF:CH₃OH. (Run 1).

time (s)	Integral IS (−120.00 ppm)	Integral 8-B-4 (−123.20 ppm)	Integral CCP (−116.45 ppm)	[mM] 8-B-4	[mM] CCP
37	1284	2450	299	39.01	2.38
74	1156	2244	526	39.68	4.65
111	1113	2185	770	40.12	7.07
148	1176	2054	1002	35.70	8.71
185	1197	2011	1250	34.33	10.67
222	1211	1713	1455	28.90	12.27
259	1172	1703	1648	29.71	14.37

Table 43. (cont.)

296	1185	1679	1854	28.96	15.99
333	1195	1251	2031	21.40	17.37
370	1202	1381	2219	23.48	18.86
407	1157	1341	2292	23.69	20.25
444	1161	1240	2452	21.83	21.59
481	1199	1194	2578	20.36	21.97
518	1165	1112	2761	19.51	24.22
555	1151	1044	2913	18.54	25.88
592	1148	965	2982	17.19	26.56
629	1159	923	3056	16.27	26.95
666	1155	869	3020	15.39	26.73
703	1166	844	3305	14.81	28.98
740	1167	799	3304	13.99	28.93
777	1183	757	3479	13.08	30.06
814	1176	719	3533	12.50	30.69
851	1160	496	3469	8.73	30.56
888	1178	461	3671	7.99	31.84
925	1196	655	3763	11.19	32.16
962	1239	598	3830	9.86	31.59
999	1191	388	3882	6.66	33.31
1036	1158	387	3831	6.83	33.83
1073	1191	347	3924	5.95	33.67
1110	1194	373	4142	6.39	35.45
1147	1169	415	4115	7.26	35.98
1184	1193	330	4223	5.66	36.19
1221	1195	419	4214	7.16	36.05
1258	1207	284	4331	4.81	36.68
1295	1200	275	4410	4.68	37.54
1332	1169	333	4375	5.81	38.24
1369	1212	300	4400	5.07	37.11
1406	1203	258	4434	4.38	37.68
1443	1201	218	4363	3.71	37.13
1480	1240	264	4504	4.36	37.13
1517	1296	294	4621	4.64	36.44
1554	1259	250	4600	4.06	37.34
1591	1204	174	4574	2.95	38.84
1628	1197	216	4627	3.69	39.51
1665	1286	165	4605	2.63	36.60
1702	1219	152	4712	2.54	39.49

Table 43. (cont.)

1739	1202	203	4691	3.45	39.88
1776	1192	202	4676	3.46	40.10
1813	1204	165	4728	2.80	40.14
1850	1242	140	4930	2.30	40.56
1887	1214	134	4711	2.25	39.66
1924	1269	129	5001	2.07	40.29
1961	1292	146	5088	2.32	40.25
1998	1237	148	4808	2.44	39.72
2035	1284	115	4945	1.83	39.37
2072	1285	137	4915	2.18	39.09
2109	1252	101	4840	1.65	39.49
2146	1252	74	4872	1.21	39.77
2183	1285	102	4855	1.63	38.61
2220	1213	74	4918	1.24	41.44
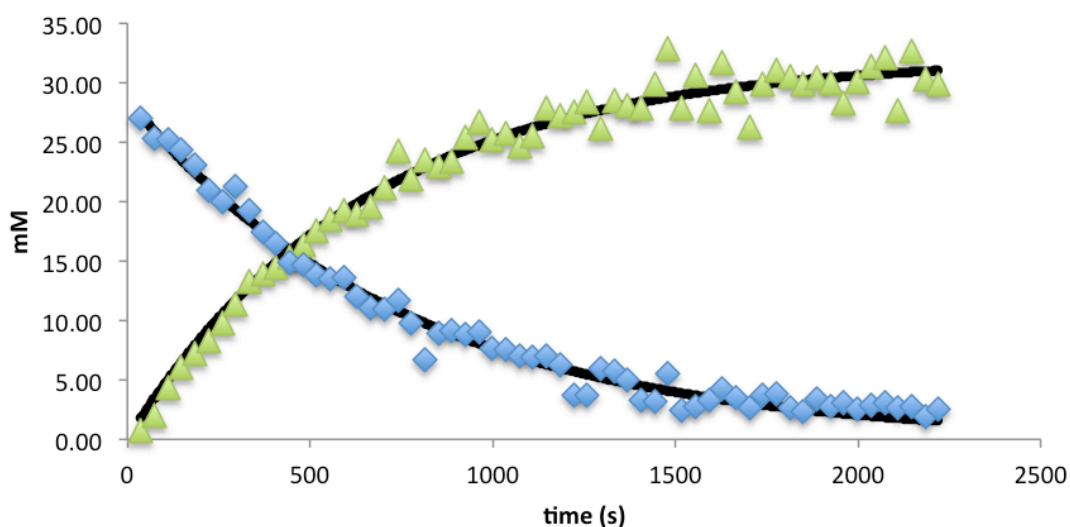
Figure 266. Decay of 8-B-4 complex **105** and formation of cross-coupling product **73** at −30 °C in THF:CH$_3$OH. (Run 2).

Table 44. Data for decay of 8-B-4 complex **105** and formation of cross-coupling product **73** at −30 °C in THF:CH$_3$OH. (Run 2).

time (s)	Integral IS (−120.00 ppm)	Integral 8-B-4 (−123.20 ppm)	Integral CCP (−116.45 ppm)	[mM] 8-B-4	[mM] CCP
37	2070	2740	148	27.05	0.73
74	1896	2350	377	25.32	2.03
111	1843	2273	787	25.22	4.37
148	1806	2154	1065	24.39	6.03
185	1930	2179	1362	23.08	7.22

Table 44 (cont.)

222	1978	2028	1597	20.96	8.25
259	1930	1884	1846	19.95	9.77
296	1804	1872	2010	21.21	11.39
333	1825	1713	2372	19.19	13.28
370	1840	1569	2511	17.43	13.95
407	1913	1542	2708	16.47	14.46
444	1934	1409	2904	14.90	15.35
481	1845	1325	2963	14.68	16.42
518	1868	1266	3206	13.85	17.54
555	1855	1229	3353	13.54	18.48
592	1826	1216	3447	13.62	19.29
629	1833	1078	3403	12.02	18.97
666	1918	1037	3668	11.05	19.54
703	1863	999	3853	10.96	21.13
740	1638	937	3892	11.70	24.28
777	1906	916	4082	9.82	21.89
814	1807	595	4162	6.73	23.54
851	1890	825	4255	8.92	23.01
888	1877	839	4287	9.14	23.34
925	1771	765	4402	8.83	25.40
962	1778	785	4637	9.02	26.65
999	1858	697	4574	7.66	25.16
1036	1785	657	4493	7.52	25.72
1073	1851	635	4461	7.01	24.64
1110	1858	631	4634	6.94	25.49
1147	1791	614	4879	7.00	27.84
1184	1893	578	5035	6.24	27.18
1221	1798	326	4853	3.70	27.59
1258	1790	322	4962	3.68	28.33
1295	1863	546	4773	5.99	26.18
1332	1797	500	5011	5.69	28.51
1369	1793	437	4934	4.98	28.12
1406	1835	299	4999	3.33	27.85
1443	1761	278	5153	3.22	29.91
1480	1543	418	4958	5.54	32.83
1517	1923	234	5239	2.49	27.84
1554	1726	236	5164	2.80	30.58
1591	1850	302	5003	3.33	27.65
1628	1746	364	5404	4.26	31.63
1665	1820	309	5217	3.47	29.29

Table 44. (cont.)

1702	1912	248	4916	2.65	26.28
1739	1797	326	5255	3.71	29.88
1776	1739	327	5287	3.85	31.08
1813	1807	235	5404	2.66	30.56
1850	1829	209	5342	2.33	29.84
1887	1874	314	5576	3.43	30.41
1924	1793	240	5261	2.74	29.99
1961	1850	282	5127	3.11	28.32
1998	1889	239	5567	2.59	30.12
2035	1772	248	5431	2.87	31.33
2072	1816	274	5713	3.08	32.15
2109	1842	241	4978	2.67	27.63
2146	1784	237	5701	2.72	32.67
2183	1901	175	5645	1.88	30.35
2220	1925	238	5631	2.53	29.90
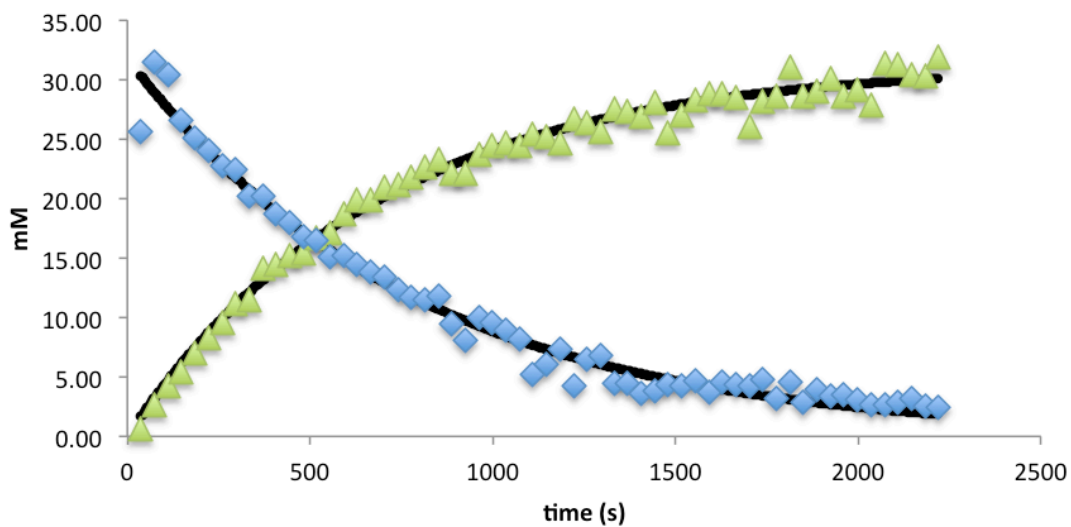
Figure 267. Decay of 8-B-4 complex **105** and formation of cross-coupling product **73** at −30 °C in THF:CH$_3$OH. (Run 3).

Table 45. Data for decay of 8-B-4 complex and formation of cross-coupling product at −30 °C in THF:CH₃OH. (Run 3).

time (s)	Integral IS (−120.00 ppm)	Integral 8-B-4 (−123.20 ppm)	Integral CCP (−116.45 ppm)	[mM] 8-B-4	[mM] CCP
37	2091	2625	135	25.66	0.66
74	1484	2282	392	31.44	2.70
111	1523	2264	639	30.40	4.29
148	1738	2262	916	26.60	5.39
185	1747	2141	1192	25.04	6.97
222	1729	2034	1411	24.04	8.34
259	1748	1943	1636	22.73	9.57
296	1702	1871	1862	22.47	11.18
333	1806	1780	2029	20.15	11.49
370	1705	1685	2363	20.21	14.17
407	1724	1577	2432	18.70	14.42
444	1712	1503	2542	17.95	15.18
481	1778	1461	2677	16.80	15.39
518	1710	1382	2791	16.52	16.68
555	1785	1318	2983	15.09	17.08
592	1717	1281	3153	15.25	18.76
629	1658	1173	3231	14.47	19.92
666	1726	1169	3364	13.85	19.92
703	1675	1100	3434	13.41	20.95
740	1714	1035	3557	12.34	21.20
777	1749	1005	3726	11.74	21.77
814	1703	952	3773	11.43	22.65
851	1655	956	3775	11.81	23.31
888	1763	811	3817	9.41	22.13
925	1735	684	3757	8.06	22.13
962	1731	846	4020	9.99	23.74
999	1696	794	4056	9.58	24.45
1036	1711	751	4125	8.97	24.64
1073	1770	712	4232	8.22	24.44
1110	1678	431	4165	5.25	25.36
1147	1682	501	4146	6.09	25.20
1184	1748	625	4225	7.31	24.71
1221	1725	356	4499	4.22	26.65
1258	1750	555	4519	6.48	26.39
1295	1709	568	4282	6.79	25.60
1332	1731	380	4656	4.49	27.49
1369	1700	373	4555	4.48	27.37

Table 45. (cont.)

1406	1805	319	4755	3.62	26.92
1443	1698	317	4669	3.81	28.09
1480	1777	378	4442	4.34	25.55
1517	1773	372	4692	4.28	27.05
1554	1740	399	4811	4.69	28.25
1591	1688	308	4766	3.73	28.85
1628	1713	384	4839	4.58	28.86
1665	1716	362	4781	4.31	28.48
1702	1867	392	4759	4.29	26.05
1739	1748	405	4817	4.73	28.16
1776	1703	264	4768	3.17	28.62
1813	1600	360	4860	4.60	31.05
1850	1716	239	4810	2.85	28.65
1887	1691	324	4801	3.91	29.02
1924	1720	288	5067	3.42	30.11
1961	1801	313	5045	3.55	28.63
1998	1746	260	4976	3.05	29.13
2035	1706	222	4654	2.66	27.88
2072	1706	223	5239	2.67	31.38
2109	1687	235	5160	2.84	31.26
2146	1723	267	5130	3.17	30.43
2183	1666	206	4947	2.53	30.35
2220	1708	203	5335	2.43	31.92

Experiment 57. Kinetic Measurement for decay of 6-B-3 complex 71 at 20 °C with 2.85 equiv of *i*-Pr₃P (Runs 1-3)

Internal Standard

1,4-Difluorobenzene, 10.22 mM
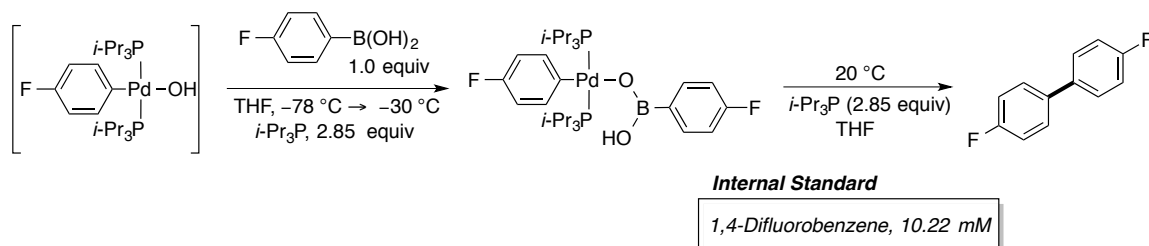
A 2-mL volumetric flask was charged with 4-fluorophenylboroxine (51.3 mg, 140 μmol, 1.0 equiv) followed by H₂O (8 μL, 420 μmol, 3.0 equiv). Then ~1 mL of THF was added and sonicated until the solid had dissolved. Once dissolved the flask was filled to the mark with THF (SDS) generating a 0.21 M solution.

A 2-mL volumetric flask was taken into the dry box and charged with [(*i*-Pr₃P)Pd(4-FC₆H₄)(μ-OH)]₂ (30.8 mg, 41 μmol, 1.0 equiv), 1,4-difluorobenzene (2.5 μL, 24 μmol) and *i*-Pr₃P (60 μL, 313 μmol, 7.63 equiv). Then the solution was diluted to the 2-mL mark.

An oven dried, 5-mm, NMR tube was taken into the dry box and 500 μL of Stock Solution was added. The tube was capped with a septum and Teflon taped. The sample was removed from the glove box and inserted into a −78 °C acetone dry-ice bath followed by the addition of the 4-fluorophenylboronic acid Stock Solution (95 μL, 20.5 μmol, 1.0 equiv) *via* a 100 μL glass syringe. The NMR tube was shaken and cleaned with a Kimwipe then placed into the NMR probe pre-cooled to −30 °C. The formation of the 6-B-3 complex was found to be complete after ~3-4 h by ^{31}P and ^{19}F NMR spectroscopy. The sample was removed from the spectrometer and placed into a −78 °C acetone dry-ice bath, followed by shaking and reinserting into the spectrometer set to 20 °C. Using the fluorine channel to collect a spectrum every 24.2 min the progress of the reaction was monitored by the decay of the 6-B-3 complex fluorine signal (−115.74 ppm) in comparison with the internal reference (1,4-difluorobenzene, −120.00 ppm). The *S*-shaped curve was fitted with OrginPro 2015 software using equation 4. Using the calculated values for k_c, q, and $[A]_0$ a maximum rate was determined using equation 5. This procedure was performed three times to obtain an average maximum rate *(44)*.

Equation 7.

$$[A] = ([A]_0 + q)\frac{[A]_0}{[A]_0 + q \cdot exp[k_c([A]_0 + q)t]}$$

391

Equation 8.

$$v = k_c \left\{ \left(\frac{[A]_0 + q}{2} \right)^2 - \left([A] - \frac{[A]_0 + q}{2} \right)^2 \right\}$$

Table 46. Calculated values from the decay of **71** with 2.85 equiv of i-Pr$_3$P.

Entry	kc	q	A$_0$ [mM]	v_{max} ($mM\,s^{-1}$)
Run 1	$(1.406 \pm 0.17) \times 10^{-5}$	9.522 ± 2.17	28.82 ± 0.77	0.00517
Run 2	$(1.384 \pm 0.15) \times 10^{-5}$	6.472 ± 1.50	26.98 ± 0.67	0.00387
Run 3	$(1.774 \pm 0.04) \times 10^{-5}$	3.796 ± 0.182	27.75 ± 0.14	0.00441

v_{max} *avg.* = **(4.48 ± 0.65) x 10^{-3} mM s^{-1}**
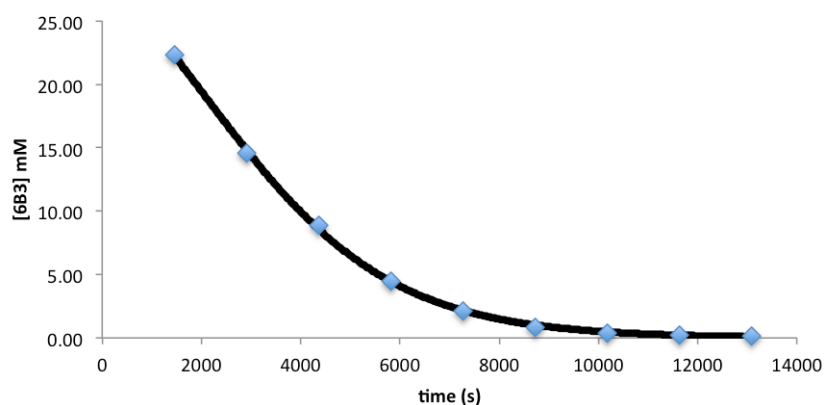
Figure 268. Decay of complex **71** with 2.85 equiv of i-Pr$_3$P (Run 1).
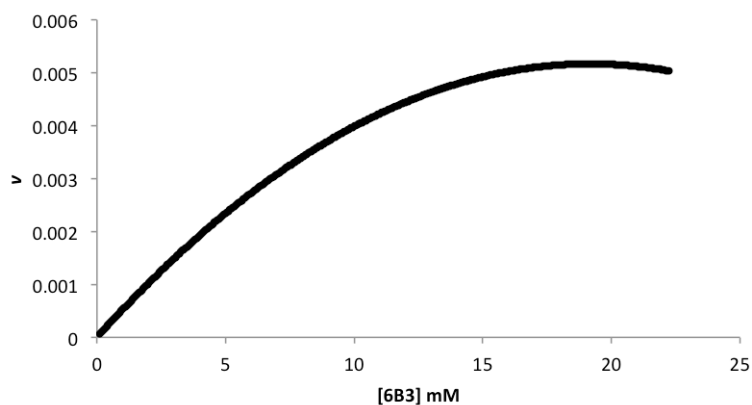
Figure 269. Rate vs. concentration of complex **71** with 2.85 equiv of i-Pr$_3$P (Run 1).

Table 47. Data for the decay of the complex **71** with 2.85 equiv of i-Pr$_3$P (Run 1).

time (s)	Integral IS (−120.00 ppm)	Integral 6-B-3 (−115.74 ppm)	[mM] 6-B-3
1454	29646	32367	22.32

Table 47. (cont.)

2908	31598	22497	14.55
4362	30620	13353	8.91
5816	31396	6839	4.45
7270	30957	3184	2.10
8724	30831	1231	0.82
10178	30781	536	0.36
11632	30538	289	0.19
13086	31559	195	0.13
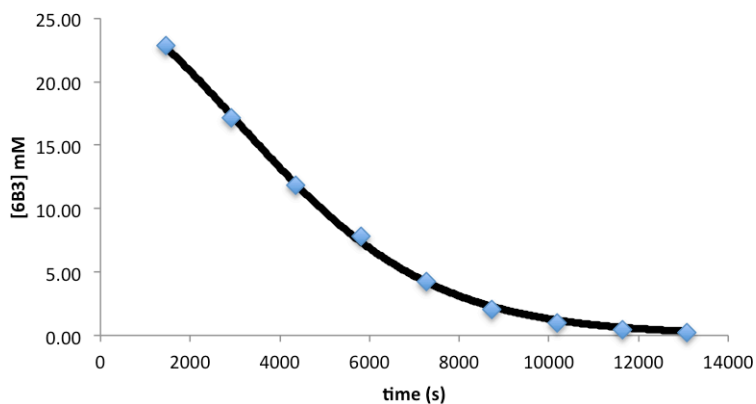
Figure 270. Decay of complex **71** with 2.85 equiv of i-Pr$_3$P (Run 2).
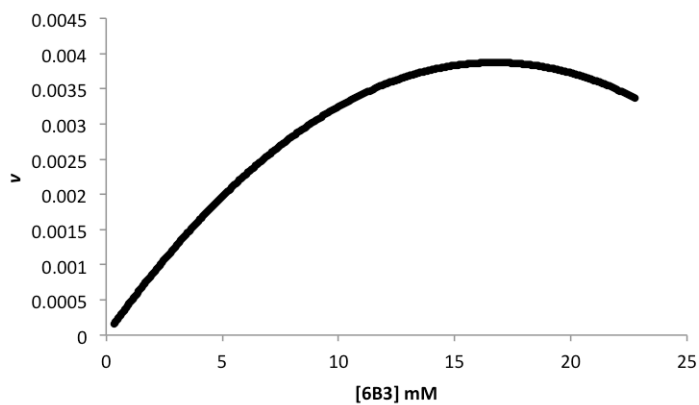
Figure 271. Rate vs. concentration of complex **71** with 2.85 equiv of i-Pr$_3$P (Run 2).

Table 48. Data for the decay of complex **71** with 2.85 equiv of i-Pr$_3$P (Run 2).

time (s)	Integral IS (−120.00 ppm)	Integral 6-B-3 (−115.74 ppm)	[mM] 6-B-3
1454	31407	35167	22.89

Table 48. (cont.)

2908	31411	26336	17.14
4362	31983	18505	11.83
5816	31075	11904	7.83
7270	30846	6398	4.24
8724	32127	3215	2.05
10178	31781	1563	1.01
11632	31837	662	0.43
13086	31864	332	0.21
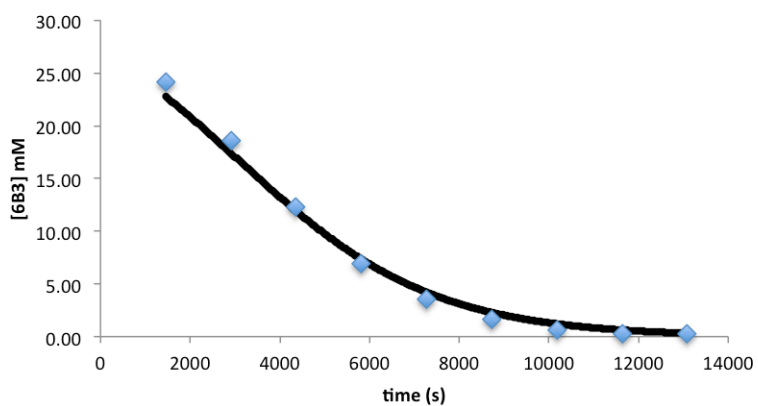
Figure 272. Decay of complex **71** with 2.85 equiv of i-Pr$_3$P (Run 3).
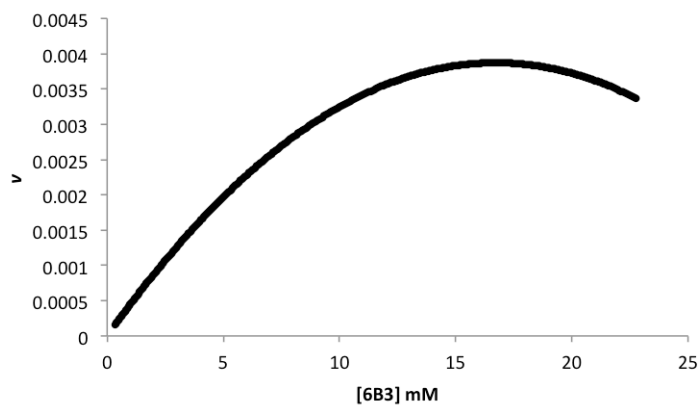
Figure 273. Rate vs. concentration of complex **71** with 2.85 equiv of i-Pr$_3$P (Run 3).

Table 49. Data for the decay of complex **71** with 2.85 equiv of *i*-Pr$_3$P (Run 3).

time (s)	Integral IS (−120.00 ppm)	Integral 6-B-3 (−115.74 ppm)	[mM] 6-B-3
1454	30648	36170	24.12
2908	29898	27158	18.57
4362	29243	17562	12.28
5816	29087	9900	6.96
7270	29253	5073	3.54
8724	29411	2326	1.62
10178	29419	953	0.66
11632	28331	428	0.31
13086	28916	352	0.25

Experiment 58. Kinetic Measurement for decay of complex 71 at 20 °C with 3.81 equiv of *i*-Pr₃P (Runs 1-3)

Internal Standard
1,4-Difluorobenzene, 10.22 mM

A 5-mL volumetric flask was charged with 4-fluorophenylboroxine (128 mg, 350 µmol, 1.0 equiv) followed by H₂O (19 µL, 1.05 mmol, 3.0 equiv). Then ~2 mL of THF was added followed by sonication until the solid had dissolved. Once dissolved the flask was filled to the mark with THF (SDS) generating a 0.21 M solution.

A 2-mL volumetric flask was taken into the dry box and charged with [(*i*-Pr₃P)Pd(4-FC₆H₄)(µ-OH)]₂ (30.8 mg, 41 µmol, 1.0 equiv), 1,4-difluorobenzene (2.5 µL, 24 µmol) and *i*-Pr₃P (75 µL, 9.54 equiv, 391 µmol) followed by dissolving with THF (SDS) to the 2-mL mark.

An oven dried, 5-mm, NMR tube was taken into the dry box and 500 µL of Stock Solution was added. The tube was capped with a septum and Teflon taped. The sample was removed from the glove box and inserted into a −78 °C acetone dry-ice bath followed by the addition of the 4-fluorophenylboronic acid Stock Solution (95 µL, 20.5 µmol, 1.0 equiv) *via* a 100 µL glass syringe. The NMR tube was shaken and cleaned with a Kimwipe then placed into the NMR probe set to −30 °C. The formation of the 6-B-3 complex was found to be complete after ~3-4 h by ^{31}P and ^{19}F NMR spectroscopy. The sample was removed from the spectrometer and placed into a −78 °C acetone dry-ice bath, followed by shaking and reinserting into the spectrometer set to 20 °C. Using the fluorine channel to collect a spectrum every 24.2 min the progress of the reaction was monitored by the decay of the 6-B-3 complex fluorine signal (−115.74 ppm) in comparison with the internal reference (1,4-difluorobenzene, −120.00 ppm). The S-shaped curve was fitted with OrginPro 2015 software using equation 3. Using the calculated values for k_c, q, and $[A]_0$ a maximum rate was determined using equation 4. This procedure was performed three times to obtain an average maximum rate.

Table 50. Calculated values from the decay of **71** with 3.81 equiv of i-Pr$_3$P.

Entry	kc	q	A_0 [mM]	v_{max} $(mM\ s^{-1})$
Run 1	$(1.534 \pm 0.16) \times 10^{-5}$	3.733 ± 0.675	25.81 ± 0.47	0.00335
Run 2	$(1.371 \pm 0.06) \times 10^{-5}$	3.965 ± 0.416	26.54 ± 0.27	0.00312
Run 3	$(1.107 \pm 0.17) \times 10^{-5}$	6.295 ± 2.10	27.93 ± 0.95	0.00324

v_{max} *avg.* = (3.24 ± 0.12) x 10^{-3} mM s^{-1}
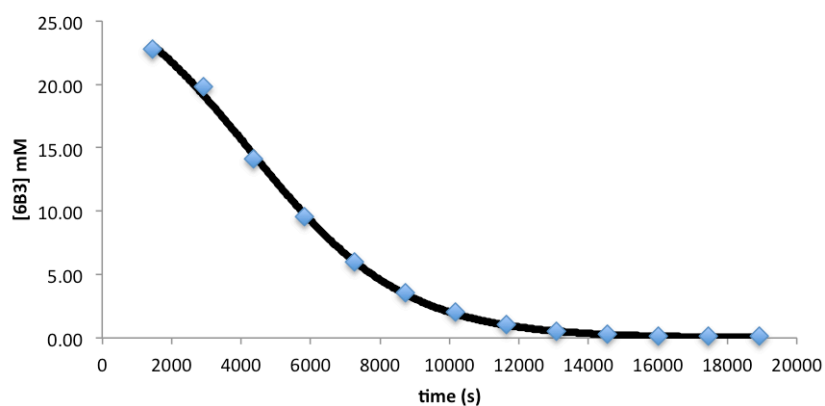
Figure 274. Decay of complex **71** with 3.81 equiv of i-Pr$_3$P (Run 1).
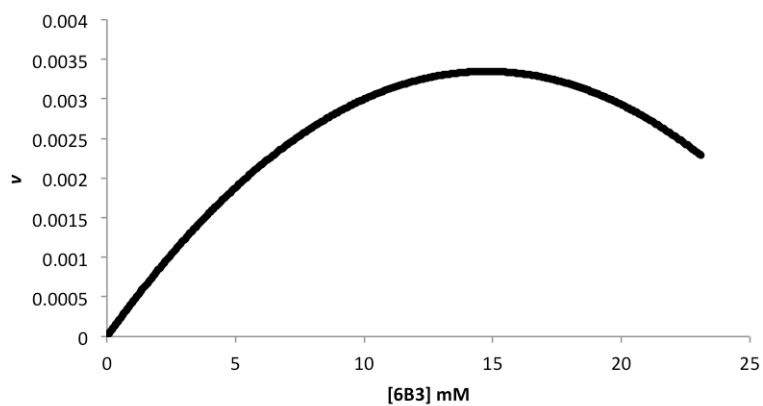
Figure 275. Rate vs. concentration of complex **71** with 3.81 equiv of i-Pr$_3$P (Run 1).

Table 51. Data for the decay of complex **71** with 3.81 equiv of i-Pr$_3$P (Run 1).

time (s)	Integral IS (−120.00 ppm)	Integral 6-B-3 (−115.74 ppm)	[mM] 6-B-3
1454	35030	39080	22.80
2908	33325	32308	19.82
4362	34793	24079	14.15
5816	35325	16544	9.57
7270	35049	10345	6.03
8724	35499	6198	3.57
10178	35962	3585	2.04
11632	34600	1850	1.09
13086	35706	924	0.53
14540	35478	543	0.31
15994	35573	303	0.17
17448	33954	309	0.19
18902	33004	211	0.13
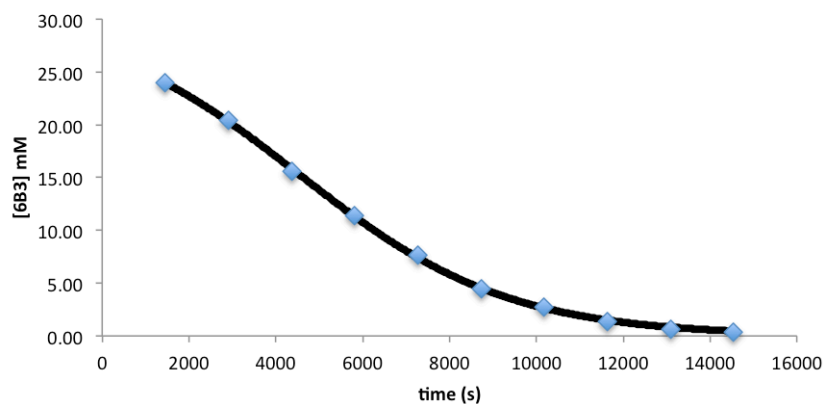
Figure 276. Decay of complex **71** with 3.81 equiv of i-Pr$_3$P (Run 2).
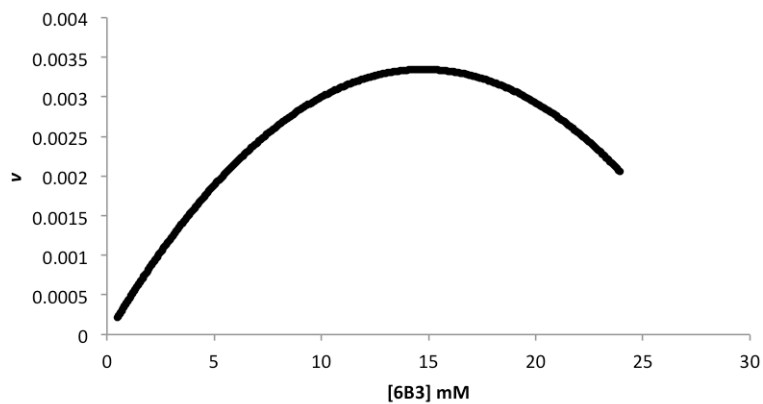
Figure 277. Rate vs. concentration of complex **71** with 3.81 equiv of i-Pr$_3$P (Run 2).

Table 52. Data for the decay of complex **71** with 3.81 equiv of *i*-Pr₃P (Run 2).

time (s)	Integral IS (−120.00 ppm)	Integral 6-B-3 (−115.74 ppm)	[mM] 6-B-3
1454	34275	40147	23.94
2908	35127	35024	20.38
4362	34579	26360	15.58
5816	34509	19197	11.37
7270	35468	13206	7.61
8724	35469	7706	4.44
10178	33612	4461	2.71
11632	34361	2309	1.37
13086	34759	1155	0.68
14540	35384	645	0.37
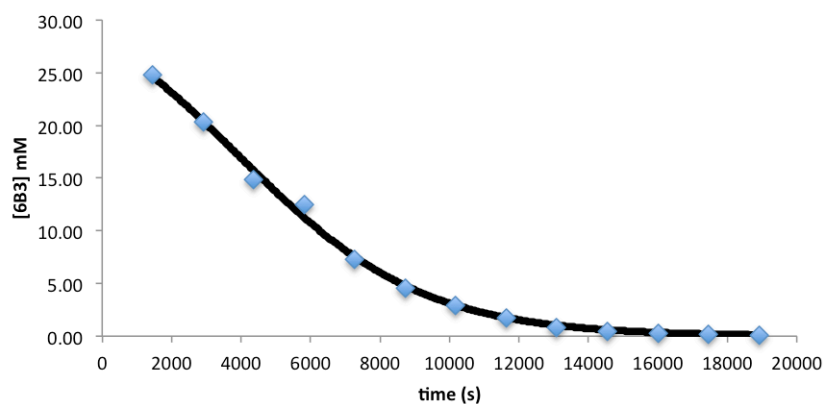
Figure 278. Decay of complex **71** with 3.81 equiv of *i*-Pr₃P (Run 3).
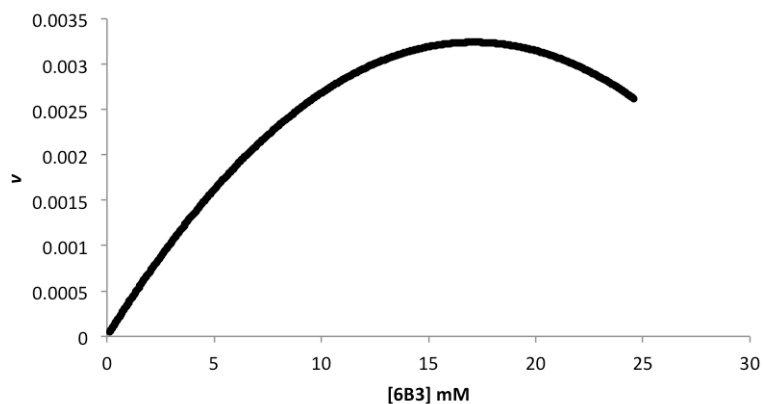
Figure 279. Rate vs. concentration of complex **71** with 3.81 equiv of *i*-Pr₃P (Run 3).

Table 53. Data for the decay of complex **71** with 3.81 equiv of *i*-Pr₃P (Run 3).

time (s)	Integral IS (−120.00 ppm)	Integral 6-B-3 (−115.74 ppm)	[mM] 6-B-3
1454	38441	46582	24.77
2908	39232	39014	20.33
4362	38963	28270	14.83
5816	37009	22677	12.52
7270	39331	13960	7.25
8724	39563	8835	4.56
10178	39531	5684	2.94
11632	39563	3428	1.77
13086	38820	1599	0.84
14540	39509	935	0.48
15994	37548	473	0.26
17448	38573	279	0.15
18902	34879	102	0.06

Experiment 59. Kinetic Measurement for decay of 6-B-3 complex 71 at 20 °C with 5.41 equiv of *i*-Pr₃P (Runs 1-3)

Internal Standard
1,4-Difluorobenzene, 10.22 mM

A 5-mL volumetric flask was charged with 4-fluorophenylboroxine (128 mg, 350 μmol, 1.0 equiv) followed by H₂O (19 μL, 1.05 mmol, 3.0 equiv). Then ~2 mL of THF was added followed by sonication until the solid had dissolved. Once dissolved the flask was filled to the mark with THF (SDS) generating a 0.21 M solution.

A 2-mL volumetric flask was taken into the dry box and charged with [(*i*-Pr₃P)Pd(4-FC₆H₄)(μ-OH)]₂ (30.8 mg, 41 μmol, 1.0 equiv), 1,4-difluorobenzene (2.5 μL, 24 μmol) and *i*-Pr₃P (100 μL, 521 μmol, 12.71 equiv) followed by dissolving with THF (SDS) to the 2-mL mark.

An oven dried, 5-mm, NMR tube was taken into the dry box and 500 μL of Stock Solution was added. The tube was capped with a septum and Teflon taped. The sample was removed from the glove box and inserted into a −78 °C acetone dry-ice bath followed by the addition of the 4-fluorophenylboronic acid Stock Solution (95 μL, 20.5 μmol, 1.0 equiv) *via* a 100 μL glass syringe. The NMR tube was shaken and cleaned with a Kimwipe then placed into the NMR probe pre-cooled to −30 °C. The formation of the 6-B-3 complex was found to be complete after ~3-4 h by ³¹P and ¹⁹F NMR spectroscopy. The sample was removed from the spectrometer and placed into a −78 °C acetone dry-ice bath, followed by shaking and reinserting into the spectrometer set to 20 °C. Using the fluorine channel to collect a spectrum every 24.2 min the progress of the reaction was monitored by the decay of the 6-B-3 complex fluorine signal (−115.74 ppm) in comparison with the internal reference (1,4-difluorobenzene, −120.00 ppm). The S-shaped curve was fitted with OrginPro 2015 software using equation 3. Using the calculated values for k_c, q, and $[A]_0$ a maximum rate was determined using equation 4. This procedure was performed three times to obtain an average maximum rate.

Table 54. Calculated values from the decay of **71** with 5.41 equiv of i-Pr$_3$P.

Entry	kc	q	A_0 [mM]	v_{max} ($mM\ s^{-1}$)
Run 1	$(6.403 \pm 0.38) \times 10^{-6}$	9.278 ± 1.07	29.31 ± 0.33	0.00238
Run 2	$(6.110 \pm 0.32) \times 10^{-6}$	9.066 ± 0.940	31.35 ± 0.31	0.00245
Run 3	$(6.968 \pm 0.64) \times 10^{-6}$	7.353 ± 1.39	30.07 ± 0.55	0.00244

v_{max} ***avg.*** $= (2.42 \pm 0.48) \times 10^{-3}$ **mM s**$^{-1}$
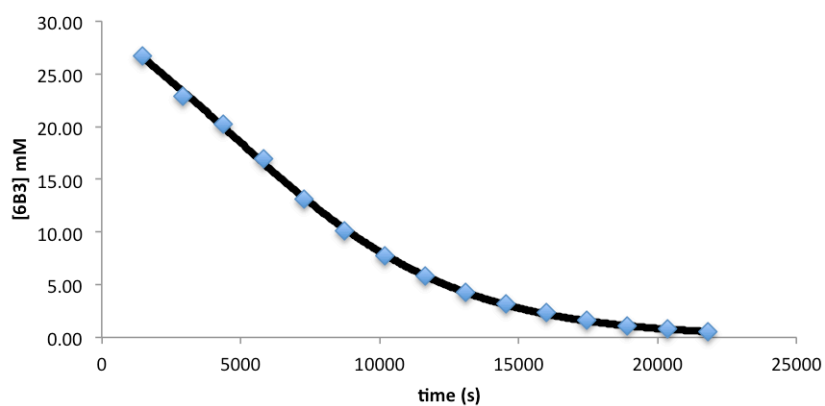
Figure 280. Decay of complex **71** with 5.41 equiv of i-Pr$_3$P (Run 1).
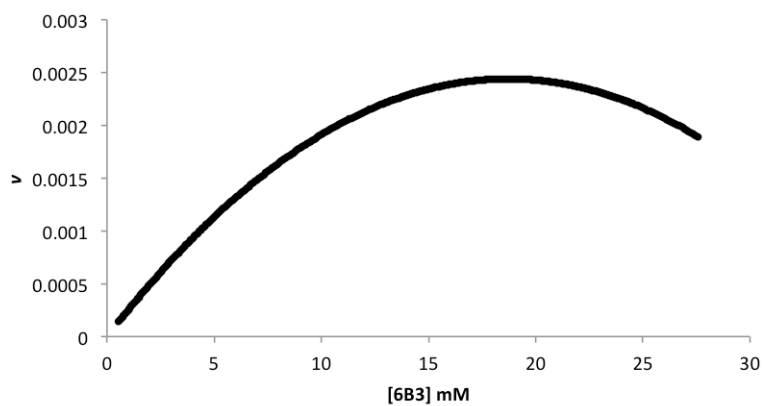
Figure 281. Rate vs. concentration of complex **71** with 5.41 equiv of i-Pr$_3$P (Run 1).

Table 55. Data for the decay of complex **71** with 5.41 equiv of *i*-Pr₃P (Run 1).

time (s)	Integral IS (−120.00 ppm)	Integral 6-B-3 (−115.74 ppm)	[mM] 6-B-3
1454	40329	52666	26.69
2908	40130	44983	22.91
4362	40446	40119	20.27
5816	39667	32861	16.93
7270	40735	26105	13.10
8724	40935	20227	10.10
10178	40786	15492	7.76
11632	41035	11708	5.83
13086	40241	8460	4.30
14540	40350	6306	3.19
15994	39945	4554	2.33
17448	40728	3239	1.63
18902	40649	2153	1.08
20356	40052	1584	0.81
21810	41339	1037	0.51
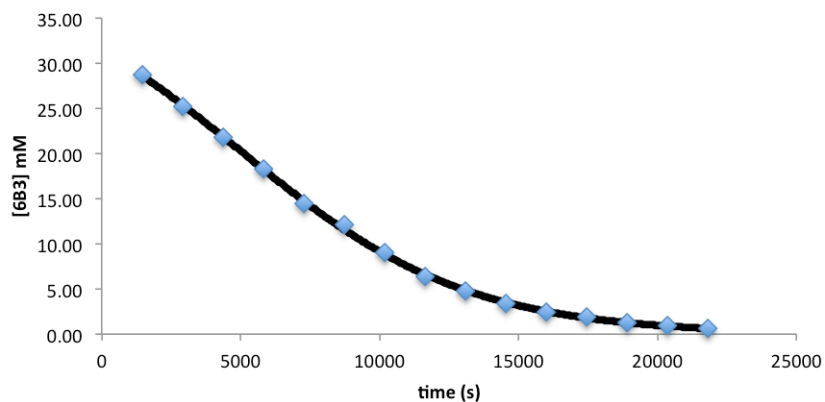
Figure 282. Decay of complex **71** with 5.41 equiv of *i*-Pr₃P (Run 2).
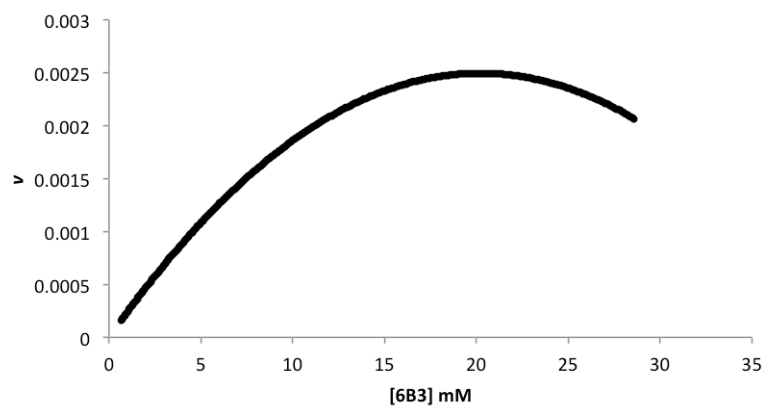
Figure 283. Rate vs. concentration of complex **71** with 5.41 equiv of *i*-Pr$_3$P (Run 2).

Table 56. Data for the decay of complex **71** with 5.41 equiv of *i*-Pr$_3$P (Run 2).

time (s)	Integral IS (−120.00 ppm)	Integral 6-B-3 (−115.74 ppm)	[mM] 6-B-3
1454	37359	52558	28.76
2908	38408	47297	25.17
4362	39290	41902	21.80
5816	39185	35051	18.28
7270	39867	28110	14.41
8724	39580	23458	12.11
10178	39561	17487	9.04
11632	40376	12630	6.39
13086	40340	9399	4.76
14540	40625	6799	3.42
15994	39346	4666	2.42
17448	39565	3614	1.87
18902	38243	2294	1.23
20356	38219	1726	0.92
21810	41804	1202	0.59
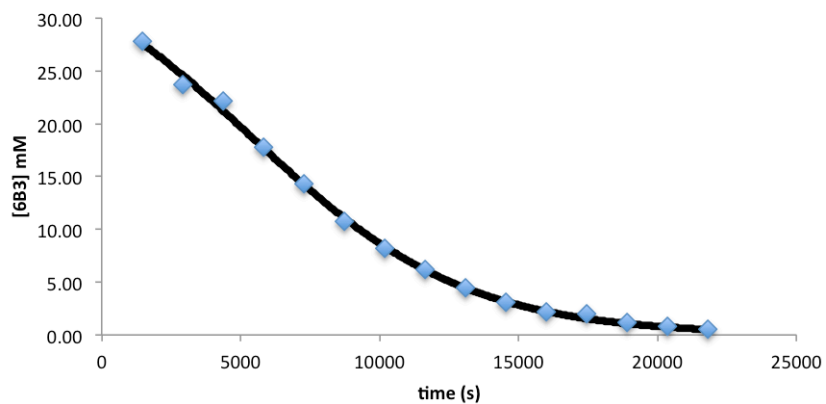
Figure 284. Decay of complex **71** with 5.41 equiv of i-Pr$_3$P (Run 3).
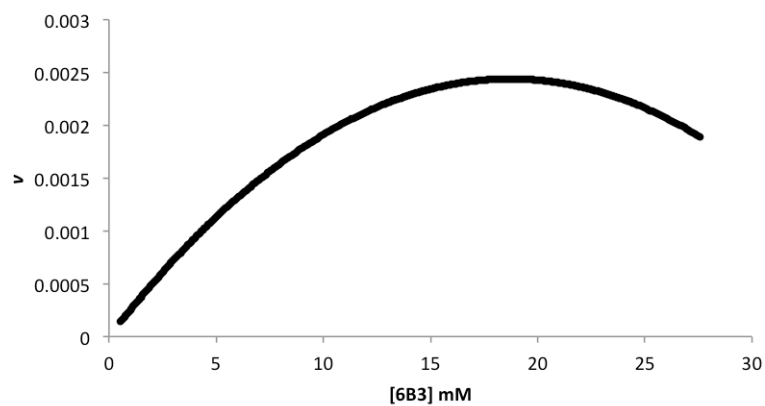
Figure 285. Rate vs. concentration of complex **71** with 5.41 equiv of i-Pr$_3$P (Run 3).

Figure 286. Data for the decay of complex **71** with 5.41 equiv of *i*-Pr₃P (Run 3).

time (s)	Integral IS (−120.00 ppm)	Integral 6-B-3 (−115.74 ppm)	[mM] 6-B-3
1454	40129	54597	27.81
2908	40099	46496	23.70
4362	40122	43386	22.10
5816	40324	34981	17.73
7270	40526	28287	14.27
8724	40861	21490	10.75
10178	40457	16243	8.21
11632	39857	12154	6.23
13086	40170	8723	4.44
14540	40631	6156	3.10
15994	41885	4434	2.16
17448	31805	3098	1.99
18902	40194	2254	1.15
20356	38405	1491	0.79
21810	39107	1110	0.58

Experiment 60. Kinetic Measurement for decay of 6-B-3 complex 51 at 20 °C with 8.62 equiv of *i*-Pr₃P (Runs 1-3)

Internal Standard
1,4-Difluorobenzene, 10.22 mM

A 5-mL volumetric flask was charged with 4-fluorophenylboroxine (128 mg, 350 µmol, 1.0 equiv) followed by H₂O (19 µL, 1.05 mmol, 3.0 equiv). Then ~2 mL of THF was added followed by sonication until the solid had dissolved. Once dissolved the flask was filled to the mark with THF (SDS) generating a 0.21 M solution.

A 2-mL volumetric flask was taken into the dry box and charged with [(*i*-Pr₃P)Pd(4-FC₆H₄)(µ-OH)]₂ (30.8 mg, 41 µmol, 1.0 equiv), 1,4-difluorobenzene (2.5 µL, 24 µmol) and *i*-Pr₃P (150 µL, 12.71 equiv, 521 µmol) followed by dissolving with THF (SDS) to the 2-mL mark.

An oven dried, 5-mm, NMR tube was taken into the dry box and 500 µL of Stock Solution was added. The tube was capped with a septum and Teflon taped. The sample was removed from the glove box and inserted into a −78 °C acetone dry-ice bath followed by the addition of the 4-fluorophenylboronic acid Stock Solution (95 µL, 20.5 µmol, 1.0 equiv) *via* a 100 µL glass syringe. The NMR tube was shaken and cleaned with a Kimwipe then placed into the NMR probe pre-cooled to −30 °C. The formation of the 6-B-3 complex was found to be complete after ~3-4 h by ³¹P and ¹⁹F NMR spectroscopy. The sample was removed from the spectrometer and placed into a −78 °C acetone dry-ice bath, followed by shaking and reinserting into the spectrometer set to 20 °C. Using the fluorine channel to collect a spectrum every 24.2 min the progress of the reaction was monitored by the decay of the 6-B-3 complex fluorine signal (−115.74 ppm) in comparison with the internal reference (1,4-difluorobenzene, −120.00 ppm). The S-shaped curve was fitted with OrginPro 2015 software using equation 4. Using the calculated values for k_c, q, and $[A]_0$ a maximum rate was determined using equation 5. This procedure was performed three times to obtain an average maximum rate.

Table 57. Calculated values from the decay of **71** with 8.62 equiv of i-Pr$_3$P.

Entry	kc	q	A_0 [mM]	v_{max} (mM s^{-1})
Run 1	$(9.050 \pm 0.61) \times 10^{-6}$	1.958 ± 0.363	23.54 ± 0.36	0.00147
Run 2	$(1.007 \pm 0.07) \times 10^{-5}$	1.880 ± 0.333	20.67 ± 0.31	0.00128
Run 3	$(8.519 \pm 0.26) \times 10^{-6}$	2.097 ± 0.171	23.13 ± 0.16	0.00136

v_{max} *avg.* $= (1.37 \pm 0.96) \times 10^{-3}$ mM s^{-1}
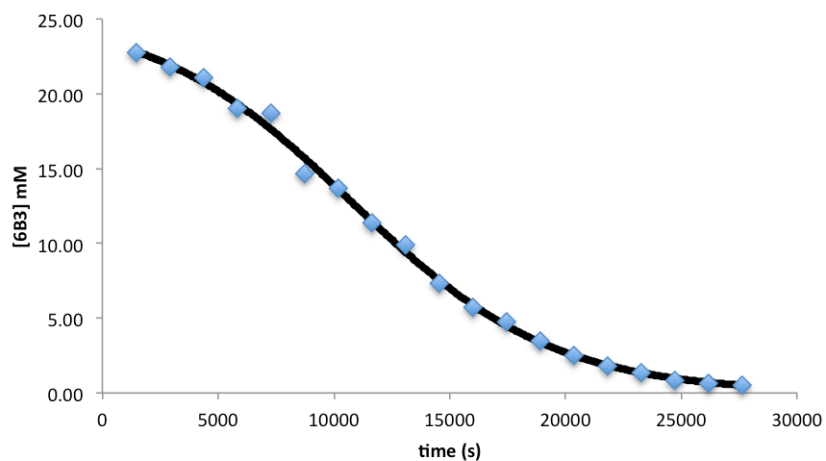
Figure 287. Decay of complex **71** with 8.62 equiv of i-Pr$_3$P (Run 1).
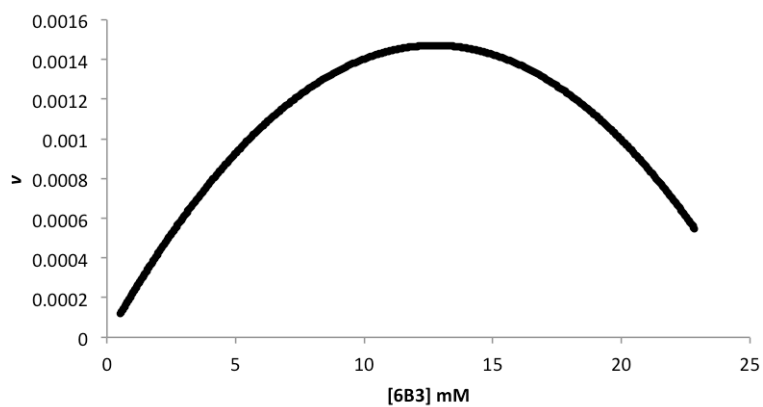
Figure 288. Rate vs. concentration of complex **71** with 8.62 equiv of i-Pr$_3$P (Run 1).

Table 58. Data for the decay of complex **71** with 8.62 equiv of i-Pr$_3$P (Run 1).

time (s)	Integral IS (−120.00 ppm)	Integral 6-B-3 (−115.74 ppm)	[mM] 6-B-3
1454	40547	45116	22.74
2908	39764	42395	21.79
4362	39764	41035	21.09
5816	40583	37791	19.03
7270	38811	35574	18.74
8724	40648	29112	14.64
10178	38418	25700	13.67
11632	39650	22079	11.38
13086	37083	17954	9.90
14540	40222	14465	7.35
15994	40383	11254	5.70
17448	37347	8730	4.78
18902	38710	6526	3.45
20356	40239	4906	2.49
21810	41672	3703	1.82
23264	38525	2602	1.38
24718	42041	1728	0.84
26172	41032	1319	0.66
27626	41947	1122	0.55
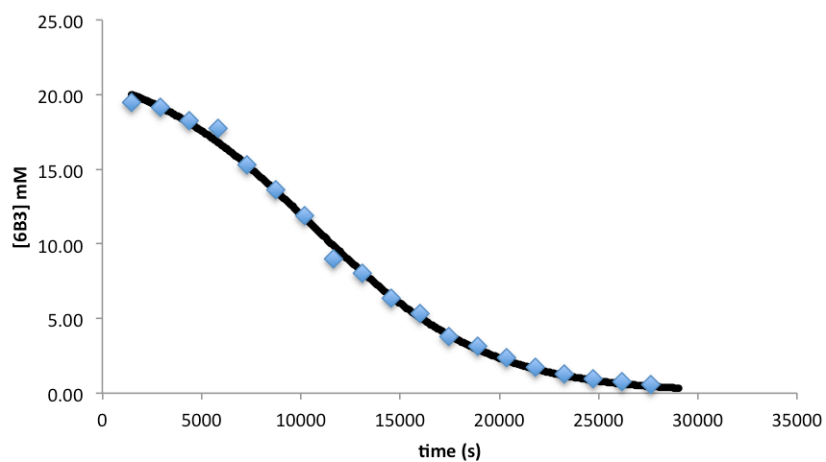
Figure 289. Decay of complex **71** with 8.62 equiv of i-Pr$_3$P (Run 2).
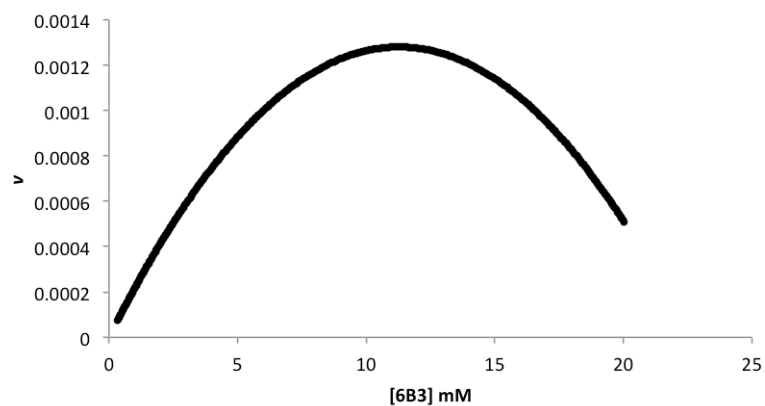
Figure 290. Rate vs. concentration of complex **71** with 8.62 equiv of *i*-Pr$_3$P (Run 2).

Table 59. Data for the decay of complex **71** with 8.62 equiv of *i*-Pr$_3$P (Run 2).

time (s)	Integral IS (−120.00 ppm)	Integral 6-B-3 (−115.74 ppm)	[mM] 6-B-3
1454	41203	39248	19.47
2908	41616	38948	19.13
4362	41048	36701	18.28
5816	38846	33690	17.73
7270	40166	30063	15.30
8724	38917	25895	13.60
10178	38570	22396	11.87
11632	41429	18240	9.00
13086	37930	14932	8.05
14540	39246	12242	6.38
15994	37415	9765	5.33
17448	39410	7290	3.78
18902	37186	5703	3.13
20356	36696	4307	2.40
21810	39014	3325	1.74
23264	40512	2556	1.29
24718	38811	1808	0.95
26172	40375	1546	0.78
27626	42380	1189	0.57
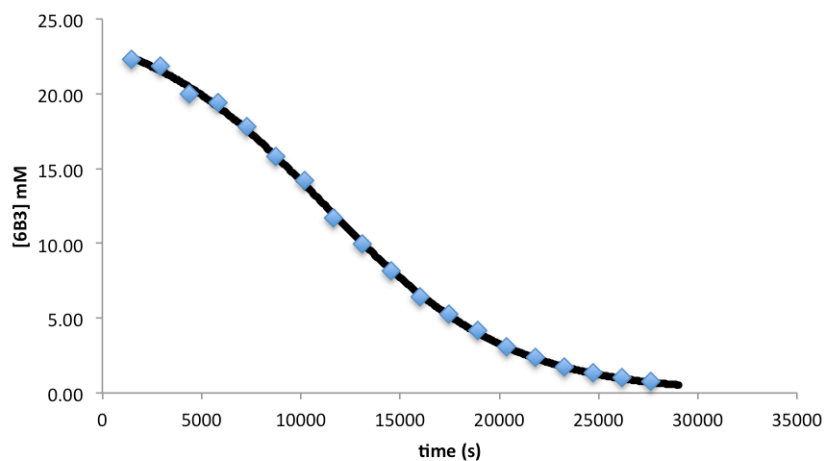
Figure 291. Decay of complex **71** with 8.62 equiv of *i*-Pr₃P (Run 3).
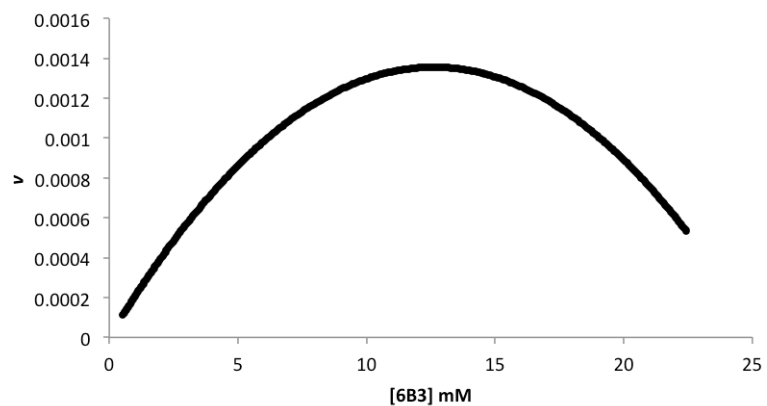
Figure 292. Rate vs. concentration of complex **71** with 8.62 equiv of *i*-Pr₃P (Run 3).

Table 60. Data for the decay of complex **71** with 8.62 equiv of *i*-Pr₃P (Run 3).

time (s)	Integral IS (−120.00 ppm)	Integral 6-B-3 (−115.74 ppm)	[mM] 6-B-3
1454	40324	44037	22.32
2908	39736	42445	21.83
4362	39773	38913	20.00
5816	39844	37822	19.40
7270	39837	34663	17.79
8724	40705	31445	15.79
10178	39659	27584	14.22
11632	41108	23599	11.73
13086	40620	19839	9.98
14540	40149	16090	8.19
15994	40481	12692	6.41
17448	39823	10265	5.27
18902	39724	8063	4.15
20356	41107	6205	3.09
21810	40457	4744	2.40
23264	41306	3551	1.76
24718	40976	2663	1.33
26172	41488	2042	1.01

Table 61. Compiled Data for Order Determination of *i*-Pr₃P.

Entry	*i*-Pr₃P [mM]	log[*i*-Pr₃P]	v_{max} *avg.* (mM s^{-1})	log[v_{max} avg]
1	97	1.988	$(4.48 \pm 0.65) \times 10^{-3}$	−2.348
2	131	2.114	$(3.24 \pm 0.12) \times 10^{-3}$	−2.490
3	185	2.267	$(2.42 \pm 0.48) \times 10^{-3}$	−2.616
4	294	2.469	$(1.37 \pm 0.96) \times 10^{-3}$	−2.863
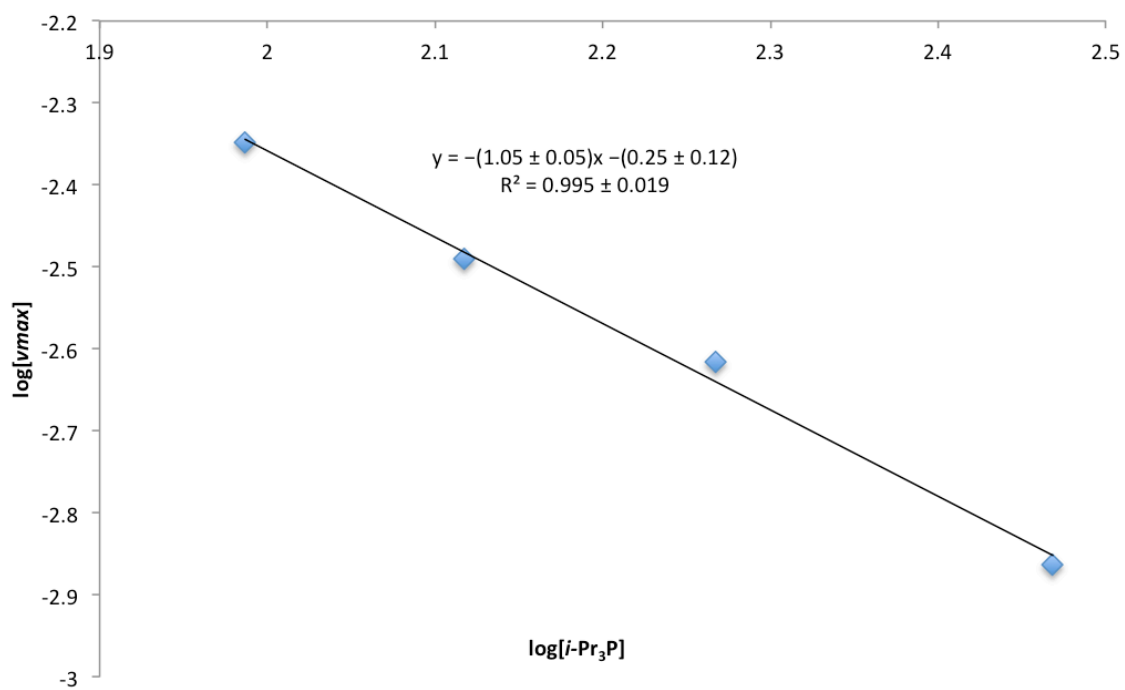
Figure 293. Order Determination of i-Pr$_3$P.

Experiment 61. Kinetic Measurement for decay of complex 51 at 20 °C with 3.81 equiv of *i*-Pr₃P and 0.25 equiv of (*i*-Pr₃P)₂Pd (Runs 1-3)
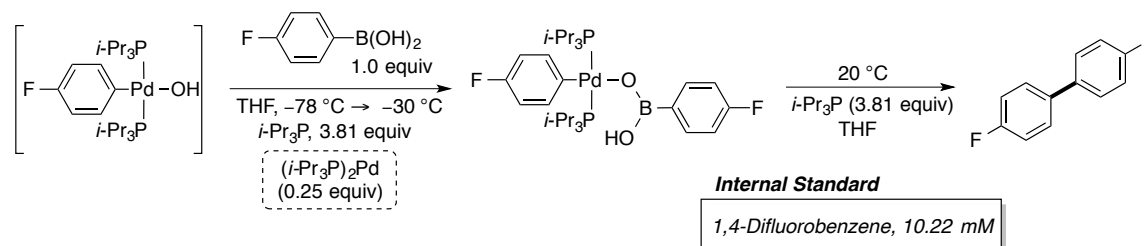
A 5-mL volumetric flask was charged with 4-fluorophenylboroxine (128 mg, 350 μmol) followed by H₂O (19 μL, 3.0 equiv, 1.05 mmol). Then ~2 mL of THF was added followed by sonication until the solid had dissolved. Once dissolved the flask was filled to the mark with THF (SDS) generating a 0.21 M solution.

A 2-mL volumetric flask was taken into the dry box and charged with [(*i*-Pr₃P)Pd(4-FC₆H₄)(μ-OH)]₂ (30.8 mg, 41 μmol), 1,4-difluorobenzene (2.5 μL, 24 μmol), (*i*-Pr₃P)₂Pd (8.7 mg, 20.4 μmol, 0.49 equiv) and *i*-Pr₃P (75 μL, 9.54 equiv, 391 μmol) followed by dissolving with THF (SDS) to the 2-mL mark.

An oven dried, 5-mm, NMR tube was taken into the dry box and 500 μL of Stock Solution was added. The tube was capped with a septum and Teflon taped. The sample was removed from the glove box and inserted into a −78 °C acetone dry-ice bath followed by the addition of the 4-fluorophenylboronic acid Stock Solution (95 μL, 20.5 μmol, 1.0 equiv) *via* a 100 μL glass syringe. The NMR tube was shaken and cleaned with a Kimwipe then placed into the NMR probe set to −30 °C. The formation of the 6-B-3 complex was found to be complete after ~3-4 h by ^{31}P and ^{19}F NMR spectroscopy. The sample was removed from the spectrometer and placed into a −78 °C acetone dry-ice bath, followed by shaking and reinserting into the spectrometer set to 20 °C. Using the fluorine channel to collect a spectrum every 24.2 min the progress of the reaction was monitored by the decay of the 6-B-3 complex fluorine signal (−115.74 ppm) in comparison with the internal reference (1,4-difluorobenzene, −120.00 ppm). The S-shaped curve was fitted with OrginPro 2015 software using equation 3. Using the calculated values for k_c, q, and $[A]_0$ a maximum rate was determined using equation 4. This procedure was performed three times to obtain an average maximum rate.

Table 62. Calculated values from the decay of **71** with 3.81 equiv of i-Pr_3P.

Entry	kc	q	A_0 [mM]	v_{max} ($mM\ s^{-1}$)
Run 1	$(1.19 \pm 0.10) \times 10^{-5}$	3.63 ± 0.75	26.96 ± 0.37	0.00279
Run 2	$(1.18 \pm 0.16) \times 10^{-5}$	3.92 ± 1.3	29.09 ± 0.89	0.00321
Run 3	$(1.31 \pm 0.26) \times 10^{-5}$	3.98 ± 1.7	24.08 ± 1.05	0.00259

v_{max} *avg.* $= (2.86 \pm 0.36) \times 10^{-3}$ mM s^{-1}
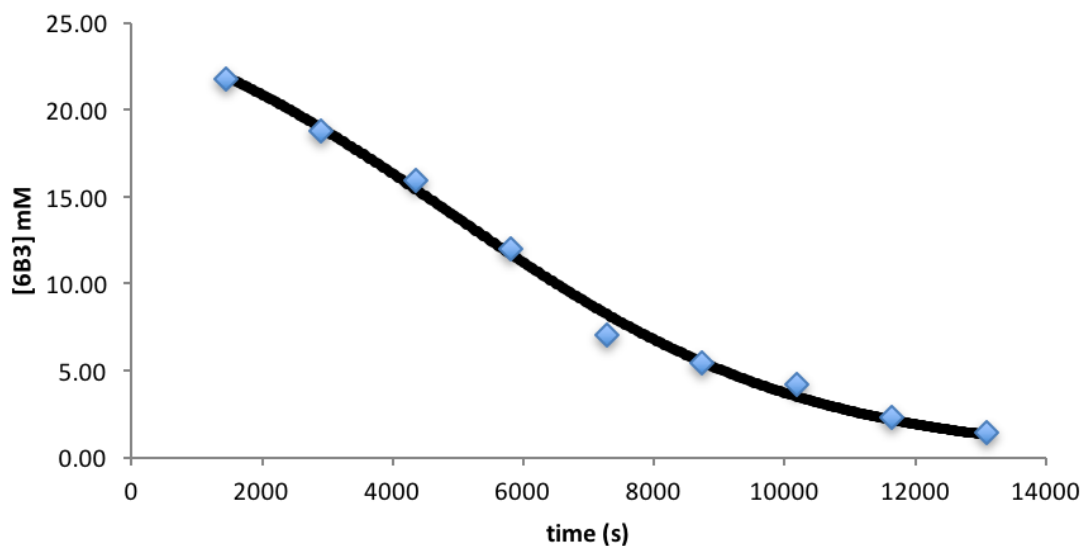
Figure 294. Decay of complex **71** with 3.81 equiv of i-Pr_3P and 0.25 equiv of $(i$-$Pr_3P)_2Pd$ (Run 1).
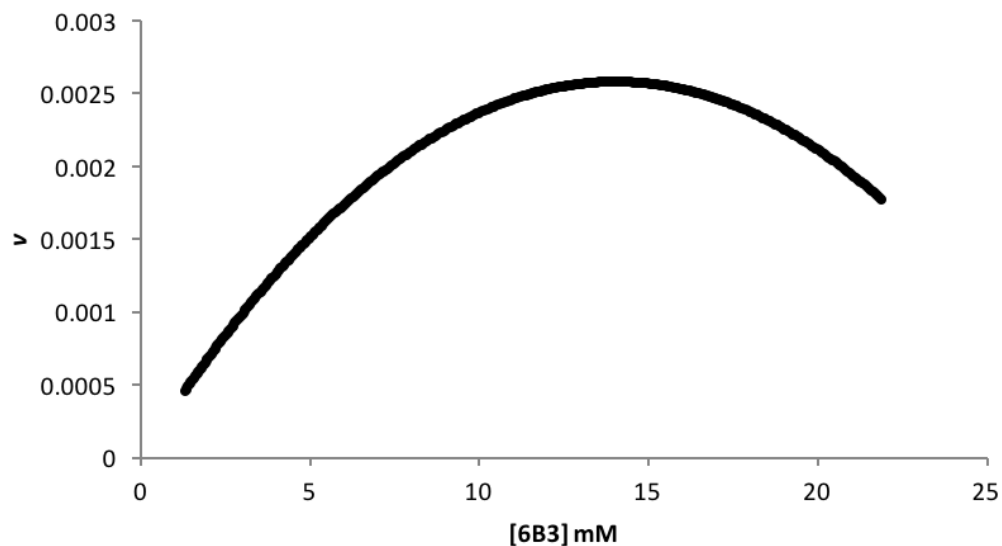
Figure 295. Rate vs. concentration of complex **71** with 3.81 equiv of i-Pr_3P and 0.25 equiv of $(i$-$Pr_3P)_2Pd$ (Run 1).

Table 63. Data for the decay of complex **71** with 3.81 equiv of i-Pr$_3$P and 0.25 equiv of (i-Pr$_3$P)$_2$Pd (Run 1).

time (s)	Integral IS (−120.00 ppm)	Integral 6-B-3 (−115.74 ppm)	[mM] 6-B-3
1454	5101	5436	22.67
2908	5019	4614	20.97
4362	5000	3903	19.28
5816	5180	3048	16.25
7270	5070	1738	13.36
8724	5108	1361	8.61
10178	3904	807	6.48
11632	5032	571	4.58
13086	4952	338	3.04
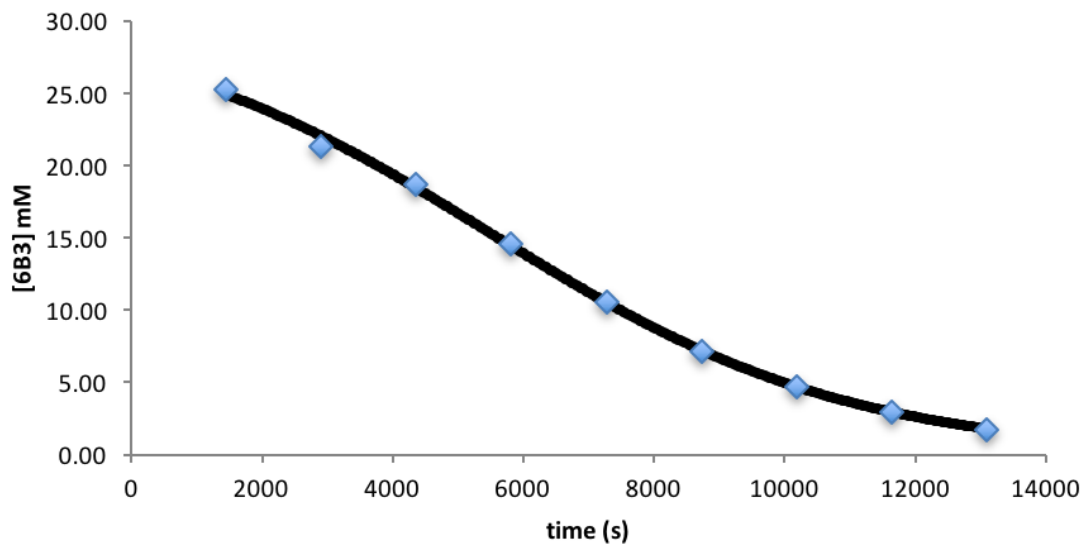
Figure 296. Decay of complex **71** with 3.81 equiv of i-Pr$_3$P and 0.25 equiv of (i-Pr$_3$P)$_2$Pd (Run 2).
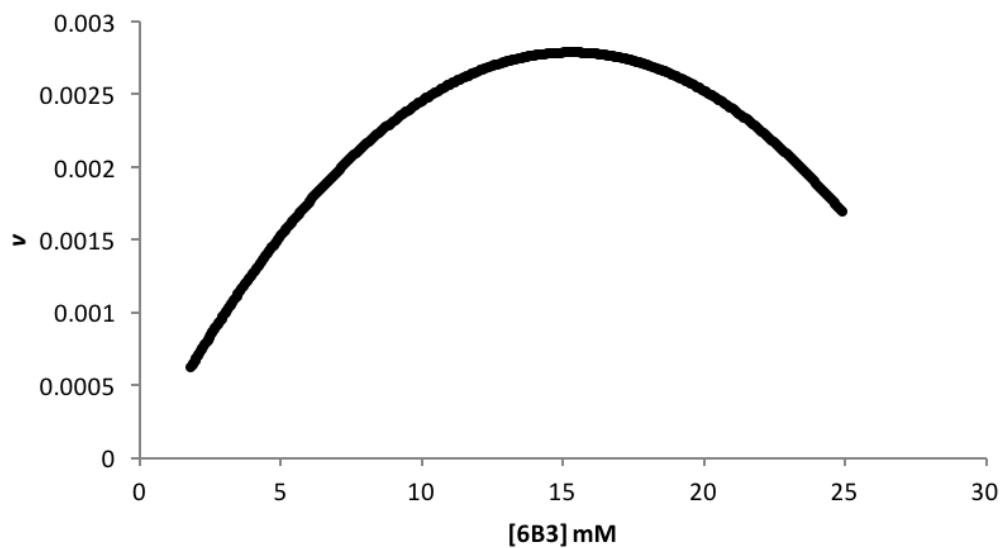
Figure 297. Rate vs. concentration of complex **71** with 3.81 equiv of *i*-Pr$_3$P and 0.25 equiv of (*i*-Pr$_3$P)$_2$Pd (Run 2).

Table 64. Data for the decay of complex **71** with 3.81 equiv of *i*-Pr$_3$P and 0.25 equiv of (*i*-Pr$_3$P)$_2$Pd (Run 2).

time (s)	Integral IS (−120.00 ppm)	Integral 6-B-3 (−115.74 ppm)	[mM] 6-B-3
1454	4764	5884	25.24
2908	4862	5073	21.33
4362	4761	4360	18.72
5816	4836	3449	14.58
7270	4784	2471	10.56
8724	4822	1679	7.12
10178	4724	1087	4.70
11632	4811	694	2.95
13086	4770	404	1.73
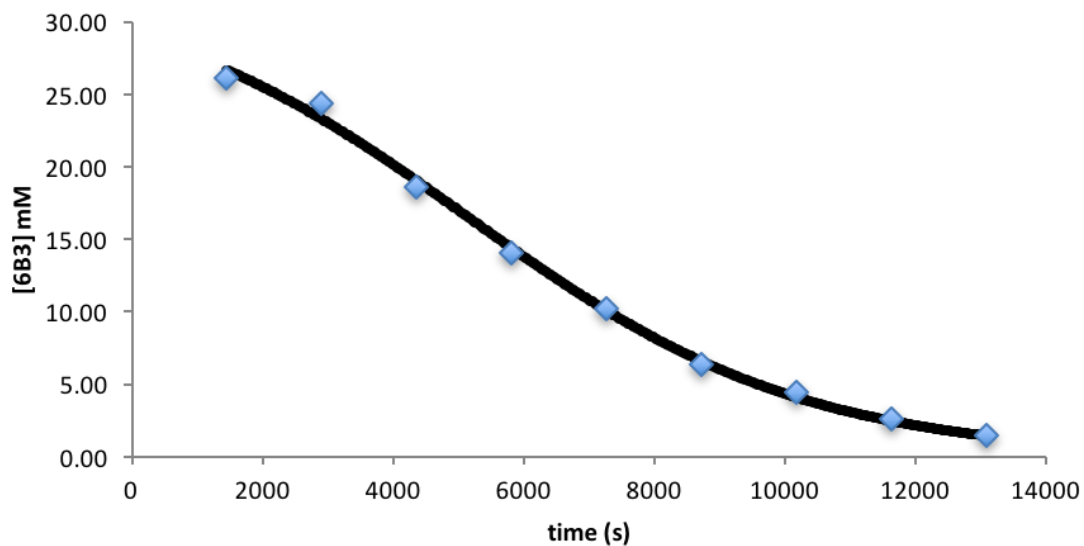
Figure 298. Decay of complex **71** with 3.81 equiv of i-Pr$_3$P and 0.25 equiv of (i-Pr$_3$P)$_2$Pd (Run 2).
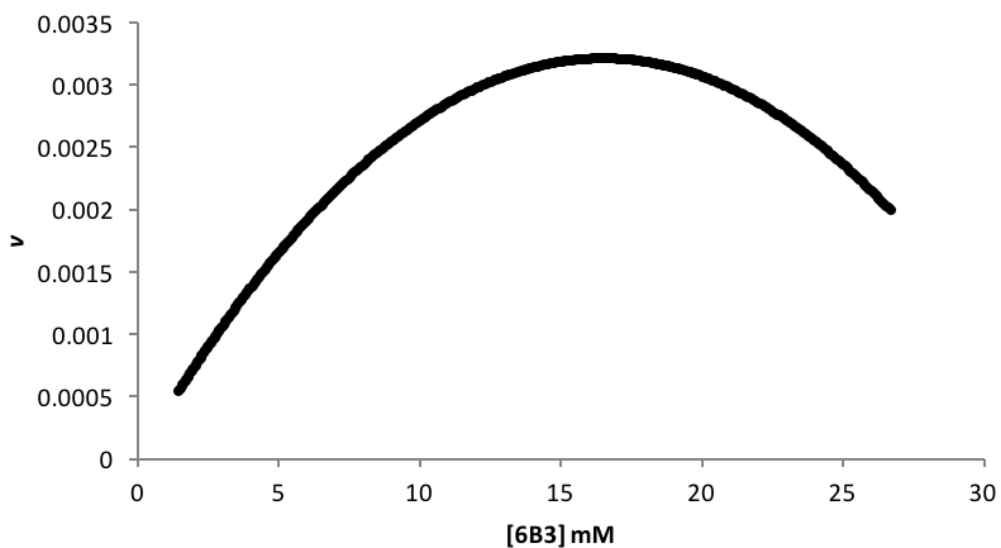
Figure 299. Rate vs. concentration of complex **71** with 3.81 equiv of i-Pr$_3$P and 0.25 equiv of (i-Pr$_3$P)$_2$Pd (Run 2).

Table 65. Data for the decay of complex **71** with 3.81 equiv of *i*-Pr$_3$P and 0.25 equiv of (*i*-Pr$_3$P)$_2$Pd (Run 2).

time (s)	Integral IS (−120.00 ppm)	Integral 6-B-3 (−115.74 ppm)	[mM] 6-B-3
1454	4377	5594	26.12
2908	4085	4879	24.41
4362	4209	3830	18.60
5816	4371	3006	14.06
7270	4237	2107	10.16
8724	4351	1357	6.37
10178	4070	879	4.41
11632	4320	543	2.57
13086	4311	314	1.49

Experiment 62. Kinetic Measurement for decay of complex 51 at 20 °C with 3.81 equiv of *i*-Pr$_3$P and 0.25 equiv of (*i*-Pr$_3$P)$_3$Pd (Runs 1-3)
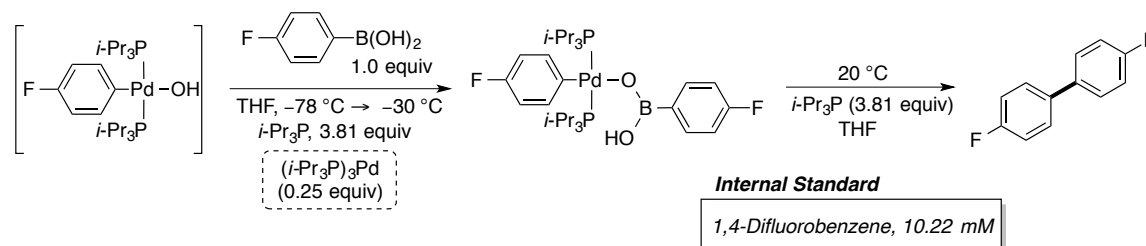
A 5-mL volumetric flask was charged with 4-fluorophenylboroxine (128 mg, 350 μmol, 1.0 equiv) followed by H$_2$O (19 μL, 1.05 mmol, 3.0 equiv). Then ~2 mL of THF was added followed by sonication until the solid had dissolved. Once dissolved the flask was filled to the mark with THF (SDS) generating a 0.21 M solution.

A 2-mL volumetric flask was taken into the dry box and charged with [(*i*-Pr$_3$P)Pd(4-FC$_6$H$_4$)(μ-OH)]$_2$ (30.8 mg, 41 μmol, 1.0 equiv), 1,4-difluorobenzene (2.5 μL, 24 μmol), (*i*-Pr$_3$P)$_3$Pd (12 mg, 20.4 μmol, 0.50 equiv) and *i*-Pr$_3$P (75 μL, 9.54 equiv, 391 μmol) followed by dissolving with THF (SDS) to the 2-mL mark.

An oven dried, 5-mm, NMR tube was taken into the dry box and 500 μL of Stock Solution was added. The tube was capped with a septum and Teflon taped. The sample was removed from the glove box and inserted into a −78 °C acetone dry-ice bath followed by the addition of the 4-fluorophenylboronic acid Stock Solution (95 μL, 20.5 μmol, 1.0 equiv) *via* a 100 μL glass syringe. The NMR tube was shaken and cleaned with a Kimwipe then placed into the NMR probe set to −30 °C. The formation of the 6-B-3 complex was found to be complete after ~3-4 h by ^{31}P and ^{19}F NMR spectroscopy. The sample was removed from the spectrometer and placed into a −78 °C acetone dry-ice bath, followed by shaking and reinserting into the spectrometer set to 20 °C. Using the fluorine channel to collect a spectrum every 24.2 min the progress of the reaction was monitored by the decay of the 6-B-3 complex fluorine signal (−115.74 ppm) in comparison with the internal reference (1,4-difluorobenzene, −120.00 ppm). The S-shaped curve was fitted with OrginPro 2015 software using equation 3. Using the calculated values for k_c, q, and $[A]_0$ a maximum rate was determined using equation 4. This procedure was performed three times to obtain an average maximum rate.

Table 66. Calculated values from the decay of **51** with 3.81 equiv of i-Pr$_3$P and 0.25 equiv of (i-Pr$_3$P)$_3$Pd.

Entry	kc	q	A$_0$ [mM]	v_{max} (s^{-1})
Run 1	$(1.45 \pm 0.09) \times 10^{-5}$	1.61 ± 0.56	23.75 ± 0.52	0.00232
Run 2	$(1.36 \pm 0.10) \times 10^{-5}$	2.24 ± 0.75	22.67 ± 0.51	0.00210
Run 3	$(1.46 \pm 0.07) \times 10^{-5}$	1.27 ± 0.18	22.93 ± 0.28	0.00214

v_{max} *avg.* = $(2.19 \pm 0.11) \times 10^{-3}$ s^{-1}
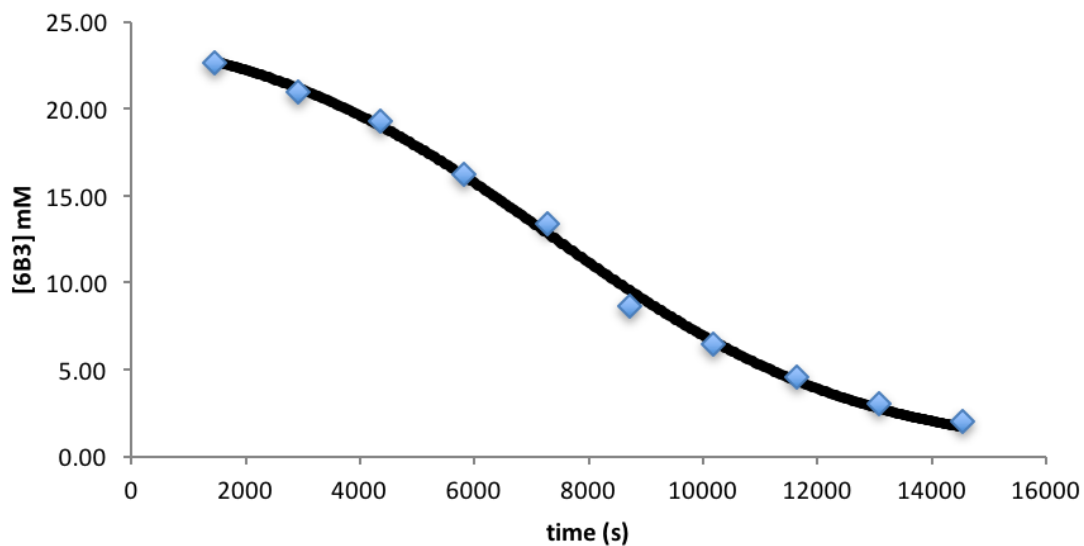
Figure 300. Decay of complex **71** with 3.81 equiv of i-Pr$_3$P and 0.25 equiv of (i-Pr$_3$P)$_3$Pd. (Run 1).
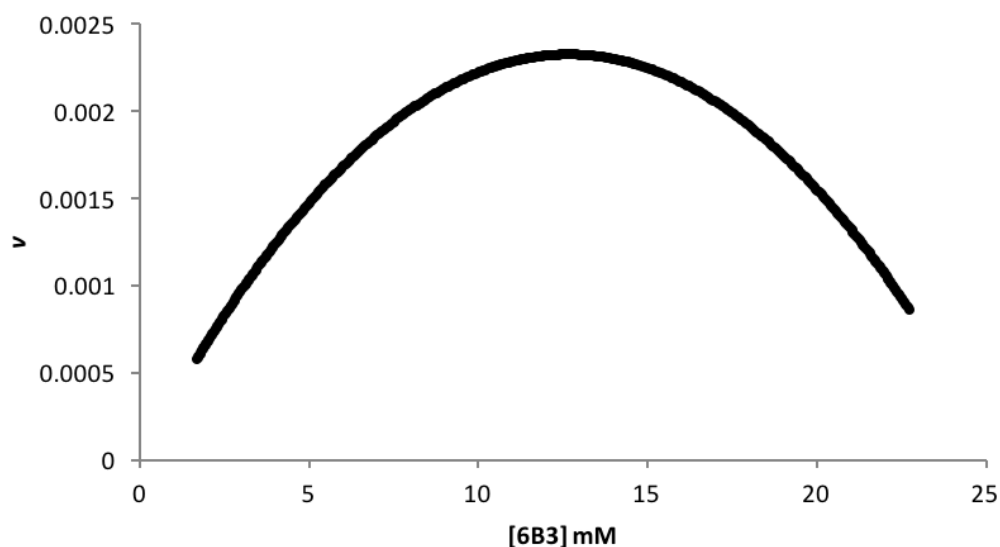
Figure 301. Rate vs. concentration of complex **71** with 3.81 equiv of *i*-Pr$_3$P and 0.25 equiv of (*i*-Pr$_3$P)$_3$Pd (Run 1).

Table 67. Data for the decay of complex **71** with 3.81 equiv of *i*-Pr$_3$P 0.25 equiv of (*i*-Pr$_3$P) (Run 1).

time (s)	Integral IS (−120.00 ppm)	Integral 6-B-3 (−115.74 ppm)	[mM] 6-B-3
1454	5092	5648	22.67
2908	5051	5182	20.97
4362	4924	4644	19.28
5816	5210	4141	16.25
7270	4905	3207	13.36
8724	5456	2299	8.61
10178	5164	1638	6.48
11632	5307	1189	4.58
13086	5376	800	3.04
14540	5131	501	2.00
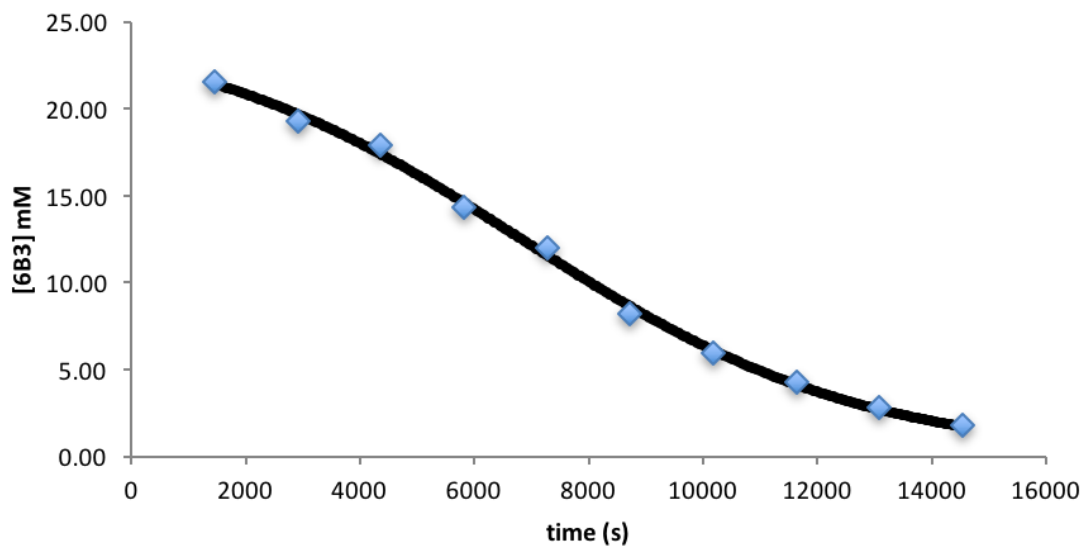
Figure 302. Decay of complex **71** with 3.81 equiv of *i*-Pr$_3$P and 0.25 equiv of (*i*-Pr$_3$P)$_3$Pd (Run 2).
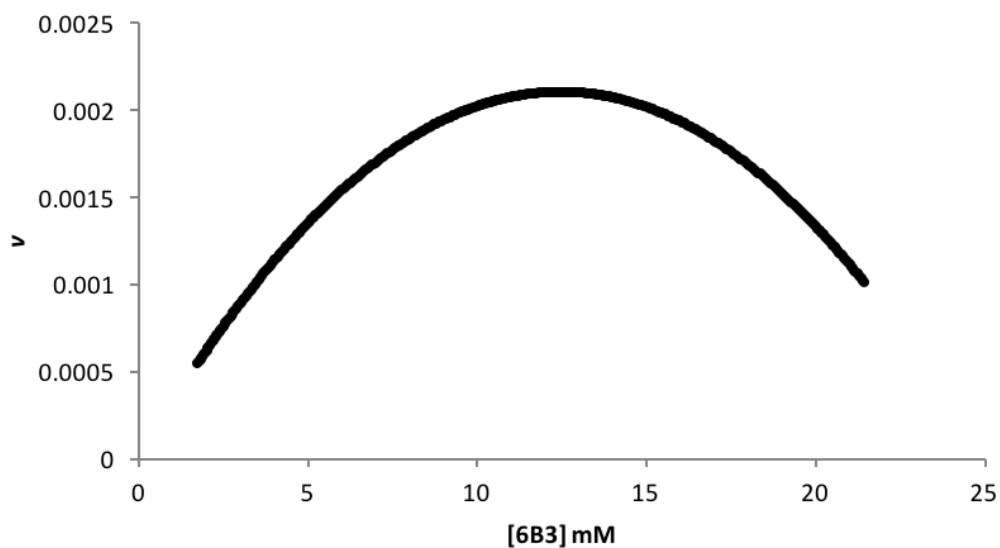
Figure 303. Rate vs. concentration of complex **71** with 3.81 equiv of *i*-Pr$_3$P and 0.25 equiv of (*i*-Pr$_3$P)$_3$Pd (Run 2).

Table 68. Data for the decay of complex **71** with 3.81 equiv of *i*-Pr₃P 0.25 equiv of (*i*-Pr₃P) (Run 2).

time (s)	Integral IS (−120.00 ppm)	Integral 6-B-3 (−115.74 ppm)	[mM] 6-B-3
1454	5327	5613	21.53
2908	5485	5173	19.28
4362	5209	4555	17.87
5816	5530	3875	14.32
7270	5410	3169	11.97
8724	5444	2189	8.22
10178	5377	1571	5.97
11632	5557	1171	4.31
13086	5582	765	2.80
14540	5465	477	1.78
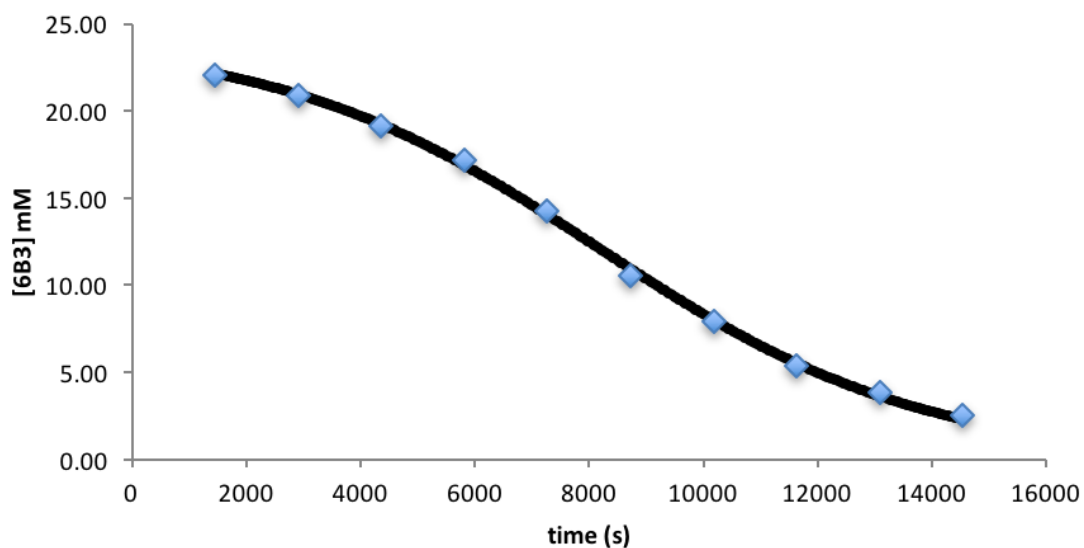
Figure 304. Decay of complex **71** with 3.81 equiv of *i*-Pr₃P and 0.25 equiv of (*i*-Pr₃P)₃Pd. (Run 3).
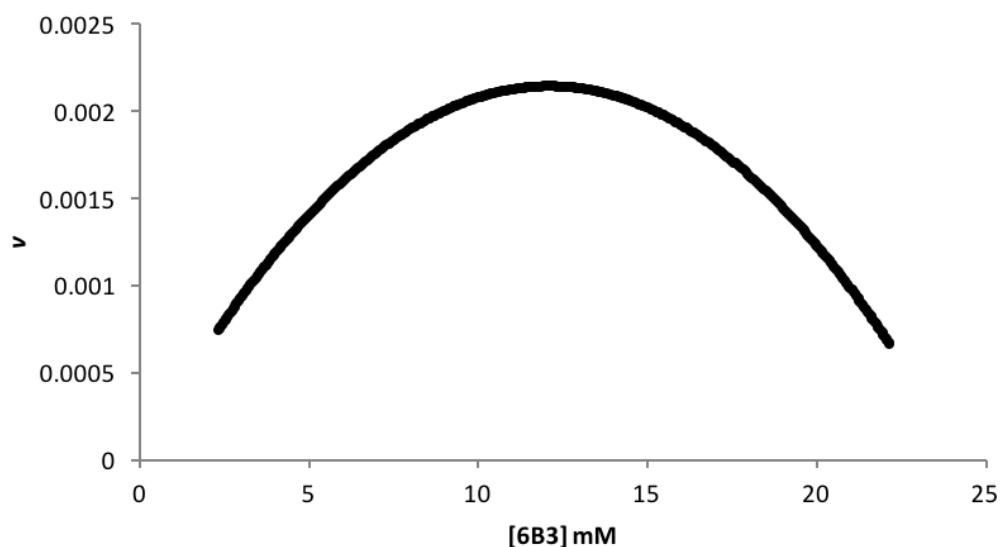
Figure 305. Rate vs. concentration of complex **71** with 3.81 equiv of i-Pr$_3$P and 0.25 equiv of (i-Pr$_3$P)$_3$Pd (Run 3).

Table 69. Data for the decay of complex **71** with 3.81 equiv of i-Pr$_3$P 0.25 equiv of (i-Pr$_3$P) (Run 3).

time (s)	Integral IS (−120.00 ppm)	Integral 6-B-3 (−115.74 ppm)	[mM] 6-B-3
1454	5487	5932	22.09
2908	5481	5607	20.91
4362	5454	5117	19.18
5816	5389	4529	17.18
7270	5311	3699	14.24
8724	5325	2753	10.57
10178	5435	2101	7.90
11632	5564	1467	5.39
13086	5571	1045	3.83
14540	5428	680	2.56

Experiment 63. Kinetic Measurement for decay of complex 71 at 20 °C with 5.41 equiv of *i*-Pr$_3$P and 10.0 equiv of water (Runs 1-3)
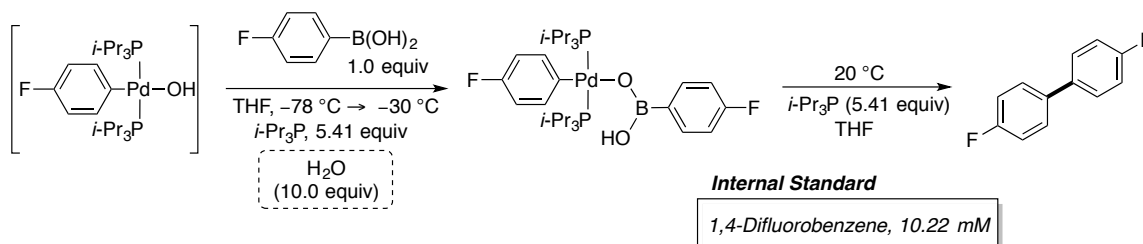
A 5-mL volumetric flask was charged with 4-fluorophenylboroxine (128 mg, 350 µmol, 1.0 equiv) followed by H$_2$O (209 µL, 11.6 mmol, 33.14 equiv). Then ~2 mL of THF was added followed by sonication until the solid had dissolved. Once dissolved the flask was filled to the mark with THF (SDS) generating a 0.21 M solution of 4-fluorophenylboronic acid and 2.1 M solution of H$_2$O.

A 2-mL volumetric flask was taken into the dry box and charged with [(*i*-Pr$_3$P)Pd(4-FC$_6$H$_4$)(µ-OH)]$_2$ (30.8 mg, 41 µmol, 1.0 equiv), 1,4-difluorobenzene (2.5 µL, 24 µmol) and *i*-Pr$_3$P (100 µL, 12.71 equiv, 521 µmol) followed by dissolving with THF (SDS) to the 2-mL mark.

An oven dried, 5-mm, NMR tube was taken into the dry box and 500 µL of Stock Solution was added. The tube was capped with a septum and Teflon taped. The sample was removed from the glove box and inserted into a −78 °C acetone dry-ice bath followed by the addition of the 4-fluorophenylboronic acid Stock Solution (95 µL, 20.5 µmol, 1.0 equiv) *via* a 100 µL glass syringe. The NMR tube was shaken and cleaned with a Kimwipe then placed into the NMR probe pre-cooled to −30 °C. The formation of the 6-B-3 complex was found to be complete after ~3-4 h by ^{31}P and ^{19}F NMR spectroscopy. The sample was removed from the spectrometer and placed into a −78 °C acetone dry-ice bath, followed by shaking and reinserting into the spectrometer set to 20 °C. Using the fluorine channel to collect a spectrum every 24.2 min the progress of the reaction was monitored by the decay of the 6-B-3 complex fluorine signal (−115.74 ppm) in comparison with the internal reference (1,4-difluorobenzene, −120.00 ppm). The S-shaped curve was fitted with OrginPro 2015 software using equation 3. Using the calculated values for k_c, q, and [A]$_0$ a maximum rate was determined using equation 4. This procedure was performed three times to obtain an average maximum rate.

Table 70. Calculated values from the decay of **71** with 5.41 equiv of i-Pr$_3$P.

Entry	kc	q	A_0 [mM]	v_{max} (s^{-1})
Run 1	$(2.707 \pm 0.228) \times 10^{-6}$	7.368 ± 1.28	33.41 ± 0.46	0.00115
Run 2	$(3.229 \pm 0.304) \times 10^{-6}$	4.433 ± 1.00	33.29 ± 0.57	0.00113
Run 3	$(3.258 \pm 0.292) \times 10^{-6}$	4.872 ± 1.00	31.49 ± 0.51	0.00108

v_{max} *avg.* = $(1.11 \pm 0.04) \times 10^{-3}$ s^{-1}
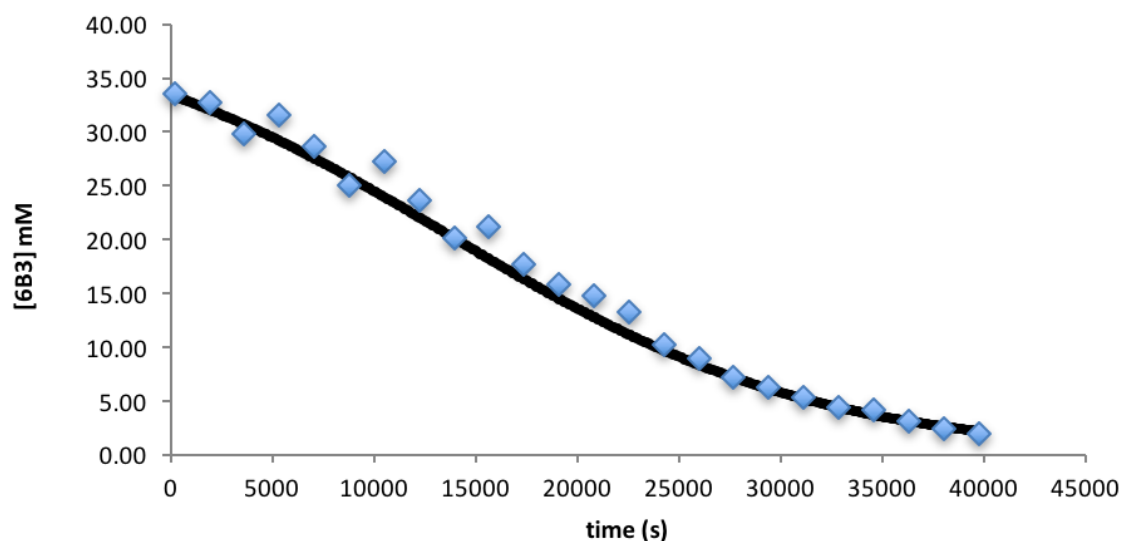
Figure 306. Decay of complex **71** with 5.41 equiv of i-Pr$_3$P and 10 equiv of H$_2$O (Run 1).
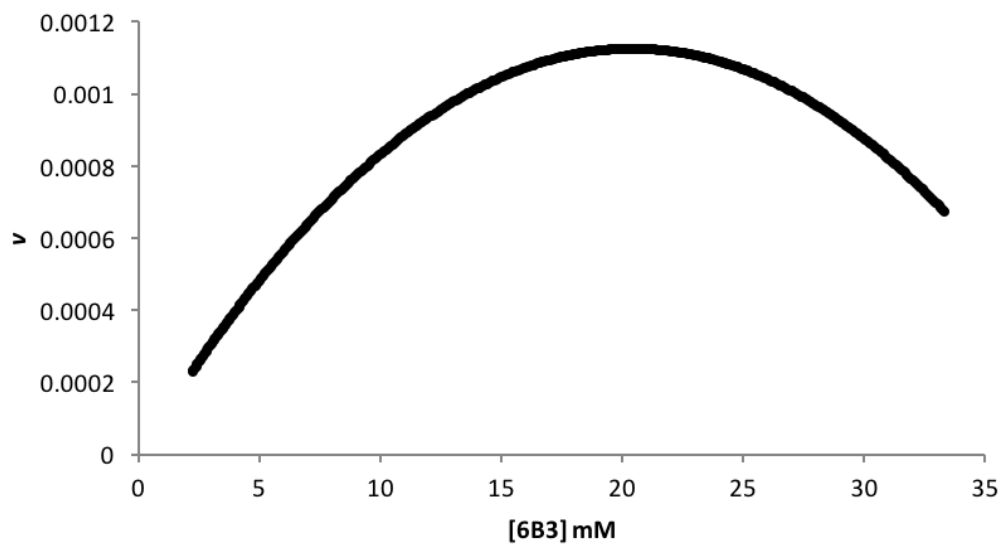
Figure 307. Rate vs. concentration of complex **71** with 5.41 equiv of i-Pr$_3$P and 10 equiv of H$_2$O (Run 1).

Table 71. Data for the decay of complex **71** with 5.41 equiv of *i*-Pr₃P and 10 equiv of H₂O (Run 1).

time (s)	Integral IS (−120.00 ppm)	Integral 6-B-3 (−115.74 ppm)	[mM] 6-B-3
172	3761	6172	33.54
1892	3671	5880	32.74
3612	3663	5344	29.82
5332	3843	5939	31.59
7052	3643	5106	28.65
8772	3772	4618	25.02
10492	3622	4831	27.26
12212	3694	4264	23.59
13932	3746	3689	20.13
15652	3615	3751	21.21
17372	3844	3326	17.69
19092	3394	2631	15.84
20812	3637	2621	14.73
22532	3533	2290	13.25
24252	3752	1886	10.27
25972	3706	1625	8.96
27692	3696	1300	7.19
29412	3666	1120	6.24
31132	3640	958	5.38
32852	3661	790	4.41
34572	3838	783	4.17
36292	3748	573	3.12
38012	3764	434	2.36
39732	3730	358	1.96
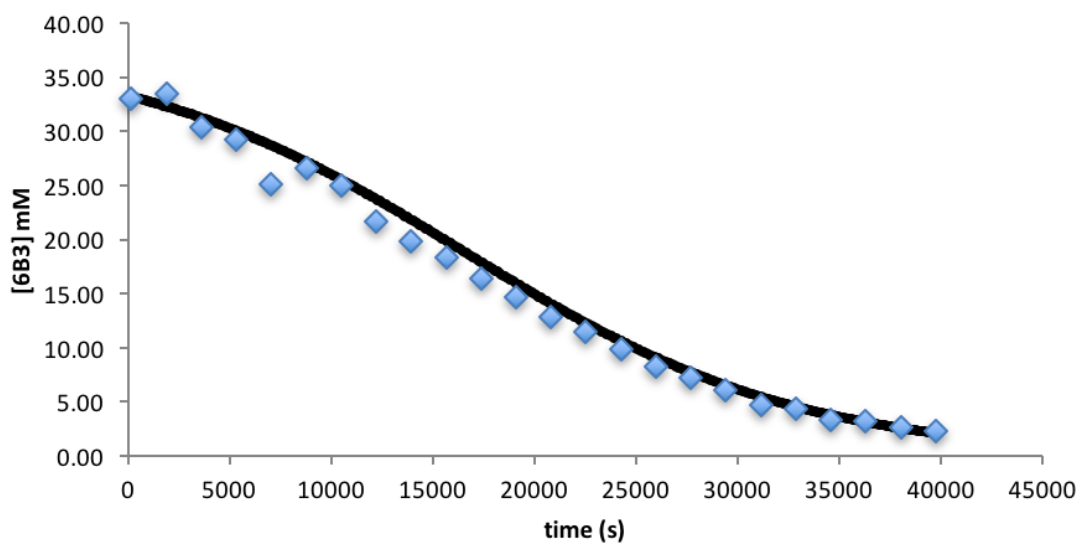
Figure 308. Decay of complex **71** with 5.41 equiv of *i*-Pr$_3$P and 10 equiv of H$_2$O (Run 2).
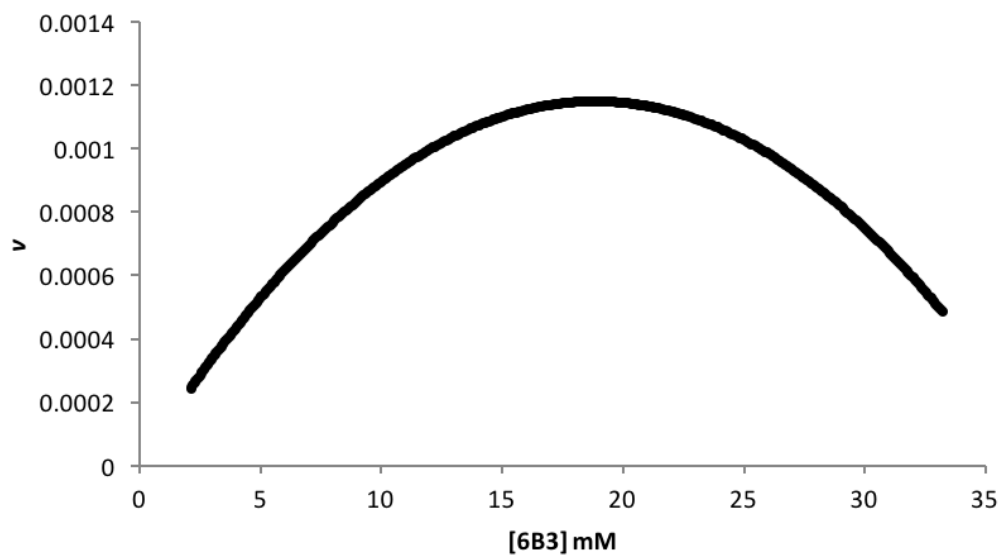
Figure 309. Rate vs. concentration of complex **71** with 5.41 equiv of *i*-Pr$_3$P and 10 equiv of H$_2$O (Run 2).

Table 72. Data for the decay of complex **71** with 5.41 equiv of i-Pr$_3$P and 10 equiv of H$_2$O (Run 2).

time (s)	Integral IS (−120.00 ppm)	Integral 6-B-3 (−115.74 ppm)	[mM] 6-B-3
172	3588	5792	33.00
1892	3279	5370	33.47
3612	3655	5428	30.36
5332	3440	4912	29.19
7052	3644	4484	25.15
8772	3425	4465	26.65
10492	3432	4196	24.99
12212	3662	3885	21.68
13932	3676	3574	19.87
15652	3661	3285	18.34
17372	3654	2927	16.37
19092	3555	2542	14.62
20812	3512	2212	12.87
22532	3538	1976	11.42
24252	3492	1693	9.91
25972	3288	1320	8.21
27692	3479	1238	7.27
29412	3586	1063	6.06
31132	3619	836	4.72
32852	3398	719	4.33
34572	3299	539	3.34
36292	3430	530	3.16
38012	3448	445	2.64
39732	3498	388	2.27
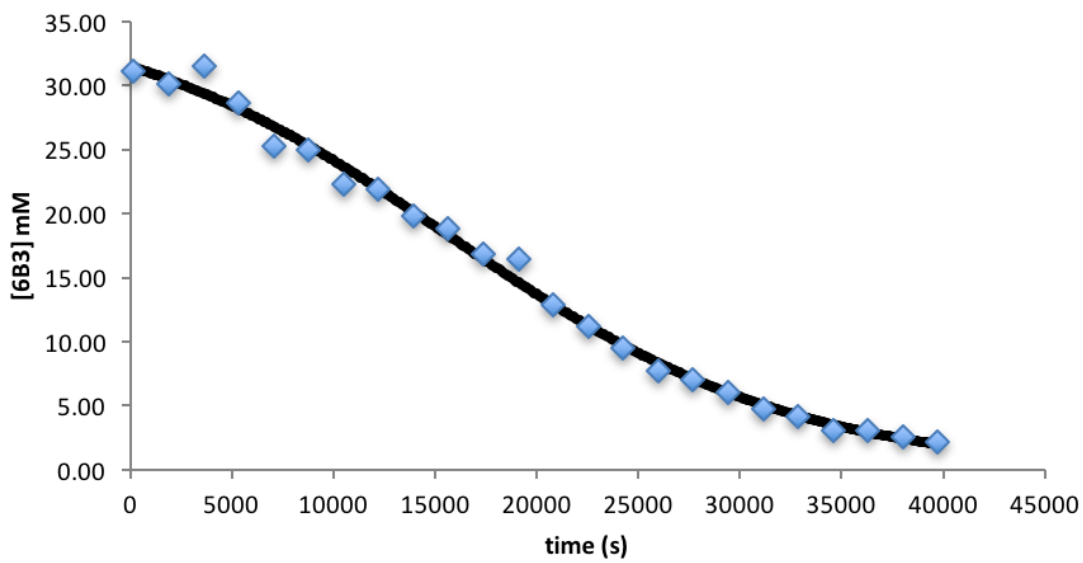
Figure 310. Decay of complex **71** with 5.41 equiv of i-Pr$_3$P and 10 equiv of H$_2$O (Run 3).
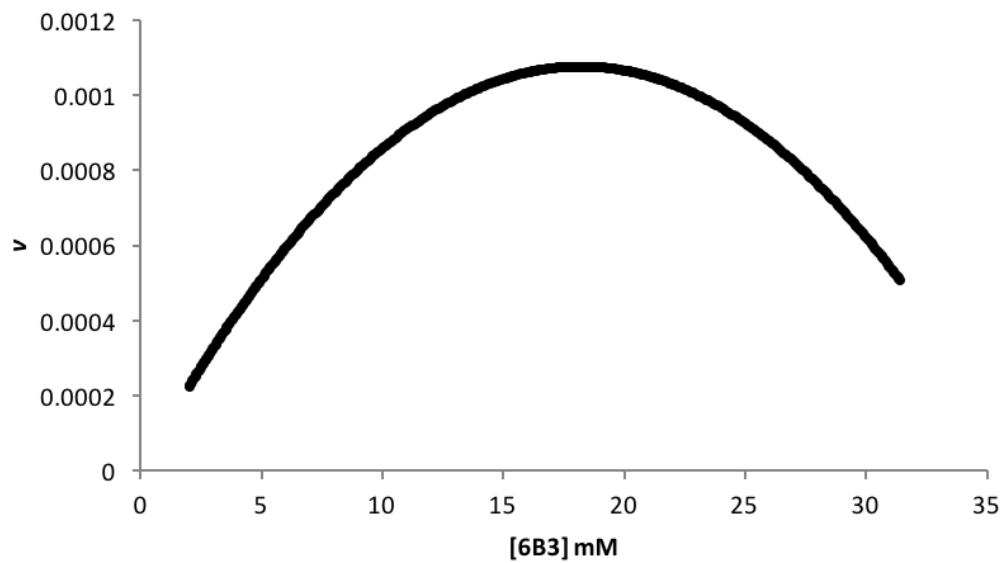
Figure 311. Rate vs. concentration of complex **71** with 5.41 equiv of i-Pr$_3$P and 10 equiv of H$_2$O (Run 3).

Table 73. Data for the decay of complex **71** with 5.41 equiv of *i*-Pr₃P and 10 equiv of H₂O (Run 3).

time (s)	Integral IS (−120.00 ppm)	Integral 6-B-3 (−115.74 ppm)	[mM] 6-B-3
172	3809	5792	31.08
1892	3639	5370	30.16
3612	3519	5428	31.53
5332	3505	4912	28.65
7052	3627	4484	25.27
8772	3654	4465	24.98
10492	3846	4196	22.30
12212	3631	3885	21.87
13932	3688	3574	19.81
15652	3562	3285	18.85
17372	3547	2927	16.87
19092	3162	2542	16.43
20812	3500	2212	12.92
22532	3617	1976	11.17
24252	3623	1693	9.55
25972	3500	1320	7.71
27692	3617	1238	7.00
29412	3588	1063	6.06
31132	3627	836	4.71
32852	3519	719	4.18
34572	3614	539	3.05
36292	3581	530	3.03
38012	3606	445	2.52
39732	3605	388	2.20

Experiment 64. Kinetic Measurement for decay of complex 71 at 20 °C from independent synthesis with 3.81 equiv of *i*-Pr$_3$P from 86 and 58.
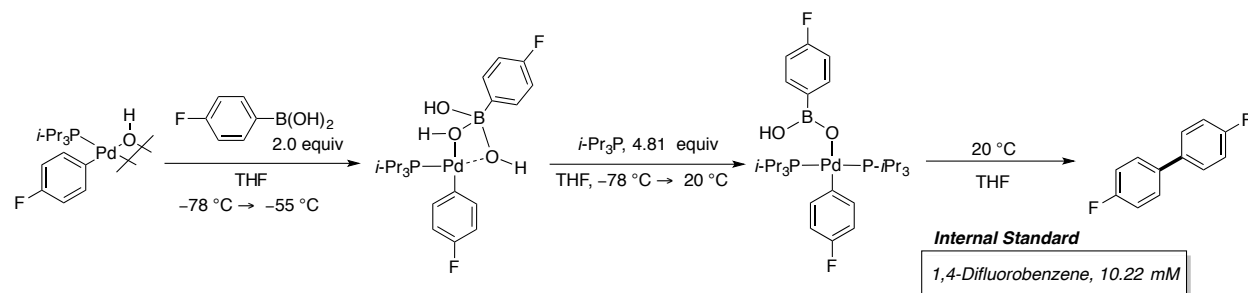
A 1-mL volumetric flask was charged with 4-fluorophenylboroxine (77.0 mg, 210 µmol, 1.0 equiv) followed by H$_2$O (11 µL, 631 µmol, 3.0 equiv). Then ~0.5 mL of THF (SDS) was added and sonicated until the solid had dissolved. Once dissolved the flask was filled to the mark with THF (SDS) generating a 0.63 M solution of 4-fluorophenylboronic acid.

A 1-mL volumetric flask was charged with *i*-Pr$_3$P (307 µL, 1.60 mmol) followed by filling to the mark with THF (SDS) generating a 1.60 M solution of *i*-Pr$_3$P.

A 2-mL volumetric flask was taken into the dry box and charged with [(*i*-Pr$_3$P)Pd(4-FC$_6$H$_4$)(µ-OH)]$_2$ (30.8 mg, 41 µmol, 1.0 equiv) and 1,4-difluorobenzene (2.5 µL, 24 µmol) followed by dissolving with THF (SDS) to the 2-mL mark. An oven dried, 5-mm, NMR tube was taken into the dry box and 500 µL of the freshly prepared solution was added. The tube was capped with a septum and Teflon taped. The sample was removed from the glove box and inserted into a −78 °C acetone dry-ice bath followed by the addition of the 4-fluorophenylboronic acid solution (35 µL, 20.5 µmol, 2.0 equiv) *via* a 100 µL glass syringe. The NMR tube was vortexed (not shaken) and cleaned with a Kimwipe followed by re-insertion into the −78 °C bath. Then 60 µL of *i*-Pr$_3$P (96 µmol, 4.81 equiv) solution was added *via* syringe and the tube was vortexed (not shaken) and placed into the NMR probe set to −55 °C. The formation of the 8-B-4 species was observed after ~10-15 min. The tube was removed and placed back into the −78 °C followed by re-insertion into the NMR probe set to 20 °C.

Using the fluorine channel to collect a spectrum every 1454 s the progress of the reaction was monitored by the decay of the 8-B-4 complex (−118.40 ppm) and formation of cross-coupling product (−116.45 ppm) in comparison with the internal reference 1,4-difluorobenzene (−120.00 ppm). The first order decay and formation profiles were fitted with OrginPro 2015 software using equations 1 and 2 respectively. This procedure was performed three times to obtain an average rate.

Table 74. Calculated values from the decay of **71** with 3.81 equiv of i-Pr$_3$P.

Entry	kc	q	A_0 [mM]	v_{max} (mM s^{-1})
Run 1	$(1.354 \pm 0.068) \times 10^{-5}$	6.090 ± 0.63	25.11 ± 0.28	0.00330
Run 2	$(1.646 \pm 0.062) \times 10^{-5}$	4.912 ± 0.40	24.02 ± 0.21	0.00344
Run 3	$(1.350 \pm 0.434) \times 10^{-5}$	4.867 ± 0.35	25.13 ± 0.18	0.00304

v_{max} **avg. = (3.26 ± 0.17) x 10^{-3} s^{-1}**
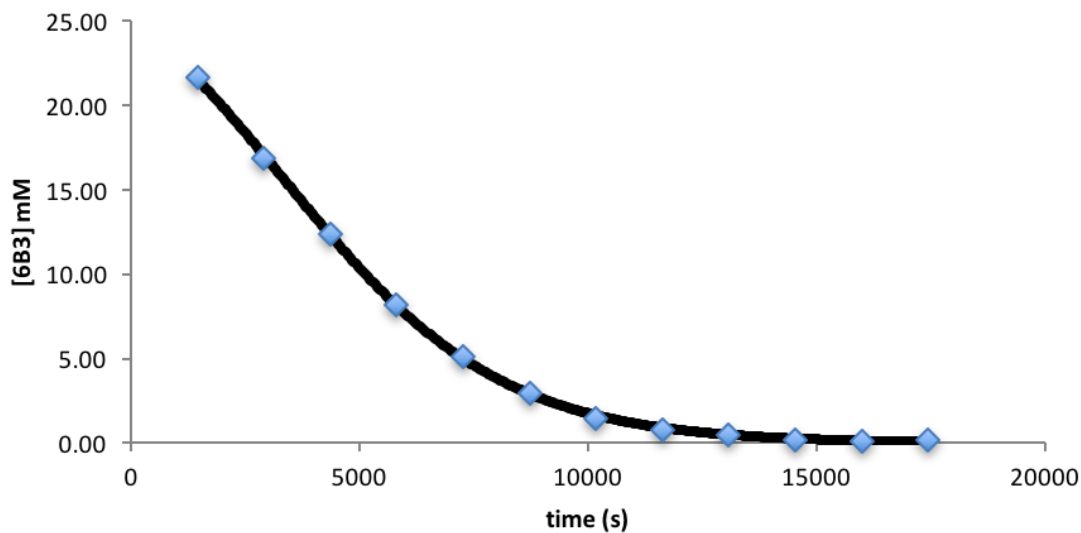
Figure 312. Decay of complex **71** with 3.81 equiv of i-Pr$_3$P (Run 1).
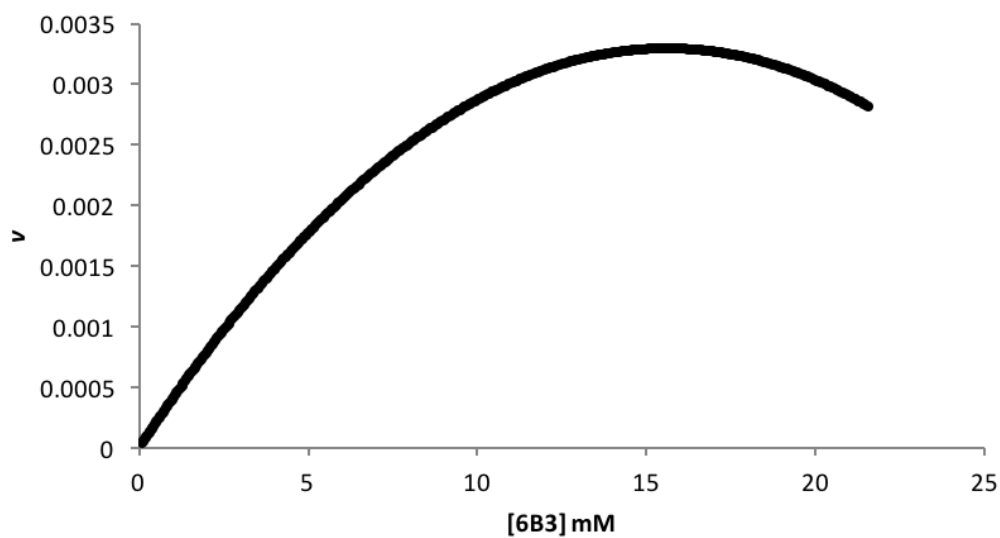
Figure 313. Rate vs. concentration of complex **71** with 3.81 equiv of i-Pr$_3$P (Run 1).

Table 75. Data for the decay of complex **71** with 3.81 equiv of *i*-Pr$_3$P (Run 1).

time (s)	Integral IS (−120.00 ppm)	Integral 6-B-3 (−115.74 ppm)	[mM] 6-B-3
1454	9530	10089	21.64
2908	9578	7894	16.84
4362	9472.69	5749.33	12.41
5816	9639.18	3854.94	8.17
7270	9602.73	2416.27	5.14
8724	9520.88	1370.62	2.94
10178	9651.22	689.682	1.46
11632	9674.15	377.682	0.80
13086	9483.52	212.826	0.46
14540	9516.06	92.4787	0.20
15994	9652.73	67.6269	0.14
17448	1785.33	14.0607	0.16
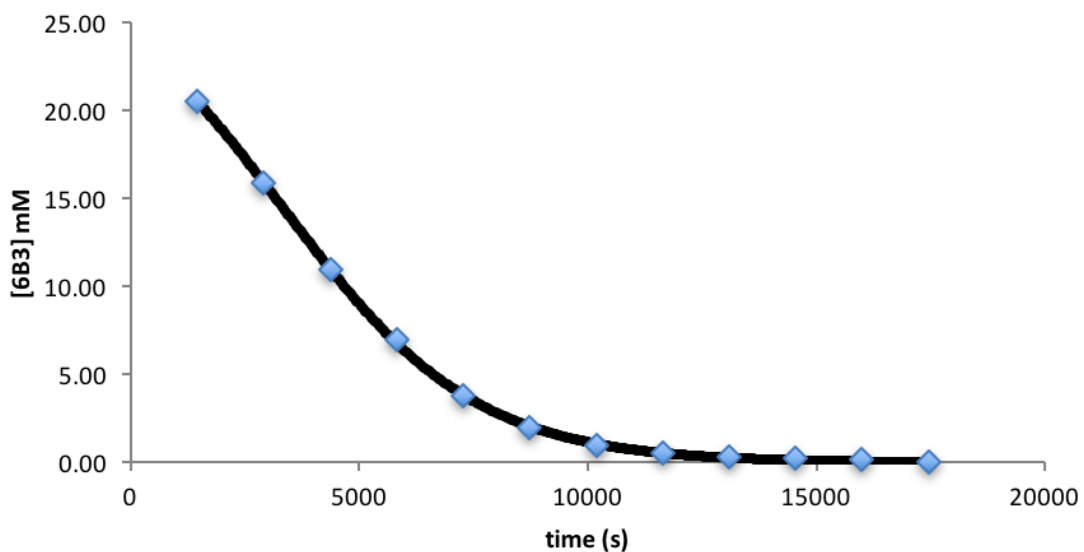
Figure 314. Decay of complex **71** with 3.81 equiv of *i*-Pr$_3$P (Run 2).
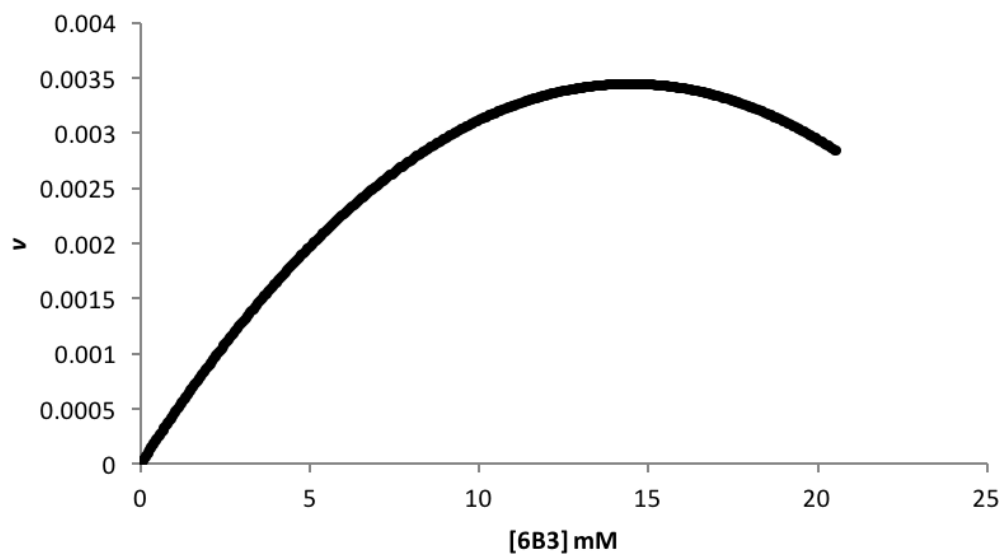
Figure 315. Rate vs. concentration of complex **71** with 3.81 equiv of *i*-Pr$_3$P (Run 2).

Table 76. Data for the decay of complex **71** with 3.81 equiv of *i*-Pr$_3$P (Run 2).

time (s)	Integral IS (−120.00 ppm)	Integral 6-B-3 (−115.74 ppm)	[mM] 6-B-3
1454	9429.91	9490.89	20.57
2908	9427.25	7322.45	15.88
4362	9498.9	5087.3	10.95
5816	9395.47	3201.72	6.97
7270	9565.18	1785.61	3.82
8724	9556.56	916.56	1.96
10178	9569.97	459.446	0.98
11632	9478.31	252.737	0.55
13086	9464.42	157.079	0.34
14540	9441.69	104.939	0.23
15994	9435.12	75.3278	0.16
17448	9591.93	30.6784	0.07
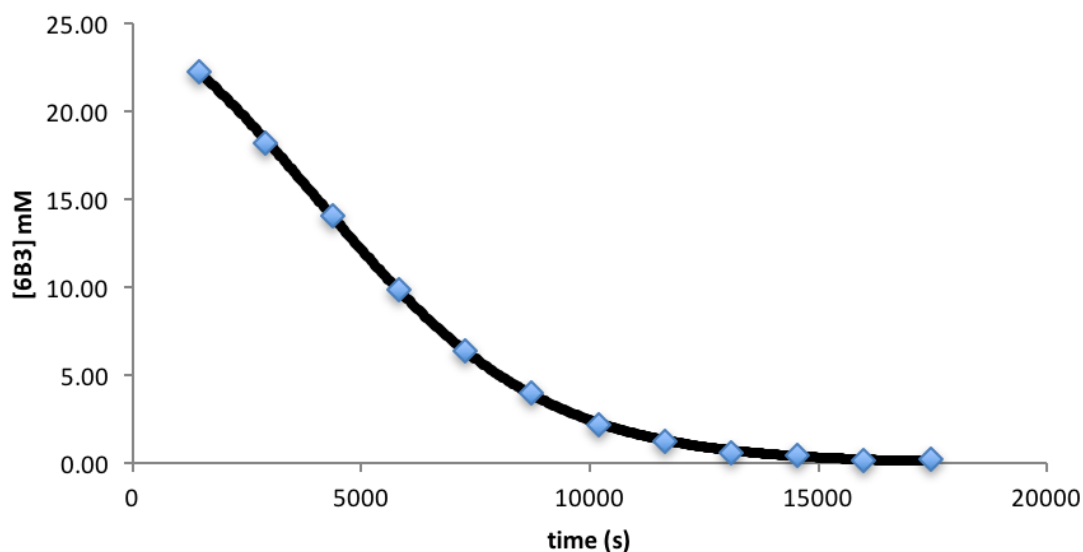
Figure 316. Decay of complex **71** with 3.81 equiv of *i*-Pr$_3$P (Run 3).
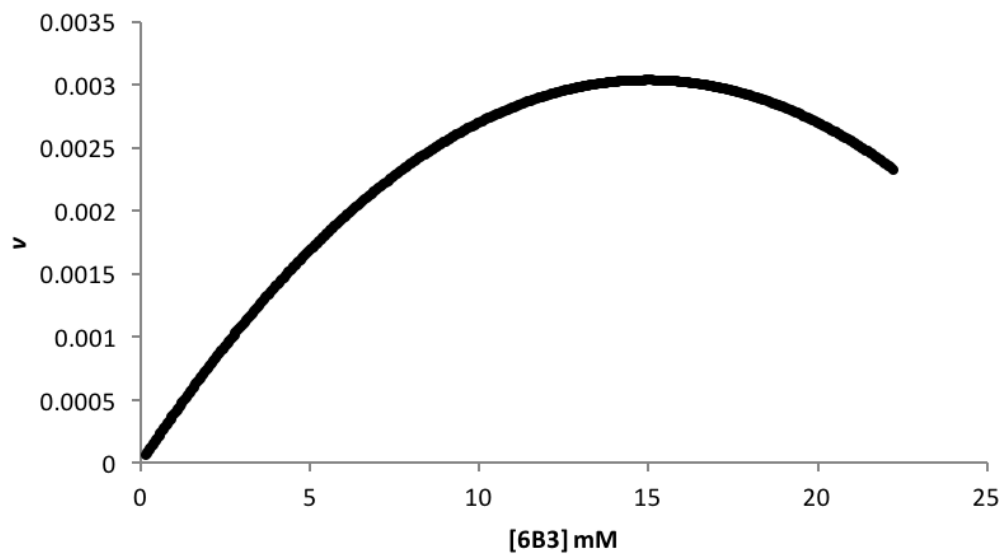
Figure 317. Rate vs. concentration of complex **71** with 3.81 equiv of *i*-Pr$_3$P (Run 3).

Table 77. Data for the decay of complex **71** with 3.81 equiv of *i*-Pr$_3$P (Run 3).

time (s)	Integral IS (−120.00 ppm)	Integral 6-B-3 (−115.74 ppm)	[mM] 6-B-3
1454	9370.46	10229.5	22.31
2908	9469.09	8453.91	18.25
4362	9325.23	6441.28	14.12
5816	9359.61	4524.27	9.88
7270	9406.12	2963.35	6.44

Table 77. (cont.)

8724	9333.19	1840.09	4.03
10178	9423.92	1029.36	2.23
11632	9351.33	568.514	1.24
13086	9438.9	296.284	0.64
14540	9406.59	203.278	0.44
15994	9489.67	81.2297	0.17
17448	9357.63	103.932	0.23

Experiment 65: Kinetic measurement for decay of 6-B-3 complex 71 at 20 °C from independent synthesis with 15.03 equiv of *i*-Pr$_3$P from 72 and 70.
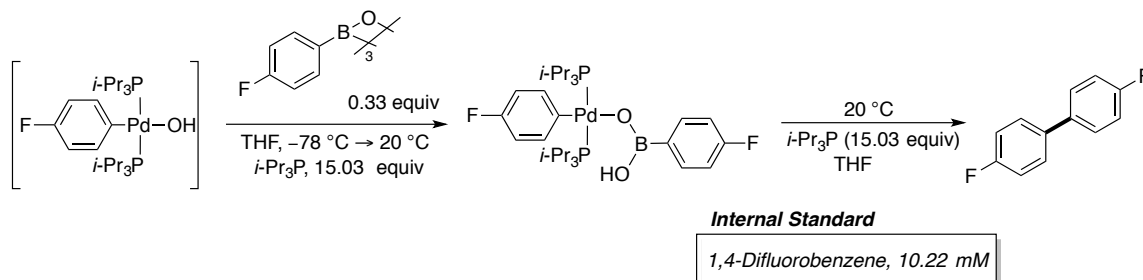
A 2-mL volumetric flask was taken into the dry box and charged with [(*i*-Pr$_3$P)Pd(4-FC$_6$H$_4$)(μ-OH)]$_2$ (30.8 mg, 41 μmol, 1.0 equiv), *i*-Pr$_3$P (250 μL, 1.30 mmol, 31.7 equiv) and 1,4-difluorobenzene (2.5 μL, 24 μmol) followed by dissolving with THF (NaK) to the 2-mL mark generating a 40.1 mM solution. An oven dried 5-mm NMR tube was charged with 4-fluorophenylboroxine (2.5 mg, 6.8 μmol) and 95μL of THF (NaK) followed by capping with a septum and Teflon taped. The sample was inserted into a -78 °C acetone dry-ice bath followed by the addition of (500 μL, 20.3 μmol, 3.0 equiv) of the arylpalladium Stock Sol. *via* a 1 mL glass syringe. The NMR tube was removed from the bath and shaken for 45 s. It was then cleaned with a Kimwipe then placed into the NMR probe set to 20 °C.

Using the fluorine channel to collect a spectrum every 1454 s, the progress of the reaction was monitored by the decay of the 6-B-3 complex (-115.75 ppm) and formation of cross-coupling product (-116.45 ppm) in comparison with the internal reference 1,4-difluorobenzene (-120.00 ppm). The first order decay and formation profiles were fitted with OrginPro 2015 software using equations **4** and **5** respectively. This procedure was performed three times to obtain an average rate.131

Table 78. Results from the cross-coupling reaction.

Entry	k (s^{-1}) (Decay **71**)	k (s^{-1}) (Form **73**)	A$_0$ [mM] (Decay **71**)	A$_0$ [mM] (Form **73**)
Run 1	$(1.184 \pm 0.008) \times 10^{-4}$	$(7.020 \pm 0.04) \times 10^{-5}$	21.47 ± 0.12	23.46 ± 0.55
Run 2	$(1.297 \pm 0.032) \times 10^{-4}$	$(7.617 \pm 0.03) \times 10^{-5}$	22.97 ± 0.44	23.63 ± 0.29
Run 3	$(1.275 \pm 0.026) \times 10^{-4}$	$(6.776 \pm 0.04) \times 10^{-5}$	22.96 ± 0.36	24.69 ± 0.56

k avg. Decay of 6-B-3 51 = (1.25 ± 0.60) x 10^{-4} s^{-1}
k avg. Formation of 53 = (7.14 ± 0.43) x 10^{-5} s^{-1}
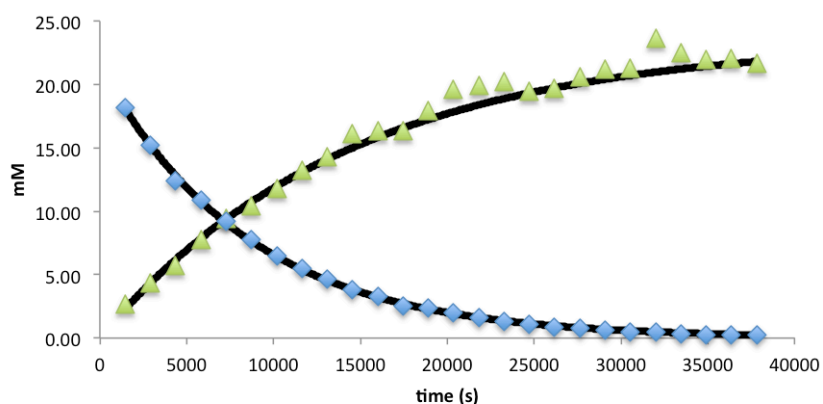
Figure 318. Decay of complex **71** and formation of **73** (Run 1).

Table 79. Data for the decay of complex **71** and formation of **73** (Run 1).

time (s)	Integral IS (−120.00 ppm)	Integral 6-B-3 (−115.75 ppm)	Integral CCP (−116.45 ppm)	[mM] 6-B-3	[mM] CCP
1454	9464	8410	2482	18.16	2.68
2908	9847	7346	4191	15.25	4.35
4362	10628	6432	5925	12.37	5.70
5816	10356	5498	7860	10.85	7.76
7270	10249	4631	9453	9.24	9.43
8724	10425	3945	10672	7.74	10.46
10178	10465	3304	12065	6.45	11.78
11632	10170	2732	13205	5.49	13.27
13086	10299	2345	14402	4.65	14.29
14540	10043	1876	15820	3.82	16.10
15994	10050	1602	16054	3.26	16.33
17448	10605	1329	16982	2.56	16.37
18902	10235	1173	17962	2.34	17.94
20356	9383	907	17990	1.98	19.59
21810	9555	769	18620	1.64	19.92
23264	9775	638	19380	1.33	20.26
24718	10264	533	19513	1.06	19.43
26172	10268	449	19784	0.89	19.69
27626	9891	376	19943	0.78	20.61
29080	10047	310	20817	0.63	21.17
30534	10070	224	20957	0.45	21.27
31988	9129	214	21109	0.48	23.63
33442	9663	169	21273	0.36	22.50

Table 79. (cont.)

34896	9778	136	21044	0.29	21.99
36350	9850	133	21217	0.28	22.01
37804	9968	119	21124	0.24	21.66
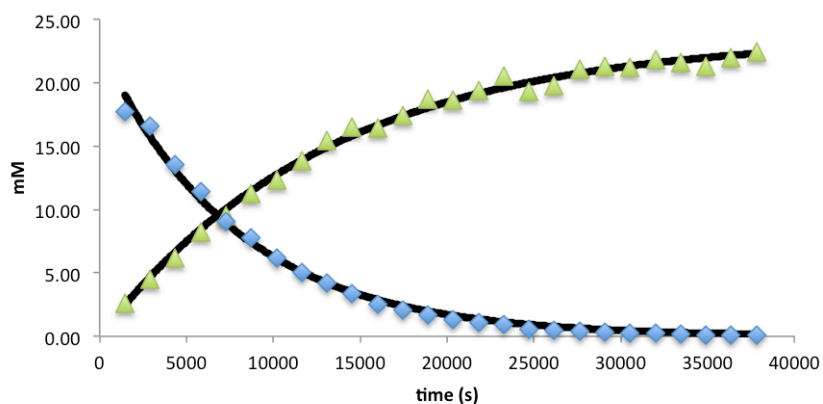
Figure 319. Decay of complex **71** and formation of **73** (Run 2).

Table 80. Data for the decay of complex **71** and formation of **73** (Run 2).

time (s)	Integral IS (−120.00 ppm)	Integral 6-B-3 (−115.75 ppm)	Integral CCP (−116.45 ppm)	[mM] 6-B-3	[mM] CCP
1454	9863	8550	2482	17.72	2.57
2908	9580	7756	4191	16.55	4.47
4362	9756	6472	5925	13.56	6.21
5816	9769	5469	7860	11.44	8.22
7270	10138	4512	9453	9.10	9.53
8724	9670	3675	10672	7.77	11.28
10178	9993	3034	12065	6.21	12.34
11632	9760	2405	13205	5.04	13.83
13086	9527	1962	14402	4.21	15.45
14540	9778	1602	15820	3.35	16.53
15994	9974	1231	16054	2.52	16.45
17448	9949	1010	16982	2.07	17.44
18902	9811	823	17962	1.72	18.71
20356	9873	628	17990	1.30	18.62
21810	9814	512	18620	1.07	19.39
23264	9644	427	19380	0.91	20.54
24718	10312	288	19513	0.57	19.34
26172	10247	247	19784	0.49	19.73

Table 80. (cont.)

27626	9677	201	19943	0.43	21.06
29080	10006	171	20817	0.35	21.26
30534	10088	105	20957	0.21	21.23
31988	9887	103	21109	0.21	21.82
33442	10077	77	21273	0.16	21.57
34896	10089	66	21044	0.13	21.32
36350	9869	47	21217	0.10	21.97
37804	9610	46	21124	0.10	22.46
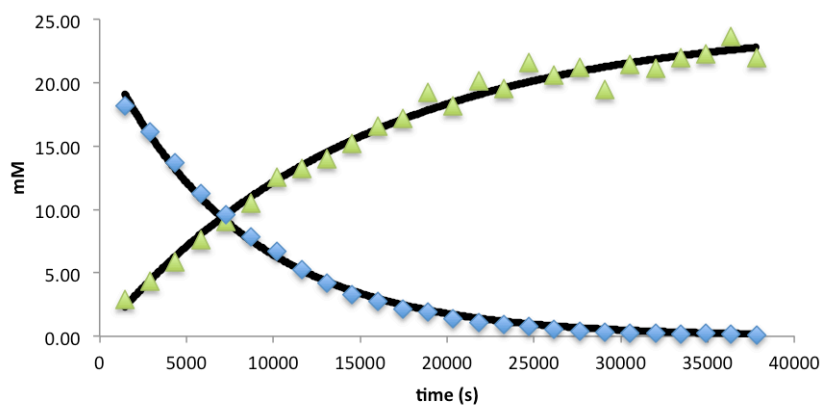
Figure 320. Decay of complex **71** and formation of **73** (Run 3).

Table 81. Data for the decay of complex **71** and formation of **73**. (Run 3).

time (s)	Integral IS (−120.00 ppm)	Integral 6-B-3 (−115.75 ppm)	Integral CCP (−116.45 ppm)	[mM] 6-B-3	[mM] CCP
1454	9801	8697	2820	18.14	2.94
2908	9797	7734	4181	16.14	4.36
4362	10000	6698	5778	13.69	5.90
5816	10036	5525	7490	11.25	7.63
7270	9973	4666	8809	9.56	9.03
8724	9949	3814	10196	7.84	10.47
10178	9698	3187	11937	6.72	12.58
11632	10023	2581	13014	5.26	13.27
13086	9999	2071	13683	4.23	13.99
14540	9963	1591	14833	3.26	15.22
15994	9874	1316	15995	2.72	16.55
17448	9912	1028	16679	2.12	17.20
18902	9323	862	17539	1.89	19.23

Table 81. (cont.)

20356	10122	674	18028	1.36	18.20
21810	9488	507	18729	1.09	20.17
23264	10092	446	19259	0.90	19.50
24718	9497	346	20068	0.74	21.59
26172	9918	273	20026	0.56	20.64
27626	9815	200	20338	0.42	21.18
29080	10288	164	19614	0.33	19.48
30534	9991	130	20975	0.27	21.46
31988	10130	106	20940	0.21	21.13
33442	9989	74	21454	0.15	21.95
34896	9797	103	21362	0.22	22.28
36350	9358	74	21648	0.16	23.64
37804	10008	42	21491	0.09	21.95

CHAPTER 8: Experimental for Chapter 4

General Experimental

Reactions were performed using glassware that had been flame-dried under vacuum or oven-dried (210 $^{\circ}$C) overnight. All reactions were conducted under an inert atmosphere using argon connected to a drying tube equipped with phosphorous pentoxide, calcium sulfate, and sodium hydroxide. Solvents used for extraction were reagent grade. Reaction solvents tetrahydrofuran (Fisher, HPLC grade), diethyl ether (Fisher, HPLC grade), toluene (Fisher, HPLC grade), hexane (Fisher, HPLC grade), and methylene chloride (Fisher, HPLC grade) were dried by percolation through two columns packed with neutral alumina under positive pressure of argon (solvent dispersion system method). Benzene (ACS grade) and pentane (ACS grade) were distilled over sodium while methanol (ACS grade) was distilled over magnesium.

Commercial reagents were purified by distillation or recrystallization prior to use unless otherwise noted. Tetrafluoroboric acid diethyl ether complex, cesium hydroxide monohydrate, isopropylmagnesium chloride solution (2M in THF), triphenylphosphine, thallium formate and trichlorophosphine, pinacol, 2-hydroxyisobutyric acid were all purchased from Aldrich. Palladium chloride was purchased from Pressure Chemical. Sodium tetraphenylboron was purchased from Mallinkrodt Chemical. 4-Fluorophenylboronic acid, 1,4-fluoroiodobenzene, 1,1'-bis(diphenylphosphino)ferrocene, and 1,4-difluorobenzene were all purchased from Oakwood Products. The following compounds were prepared by literature methods, 4-fluorophenylboroxine,[132] potassium 4-fluorophenyltrihydroxyboronate,[133] bromo(4-fluorophenyl)(tri-*tert*-butylphosphine)palladium[134] and allylcyclopentyl-palladium(II).[135]

^{1}H, ^{13}C, ^{19}F, and ^{31}P, spectra were recorded on a Varian Unity, Agilent, or Bruker Avance 600 MHz spectrometers (^{1}H, 151 MHz; ^{13}C, 565 MHz; ^{19}F, 243 MHz; ^{31}P, 193 MHz). ^{11}B NMR spectra were reordered on a Varian Unity 400 MHz (^{11}B NMR, 129 MHz).

Spectra are referenced to residual chloroform (7.26 ppm, ^{1}H; 77.00 ppm, ^{13}C), residual THF (1.72 ppm, ^{1}H; 68.21 ppm, ^{13}C), 1,4-difluorobenzene (–120.00 ppm, ^{19}F), Ph$_4$BNa (−6.14 ppm, ^{11}B), triisopropylphosphine (19.00 ppm, ^{31}P), and external HBF$_4$•OEt$_2$ (0.00 ppm, ^{11}B). Chemical shifts are reported in ppm, multiplicities are indicated by s (singlet), d (doublet), t (triplet), q (quartet), p (pentet), h (hextet), m (multiplet) and br (broad). Coupling constants, *J*, are reported in Hertz.

Experiment 66: Reaction of complex 70 with 117 and 4.0 equiv of *i*-Pr₃P.
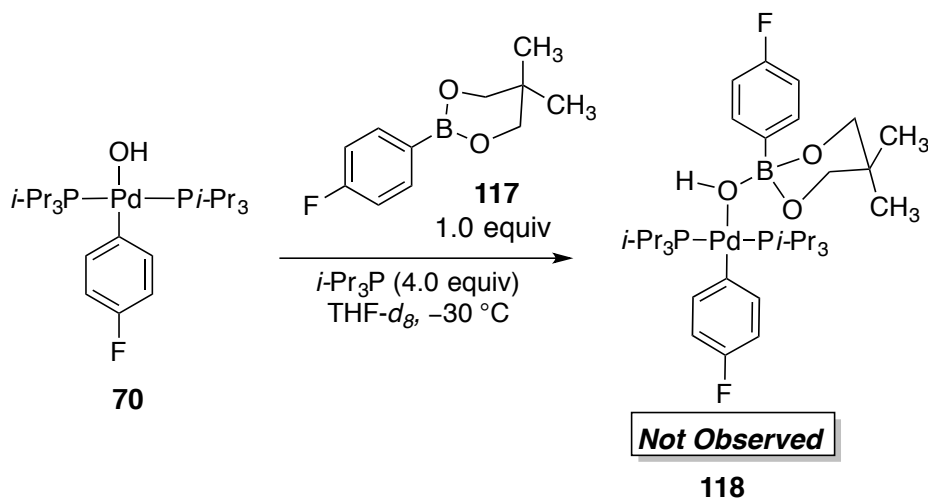
An oven-dried, 5-mm, NMR tube was taken into the glove box and both [(*i*-Pr₃P)Pd(4-FC₆H₄)(μ-OH)]₂ (7.58 mg, 10 μmol, 1.0 equiv) and *i*-Pr₃P (12 μL, 60 μmol, 6.0 equiv) were added, followed by the addition of 500 μL of freshly distilled (NaK) THF-*d₈*. The tube was capped with a septum and Teflon taped, then the tube was shaken and placed into a −78 °C dry-ice acetone bath followed by the addition of 4-fluorophenylneopentyl boronate (4.2 mg, 20 μmol, 2.0 equiv) dissolved in THF (100 μL). The tube was shaken, and quickly cleaned with a Kimwipe and placed into the probe of the NMR spectrometer pre-cooled to −30 °C.
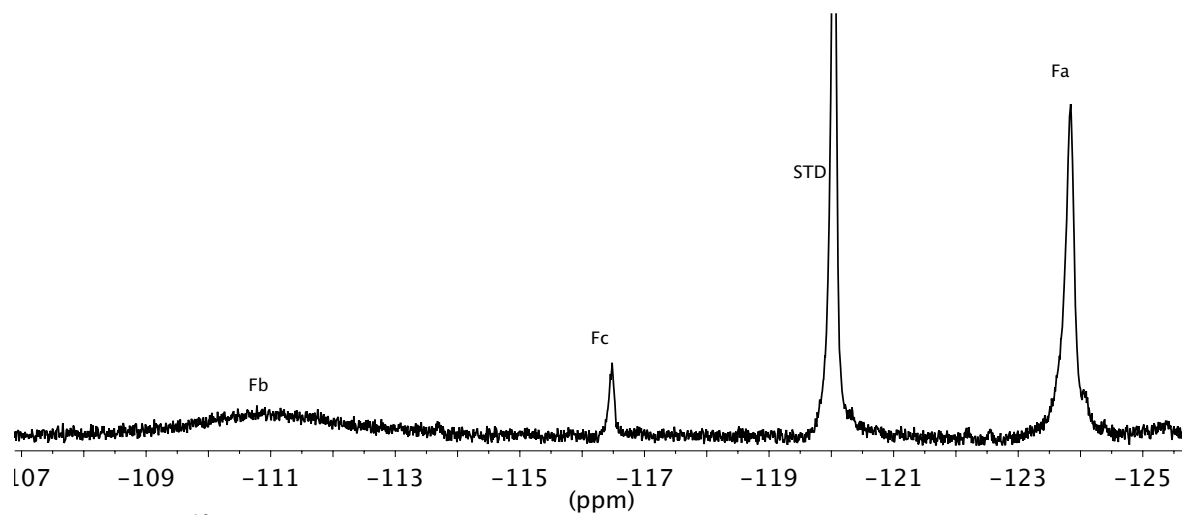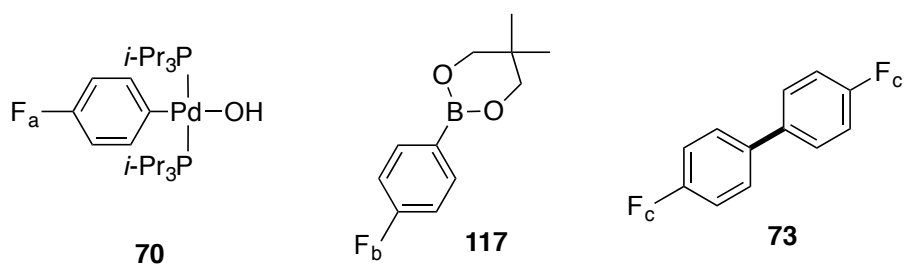
Figure 321. ^{19}F NMR spectrum of **70** and **117** at −30 °C, referenced to 1,4-diflurobenzene (−120.00 ppm).

Experiment 67: Reaction of complex 70 with 119 and 3.0 equiv of *i*-Pr$_3$P.
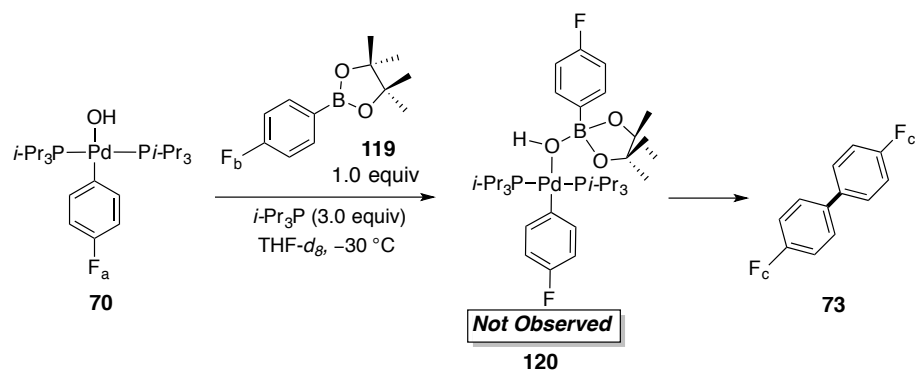
An oven-dried, 5-mm, quartz NMR tube was taken into the glove box and both [(*i*-Pr$_3$P)Pd(4-FC$_6$H$_4$)(μ-OH)]$_2$ (7.58 mg, 10 μmol, 1.0 equiv) and *i*-Pr$_3$P (10 μL, 50 μmol, 5.0 equiv) were added, followed by the addition of 600 μL of freshly distilled (NaK) THF-d_8. The tube was capped with a septum and Teflon taped, then the tube was shaken and placed into a −78 °C dry-ice acetone bath followed by the addition of 4-fluorophenylpinacol boronate (4.5 mg 20 μmol, 2.0 equiv) dissolved in THF (100 μL). The tube was shaken, and quickly cleaned with a Kimwipe and placed into the probe of the NMR spectrometer pre-cooled to −30 °C. Substantial cross-coupling product **73** was observed by fluorine NMR.
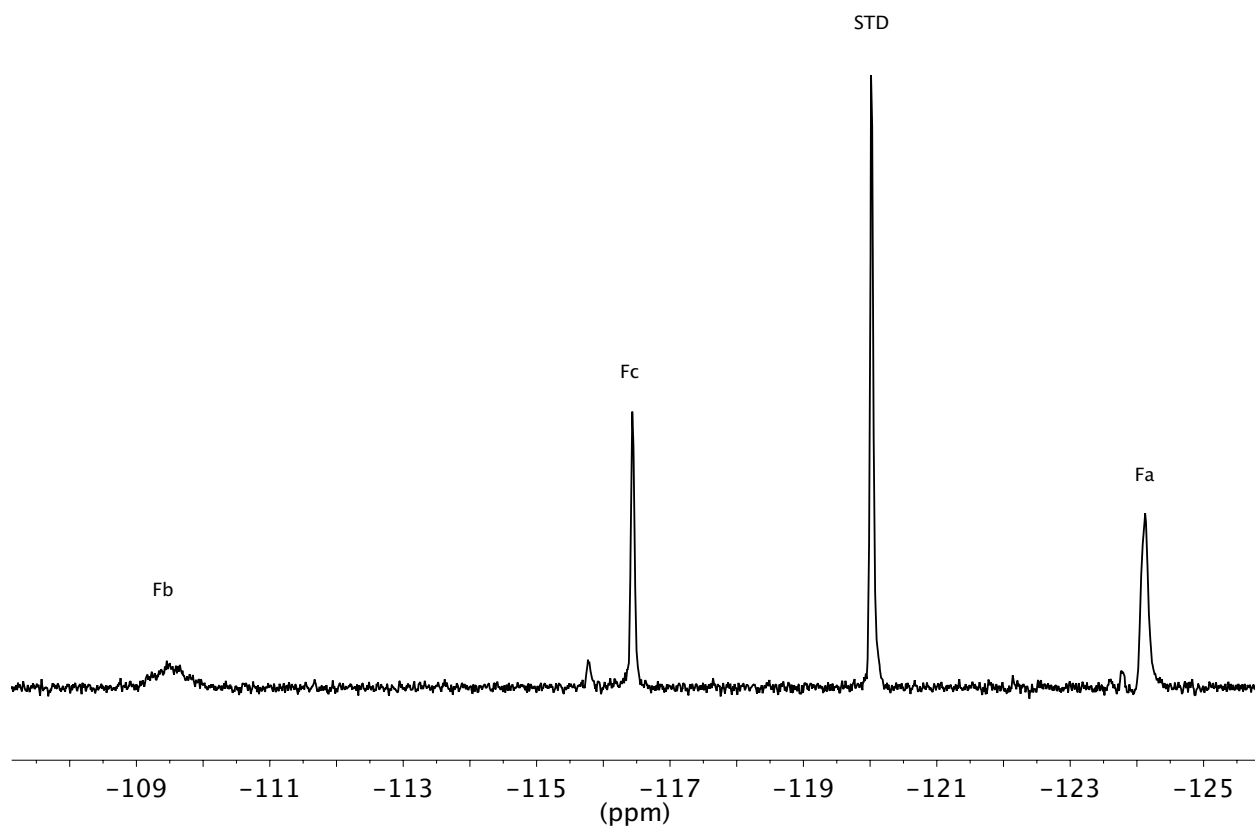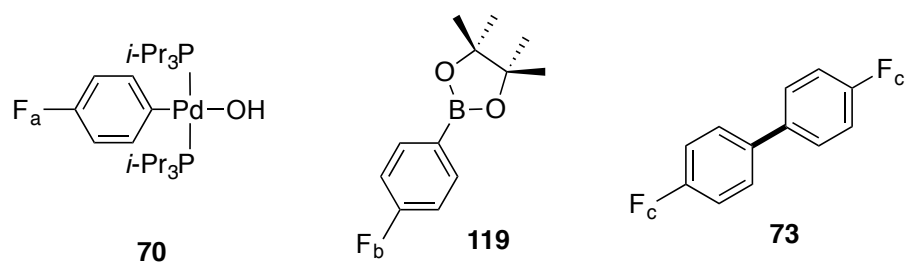
Figure 322. ^{19}F NMR spectrum of **70** and **119** at −30 °C, referenced to 1,4-difluorobenzene (−120.00 ppm).

Experiment 68: Addition of 121 into 70.

An oven-dried, 5-mm, NMR tube was taken into the glove box and both [(*i*-Pr$_3$P)Pd(4-FC$_6$H$_4$)(μ-OH)]$_2$ (7.58 mg, 10 μmol, 1.0 equiv) and *i*-Pr$_3$P (19 μL, 100 μmol, 10.0 equiv) were added, followed by the addition of 500 μL of freshly distilled (NaK) THF-d_8. The tube was capped with a septum and Teflon taped, then the tube was shaken and placed into a −78 °C dry-ice acetone bath followed by the addition of 4-fluorophenylcatechol boronate (4.3 mg, 20 μmol, 2.0 equiv) dissolved in THF (100 μL). The tube was shaken, and quickly cleaned with a Kimwipe and placed into the probe of the NMR spectrometer pre-cooled to −60 °C. Multiple specie were present by ^{19}F NMR spectroscopy.

Figure 323. ^{19}F NMR spectrum of **121** and **70** at −60 °C, referenced to 1,4-diflurobenzene (−120.00 ppm).

451

Experiment 69: RI-NMR injection of 121 into 70.

An oven-dried, 5-mm, quartz NMR tube was taken into the glove box and both [(*i*-Pr$_3$P)Pd(4-FC$_6$H$_4$)(μ-OH)]$_2$ (7.58 mg, 10 μmol, 1.0 equiv) and *i*-Pr$_3$P (19 μL, 100 μmol, 10.0 equiv) were added, followed by the addition of 500 μL of freshly distilled (NaK) THF-d_8. The tube was capped with a septum and Teflon taped, then the tube was shaken and placed into a −78 °C dry-ice acetone bath followed by the addition of 4-fluorophenylcatechol boronate (4.3 mg, 20 μmol, 2.0 equiv) dissolved in THF (100 μL). The tube was shaken, and quickly cleaned with a Kimwipe and placed into the probe of the NMR spectrometer pre-cooled to −60 °C. Multiple specie were present by ^{19}F NMR spectroscopy.

Figure 324. ^{19}F NMR spectrum of **121** and **70** at -60 °C, referenced to 1,4-diflurobenzene (-120.00 ppm).
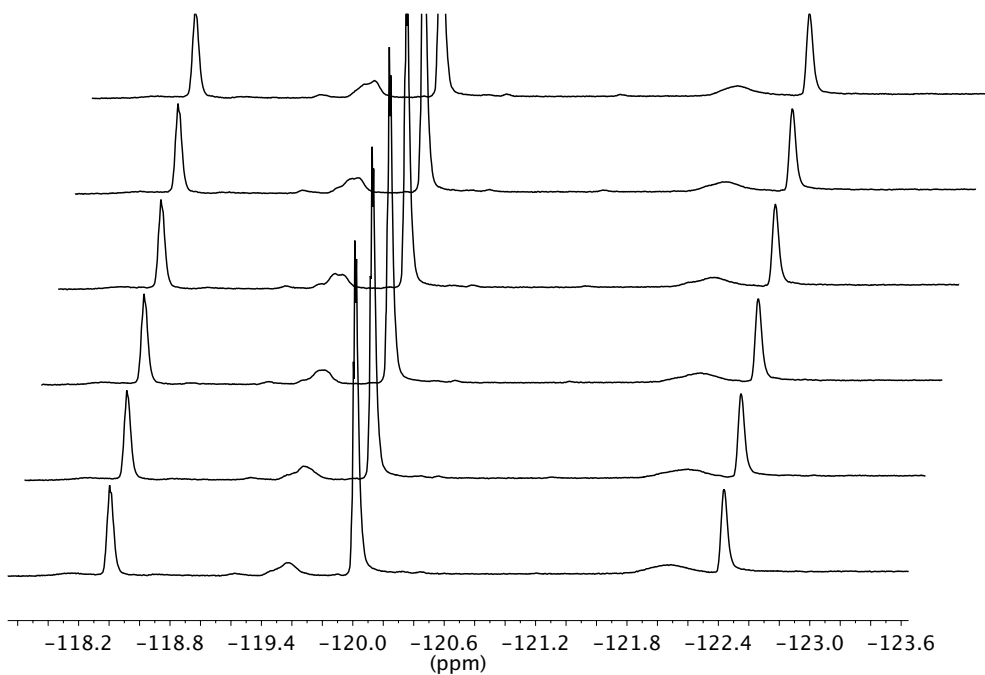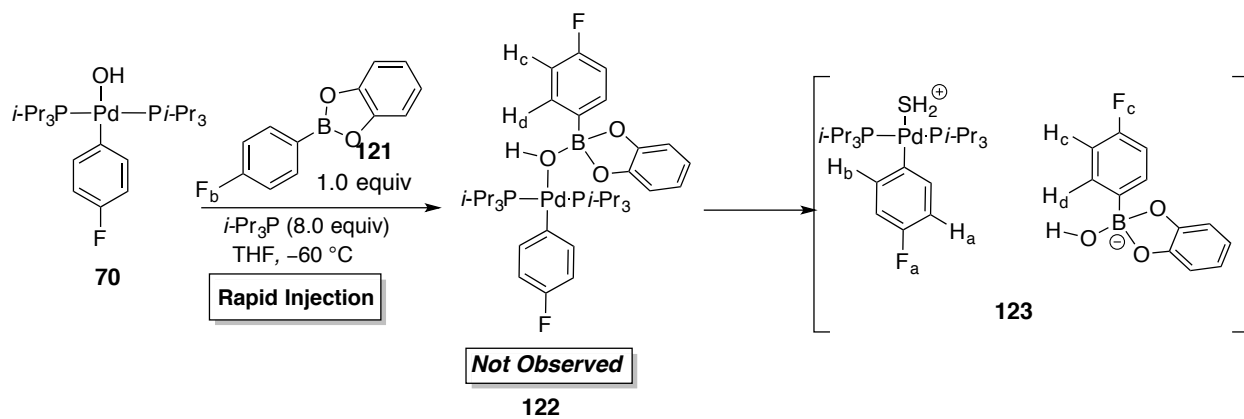
Figure 325. ^{19}F NMR spectra of **121** and **70** at −60 °C, referenced to 1,4-diflurobenzene (−120.00 ppm).
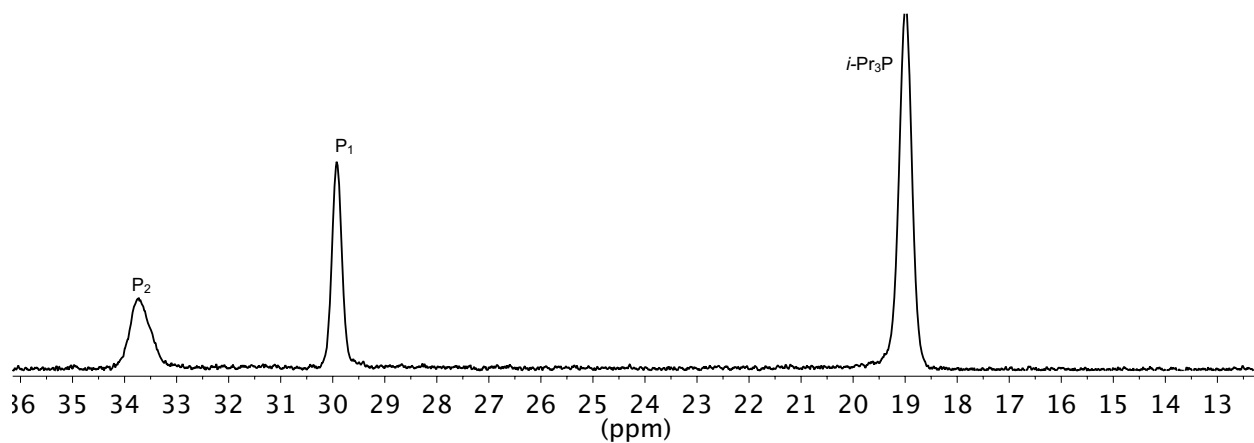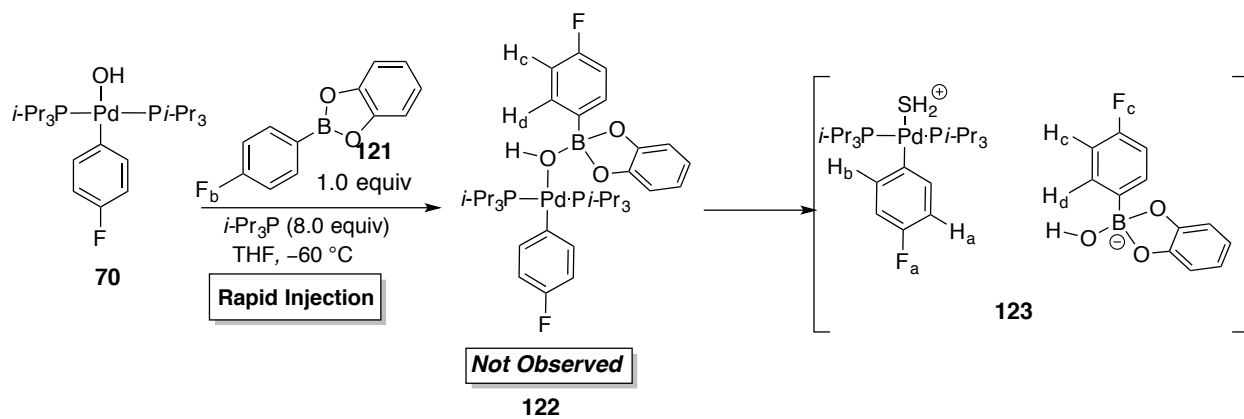
Figure 326. ^{31}P NMR spectra of **121** and **70** at −60 °C, referenced i-Pr$_3$P (−19.00 ppm).

Experiment 70: Preparation of 8-B-4 complex 129 in THF

80   **129**
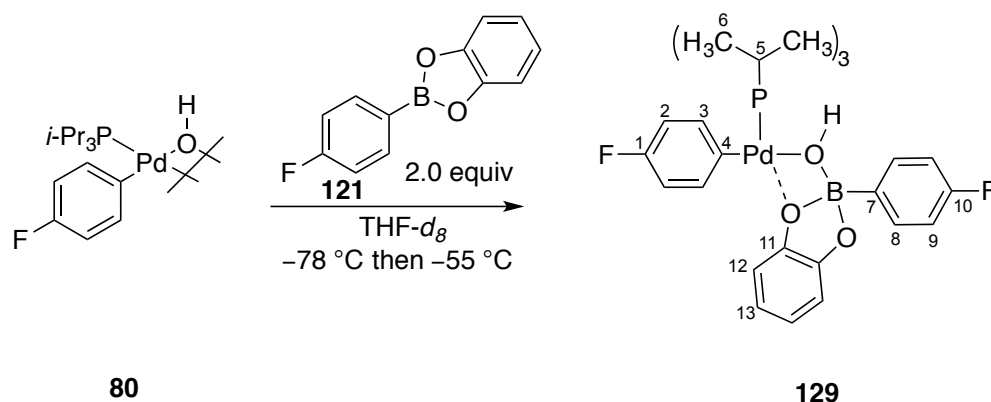
An oven-dried, NMR tube was charged with catechol 4-fluorophenylboronic ester (44 mg, 120 μmol, 1.0 equiv) and 500 μL of THF-d_8 yielding a 0.72 M solution.

An oven dried, 5-mm, Quartz NMR tube was charged with [(i-Pr$_3$P)Pd(4-FC$_6$H$_4$)(μ-OH)]$_2$ (7.58 mg, 10 μmol, 1.0 equiv) and 500 μL of THF-d_8 followed by sonication for ~2 min. The tube was shaken and placed into a −78 °C dry-ice acetone bath followed by the addition of the catechol 4-fluorophenylboronic ester (95 μL, 20 μmol, 2.0 equiv) solution. The tube was vortexed (not shaken) quickly cleaned with a Kimwipe and placed into the −78 °C bath. The tube was then placed into the probe of the NMR spectrometer pre-cooled to −55 °C. The sample was found to be stable for ~3-4 h at −55 °C. The complex was characterized *via* 1D and 2D NMR experiments over a course of multiple experiments.

Data for **129**:

^{1}H NMR: (600 MHz, THF-d_8)

7.66 (m, 2 HC(8)), 7.31 (m, 2 HC(3)), 6.90 (m, 2 HC(9)), 6.82 (m, 2 CH(2)), 6.38 (m, 2 CH(12)), 6.20 (m, 2 CH(13)), 5.00 (broad, HO), 2.28 (m, 6 HC(5)), 1.24 (m, 36 HC(6))

^{13}C NMR: (151 MHz, THF-d_8)

164.64, 163.06 (d, ^1J(F-C) = 241 Hz, 1 C(10)), 163.80, 162.20 (d, ^1J(F-C) = 240 Hz, 1 C(1)), 153.88 (s, 2 C(11)), 144.52 (Obs. in HMBC, 1 C(4)), 138.02 (m, 2 C(8)), 136.85 (Obs. in HMBC, 1 C(7)), 135.02, 134.98 (d, ^3J(F-C) = 7 Hz 2 C(3)), 119.28 (s, 2 C(12)), 115.48, 115.34 (d, ^2J(F-C) = 18 Hz, 2 C(9)), 114.88, 114.75 (d, ^2J(F-C) = 18 Hz, 2 C(2)), 110.83 (s, 2 C(13)), 25.88 (UD, 3 C(5)), 20.19 (s, 6 C(6))

<u>^{19}F NMR:</u>   (565 MHz, THF-d_8)

−117.43 (s, FC(10)), −120.77 (s, FC(1)),

<u>^{31}P NMR:</u>   (243 MHz, THF-d_8)

51.85 (s, 1 P(Pd))

<u>^{11}B NMR:</u>   (129 MHz, THF-d_8)

12 ppm (br, 1 B(O))
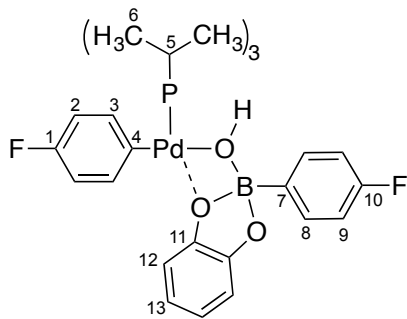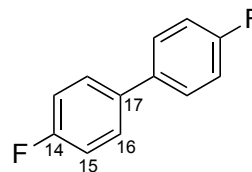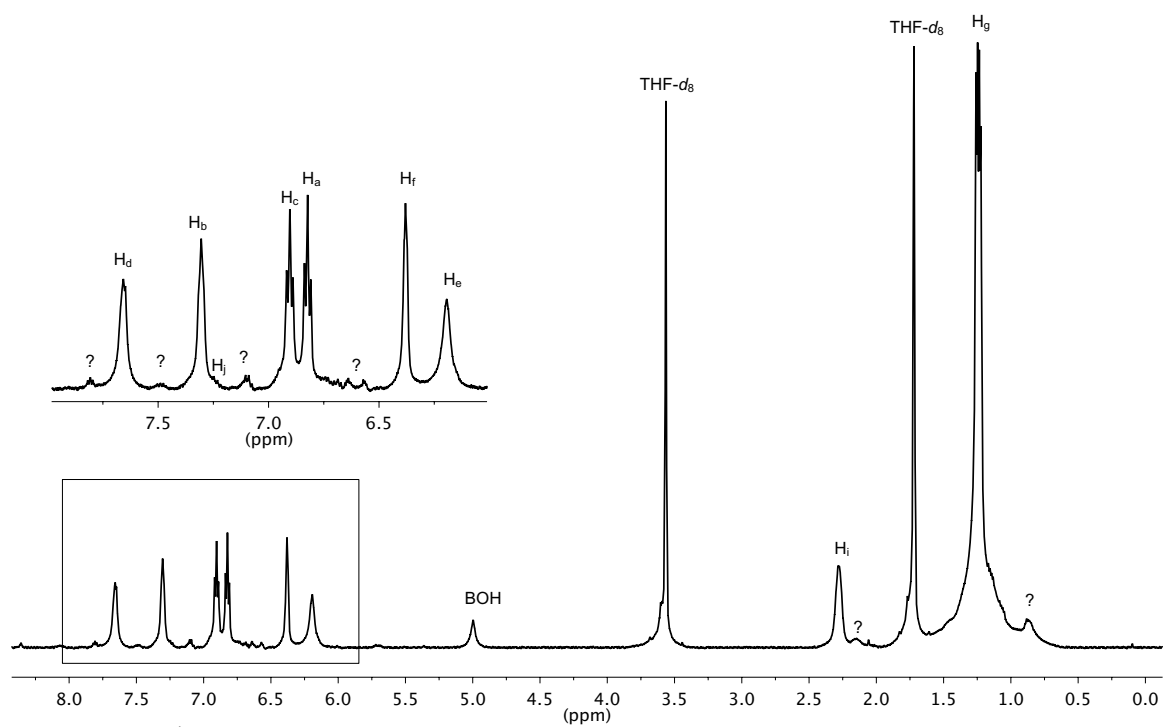
Figure 327. ^{1}H NMR spectrum of **129** at −55 °C, referenced to THF-d_8 (1.72 ppm).
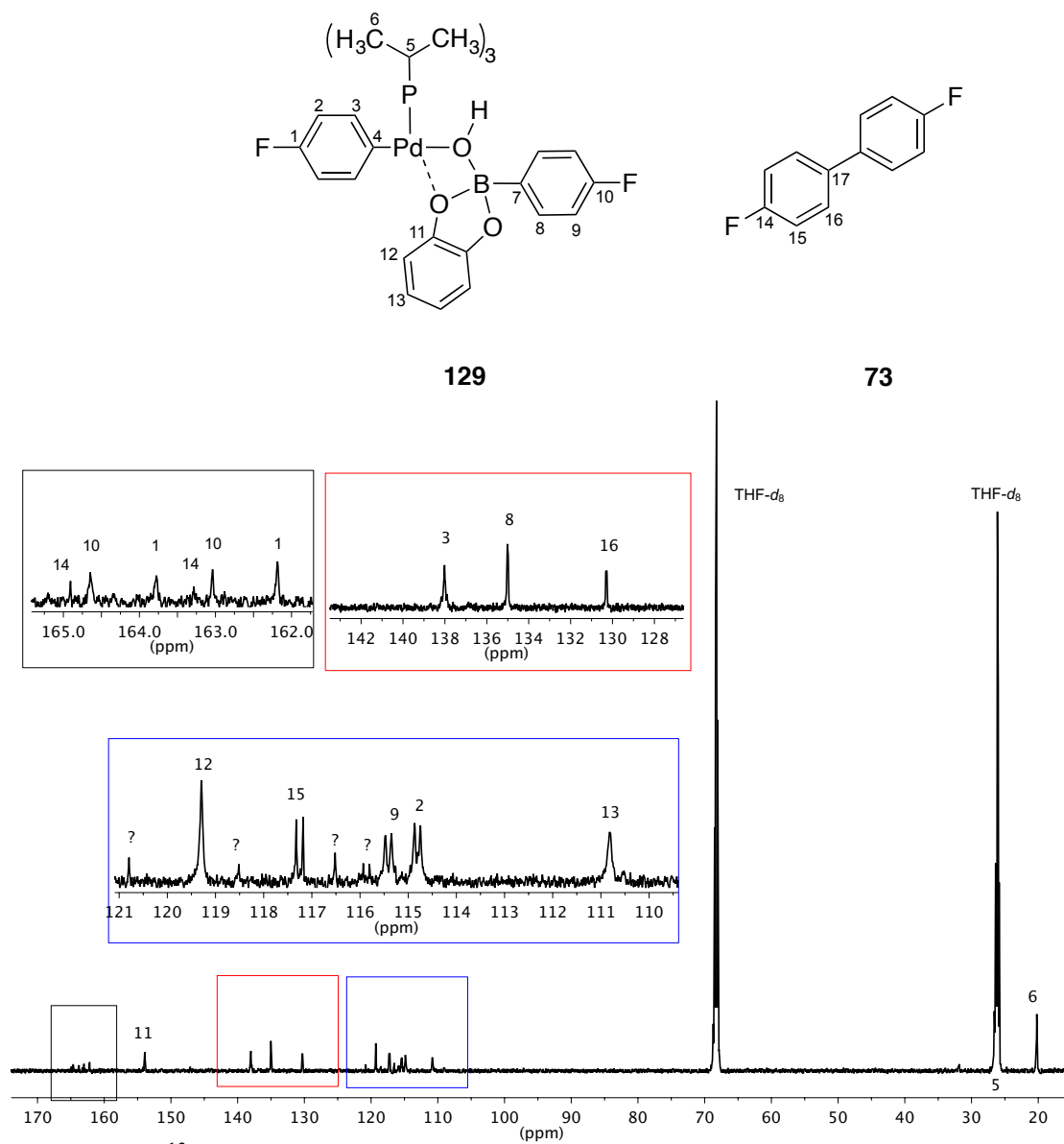
Figure 328. ^{13}C NMR spectrum of **129** at −55 °C, referenced to THF-d_8 (68.21 ppm).
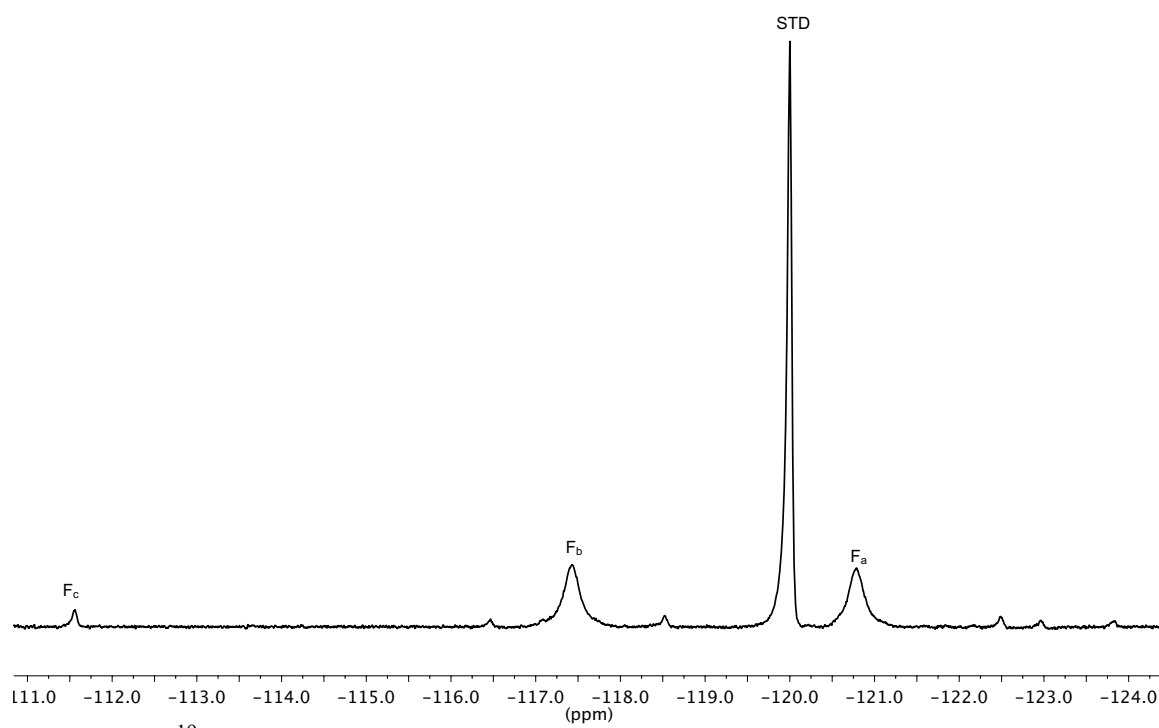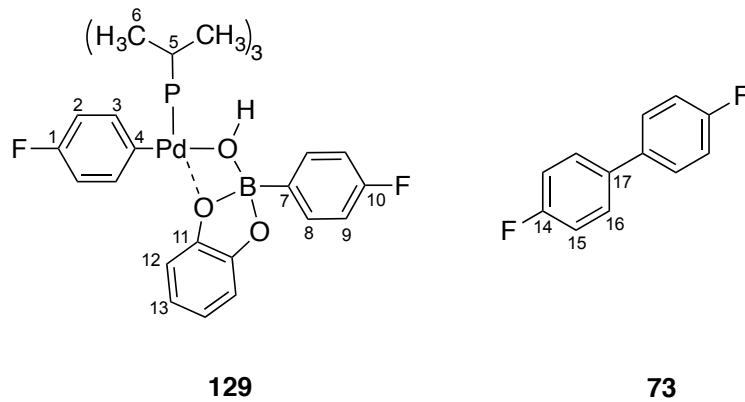
Figure 329. ^{19}F NMR spectrum of **129** at −55 °C, referenced to 1,4-difluorobenzene (−120 ppm).

129

73

60 55 50 45 40 35 30 25 20 15 10 5 0 −5 −10 −15 −20 −25 −30
(ppm)
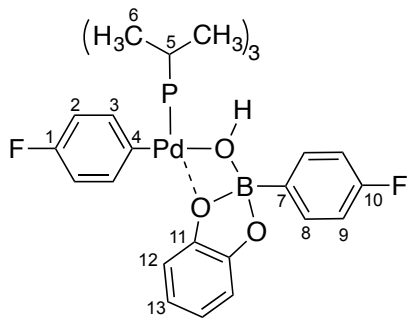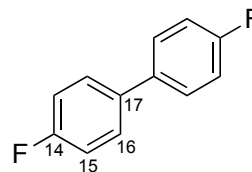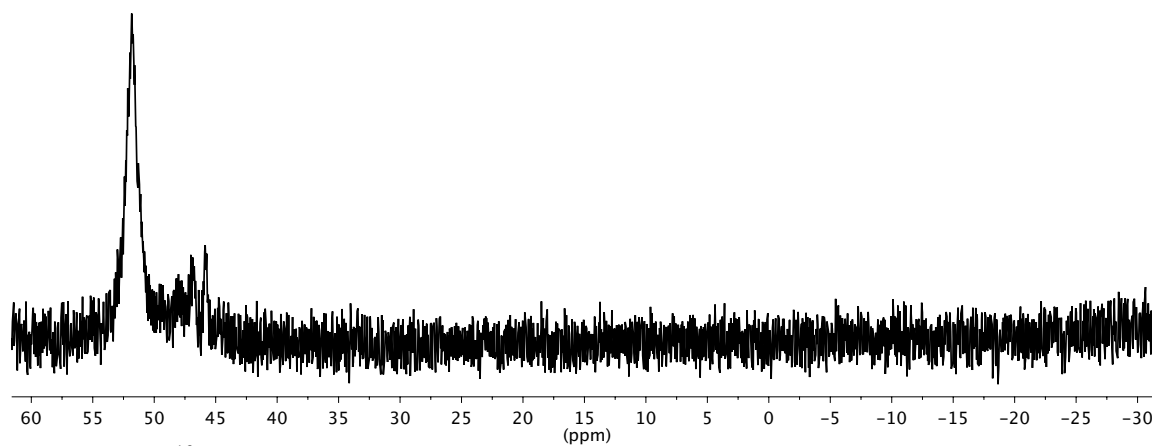
Figure 330. ^{19}F NMR spectrum of **129** at −55 °C, referenced externally to *i*-Pr$_3$P (19 ppm).
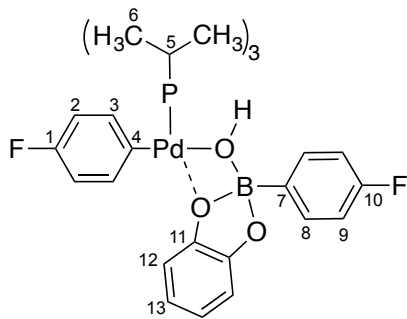
129
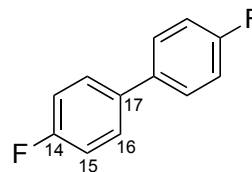
73
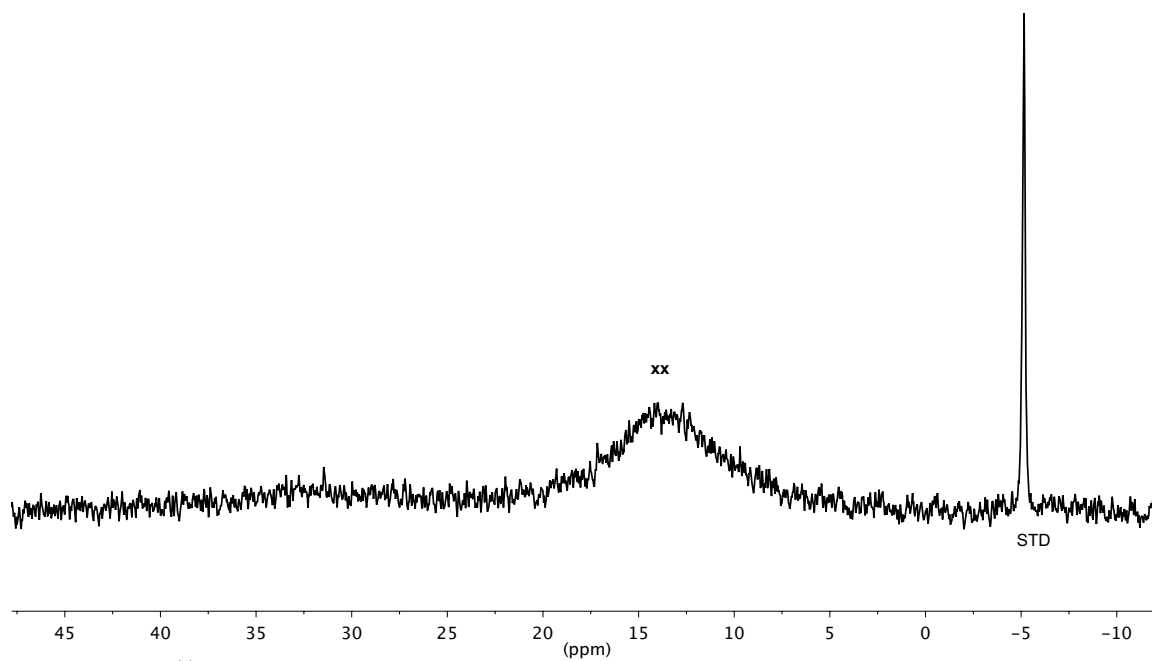
Figure 331. ^{11}B NMR spectrum of **129** at −55 °C, referenced to Ph$_4$BNa (−6.14 ppm).
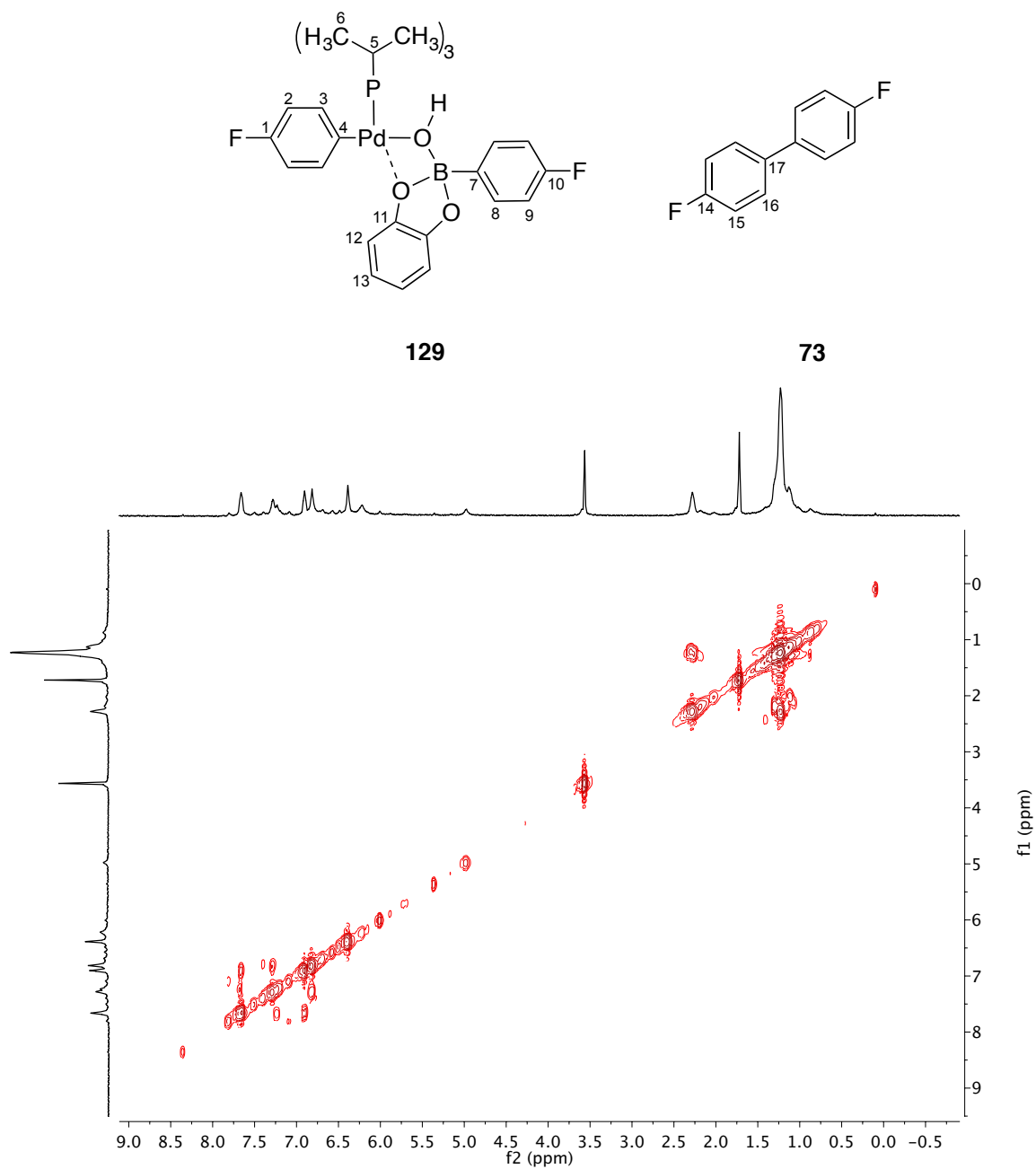
Figure 332. COSY NMR spectrum of **xx** at −55 °C, referenced to THF-d_8 (1.72 ppm).
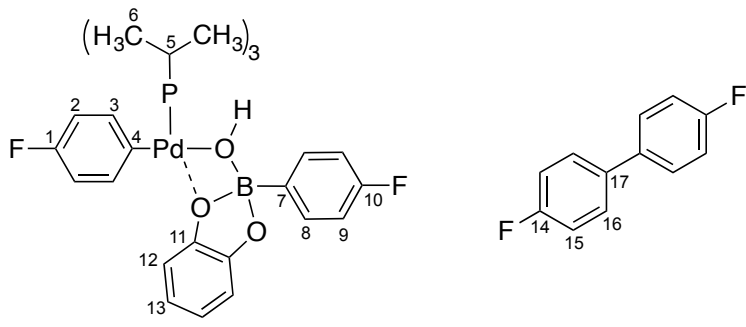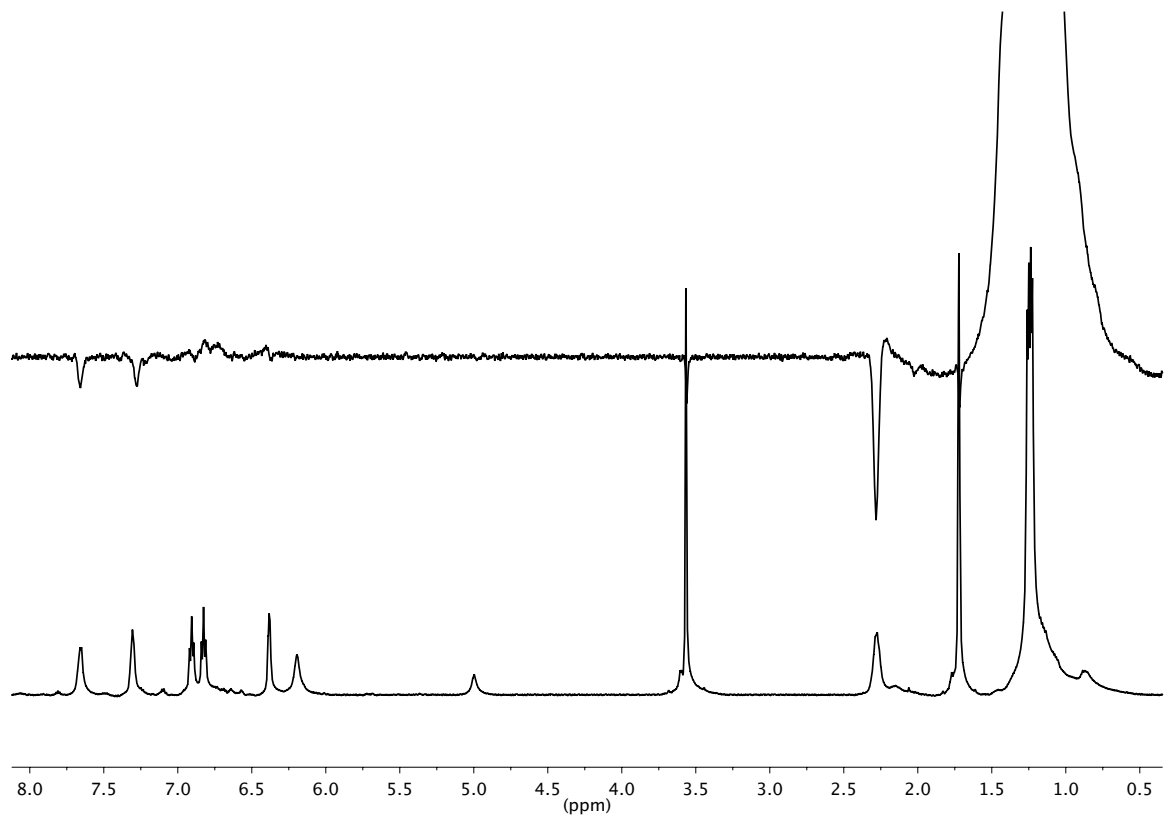
Figure 333. 1D-Phase cycled NOE spectrum at −55 °C (CH$_3$ irradiated at 1.24 ppm) (TOP) and ^{1}H NMR spectrum (bottom) at −55 °C, referenced to THF-d_8 (1.72 ppm).
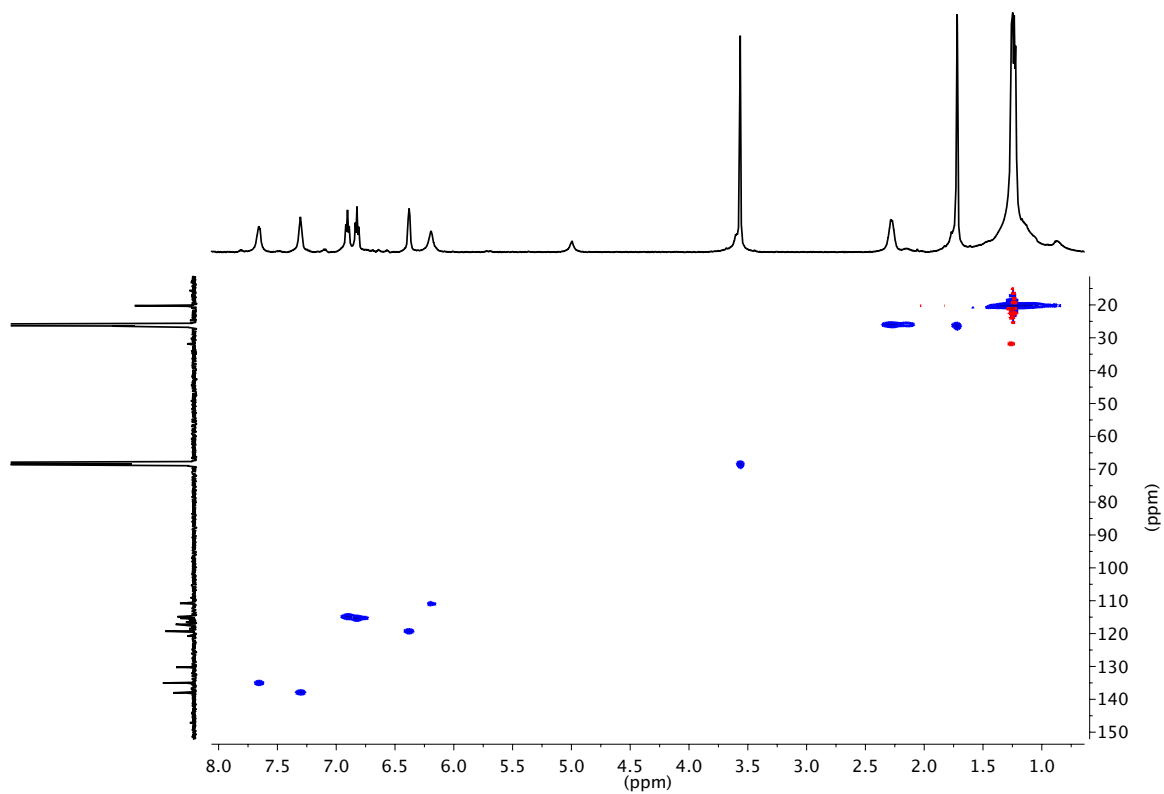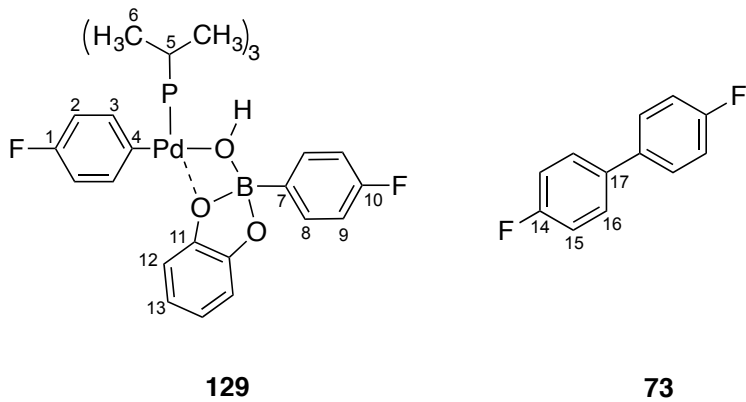
Figure 334. gHSQC spectrum of **129** at −55 °C, referenced to THF-d_8 (1.72 and 68.21 ppm).

465
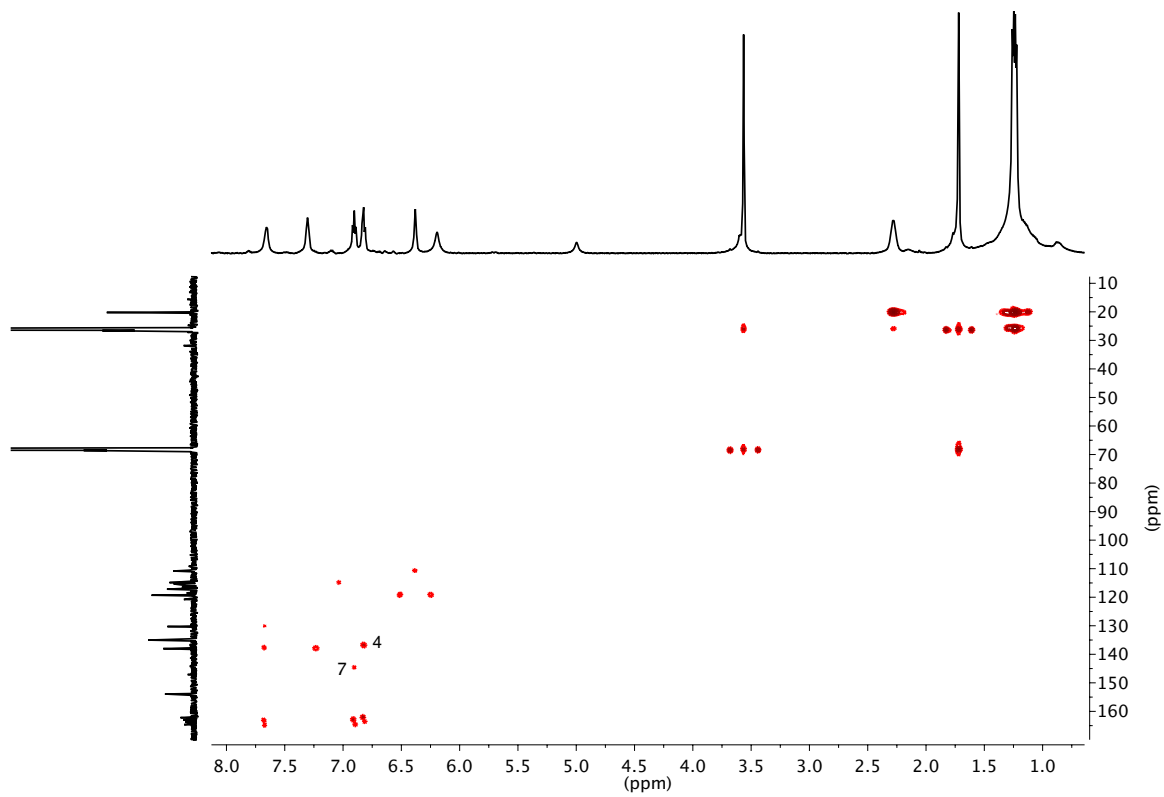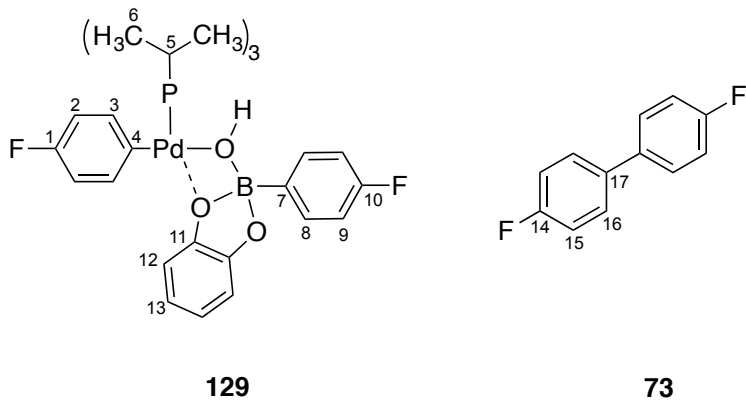
Figure 335. gHMBC spectrum of **129** at −55 °C, referenced to THF-d_8 (1.72 and 68.21 ppm).

466

Experiment 71: Preparation of 8-B-4 complex 132 in THF
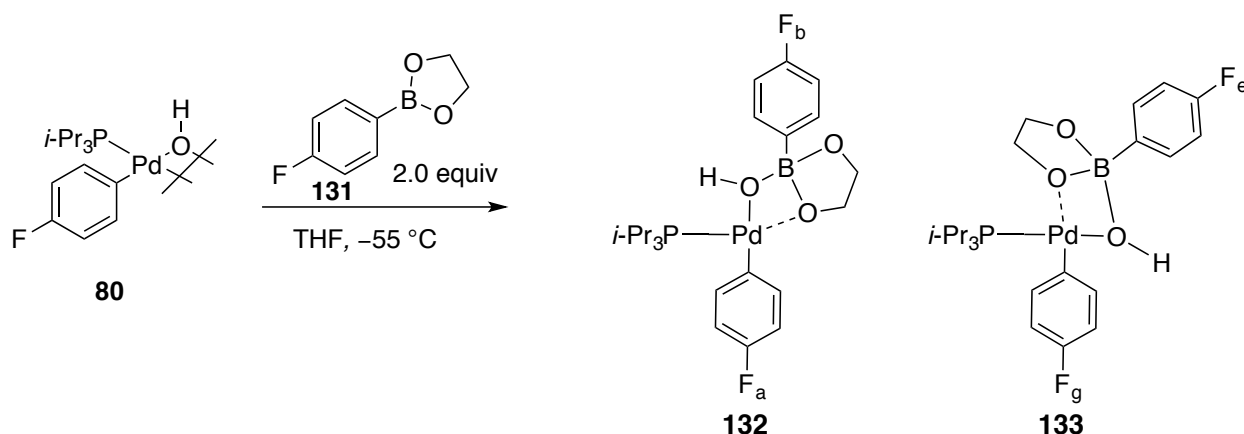
An oven-dried, 5-mm, NMR tube was charged with freshly sublimed 4-fluorophenylboronic acid glycol ester (20 mg, 120 μmol, 1.0 equiv) followed by the addition of 500 μL of THF (NaK) yielding a 4-fluorophenylboronic acid solution (0.72 M).

An oven dried, 5-mm, NMR tube as charged with [(i-Pr₃P)Pd(4-FC₆H₄)(μ-OH)]₂ (7.58 mg, 10 μmol, 1.0 equiv) and 500 THF (NaK) followed by sonication for ~2 min. The tube was placed into a −78 °C dry-ice acetone bath followed by the addition of 4-fluorophenylboronic acid glycol ester solution (95 μL, 20 μmol, 2.0 equiv). The tube was vortexed (not shaken) quickly cleaned with a Kimwipe and placed into the −78 °C bath. The tube was then placed into the probe of the NMR spectrometer pre-cooled to −55 °C. The sample was found to be stable for ~3-4 h at −55 °C. The complex was characterized *via* 1D experiments over a course of multiple experiments.

Data for **132**:

^{19}F NMR: (565 MHz, THF-d_8)

−118.65 (s, FC(10)), −121.64 (s, FC(1)),

^{31}P NMR: (243 MHz, THF-d_8)

56.00 (s, 1 P(Pd))
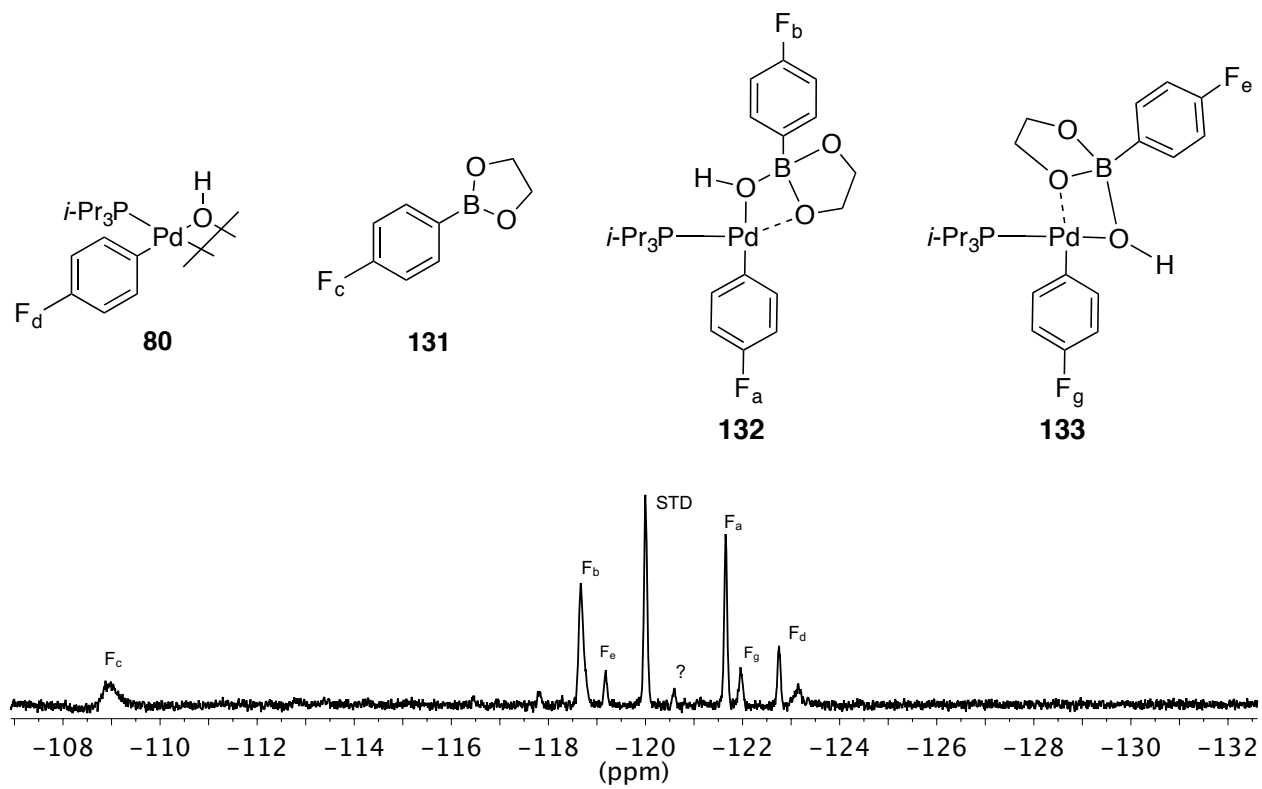
Figure 336. ^{1}H NMR spectrum of **132** at −55 °C, referenced to THF-d_8 (1.72 ppm).

468
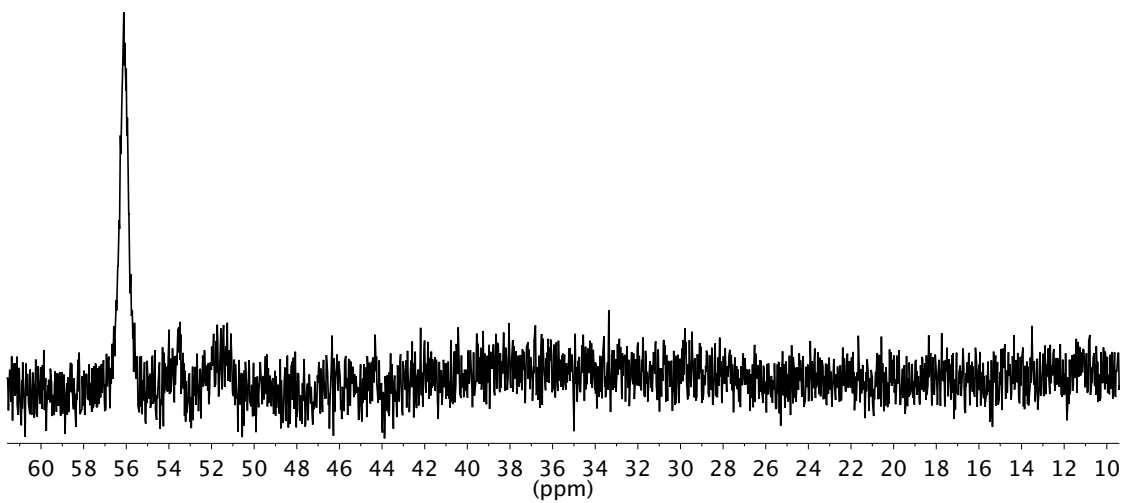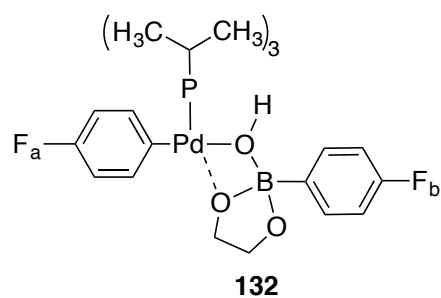
Figure 337. ^{31}P NMR spectrum of **132** at −55 °C, externally referenced to *i*-Pr$_3$P (19.00 ppm).

Experiment 72: Addition of 117 to 80

An oven-dried, 5-mm, NMR tube was charged with 4-fluorophenylboronic neopently acid solution (22 mg, 105 μmol) and 500 μL of THF (NaK) followed by sonication until the solid had dissolved yielding a 0.21 M solution.

An oven dried, 5-mm, NMR tube as charged with [(*i*-Pr$_3$P)Pd(4-FC$_6$H$_4$)(μ-OH)]$_2$ (7.58 mg, 10 μmol, 1.0 equiv) and 500 THF (NaK) followed by sonication for ~2 min. The tube was placed into a −78 °C dry-ice acetone bath followed by the addition of 4-fluorophenylboronic neopently acid solution (95 μL, 20 μmol, 2.0 equiv). The tube was vortexed (not shaken) quickly wiped with a Kimwipe and placed into the probe of the NMR spectrometer pre-cooled to −55 °C. No intermediate was observed *via* ^{19}F NMR. The reaction mixture was found to give cross-coupled product slowly at −55 °C thus it was warmed to −30 °C where cross-coupled product was observed over ~20 min.
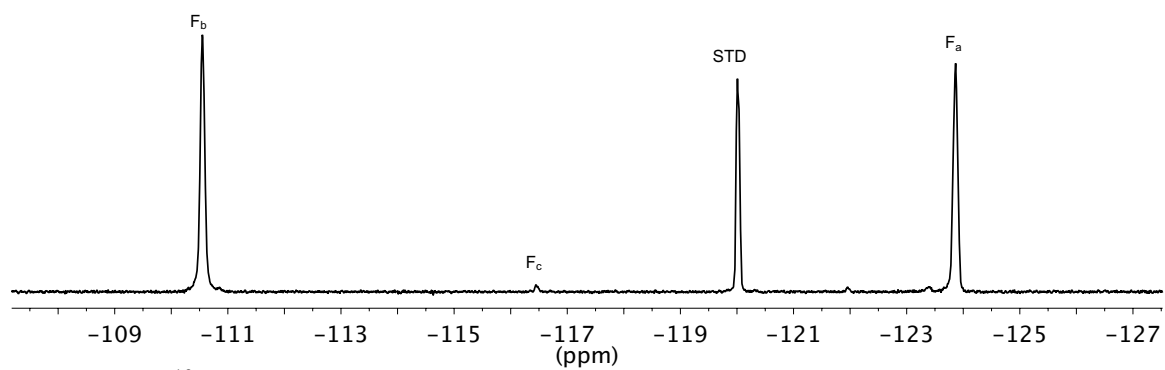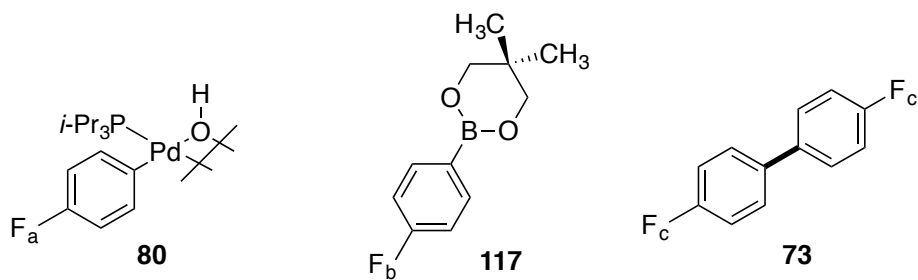
Figure 338. ^{19}F NMR spectrum of **117** and **80** at −55 °C, referenced to 1,4-difluorobenzene (−120 ppm).
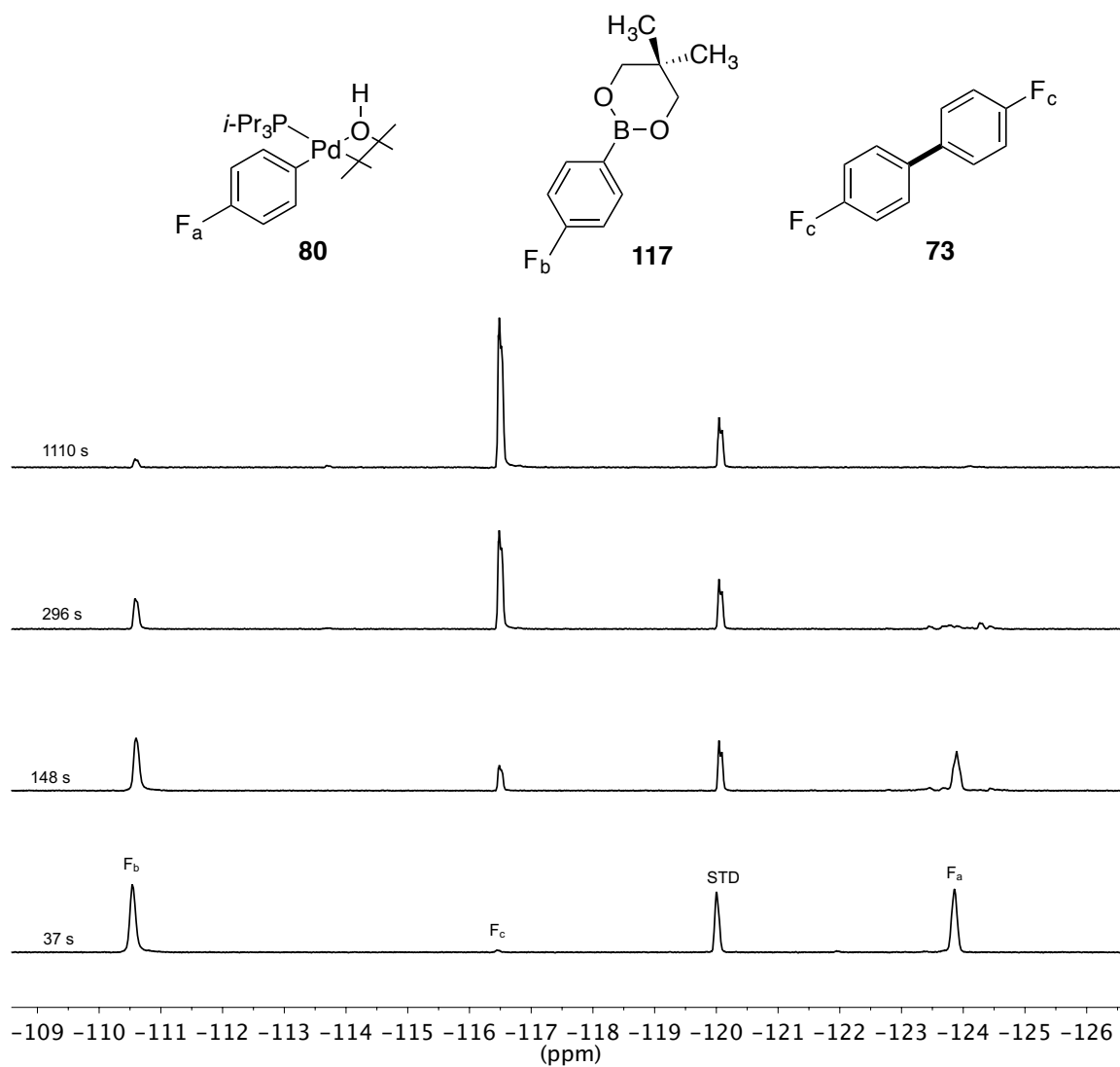
Figure 339. Cross-coupled product **73** formation at −30 °C, referenced to 1,4-difluorobenzene (−120 ppm).

472

Experiment 73: Reaction of complex 80 with 119
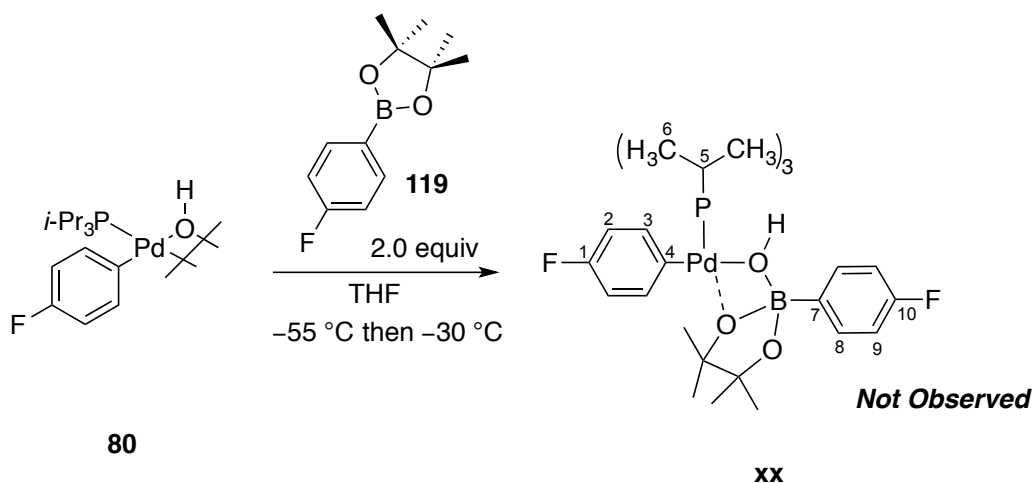
An oven-dried, 5-mm, NMR tube was charged with 4-fluorophenylboronic pinacol acid solution (23 mg, 105 μmol) and 500 μL of THF (NaK) followed by sonication until the solid had dissolved yielding a 0.21 M solution.

An oven dried, 5-mm, NMR tube as charged with $[(i\text{-Pr}_3P)Pd(4\text{-FC}_6H_4)(\mu\text{-OH})]_2$ (7.58 mg, 10 μmol, 1.0 equiv) and 1,4-difluorobenzene (0.5 μL, 4.8 μmol) followed by 500 μL of THF (NaK). The tube was placed into a −78 °C dry-ice acetone bath followed by the addition of 4-fluorophenylboronic pinacol acid solution (95 μL, 20 μmol, 2.0 equiv). The tube was vortexed (not shaken) quickly wiped with a Kimwipe and placed into the probe of the NMR spectrometer pre-cooled to −55 °C. No intermediate was observed *via* ^{19}F NMR. The reaction mixture was found to give cross-coupled product slowly −30 °C where cross-coupled product was observed over ~4.5 hr.
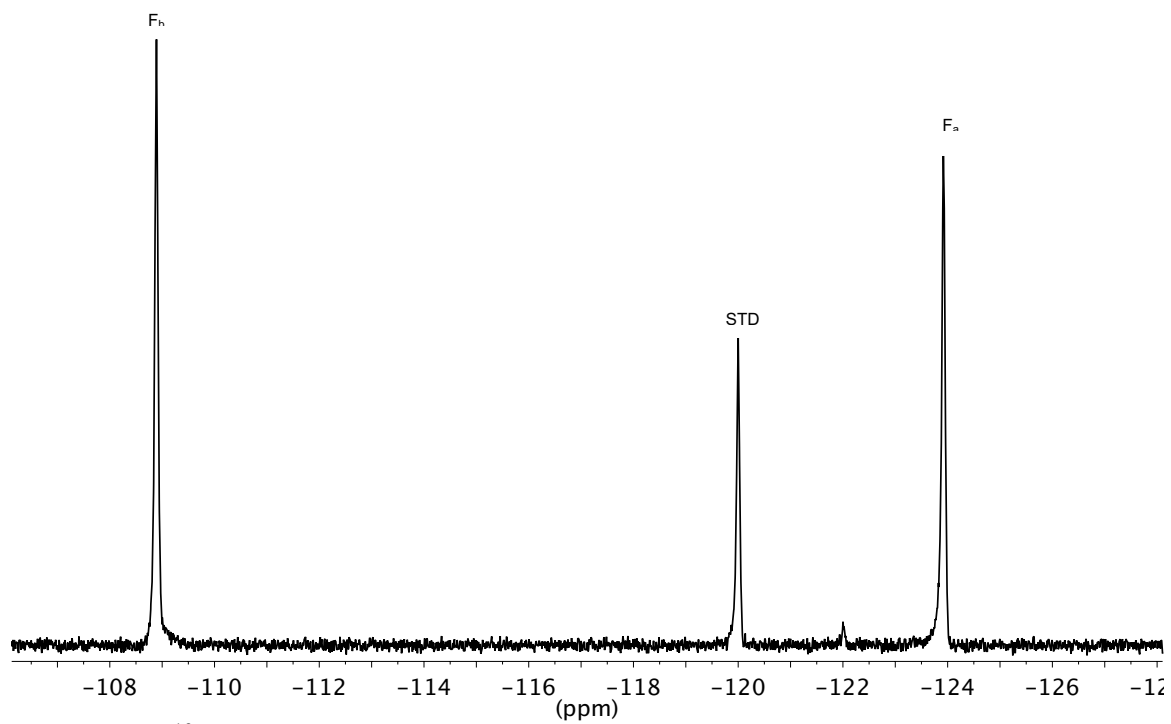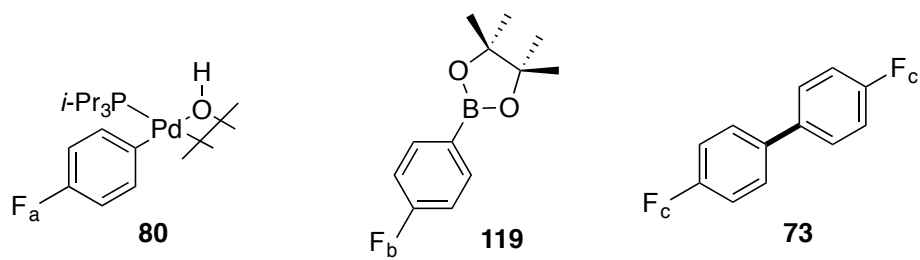
Figure 340. ^{19}F NMR spectrum of **119** and **80** at −55 °C, referenced to 1,4-difluorobenzene (−120 ppm).
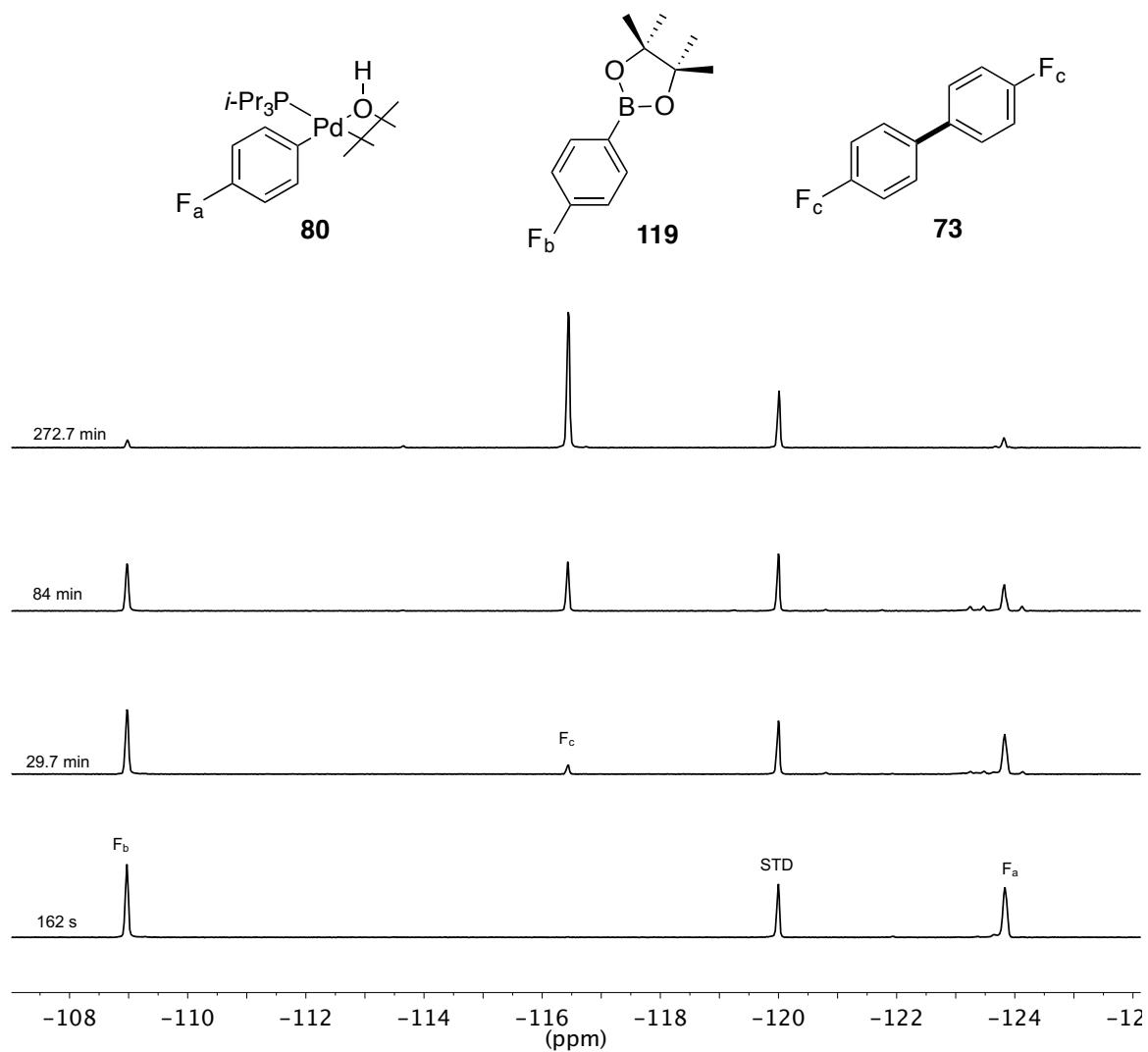
Figure 341. Cross-coupled product **73** formation at −30 °C, referenced to 1,4-difluorobenzene (−120 ppm).

Experiment 74: Preparation of 8-B-4 complex 135

A 1-mL volumetric flask was charged with freshly sublimed 2-hydroxy-2-methylpropanoic acid 4-fluorophenylboronate (44.0 mg, 210 μmol). Then ~0.5 mL of THF (NaK) was added and sonicated until the solid had dissolved. Once dissolved the flask was filled to the mark with THF (NaK) generating a 0.21 M solution of 2-hydroxy-2-methylpropanoic acid 4-fluorophenylboronate.

A 2-mL volumetric flask was taken into the dry box and charged with [(i-Pr$_3$P)Pd(4-FC$_6$H$_4$)(μ-OH)]$_2$ (30.8 mg, 41 μmol) and 1,4-difluorobenzene (2.5 μL, 24 μmol) followed by dissolving with THF (NaK) to the 2-mL mark. An oven dried, 5-mm, NMR tube was taken into the dry box and 500 μL of the freshly prepared solution was added. The tube was capped with a septum and Teflon taped. The sample was removed from the glove box and inserted into a −78 °C acetone dry-ice bath followed by the addition of the 2-hydroxy-2-methylpropanoic acid 4-fluorophenylboronate solution (95 μL, 20.5 μmol, 2.0 equiv) *via* a 100 μL glass syringe. The NMR tube was vortexed (not shaken) and cleaned with a Kimwipe followed by re-insertion into the −78 °C bath. Then the tube was placed into the NMR probe set to −30 °C. Two broad ^{19}F NMR signals were observed after the addition.

Data for **135**:

^{19}F NMR: (565 MHz, THF-d_8)

−117.53 (s, FC(10)), −116.74 (s, FC(1)),

135
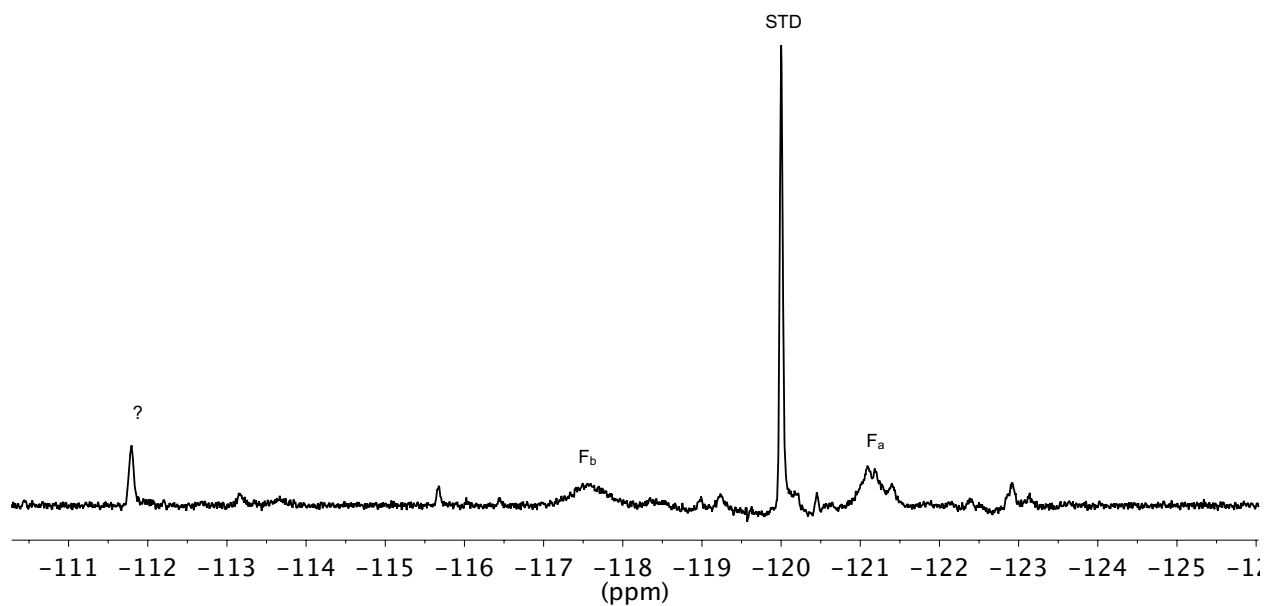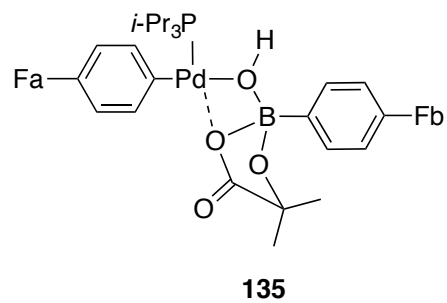
Figure 342. ^{19}F NMR spectrum of **135** at −55 °C, referenced to 1,4-difluorobenzene (−120 ppm).

Experiment 75: Injection of oxalic acid 137
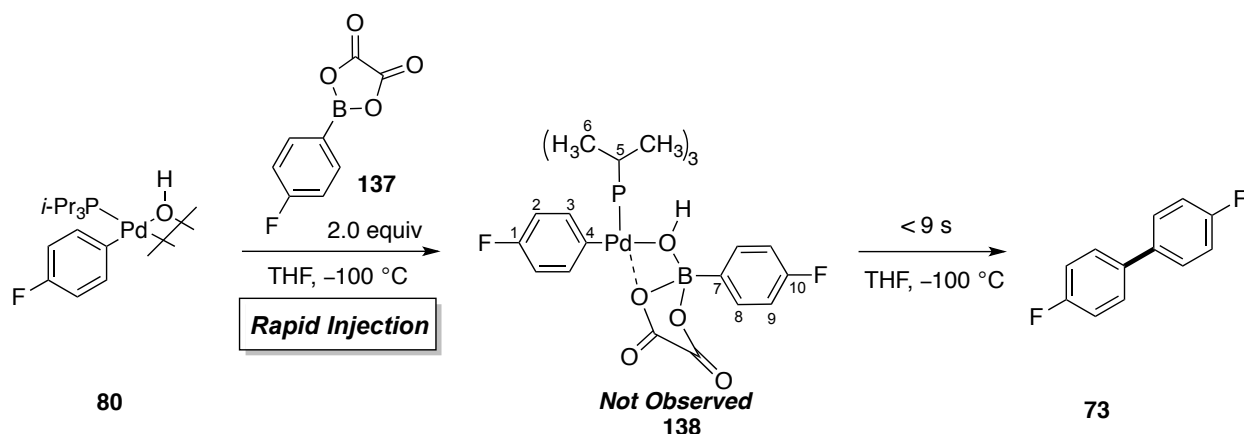
A 50-mL volumetric flask was charged with oxalic acid 4-fluorophenylboronate (0.97 g, 5 mmol). Then ~15 mL of THF (NaK) was added and sonicated until the solid had dissolved. Once dissolved the flask was filled to the mark with THF (NaK) generating a 0.1 M solution of oxalic acid 4-fluorophenylboronate. The rapid injection apparatus was then charged with the solution.

A 2-mL volumetric flask was charged with $[(i\text{-Pr}_3P)Pd(4\text{-FC}_6H_4)(\mu\text{-OH})]_2$ (38.3 mg, 50.5 μmol) and 1,4-difluorobenzene (3 μL, 29 μmol) followed by dissolving with THF (NaK) to the 2-mL mark. An oven dried, 5-mm, NMR tube was taken into the dry box and 395 μL of the freshly prepared solution was added. The tube was capped with a septum and Teflon taped. The sample was removed from the glove box and inserted into a −78 °C acetone dry-ice bath followed by insertion into the NMR probe with the cap off set to −100 °C. Then the injector system was lowered into the magnet and allowed to cool for 15 min. Then 200 μL (2.0 equiv, 20 μmol) of the oxalic acid 4-fluorophenylboronate solution was injected at a rate of 50 μL/s over 5 s. The first ^{19}F NMR spectrum displayed only cross-coupled product **73**.
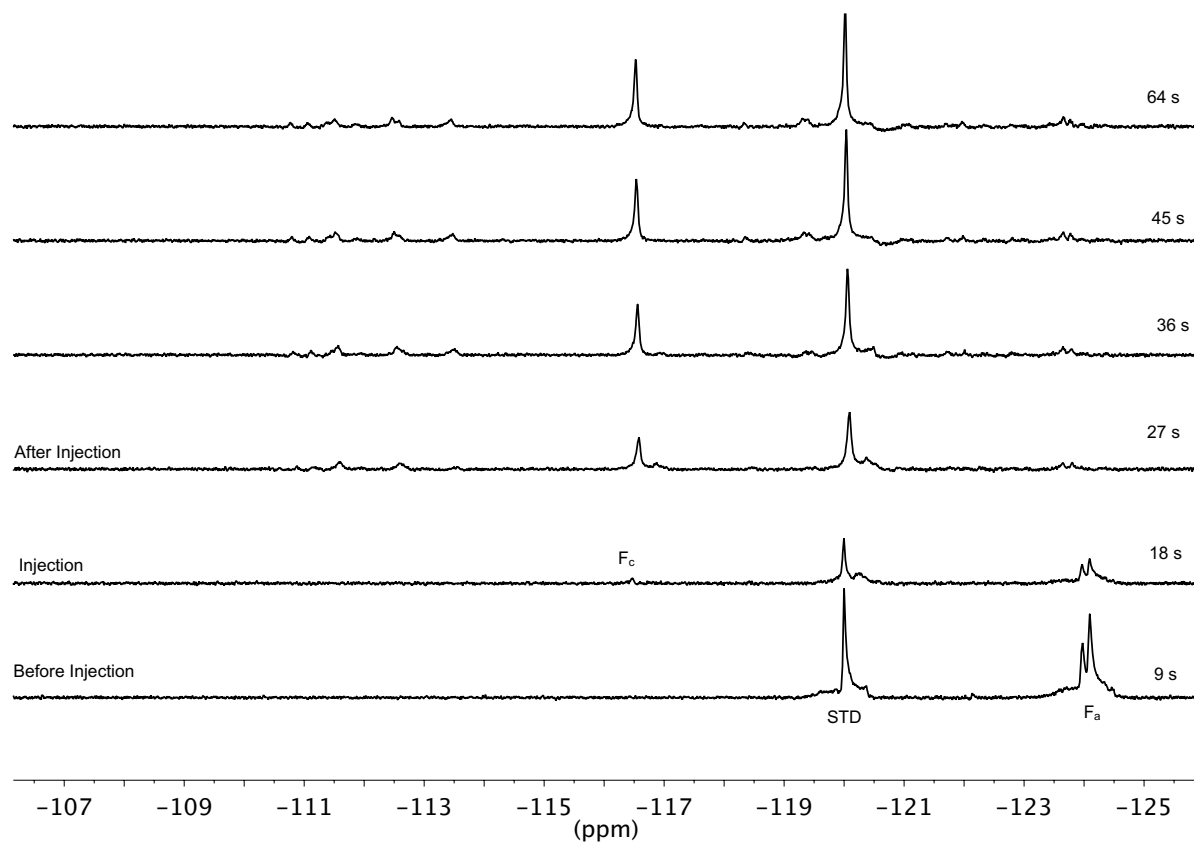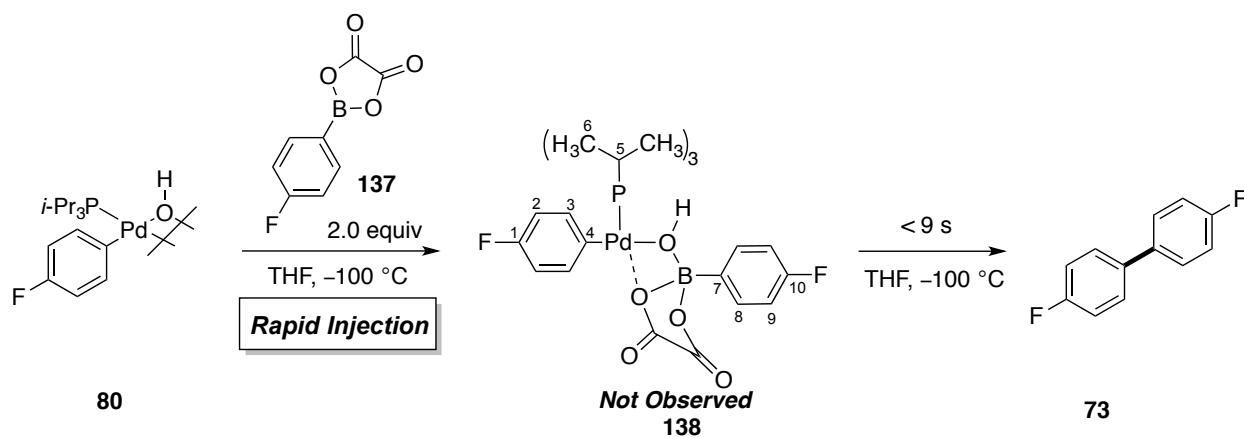
Figure 343. ^{19}F NMR spectra (RI-NMR) of **80** with **137** at −100 °C, referenced to 1,4-difluorobenzene (−120 ppm).

Experiment 76: Cross-coupling formation from complex 129 in THF

80   **129**   **73**

Internal Standard

1,4-Difluorobenzene, 10.22 mM
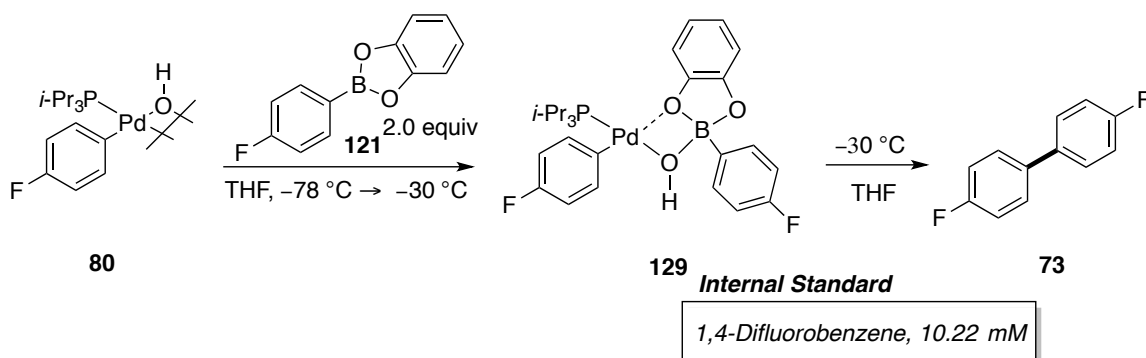
A oven dried 5-mm NMR tube was charged with freshly sublimed 4-fluorophenylboronic acid catechol ester (23 mg, 107 μmol) followed by 500 μL of THF (NaK) generating a 21 mM solution.

A 2-mL volumetric flask was taken into the dry box and charged with [(*i*-Pr$_3$P)Pd(4-FC$_6$H$_4$)(μ-OH)]$_2$ (30.8 mg, 41 μmol) and 1,4-difluorobenzene (2.5 μL, 24 μmol) followed by dissolving with THF (SDS) to the 2-mL mark. An oven dried, 5-mm, NMR tube was taken into the dry box and 500 μL of the freshly prepared solution was added. The tube was capped with a septum and Teflon taped. The sample was removed from the glove box and inserted into a −78 °C acetone dry-ice bath followed by the addition of (95 μL, 20.3 μmol, 2.0 equiv) of 4-fluorophenylboronic acid catechol ester Stock Sol. *via* a 100 μL glass syringe. The NMR tube was vortexed (not shaken), and cleaned with a Kimwipe then placed into the NMR probe set to −30 °C.

Using the fluorine channel to collect a spectrum every 37 s, the progress of the reaction was monitored by the decay of the ester complex (−117.36 ppm) and formation of cross-coupling product (−116.45 ppm) in comparison with the internal reference 1,4-difluorobenzene (−120.00 ppm). The first order decay and formation profiles were fitted with OrginPro 2015 software using equations **1** and **2** respectively. This procedure was performed three times to obtain an average rate.[136] The rate obtained was used to calculate ΔG‡ using the Eyring equation 3.

Equation 9.

$$[A] = [A]_0 e^{-kt}$$

Equation 10.

$$[P] = [A]_0(1 - e^{-kt})$$

Equation 11.

$$k = \frac{K_B T}{h} e^{\frac{-\Delta G^{\ddagger}}{RT}}$$

Table 82. Results from the cross-coupling reaction.

Entry	$k\,(s^{-1})$ (Decay 8-B-4)	$k\,(s^{-1})$ (Form CCP)	A_0 [mM] (Decay 8-B-4)	A_0 [mM] (Form CCP)
Run 1	$(2.98 \pm 0.19) \times 10^{-3}$	$(2.06 \pm 0.74) \times 10^{-3}$	24.44 ± 0.67	22.88 ± 0.26
Run 2	$(3.35 \pm 0.13) \times 10^{-3}$	$(2.34 \pm 0.10) \times 10^{-3}$	30.31 ± 0.86	23.28 ± 0.30
Run 3	$(3.08 \pm 0.14) \times 10^{-3}$	$(3.00 \pm 0.12) \times 10^{-3}$	27.79 ± 0.90	18.91 ± 0.19

k avg. Decay of 8-B-4 = (2.74 ± 0.32) x 10^{-3} s^{-1}
k avg. Formation of CCP = (2.60 ± 0.17) x 10^{-3} s^{-1}
$\Delta G^{\ddagger}$ = (16.99 ± 0.06) kcal/mol at −30 °C
$\Delta G^{\ddagger}$ = Calculated = (17.7) kcal/mol at −30 °C
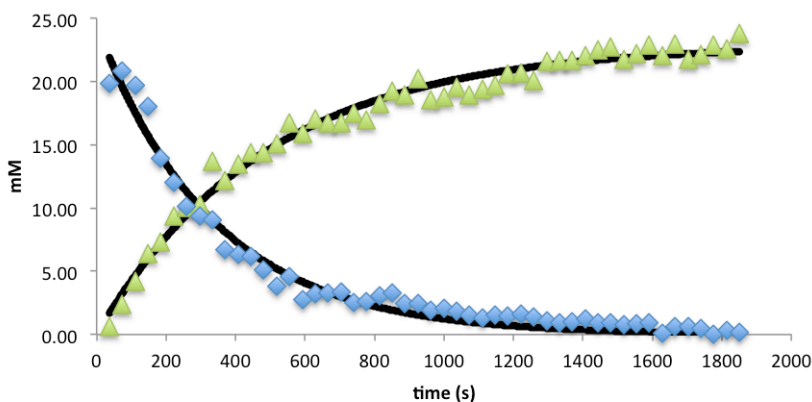
Figure 344. Decay of complex **129** and formation of **73** (Run 1).

Table 83. Data for the decay of complex **129** and formation of **73** (Run 1).

time (s)	Integral IS (−120.00 ppm)	Integral **129** (−117.36 ppm)	Integral **73** (−116.45 ppm)	[mM] **129**	[mM] **73**
37	1929	1871	121	19.82	0.64
74	1613	1644	380	20.83	2.40
111	1558	1499	644	19.67	4.22
148	1448	1274	905	17.98	6.39
185	1502	1025	1078	13.95	7.34
222	1491	878	1371	12.04	9.40
259	1499	742	1474	10.13	10.05

Table 83. (cont.)

296	1563	718	1572	9.39	10.28
333	1305	579	1752	9.08	13.72
370	1546	507	1845	6.70	12.20
407	1494	465	1966	6.36	13.45
444	1424	431	2005	6.19	14.40
481	1479	371	2080	5.12	14.37
518	1481	279	2181	3.85	15.05
555	1395	313	2279	4.59	16.70
592	1496	204	2322	2.79	15.87
629	1403	221	2338	3.22	17.03
666	1504	243	2461	3.30	16.72
703	1480	242	2418	3.34	16.70
740	1438	181	2466	2.57	17.52
777	1537	193	2545	2.57	16.93
814	1443	215	2573	3.04	18.23
851	1420	230	2671	3.31	19.22
888	1467	174	2719	2.42	18.94
925	1375	165	2725	2.45	20.26
962	1467	135	2663	1.88	18.55
999	1475	148	2710	2.05	18.78
1036	1438	129	2747	1.84	19.52
1073	1500	113	2776	1.54	18.91
1110	1486	94	2819	1.29	19.39
1147	1449	111	2792	1.57	19.69
1184	1428	102	2881	1.45	20.63
1221	1446	115	2925	1.62	20.68
1258	1447	100	2840	1.41	20.06
1295	1374	72	2905	1.08	21.61
1332	1396	64	2956	0.94	21.64
1369	1347	69	2859	1.05	21.70
1406	1369	85	2952	1.27	22.04
1443	1337	62	2949	0.95	22.54
1480	1337	60	2978	0.91	22.76
1517	1402	51	2980	0.74	21.73
1554	1390	57	3018	0.83	22.19
1591	1366	63	3059	0.94	22.88
1628	1386	7	2993	0.10	22.06
1665	1381	42	3100	0.63	22.94
1702	1412	43	3000	0.62	21.71
1739	1412	32	3061	0.46	22.16

Table 83. (cont.)

1776	1358	1	3038	0.01	22.86
1813	1383	21	3051	0.31	22.55
1850	1338	10	3113	0.15	23.77
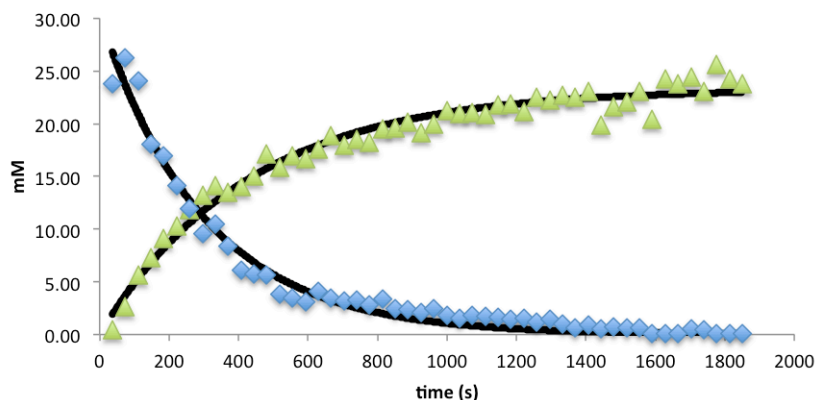
Figure 345. Decay of complex **129** and formation of **73** (Run 2).

Table 84. Data for the decay of complex **129** and formation of **73** (Run 2).

time (s)	Integral IS (−120.00 ppm)	Integral **129** (−117.36 ppm)	Integral **73** (−116.45 ppm)	[mM] **129**	[mM] **73**
37	1818	2120	79	23.83	0.44
74	1327	1703	346	26.22	2.67
111	1254	1478	691	24.10	5.63
148	1270	1122	903	18.05	7.27
185	1322	1097	1178	16.97	9.11
222	1357	939	1366	14.14	10.29
259	1342	782	1549	11.92	11.80
296	1308	615	1694	9.60	13.24
333	1293	663	1787	10.47	14.12
370	1451	596	1920	8.39	13.53
407	1507	452	2073	6.13	14.06
444	1465	414	2159	5.77	15.06
481	1291	359	2162	5.68	17.11
518	1489	276	2308	3.79	15.85
555	1461	245	2421	3.42	16.94
592	1503	228	2446	3.10	16.63
629	1529	306	2633	4.09	17.60
666	1391	233	2562	3.42	18.82
703	1536	238	2692	3.17	17.91
740	1545	245	2793	3.25	18.47

Table 84. (cont.)

777	1554	216	2776	2.84	18.26
814	1420	235	2711	3.38	19.51
851	1517	179	2903	2.42	19.56
888	1480	170	2909	2.35	20.09
925	1522	159	2844	2.14	19.10
962	1489	182	2910	2.50	19.98
999	1532	138	3178	1.84	21.19
1036	1589	120	3255	1.55	20.94
1073	1418	126	2923	1.82	21.06
1110	1504	124	3072	1.69	20.88
1147	1531	126	3266	1.68	21.80
1184	1549	113	3319	1.49	21.90
1221	1479	114	3065	1.57	21.18
1258	1540	88	3393	1.16	22.52
1295	1483	105	3220	1.45	22.20
1332	1577	78	3497	1.02	22.66
1369	1519	50	3341	0.67	22.48
1406	1472	65	3326	0.91	23.09
1443	1484	39	2889	0.54	19.90
1480	1504	51	3181	0.70	21.61
1517	1539	47	3315	0.62	22.02
1554	1392	45	3136	0.66	23.03
1591	1532	8	3060	0.10	20.41
1628	1452	6	3443	0.08	24.24
1665	1523	4	3545	0.05	23.79
1702	1499	42	3577	0.57	24.39
1739	1522	32	3435	0.43	23.06
1776	1303	5	3261	0.08	25.58
1813	1433	5	3400	0.07	24.24
1850	1459	8	3393	0.11	23.77
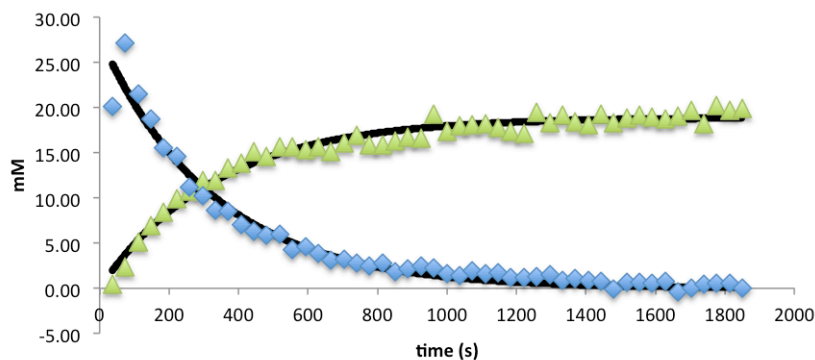
Figure 346. Decay of complex **129** and formation of **73** (Run 3).

Table 85. Data for the decay of complex **129** and formation of **73**. (Run 3).

time (s)	Integral IS (−120.00 ppm)	Integral **129** (−117.36 ppm)	Integral **73** (−116.45 ppm)	[mM] **129**	[mM] **73**
37	1922	1895	76	20.16	0.40
74	1311	1743	303	27.16	2.36
111	1319	1384	667	21.45	5.17
148	1367	1253	926	18.73	6.92
185	1421	1078	1170	15.51	8.41
222	1275	913	1239	14.63	9.93
259	1417	777	1500	11.21	10.82
296	1376	689	1610	10.23	11.95
333	1482	626	1729	8.64	11.92
370	1448	605	1881	8.54	13.28
407	1497	517	2032	7.06	13.87
444	1423	442	2106	6.35	15.12
481	1502	432	2145	5.88	14.60
518	1443	419	2214	5.93	15.68
555	1514	318	2323	4.30	15.68
592	1573	358	2359	4.65	15.33
629	1616	304	2471	3.85	15.63
666	1679	260	2492	3.16	15.17
703	1643	257	2578	3.20	16.04
740	1575	214	2611	2.77	16.94
777	1662	205	2588	2.52	15.92
814	1735	235	2690	2.77	15.85
851	1739	157	2774	1.84	16.30
888	1718	181	2810	2.15	16.72

Table 85. (cont.)

925	1780	213	2903	2.44	16.66
962	1526	173	2870	2.31	19.23
999	1732	135	2940	1.60	17.35
1036	1687	119	2972	1.44	18.01
1073	1678	160	2964	1.95	18.06
1110	1710	132	3048	1.58	18.21
1147	1700	145	2953	1.74	17.75
1184	1819	105	3098	1.18	17.41
1221	1824	109	3065	1.22	17.18
1258	1657	106	3156	1.31	19.47
1295	1723	126	3094	1.50	18.35
1332	1685	76	3153	0.92	19.13
1369	1766	90	3187	1.05	18.45
1406	1780	78	3148	0.90	18.08
1443	1683	66	3166	0.81	19.23
1480	1778	-3	3186	-0.03	18.31
1517	1793	59	3312	0.67	18.88
1554	1662	52	3124	0.64	19.21
1591	1733	49	3212	0.58	18.94
1628	1731	64	3183	0.76	18.79
1665	1744	-37	3248	-0.43	19.04
1702	1709	3	3299	0.04	19.73
1739	1801	37	3211	0.42	18.22
1776	1698	42	3365	0.51	20.25
1813	1775	48	3422	0.55	19.70
1850	1714	2	3345	0.03	19.94

Experiment 77: Cross-coupling formation from complex 132 in THF
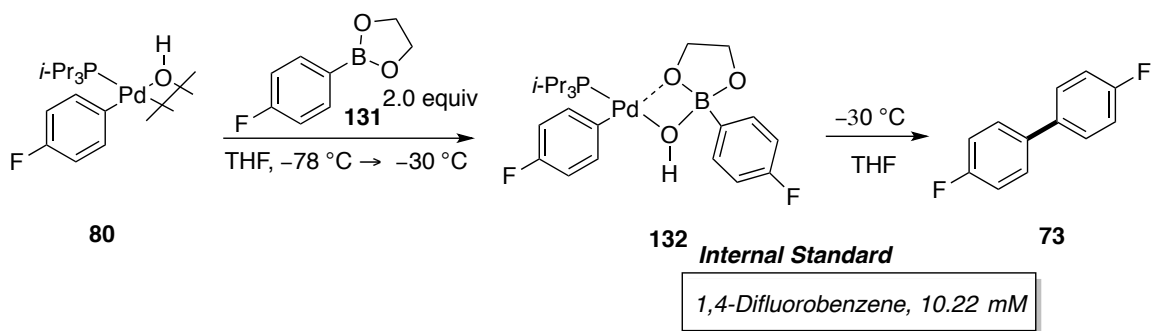
A oven dried 1 mL volumetric flask was charged with freshly sublimed 4-fluorophenylboronic acid glycol ester (34.8 mg, 210 μmol) followed by filling to the mark with THF (NaK) generating a 0.21 M solution.

A 2-mL volumetric flask was taken into the dry box and charged with [(*i*-Pr$_3$P)Pd(4-FC$_6$H$_4$)(μ-OH)]$_2$ (30.8 mg, 41 μmol) and 1,4-difluorobenzene (2.5 μL, 24 μmol) followed by dissolving with THF (NaK) to the 2-mL mark. An oven dried, 5-mm, NMR tube was taken into the dry box and 500 μL of the freshly prepared solution was added. The tube was capped with a septum and Teflon taped. The sample was removed from the glove box and inserted into a −78 °C acetone dry-ice bath followed by the addition of (95 μL, 20.3 μmol, 2.0 equiv) of 4-fluorophenylboronic acid glycol ester Stock Sol. *via* a 100 μL glass syringe. The NMR tube was vortexed (not shaken), and cleaned with a Kimwipe then placed into the NMR probe set to −30 °C.

Using the fluorine channel to collect a spectrum every 9 s, the progress of the reaction was monitored by the formation of cross-coupling product (−116.45 ppm) in comparison with the internal reference 1,4-difluorobenzene (−120.00 ppm). The first order formation profiles were fitted with OrginPro 2015 software using equation **2**. This procedure was performed three times to obtain an average rate.[136]

Table 86. Results from the cross-coupling reaction.

Entry	k (s^{-1}) (Form CCP)	A_0 [mM] (Form CCP)
Run 1	(1.33 ± 0.36) x 10^{-2}	30.11 ± 0.18
Run 2	(1.32 ± 0.39) x 10^{-2}	30.43 ± 0.20
Run 3	(1.34 ± 0.38) x 10^{-2}	30.35 ± 0.19

***k* avg. Formation of CCP = (1.33 ± 0.07) x 10^{-2} s^{-1}**
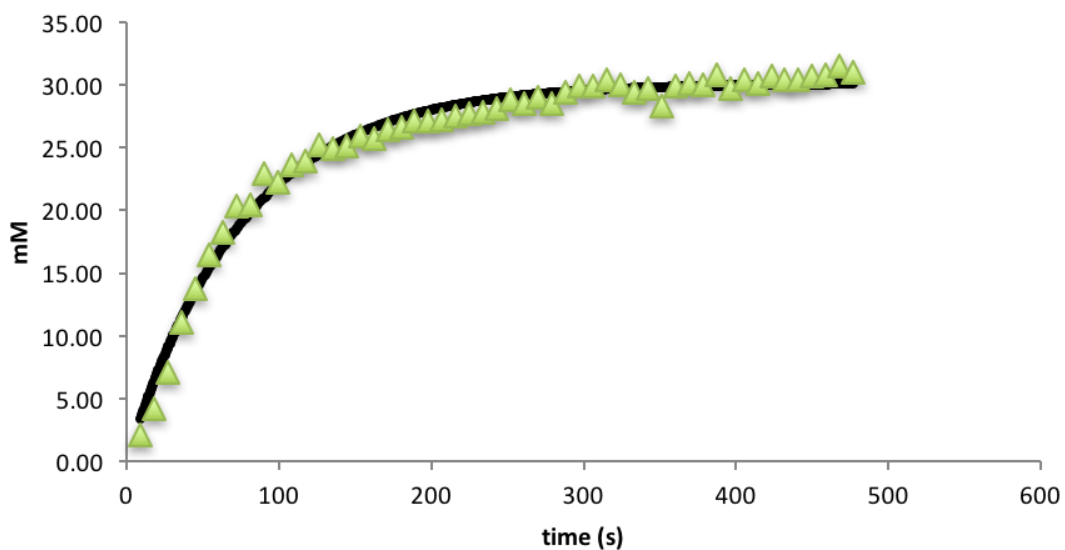
Figure 347. Formation of **73** from **132**. (Run 1).

Table 87. Data for the formation of **73** from **132**. (Run 1).

time (s)	Integral IS (-120.00 ppm)	Integral **73** (-116.45 ppm)	[mM] **73**
9	254.764	51.7227	2.07
18	253.934	105.717	4.25
27	242.048	169.056	7.14
36	237.523	256.964	11.06
45	239.187	322.273	13.77
54	233.392	375.806	16.46
63	234.333	418.953	18.27
72	232.435	462.001	20.31
81	235.098	470.89	20.47
90	227.69	511.5	22.96
99	238.008	516.946	22.20
108	228.403	528.615	23.65

Table 87. (cont.)

117	232.611	543.742	23.89
126	226.054	558.612	25.26
135	234.131	569.999	24.88
144	236.392	580.296	25.09
153	232.516	589.523	25.91
162	235.137	590.637	25.67
171	235.148	606.981	26.38
180	234.187	609.319	26.59
189	231.285	612.839	27.08
198	233.59	620.06	27.13
207	232.709	619.637	27.21
216	227.967	613.949	27.52
225	233.371	631.827	27.67
234	231.194	629.206	27.81
243	234.184	644.014	28.11
252	230.052	648.808	28.82
261	233.181	650.712	28.52
270	230.534	655.002	29.04
279	229.192	639.118	28.50
288	230.505	663.478	29.42
297	229.098	670.623	29.92
306	230.742	674.126	29.86
315	227.534	675.651	30.35
324	229.801	675.306	30.03
333	230.279	661.896	29.38
342	232.72	676.732	29.72
351	242.488	670.988	28.28
360	233.627	684.117	29.93
369	230.73	678.815	30.07
378	236.296	693.288	29.99
387	232.105	699.037	30.78
396	238.934	695.411	29.75
405	229.191	682.122	30.42
414	234.281	690.056	30.10
423	232.875	699.447	30.70
432	234.495	697.668	30.41
441	231.566	688.503	30.39
450	235.037	706.371	30.71
459	231.083	697.322	30.84
468	231.274	713.147	31.51

Table 87. (cont.)

477	235.33	712.844	30.96
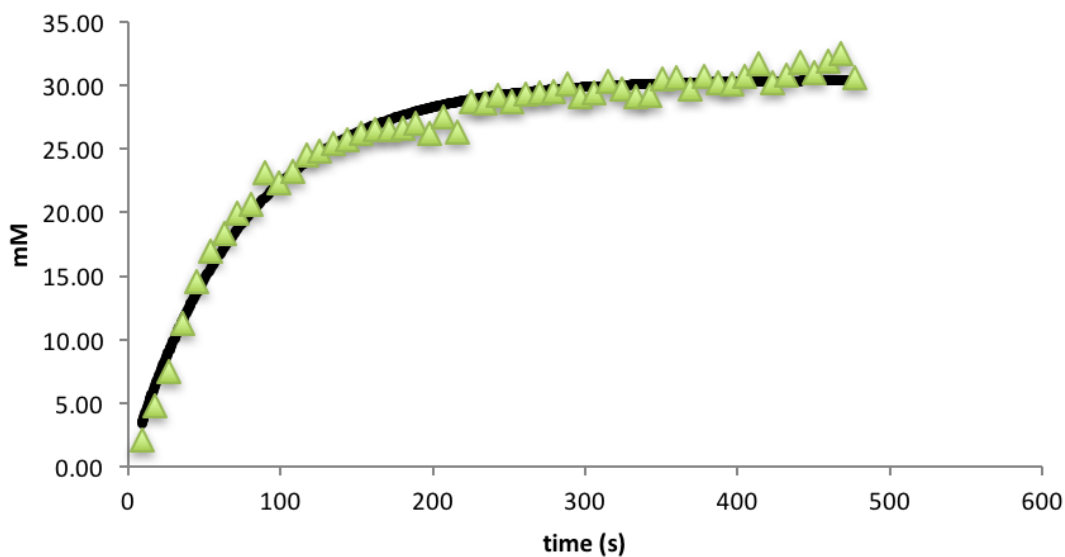
Figure 348. Formation of **73** from **132**. (Run 2).

Table 88. Data for the formation of **73** from **132**. (Run 2).

time (s)	Integral IS (−120.00 ppm)	Integral **73** (−116.45 ppm)	[mM] **73**
9	261.868	53.9886	2.11
18	262.268	124.107	4.84
27	260.043	190.318	7.48
36	243.875	270.19	11.32
45	248.723	353.392	14.52
54	242.33	401.879	16.95
63	243.175	436.499	18.34
72	246.249	479.677	19.91
81	244.336	493.34	20.64
90	236.338	535.952	23.18
99	247.321	540.02	22.32
108	245.146	555.945	23.18
117	242.596	582.907	24.56
126	245.687	596.595	24.82
135	242.225	602.626	25.43
144	245.859	619.099	25.74

Table 88. (cont.)

153	243.452	625.253	26.25
162	246.55	638.474	26.47
171	244.088	633.735	26.53
180	240.185	625.758	26.63
189	246.122	650.323	27.00
198	249.372	638.632	26.17
207	245.259	660.012	27.50
216	254.339	655.144	26.33
225	243.409	683.409	28.69
234	241.163	675.558	28.63
243	243.272	695.035	29.20
252	243.082	683.054	28.72
261	239.265	686.527	29.32
270	242.113	696.669	29.41
279	237.811	686.316	29.49
288	234.649	690.851	30.09
297	247.493	704.377	29.09
306	247.208	711.701	29.42
315	241.088	714.101	30.27
324	245.525	714.107	29.72
333	244.302	695.637	29.10
342	250.626	717.251	29.25
351	243.698	726.074	30.45
360	240.996	722.319	30.63
369	246.903	717.01	29.68
378	242.446	729.313	30.74
387	243.764	720.28	30.20
396	251.294	740.136	30.10
405	242.181	726.809	30.67
414	240.546	746.57	31.72
423	243.708	720.8	30.23
432	247.424	745.58	30.80
441	241.545	751.145	31.78
450	245.797	746.419	31.04
459	238.78	744.595	31.87
468	236.293	750.547	32.46
477	247.624	740.784	30.57
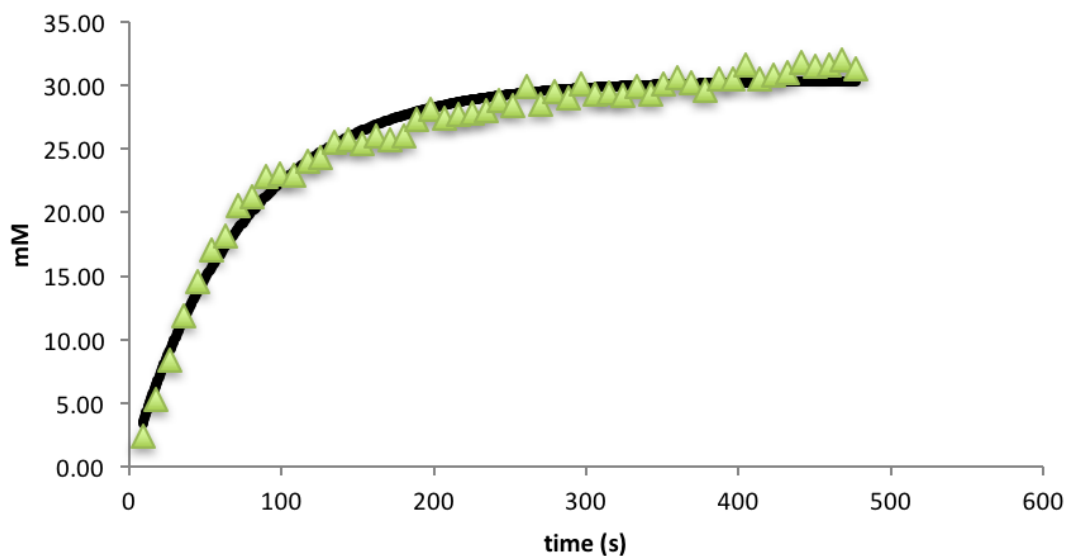
Figure 349. Formation of **73** from **132**. (Run 3).

Table 89. Data for the formation of **73** from **132**. (Run 3).

time (s)	Integral IS (−120.00 ppm)	Integral **73** (−116.45 ppm)	[mM] **73**
9	249.188	59.0079	2.42
18	241.209	125.223	5.31
27	243.152	200.677	8.43
36	238.157	277.485	11.91
45	237.943	338.726	14.55
54	234.895	392.689	17.09
63	239.766	425.069	18.12
72	236.897	477.002	20.58
81	235.396	488.568	21.21
90	233.489	521.558	22.83
99	238.723	538.537	23.06
108	236.351	529.852	22.91
117	231.33	544.719	24.07
126	233.032	554.233	24.31
135	233.472	582.389	25.49
144	235.166	590.639	25.67
153	233.471	579.779	25.38
162	231.962	589.994	25.99
171	242.52	611.337	25.76
180	235.726	600.135	26.02

Table 89. (cont.)

189	231.254	617.317	27.28
198	226.977	623.414	28.07
207	230.234	618.42	27.45
216	232.818	630.779	27.69
225	235.152	639.05	27.77
234	233.124	637.877	27.96
243	232.54	654.291	28.76
252	231.494	642.834	28.38
261	226.529	663.506	29.93
270	237.744	663.955	28.54
279	231.08	667.063	29.50
288	230.365	652.795	28.96
297	229.645	677.351	30.14
306	234.402	672.075	29.30
315	235.703	677.096	29.36
324	236.671	676.298	29.20
333	230.738	675.573	29.92
342	236.998	678.357	29.25
351	233.149	687.08	30.12
360	231.769	694.848	30.64
369	234.251	692.478	30.21
378	237.688	689.465	29.65
387	233.293	695.658	30.48
396	233.764	697.893	30.51
405	229.484	708.601	31.56
414	234.681	700.168	30.49
423	232.796	701.577	30.80
432	232.625	705.728	31.01
441	230.488	715.812	31.74
450	231.489	714.224	31.53
459	232.758	719.151	31.58
468	230.39	721.39	32.00
477	235.21	720.426	31.30

Experiment 78: Cross-coupling formation from complex 105 in THF
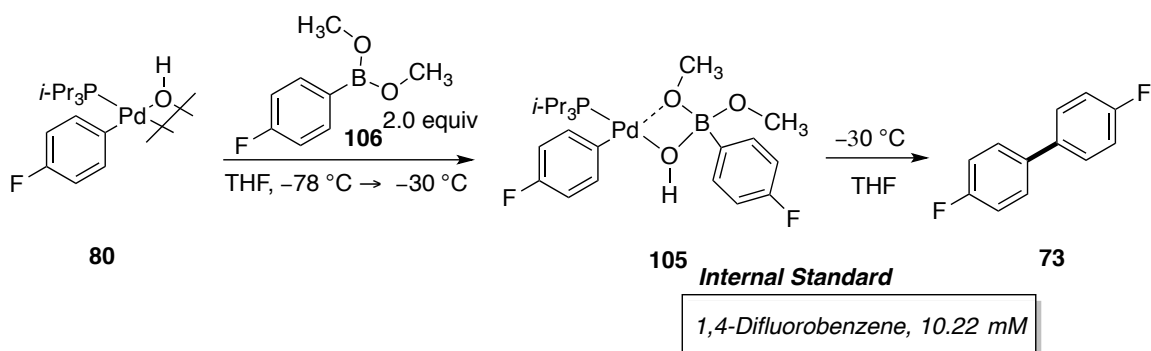
A oven dried 1 mL volumetric flask was charged with freshly distilled 4-fluorophenylboronic acid methyl ester (35 mg, 210 μmol) followed by filling to the mark with THF (NaK) generating a 0.21 M solution.

A 2-mL volumetric flask was taken into the dry box and charged with [(i-Pr$_3$P)Pd(4-FC$_6$H$_4$)(μ-OH)]$_2$ (30.8 mg, 41 μmol) and 1,4-difluorobenzene (2.5 μL, 24 μmol) followed by dissolving with THF (NaK) to the 2-mL mark. An oven dried, 5-mm, NMR tube was taken into the dry box and 500 μL of the freshly prepared solution was added. The tube was capped with a septum and Teflon taped. The sample was removed from the glove box and inserted into a −78 °C acetone dry-ice bath followed by the addition of (95 μL, 20.3 μmol, 2.0 equiv) of 4-fluorophenylboronic acid glycol ester Stock Sol. *via* a 100 μL glass syringe. The NMR tube was vortexed (not shaken), and cleaned with a Kimwipe then placed into the NMR probe set to −30 °C.

Using the fluorine channel to collect a spectrum every 9 s, the progress of the reaction was monitored by the formation of cross-coupling product (−116.45 ppm) in comparison with the internal reference 1,4-difluorobenzene (−120.00 ppm). The first order formation profiles were fitted with OrginPro 2015 software using equation **1**. This procedure was performed three times to obtain an average rate.[136]

Table 90. Results from the cross-coupling reaction.

Entry	k (s^{-1}) (Form CCP)	A_0 [mM] (Form CCP)
Run 1	$(1.53 \pm 0.64) \times 10^{-2}$	38.47 ± 0.34
Run 2	$(0.99 \pm 0.33) \times 10^{-2}$	26.45 ± 0.24
Run 3	$(1.20 \pm 0.28) \times 10^{-2}$	25.96 ± 0.15

***k* avg. Formation of CCP = (1.24 ± 0.02) x 10^{-2} s^{-1}**
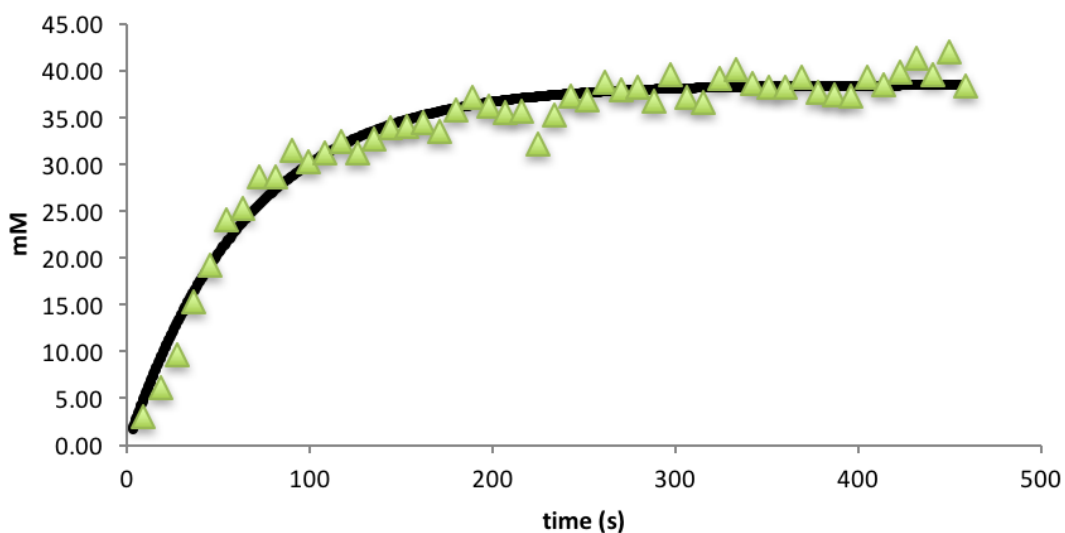
Figure 350. Formation of **73** from **105**. (Run 1).

Table 91. Data for the formation of **73** from **105**. (Run 1).

time (s)	Integral IS (-120.00 ppm)	Integral **73** (-116.45 ppm)	[mM] **73**
9	174.335	51.7227	3.03
18	174.486	105.717	6.19
27	179.253	169.056	9.64
36	171.265	256.964	15.33
45	171.134	322.273	19.25
54	159.418	375.806	24.09
63	169.331	418.953	25.29
72	164.502	462.001	28.70
81	168.014	470.89	28.64
90	165.897	511.5	31.51
99	174.625	516.946	30.25
108	172.84	528.615	31.26

Table 91. (cont.)

117	171.342	543.742	32.43
126	183.366	558.612	31.13
135	177.998	569.999	32.73
144	174.743	580.296	33.94
153	177.122	589.523	34.02
162	175.495	590.637	34.40
171	184.924	606.981	33.55
180	174.349	609.319	35.72
189	168.978	612.839	37.07
198	174.982	620.06	36.22
207	178.34	619.637	35.51
216	176.176	613.949	35.62
225	200.702	631.827	32.17
234	182.541	629.206	35.23
243	176.634	644.014	37.26
252	179.604	648.808	36.92
261	171.379	650.712	38.80
270	176.391	655.002	37.95
279	170.987	639.118	38.20
288	184.331	663.478	36.79
297	173.333	670.623	39.54
306	185.493	674.126	37.14
315	188.88	675.651	36.56
324	176.138	675.306	39.18
333	168.491	661.896	40.15
342	178.823	676.732	38.68
351	179.612	670.988	38.18
360	183.001	684.117	38.21
369	176.795	678.815	39.24
378	187.816	693.288	37.73
387	191.376	699.037	37.33
396	190.561	695.411	37.30
405	177.251	682.122	39.33
414	183.018	690.056	38.53
423	179.591	699.447	39.80
432	172.457	697.668	41.34
441	177.685	688.503	39.60
450	172.05	706.371	41.96
459	185.761	697.322	38.36
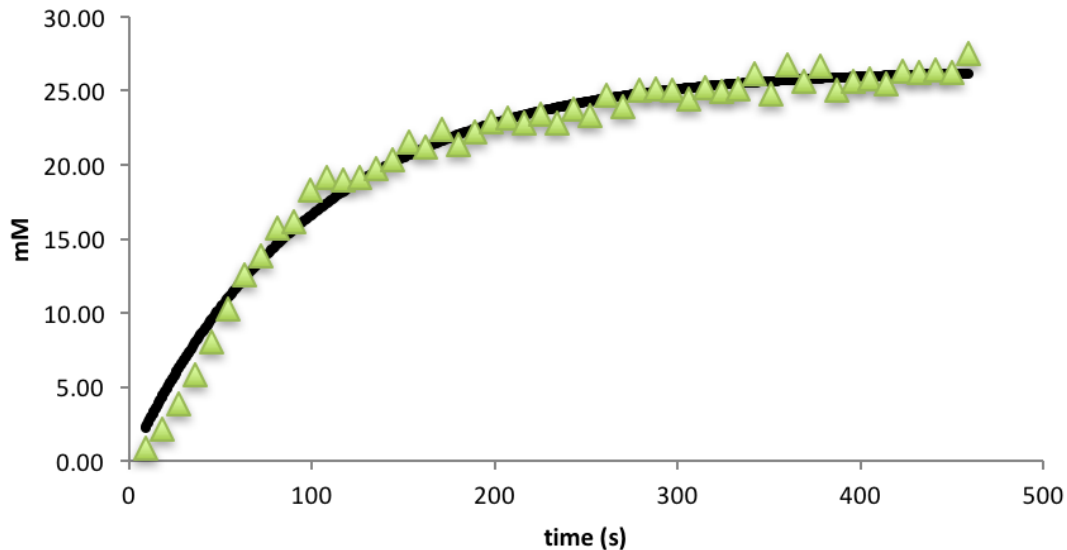
Figure 351. Formation of **73** from **105**. (Run 2).

Table 92. Data for the formation of **73** from **105**. (Run 2).

time (s)	Integral IS (−120.00 ppm)	Integral **73** (−116.45 ppm)	[mM] **73**
9	286.699	23.7818	0.85
18	268.384	56.2848	2.14
27	256.513	96.5488	3.85
36	252.627	144.27	5.84
45	242.445	190.577	8.03
54	236.901	238.605	10.29
63	229.555	281.477	12.53
72	236.473	320.34	13.84
81	226.774	349.884	15.77
90	239.885	379.419	16.16
99	222.87	398.929	18.29
108	223.349	418.961	19.17
117	232.38	432.131	19.00
126	243.28	454.844	19.11
135	243.879	470.601	19.72
144	237.742	473.674	20.36
153	233.078	490.947	21.53
162	244.254	505.784	21.16
171	235.238	514.473	22.35

Table 92 (cont.)

180	246.936	516.785	21.39
189	244.266	530.645	22.20
198	237.056	530.64	22.88
207	243.463	552.218	23.18
216	245.653	548.114	22.80
225	241.901	554.108	23.41
234	248.438	554.019	22.79
243	245.185	569.938	23.76
252	244.014	556.943	23.33
261	238.265	576.35	24.72
270	244.301	571.716	23.92
279	237.646	582.347	25.04
288	242.073	594.51	25.10
297	241.57	591.118	25.01
306	249.979	598.085	24.45
315	243.872	601.185	25.19
324	246.099	601.584	24.98
333	248.435	609.716	25.08
342	239.981	613.892	26.14
351	250.93	608.418	24.78
360	233.038	609.384	26.72
369	245.144	615.556	25.66
378	240.198	627.347	26.69
387	250.854	615.173	25.06
396	242.62	608.455	25.63
405	247.664	625.794	25.82
414	250.487	623.265	25.43
423	244.58	628.916	26.28
432	246.682	632.833	26.22
441	247.708	640.468	26.42
450	249.835	641.178	26.23
459	238.466	642.515	27.54
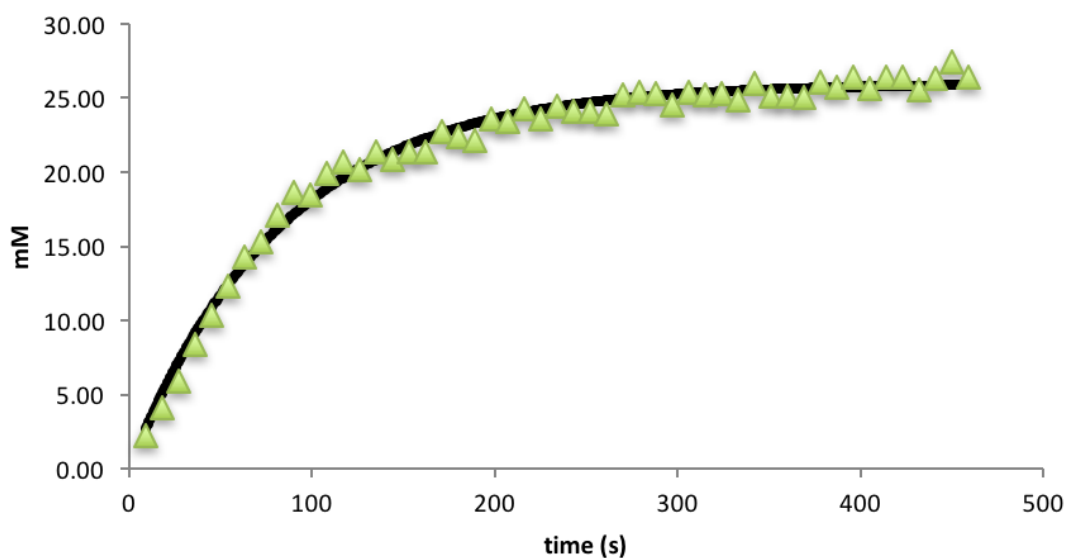
Figure 352. Formation of **73** from **105**. (Run 3).

Table 93. Data for the formation of **73** from **105**. (Run 3).

time (s)	Integral IS (−120.00 ppm)	Integral **73** (−116.45 ppm)	[mM] **73**
9	252.385	56.3024	2.28
18	245.733	99.0967	4.12
27	251.998	146.509	5.94
36	230.427	189.39	8.40
45	240.173	242.45	10.32
54	235.646	283.125	12.28
63	231.642	323.488	14.27
72	235.341	352.776	15.32
81	228.64	382.355	17.09
90	220.619	402.331	18.64
99	233.768	422.28	18.46
108	228.898	446.199	19.92
117	225.432	456.824	20.71
126	236.636	466.487	20.15
135	232.084	484.811	21.35
144	238.281	485.816	20.84
153	240.04	502.031	21.37
162	244.078	510.867	21.39
171	237.383	527.723	22.72
180	243.916	533.699	22.36

Table 93 (cont.)

189	249.322	540.241	22.15
198	236.922	546.83	23.59
207	237.426	544.542	23.44
216	237.074	563.122	24.28
225	243.354	562.238	23.61
234	235.951	564.756	24.46
243	243.232	573.216	24.09
252	244.031	574.948	24.08
261	246.22	575.941	23.91
270	239.552	591.453	25.23
279	237.242	588.048	25.33
288	237.975	589.196	25.30
297	246.152	590.47	24.52
306	238.582	592.531	25.38
315	240.769	594.482	25.23
324	241.415	596.474	25.25
333	250.535	610.148	24.89
342	240.635	611.858	25.99
351	248.039	610.358	25.15
360	247.69	608.081	25.09
369	249.286	610.176	25.02
378	242.667	618.706	26.06
387	246.132	618.278	25.67
396	246.574	637.26	26.41
405	249.662	626.978	25.67
414	245.713	634.661	26.40
423	244.116	630.68	26.40
432	253.404	632.711	25.52
441	244.789	630.596	26.33
450	235.549	632.564	27.45
459	245.831	633.967	26.36

Experiment 79: Cross-coupling formation from 72 and 80 at −30 °C.
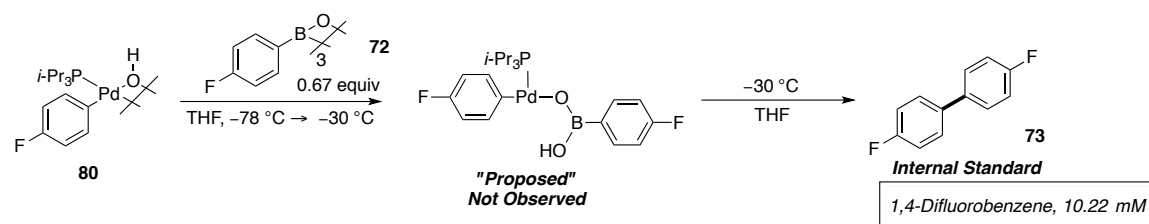
A 5-mL volumetric flask was charged with 4-flurophenylboroxine (128 mg, 350 µmol) followed by 2-3 mL of THF (NaK). Then sonication was performed (~10 min) until the solid had dissolved. Once dissolved the flask was filled to the mark with THF (NaK) generating a 20.5 mM solution.

A 2-mL volumetric flask was taken into the dry box and charged with [(i-Pr$_3$P)Pd(4-FC$_6$H$_4$)(µ-OH)]$_2$ (30.8 mg, 41 µmol) and 1,4-difluorobenzene (2.5 µL, 24 µmol) followed by dissolving with THF (SDS) to the 2-mL mark. An oven dried, 5-mm, NMR tube was taken into the dry box and 500 µL of the freshly prepared solution was added. The tube was capped with a septum and Teflon taped. The sample was removed from the glove box and inserted into a −78 °C acetone dry-ice bath followed by the addition of (95 µL, 20.5 µmol, 0.67 equiv) of 4-fluorophenylboroxine Stock Solution *via* a µL glass syringe. The NMR tube was vortexed (not shaken) and cleaned with a Kimwipe then placed into the NMR probe set to −30 °C.

Using the fluorine channel to collect a spectrum every 37 s the progress of the reaction was monitored by the formation of cross-coupling product fluorine signal (−116.45 ppm) in comparison with the internal reference 1,4-difluorbenzene (−120.00 ppm). The first order formation profile was fitted with OrginPro 2015 software using equation 12. This procedure was performed three times to obtain an average rate.

Equation 12.

$$[P] = [A]_0(1 - e^{-kt})$$

Table 94. Results from cross-coupling reaction.

Entry	$k \, (\mathrm{s}^{-1})$ (Form CCP)	$A_0 \, [\mathrm{mM}]$ (Form CCP)
Run 1	$(5.99 \pm 0.03) \times 10^{-3}$	19.01 ± 0.19
Run 2	$(4.57 \pm 0.02) \times 10^{-3}$	23.58 ± 0.20
Run 3	$(5.60 \pm 0.09) \times 10^{-3}$	23.69 ± 0.15

k avg. Formation of CCP = $(5.39 \pm 0.07) \times 10^{-3} \, \mathrm{s}^{-1}$
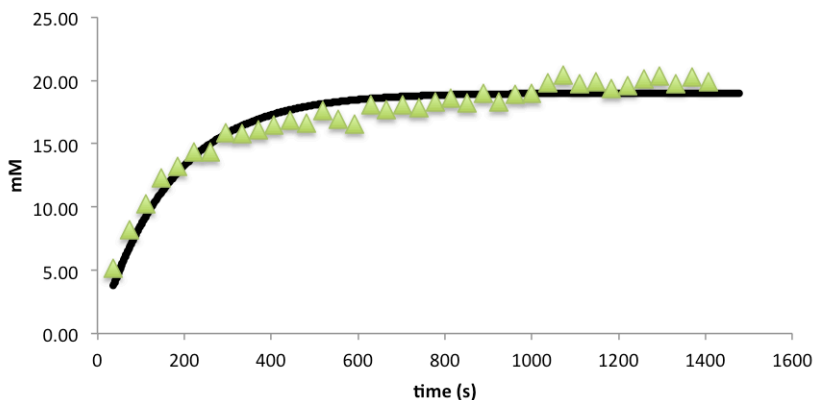
Figure 353. Formation of cross-coupled product from **73** (Run 1).

Table 95. Data for formation of cross-coupled product from **73** (Run 1).

time (s)	Integral IS (−120.00 ppm)	Integral **73** (−116.45 ppm)	[mM] **73**
37	2324	1176	5.17
74	1922	1545	8.22
111	1993	1993	10.22
148	1935	2330	12.30
185	2022	2621	13.25
222	2019	2839	14.37
259	2012	2826	14.35
296	1964	3053	15.88
333	2017	3120	15.81
370	2008	3170	16.13
407	1997	3227	16.51
444	1979	3264	16.85
481	2034	3310	16.63
518	1973	3409	17.65
555	2047	3391	16.93

Table 95. (cont.)

592	2063	3345	16.57
629	1987	3506	18.04
666	2018	3498	17.72
703	2012	3558	18.07
740	2022	3536	17.87
777	2021	3622	18.32
814	2018	3674	18.60
851	2025	3612	18.23
888	1988	3695	19.00
925	2086	3735	18.30
962	2053	3802	18.93
999	2025	3759	18.98
1036	2007	3893	19.82
1073	2009	4021	20.45
1110	2027	3911	19.72
1147	2059	4002	19.87
1184	2089	3951	19.33
1221	2074	3979	19.60
1258	2042	4023	20.13
1295	2015	4005	20.31
1332	2089	4034	19.73
1369	2054	4068	20.24
1406	2061	4005	19.86
1443	2102	4034	19.61
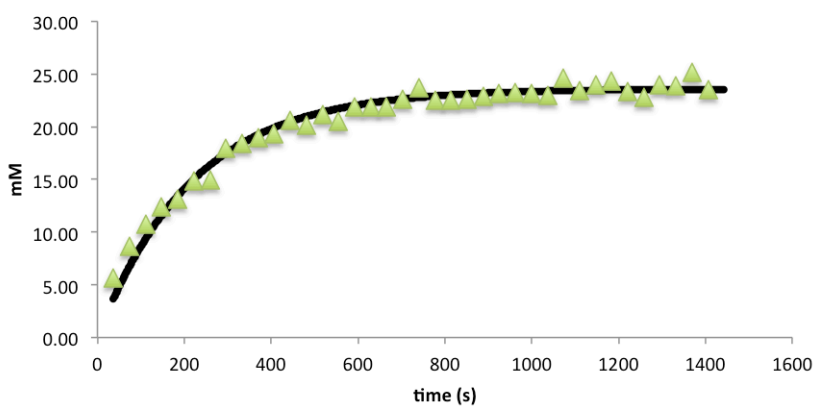
Figure 354. Formation of cross-coupled product from **73** (Run 2).

Table 96. Data for formation of cross-coupled product from **73** (Run 2).

time (s)	Integral IS (−120.00 ppm)	Integral **73** (−116.45 ppm)	[mM] **73**
37	1834	1013	5.64
74	1615	1363	8.62
111	1611	1694	10.75
148	1586	1924	12.40
185	1655	2121	13.10
222	1593	2311	14.82
259	1633	2384	14.92
296	1473	2589	17.96
333	1570	2822	18.37
370	1571	2917	18.98
407	1586	3000	19.34
444	1560	3140	20.58
481	1563	3083	20.16
518	1556	3223	21.17
555	1595	3195	20.47
592	1549	3317	21.88
629	1584	3385	21.84
666	1568	3353	21.85
703	1533	3391	22.61
740	1479	3434	23.73
777	1559	3435	22.53
814	1546	3410	22.54
851	1575	3481	22.59
888	1578	3529	22.86
925	1570	3556	23.15
962	1547	3516	23.23
999	1557	3531	23.17
1036	1572	3525	22.92
1073	1490	3591	24.64
1110	1565	3582	23.39
1147	1537	3608	23.98
1184	1578	3755	24.32
1221	1585	3620	23.35
1258	1585	3535	22.80
1295	1519	3566	24.00
1332	1557	3632	23.84
1369	1477	3629	25.11
1406	1589	3650	23.48
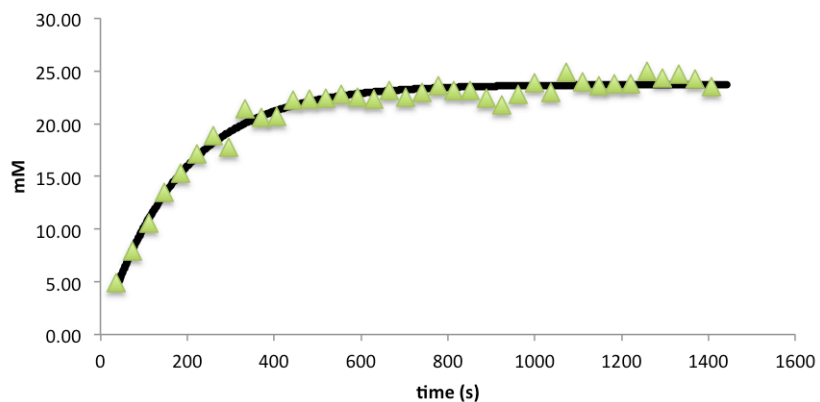
Figure 355. Formation of cross-coupled product from **73** (Run 3).

Table 97. Data for formation of cross-coupled product from **73** (Run 3).

time (s)	Integral IS (−120.00 ppm)	Integral **73** (−116.45 ppm)	[mM] **73**
37	1826	886	4.96
74	1711	1327	7.93
111	1704	1755	10.52
148	1656	2187	13.50
185	1600	2394	15.29
222	1651	2775	17.17
259	1627	2999	18.83
296	1672	2903	17.75
333	1588	3334	21.45
370	1568	3161	20.61
407	1630	3300	20.70
444	1642	3578	22.26
481	1629	3560	22.33
518	1598	3508	22.44
555	1558	3470	22.76
592	1607	3535	22.49
629	1601	3495	22.31
666	1655	3754	23.18
703	1605	3537	22.52
740	1589	3570	22.97
777	1631	3760	23.57
814	1643	3721	23.14
851	1647	3736	23.18
888	1637	3594	22.45
925	1676	3567	21.75

Table 97. (cont.)

962	1648	3668	22.75
999	1624	3792	23.86
1036	1641	3688	22.97
1073	1584	3857	24.89
1110	1553	3639	23.95
1147	1600	3700	23.63
1184	1651	3847	23.81
1221	1637	3811	23.79
1258	1595	3900	25.00
1295	1644	3912	24.31
1332	1546	3737	24.70
1369	1583	3759	24.26
1406	1638	3766	23.50
1443	1649	3903	24.19

Experiment 80: Cross-coupling formation from complex 135 in THF

A 1-mL volumetric flask was charged with freshly sublimed 2-hydroxy-2-methylpropanoic acid 4-fluorophenylboronate (44.0 mg, 210 μmol). Then ~0.5 mL of THF (NaK) was added and sonicated until the solid had dissolved. Once dissolved the flask was filled to the mark with THF (NaK) generating a 0.21 M solution of 2-hydroxy-2-methylpropanoic acid 4-fluorophenylboronate.

A 2-mL volumetric flask was taken into the dry box and charged with [(*i*-Pr$_3$P)Pd(4-FC$_6$H$_4$)(μ-OH)]$_2$ (30.8 mg, 41 μmol) and 1,4-difluorobenzene (2.5 μL, 24 μmol) followed by dissolving with THF (NaK) to the 2-mL mark. An oven dried, 5-mm, NMR tube was taken into the dry box and 500 μL of the freshly prepared solution was added. The tube was capped with a septum and Teflon taped. The sample was removed from the glove box and inserted into a −78 °C acetone dry-ice bath followed by the addition of the 2-hydroxy-2-methylpropanoic acid 4-fluorophenylboronate solution (95 μL, 20.5 μmol, 2.0 equiv) *via* a 100 μL glass syringe. The NMR tube was vortexed (not shaken) and cleaned with a Kimwipe followed by re-insertion into the −78 °C bath. Then the tube was placed into the NMR probe set to −30 °C.

Using the fluorine channel to collect a spectrum every 101 s the progress of the reaction was monitored by the and formation of cross-coupling product (−116.45 ppm) in comparison with the internal reference 1,4-difluorobenzene (−120.00 ppm). The first order decay and formation profiles were fitted with OrginPro 2015 software using equations 1 and 2 respectively. This procedure was performed three times to obtain an average rate.

Table 98. Results from the cross-coupling reaction.

Entry	k (s^{-1}) (Form CCP)	A_0 [mM] (Form CCP)
Run 1	$(2.59 \pm 0.05) \times 10^{-4}$	11.56 ± 0.13
Run 2	$(2.63 \pm 0.11) \times 10^{-4}$	12.23 ± 0.35
Run 3	$(1.84 \pm 0.05) \times 10^{-2}$	10.63 ± 0.18

k avg. Formation of CCP = (2.26 ± 0.31) x 10^{-4} s^{-1}
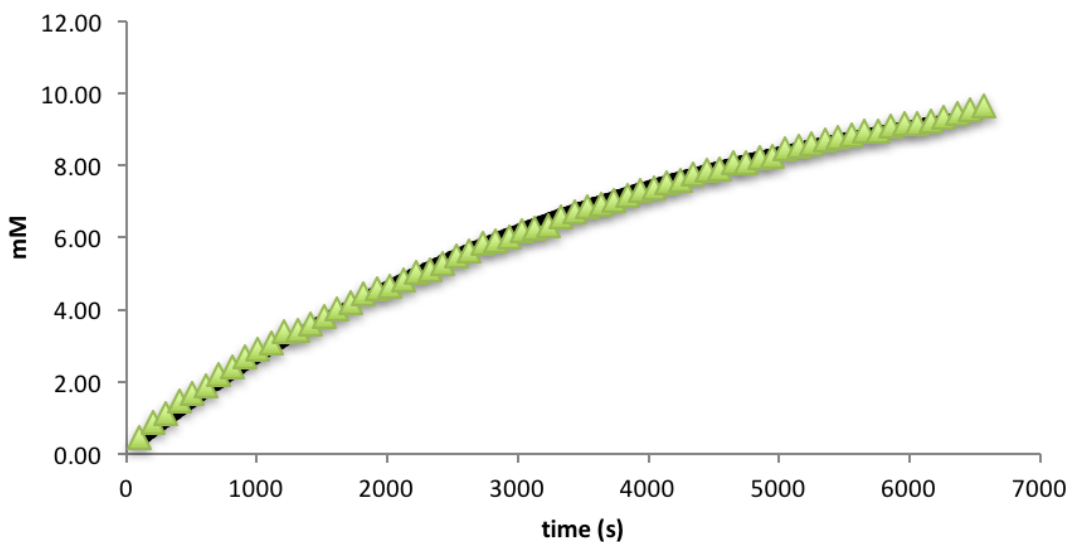
Figure 356. Formation of **73** from **135**. (Run 3).

Table 99. Data for the formation of **73** from **135**. (Run 3).

time (s)	Integral IS (−120.00 ppm)	Integral **73** (−116.45 ppm)	[mM] **73**
101	286.699	37.0951	0.14
202	268.384	119.789	0.61
303	256.513	172.32	0.67
404	252.627	211.216	0.82
505	242.445	266.369	1.04
606	236.901	337.288	1.44
707	229.555	365.777	1.43
808	236.473	388.161	1.55
909	226.774	437.934	1.76
1010	239.885	499.11	2.01
1111	222.87	520.427	2.09

Table 99. (cont.)

1212	223.349	585.01	2.34
1313	232.38	605.499	2.38
1414	243.28	657.95	2.55
1515	243.879	676.203	2.67
1616	237.742	712.489	2.83
1717	233.078	763.338	2.98
1818	244.254	778.389	3.04
1919	235.238	810.986	3.20
2020	246.936	845.311	3.30
2121	244.266	880.017	3.44
2222	237.056	900.474	3.47
2323	243.463	944.449	3.69
2424	245.653	981.717	3.84
2525	241.901	1002.45	3.93
2626	248.438	1044.36	4.06
2727	245.185	1057.39	4.13
2828	244.014	1098.17	4.28
2929	238.265	1128.31	4.39
3030	244.301	1141.91	4.47
3131	237.646	1165.13	4.58
3232	242.073	1186.96	4.65
3333	241.57	1210.98	4.79
3434	249.979	1245.49	4.88
3535	243.872	1276.66	5.02
3636	246.099	1299.93	5.07
3737	248.435	1327.28	5.20
3838	239.981	1352	5.31
3939	250.93	1369.6	5.34
4040	233.038	1382.4	5.41
4141	245.144	1426.38	5.59
4242	248.435	1461.61	5.77
4343	248.435	1447.35	5.71
4444	239.981	1493.86	5.87
4545	250.93	1537.23	6.02
4646	233.038	1521.42	5.97
4747	245.144	1559.94	6.10
4848	240.198	1565.6	6.20
4949	250.854	1620.02	6.35
5050	239.981	1626.52	6.38

Table 99. (cont.)

5151	250.93	1660.2	6.60
5252	248.435	1655.93	6.55
5353	239.981	1685.55	6.68
5454	250.93	1702.58	6.72
5555	233.038	1756.36	6.87
5656	245.144	1745.21	6.89
5757	240.198	1775.18	6.95
5858	250.854	1787.06	6.99
5959	233.038	1824.58	7.21
6060	245.144	1832.45	7.24
6161	240.198	1849.86	7.29
6262	250.854	1846.7	7.35
6363	240.198	1861.84	7.38
6464	250.854	1880.9	7.39
6565	242.62	1909.08	7.60

Experiment 81: Preparation of 4-fluorophenylglycol ester
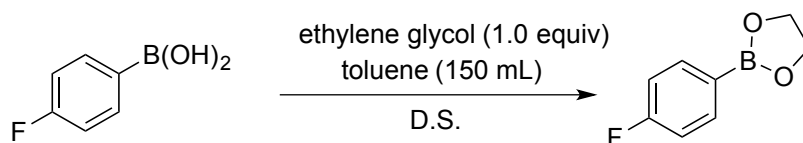
A 250-mL, round-bottomed flask was charged with a magnetic stir bar, 4-fluorophenyl boronic acid (4.2 g, 30 mmol, 1.0 equiv), ethylene glycol (1.86 g, 30 mmol, 1.0 equiv) and 150 mL of toluene (SDS). A dean stark trap apparatus filled with 4 Å molecular sieves was fitted and the reaction was refluxed for 16 h. Toluene was removed by roto-evaporation and the remaining solid was sublimed at 60 °C under high vacuum yielding a white powder 1.45 g, 72%. The spectra matched those previously published by Sigman and co-workers.[137]

Experiment 82: Preparation of 2-hydroxy-2-methyl propanoic ester 134
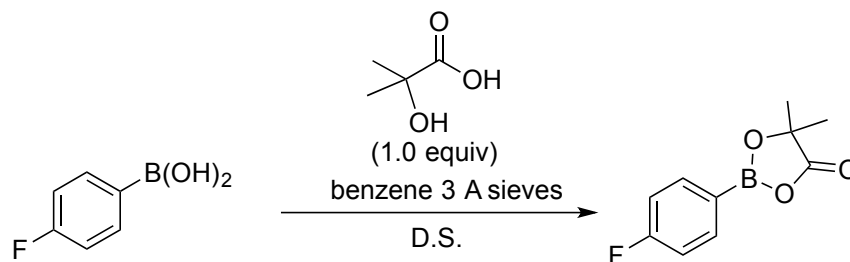
A 500-mL, round-bottomed flask was charged with a magnetic stir bar, 4-fluorophenyl boronic acid (1.0 g, 8.2 mmol, 1.0 equiv), 2-hydroxy-2-methyl propanoic (0.86 g, 8.2 mmol, 1.0 equiv) and 150 mL of benzene. A dean stark trap apparatus filled with 3 Å molecular sieves was fitted and the reaction was refluxed for 15 h. Benzene was removed by roto-evaporation and the remaining solid was sublimed at 50 °C under high vacuum yielding a white powder 1.04 g, 61%.

Experiment 83: Preparation of oxalic acid ester 137
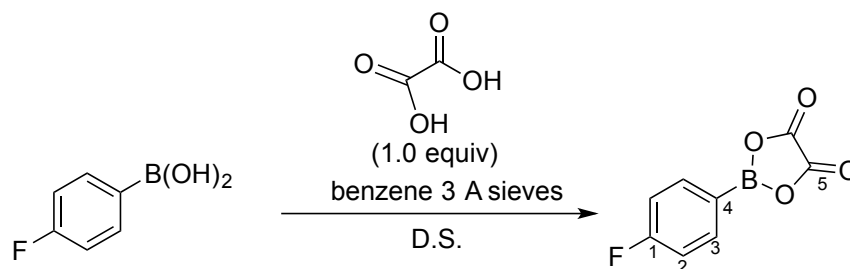
A 250-mL, round-bottomed flask was charged with a magnetic stir bar, 4-fluorophenyl boronic acid (4.2 g, 30 mmol, 1.0 equiv), oxalic acid dihydrate (3.78 g, 30 mmol, 1.0 equiv) and 150 mL of benzene. A dean stark trap apparatus filled with 3 Å molecular sieves was fitted and the reaction was refluxed for 16 h. A white powder was observed it was collected and washed with hot benzene to yield 0.83 g, 14%.

Data for **137**:

^{1}H NMR:	(600 MHz, THF-d_8)
	8.39 (m, 2 HC(3)), 7.23 (m, 2 HC(2)),
^{19}F NMR:	(565 MHz, THF-d_8)
	−108.8 (s, FC(1))
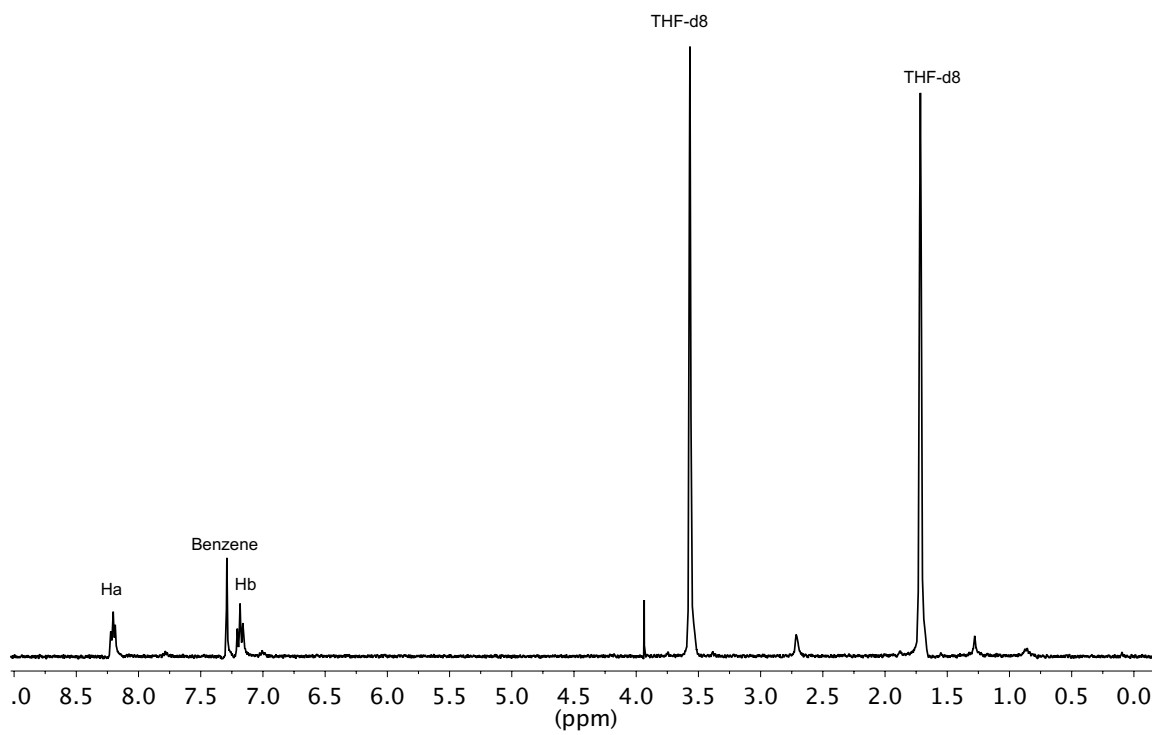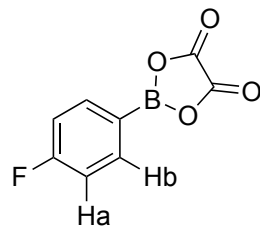
Figure 357. ^{1}H NMR spectrum of **137**.
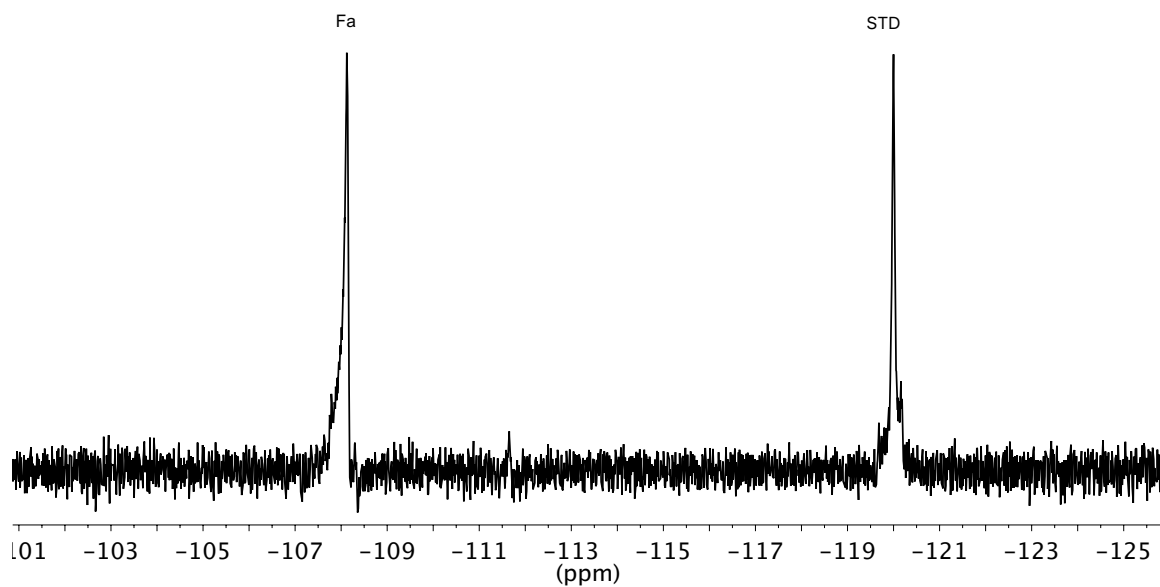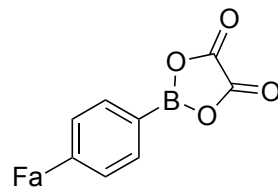
Figure 358. ^{19}F NMR spectrum of **137** −100 °C, referenced to 1,4-diflurobenzene (−120.00 ppm).

513

REFERENCES:

(1)   (a) Chemla, F.; Ferreira, F.; Perez-Luna, A.; Micouin, L.; Jackowski, O. *Metal-Catalyzed Cross-Coupling Reactions and More, 3ⁿᵈ Edition;* de Meijere A., Bräse, S., Oestreich, M., Eds.; Wiley-VCH: Weinheim, Germany, 2014; Vol. 1, Chapter. 5. (b) Heravi, M. M.; Hajiabbasi, P. *Monatsh. Chem. Mon.* **2012**, *143*, 1575-1592.

(2)   (a) Lee, J. C. H.; Hall, D. G. *Metal-Catalyzed Cross-Coupling Reactions and More, 3ⁿᵈ Edition;* de Meijere A., Bräse, S., Oestreich, M., Eds.; Wiley-VCH: Weinheim, Germany, 2014, Vol. 1. Chapter 2. (b) Lennox, A. J. J.; Lloyd-Jones, G. C. *Chem. Soc. Rev.* **2014**, *43*, 412-443. (c) Miyaura, N.; Suzuki, A. *Chem. Rev.* **1995**, *95*, 2457-2483.

(3)   (a) Martín-Matute, B.; Szabó, K. J.; Mitchell, T. N.; *Metal-Catalyzed Cross-Coupling Reactions and more, 3ⁿᵈ Edition;* de Meijere A., Bräse, S., Oestreich, M., Eds.; Wiley-VCH: Weinheim, Germany, 2014, Vol. 2, Chapter 6. (b) Farina, V.; Krishnamurthy, V; Scott, W. J. *Org. React.* **2004**, *50,* Vol. 1.

(4)   (a) Chang, W. T. T.; Smith, R. C.; Regens, C. S.; Bailey, A. D.; Werner, N. S.; Denmark, S. E. *Org. React.* **2011**, *75*, Chapter 3. (b) Denmark, S.E.; Sweis, R.F. *Metal-Catalyzed Cross-Coupling Reactions and more, 3ⁿᵈ Edition;* de Meijere A., Bräse, S., Oestreich, M., Eds.; Wiley-VCH: Weinheim, Germany, 2014, Vol. 2, Chapter 7.

(5)   (a) Xu, S.; Kamada, H.; Kim, E. H.; Oda, A.; Negishi, E. *Metal-Catalyzed Cross-Coupling Reactions and more, 3ⁿᵈ Edition;* de Meijere A., Bräse, S., Oestreich, M., Eds.; Wiley-VCH: Weinheim, Germany, 2014, Vol. 1, Chapter 3. (b) Phapale, V. B.; Cárdenas, D. J.; *Chem. Soc. Rev.* **2009**, *38*, 1598-1607.

(6)   (a) Suzuki, A., *Angew. Chem., Int. Ed.* **2011**, *50*, 6722-6737. (b) Seechurn, C. C. C. J.; Kitching, M. O.; Colacot, T. J., Snieckus, V., *Angew. Chem., Int. Ed.* **2012**, *51*, 5062-5085.

(7)   Picquet, M. *Organometallics as Catalysts in the Fine Chemical Industry.* Matthias, B.; Blaser, H.U. Springer: Berlin Heidelberg, 2013, Vol. 42, Chapter 1.

(8)   (a) Magano, J.; Dunetz, J. R. *Chem. Rev.* **2011,** *111*, 2177-2250. (b) Torborg, C.; Beller, M. *Adv. Synth. Catal.* **2009**, *351*, 3027-3043. (c) Corbet, J.-P.; Mignani, G. *Chem. Rev.* **2006**, *106*, 2651-2710. (d) Lipton, M. F.; Mauragis, M. A.; Maloney, M. T.; Veley, M. F.; VanderBor, D. W.; Newby, J. J.; Appell, R. B.; Daugs, E. D.; *Org Proc. Res. Dev.* **2003**, *7*, 385-392.

(9)   Stille, J. K.; Lau, K.S.Y. *Acc. Chem. Res.* **1977**, *10*, 434-442.

(10)   Shekhar, S.; Hartwig, J. F. *J. Am. Chem. Soc.* **2004**, *126*, 13016-13027.

(11)   (a) Tymonko, S. A.; Smith, R. C.; Ambrosi, A.; Denmark, S. E. *J. Am. Chem. Soc.* **2015**, *137*, 6192-9199. (b) Tymonko, S. A.; Smith, R. C.; Ambrosi, A.; Ober, M. H.; Wang, H.; Denmark, S. E. *J. Am. Chem. Soc.* **2015**, *137*, 6200-6218.

(12)   Heck, R.F. *J. Am. Chem. Soc.* **1969**, *91*, 6707-6714.

(13)   Jutand, A., Mechanisms of the Mizoroki–Heck Reaction. In *The Mizoroki–Heck Reaction*, John Wiley & Sons, Ltd: 2009; pp 1-50

(14)   Fitton, P.; Rick, E. A. *J. Organometal. Chem.* **1971**, *28*, 287-291.

(15)   (a) Fauvarque, J. F.; Pfluger, F.; Troupel, M., *J. Organomet. Chem.* **1981,** *208* (3), 419-27. (b) Amatore, C.; Jutand, A., *J. Organomet. Chem.* **1999,** *576*, 254-278.

(16)   Vicente, J.; Arcas, A.; Bautista, D. *Organometallics* **1997**, *16*, 2127-2138.

(17)   Fu, G. C., *Acc. Chem. Res.* **2008,** *41*, 1555-1564.

(18)   Old, D. W.; Wolfe, J. P.; Buchwald, S. L., *J. Am. Chem. Soc.* **1998,** *120*, 9722-9723.

(19)   (a) Paul, F.; Patt, J.; Hartwig, J. F., *J. Am. Chem. Soc.* **1994,** *116*, 5969-5970 (b) Paul, F.; Patt, J.; Hartwig, J. F.,. *Organometallics* **1995,** *14*, 3030-30399. (c) Hartwig, J. F.; Paul, F.,. *J. Am. Chem. Soc.* **1995,** *117*, 5373-5374.

(20)   Stambuli, J. P.; Buehl, M.; Hartwig, J. F., *J. Am. Chem. Soc.* **2002,** *124*, 9346-9347.

(21)   Gillie, A.; Stille, J. K., Mechanisms of 1,1-reductive elimination from palladium. *J. Am. Chem. Soc.* **1980,** *102*, 4933-4941.

(22)   Ozawa, F.; Ito, T.; Nakamura, Y.; Yamamoto, A., *Bull. Chem. Soc. Jpn.* **1981,** *54*, 1868-1880.

(23)   Shekhar, S.; Hartwig, J. F., *J. Am. Chem. Soc.* **2004,** *126*, 13016-13027.

(24)   (a) Kosugi, M.; Shimizu, Y.; Migita, T., *J. Organomet. Chem.* **1977,** *129*, C36-C38. (b) Kosugi, M.; Shimizu, Y.; Migita, T., *Chem. Lett.* **1977**, 1423-1424.

(25)   Milstein, D.; Stille, J. K., *J. Am. Chem. Soc.* **1978,** *100*, 3636-3638.

(26)   Stille, J. K., *Angew. Chem.* **1986,** *98,* 504-519.

(27)   Farina, V.; Krishnamurthy, V.; Scott, W. J., The Stille Reaction. In *Organic Reactions*, John Wiley & Sons, Inc.: 2004.

(28)   Labadie, J. W.; Stille, J. K., *J. Am. Chem. Soc.* **1983,** *105*, 6129-37.

(29)   Casado, A.L.; Espinet, P. *J. Am. Chem. Soc.* **1998**, *120*, 8978-8985.

(30)   (a) Farina, V.; Baker, S. R.; Benigni, D.; Sapino, C., Jr., *Tetrahedron Lett.* **1988,** *29*, 5739-42. (b) Green, R. J.; Anderson, S. L., *Int. Rev. Phys. Chem.* **2001,** *20*, 165-188.

(31)   Louie, J.; Hartwig, J. F., *J. Am. Chem. Soc.* **1995,** *117*, 11598-11599.

(32)   Farina, V.; Krishnan, B.,. *J. Am. Chem. Soc.* **1991,** *113*, 9585-9595.

(33)   Tamao, K.; Yoshida, J.; Yamamoto, H.; Kakui, T.; Matsumoto, H.; Takahashi, M.; Kurita, A.; Murata, M.; Kumada, M., *Organometallics* **1982,** *1*, 355-68.

(34)   Hatanaka, Y.; Hiyama, T., *J. Org. Chem.* **1988,** *53*, 918-920.

(35)   Sugiyama, A.; Ohnishi, Y.-y.; Nakaoka, M.; Nakao, Y.; Sato, H.; Sakaki, S.; Nakao, Y.; Hiyama, T., *J. Am. Chem. Soc.* **2008,** *130*, 12975-12985.

(36)   Amatore, C.; Grimaud, L.; Le Duc, G.; Jutand, A., *Angew. Chem., Int. Ed.* **2014,** *53*, 6982-6985.

(37)   Denmark, S.E.; Smith, R.C. *J. Am. Chem. Soc.* **2010**, *132*, 1243-1245.

(38)   Martin, J. C.; Arduengo, A. J., Lau, W.; Alegria, A.; Kochi, J. K. *J. Am. Chem. Soc.* **1980**, *102,* 7753-7759.

(39)   For an excellent summary of the current state of understanding of transmetalation in the Suzuki-Miyaura reaction see: Lennox, A. J. J.; Lloyd-Jones, G. C. *Angew. Chem., Int. Ed.* **2013,** *52,* 7362 – 7370.

(40)   Matos, K.; Soderquist, J. A. Alkylboranes in the Suzuki−Miyaura Coupling: *J. Org. Chem.* **1998**, *63*, 461-470.

(41)   Ortuño, M.A.; Liedós, A.; Maseras, F.; Ujaque, G. *ChemCatChem*, **2014**, *6*, 3132-3138.

(42)   These conclusions have also been reached in similar DFT investigations: (a) Sicre, C.; Braga, A. A. C.; Maseras, F.; Cid, M. M. *Tetrahedron*, **2008**, *64*, 7437-7443. (b) Sumimoto, M.; Iwane, N.; Takahama, T.; Sakaki, S. *J. Am. Chem. Soc.* **2004**, *126*, 10457-10471. (c) Goossen, L. J.; Koley, D.; Hermann, H. J.; Thiel, W. *J. Am. Chem. Soc.* **2005**, *127*, 11102-11114. (d) Goossen, L. J.; Koley, D.; Hermann, H. L.; Thiel, W. *Organometallics* **2006**, *25*, 54-67.

(43)   Jover, J.; Fey, N.; Purdie, M.; Lloyd-Jones, G. C. Harvey, J. N. *J. Mol. Cat. A.* **2010**, *324*, 39-47.

(44)   Carrow, B. P.; Hartwig, J. F. *J. Am. Chem. Soc.* **2011**, *133*, 2116-2119.

(45)   (a) Amatore, C.; Jutand, A.; Le Duc, G. *Chem. Eur. J.* **2011**, *17*, 2492-2503. (b) Amatore, C.; Jutand, A.; Le Duc, G. *Chem. Eur. J.* **2011**, *81*, 1573-1574. (c) Amatore, C.; Jutand, A.; Le Duc, G. *Angew. Chem. Int Ed.* **2012**, *124*, 1408-1411.

(46)   Schimidt, A. F.; Kurokhtina, A. A.; Larina, E. V. *Russ. J. Gen. Chem.* **2011**, *81*, 1573-1574.

(47)   (Ph₃P)₂PdPhOH was generated in situ by reacting [(Ph₃P)PdPh(OH)]₂ in the presence of excess Ph₃P.

(48)   Aliprantis, A. O; Canary, J. W. *J. Am. Chem. Soc.* **1994**, *116*, 6985-6986.

(49)   (a) Denmark, S. E.; Williams, B. J.; Eklov, B. M.; Pham, S. M.; Beutner, G. L. *J. Org. Chem.* **2010**, *75*, 5558-5572. (b) Bartholomew, E. R.; Bertz, S. H.; Cope, S. K.; Murphy, M. D.; Ogle, C. A.; Thomas, A. A. *Chem. Commun.* **2010**, *46*, 1253-1254.

(50)   McGarrity, J. F.; Prodolliet, J.; Smyth, T. *Org. Magn. Reson.* **1981**, *17*, 59-65.

(51)   A preliminary communication of some of these results have already appeared. Thomas, A. A.; Denmark, S.E. *Science,* **2016**, *352*, 329-332.

(52)   Osakada, K.; Onodera, H.; Nishihara, Y. *Organometallics*, **2005**, *24*, 3815-3817.

(53)   Zhao, P.; Incarvito, C. D.; Hartwig, J. F. *J. Am. Chem. Soc,* **2007,** *129*, 1876-1877.

(54)   For a complete, tabular listing of all chemical shifts, see Supporting Information.

(55)   Sekiya, A.; Ishikawa, N., *J. Organomet. Chem.* **1976,** *118*, 349-54.

(56)   Driver, M. S.; Hartwig, J. F., *Organometallics* **1997,** *16*, 5706-5715.

(57)   Grushin, V. V.; Alper, H., *Organometallics* **1993,** *12*, 1890-901.

(58)   Grushin, V. V.; Alper, H., *Organometallics* **1996**, *15*, 5242-5245.

(59)   The addition of excess *i*-Pr₃P to the system was found to suppress the formation of cross-coupling product **73** and stabilize any intermediates formed during the reaction.

(60)   Nishihara, Y.; Onodera, H.; Osakada, K. *Chem. Commun.* **2004**, 192-193.

(61)   Weber, E.; Skobridis, K.; Ouchi, M.; Hakushi, T.; Inoue, Y. *Bull. Chem. Soc. Jpn.* **1990**, *63*, 3670-3677.

(62)   (a) Ludwig, M.; Stromberg, S.; Svensson, M.; Åkermark, B. *Orgaonometallics* **1999**, *18*, 970. (b) Alcazar-Roman, L. M.; Hartwig, J. F. *Organometallics* **2002**, *21*, 491.

(63)   Brown, H.C. *J. Am. Chem. Soc.* **1945**, *67*, 374-378.

(64)   For related 2:1 palladium complexes with acetate ligands see: Stephenson, T. A.; Morehouse, S. M. (Mrs.), Powell, A. R.; Heffer, J. P.; Wilkinson, G. *J. Chem. Soc.* **1965**, 3632-3640

(65)   Amatore, C.; Carre, E.; Jutand, A.; M'Barki, M. A.; Meyer, G. *Organometallics* **1995**, *14*, 5605.

(66)   (a) Barrios-Landeros, F.; Carrow, B.P.; Hartwig, J.F. *J. Am. Chem. Soc.* **2008**, *130,* 5842-5843. (b) Shekhar, S.; Hartwig, J. F. *Organometallics* **2007**, *26*, 340.

(67)   Ruiz, J.; Martinez, M. T.; Vicente, C.; Rodriguez, V.; Lopez, G.; Perez, J.; Chaloner, P. A.; Hitchcock, P. B., *Z. Anorg. Allg. Chem.* **2005,** *631*, 2227-2231.

(68)   Brown, H. C. *J. Am. Chem. Soc.* **1945**, *67*, 374-378.

(69)   Hayashi, Y.; Wada, S.; Yamashita, M.; Nozaki, K. *Organometallics,* **2012**, *31*, 1073-1081.

(70)   Schott, D.; Pregosin, P. S.; Veiros, L.; Calhorda, M. J. *Organometallics,* **2005**, *24*, 5710-5717.

(71)   Arrechea, P.L.; Buchwald, S.L. *J. Am. Chem. Soc.* **2016**, *138*, 12486-12493.

(72)   Cardenas, D. J.; Mateo, C.; Echavarren, A. M., Synthesis of oxa- and azapalladacycles from organostannanes. *Angew. Chem.* **1994,** *106*, 2529-2531

516

(73) Mateo, C.; Cardenas, D. J.; Fernandez-Rivas, C.; Echavarren, A. M., *Chem. - Eur. J.* **1996,** *2*, 1596-1606.

(74) See: Denmark, S. E.; Smith, R. C.; Chang, W.-T. T. *Tetrahedron* **2011**, *67*, 4391-4396.

(75) Schmid, R.; Sapunov, V. N.; in *Non-Formal Kinetics in Search for Chemical Reaction Pathways*; Ebel, H. F., Ed.; Verlag Chemie:Weinheim, 1982; Vol. 14. Chapter 3.

(76) Wei, C. S.; Davies, G. H. M.; Soltani, O.; Albrecht, J.; Gao, Q.; Pathirana, C.; Hsiao, Y.; Tummala, S.; Eastgate, M. D., *Angew. Chem., Int. Ed.* **2013,** *52*, 5822-5826.

(77) De Graaf, W.; Boersma, J.; Smeets, W. J. J.; Spek, A. L.; Van Koten, G., *Organometallics* **1989,** *8*, 2907-2917.

(78) Kuran, W.; Musco, A., *Inorg. Chim. Acta* **1975,** *12*, 187-193.

(79) Tymonko, S. A.; Smith, R. C.; Ambrosi, A.; Ober, M. H.; Wang, H.; Denmark, S. E. *J. Am. Chem. Soc.* **2015**, *137*, 6200-6218.

(80) Appleton, T. G.; Clark, H. C.; Manzer, L. E. *Coord. Chem. Rev.* **1973**, *10*, 335-422.

(81) The same strategy was used in the computational analysis of cross coupling of arylpalladium arylsilanolates to account for the high-energy dimethylsilanone species formed directly from transmetalation.[11b]

(82) Miyaura, N.; Suzuki, A. *Chem. Rev.* **1995**, *95*, 2457-2483.

(83) Hall, D. G., Structure, Properties, and Preparation of Boronic Acid Derivatives. In *Boronic Acids*, Wiley-VCH Verlag GmbH & Co. KGaA: 2011; pp 1-133.

(84) Miyaura, N.; Yanagi, T.; Suzuki, A., *Synth. Commun.* **1981,** *11*, 513-19.

(85) Hafner, A.; Meisenbach, M.; Sedelmeier, J., *Org. Lett.* **2016,** *18* , 3630-3633.

(86) Molander, G.A.; Trice, S.L.J.; Dreher, S.D. *J. Am. Chem. Soc.* **2010**, *132*, 17701-17703.

(87) Larsen, R.D.; King, A.O.; Chen, C.Y.; Corley, E.G.; Foster, B.S.; Roberts, F.E.; Yang, R.C.; Lieberman, D.R.; Reamer, R.A. *J. Org. Chem.* **1994**, *59*, 6391-6394.

(88) Lennox, A.J.; Lloyd-Jones, G.C. *Isr. J. Chem.* **2010**, *50*, 664-674.

(89) Sonogashira, K.; Tohda, Y.; and Hagihara, N; *Tetrahedron Lett.*, **1975** 4467–4470.

(90) Glasnov, T.N.; Kappe, C.O.; *Adv. Synth. Catal.* **2010**, *352*, 3089-3097.

(91) Kasai, Y.; Ito, T.; Sasaki, M. *Org. Lett.* **2012**, *14*, 3186-3189.

(92) Lennox, A.J.J.; Lloyd-Jones, G.C. *Chem. Soc. Rev.* **2014**, *43*, 412-443.

(93) Brown, HC.; Zweifel, G. *J. Am. Chem. Soc.* **1959**, *81*, 241-247.

(94) Ishiyama, T.; Murata, M.; Miyaura, N. *J. Org. Chem.*, **1995**, *60*, 7508-7510.

(95) Kinuta, H.; Tobisu, M.; Chatani, N., *J. Am. Chem. Soc.* **2015,** *137*, 1593-1600.

(96) Kruger, A.W.; Rozema, M.J.; Chu-Kung, A.; Gandarilla, J.; Haight, A.R., Kotecki, B. J.; Richter, S.M.; Schwartz, A.M.; and Wang, Z. *Org. Process Res. Dev.,* **2009**, *13*, 1419–1425.

(97) Stewart, G.W.; Brands, K.M.J.; Brewer, S.E.; Cowden, C.J., Davies, A.J.; Edwards, J.S.; Gibson, A.W.; Hamilton, S.E.; Katz, J.D., Keen, S.P.; Mullens, P.R.; Scott, J.P., Wallace, D.J.; and Wise, C.S. *Org. Process Res. Dev.,* **2010,** *14*, 849–858.

(98) De Koning, P.D.; McAndrew, D.; Moore, R., Moses, I.B.; Boyles, D.C.; Kissick, K.; Stanchina, C.L.; Cuthbertson, T.; Kamatani, A.; Rahman, L.; Rodriguez, R.; Urbina, A.; Sandoval, A.; and Rose, P.R. *Org. Process Res. Dev.*, **2011,** *15*, 1018–1026.

(99) Li, J.; Grillo, A.S.; Burke, M.D. *Acc Chem Rev* **2015**, *48*,2297-2307

(100) Molander, G.A.; Rivero, M.R. *Org. Lett.* **2002**, *4*, 107-109.

(101) Worely, E.M.; Roy, J. Burke, M.D. *Nature Chem.* **2014**, *6*, 484-491.

(102) Gillis, E.P.; Burke, M.D. *J. Am. Chem. Soc.* **2007**, *129*, 6716-6717.

(103) Knapp, D.M.; Gillis, E.P. Burke, M.D. *J.Am. Chem. Soc.* **2009**, *131*, 6961-6963.

(104) Gonzalez, J. A.; Ogba, O. M.; Morehouse, G. F.; Rosson, N.; Houk, K. N.; Leach, A. G.; Cheong, P. H. Y.; Burke, M. D.; Lloyd-Jones, G. C., *Nat. Chem.* **2016,** *8* (11), 1067-1075.

(105) Chambers, R.D.; Clark, H.C.; Willis, C.J. *J. Am. Chem. Soc.* **1960**, *82*, 5298-5301.

(106) Dares, S.; Genet, J.P.; Brayer, J.L.; Demoute, J.P. *Tetrahedron Lett.* **1997**, *38*, 4393-4396.

(107) Molander, G.A. Petrillo, D.E. *J. Am. Chem. Soc.* **2006**, *128*, 9634-9635.

(108) Darses, S.; Genet, J.P. *Chem. Rev.***2008**, *108*, 288-325.

(109) Vedejs, E.; Chapman, W.; Fields, S.C.; Lin, S. Schrimpf, M.R. *J. Org. Chem.* **1995**, *60,* 3020-3027.

(110) Lennox, A.J.; Lloyd-Jones, G.C. *Angew. Chem. Int. Ed.* **2012**, *51*, 9385-9388.

(111) Dumrath, A.; Lübbe, C.; Beller, M., Palladium-Catalyzed Cross-Coupling Reactions – Industrial Applications. In *Palladium-Catalyzed Coupling Reactions*, Wiley-VCH Verlag GmbH & Co. KGaA: 2013; pp 445-489.

(112) Grosjean, C., Henderson, A.P., Herault, D., Ilyashenko, G., Knowles, J.P., Whiting, A., and Wright, A.R. *Org. Process Res. Dev* **2009**, *13*, 434–441.

(113) Molander, G.A.; Dehmel, F. *J. Am. Chem. Soc.* **2004**, *126*, 10313-10318.

(114) Lennox, A.J.J.; Lloyd-Jones, G.C. *J. Am. Chem. Soc.* **2012**, *134*, 7431-7441

(115) A preliminary communication of some of these results have already appeared. Thomas, A. A.; Denmark, S.E. *Science*, **2016**, *352*, 329-332.

(116) Lennox, A. J. J.; Lloyd-Jones, G. C. *Chem. Soc. Rev.* **2014**, *43*, 412-443.

(117) Hartley, F.R. *The Chemistry of Platinum and Palladium* Robinson, P.L. Ed. Wiley-VCH, New York, 1973

(118) Clark, H.C.; Manzer, L.E. *J. Organomet. Chem.* **1973**, *59*, 411.

(119) Appleton, T.G.; Clark, H.C.; Manzer, L.E. *J. Organomet. Chem.* **1974**, *65*, 275.

(120) Arnold, D.P.; Bennett, M.A. *J. Organomet. Chem.* **1980**, *199*, 119.

(121) Khan, H.; Badshah, A.; Murtaz, G.; Said, M.; Zia ur, R.; Neuhausen, C.; Todorova, M.; Jean-Claude, B. J.; Butler, I. S. *Eur. J. Med. Chem.* **2011**, *46*, 4071-4077.

(122) Jordan-Hore, J.A.; Sanderson, J.N.; Lee, A.L. **2012**, *14*, 2508-2511.

(123) Carrow, B. P.; Hartwig, J. F. *J. Am. Chem. Soc.* **2011**, *133*, 2116-2119.

(124) Tymonko, S.A.; Smith, R.C.; Ambrosi, A.; Ober, M.H.; Wang, H. Denmark, S.E. *J. Am. Chem. Soc.* **2015**, *137*, 6200-6218.

(125) Tatsuno, Y.; Yoshida, T.; Otsuka, S. *Inorg. Synth.* **1990**, *28*, 342-345.

(126) Khan, H.; Badshah, A.; Murtaz, G.; Said, M.; Rehman, Z.; Neuhausen, C.; Todorova, M.; Jean-Claude, B.J.; Butler, I.S. *Eur. J. Med. Chem.* **2011**, *46*, 4071-4077.

(127) Grushin, V.V.; Alper, H *Organometallics*, **1996**, *15*, 5242-5245.

(128) Kuran, W.; Musco, A. *Inorganic Chimica Acta,* **1975**, *187-193*.

(129) Sola, E.; Navarro, J.; López, J.A.; Lahoz, F.J.; Oro, L.A.; Werner, H. *Organometallics*, **1999**, *18*, 3534-3546.

(130) Olah, G.A.; McFarland, C.W. *J. Org. Chem.* **1969***, 34*, 1832-1834.

(131) Schmid, R.; Sapunov, V. N.; in *Non-Formal Kinetics in Search for Chemical Reaction Pathways*; Ebel, H. F., Ed.; Verlag Chemie:Weinheim, 1982; Vol. 14. Chapter 3.

(132) Jordan-Hore, J.A.; Sanderson, J.N.; Lee, A.L. **2012**, *14*, 2508-2511.

(133) Carrow, B. P.; Hartwig, J. F. *J. Am. Chem. Soc.* **2011**, *133*, 2116-2119.

(134) Tymonko, S.A.; Smith, R.C.; Ambrosi, A.; Ober, M.H.; Wang, H. Denmark, S.E. *J. Am. Chem. Soc.* **2015**, *137*, 6200-6218.

(135) Tatsuno, Y.; Yoshida, T.; Otsuka, S. *Inorg. Synth.* **1990**, *28*, 342-345.

(136) R. Schmid, V. N. Sapunov, in *Non-Formal Kinetics in Search for Chemical Reaction*

(137) Iwai, Y.; Gligorich, K.M.; Sigman, S.M. *Angew. Chem. Int. Ed.* **2008**, *47*, 3219-3222.